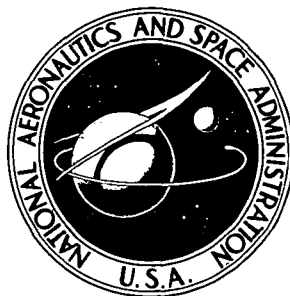


~~CONFIDENTIAL~~

NASA TECHNICAL
MEMORANDUM

NASA TM X-2759



NASA TM X-2759

DOWNGRADED TO *unclassified*
BY AUTHORITY OF NASA CLASSIFICATION
CHANGE NOTICES NO. *240* DATE *30 sep 76*
ITEM NO. *41*

~~CONFIDENTIAL~~ CLASSIFIED
BY ~~Henry A. Fedruk~~
SUBJECT TO GENERAL DECLASSIFICATION SCHEDULE OF
EXECUTIVE ORDER 11652 AUTOMATICALLY DOWNGRADED
AT TWO YEAR INTERVALS AND DECLASSIFIED ON DEC 31
1979

A WIND-TUNNEL INVESTIGATION
OF THE APPLICATION OF THE
NASA SUPERCRITICAL AIRFOIL TO
A VARIABLE-WING-SWEEP FIGHTER AIRPLANE

by Theodore G. Ayers
Langley Research Center
Hampton, Va. 23365

NATIONAL AERONAUTICS AND SPACE ADMINISTRATION • WASHINGTON, D. C. • JULY 1973

~~CONFIDENTIAL~~

1. Report No. NASA TM X-2759	2. Government Accession No.	3. Recipient's Catalog No.
4. Title and Subtitle A WIND-TUNNEL INVESTIGATION OF THE APPLICATION OF THE NASA SUPERCRITICAL AIRFOIL TO A VARIABLE-WING-SWEEP FIGHTER AIRPLANE (U)		5. Report Date July 1973
		6. Performing Organization Code
7. Author(s) Theodore G. Ayers		8. Performing Organization Report No. L-8689
		10. Work Unit No. 760-64-01-05
9. Performing Organization Name and Address NASA Langley Research Center Hampton, Va. 23665		11. Contract or Grant No.
		13. Type of Report and Period Covered Technical Memorandum
12. Sponsoring Agency Name and Address National Aeronautics and Space Administration Washington, D.C. 20546		14. Sponsoring Agency Code

15. Supplementary Notes

16. Abstract

An investigation was conducted in the Langley 8-foot transonic pressure tunnel and the Langley Unitary Plan wind tunnel to evaluate the effectiveness of three variations of the NASA supercritical airfoil as applied to a model of a variable-wing-sweep fighter airplane. Wing panels incorporating conventional NACA 64A-series airfoil with 0.20 and 0.40 camber were used as bases of reference for this evaluation. Static force and moment measurements were obtained for wing leading-edge sweep angles of 26°, 33°, 39°, and 72.5°. Fluctuating wing-root-bending-moment data were obtained at subsonic speeds to determine buffet characteristics. Subsonic data were also obtained for determining the effects of wing transition location and spoiler deflection. Limited lateral directional data are included for the conventional 0.20 cambered wing and the supercritical wing.

CLASSIFICATION CHANGE

To **UNCLASSIFIED**
 By authority of NASA HDQ. T.D. 77-163
 Changed by L. Shirley Date 6-15-76
 Classified Document Master Control Station, NASA
 Scientific and Technical Information Facility

17. Key Words (Suggested by Author(s))
 Transonic aerodynamics
 Supercritical wing
 Variable sweep fighter aircraft

19. Security Classif. (of this report) Confidential	20. Security Classif. Unclassified
---	---------------------------------------

~~"NATIONAL SECURITY INFORMATION"~~
 Unauthorized Disclosure Subject to Criminal Sanctions.

[REDACTED]

A WIND-TUNNEL INVESTIGATION OF THE
APPLICATION OF THE NASA SUPERCRITICAL AIRFOIL TO A
VARIABLE-WING-SWEEP FIGHTER AIRPLANE*

By Theodore G. Ayers
Langley Research Center

SUMMARY

An investigation has been conducted in the Langley 8-foot transonic pressure tunnel and the Langley Unitary Plan wind tunnel to evaluate the effectiveness of three variations of the NASA supercritical airfoil as applied to a model of a variable-wing-sweep fighter airplane. Wing panels incorporating conventional NACA 64A-series airfoils with 0.20 and 0.40 camber were used as bases of reference for this evaluation. Static force and moment measurements were obtained for wing leading-edge sweep angles of 26° , 33° , and 39° at subsonic speeds and for a wing leading-edge sweep angle of 72.5° at transonic and supersonic speeds. In addition, fluctuating wing-root-bending-moment data were obtained at subsonic speeds to determine buffet characteristics.

The results of this evaluation indicate that increasing the conventional camber had little effect on the cruise Mach number but did reduce the trimmed drag characteristics in the moderate- to high-lift range and did increase the buffet onset lift coefficient at subsonic speeds. An increase in the cruise Mach number capability of about 0.10 was noted for the model with the supercritical wing as compared with the wings incorporating conventional NACA 64A-series airfoils. Substantial reductions in the moderate- to high-lift trimmed drag characteristics were achieved with the supercritical wing at the higher subsonic speeds. The lift coefficient for buffet onset was increased significantly with the supercritical wing for a leading-edge sweep angle of 26° at Mach numbers of 0.75 and above. The low-speed (Mach number = 0.60) drag characteristics were somewhat higher and the buffet-onset lift coefficient somewhat lower for the supercritical wing as compared with the conventional 0.40 cambered wing although these characteristics were improved by the use of trailing-edge flaps. At supersonic speeds, the trimmed drag characteristics for the supercritical wing were slightly higher than those for the wings incorporating conventional camber. No adverse yaw characteristics were noted for the supercritical wing at the test conditions for which data were obtained.

*Title, Unclassified.

[REDACTED]

~~CONFIDENTIAL~~

INTRODUCTION

The current emphasis on fighter aircraft capable of achieving high maneuver load factors for air-to-air combat at high subsonic speeds has created a need for basic research in the areas of buffet and high-lift drag at transonic speeds. The stringent requirements placed on these aircraft also are such that methods must be found to reduce the drag and airplane buffeting associated with shock-induced boundary-layer separation of the wing flow at high maneuvering lift coefficients. Although twist, camber, and sweep have a favorable effect on the wing flow characteristics, the use of these methods alone does not fully solve the basic supercritical flow problem. Two-dimensional results for recently developed integral supercritical airfoils (ref. 1) have indicated that substantial improvements in aircraft performance at high subsonic speeds might be achieved by special shaping of the airfoil to improve the supercritical flow above the upper surface. Three-dimensional wind-tunnel and flight-test results are included in references 2 to 5 for airplane configurations intended to demonstrate the potential of the supercritical airfoil for improving wing structural efficiency and airplane cruise speed.

As is well known, at supercritical Mach numbers a broad region of supersonic flow extends vertically from an airfoil. This region of supersonic flow is usually terminated by a shock wave causing an energy loss and therefore a drag increase. In addition, the shock wave produces a positive pressure gradient at the airfoil surface which may cause separation of the boundary layer with an associated large increase in drag. This shock-induced separation occurs initially on an airfoil because the low-momentum air of the boundary layer cannot traverse the pressure rise through the shock wave superimposed on the subcritical pressure recovery. The special shaping of the supercritical airfoil upper surface reduces both the extent and strength of the shock wave and also reduces the adverse pressure gradient behind the shock wave with corresponding reductions in the drag. To compensate for the reduced lift on the upper surface of the supercritical airfoil resulting from the reduced curvature, the airfoil has increased camber near the trailing edge. Unpublished two-dimensional results have indicated a delay in the drag-rise Mach number of about 0.10 as compared with a conventional 6-series airfoil. In addition, a significant delay in the Mach number for buffet onset at a given lift coefficient was noted as well as an increase in the maximum lift coefficient for buffet onset.

On the basis of the two-dimensional results, a program was initiated by the NASA to investigate the three-dimensional characteristics of a variable-wing-sweep fighter airplane model incorporating the supercritical airfoil. A variable-wing-sweep model was chosen because of the large leading-edge radius of the supercritical airfoil which must be swept behind the Mach line for operation at supersonic speeds. The purpose of this paper is to present the results of this three-dimensional investigation. Data are also included for a NACA 64A-series airfoil with 0.20 and 0.40 camber to indicate the improvements in

~~CONFIDENTIAL~~

high-lift characteristics which might be expected from an increase in conventional camber. Data are included herein for the effects of wing section geometry, wing incidence angle, trailing-edge flap deflection, and wing leading-edge sweep angle. Limited data are included for the effects of horizontal-tail deflection and transition location.

SYMBOLS

The results as presented herein are referred to the body-axis system with the exception of the lift and drag coefficients which are referred to the stability-axis system. The moment center was located at a point 55.174 cm (21.722 in.) rearward of the nose ($0.45c$, $\Lambda = 16^\circ$) along the model reference line. (See fig. 1.) All coefficients are based on the geometry of the model having a wing-leading-edge sweep of 16° . Data were obtained in U.S. Customary Units and are presented herein in both SI and U.S. Customary Units. The coefficients and symbols used herein are defined as follows:

b	wing span, 80.010 cm (31.500 in.)
C_D	drag coefficient, $\frac{\text{Drag}}{qS}$
C_L	lift coefficient, $\frac{\text{Lift}}{qS}$
C_l	rolling-moment coefficient, $\frac{\text{Rolling moment}}{qSb}$
$C_{l\beta}$	lateral stability parameter, $\frac{\Delta C_l}{\Delta\beta}$, per deg
C_m	pitching-moment coefficient, $\frac{\text{Pitching moment}}{qS\bar{c}}$
C_n	yawing-moment coefficient, $\frac{\text{Yawing moment}}{qSb}$
$C_{n\beta}$	directional stability parameter, $\frac{\Delta C_n}{\Delta\beta}$, per deg
C_Y	side-force coefficient, $\frac{\text{Side force}}{qS}$
$C_{Y\beta}$	side-force parameter, $\frac{\Delta C_Y}{\Delta\beta}$, per deg
c	local chord, cm (in.)
\bar{c}	wing mean aerodynamic chord, 11.483 cm (4.521 in.)

- i_w incidence of wing reference plane at pivot relative to model reference line
(positive when trailing edge is down), deg
- L/D lift-drag ratio
- M free-stream Mach number
- M_b root-mean-square output of wing bending gage, N-m (lb-in.)
- p_t stagnation pressure, kN/m^2 (lb/ft²)
- q free-stream dynamic pressure, N/m^2 (lb/ft²)
- R Reynolds number based on \bar{c}
- S wing area including fuselage intercept, 846.319 cm^2 (0.911 ft^2)
- T_t stagnation temperature, K ($^{\circ}F$)
- t/c thickness-chord ratio
- x, y, z distances along the X-, Y-, and Z-axes, respectively, cm (in.)
- α angle of attack referred to model reference line, deg
- β angle of sideslip referred to model plane of symmetry (positive when nose is left), deg
- δ_f trailing-edge flap deflection (positive when trailing edge is down), deg
- δ_h horizontal-tail deflection angle referred to respective wing reference plane (positive when trailing edge is down), deg
- δ_s spoiler deflection (positive when trailing edge is up), deg
- Λ leading-edge sweep angle of outboard wing panel, deg

Subscripts:

l lower

4

trim trimmed condition

u upper

MODEL DESCRIPTION

The general arrangement of the 1/24-scale model utilized for this investigation is shown in figure 1 and photographs are presented as figure 2. The model has an inboard wing pivot located longitudinally at model station 55.756 cm (21.951 in.) and laterally at 7.440 cm (2.929 in.) outboard of the model plane of symmetry. Provisions were made for manually varying the leading-edge sweep of the outboard wing panels from 16° to 72.5° and for varying the wing incidence angle, at the wing pivot, from 1° to -3° with respect to the model reference plane. Data were obtained during this investigation for leading-edge sweep angles of 26° , 33° , and 39° with various wing incidence angles at subsonic speeds and for a leading-edge sweep angle of 72.5° and a wing incidence angle of 1° at transonic and supersonic speeds. Five wings identical in planform and thickness ($t/c \approx 0.11$ at pivot and $t/c \approx 0.10$ at tip; parallel to free stream $\Lambda = 16^\circ$) were tested during the present investigation. Sketches of the airfoil shapes at approximately the mid-span of the panels for four of these wings are shown in figure 3. This series of wings comprised of two conventional wings, one incorporating NACA 64A2XX airfoils; the other incorporating NACA 64A4XX airfoils, and three wings incorporating variations of the supercritical airfoil.

The first wing consisted of a modified NACA 64A-series airfoil with 0.2 camber (NACA 64A2XX) outboard of the wing pivot and parallel to the free stream ($\Lambda = 16^\circ$). (See table I for coordinates.) This wing was uniformly twisted about the 26.146-percent chord line; the twist varying from 0° at the pivot to -4° at the tip. The area of the trailing edge of the wing, bounded by span stations 10.579 cm (4.165 in.) and 17.043 cm (6.710 in.) and the 65-percent chord line, was modified as shown in figure 4 to allow the wing to clear the engine ducts when the leading-edge sweep was 72.5° . This basic wing was tested with 1° of wing incidence only.

The second wing consisted of conventional NACA 64A-series airfoil sections with 0.40 camber (NACA 64A4XX) outboard of span station 12.700 cm (5.00 in.) and parallel to the free stream ($\Lambda = 16^\circ$). The airfoils inboard of this span station were modified NACA 64A-series with 0.20 camber; this change was incorporated into the wing to allow testing without altering the model geometry in the area of the wing glove juncture. This wing did not have the trailing-edge modification which was incorporated into the NACA 64A2XX wing. In addition, this wing was twisted in a manner similar to the 0.20 cambered wing; however, the twist was increased to -6° at the tip to improve the spanwise load distribution for the high-lift maneuver cases at the higher subsonic Mach numbers.

~~SECRET~~

The airfoil coordinates for this wing are given in table II. Data were obtained for this wing with incidence angles of $\pm 1^\circ$ with $\Lambda = 26^\circ$ and for -1° with $\Lambda = 33^\circ$ and 39° .

Supercritical wing A consisted of constant spanwise section geometry outboard of span station 12.700 cm (5.00 in.). (See table III for coordinates.) The twist distribution for this wing was the same as that for the 0.40 cambered wing, that is, 6° of uniform twist from the pivot to the tip. All data presented herein for supercritical wing A were obtained with 1° of wing incidence.

Supercritical wing B, as well as wing C to be described below, was developed through a series of exploratory tests and only the data for the final shapes are presented herein. These exploratory tests were conducted with 26° of leading-edge sweep on the outboard panels, the design criteria being reduced high-lift ($C_L = 0.90$) drag at $M = 0.85$ and $M = 0.91$ without adversely affecting the $M = 0.85$ cruise drag. The airfoil geometry for supercritical wing B (table IV) differed from supercritical wing A primarily in that the lower surface of supercritical wing B was modified to eliminate boundary-layer separation on that surface at the higher Mach numbers and the upper surface was modified near the wing-glove juncture to improve the shock-wave pattern. In addition, the wing trailing-edge angle was increased somewhat to improve the lift effectiveness. Data were obtained for $\pm 1^\circ$ of incidence with this wing.

Supercritical wing C consisted of further modifications which essentially resulted in a variation in the spanwise airfoil geometry. The trailing-edge angle was decreased inboard and increased outboard in an attempt to improve the upper surface pressure distributions, particularly for the higher wing-sweep angles of 33° and 39° . The lower surface was modified near the tip to eliminate a local shock formation on this surface and the trailing-edge thickness was increased to alleviate the structural problems associated with a very thin trailing edge. Coordinates for supercritical wing C are given in table V. Data were obtained for this wing with -3° of incidence only.

Provisions were made for testing the supercritical wing with various full-span trailing-edge flap deflections. The desired flap deflections were obtained by machining grooves into the upper and lower surface of the wing panels at the 80-percent chord line and rotating the last 20-percent chord of the wing panels about the mean line of the airfoil at 0.80c. Data were obtained for supercritical wing B with 5° and 10° of flap rotation at subsonic speeds and with -5° of flap rotation at the higher supersonic speeds.

The horizontal tails were mounted in the wing chord plane and consisted of biconvex airfoil sections, parallel to the free stream. The vertical tail consisted of 3.2-percent-thick modified biconvex airfoils parallel to the free stream. Twin ventral fins were mounted on the lower aft fuselage and canted outward 30° from the model plane of symmetry.

APPARATUS AND PROCEDURES

Facilities

The transonic tests ($M = 0.60$ to $M = 1.20$) were conducted in the Langley 8-foot transonic pressure tunnel (ref. 6) which is a single-return tunnel having a rectangular slotted test section to permit continuous operation through the transonic speed range. The stagnation temperature and dewpoint were maintained at values sufficient to avoid significant condensation effects throughout the tests. The supersonic tests ($M = 1.60$ to $M = 2.50$) were conducted in the low Mach number test section of the Langley Unitary Plan wind tunnel (also in ref. 6) which is a variable-pressure, continuous-flow tunnel permitting a continuous variation in Mach number from about 1.50 to 2.90 by the use of an asymmetric sliding-block-type nozzle upstream of the test section. For the supersonic tests, the dewpoint, measured at stagnation pressure, was maintained below 239 K (-30° F) in order to insure negligible condensation effects.

The following table presents the conditions (unless otherwise noted in the figures) at which the tests were conducted:

M	T_t		p_t		R based on \bar{c}
	K	$^{\circ}$ F	kN/m ²	lb/ft ²	
0.60	322	120	160.4	3350	1.88×10^6
.70	↓	↓	159.8	3337	2.07×10^6
.75	↓	↓	153.0	3195	↓
.77	↓	↓	147.7	3085	↓
.80	↓	↓	147.7	3085	↓
.85	↓	↓	143.5	2997	↓
.88	↓	↓	141.2	2950	↓
.91	↓	↓	140.3	2930	↓
.95	↓	↓	100.1	2090	1.51×10^6
1.00	↓	↓	98.5	2058	↓
1.03	↓	↓	98.1	2048	↓
1.20	↓	↓	96.2	2009	↓
1.60	339	150	81.9	1712	1.13×10^6
2.16	↓	↓	102.5	2141	↓
2.50	↓	↓	121.4	2535	↓

Boundary-Layer Transition

Transition was fixed on the upper and lower surfaces of the outboard wing panels for most of the subsonic and transonic tests by using the techniques discussed in reference 7 to simulate the full-scale Reynolds number boundary-layer separation characteristics. To maintain laminar flow ahead of the trip, as required by this technique, the model surface was maintained in an exceptionally smooth condition throughout the tests. For the data presented herein with the transition rearward, the upper surface trip location varied from 35- to 40-percent chord at the mean aerodynamic chord and the tip, respectively, and the lower surface trip location varied from 30- to 35-percent chord at the mean aerodynamic chord and the tip, respectively. By using the fluorescent oil film technique (ref. 8) to observe boundary-layer flow patterns, laminar separation was observed ahead of the upper surface trip outboard of the wing-glove juncture for wing-sweep angles of 26° , 33° , and 39° . The trips for this inboard region were located at about 5-percent chord at the wing-glove juncture and were angled rearward to intersect the aft trip at a point 7.62 cm (3.0 in.), 11.43 cm (4.5 in.), and 15.24 cm (6.0 in.) outboard of the wing-glove juncture and along the span for leading-edge sweep angles of 26° , 33° , and 39° , respectively. In addition, laminar separation was observed across the span where a strong adverse pressure gradient occurred ahead of the trip. In most of these cases the upper surface transition was moved forward to about the 5-percent chord to insure that a turbulent boundary layer existed forward of this adverse pressure gradient.

Measurements

Six-component static aerodynamic force and moment measurements were obtained by means of an electrical strain-gage balance located within the fuselage cavity. The measurements were taken over an angle-of-attack range from about 0° to 12° for wing-leading-edge sweep angles of 26° , 33° , and 39° at Mach numbers from 0.60 to 0.91 and for a wing-leading-edge sweep angle of 72.5° at Mach numbers from 0.95 to 2.50. Limited measurements were obtained at sideslip angles of $\pm 5^{\circ}$ for a wing-leading-edge sweep of 33° at Mach numbers of 0.85 and 0.91. Total and static pressures were measured at the duct exits to determine internal duct drag. Additional pressures were measured at the balance chamber and nozzle exit plug bases.

The buffet information included herein was obtained by the wing-root-bending gage technique described in references 9 and 10. The wing gages located in the position shown in figure 3 consisted of four active strain gages forming a complete bending-moment bridge. The results, as presented in this paper, represent the average root-mean-square values of the fluctuating wing-root-bending moments integrated over a 45-second sampling time.

Corrections

The drag coefficient C_D has been corrected for internal flow through the ducts. The drag data have also been adjusted to the condition of free-stream static pressure acting over the fuselage cavity and nozzle-exit plug bases.

Because of the high loads imposed on the model in the transonic speed range and the necessity for obtaining data at angles of attack where severe model buffeting occurred, a model sting arrangement was chosen in which the sting diameter was increased, by a tapered section, immediately aft of the model base. The proximity of the sting taper to the model base produced a positive pressure field, at subsonic and transonic speeds, which affected the axial-force and pitching-moment measurements. In order to determine correctly the pitch requirements for trim, the pitching-moment coefficients have been adjusted by incremental values determined from unpublished data obtained from previous tests of the basic configuration using a model sting which did not adversely affect the strain-gage data. The drag data have not been adjusted for this adverse pressure field and are therefore invalid insofar as absolute values are concerned. However, the buoyancy effect would be the same for all configurations and the incremental drag values are therefore accurate. No buoyancy corrections were required for the data obtained at Mach numbers from 1.60 to 2.50.

The measured angles of attack and sideslip have been corrected for model support sting and balance deflections occurring upstream of the angle-measurement device as a result of aerodynamic loads on the model. The angles of attack, sideslip, and control deflections are estimated to be accurate to within $\pm 0.1^\circ$; the Mach numbers, within ± 0.002 at transonic speeds and ± 0.015 at supersonic speeds.

PRESENTATION OF RESULTS

The results of this investigation are presented in the following figures:

	Figure
Longitudinal aerodynamic characteristics ($\beta = 0^\circ$) of configuration for -	
$\Lambda = 26^\circ$ for -	
Comparison of NACA 64A2XX and supercritical airfoils	5
Comparison of NACA 64A2XX and NACA 64A4XX airfoils	6
$\Lambda = 33^\circ$ for -	
Comparison of NACA 64A2XX and supercritical airfoils	7
Comparison of NACA 64A2XX and NACA 64A4XX airfoils	8
$\Lambda = 39^\circ$ for -	
Comparison of NACA 64A2XX, supercritical, and NACA 64A4XX airfoils	9

Longitudinal aerodynamic characteristics ($\beta = 0^\circ$) for -

$\Lambda = 26^\circ$ for -

Effect of trailing-edge flaps on configuration with supercritical airfoil B . . .	10
Effect of fuselage fairing on configuration with NACA 64A2XX airfoil	11
Effect of transition location on configuration with NACA 64A2XX airfoil . . .	12
Effect of transition location on configuration with supercritical airfoil B . . .	13
Effect of transition location on configuration with supercritical airfoil C . . .	14

$\Lambda = 39^\circ$ for -

Effect of transition location on configuration with supercritical airfoil B . . .	15
---	----

Effect of horizontal-tail deflection on longitudinal aerodynamic characteristics for -

$\Lambda = 26^\circ$ for -

Configuration with NACA 64A2XX airfoil. $i_w = 1^\circ$	16
Configuration with supercritical airfoil B. $i_w = -1^\circ$	17
Configuration with NACA 64A4XX airfoil. $i_w = 1^\circ$	18
Configuration with NACA 64A4XX airfoil. $i_w = -1^\circ$	19

$\Lambda = 33^\circ$ for -

Configuration with supercritical airfoil B. $i_w = 1^\circ$	20
Configuration with supercritical airfoil C. $i_w = -3^\circ$	21
Configuration with NACA 64A4XX airfoil. $i_w = 1^\circ$	22

$\Lambda = 39^\circ$ for -

Configuration with supercritical airfoil B. $i_w = -1^\circ$	23
Configuration with NACA 64A4XX airfoil. $i_w = -1^\circ$	24

Buffet characteristics of configuration with -

$\Lambda = 26^\circ$ for -

Comparison of NACA 64A2XX and supercritical airfoils	25
Comparison of NACA 64A2XX and NACA 64A4XX airfoils	26

$\Lambda = 33^\circ$ for -

Comparison of NACA 64A2XX and supercritical airfoils	27
Comparison of NACA 64A2XX and NACA 64A4XX airfoils	28

$\Lambda = 39^\circ$ for -

Comparison of NACA 64A2XX, supercritical, and NACA 64A4XX airfoils . . .	29
--	----

Buffet characteristics for -

$\Lambda = 26^\circ$ for -

Effect of trailing-edge flaps on configuration with supercritical airfoil B . . .	30
Effect of transition location on configuration with NACA 64A2XX airfoil . . .	31
Effect of transition location on supercritical airfoil B	32
Effect of transition location on configuration with supercritical airfoil C . . .	33

$\Lambda = 39^\circ$ for -

Effect of transition location on configuration with supercritical airfoil B . . . 34

Comparison of longitudinal aerodynamic characteristics of configuration with NACA 64A2XX, supercritical B, and NACA 64A4XX airfoils with -

$\Lambda = 72.5^\circ$ for -

$\delta_h = \text{Off}$, transition rearward, fuselage fairing on 35

$\delta_h = 0^\circ$, transition rearward, fuselage fairing on 36

$\delta_h = \text{Off}$, transition forward, fuselage fairing off 37

$\delta_h = 0^\circ$, transition forward, fuselage fairing off 38

$\delta_h = -10^\circ$, transition forward, fuselage fairing off 39

Lateral-directional aerodynamic characteristics for -

$\Lambda = 33^\circ$ for -

Configuration with NACA 64A2XX airfoil. $i_w = 1^\circ$ 40

Configuration with supercritical airfoil B. $i_w = 1^\circ$ 41

Configuration with supercritical airfoil B. $i_w = -1^\circ$ 42

Effect of spoiler deflection on configuration with supercritical airfoil B.

$\Lambda = 26^\circ$ 43

Summary of aerodynamic characteristics -

Variation of trimmed C_D with M for -

$C_L = 0.50$ 44

$C_L = 0.90$ 45

Variation of C_m with M for -

$C_L = 0.50$ 46

$C_L = 0.90$ 47

Variation of α with M for -

$C_L = 0.50$ 48

$C_L = 0.90$ 49

Variation of sideslip derivatives with C_L 50

Trimmed lift-drag polars. $\Lambda = 39^\circ$, $M = 0.90$ 51

DISCUSSION OF RESULTS

Early in the test program a fairing was added to the fuselage sides as shown in figure 1 to improve the wing lower surface flow near the wing-body juncture. For the more important comparisons presented herein, this fairing was on the model; however, some data are presented for the model without the fairing. To provide the reader with incremental values, data are presented in figure 11 for the basic configuration with and without

~~CONFIDENTIAL~~

this fairing. Unless otherwise noted all data presented herein are for the configurations without the fuselage fairing.

Because of the scope of this investigation, it became prohibitive to obtain horizontal-tail deflection data for all the configurations at all test conditions. For those configurations where no trim data were obtained, the trimmed drag characteristics, presented in figures 44, 45, and 51, were obtained by using incremental values from configurations and test conditions which most nearly represented the configuration to be trimmed.

Although an attempt was made to obtain all the basic comparison data, for a given wing-sweep angle, at the same horizontal-tail deflection angle, some data were inadvertently obtained with inconsistent horizontal-tail settings. The reader is therefore cautioned to note the horizontal-tail deflection angle listed in the figure key when using the basic comparison data presented herein. The reader is also cautioned to note that the horizontal-tail deflection angles were all referenced to the respective wing chord plane in an attempt to provide data with consistent wing-tail relationships and to provide pitching-moment levels approximately the same for all configurations.

The reader will also note that the wing incidence angle was varied during the investigation. This variation was made in an attempt to have the fuselage angles of attack for the various supercritical wing configurations match those for the configuration with the NACA 64A4XX airfoil at the cruise condition. However, the final incidence angle for the supercritical wing was determined from a compromise of the cruise and maneuver drag characteristics.

For the data presented in the analysis figures (figs. 44 to 51), no attempt has been made to adjust the results for transition location. However, the data presented in figures 12 to 15 indicate that the general conclusions would not be affected if these adjustments were made. The reader can therefore refer back to the basic data included in figures 5 to 9 for the transition locations for the various wings.

Cruise Mach Number

The trimmed drag characteristics for four of the wings utilized in the present investigation are summarized in figure 44 for a cruise lift coefficient of 0.50. The results obtained for the 0.40 cambered wing with $i_w = -1^\circ$, which has better high-speed maneuver characteristics than the same wing with $i_w = 1^\circ$, show little or no improvement in aerodynamic range factor $M(L/D)$ over the 0.20 cambered wing throughout the Mach number and wing-sweep ranges for which data were obtained.

The results obtained for supercritical wing C, $i_w = -3^\circ$, indicate an increase in the cruise Mach number of about 0.10 as compared with the conventional wings. It will be noted that there is a slight drag penalty associated with the supercritical wing at the cruise

████████████████████

Mach number. However, in spite of this penalty, the supercritical wing C provides an increase in the aerodynamic range factor of somewhat more than 10 percent. It should also be pointed out that in every instance the results for supercritical wing C show improvements over supercritical wing B. The pitching-moment characteristics summarized in figure 46 show more negative values of C_m for the supercritical wings; however, the trim drag penalties are generally very small at the subsonic cruise lift conditions.

High-Lift Drag at High Subsonic Mach Numbers

The trimmed drag characteristics presented in figure 45 for a lift coefficient of 0.90 indicate that the 0.40 cambered NACA 64A-series wing effectively reduced the drag as compared with the 0.20 cambered wing throughout the Mach number and wing-sweep ranges of the investigation. Analysis of the data presented in figures 6, 8, and 9 indicates that the drag improvements obtained with the 0.40 cambered wing are considerably less at moderate lift coefficients and in the low-lift range the increased camber results in drag penalties.

The results presented in figure 45(a) for the 0.40 cambered NACA 64A-series wing at a leading-edge sweep angle of 26° indicate that the use of $i_w = -1^\circ$ provides lower drag at high lift in the Mach number range from 0.75 to 0.90 than $i_w = 1^\circ$. In essence, the more negative wing incidence increases the effective twist and thereby unloads the wing tips and reduces the tendency toward tip stall, particularly at the higher wing-sweep angles. Only the negative incidence ($i_w = -1^\circ$) was used for tests of the wing with 0.40 camber at the higher leading-edge sweep angles of 33° and 39° .

The results obtained for supercritical wings B and C are also presented in figure 45 and indicate substantial drag reductions at Mach numbers above 0.76 as compared with those for the 0.40 cambered wing. Again, as was noted for the cruise condition, supercritical wing C indicates lower drag levels than supercritical wing B throughout the Mach number and wing-sweep ranges of the investigation.

Data presented in figures 5 and 7 indicate that reducing the incidence of supercritical wing B from 1° to -1° provides substantially lower drag at high lift coefficients throughout the Mach number range. For supercritical wing C, the incidence angle was further reduced to -3° to provide more nearly the same fuselage angle of attack for a given lift coefficient as for the 0.40 cambered wing (fig. 49).

Again, as at cruise lift coefficients, the pitching moments for the configurations with the supercritical wings are more negative than for the conventional wings. (See fig. 47.) However, for the higher Mach numbers where the drag penalties associated with providing trim are greatest, the differences in pitching moment for the supercritical and conventional wings are generally relatively small.

~~SECRET~~

To provide an indication of the general effectiveness of the supercritical airfoil in reducing drag at $M = 0.90$, a condition of primary interest to the military services, trimmed drag polars for the condition obtained from cross plots of the measured data are presented in figure 51. The comparison is made for a leading-edge sweep angle of 39° which results in the lowest drag for the NACA 64A-series and supercritical C wings at this Mach number. Although the reductions in drag indicated are substantial, significantly greater improvements were obtained with the supercritical wing at Mach numbers of 0.80 and 0.85 for the most satisfactory sweep angles for these conditions (figs. 44 and 45).

High-Lift Drag at Moderate Subsonic Mach Numbers

The results of figure 45 indicate that for a sweep angle of 26° , the drag at high lift for the supercritical wings is greater than for the 0.40 camber NACA 64A-series wing at Mach numbers less than 0.76. The results presented in figure 10 indicate that simple trailing-edge flap deflections can substantially improve the high-lift characteristics of the supercritical wing at the lower speeds. Also, the results of several other investigations of leading-edge flap deflections on uncambered conventional sections suggest that the low-speed characteristics for the supercritical wing could probably be significantly improved by such a device.

Drag at Supersonic Mach Numbers

The aerodynamic characteristics obtained at supersonic Mach numbers are presented in figures 35 to 39 for a wing leading-edge sweep angle of 72.5° . Because of the proximity of the horizontal tail to the wing chord plane, it was believed that a wing-tail interference might exist for the 72.5° sweep condition. For this reason the supersonic tests were conducted with the horizontal tail on and off. Additional data were also obtained for a horizontal-tail deflection angle of -10° at the higher supersonic speeds.

The drag characteristics obtained at a Mach number of 1.20 for the configurations without the horizontal tail are presented in figure 35. These data show nearly identical drag levels for the conventional 0.20 cambered wing and the supercritical wing. Somewhat better drag characteristics are noted for the 0.40 cambered wing as compared with the 0.20 cambered wing.

The results obtained at the higher supersonic Mach numbers (figs. 37, 38, and 39) in general indicate higher drag levels for supercritical wing B as compared with the 0.20 cambered wing. It will be noted, however, that the pitching moments for supercritical wing B are somewhat more positive than those for the NACA 64A-series wings and this wing would therefore have a lower trim drag penalty. It should also be pointed out that the data presented in figures 37, 38, and 39 for the supercritical wing B were obtained

In many instances, high values of the fluctuating wing-root-bending moments were noted for all the wings at relatively low lift coefficients, particularly at the higher Mach numbers. It is believed that these high bending-moment values are the result of lower surface separation and that in the case of the supercritical wings, this separation could probably be eliminated by negative flap deflections or higher sweep angles.

Lateral Characteristics

The very limited data obtained at sideslip angles and summarized in figure 50 indicate no adverse effects for supercritical wing B as compared with the NACA 64A-series wing with 0.20 camber.

Limited data were obtained at low Mach numbers to determine the effect of spoiler deflection, for lateral control, on supercritical wing B (fig. 43). In general, the results indicate that the spoiler deflection is very effective in providing lateral control for the supercritical wing.

Transition Location Effects

The effects of wing upper surface transition location on the longitudinal aerodynamic characteristics of the configuration with the 0.20 cambered wing are presented in figure 12. These data indicate increased drag and substantially altered pitching-moment characteristics at supercritical Mach numbers when the transition trip is moved forward. This forward location of the transition trip increases the relative boundary-layer thickness as compared with full-scale conditions and results in more severe shock-induced separation. For the supercritical wings at some Mach numbers, the shock wave moves from near the leading edge to a well aft position as the angle of attack is increased and for these test conditions the correct transition trip location is in doubt. In most cases, data were obtained with both forward and rearward trip locations. Some of the results are presented in figures 13, 14, and 15.

The effect of wing upper surface transition location on the buffet characteristics of the configuration with the 0.20 cambered wing with a leading-edge sweep angle of 26° is presented in figure 31. These data are of interest in that moving the transition forward results in higher buffet onset lift coefficients at the Mach numbers where supercritical flow exists over the wing. It appears that the thicker boundary layer associated with the greater chordwise extent of turbulent flow for the forward transition may attenuate the fluctuations associated with shock—boundary-layer interaction and thus provide results which may be more favorable than those which would be obtained in flight. For this reason, extreme caution should be used in obtaining and interpreting wind-tunnel results using the wing-root-bending-moment technique.

CONCLUSIONS

An investigation has been conducted in the Langley 8-foot transonic pressure tunnel and the Langley Unitary Plan wind tunnel to evaluate the effectiveness of three variations of the NASA supercritical airfoil as applied to a model of a variable-wing-sweep fighter airplane. Wing panels incorporating conventional NACA 64A-series airfoils with 0.20 and 0.40 camber were used as bases of reference for this evaluation. Static force and moment measurements were obtained for wing leading-edge sweep angles of 26° , 33° , and 39° at subsonic speeds and for a wing leading-edge sweep of 72.5° at transonic and supersonic speeds. In addition, fluctuating wing-root-bending-moment data were obtained at subsonic speeds to determine buffet characteristics. The following conclusions are indicated:

1. Increasing the conventional camber had little effect on the cruise Mach number but did reduce the trimmed drag characteristics in the moderate- to high-lift range and increased the buffet onset lift coefficient at subsonic speeds.
2. An increase in the cruise Mach number capability of about 0.10 was noted for the model with the supercritical wing as compared with the wings incorporating conventional NACA 64A-series airfoils.
3. Substantial reductions in the moderate- to high-lift trimmed drag characteristics were achieved with the supercritical wing at the higher subsonic speeds.
4. The lift coefficient for buffet onset was increased significantly with the supercritical wing for a leading-edge sweep angle of 26° at Mach numbers of 0.75 and above.
5. The low-speed (Mach number = 0.60) drag characteristics were somewhat higher and the buffet onset lift coefficient somewhat lower for the supercritical wing as compared with the conventional 0.40 cambered wing although these characteristics were improved by the use of trailing-edge flaps.
6. At supersonic speeds, the trimmed drag characteristics for the supercritical wing were slightly higher than those for the wings incorporating conventional camber.
7. No adverse yaw characteristics were noted for the supercritical wing at the test conditions for which the data were obtained.

Langley Research Center,
National Aeronautics and Space Administration,
Hampton, Va., March 16, 1973.

~~CONFIDENTIAL~~

REFERENCES

1. Harris, Charles D.: Aerodynamic Characteristics of Two NASA Supercritical Airfoils With Different Maximum Thicknesses. NASA TM X-2532, 1972.
2. Ferris, James C.: Static Aerodynamic Characteristics of a Model With a 17-Percent-Thick Supercritical Wing. NASA TM X-2551, 1972.
3. Bartlett, Dennis W.; and Re, Richard J.: Wind-Tunnel Investigation of Basic Aerodynamic Characteristics of a Supercritical-Wing Research Airplane Configuration. NASA TM X-2470, 1972.
4. Anon.: Supercritical Wing Technology - A Progress Report on Flight Evaluations. NASA SP-301, 1972.
5. Palmer, W. E.; Elliott, D. W.; and White, J. E.: Flight and Wind Tunnel Evaluation of a 17% Thick Supercritical Airfoil on a T-2C Airplane. NR71H-150 (Contract N00019-70-C-0474), North American Rockwell Corp., July 31, 1971.
Vol. I - Basic Report. (Available from DDC as AD 517 436L.)
Vol. II - Flight Measured Wing Wake Profiles and Surface Pressures.
(Available from DDC as AD 517 437L.)
6. Pirrello, C. J.; Hardin, R. D.; Heckart, M. V.; and Brown, K. R.: An Inventory of Aeronautical Ground Research Facilities. Vol. I - Wind Tunnels. NASA CR-1874, 1971.
7. Loving, Donald L.: Wind-Tunnel—Flight Correlation of Shock-Induced Separated Flow. NASA TN D-3580, 1966.
8. Loving, Donald L.; and Katzoff, S.: The Fluorescent-Oil Film Method and Other Techniques for Boundary-Layer Flow Visualization. NASA MEMO 3-17-59L, 1959.
9. Davis, Don D., Jr.; and Huston, Wilber B.: The Use of Wind Tunnels To Predict Flight Buffet Loads. NACA RM L57D25, 1957.
10. Ray, Edward J.: Techniques for Determining Buffet Onset. NASA TM X-2103, 1970.

TABLE I. - AIRFOIL COORDINATES FOR NACA 64A2XX

$(x/c)_u$ and l	y = 10.548 cm (4.153 in.) c = 13.127 cm (5.168 in.)		y = 40.005 cm (15.750 in.) c = 5.174 cm (2.037 in.)	
	$(z/c)_u$	$(z/c)_l$	$(z/c)_u$	$(z/c)_l$
0	0.0025	0.0025	0.0790	0.0790
.008	.0128	-.0066	.0918	.0682
.012	.0163	-.0093	.0957	.0663
.025	.0230	-.0137	.1046	.0638
.050	.0337	-.0205	.1159	.0619
.070	.0406	-.0246	.1232	.0619
.100	.0490	-.0298	.1316	.0628
.150	.0586	-.0356	.1433	.0653
.200	.0646	-.0385	.1527	.0673
.300	.0693	-.0408	.1674	.0717
.400	.0708	-.0399	.1772	.0785
.500	.0689	-.0366	.1811	.0889
.600	.0617	-.0296	.1811	.1021
.700	.0509	-.0203	.1782	.1168
.750	.0441	-.0157	.1733	.1247
.800	.0368	-.0112	.1728	.1316
.850	.0290	-.0070	.1689	.1379
.900	.0211	-.0031	.1649	.1443
.950	.0128	.0006	.1586	.1507
1.000	.0046	.0039	.1581	.1561
L.E. radius	0.0085c		0.0118c	

TABLE II. - AIRFOIL COORDINATES FOR NACA 64A4XX

$(x/c)_u$ and l	$y = 10.584 \text{ cm (4.167 in.)}$ $c = 13.081 \text{ cm (5.150 in.)}$		$y = 12.700 \text{ cm (5.000 in.)}$ $c = 12.530 \text{ cm (4.933 in.)}$		$y = 14.181 \text{ cm (5.583 in.)}$ $c = 12.146 \text{ cm (4.782 in.)}$		$y = 40.005 \text{ cm (15.750 in.)}$ $c = 5.159 \text{ cm (2.031 in.)}$	
	$(z/c)_u$	$(z/c)_l$	$(z/c)_u$	$(z/c)_l$	$(z/c)_u$	$(z/c)_l$	$(z/c)_u$	$(z/c)_l$
0.008	0.0016	0.0016	0.0045	0.0045	0.0065	0.0065	0.0817	0.0817
.025	.0254	-.0138	.0266	-.0097	.0295	-.0079	.1014	.0684
.050	.0375	-.0208	.0375	-.0162	.0404	-.0123	.1147	.0684
.101	.0534	-.0301	.0535	-.0221	.0558	-.0163	.1329	.0694
.200	.0691	-.0361	.0730	-.0272	.0765	-.0199	.1610	.0748
.301	.0715	-.0365	.0811	-.0280	.0882	-.0207	.1802	.0837
.401	.0732	-.0357	.0851	-.0253	.0939	-.0188	.1955	.0960
.501	.0728	-.0320	.0843	-.0213	.0926	-.0125	.2033	.1108
.601	.0654	-.0264	.0776	-.0148	.0853	-.0050	.2053	.1275
.702	.0538	-.0190	.0659	-.0069	.0738	.0033	.2053	.1443
.802	.0388	-.0107	.0503	0	.0583	.0105	.2019	.1590
.901	.0221	-.0025	.0320	.0063	.0381	.0134	.1935	.1723
1.000	.0070	.0058	.0124	.0111	.0153	.0140	.1851	.1822
L.E. radius	0.0078c		0.0077c		0.0077c		0.0069c	

TABLE III. - AIRFOIL COORDINATES FOR SUPERCRITICAL WING A

(x/c) _{u and l}	y = 8.839 cm (3.48 in.) c = 12.913 cm (5.084 in.)		y = 9.870 cm (3.886 in.) c = 13.310 cm (5.240 in.)		y = 10.549 cm (4.153 in.) c = 13.127 cm (5.168 in.)		y = 40.005 cm (15.750 in.) c = 5.159 cm (2.031 in.)			
	(z/c) _u	(z/c) _l	(z/c) _u	(z/c) _l	(z/c) _u	(z/c) _l	(x/c) _u	(z/c) _u	(x/c) _l	(z/c) _l
0	0	0	0	0	0.0015	0.0015	0	0.0921	0	0.0921
.0074	.0175	-.0175	.0175	-.0175	.0190	-.0161	.0059	.0950	.0094	.0625
.0120	.0214	-.0216	.0216	-.0216	.0230	-.0199	.0103	.0990	.0148	.0596
.0250	.0275	-.0281	.0277	-.0281	.0292	-.0265	.0222	.1053	.0276	.0551
.0370	.0317	-.0325	.0317	-.0324	.0333	-.0308	.0345	.1102	.0404	.0522
.0500	.0346	-.0358	.0347	-.0359	.0364	-.0341	.0468	.1147	.0532	.0507
.0750	.0393	-.0407	.0393	-.0408	.0412	-.0391	.0714	.1216	.0788	.0487
.1000	.0429	-.0445	.0427	-.0445	.0447	-.0426	.0960	.1275	.1044	.0483
.1250	.0454	-.0472	.0454	-.0471	.0474	-.0453	.1206	.1324	.1295	.0483
.1500	.0476	-.0494	.0475	-.0492	.0495	-.0474	.1452	.1369	.1546	.0487
.1750	.0494	-.0509	.0492	-.0510	.0513	-.0490	.1704	.1413	.1797	.0502
.2000	.0507	-.0521	.0508	-.0521	.0528	-.0501	.1950	.1452	.2048	.0512
.2500	.0527	-.0539	.0529	-.0540	.0550	-.0517	.2447	.1521	.2550	.0551
.3000	.0539	-.0549	.0540	-.0548	.0563	-.0524	.2949	.1585	.3063	.0497
.3500	.0547	-.0549	.0548	-.0550	.0573	-.0524	.3447	.1645	.3550	.0650
.4000	.0551	-.0541	.0550	-.0540	.0577	-.0515	.3949	.1699	.4047	.0709
.4500	.0559	-.0523	.0557	-.0525	.0586	-.0495	.4446	.1748	.4549	.0203
.500	.0543	-.0498	.0542	-.0496	.0571	-.0468	.4948	.1797	.5047	.0135
.550	.0533	-.0454	.0532	-.0454	.0563	-.0424	.5451	.1841	.5544	.0946
.575	.0527	-.0427	.0527	-.0426	.0557	-.0395	.5697	.1861	.5790	.0995
.600	.0519	-.0389	.0519	-.0389	.0550	-.0358	.5948	.1939	.6032	.1053
.625	.0511	-.0342	.0511	-.0342	.0544	-.0310	.6199	.1901	.6283	.1123
.650	.0502	-.0281	.0500	-.0282	.0534	-.0250	.6450	.1915	.6524	.1206
.675	.0490	-.0214	.0489	-.0216	.0522	-.0182	.6701	.1935	.6770	.1295
.700	.0476	-.0149	.0475	-.0149	.0511	-.0114	.6952	.1950	.7011	.1379
.725	.0460	-.0090	.0460	-.0092	.0495	-.0056	.7203	.1960	.7258	.1457
.750	.0443	-.0037	.0443	-.0036	.0478	-.0002	.7454	.1969	.7504	.1531
.775	.0421	.0010	.0422	.0010	.0459	.0046	.7710	.1979	.7750	.1600
.800	.0397	.0051	.0397	.0052	.0435	.0087	.7962	.1984	.7996	.1659
.825	.0370	.0087	.0370	.0086	.0406	.0124	.8213	.1984	.8242	.1718
.850	.0336	.0110	.0338	.0111	.0373	.0149	.8469	.1979	.8488	.1768
.875	.0299	.0130	.0300	.0130	.0339	.0165	.8720	.1969	.8735	.1807
.900	.0256	.0136	.0256	.0135	.0294	.0174	.8976	.1955	.8986	.1837
.925	.0205	.0128	.0204	.0126	.0244	.0166	.9233	.1935	.9237	.1856
.950	.0144	.0102	.0143	.0101	.0184	.0143	.9483	.1910	.9493	.1856
.975	.0075	.0055	.0074	.0055	.0116	.0097	.9744	.1871	.9744	.1841
1.000	-.0008	-.0018	-.0008	-.0017	.0035	.0023	1.000	.1822	1.000	.1797
L.E. radius	0.0246c		0.0244c		0.0246c		0.0212c			

~~CONFIDENTIAL~~

TABLE IV. - AIRFOIL COORDINATES FOR SUPERCRITICAL WING B

$(x/c)_u$ and l	y = 9.888 cm (3.893 in.) c = 13.317 cm (5.243 in.)		y = 17.127 cm (6.743 in.) c = 11.336 cm (4.463 in.)		y = 24.519 cm (9.653 in.) c = 9.332 cm (3.674 in.)		y = 36.101 cm (14.213 in.) c = 6.187 cm (2.436 in.)	
	$(z/c)_u$	$(z/c)_l$	$(z/c)_u$	$(z/c)_l$	$(z/c)_u$	$(z/c)_l$	$(z/c)_u$	$(z/c)_l$
0	0.0000	0.0000	0.0090	0.0090	0.0223	0.0223	0.0595	0.0595
.0125	.0217	-.0217	.0305	-.0127	.0439	.0013	.0800	.0387
.025	.0285	-.0300	.0374	-.0203	.0505	-.0055	.0868	.0325
.050	.0367	-.0396	.0459	-.0289	.0588	-.0136	.0965	.0261
.075	.0416	-.0461	.0509	-.0348	.0642	-.0191	.1026	.0222
.100	.0448	-.0503	.0545	-.0388	.0676	-.0225	.1074	.0201
.150	.0487	-.0557	.0592	-.0430	.0734	-.0259	.1150	.0195
.200	.0509	-.0579	.0628	-.0446	.0774	-.0267	.1215	.0216
.250	.0518	-.0578	.0651	-.0442	.0807	-.0255	.1273	.0247
.300	.0524	-.0567	.0669	-.0426	.0832	-.0235	.1325	.0292
.350	.0526	-.0545	.0685	-.0400	.0856	-.0207	.1373	.0345
.400	.0523	-.0514	.0694	-.0364	.0876	-.0162	.1414	.0401
.450	.0519	-.0473	.0704	-.0319	.0895	-.0113	.1456	.0466
.500	.0511	-.0420	.0710	-.0267	.0909	-.0055	.1493	.0542
.550	.0500	-.0361	.0709	-.0209	.0917	.0010	.1522	.0630
.600	.0484	-.0298	.0704	-.0139	.0920	.0089	.1546	.0733
.625	.0473	-.0260	.0700	-.0098	.0919	.0131	.1554	.0789
.650	.0462	-.0223	.0693	-.0055	.0917	.0175	.1560	.0848
.675	.0449	-.0183	.0684	-.0006	.0913	.0233	.1564	.0916
.700	.0436	-.0146	.0672	.0046	.0907	.0294	.1569	.0988
.725	.0419	-.0102	.0657	.0100	.0897	.0353	.1569	.1049
.750	.0402	-.0058	.0641	.0158	.0886	.0410	.1569	.1123
.775	.0382	-.0017	.0622	.0205	.0871	.0463	.1569	.1185
.800	.0358	.0022	.0601	.0250	.0854	.0512	.1564	.1244
.825	.0335	.0058	.0574	.0287	.0832	.0550	.1558	.1295
.850	.0309	.0086	.0544	.0320	.0807	.0585	.1548	.1341
.875	.0278	.100	.0512	.0337	.0780	.0605	.1532	.1376
.900	.0242	.0103	.0472	.0344	.0746	.0614	.1513	.1402
.925	.0201	.0093	.0425	.0338	.0705	.0613	.1482	.1406
.950	.0154	.0071	.0370	.0316	.0655	.0593	.1445	.1388
.975	.0093	.0037	.0296	.0269	.0588	.0550	.1396	.1355
1.000	.0010	0	.0215	.0202	.0505	.0493	.1324	.1305
L.E. radius	0.0246c		0.0242c		0.0237c		0.0221c	

~~CONFIDENTIAL~~

TABLE V.- AIRFOIL COORDINATES FOR SUPERCRITICAL WING C

$(x/c)_{u \text{ and } l}$	$y = 9.888 \text{ cm (3.893 in.)}$ $c = 13.317 \text{ cm (5.243 in.)}$		$y = 17.127 \text{ cm (6.743 in.)}$ $c = 11.336 \text{ cm (4.463 in.)}$		$y = 24.519 \text{ cm (9.653 in.)}$ $c = 9.332 \text{ cm (3.674 in.)}$		$y = 36.101 \text{ cm (14.213 in.)}$ $c = 6.187 \text{ cm (2.436 in.)}$	
	$(z/c)_u$	$(z/c)_l$	$(z/c)_u$	$(z/c)_l$	$(z/c)_u$	$(z/c)_l$	$(z/c)_u$	$(z/c)_l$
0	0.0000	0.0000	0.0090	0.0090	0.0223	0.0223	0.0595	0.0595
.0125	.0217	-.0217	.0305	-.0127	.0439	.0013	.0800	.0387
.025	.0286	-.0275	.0376	-.0197	.0504	-.0049	.0874	.0341
.050	.0362	-.0366	.0455	-.0291	.0582	-.0133	.0961	.0287
.075	.0406	-.0425	.0502	-.0350	.0638	-.0188	.1022	.0259
.100	.0441	-.0471	.0538	-.0385	.0675	-.0220	.1071	.0238
.150	.0488	-.0526	.0589	-.0430	.0732	-.0253	.1145	.0226
.200	.0521	-.0557	.0625	-.0444	.0773	-.0261	.1207	.0238
.250	.0540	-.0561	.0650	-.0441	.0803	-.0253	.1268	.0263
.300	.0560	-.0549	.0668	-.0426	.0827	-.0237	.1318	.0291
.350	.0562	-.0530	.0679	-.0401	.0846	-.0210	.1367	.0333
.400	.0557	-.0504	.0686	-.0365	.0868	-.0171	.1412	.0382
.450	.0545	-.0463	.0692	-.0323	.0882	-.0122	.1453	.0442
.500	.0528	-.0416	.0692	-.0271	.0898	-.0065	.1490	.0521
.550	.0505	-.0359	.0690	-.0213	.0901	.0005	.1527	.0612
.600	.0479	-.0288	.0681	-.0139	.0901	.0082	.1552	.0718
.625	.0463	-.0248	.0677	-.0101	.0898	.0128	.1564	.0776
.650	.0444	-.0212	.0668	-.0060	.0895	.0174	.1572	.0833
.675	.0429	-.0168	.0659	-.0011	.0890	.0229	.1580	.0899
.700	.0410	-.0132	.0645	.0040	.0882	.0283	.1585	.0960
.725	.0390	-.0093	.0630	.0096	.0871	.0338	.1585	.1026
.750	.0374	-.0060	.0614	.0142	.0857	.0392	.1582	.1096
.775	.0349	-.0028	.0592	.0190	.0841	.0444	.1580	.1162
.800	.0324	.0000	.0569	.0229	.0819	.0484	.1572	.1219
.825	.0298	.0028	.0542	.0262	.0797	.0520	.1560	.1264
.850	.0269	.0047	.0513	.0287	.0770	.0544	.1544	.1305
.875	.0240	.0065	.0482	.0302	.0740	.0561	.1523	.1338
.900	.0200	.0068	.0439	.0305	.0700	.0563	.1494	.1351
.925	.0162	.0065	.0388	.0287	.0648	.0550	.1461	.1351
.950	.0118	.0052	.0329	.0255	.0593	.0517	.1420	.1326
.975	.0065	.0021	.0258	.0202	.0520	.0455	.1355	.1283
1.000	.0005	-.0025	.0175	.0135	.0435	.0385	.1280	.1220
L.E. radius	0.0246c		0.0242c		0.0237c		0.0221c	

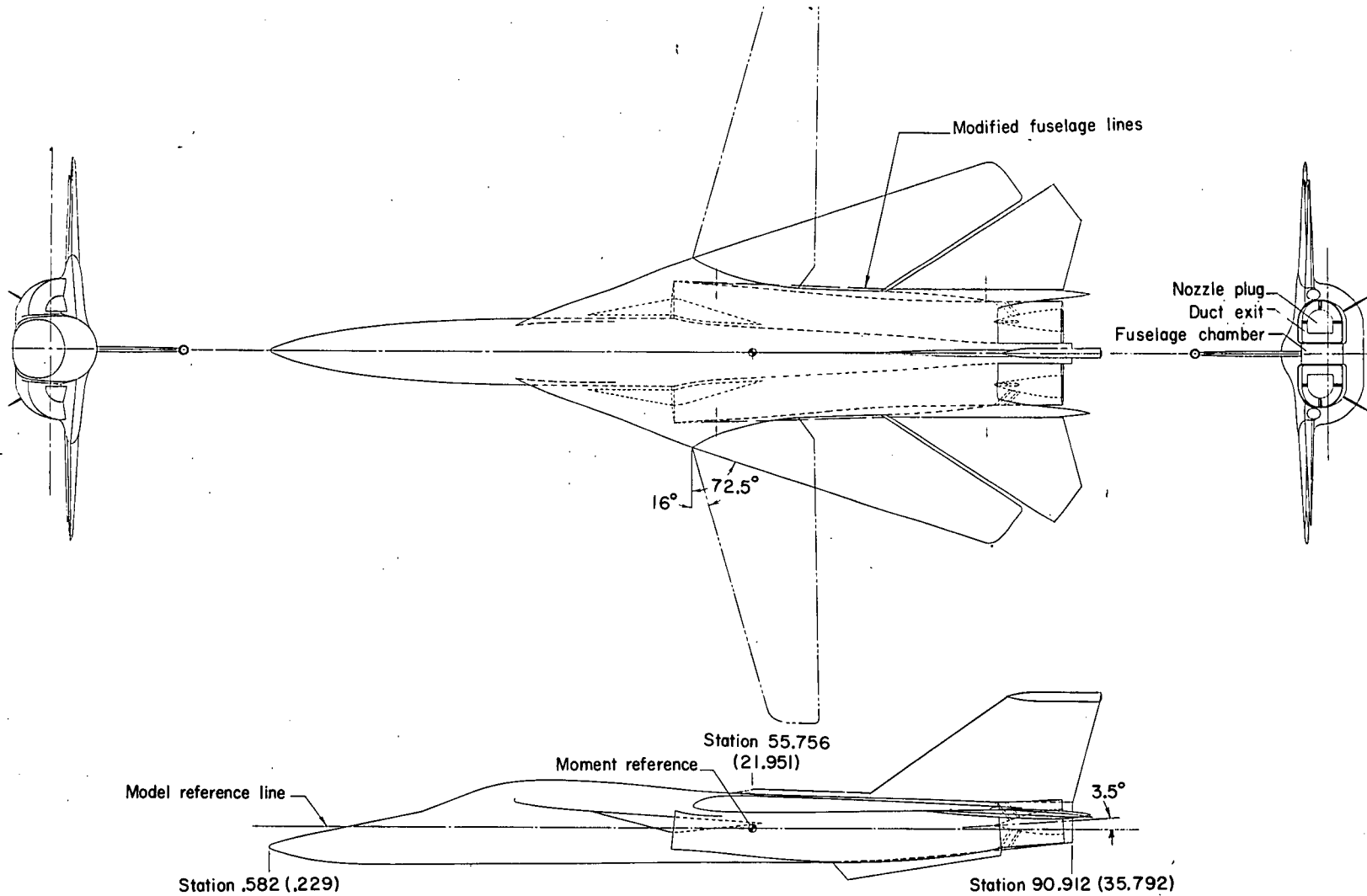
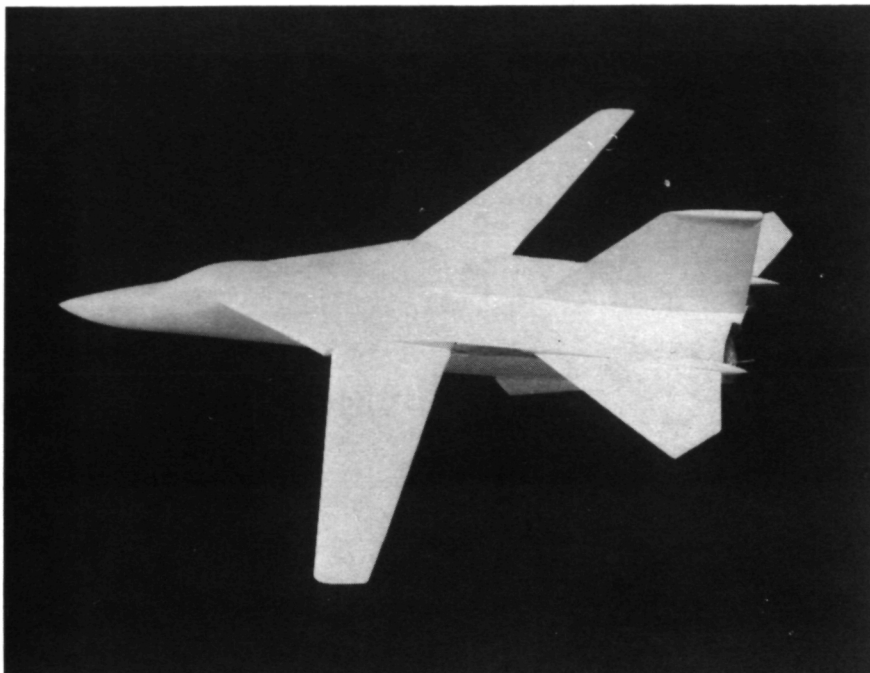
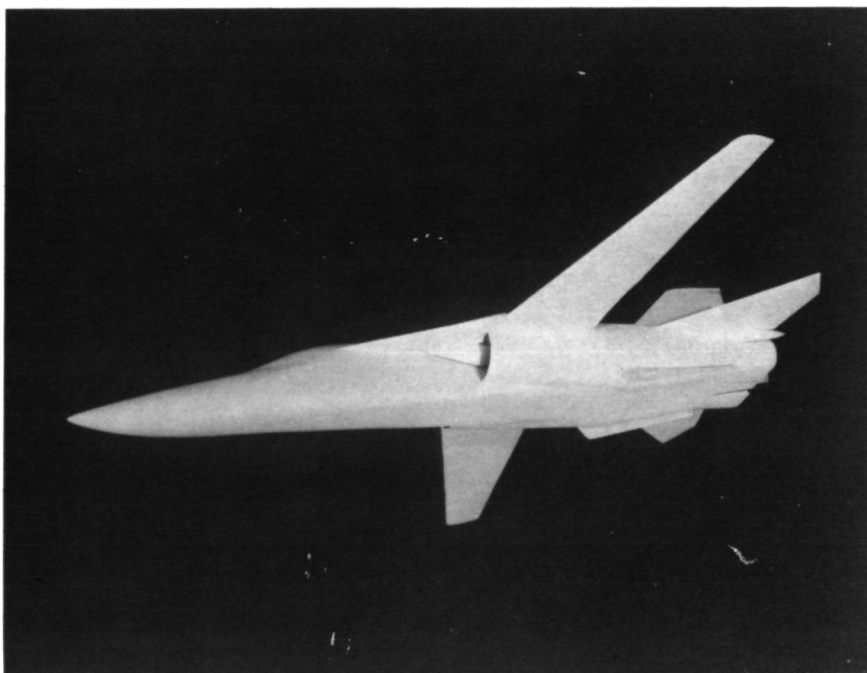


Figure 1.- General arrangement of 1/24-scale model variable-sweep fighter airplane. All linear dimensions in centimeters with inches in parentheses unless otherwise noted.

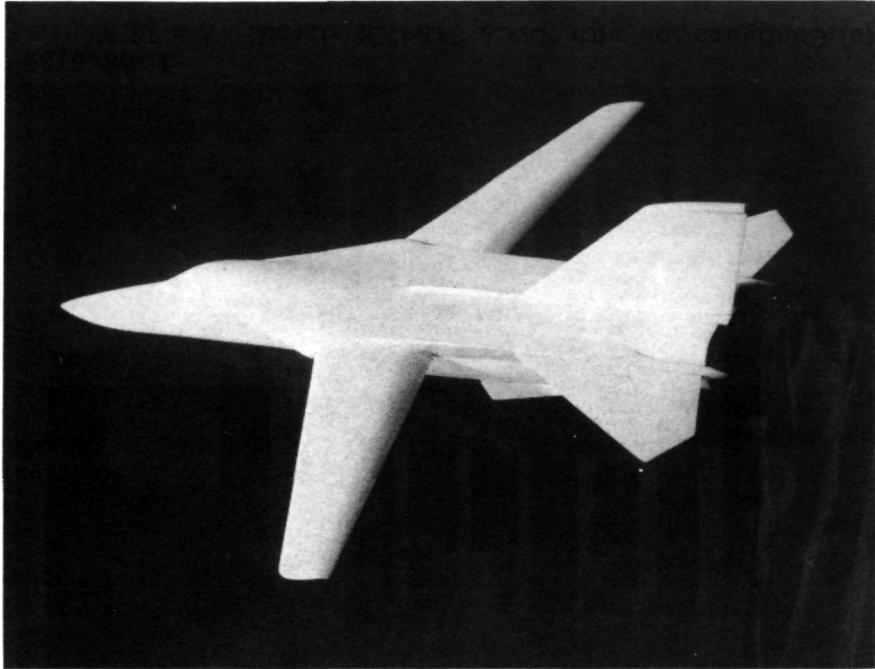


L-68-3940

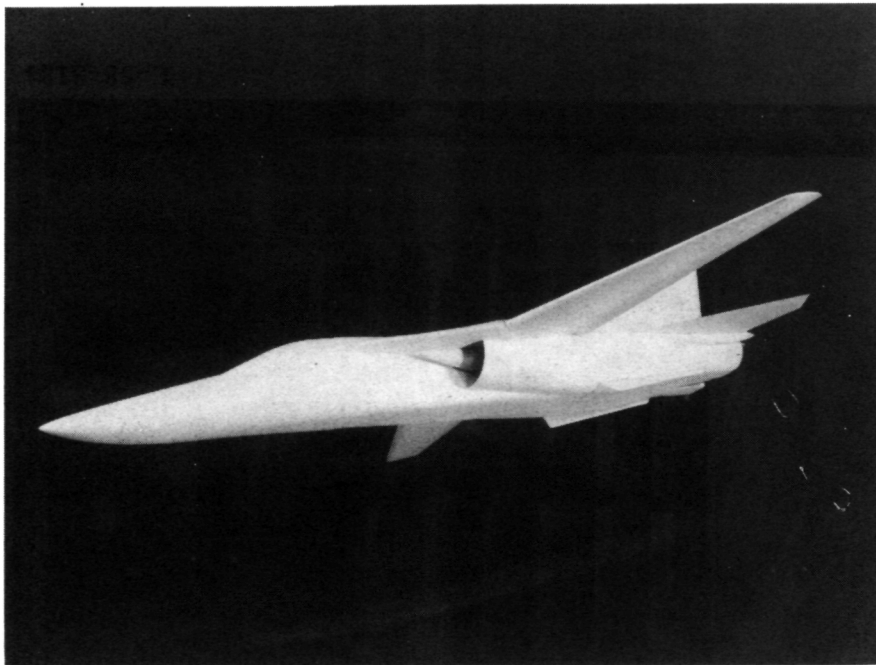


(a) Configuration with NACA 64A2XX airfoil. $\Lambda = 26^\circ$. L-68-3941

Figure 2. - Wind-tunnel models.



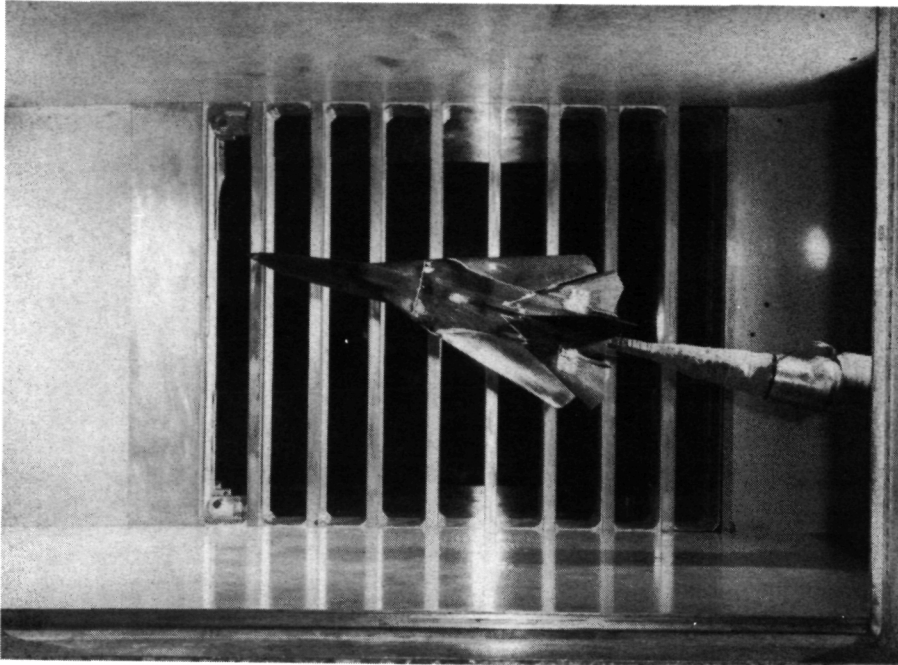
L-68-3943



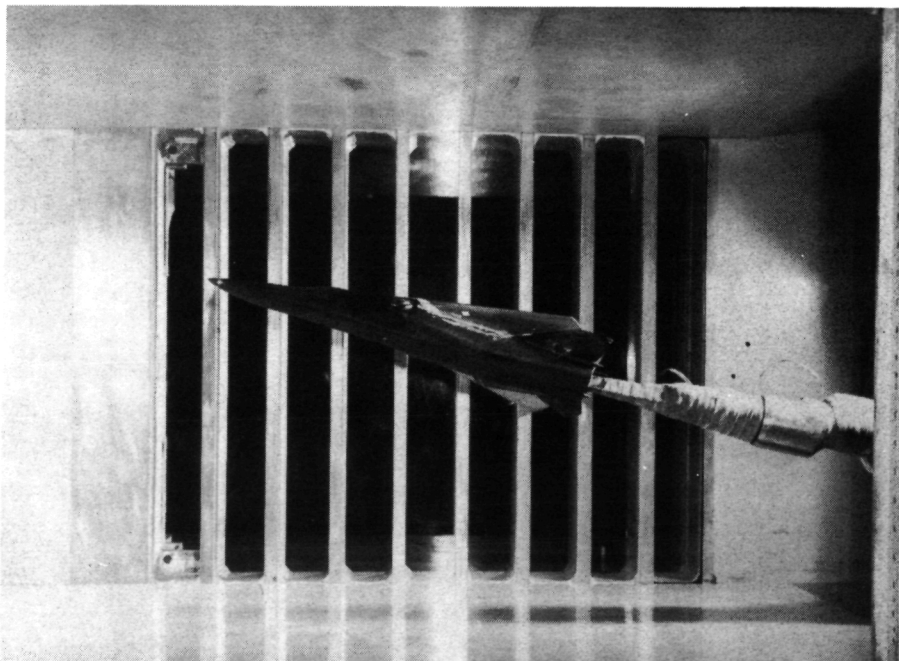
(b) Configuration with supercritical airfoil B. $\Lambda = 26^\circ$. L-68-3942

Figure 2. - Continued.

~~CONFIDENTIAL~~



L-68-3134



L-68-3135

(c) Configuration with NACA 64A4XX airfoil. $\Lambda = 72.5^\circ$.

Figure 2.- Concluded.

~~CONFIDENTIAL~~

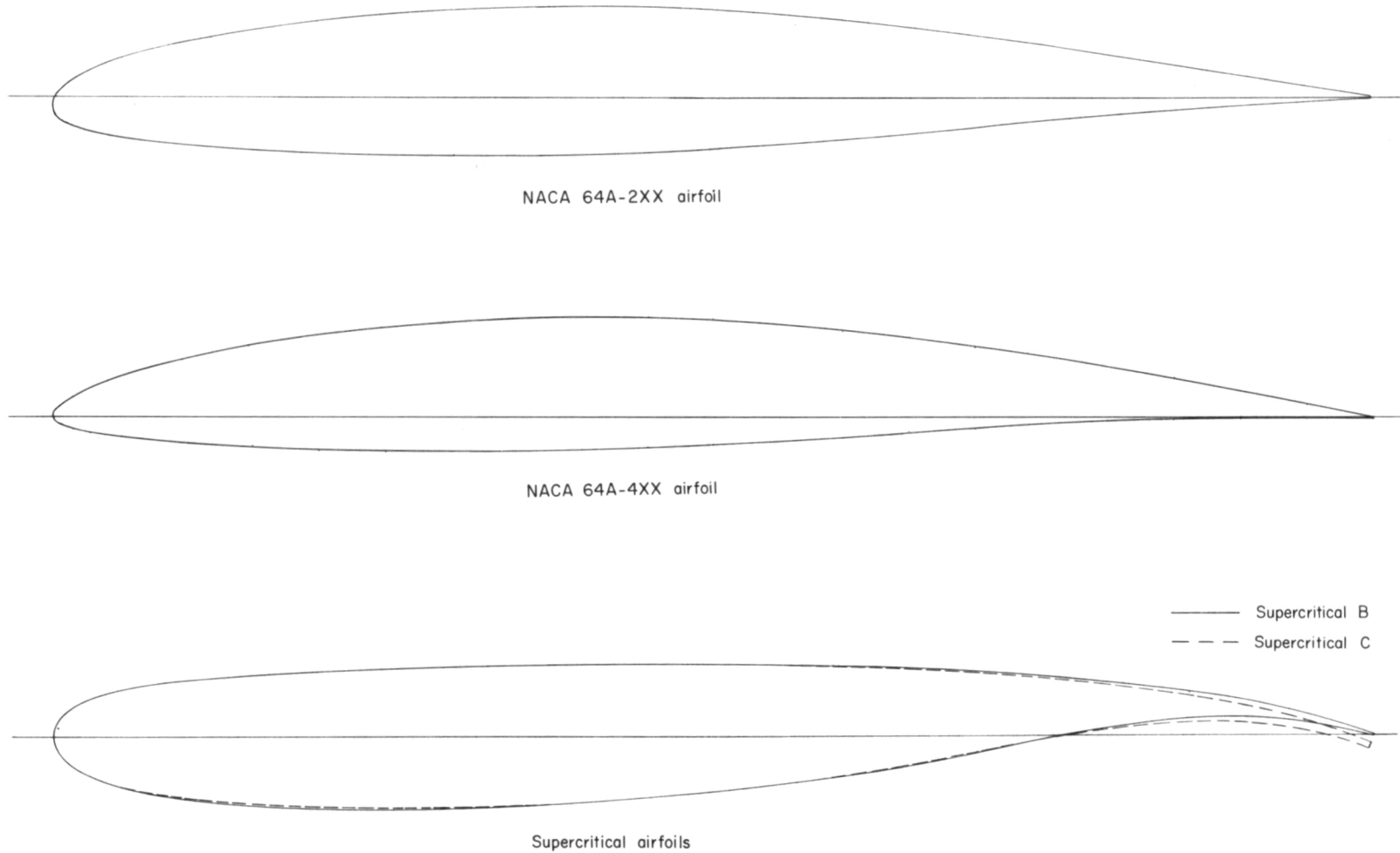


Figure 3.- Wing airfoil shapes at model span station 24.519 cm (9.653 in.). $\Lambda = 16^{\circ}$.

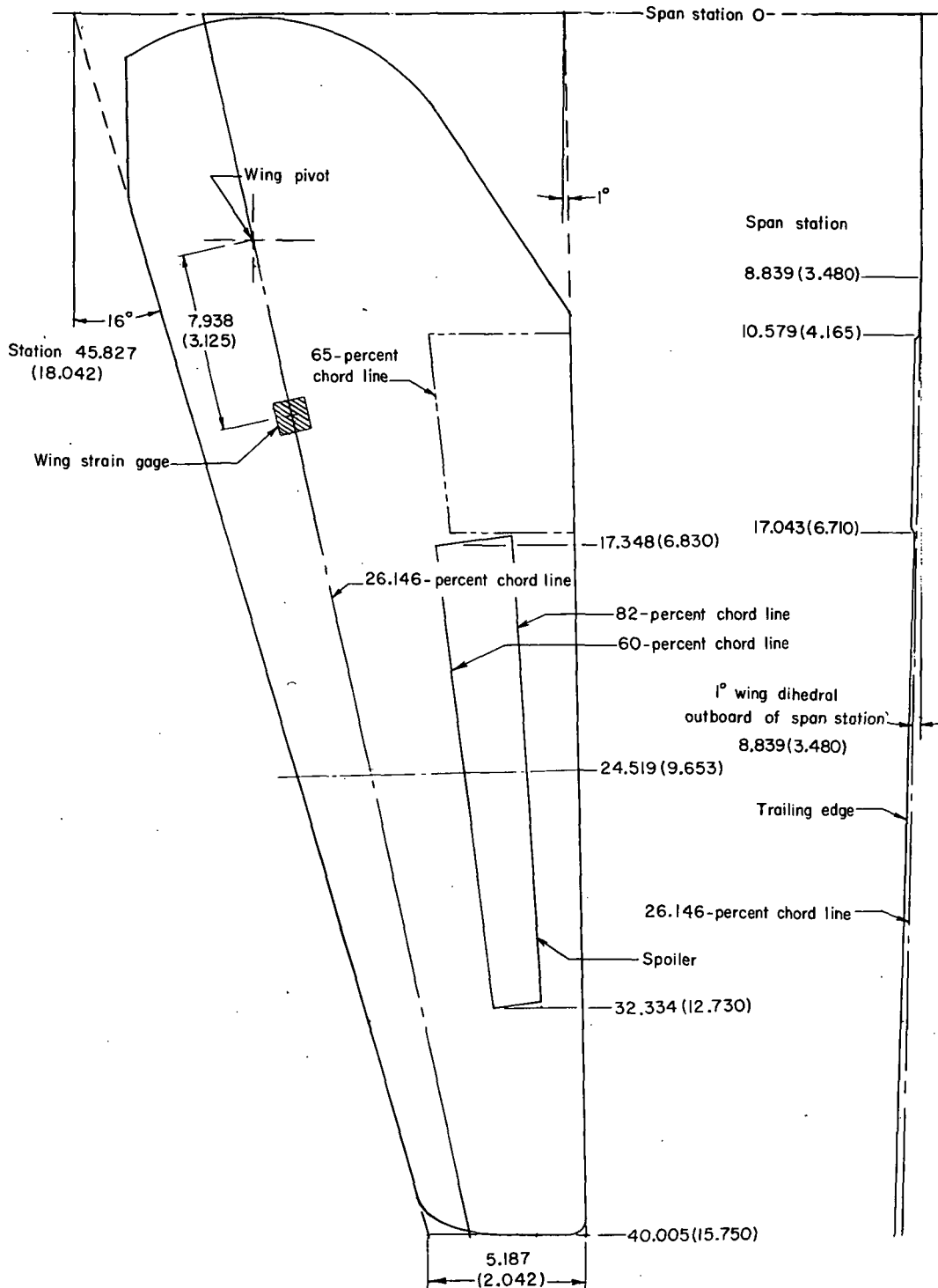
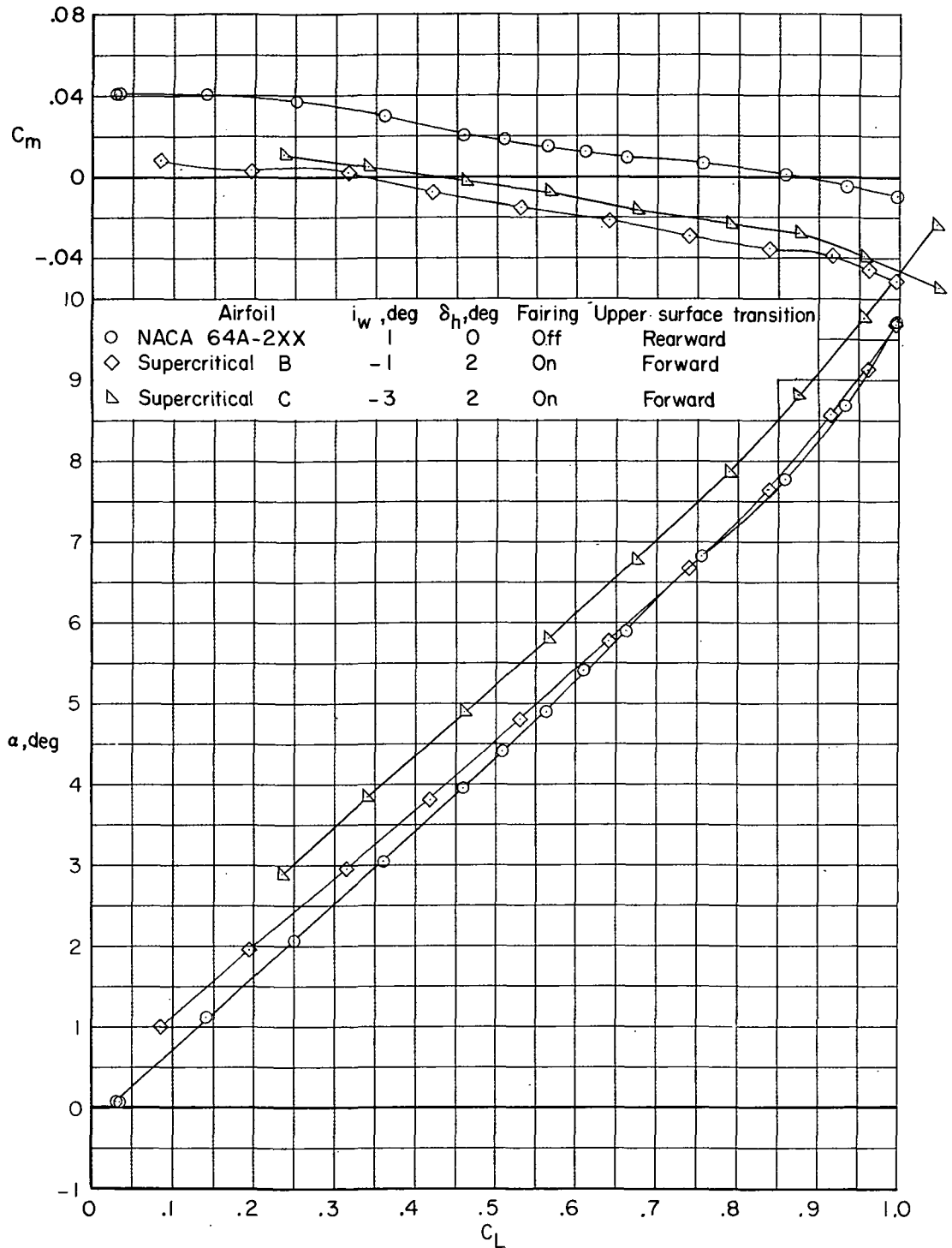
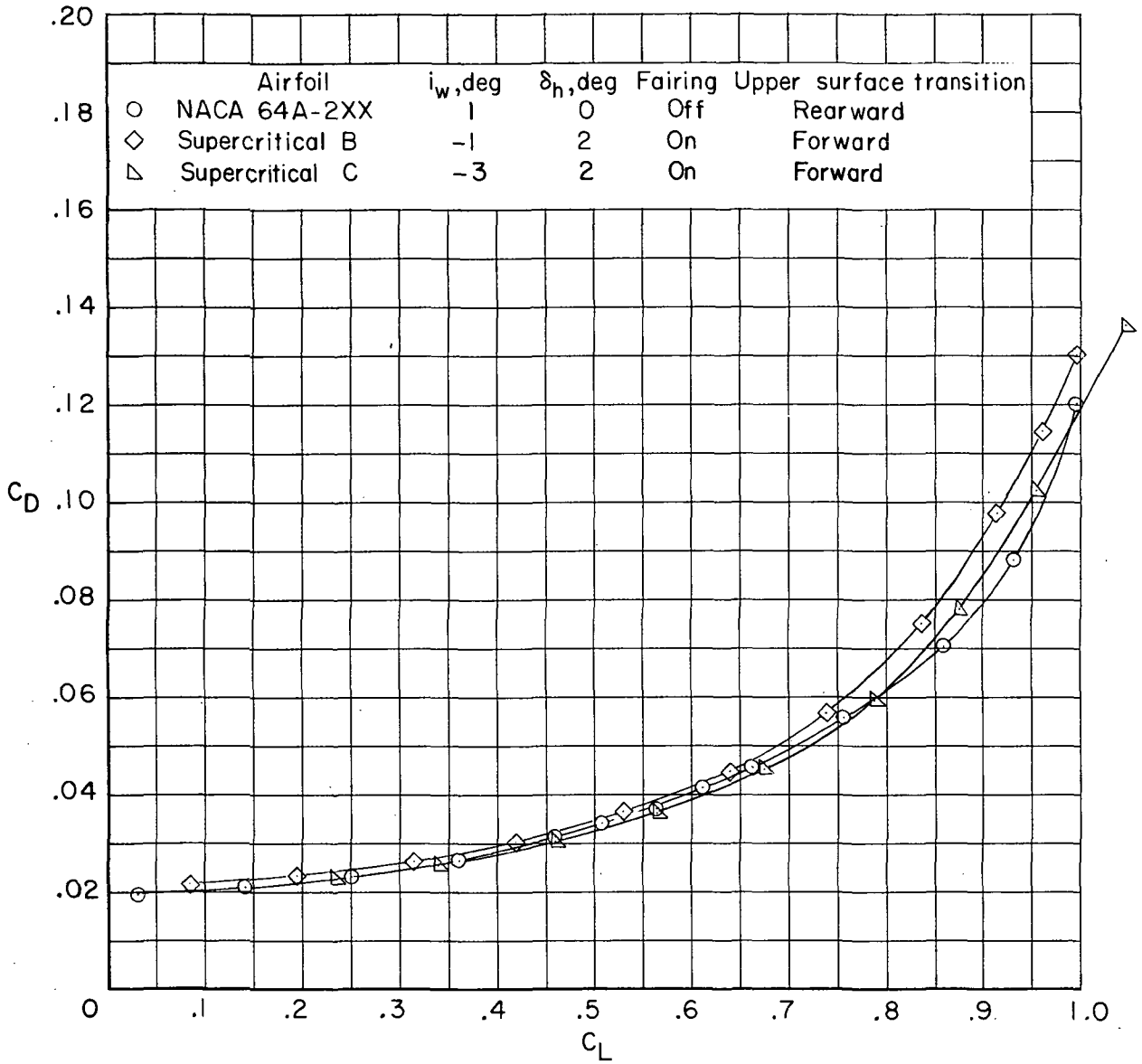


Figure 4. - Wing details. All linear dimensions in centimeters with inches in parentheses unless otherwise noted.



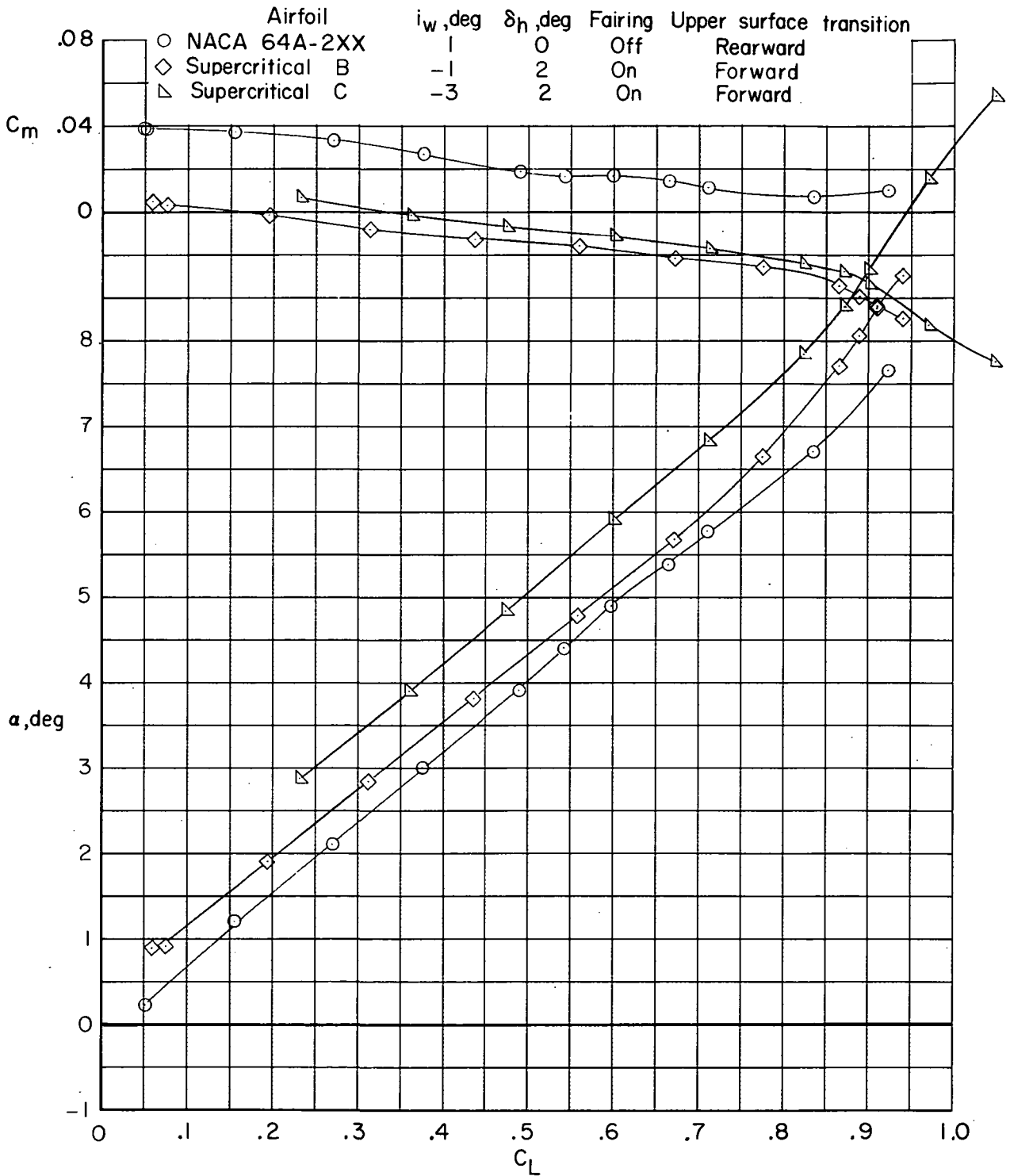
(a) $M = 0.60$.

Figure 5.- Comparison of longitudinal aerodynamic characteristics for configuration with NACA 64A2XX and supercritical airfoils. $\Lambda = 26^\circ$.



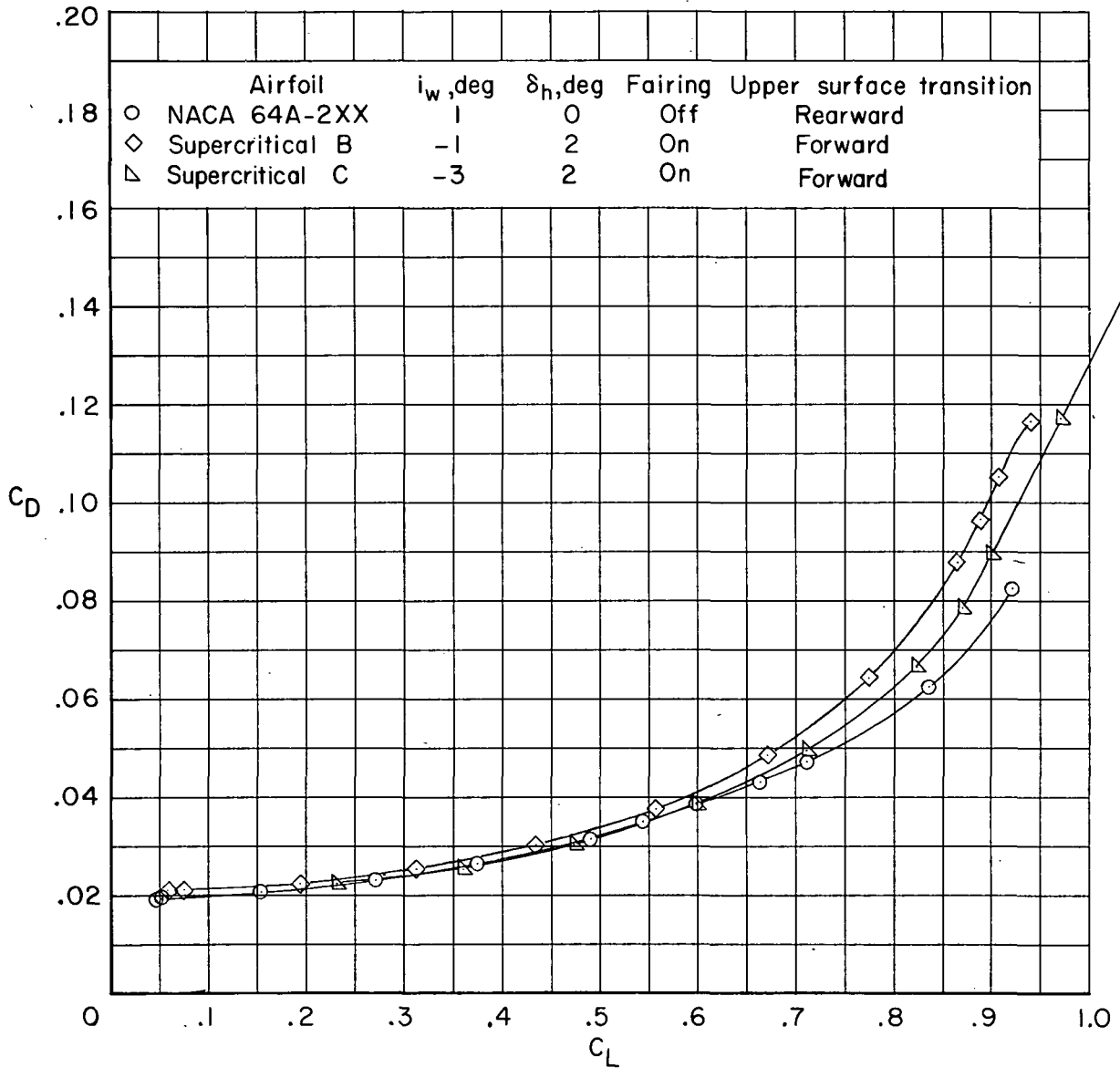
(a) $M = 0.60$. Concluded.

Figure 5. - Continued.



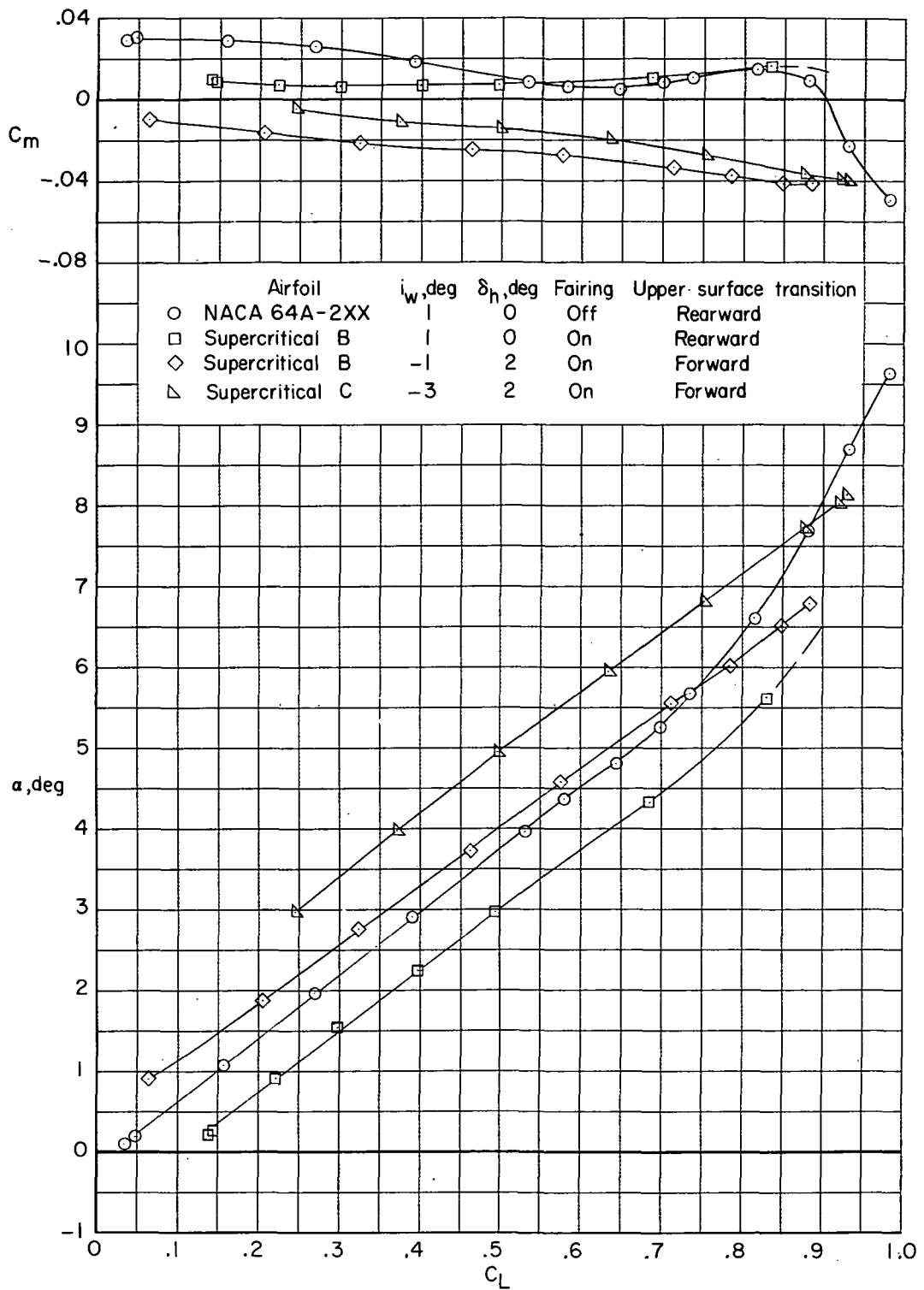
(b) $M = 0.70$.

Figure 5.- Continued.



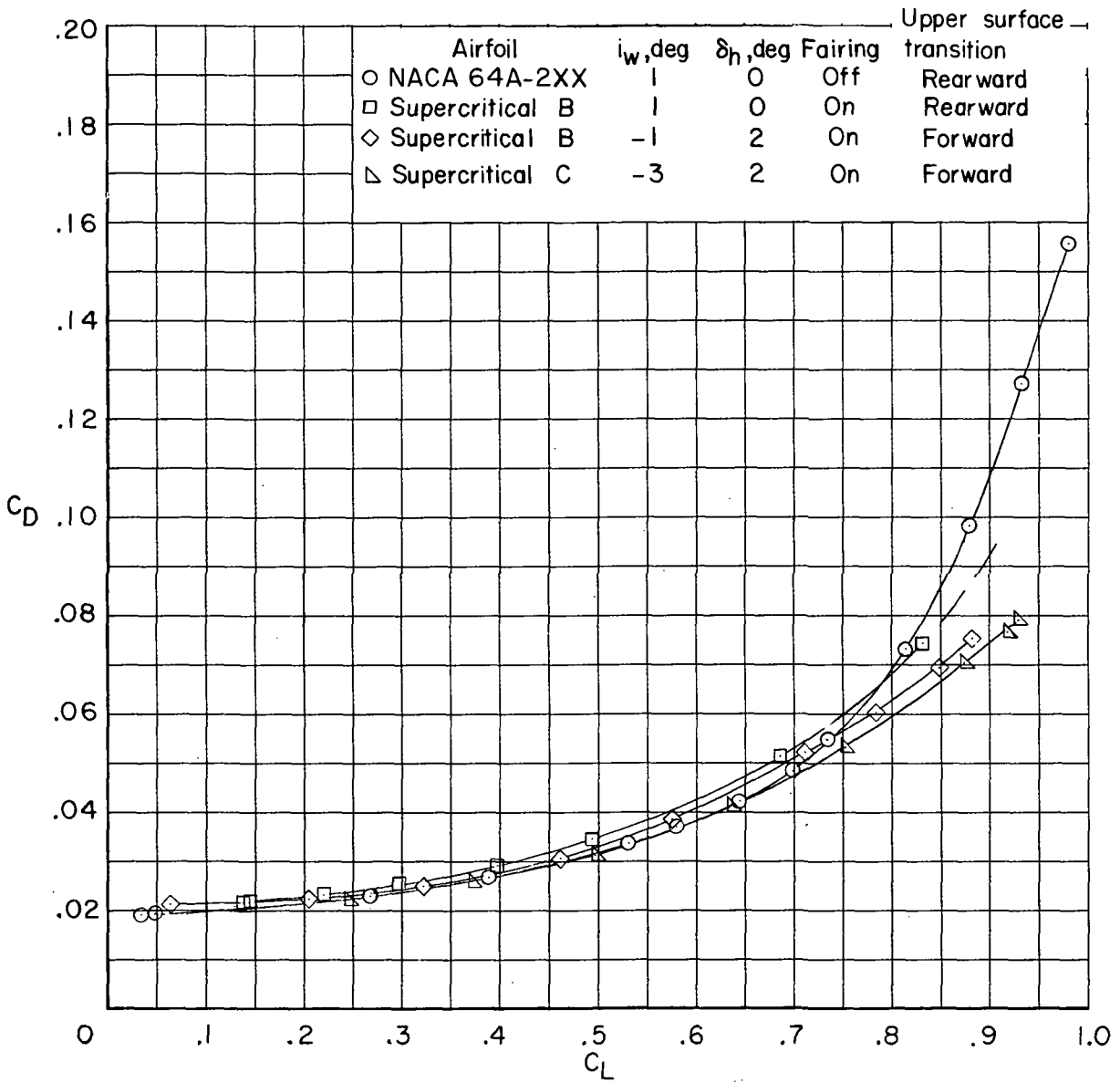
(b) $M = 0.70$. Concluded.

Figure 5.- Continued.



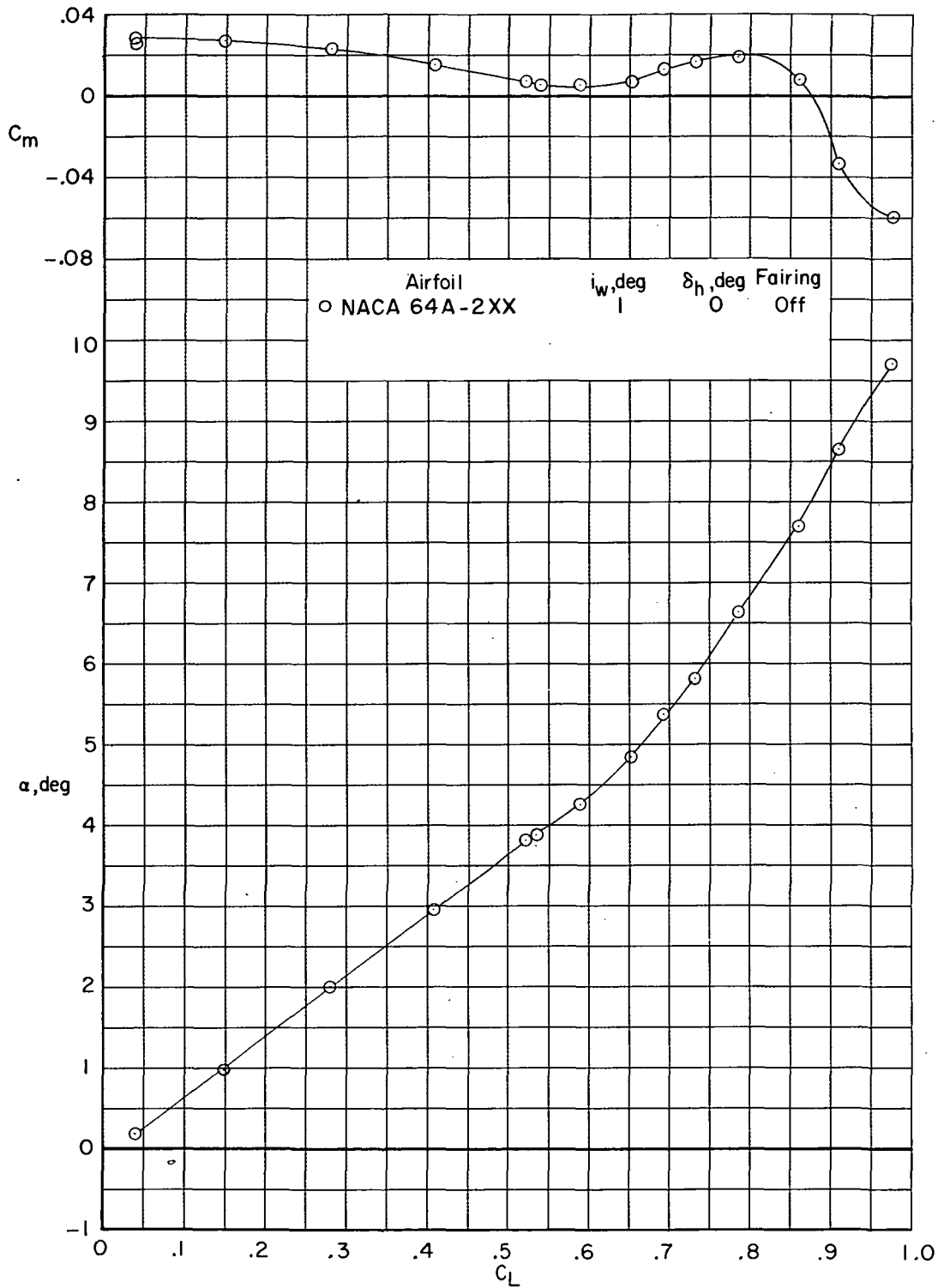
(c) $M = 0.75$.

Figure 5. - Continued.



(c) $M = 0.75$. Concluded.

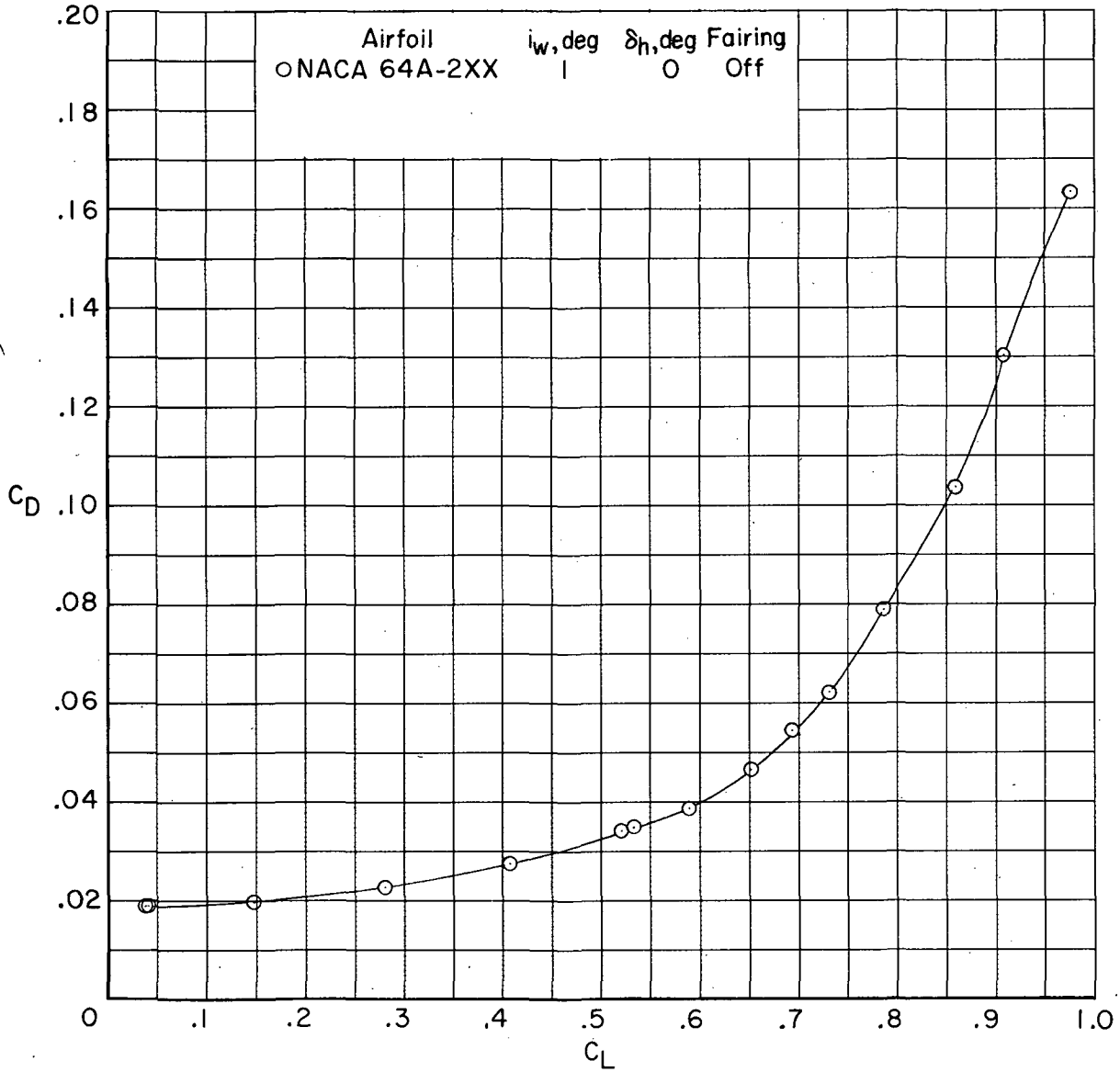
Figure 5. - Continued.



(d) $M = 0.77$. Transition rearward.

Figure 5. - Continued.

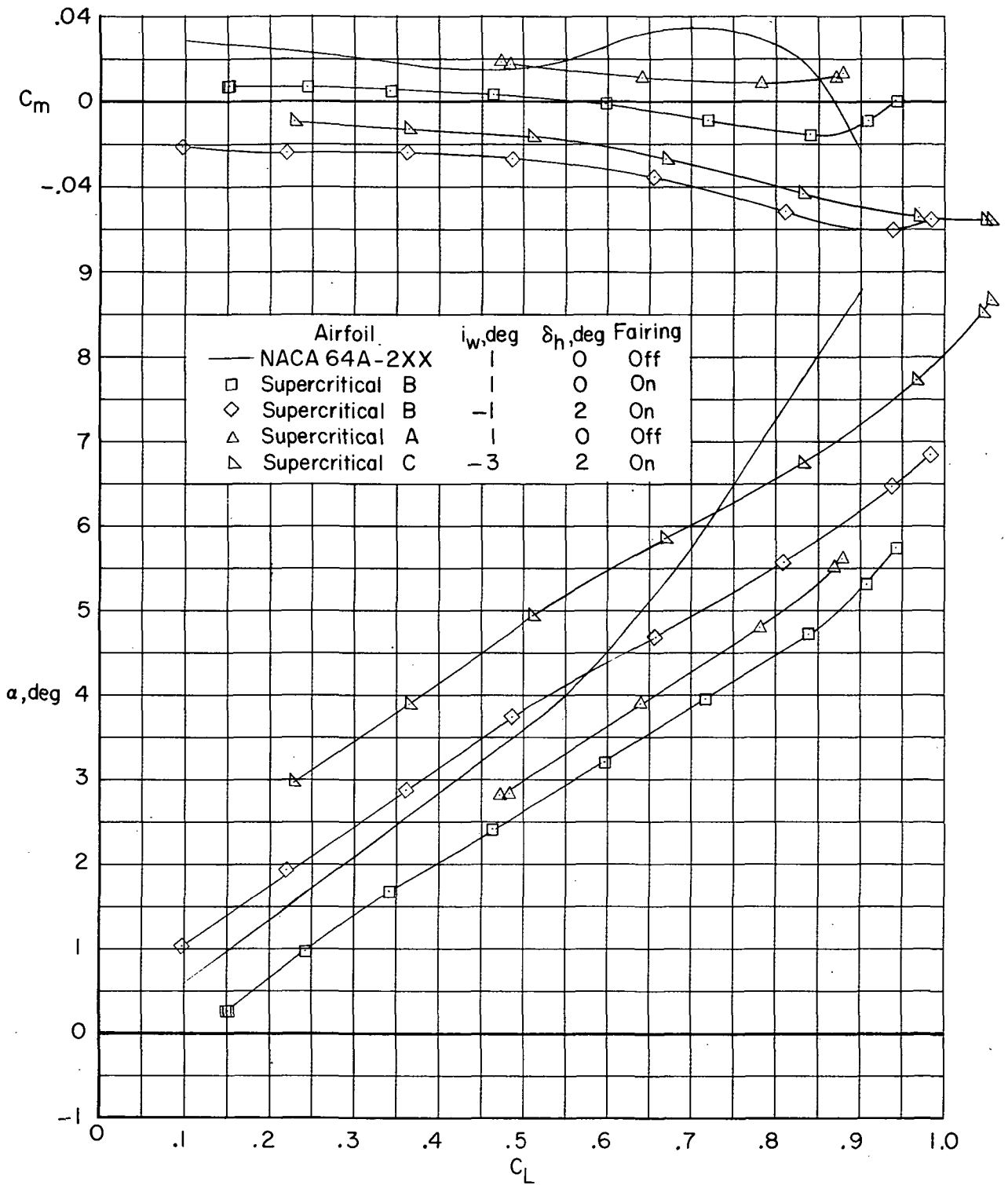
~~CONFIDENTIAL~~



(d) $M = 0.77$. Transition rearward. Concluded.

Figure 5. - Continued.

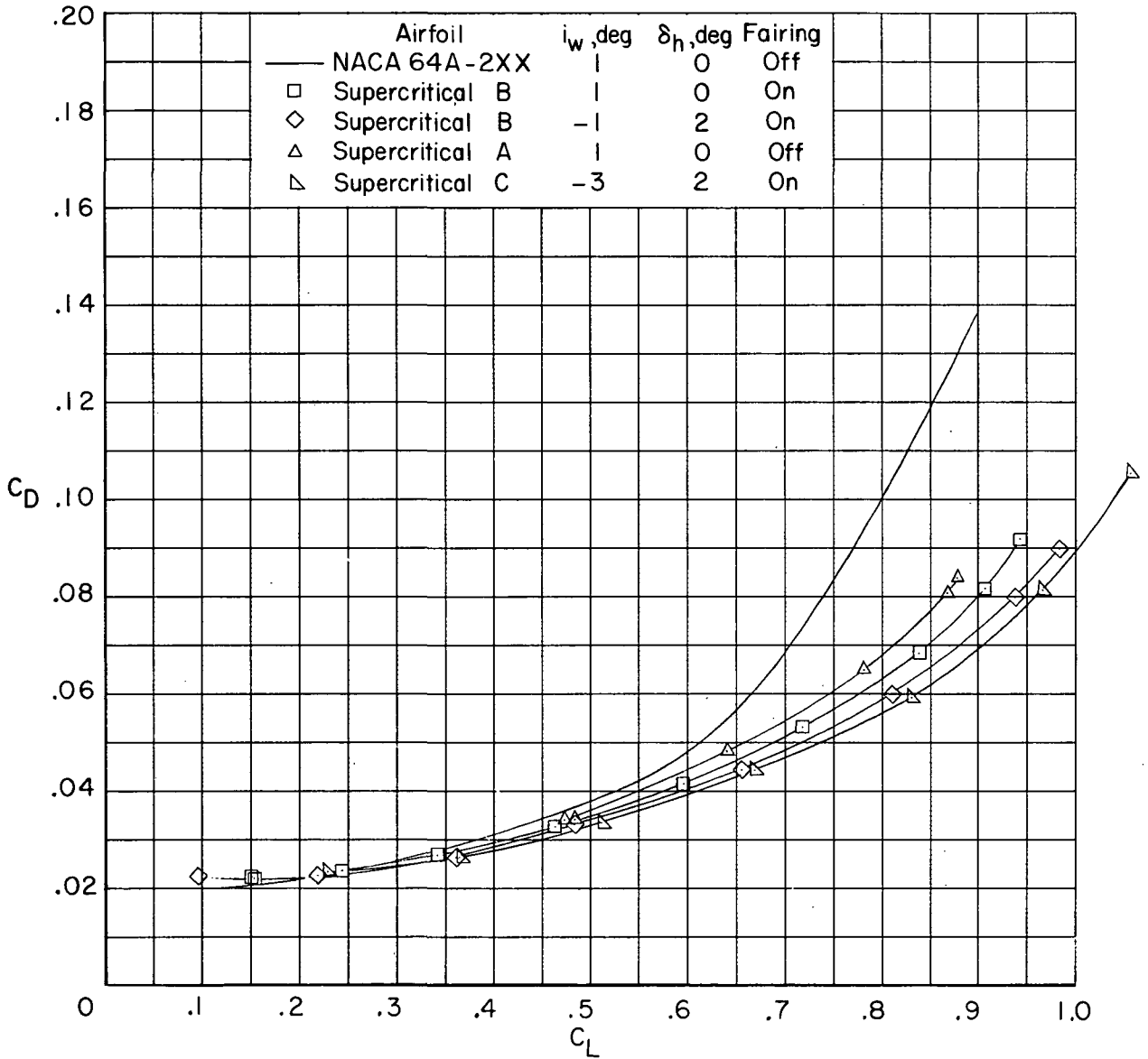
~~CONFIDENTIAL~~



(e) $M = 0.80$. Transition rearward.

Figure 5.- Continued.

~~CONFIDENTIAL~~

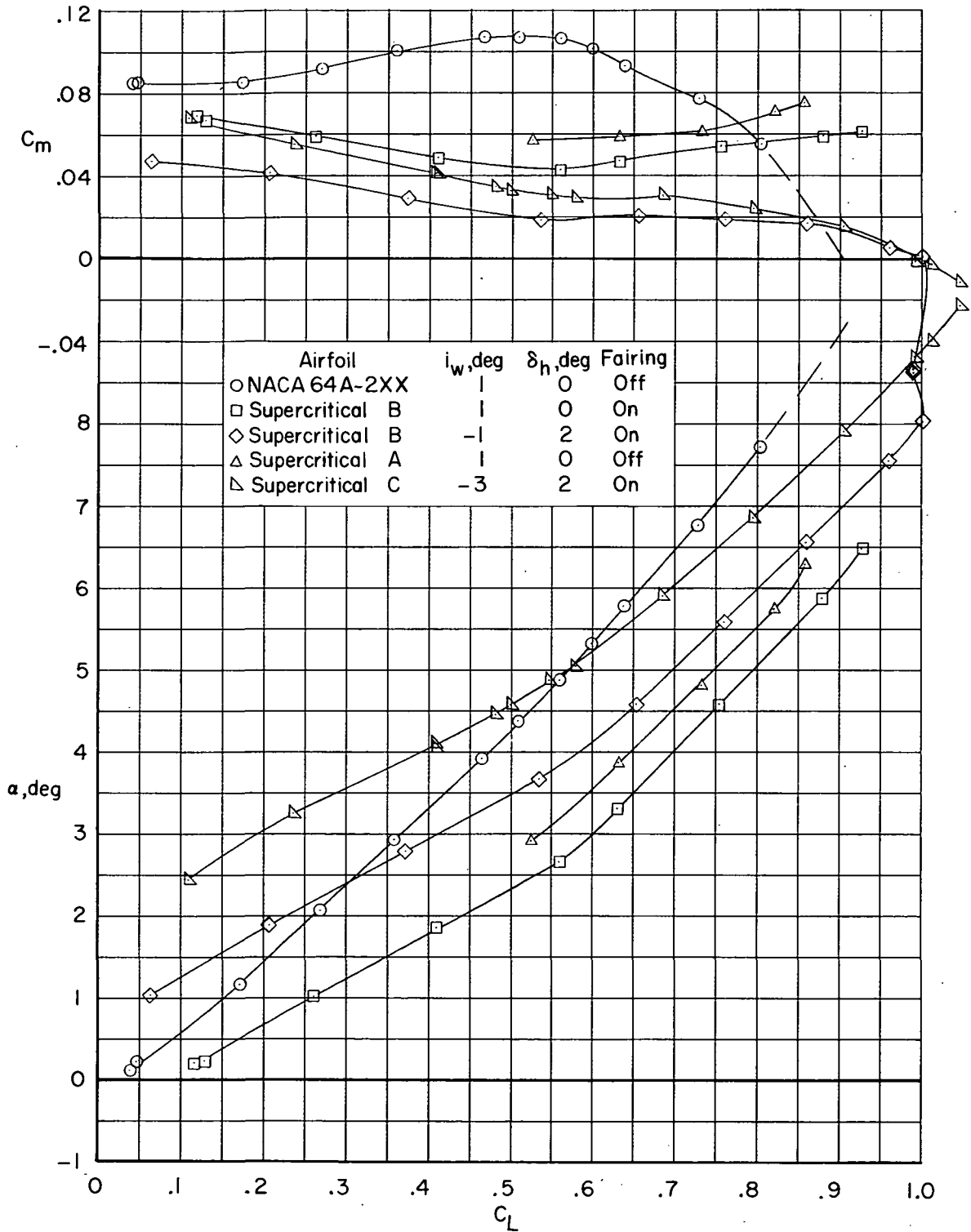


(e) $M = 0.80$. Transition rearward. Concluded.

Figure 5.- Continued.

~~CONFIDENTIAL~~

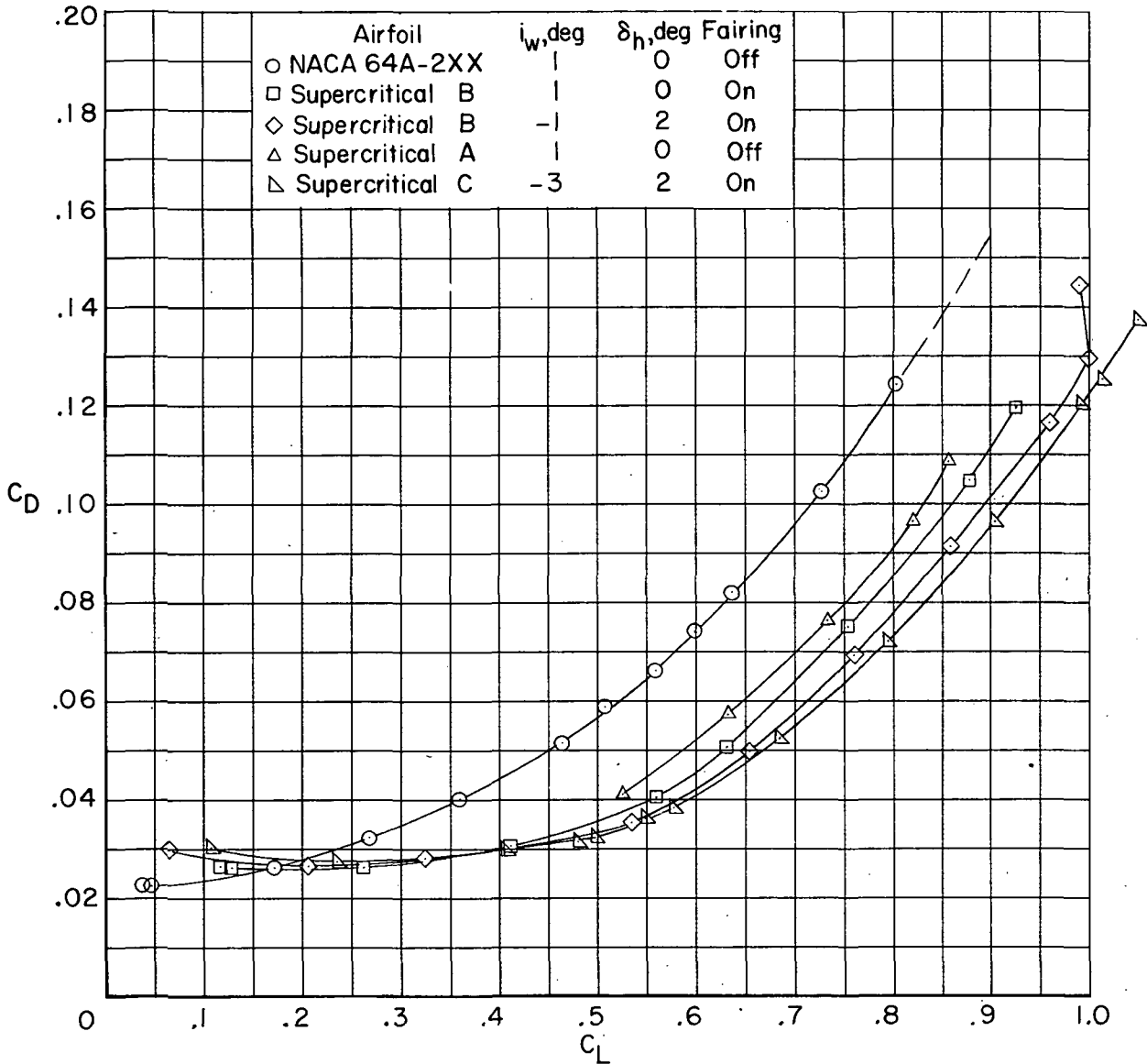
~~CONFIDENTIAL~~



(f) $M = 0.85$. Transition rearward.

Figure 5. - Continued.

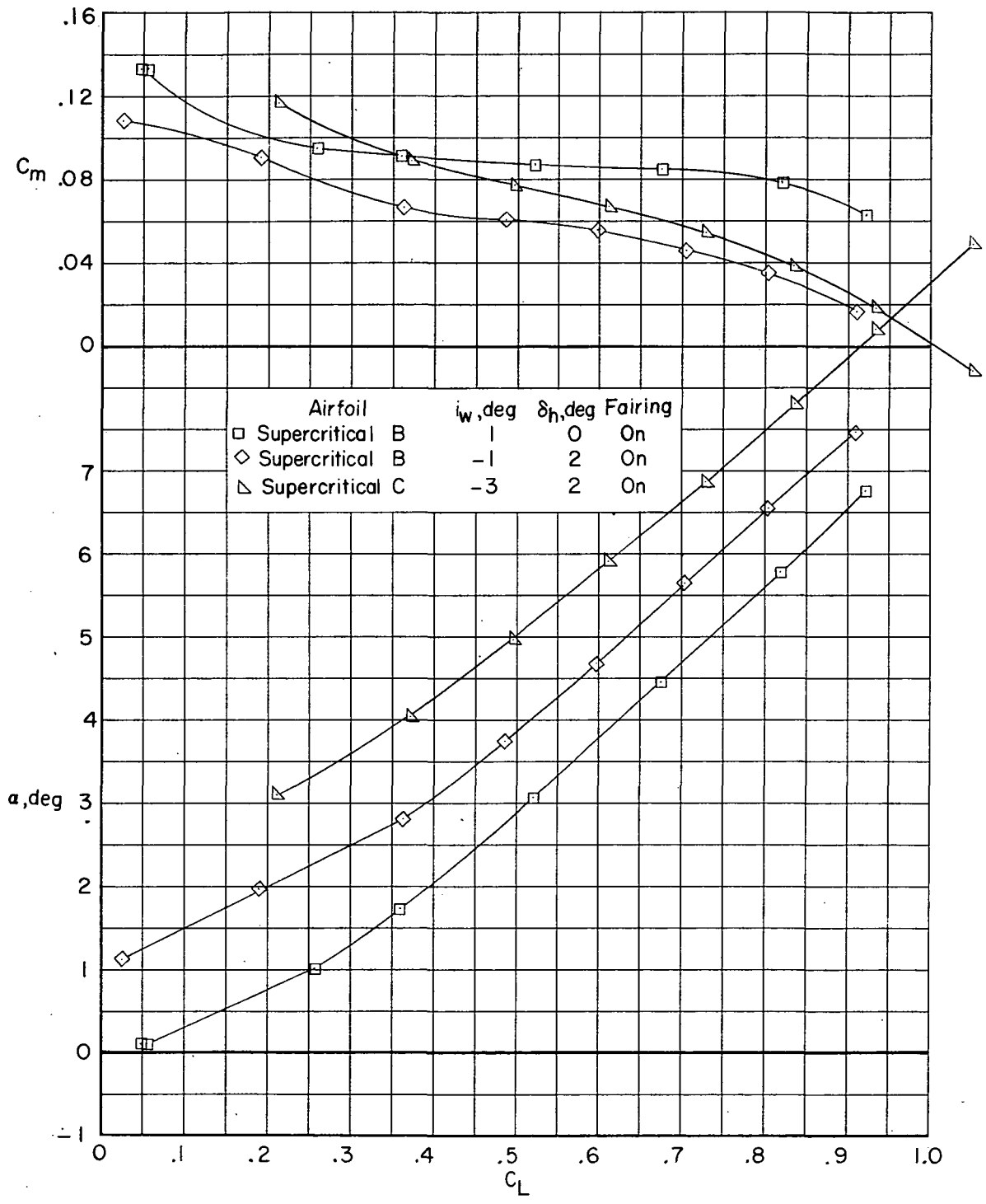
~~CONFIDENTIAL~~



(f) $M = 0.85$. Transition rearward. Concluded.

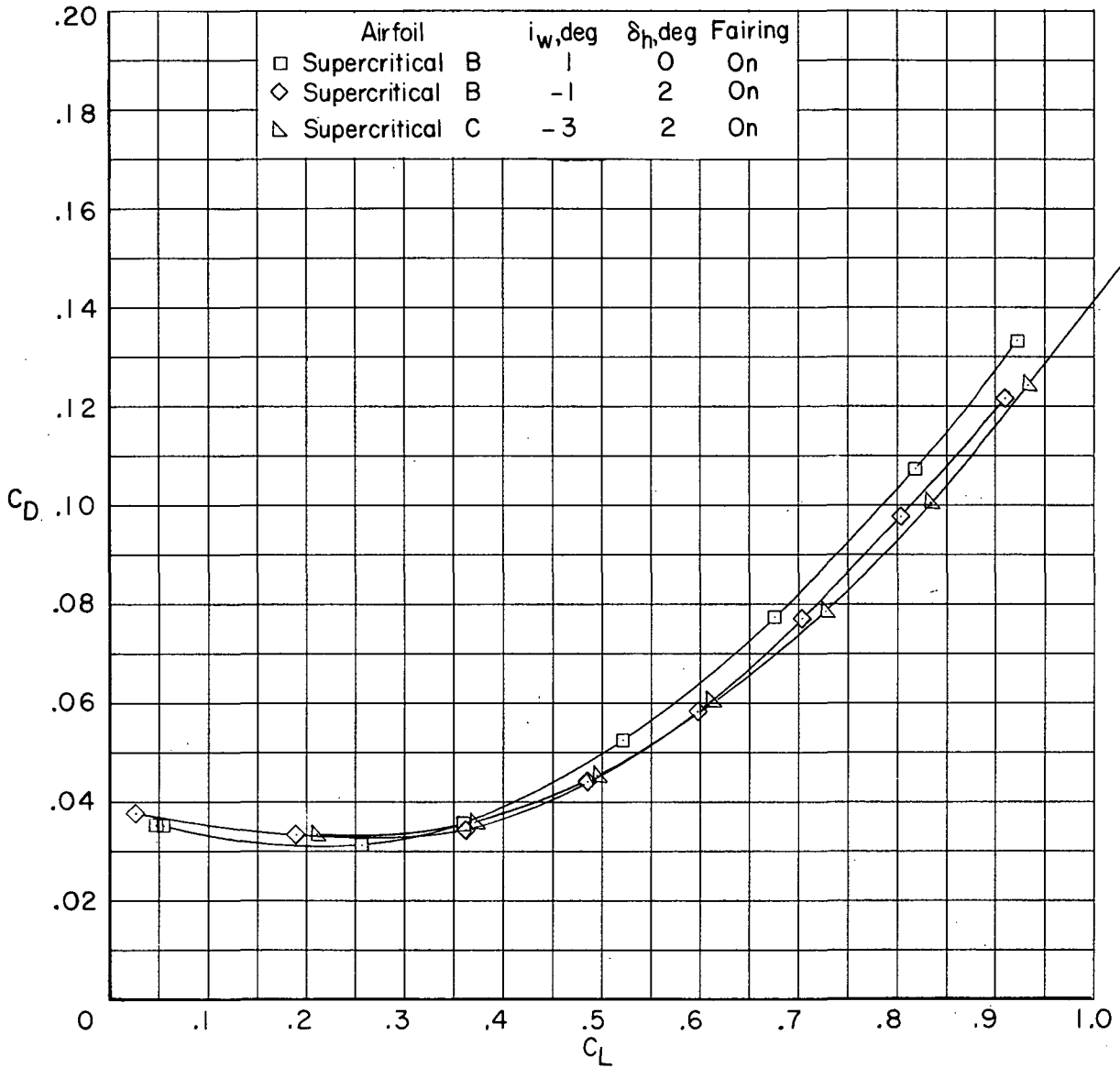
Figure 5.- Continued.

~~CONFIDENTIAL~~



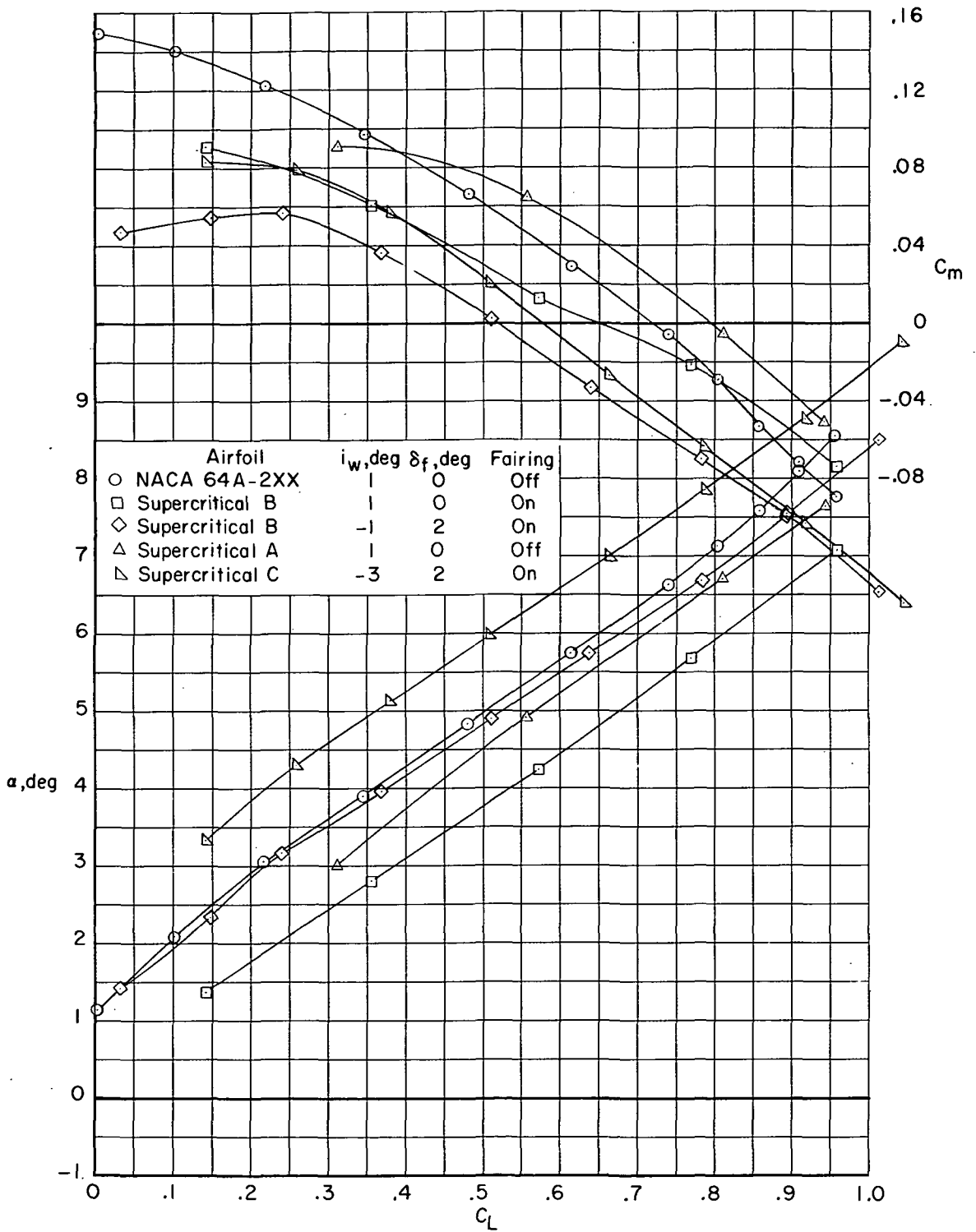
(g) $M = 0.88$. Transition rearward.

Figure 5.- Continued.



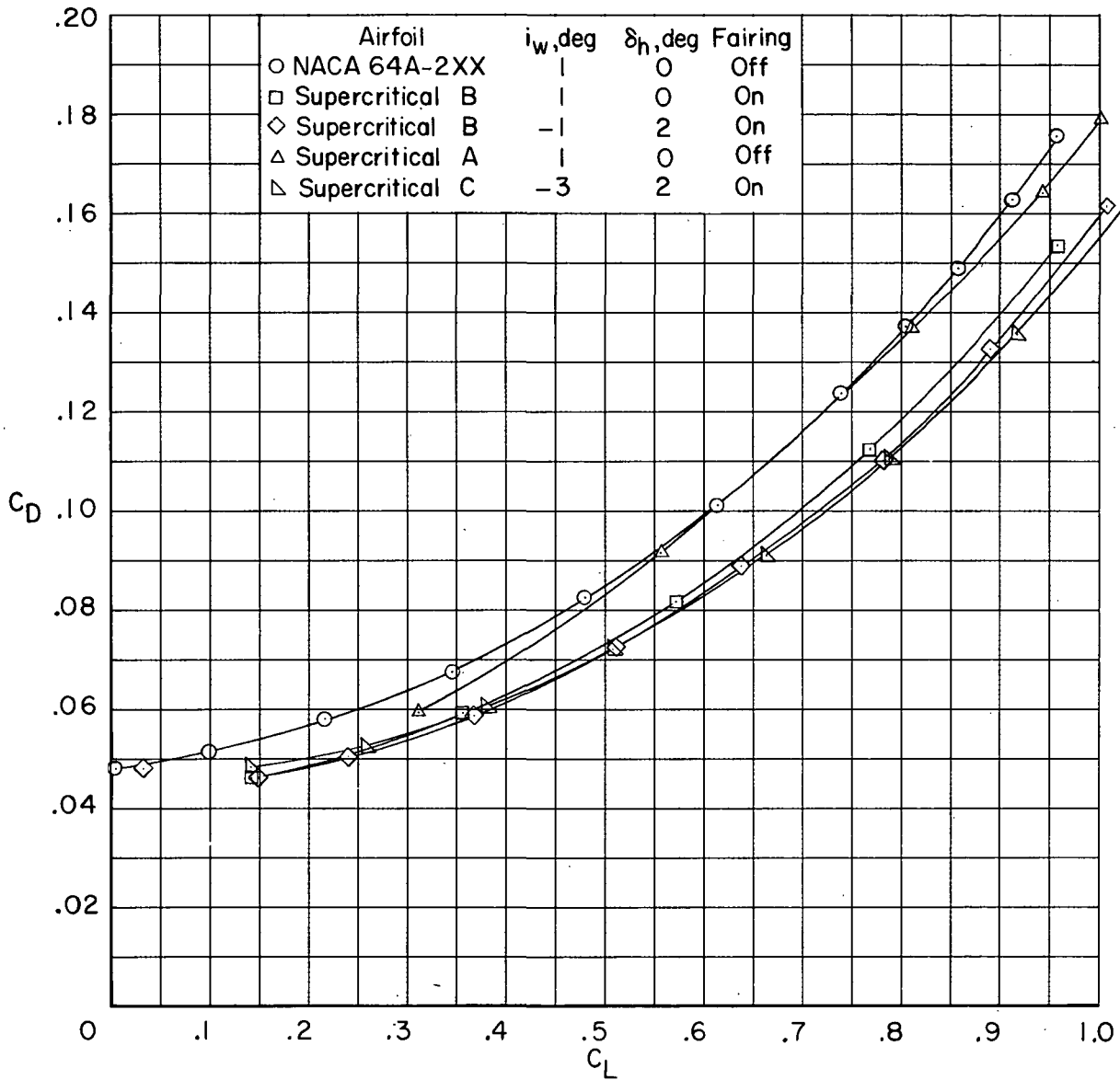
(g) $M = 0.88$. Transition rearward. Concluded.

Figure 5. - Continued.



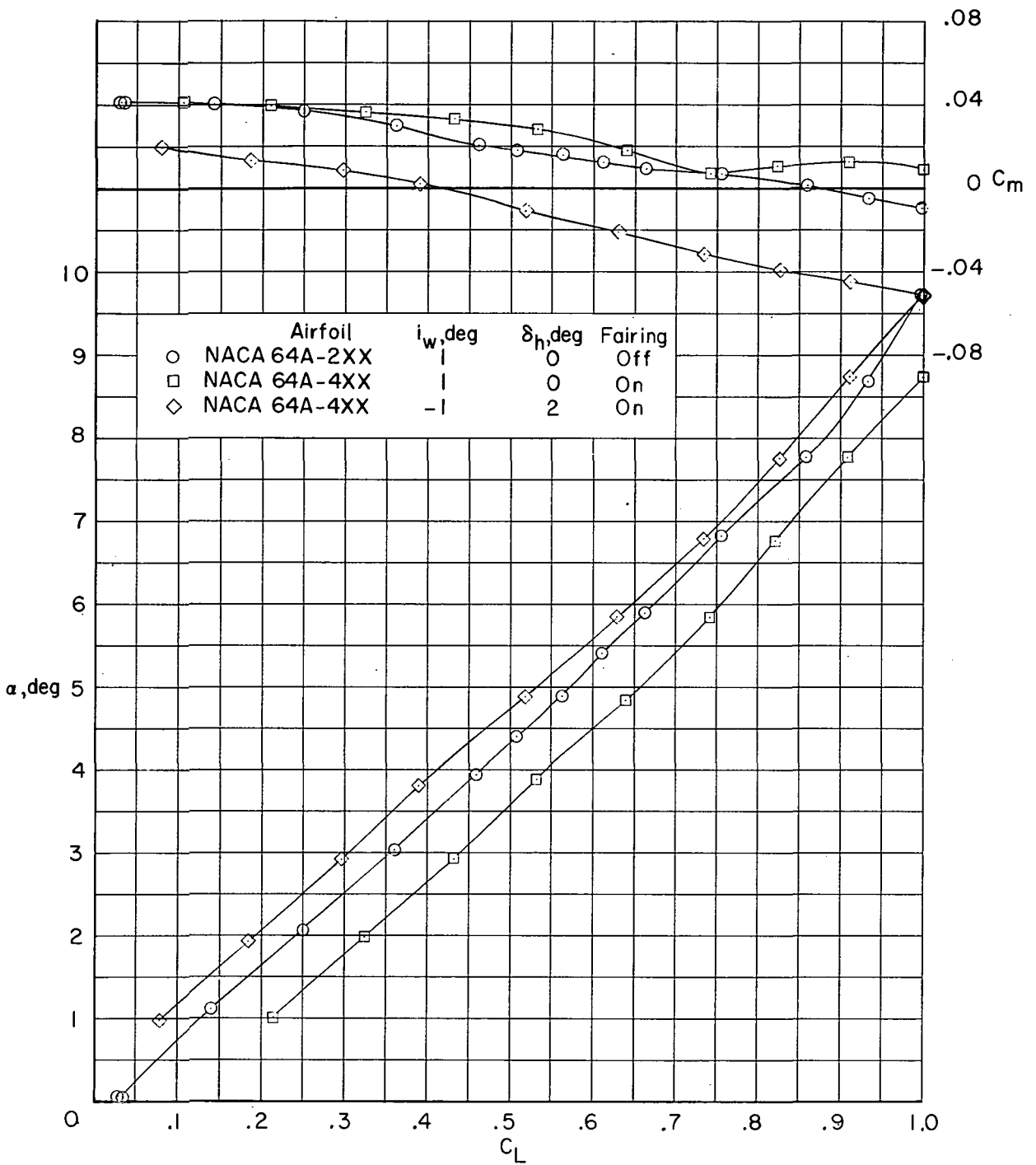
(h) $M = 0.91$. Transition rearward.

Figure 5.- Continued.



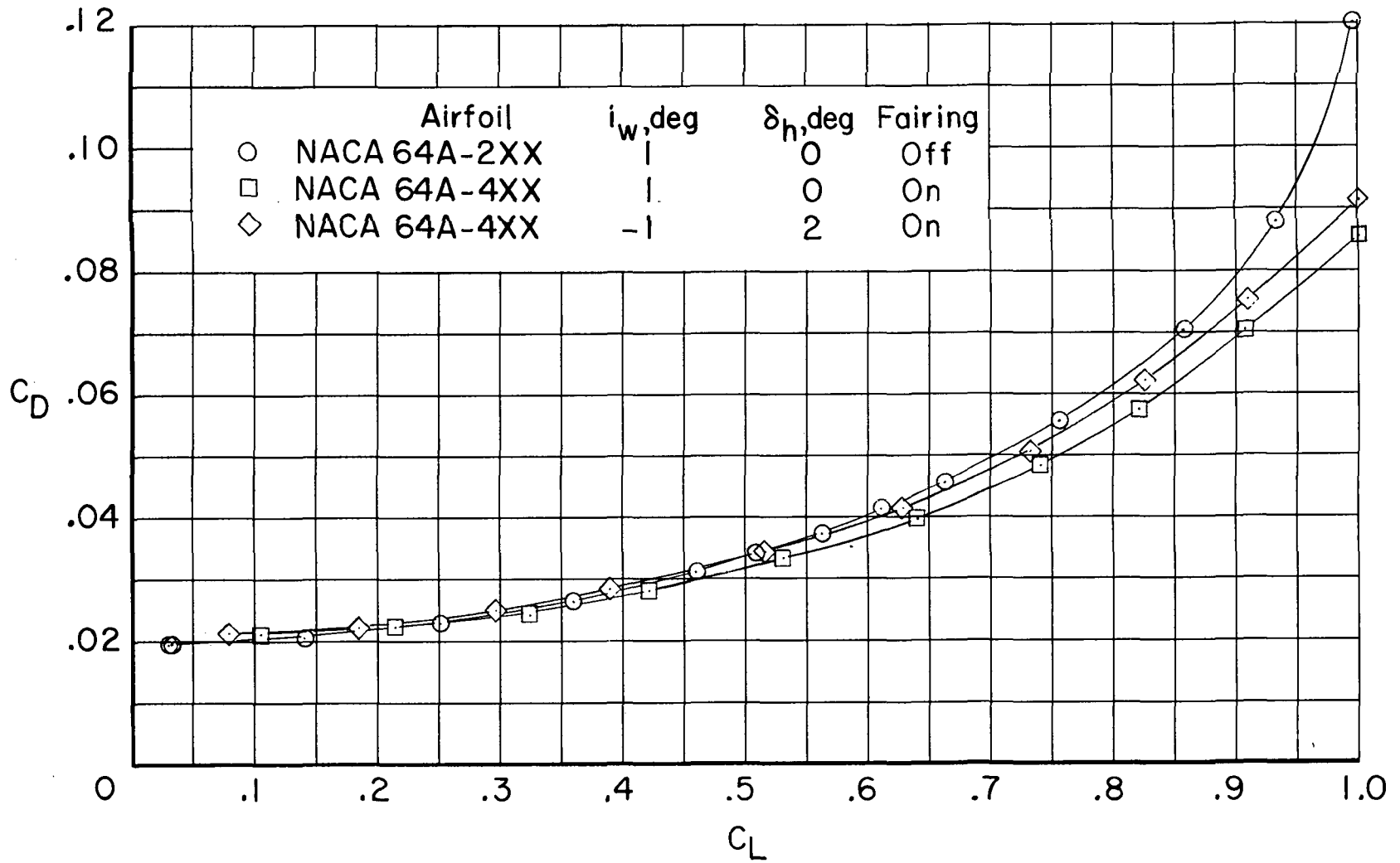
(h) $M = 0.91$. Transition rearward. Concluded.

Figure 5.- Concluded.



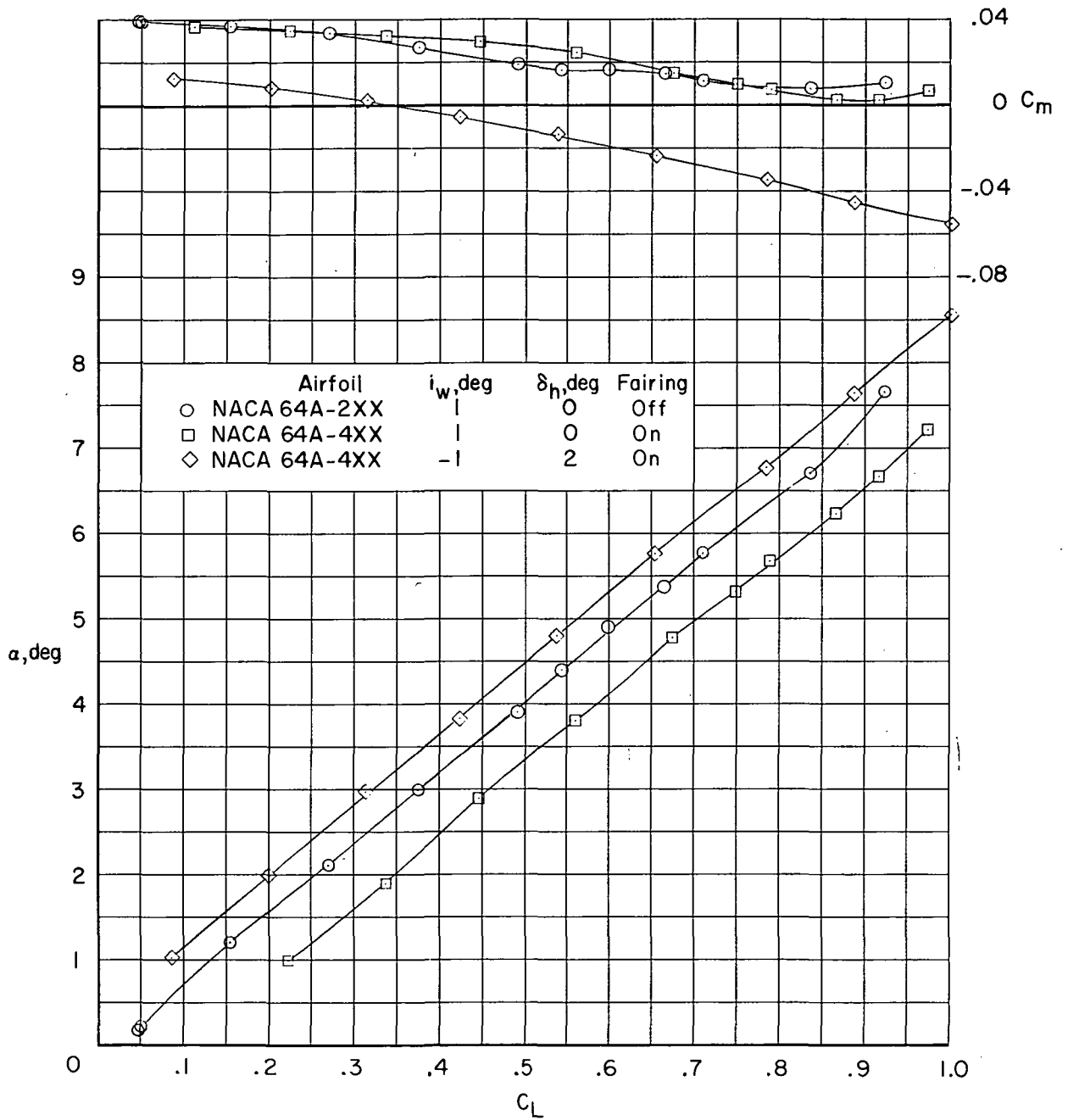
(a) $M = 0.60$.

Figure 6.- Comparison of longitudinal aerodynamic characteristics for configuration with NACA 64A2XX and NACA 64A4XX airfoils and transition rearward. $\Lambda = 26^\circ$.



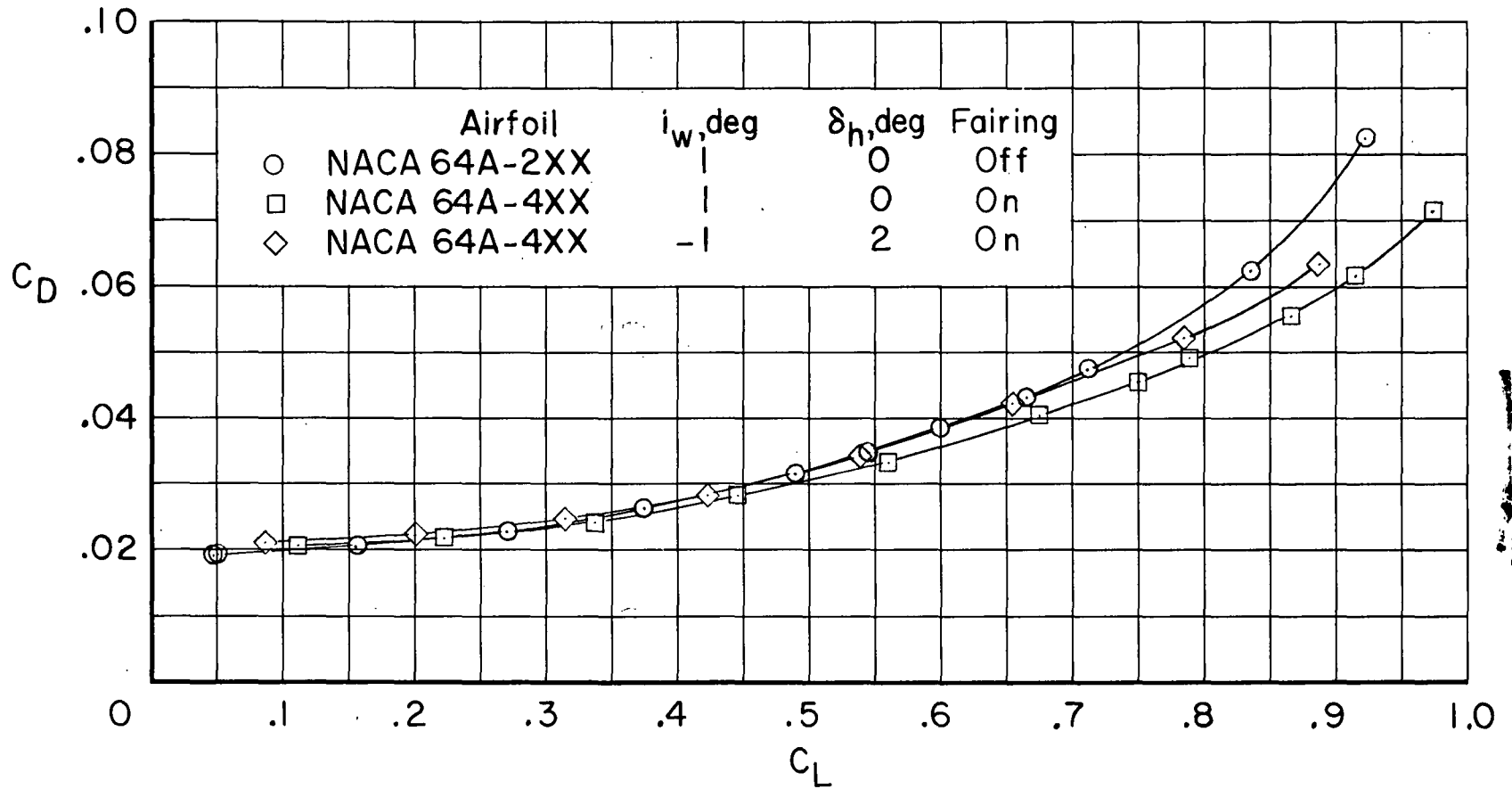
(a) $M = 0.60$. Concluded.

Figure 6.- Continued.



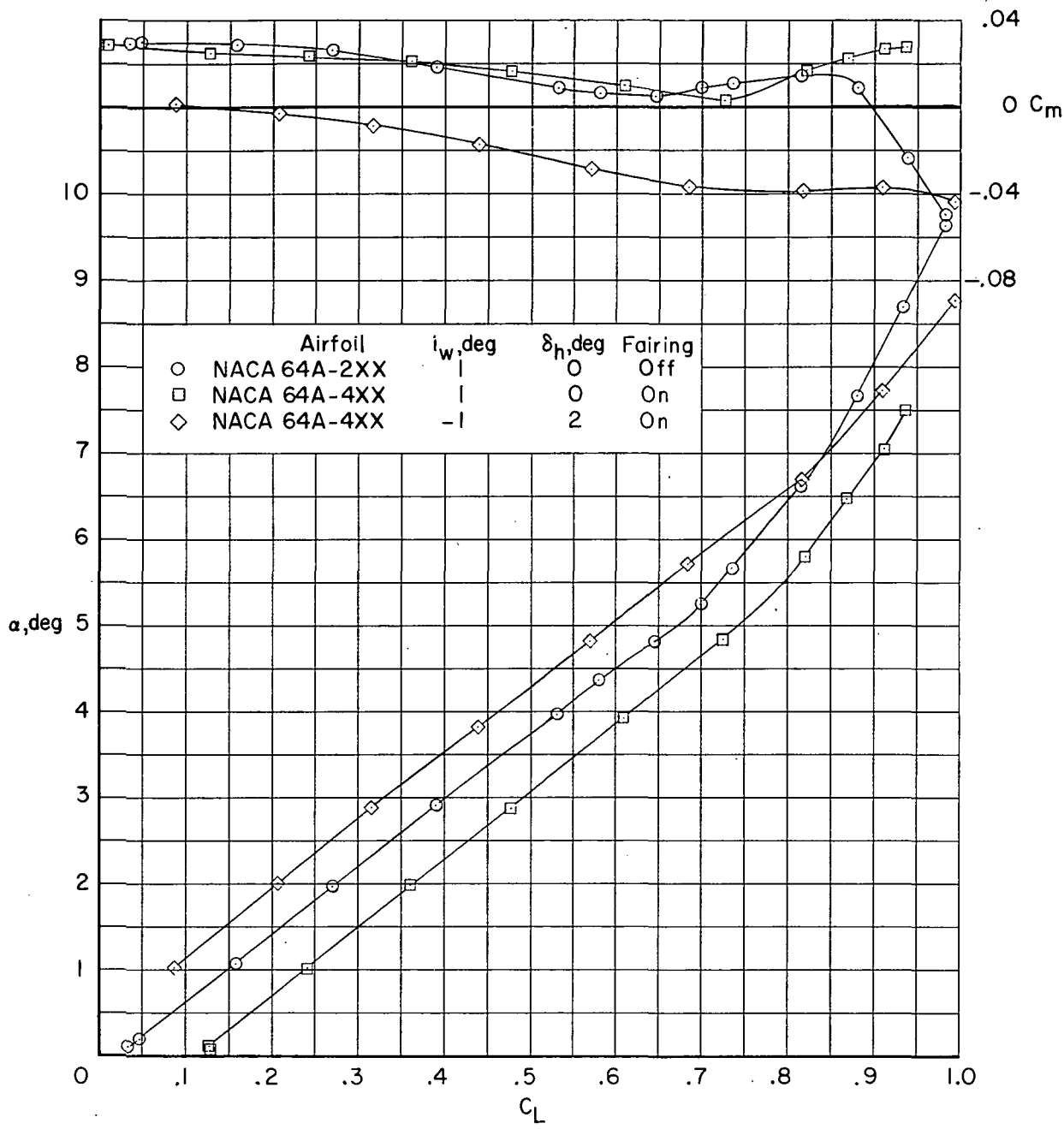
(b) $M = 0.70$.

Figure 6. - Continued.



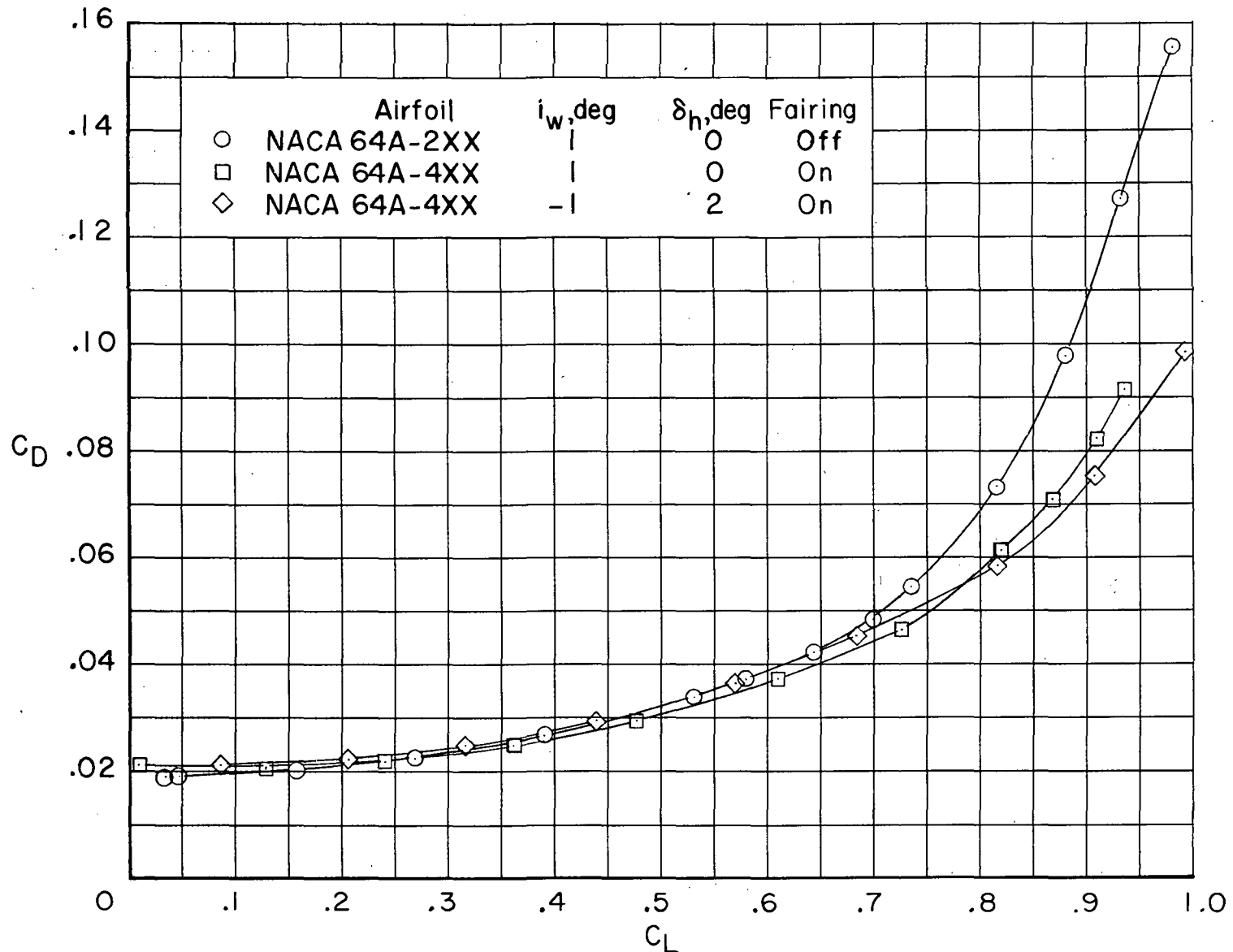
(b) $M = 0.70$. Concluded.

Figure 6. - Continued.



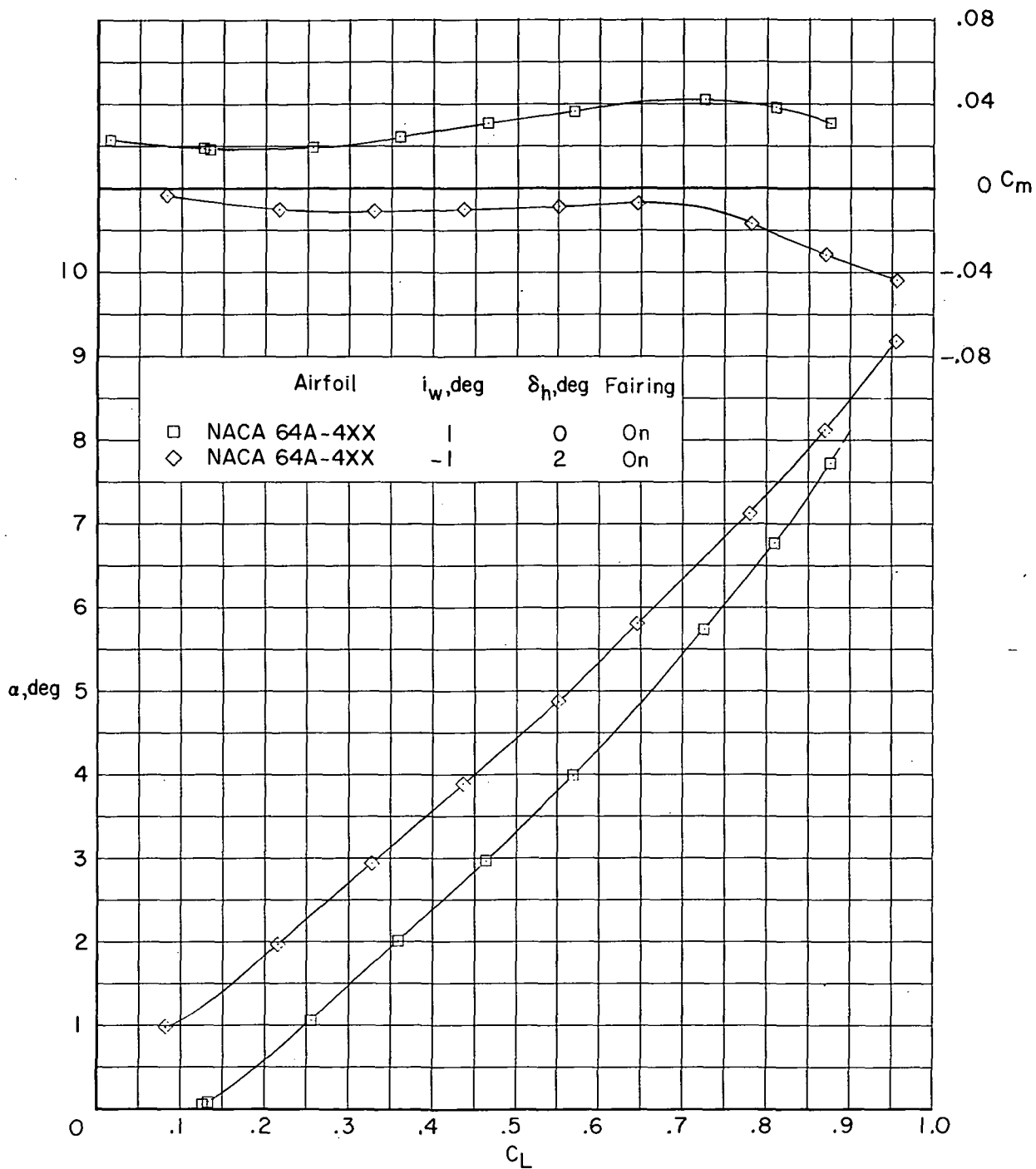
(c) $M = 0.75$.

Figure 6. - Continued.



(c) $M = 0.75$. Concluded.

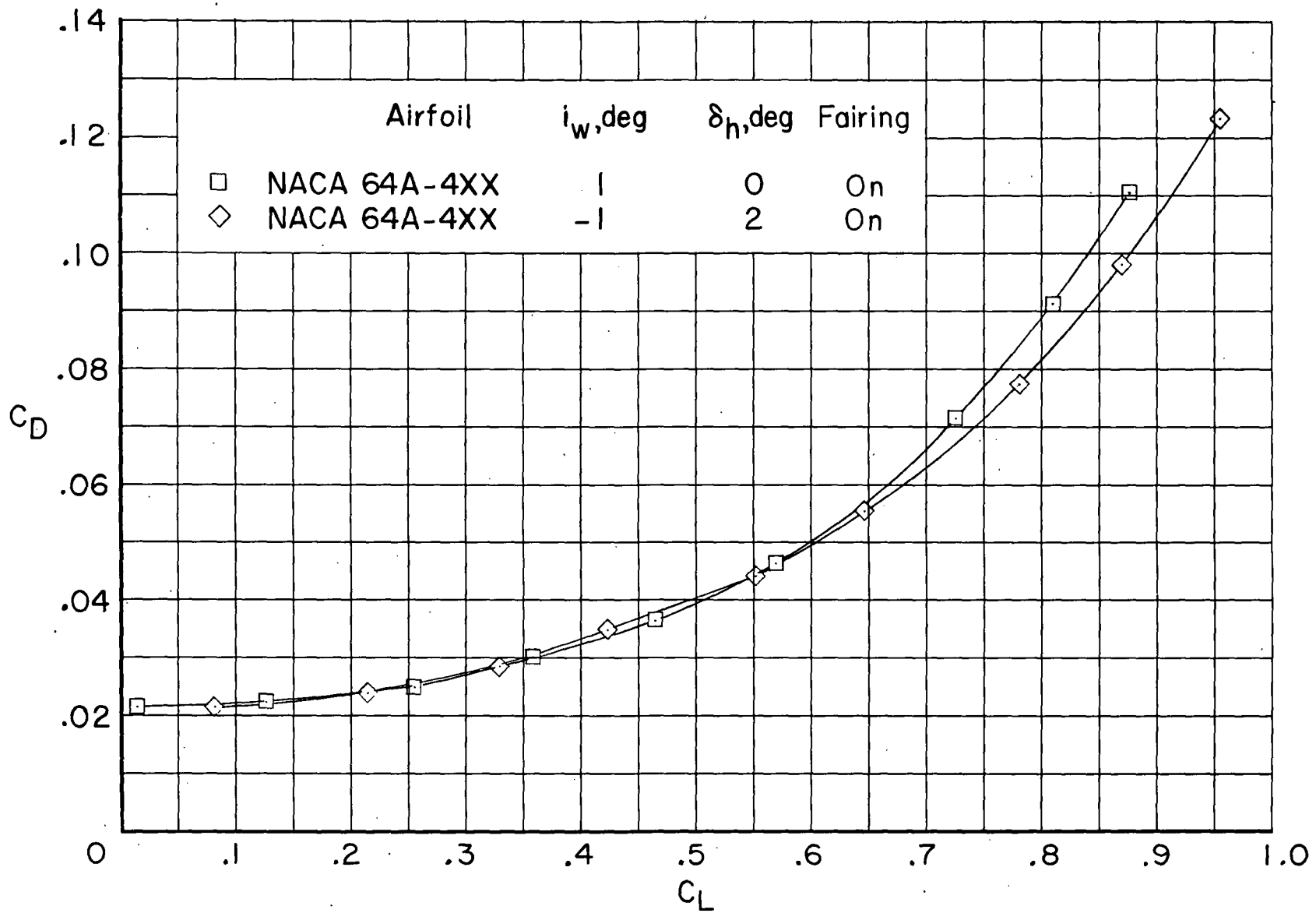
Figure 6.- Continued.



(d) $M = 0.80$.

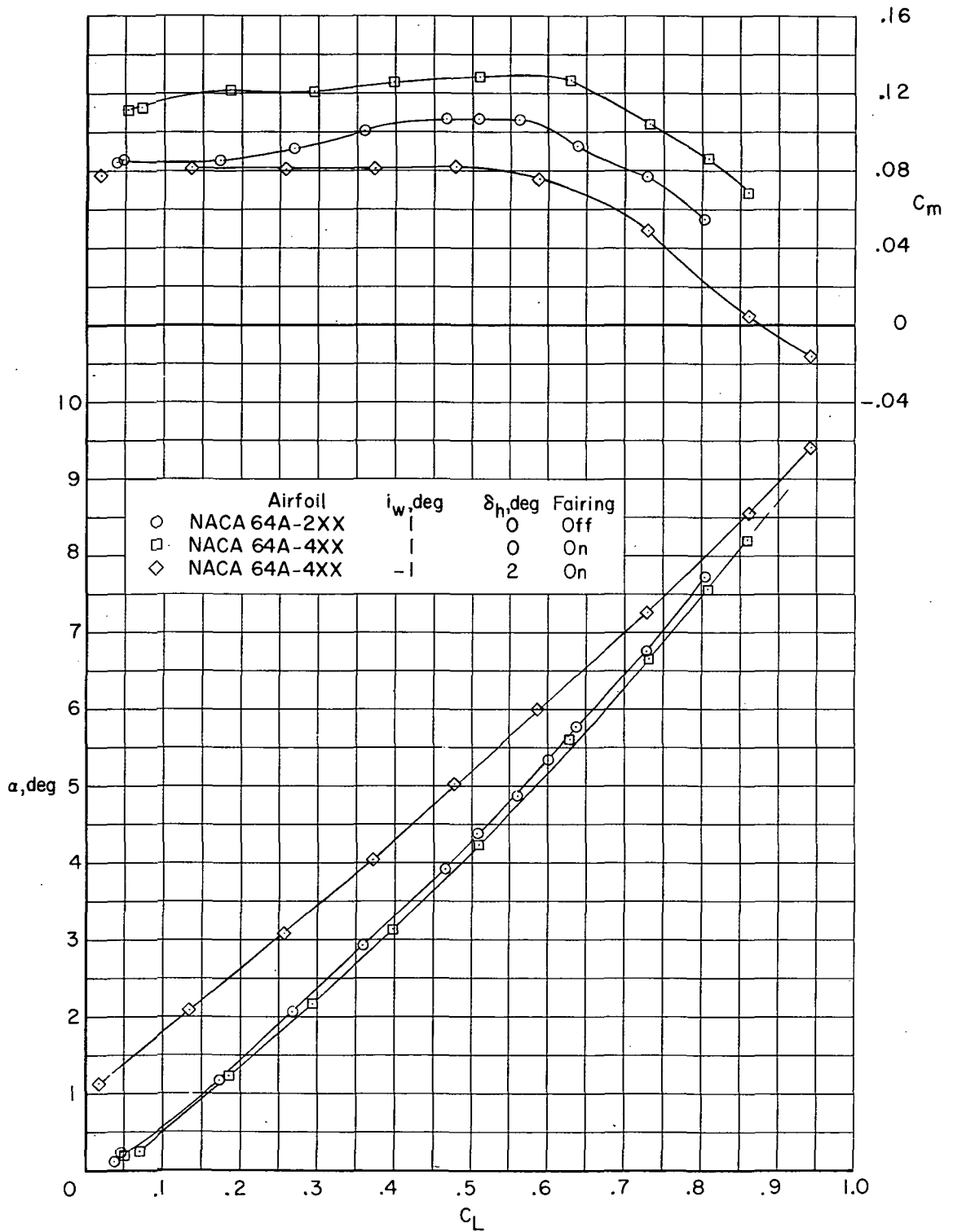
Figure 6. - Continued.

CONFIDENTIAL



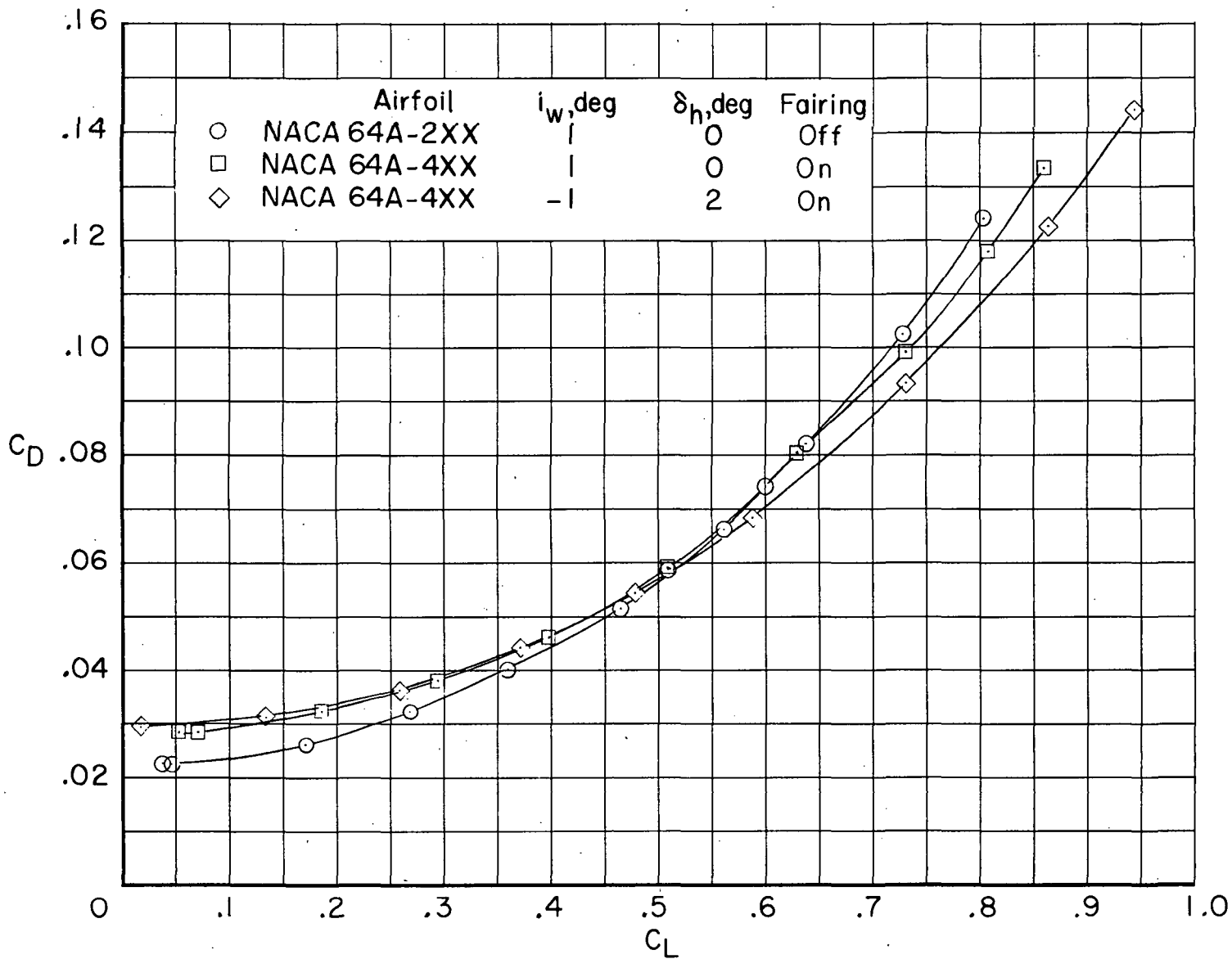
(d) $M = 0.80$. Concluded.

Figure 6.- Continued.



(e) $M = 0.85$.

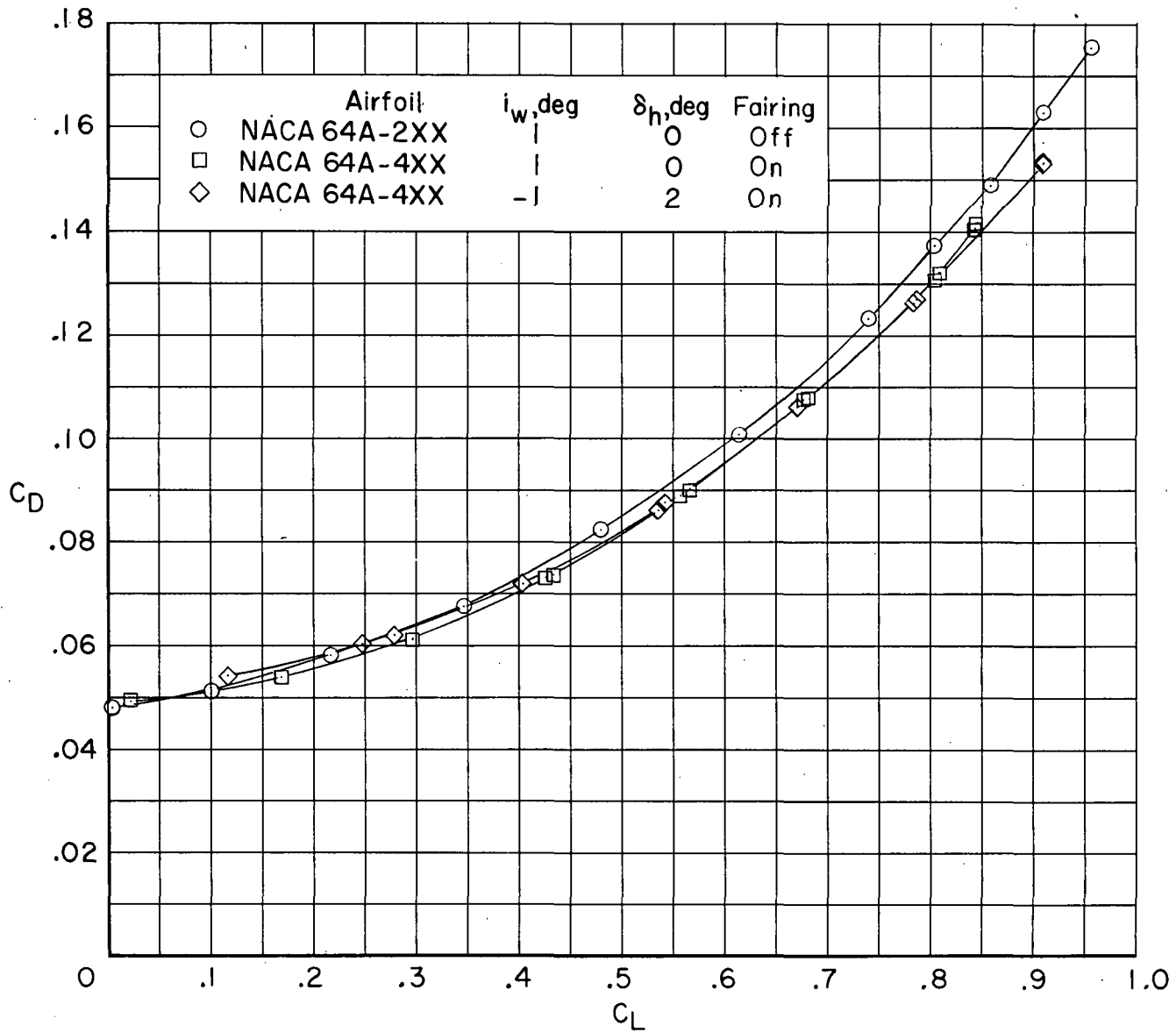
Figure 6.- Continued.



(e) $M = 0.85$. Concluded.

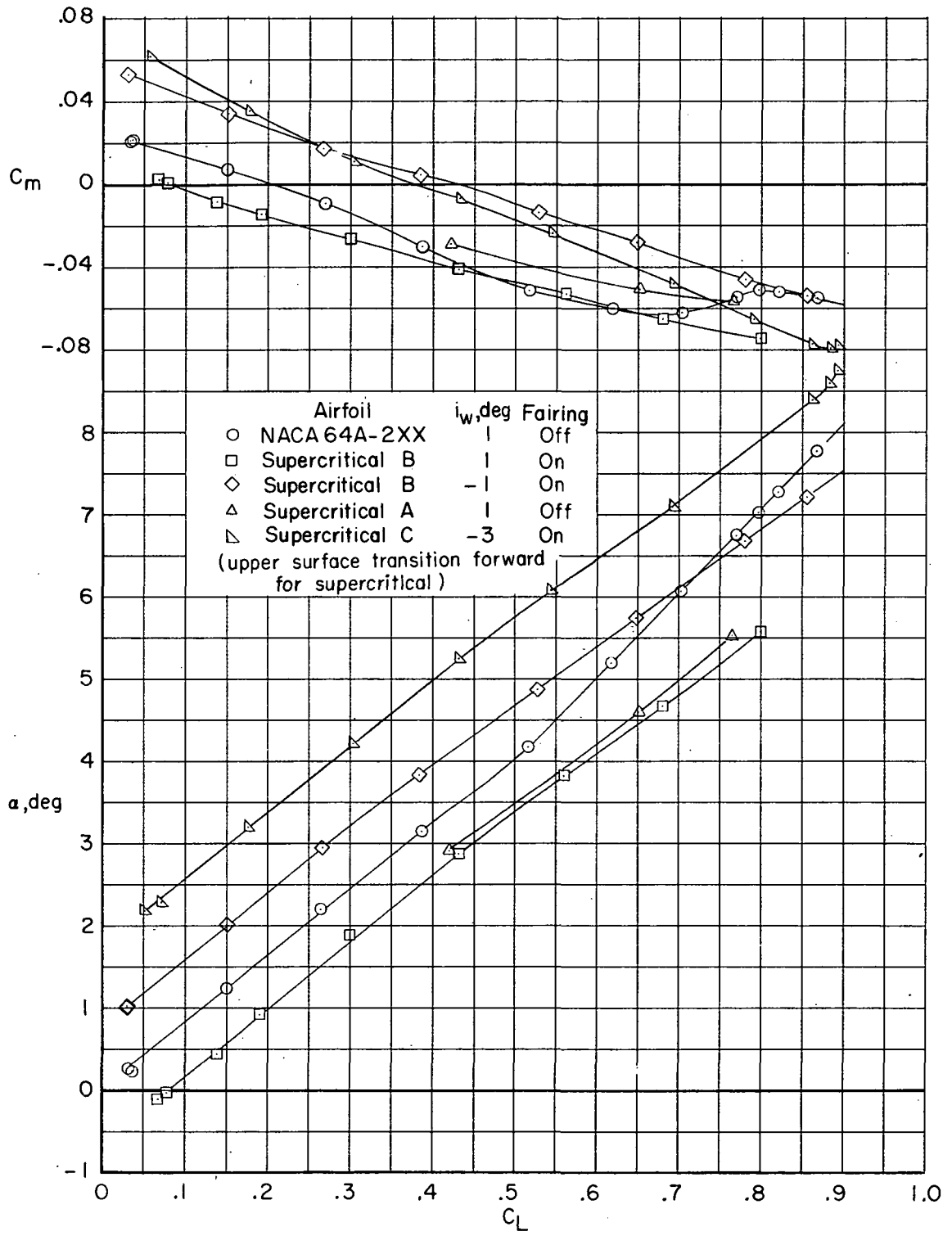
Figure 6. - Continued.

Page intentionally left blank



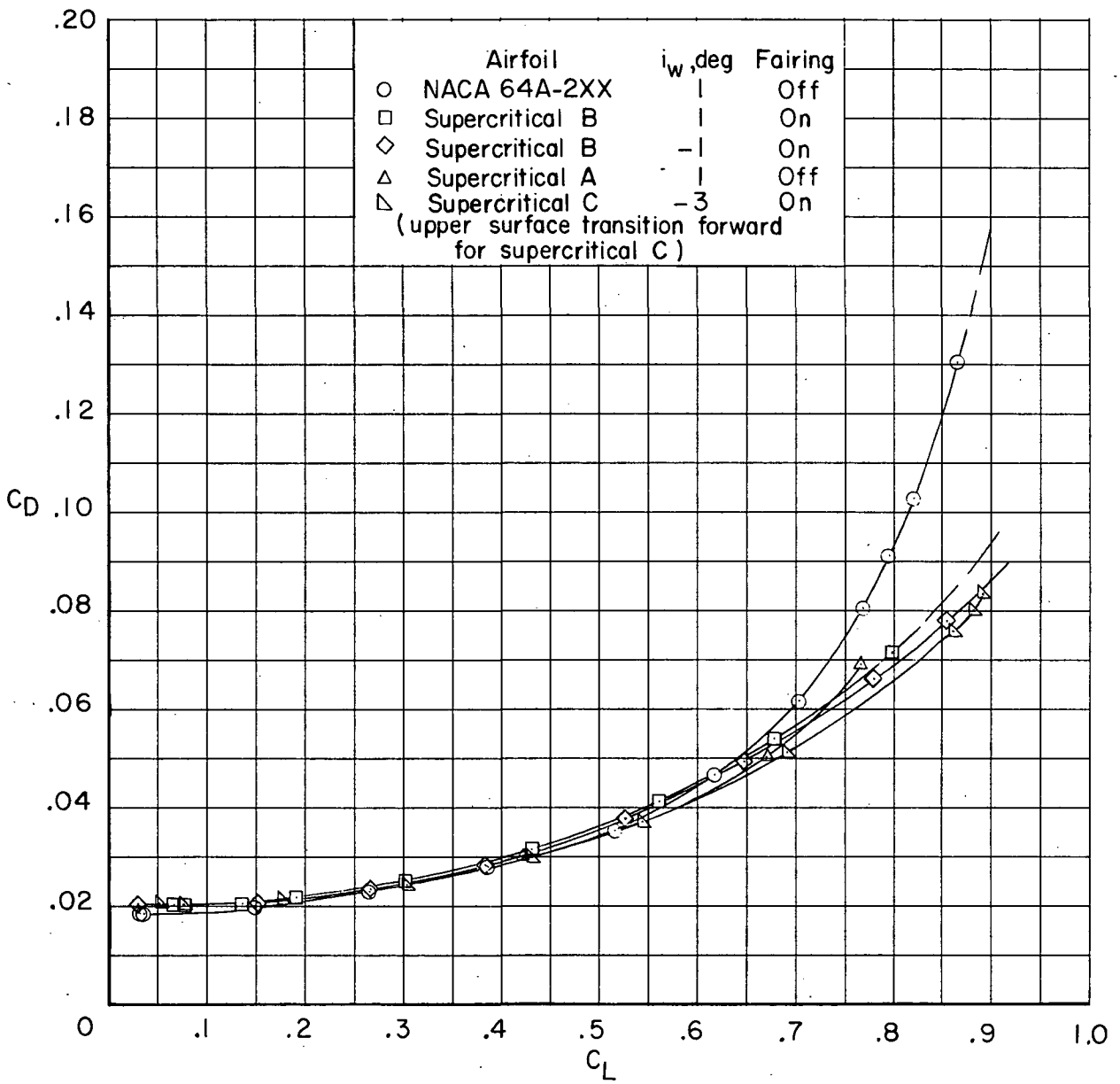
(f) $M = 0.91$. Concluded.

Figure 6.- Concluded.



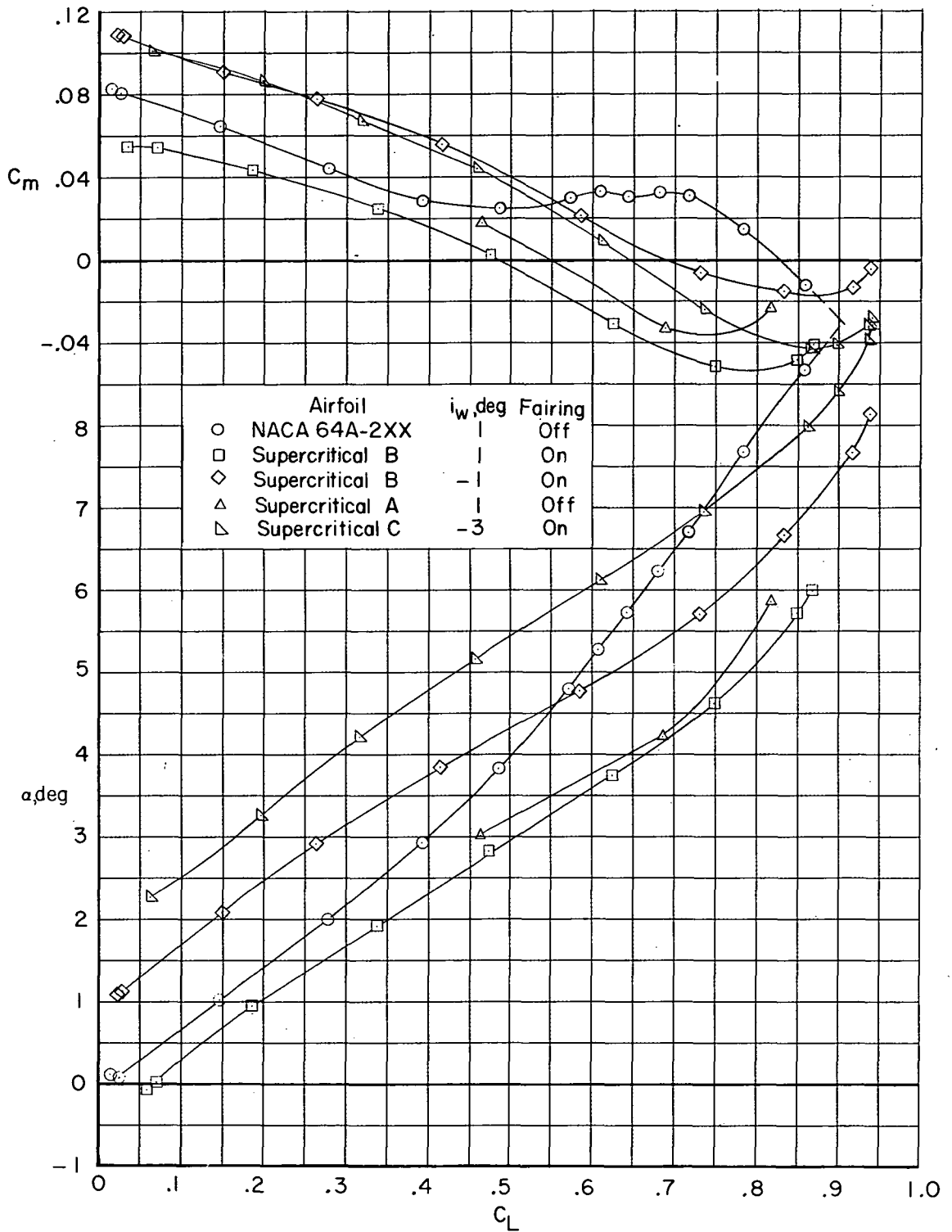
(a) $M = 0.80$.

Figure 7. - Comparison of longitudinal aerodynamic characteristics for configuration with NACA 64A2XX and supercritical airfoils with transition rearward except as noted. $\Lambda = 33^\circ$; $\delta_h = 0^\circ$.



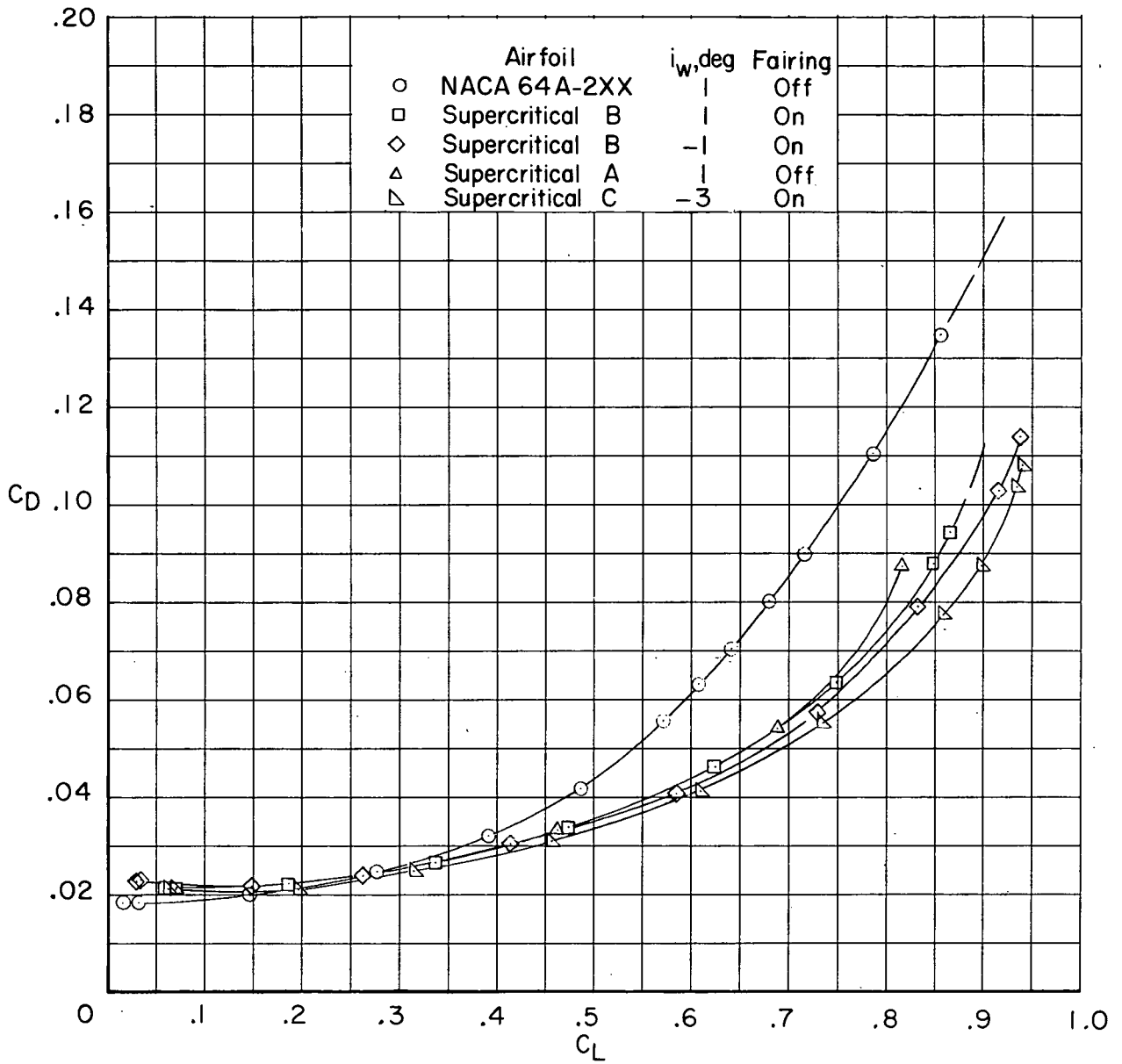
(a) $M = 0.80$. Concluded.

Figure 7.- Continued.



(b) $M = 0.85$.

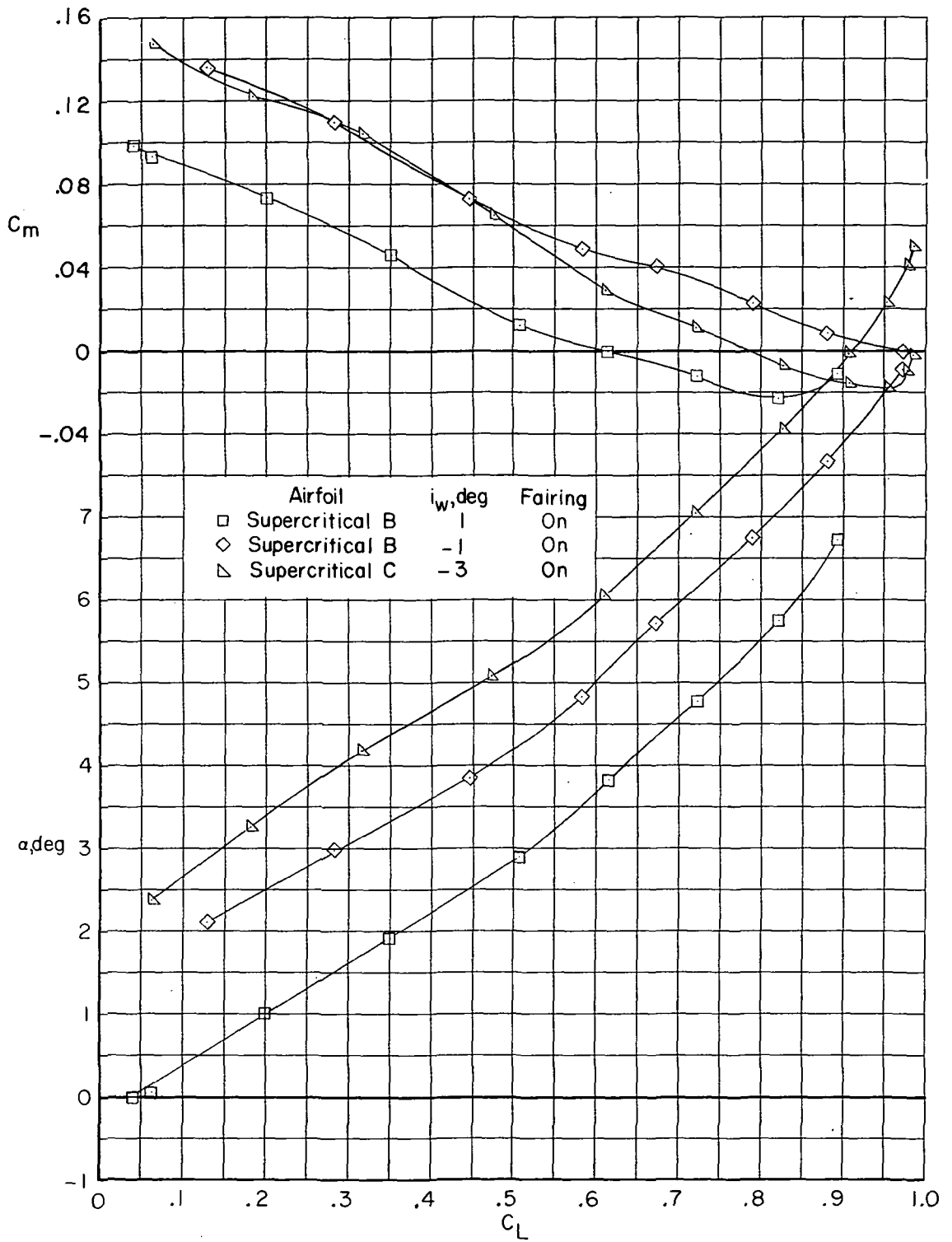
Figure 7. - Continued.



(b) $M = 0.85$. Concluded.

Figure 7.- Continued.

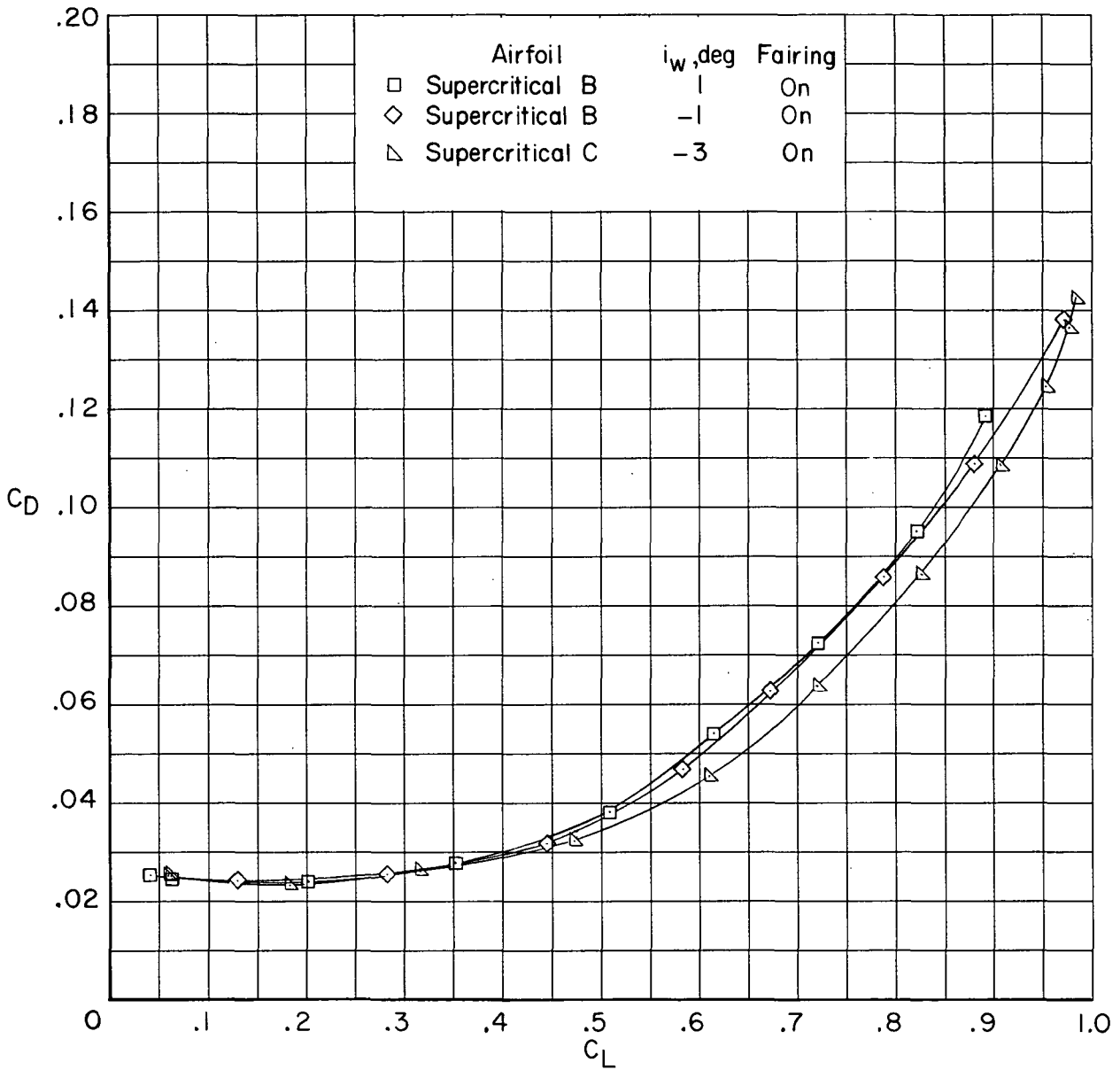
~~CONFIDENTIAL~~



(c) $M = 0.88$.

Figure 7.- Continued.

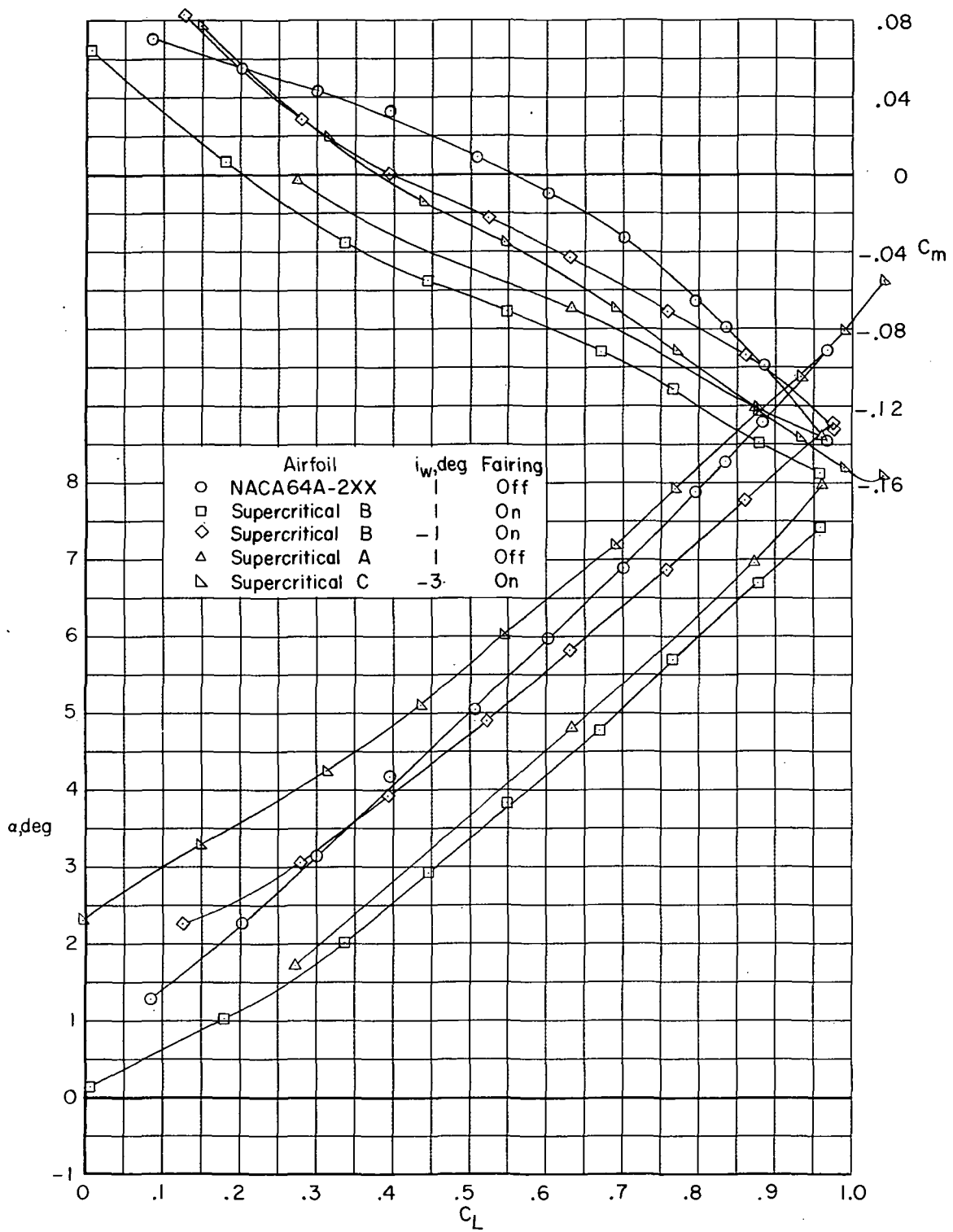
~~CONFIDENTIAL~~



(c) $M = 0.88$. Concluded.

Figure 7.- Continued.

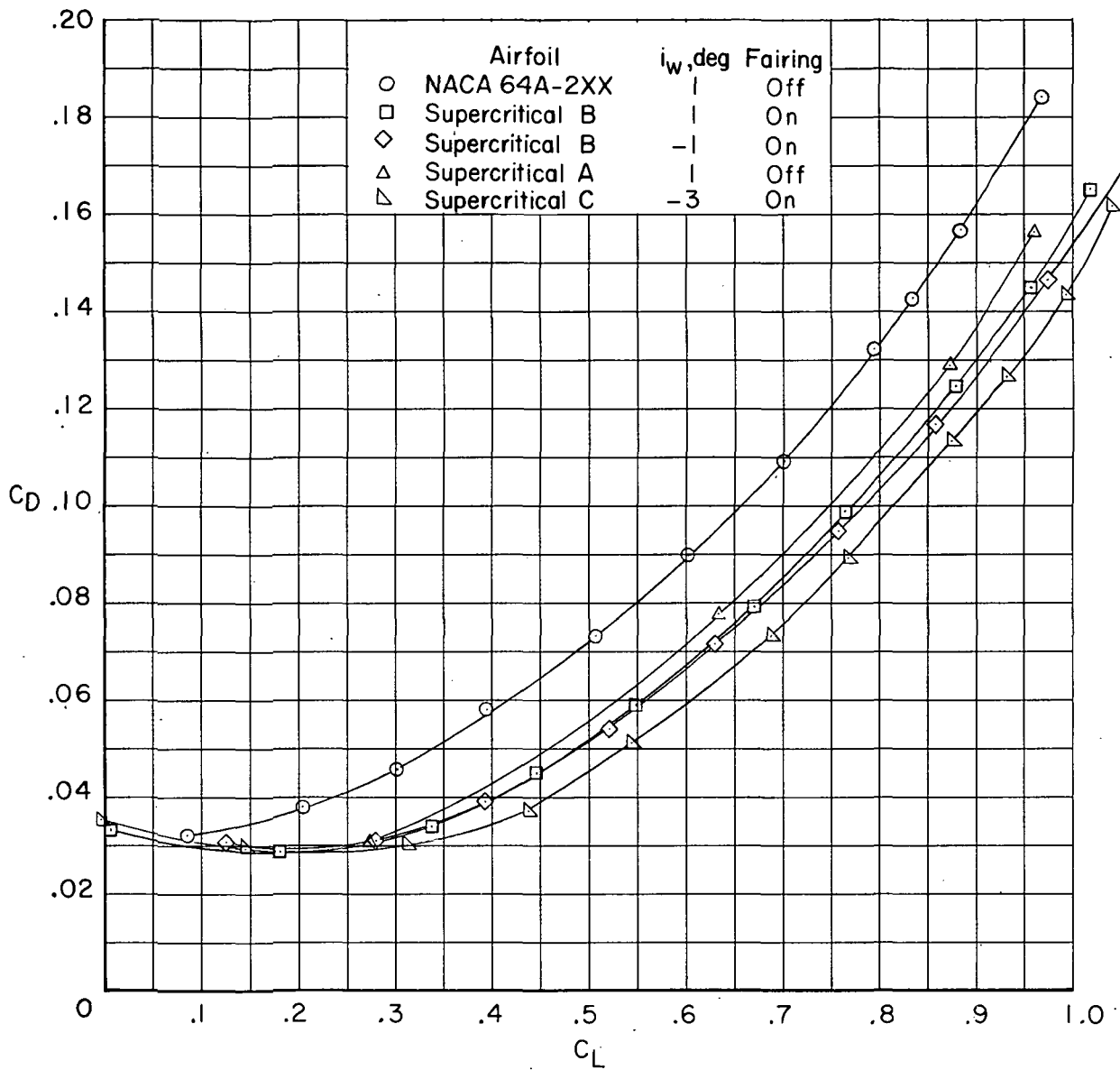
~~CONFIDENTIAL~~



(d) $M = 0.91$.

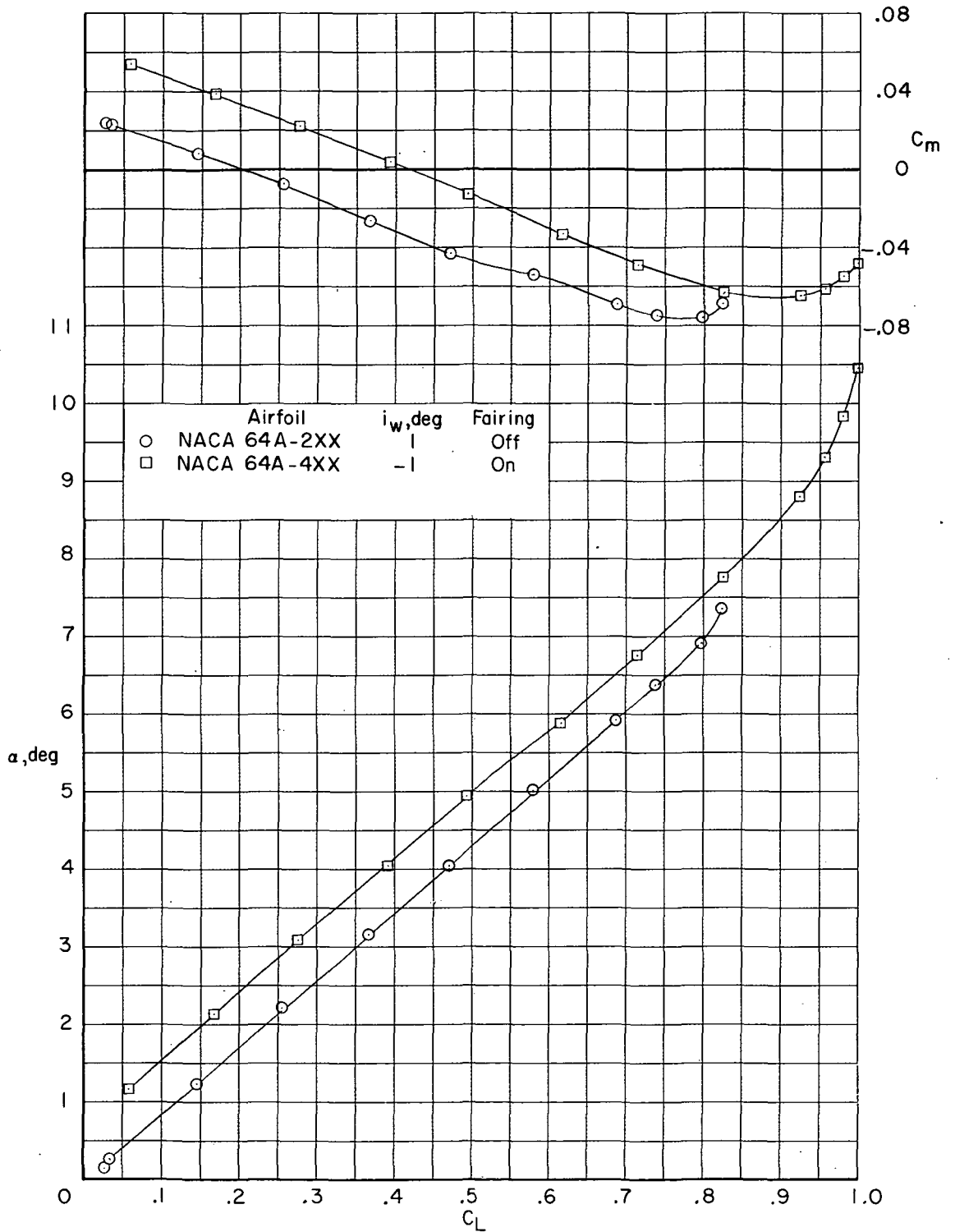
Figure 7. - Continued.

~~CONFIDENTIAL~~



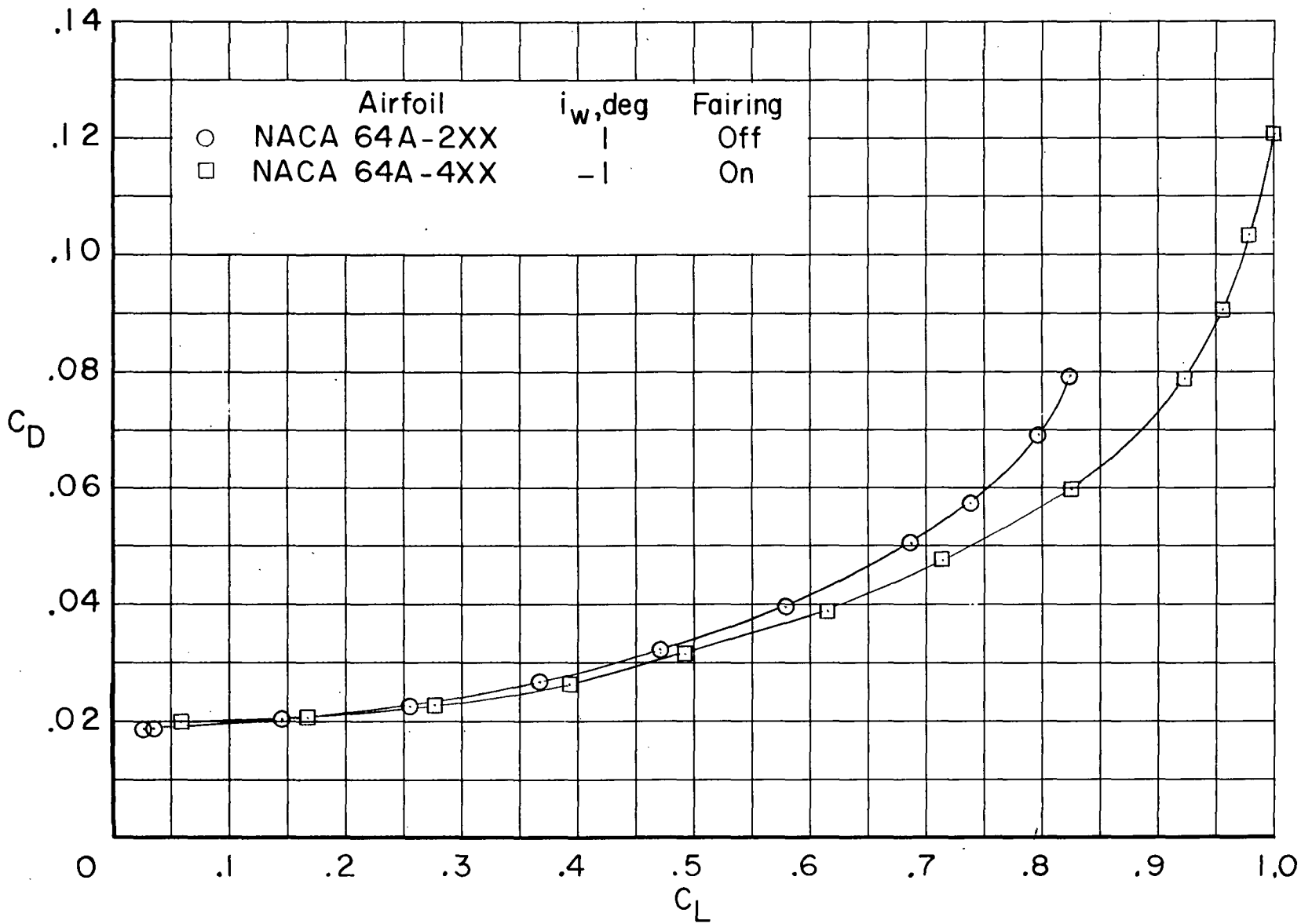
(d) $M = 0.91$. Concluded.

Figure 7.- Concluded.



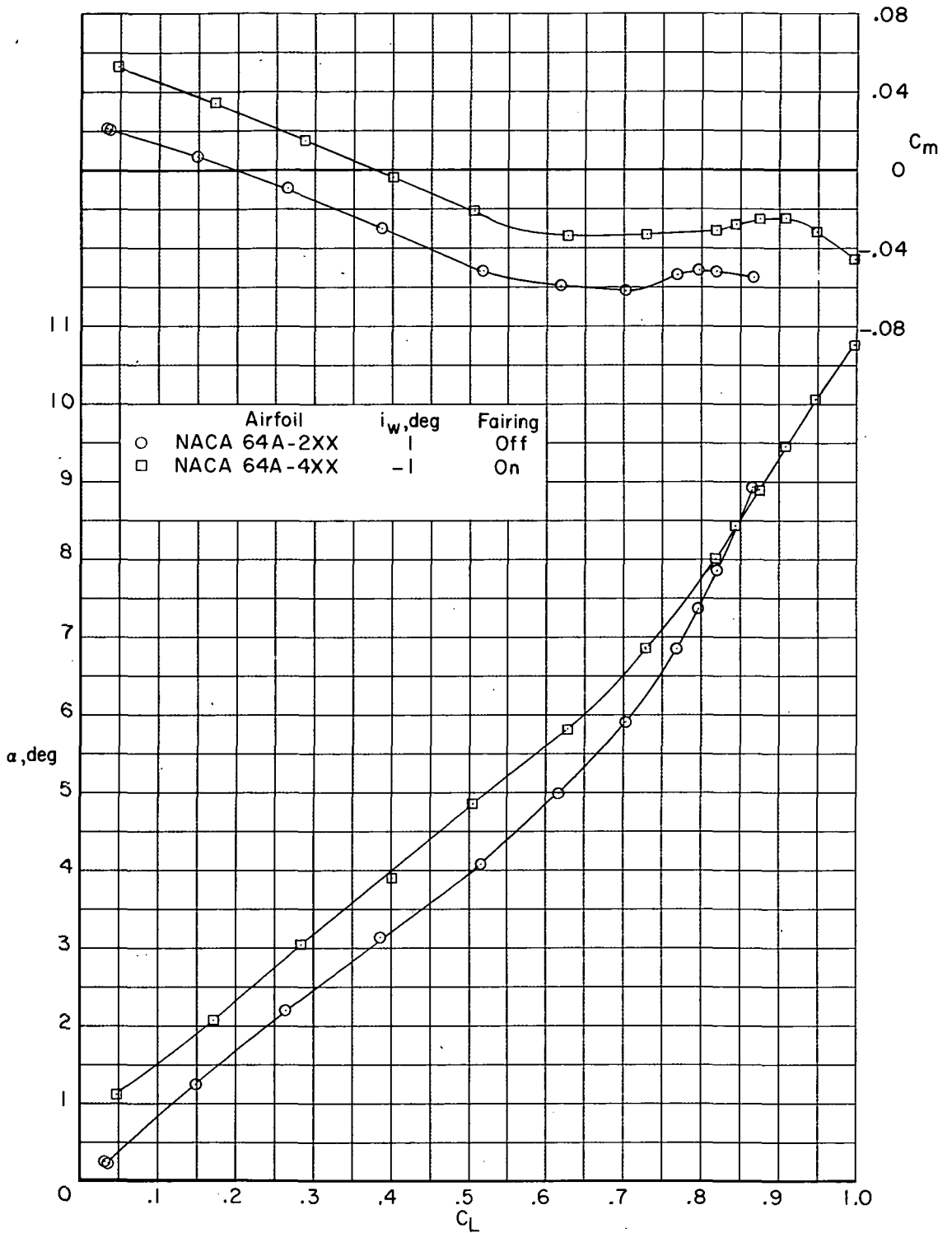
(a) $M = 0.75$.

Figure 8.- Comparison of longitudinal aerodynamic characteristics for configuration with NACA 64A2XX and NACA 64A4XX airfoils and transition rearward. $\Lambda = 33^\circ$; $\delta_h = 0^\circ$.



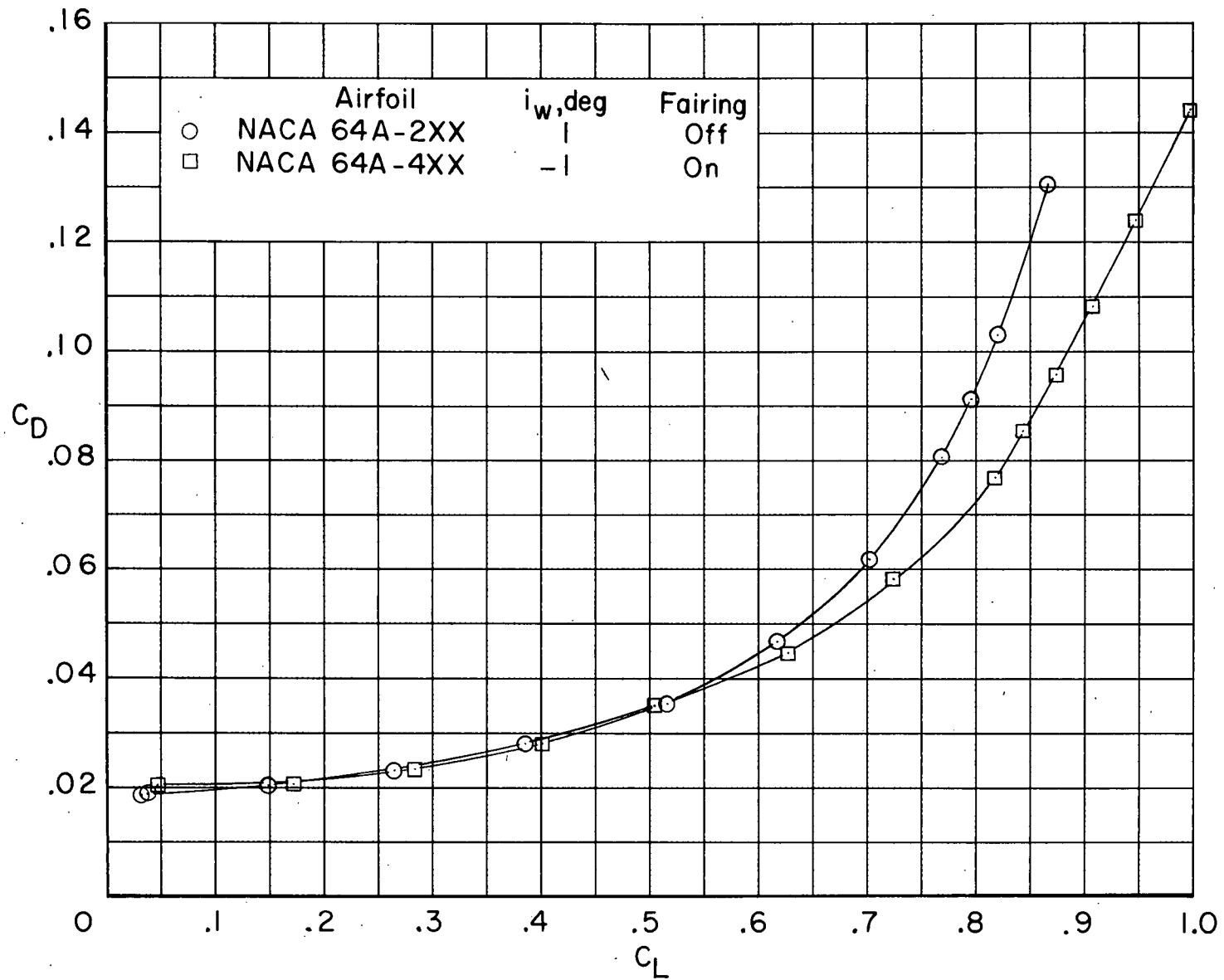
(a) $M = 0.75$. Concluded.

Figure 8.- Continued.



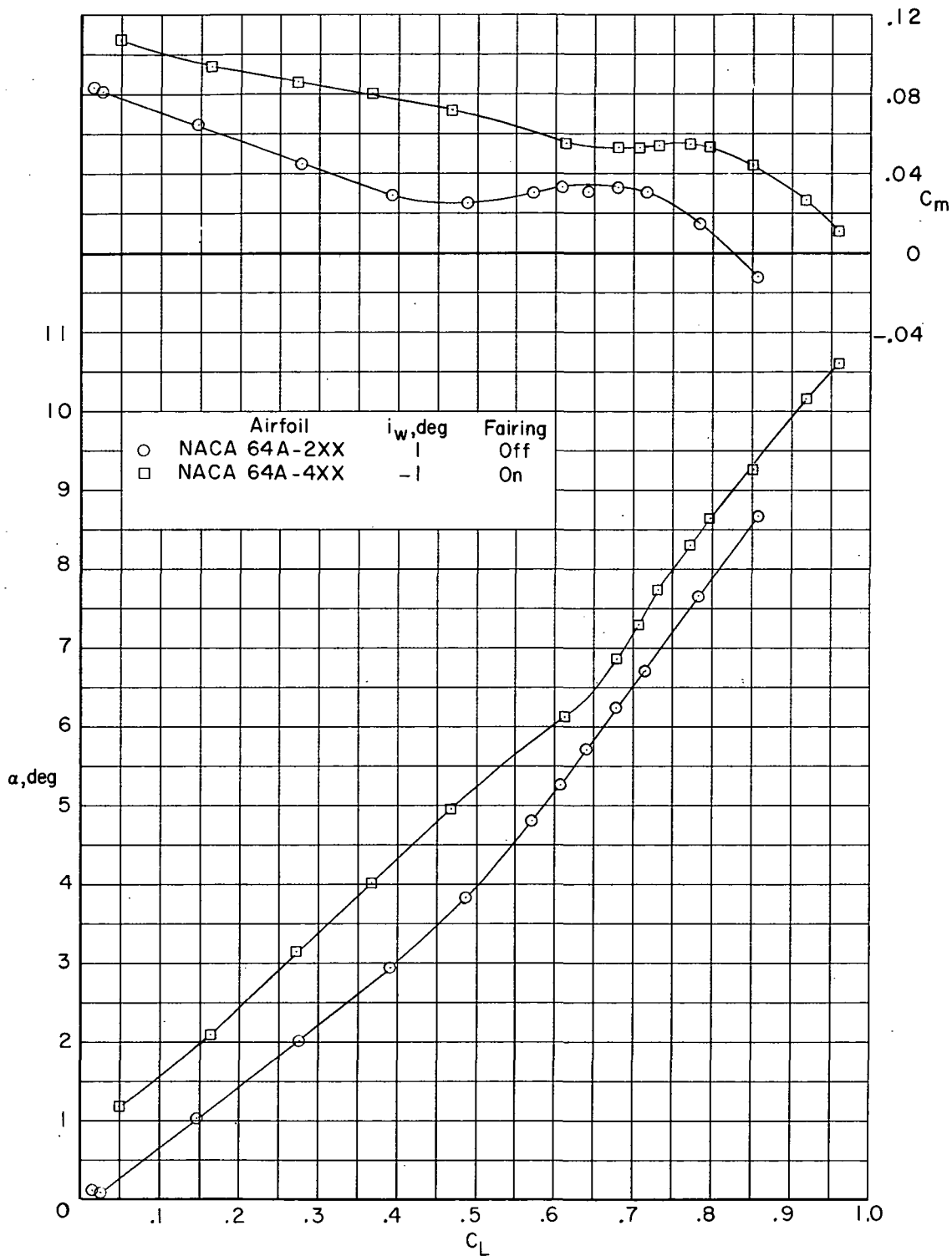
(b) $M = 0.80$.

Figure 8. - Continued.



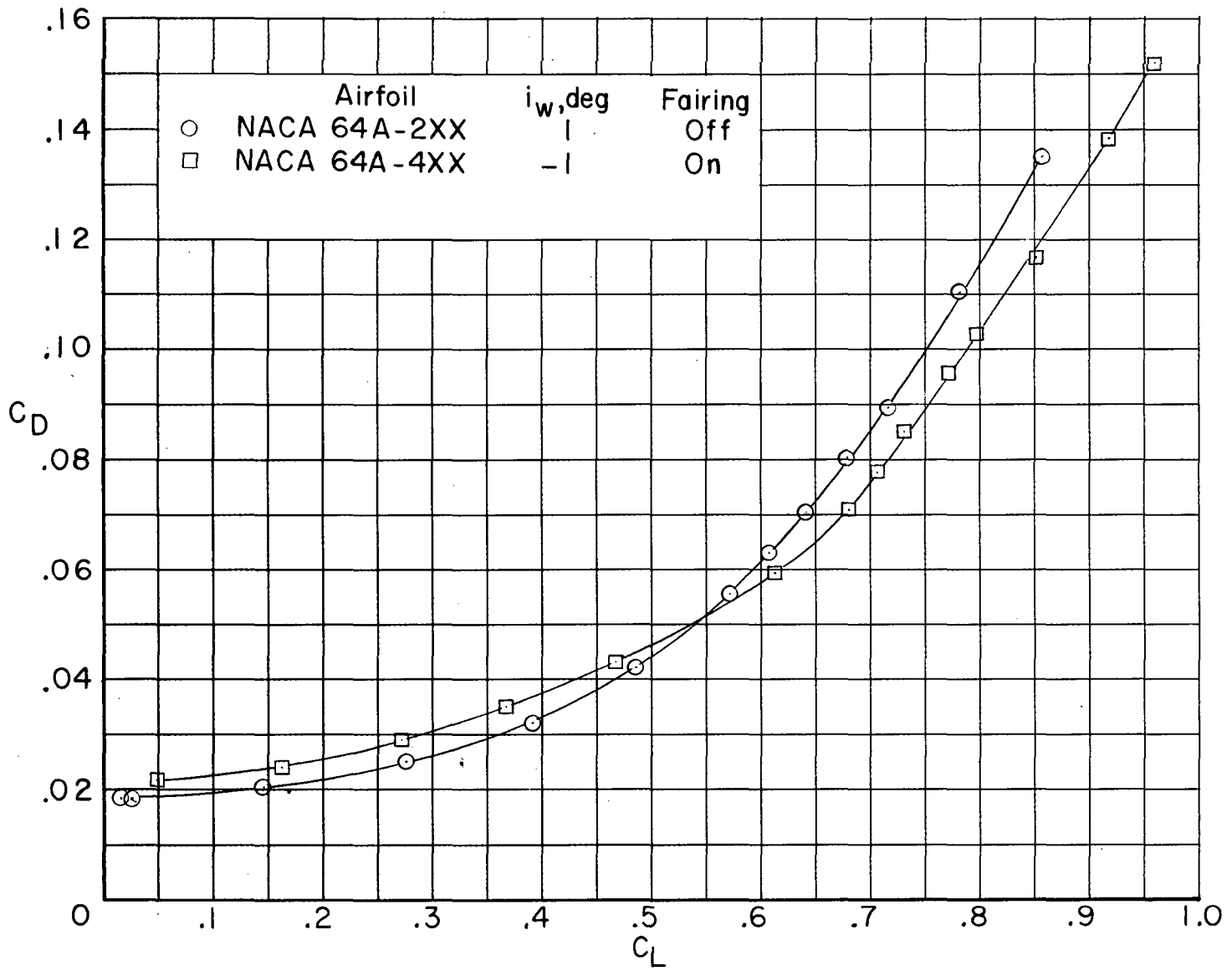
(b) $M = 0.80$. Concluded.

Figure 8. - Continued.



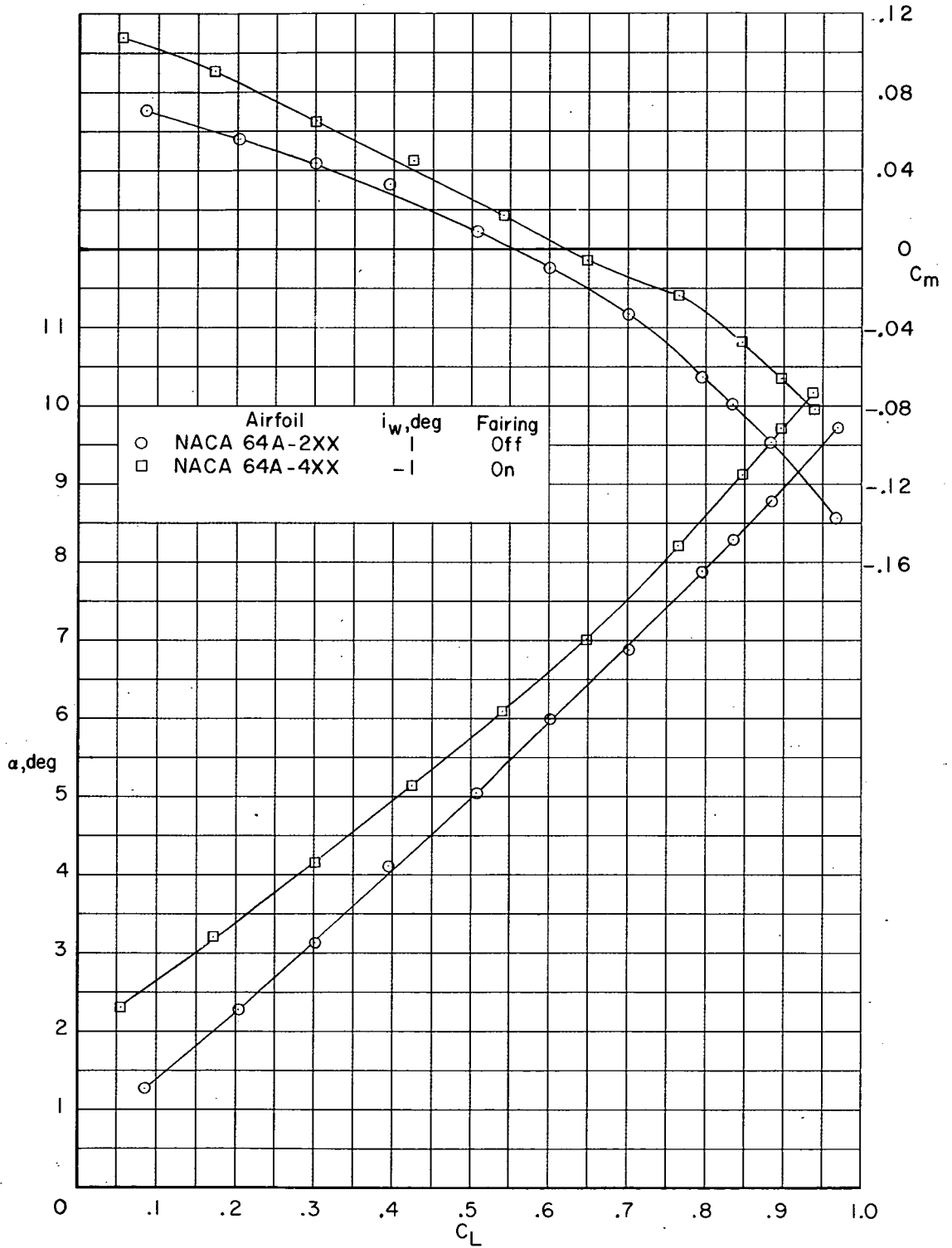
(c) $M = 0.85$.

Figure 8. - Continued.



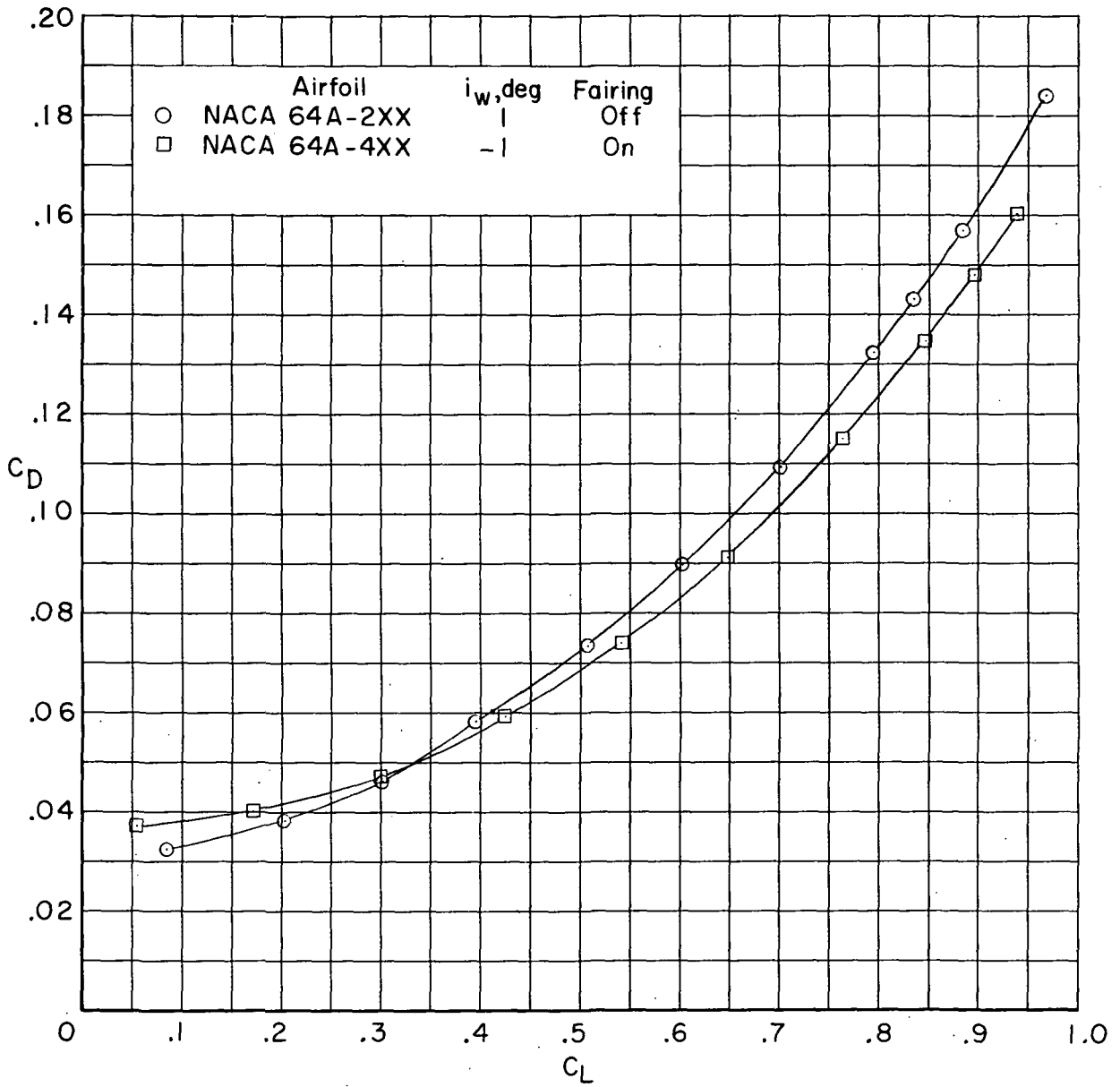
(c) $M = 0.85$. Concluded.

Figure 8.- Continued.



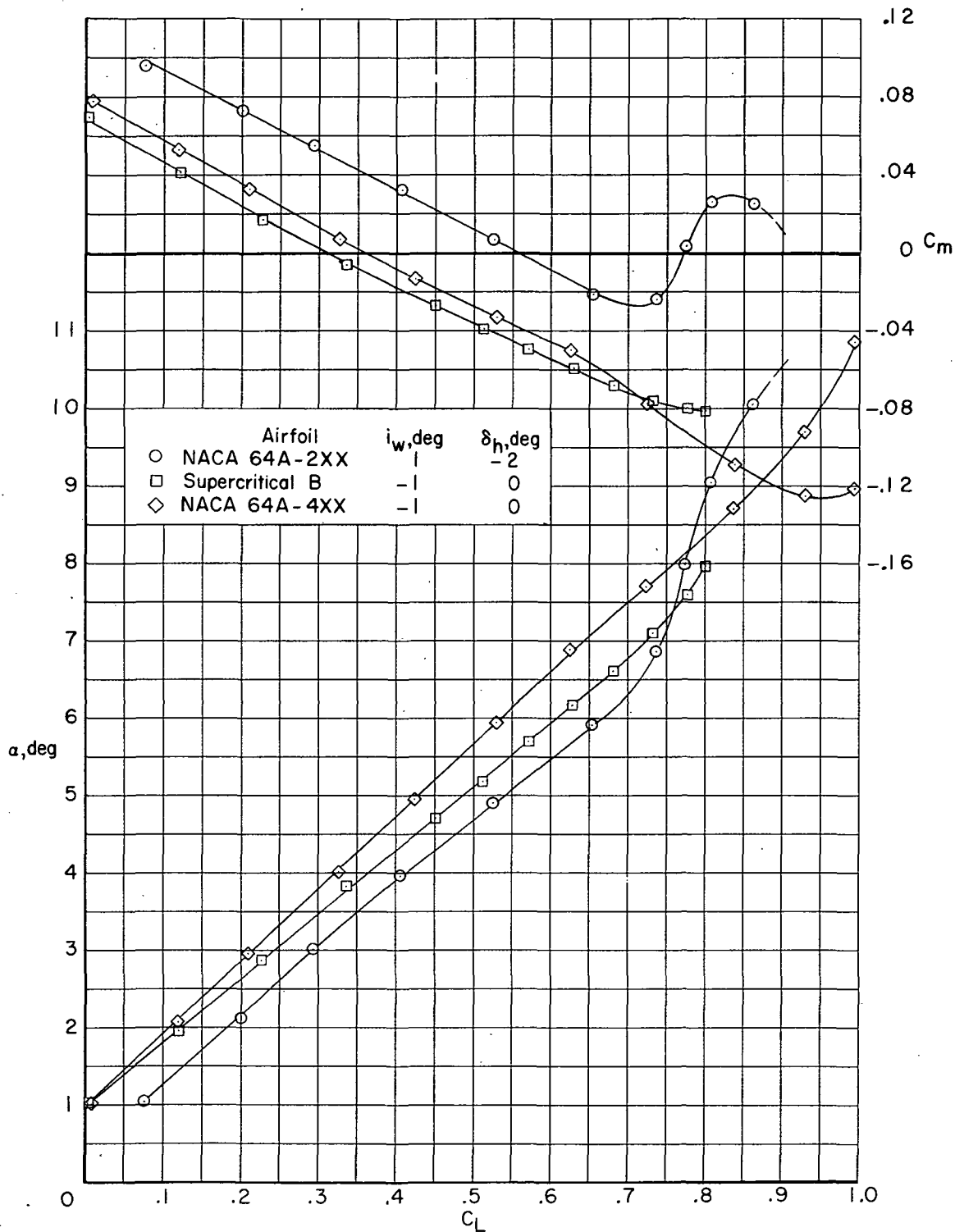
(d) $M = 0.91$.

Figure 8. - Continued.



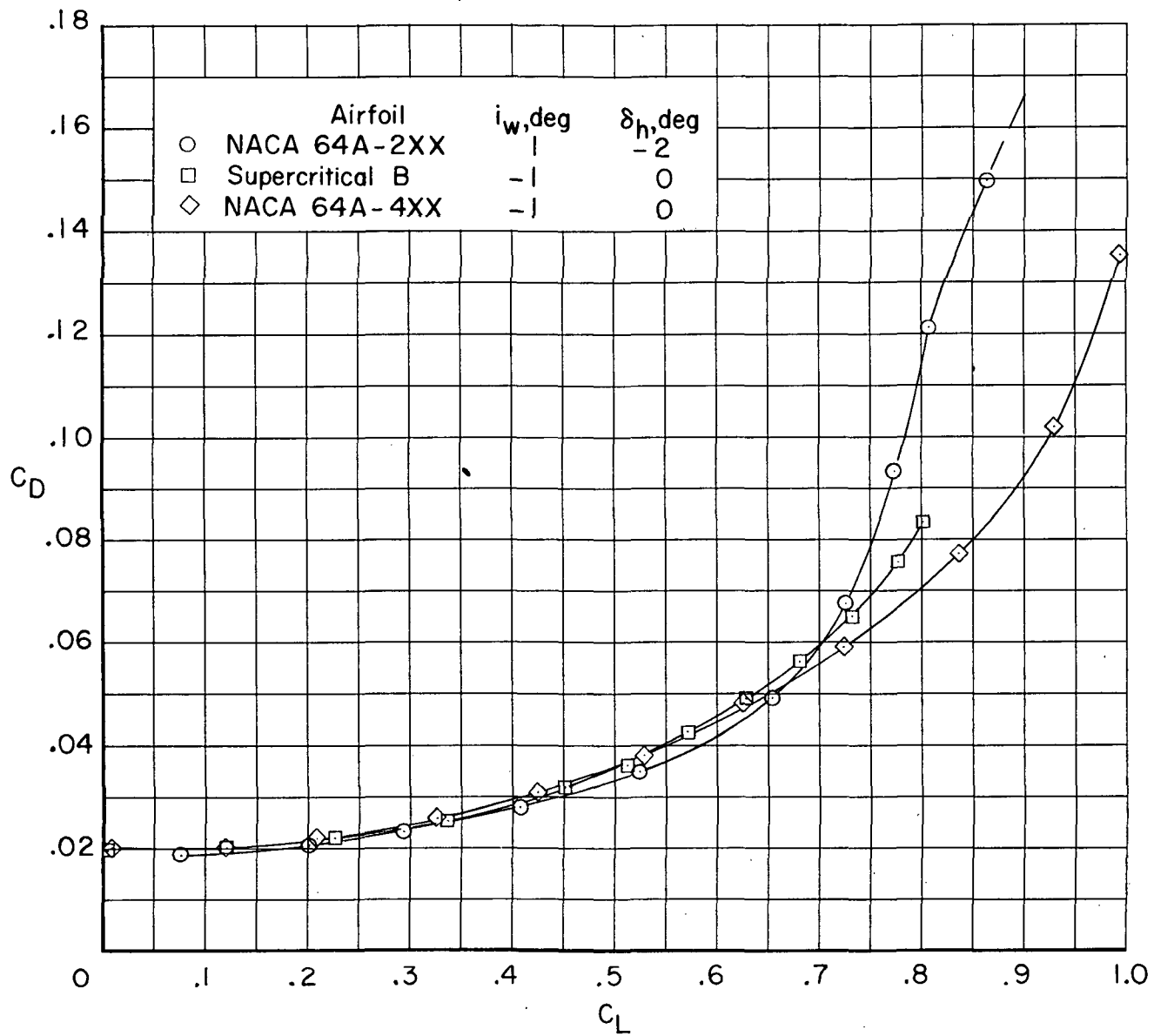
(d) $M = 0.91$. Concluded.

Figure 8. - Concluded.



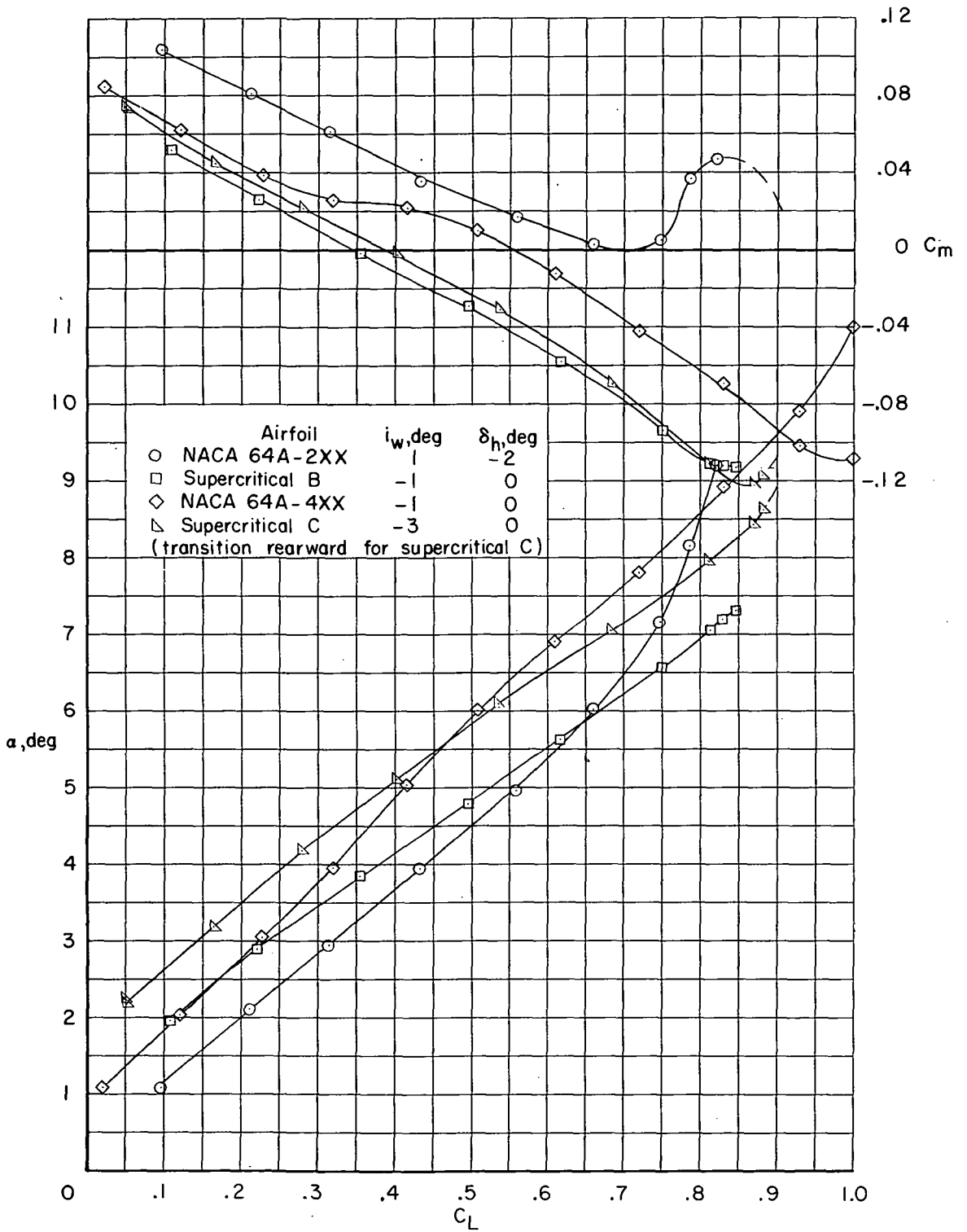
(a) $M = 0.80$.

Figure 9. - Comparison of longitudinal aerodynamic characteristics for configuration with NACA 64A2XX, NACA 64A4XX, and supercritical airfoils and fuselage fairing on upper surface transition forward except as noted. $\Lambda = 39^\circ$.



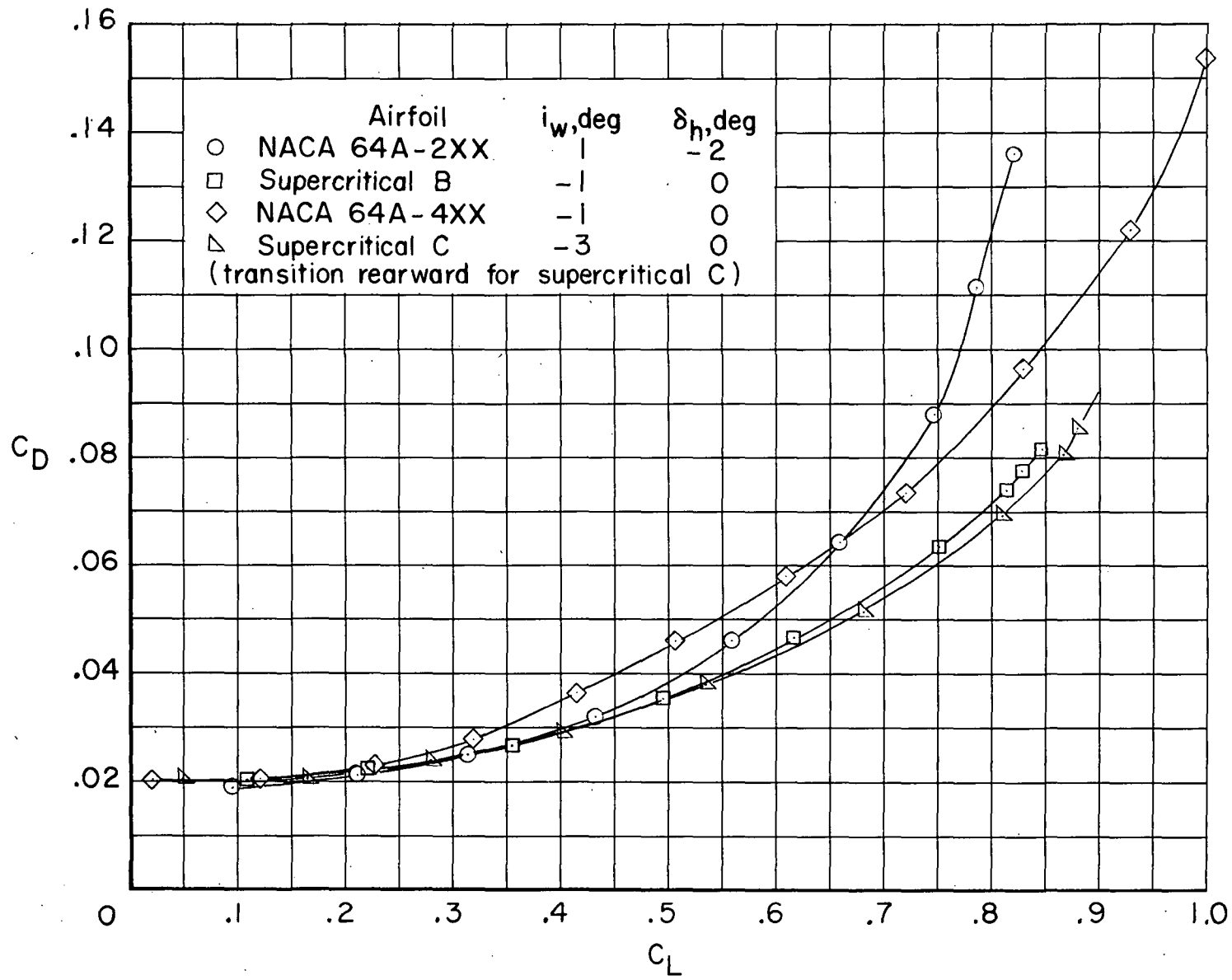
(a) $M = 0.80$. Concluded.

Figure 9. - Continued.



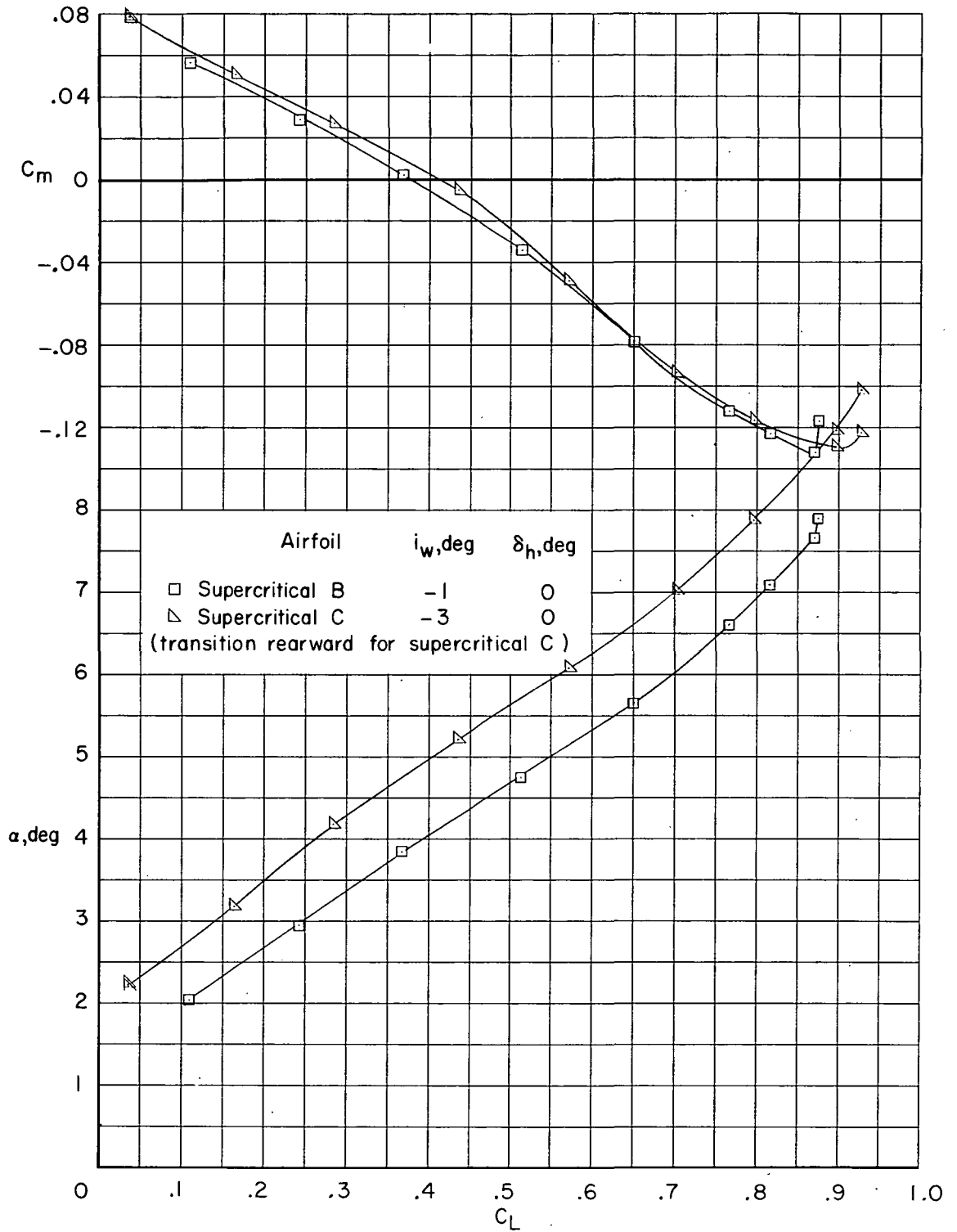
(b) $M = 0.85$.

Figure 9. - Continued.



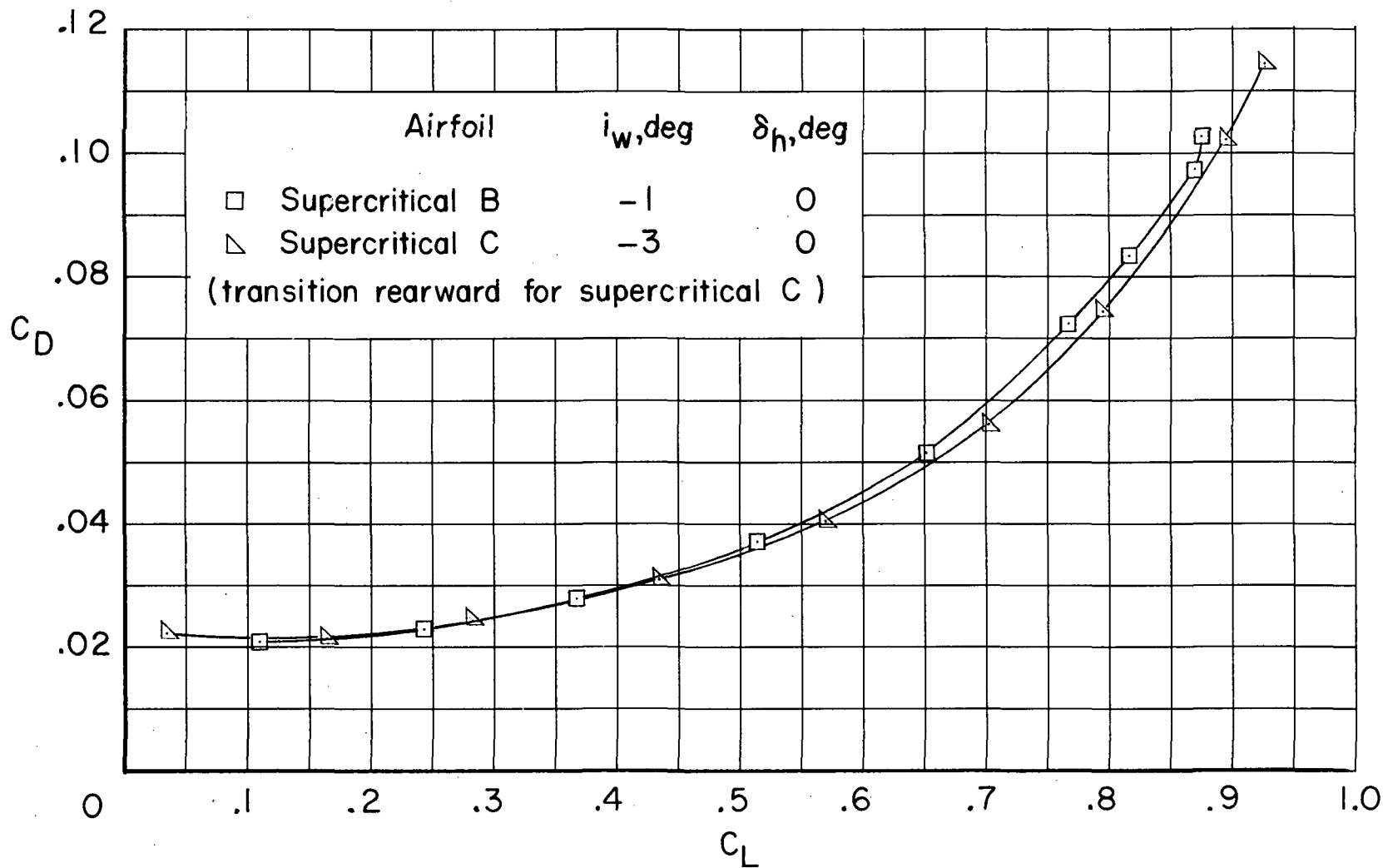
(b) $M = 0.85$. Concluded.

Figure 9.- Continued.



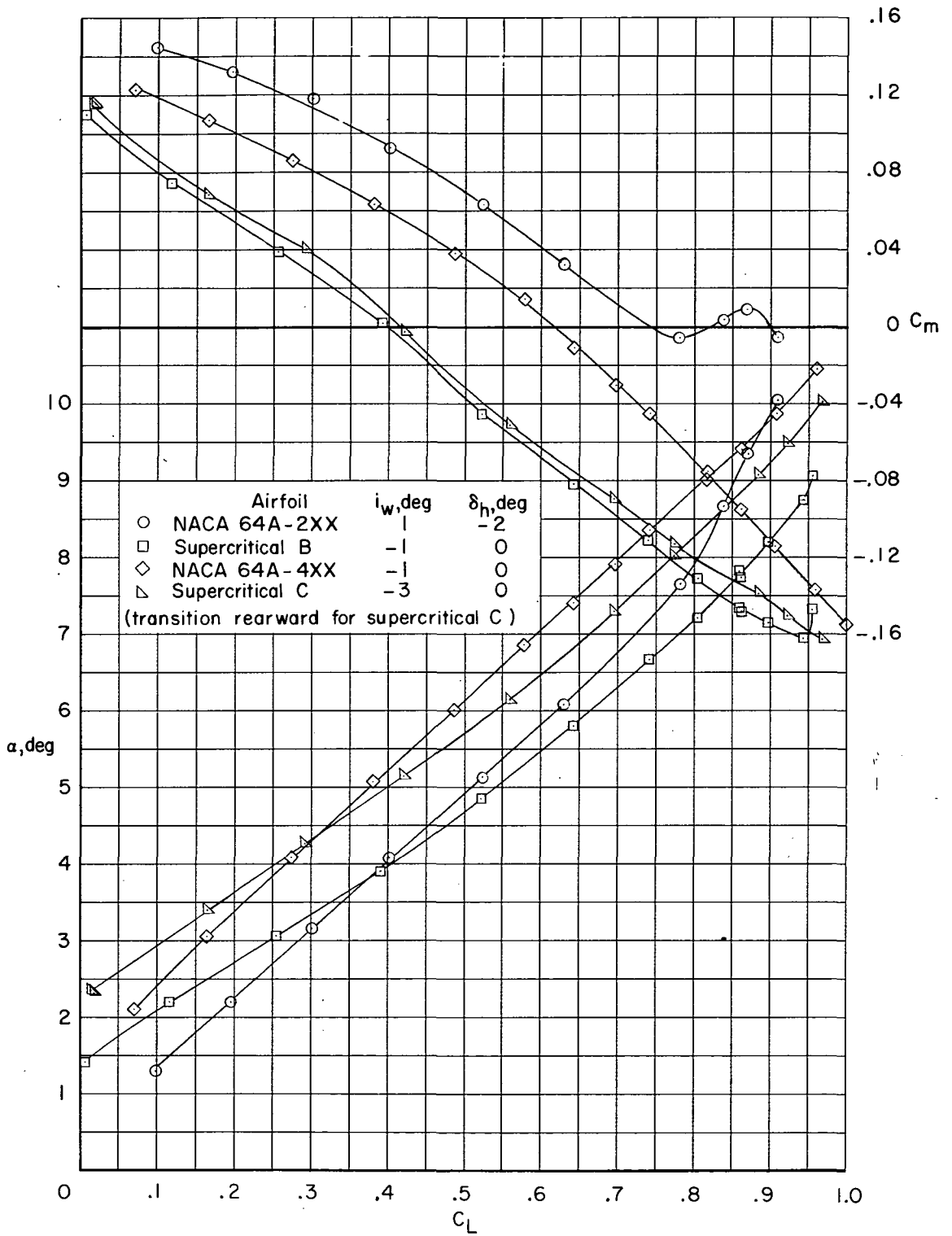
(c) $M = 0.88$.

Figure 9. - Continued.



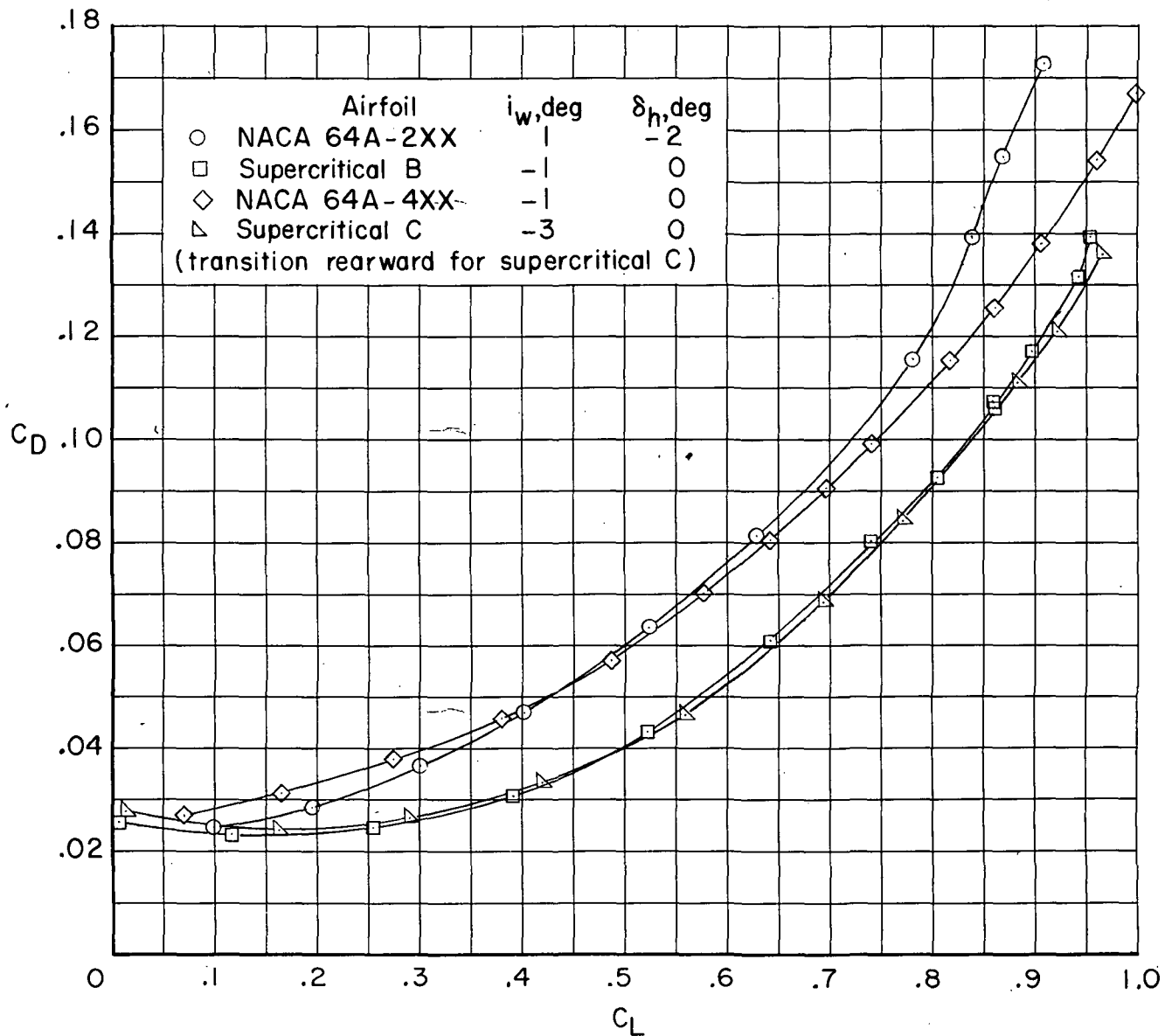
(c) $M = 0.88$. Concluded.

Figure 9.- Continued.



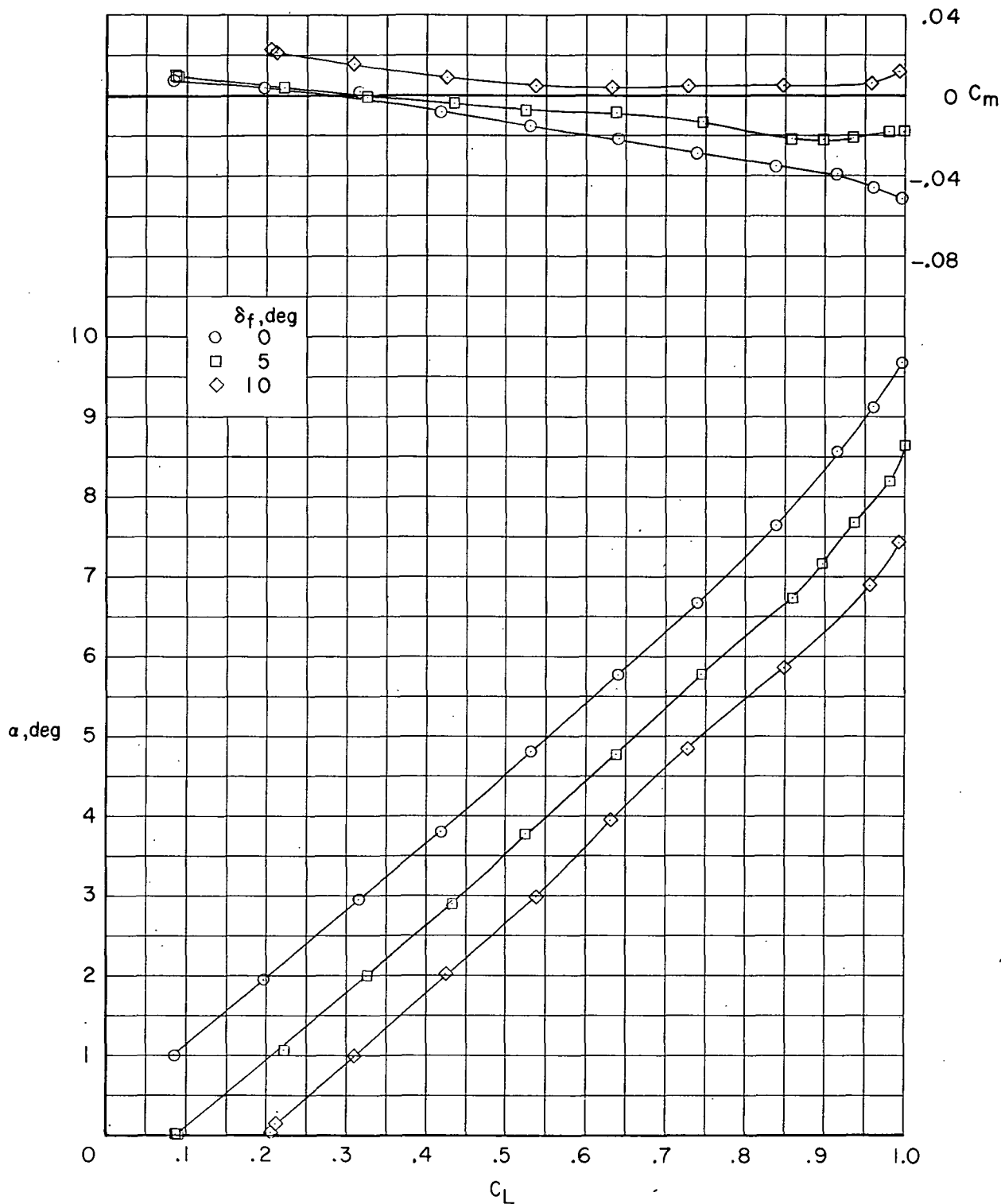
(d) $M = 0.91$.

Figure 9. - Continued.



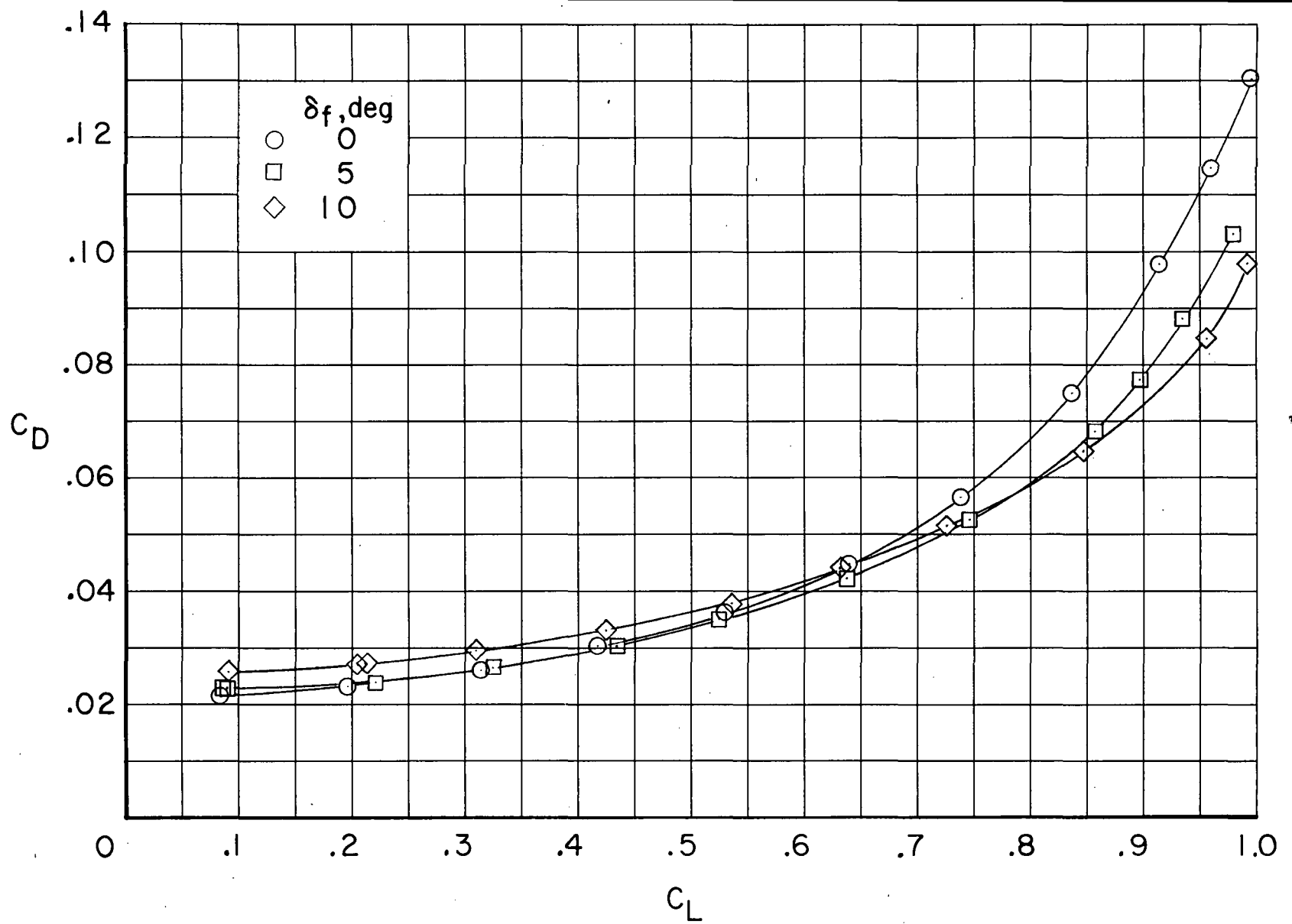
(d) $M = 0.91$. Concluded.

Figure 9.- Concluded.



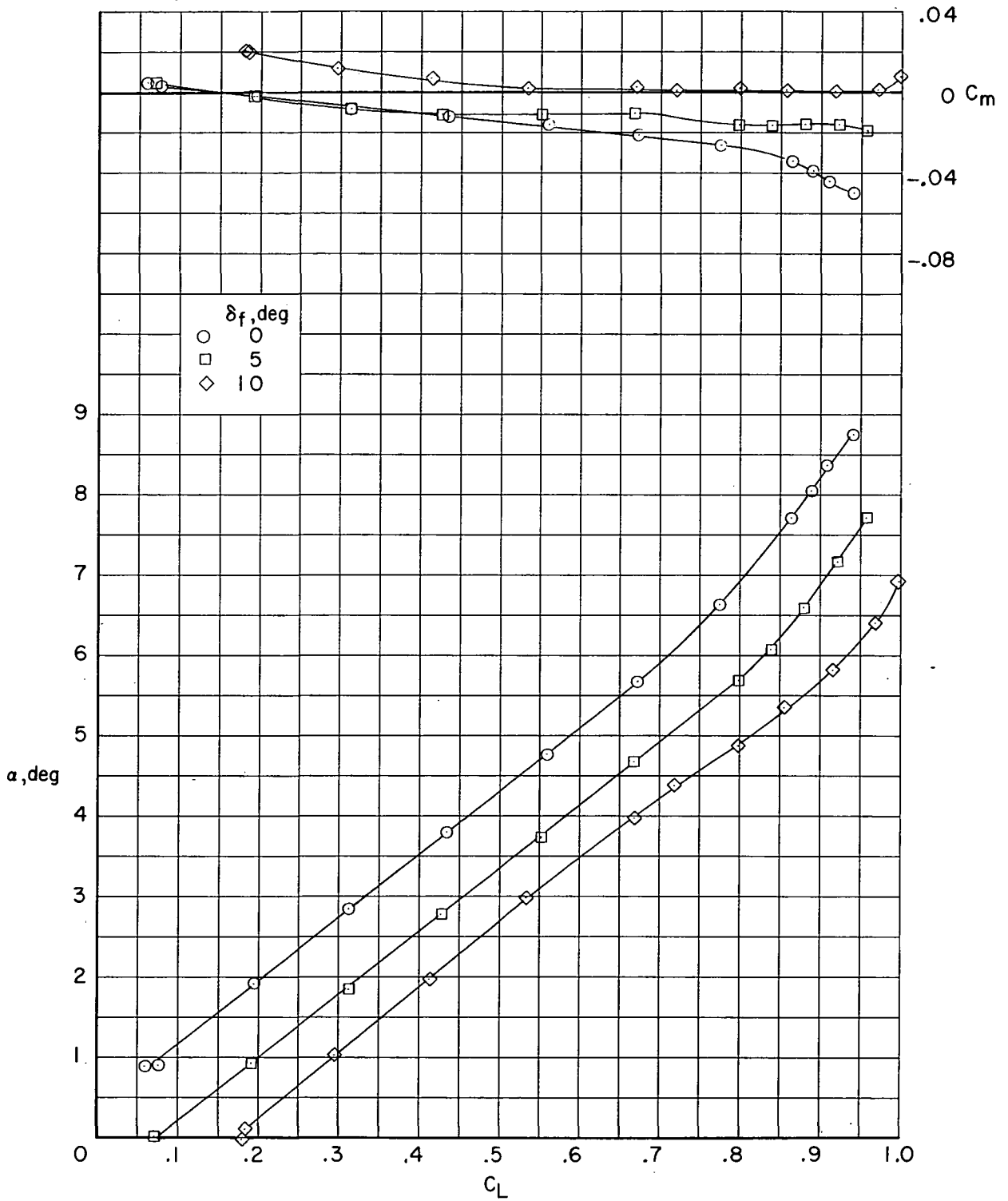
(a) $M = 0.60$. Upper surface transition forward.

Figure 10.- Effect of trailing-edge flaps on longitudinal aerodynamic characteristics of configuration with supercritical airfoil B and fuselage fairing. $\Lambda = 26^\circ$; $\delta_h = 2^\circ$; $i_w = -1^\circ$.



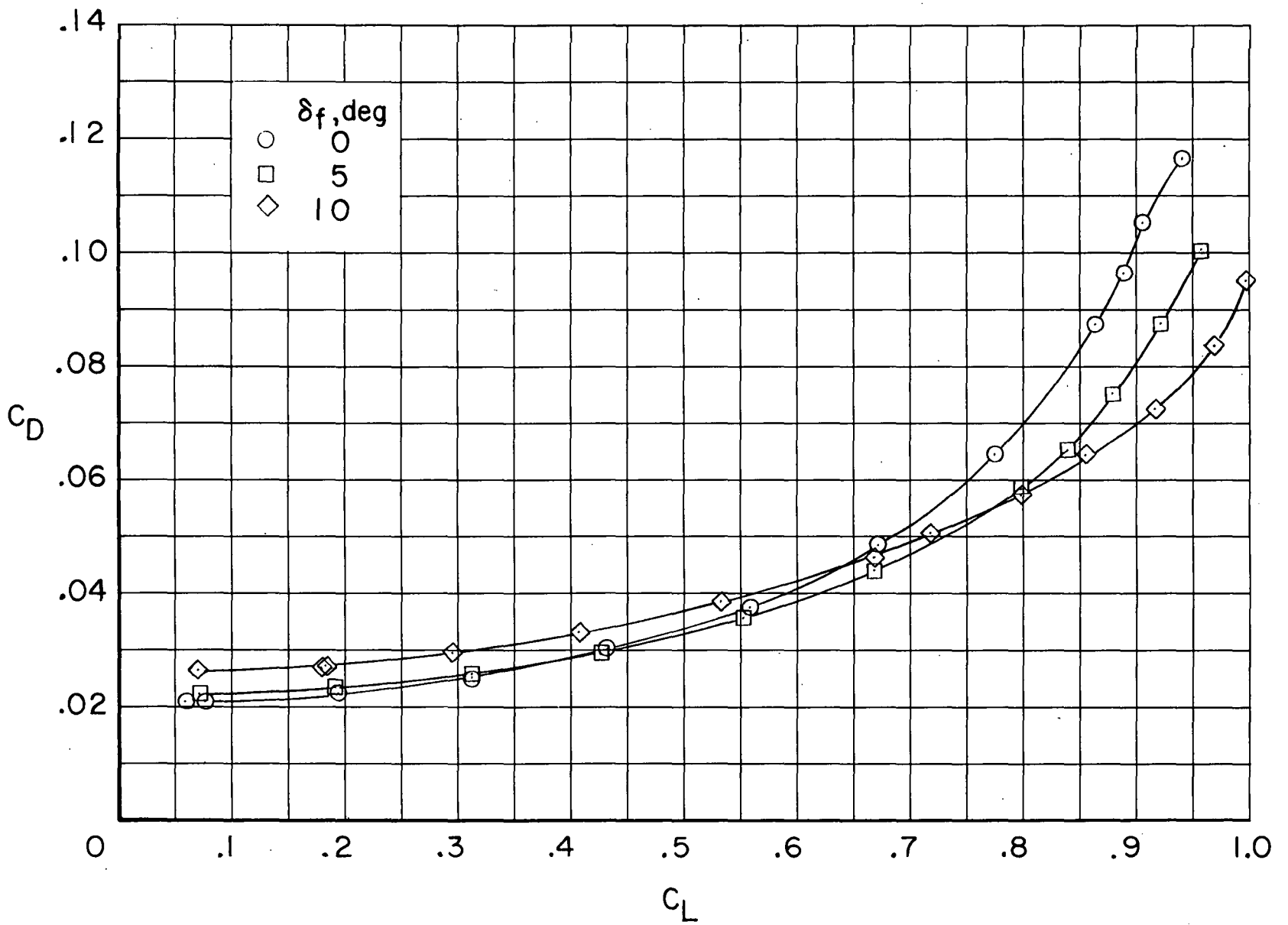
(a) $M = 0.60$. Upper surface transition forward. Concluded.

Figure 10.- Continued.



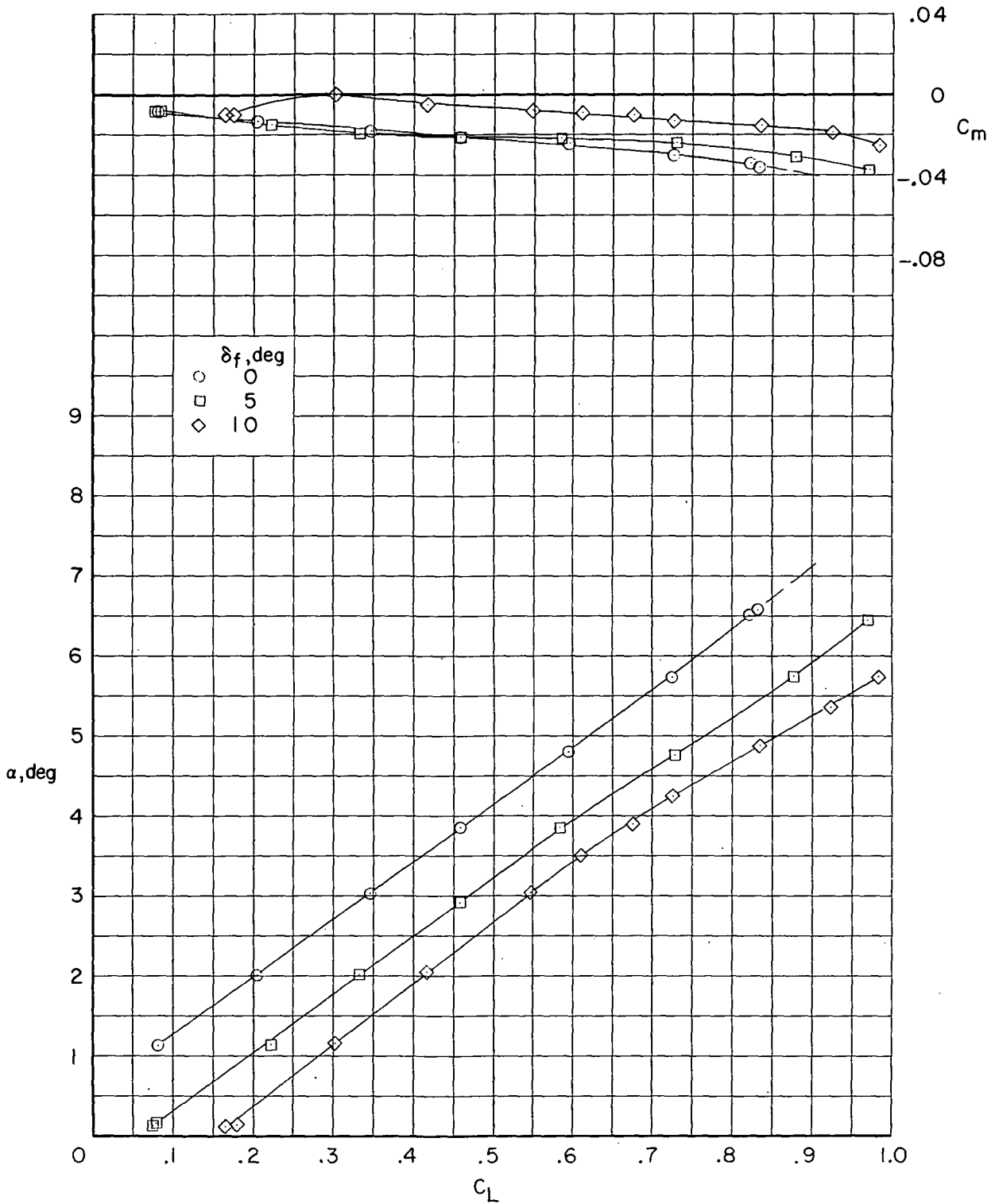
(b) $M = 0.70$. Upper surface transition forward.

Figure 10.- Continued.



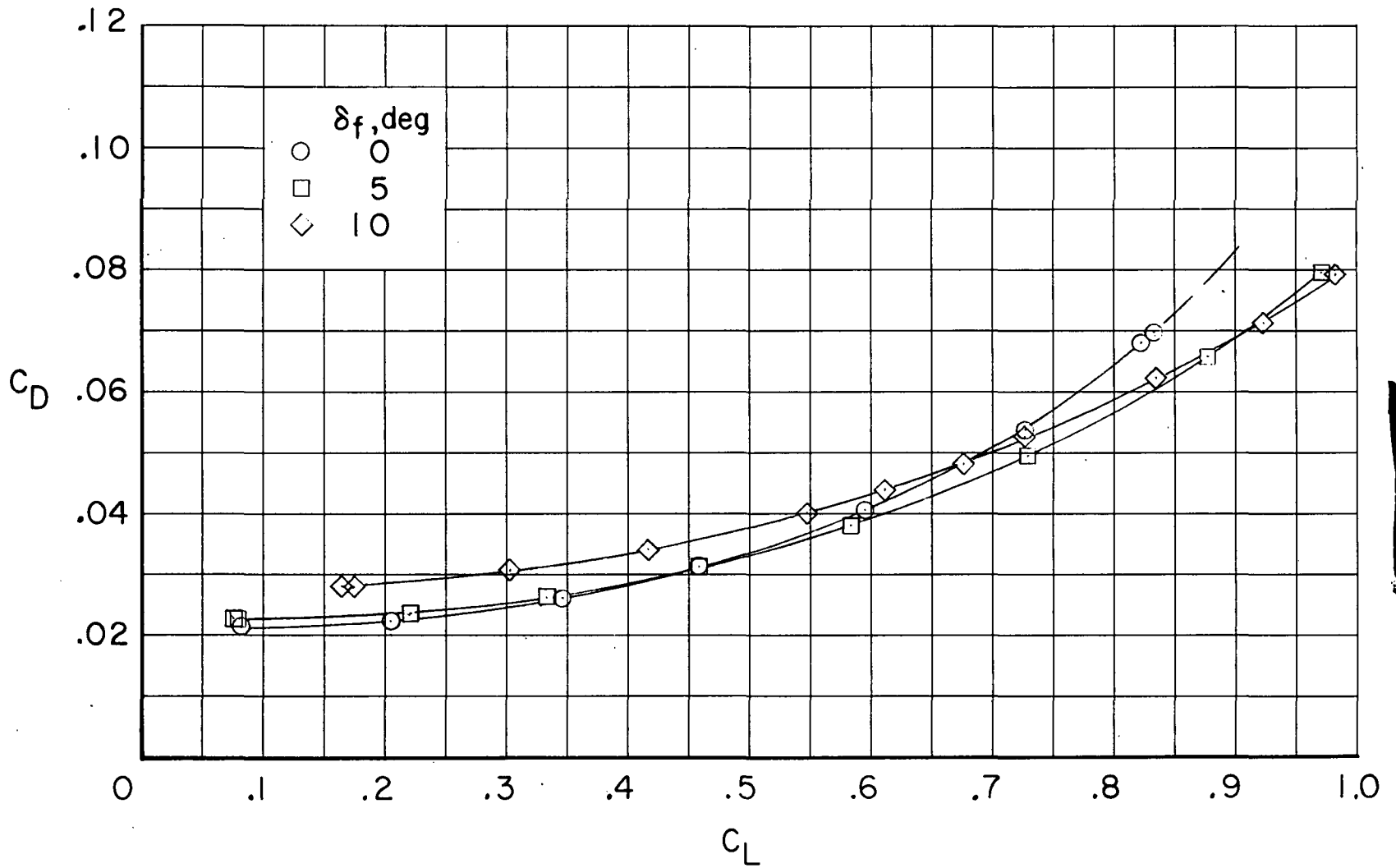
(b) $M = 0.70$. Upper surface transition forward. Concluded.

Figure 10.- Continued.



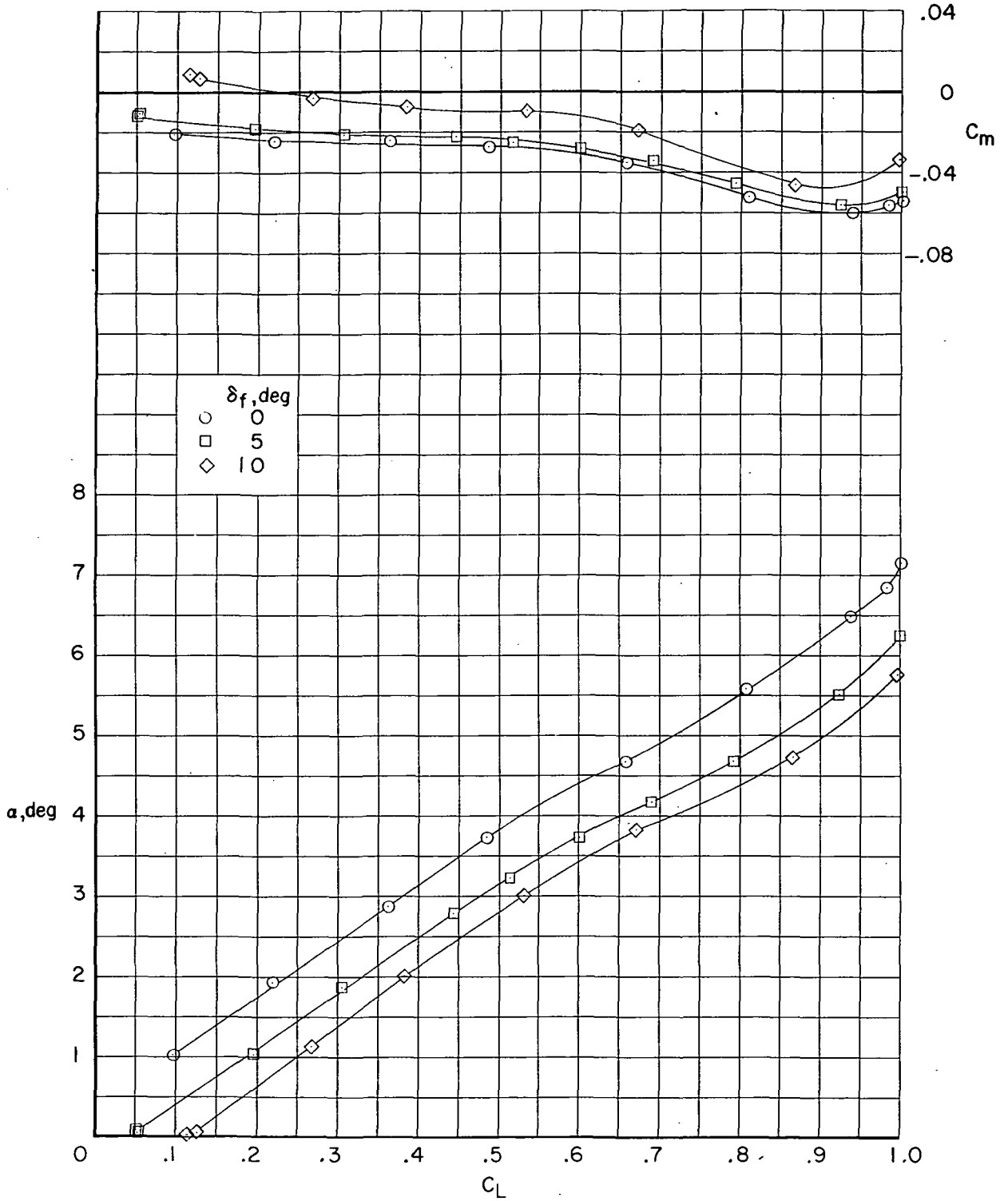
(c) $M = 0.75$. Upper surface transition forward.

Figure 10.- Continued.



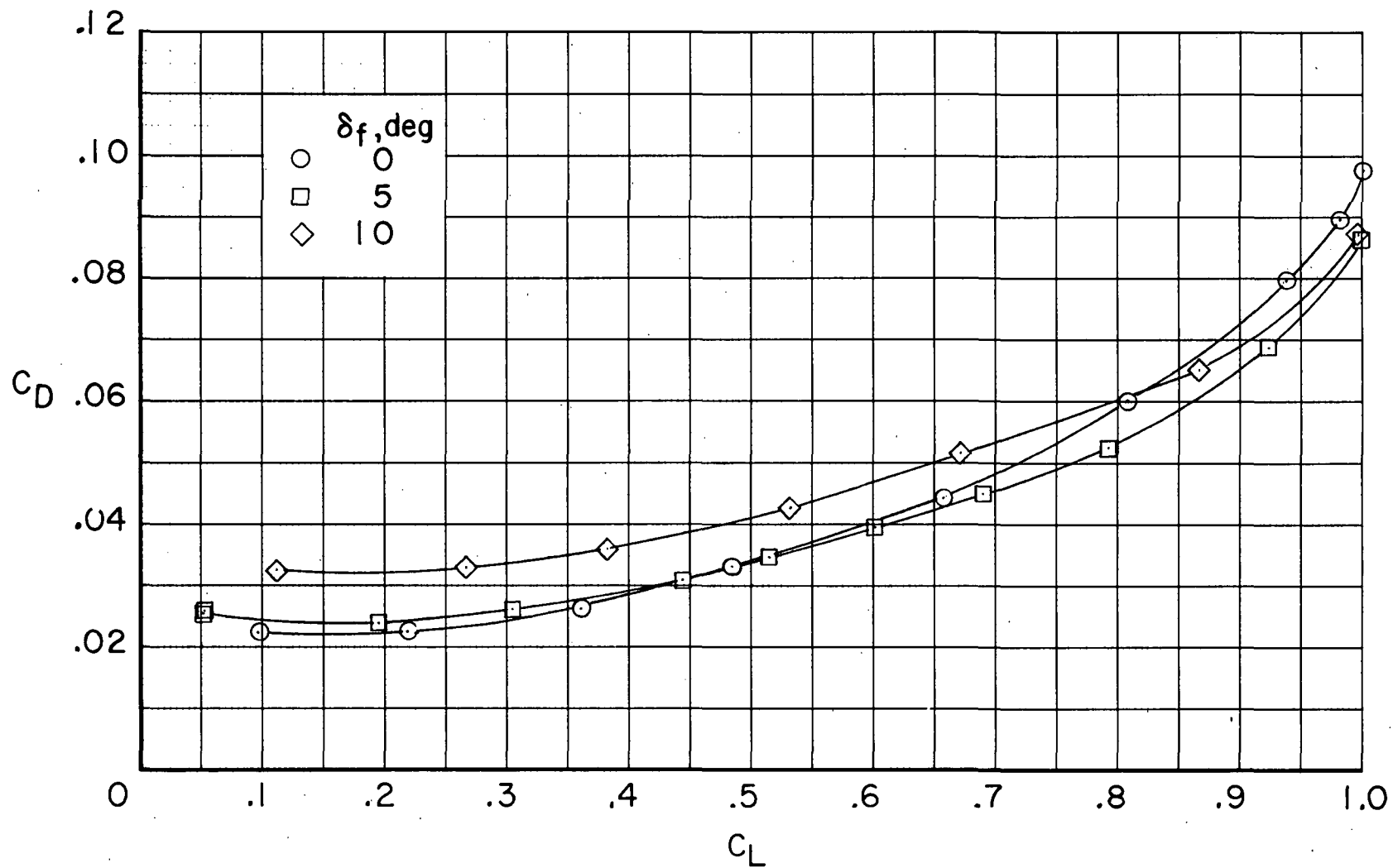
(c) $M = 0.75$. Upper surface transition forward. Concluded.

Figure 10. - Continued.



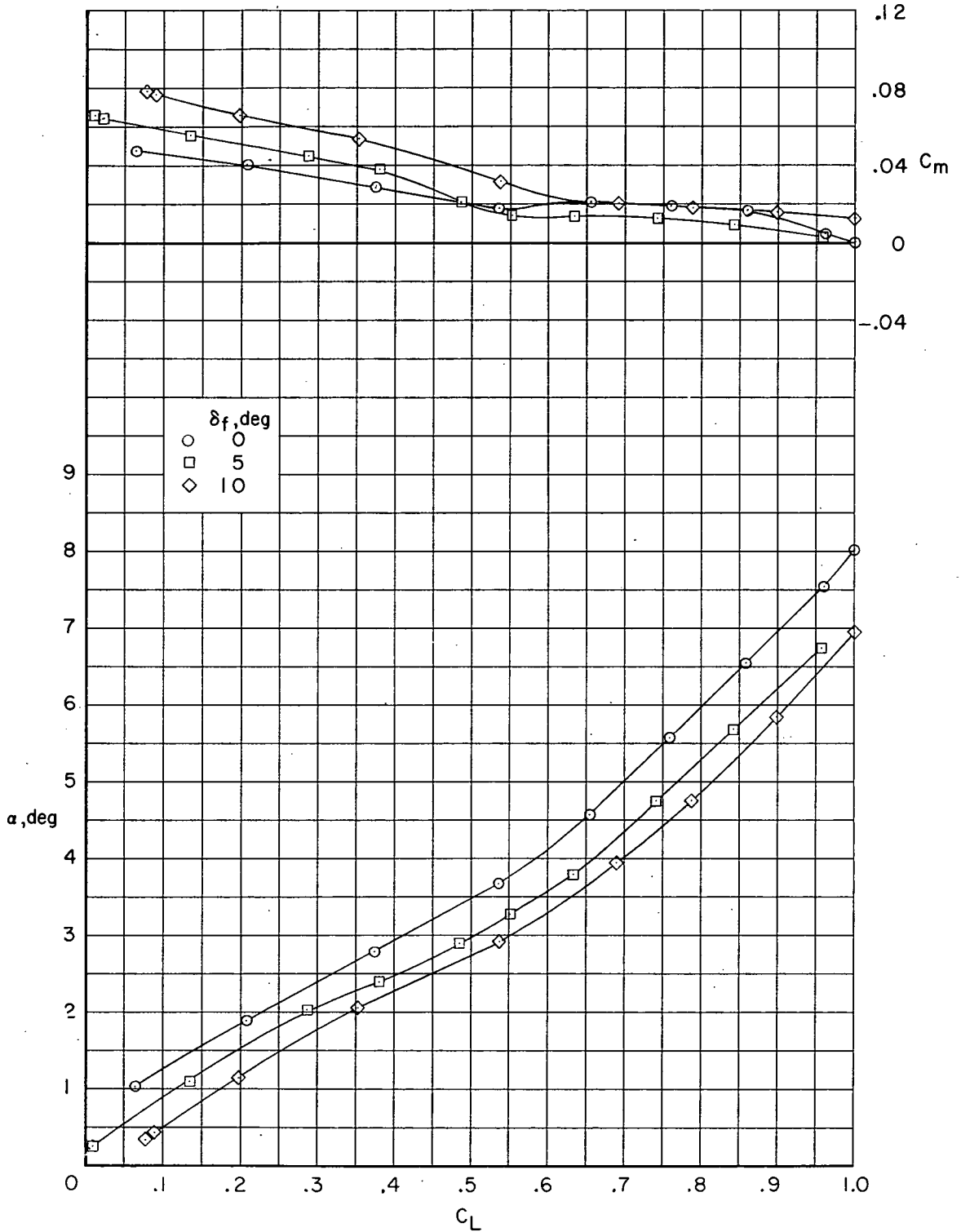
(d) $M = 0.80$. Transition rearward.

Figure 10. - Continued.



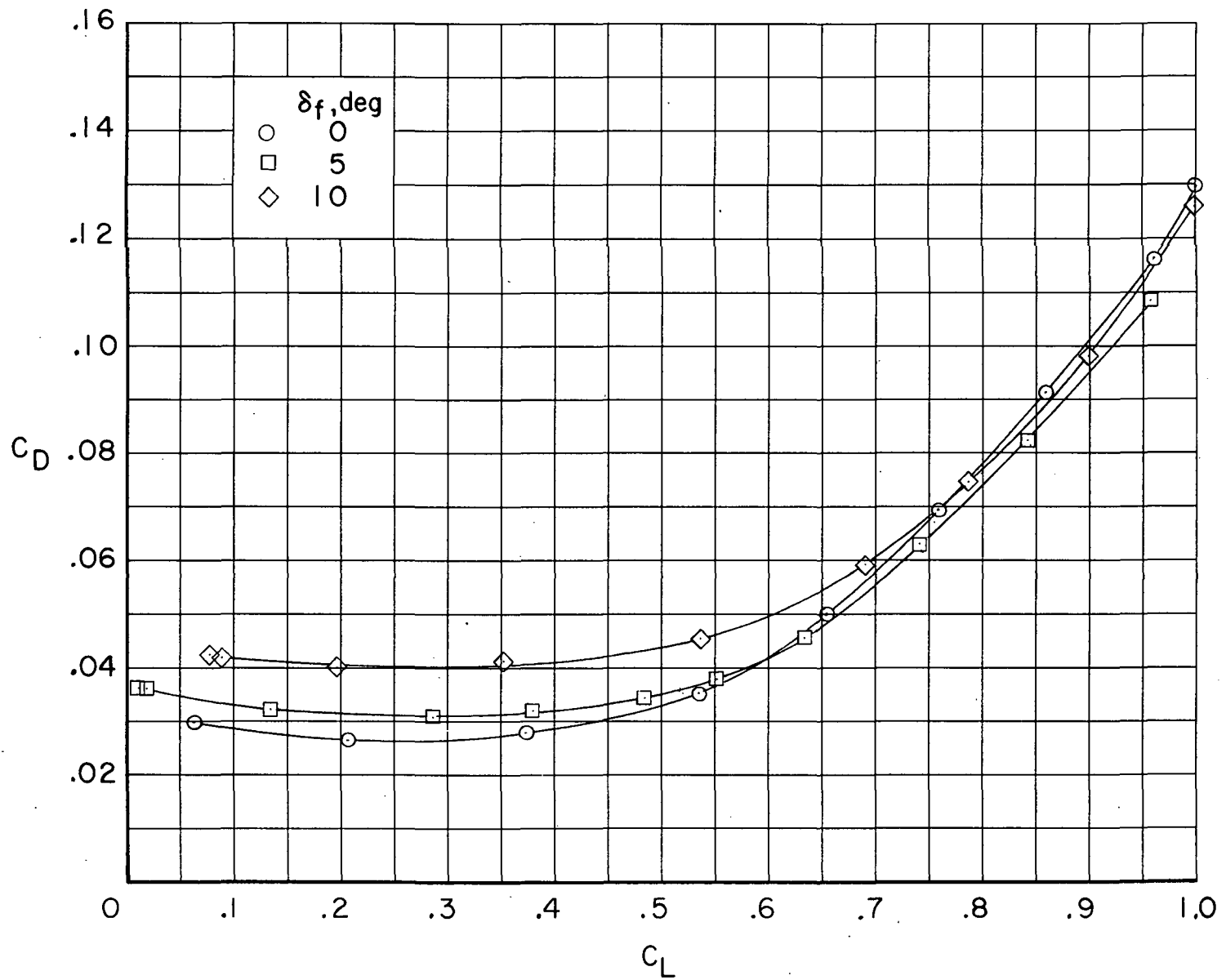
(d) $M = 0.80$. Transition rearward. Concluded.

Figure 10.- Continued.



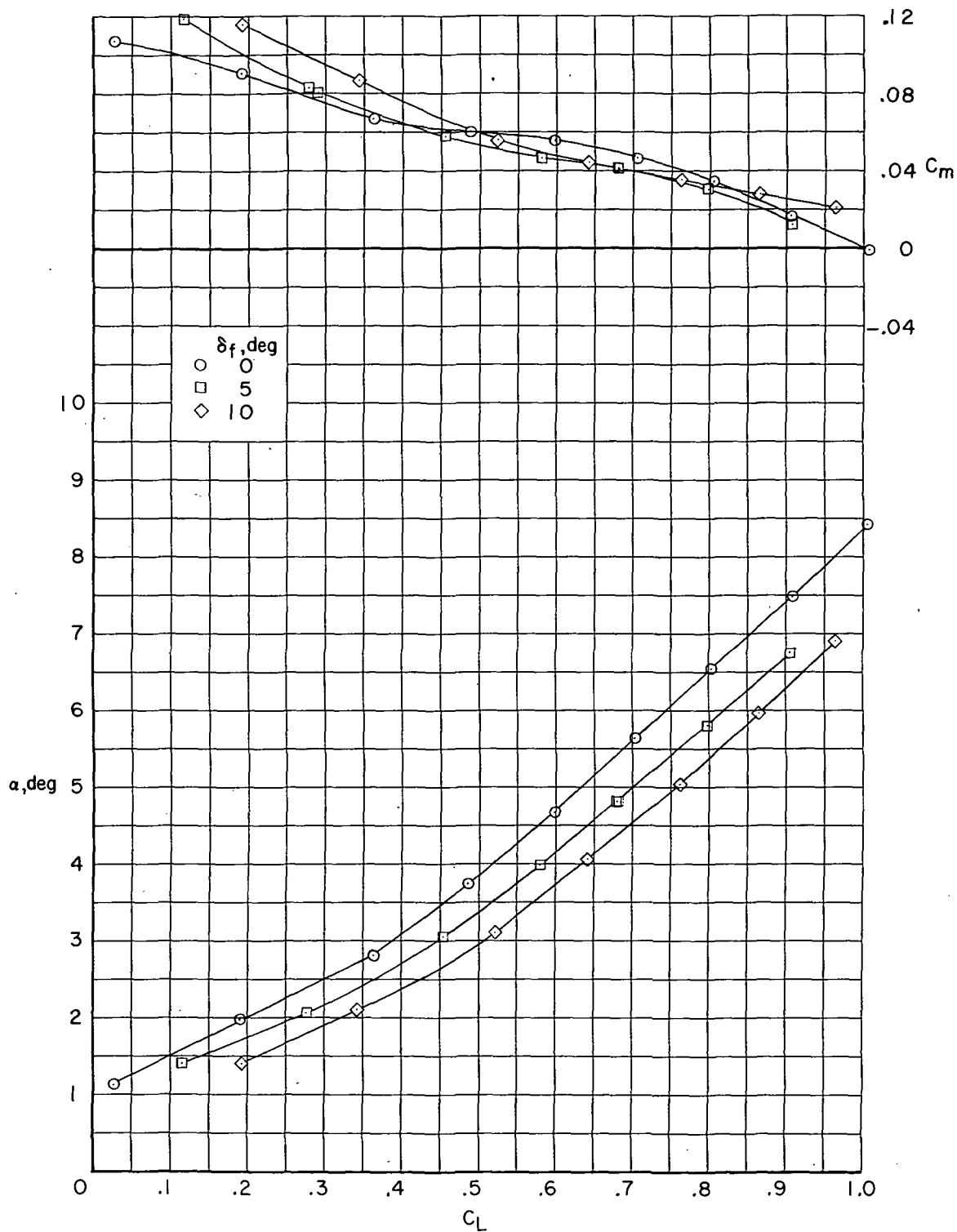
(e) $M = 0.85$. Transition rearward.

Figure 10.- Continued.



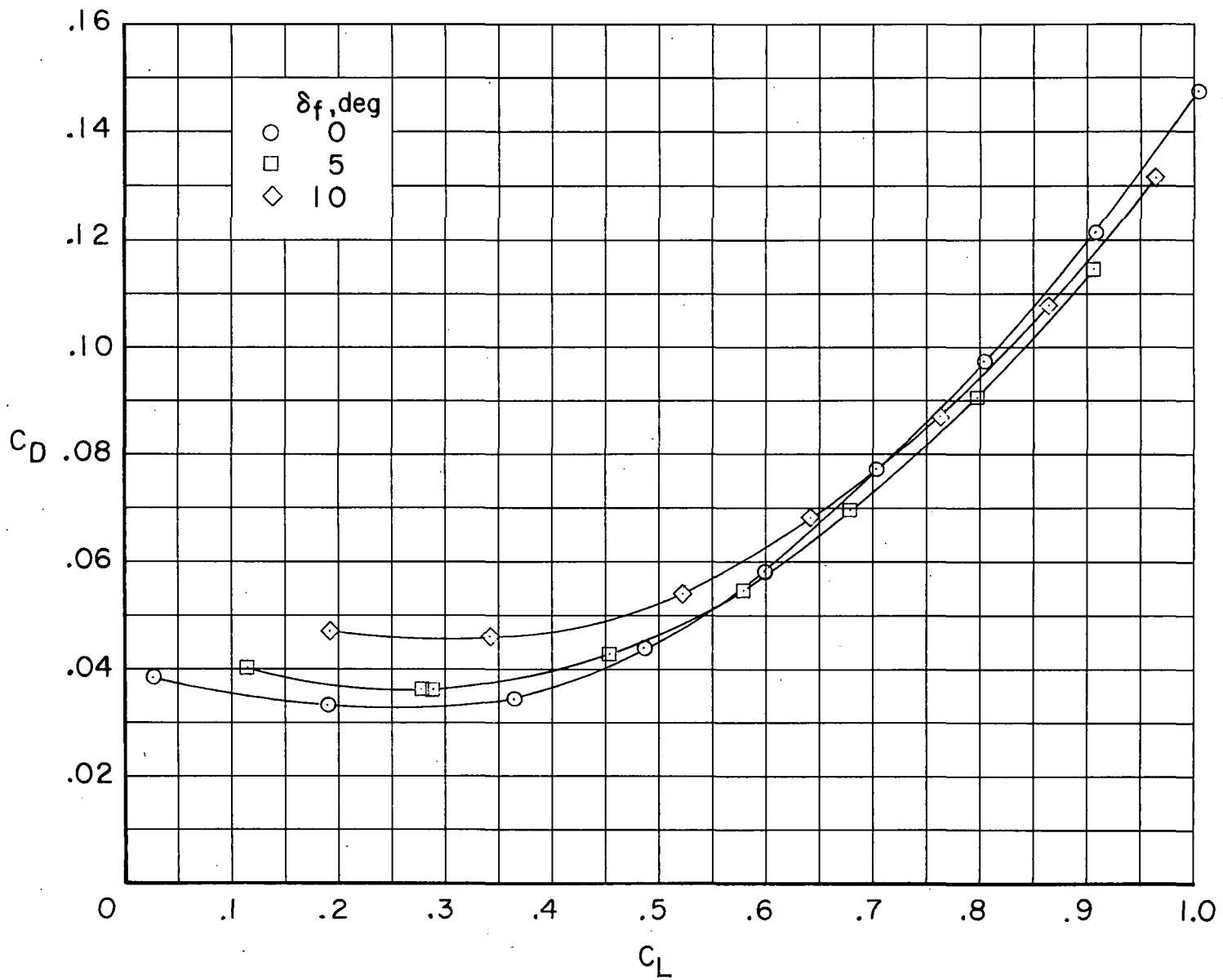
(e) $M = 0.85$. Transition rearward. Concluded.

Figure 10. - Continued.



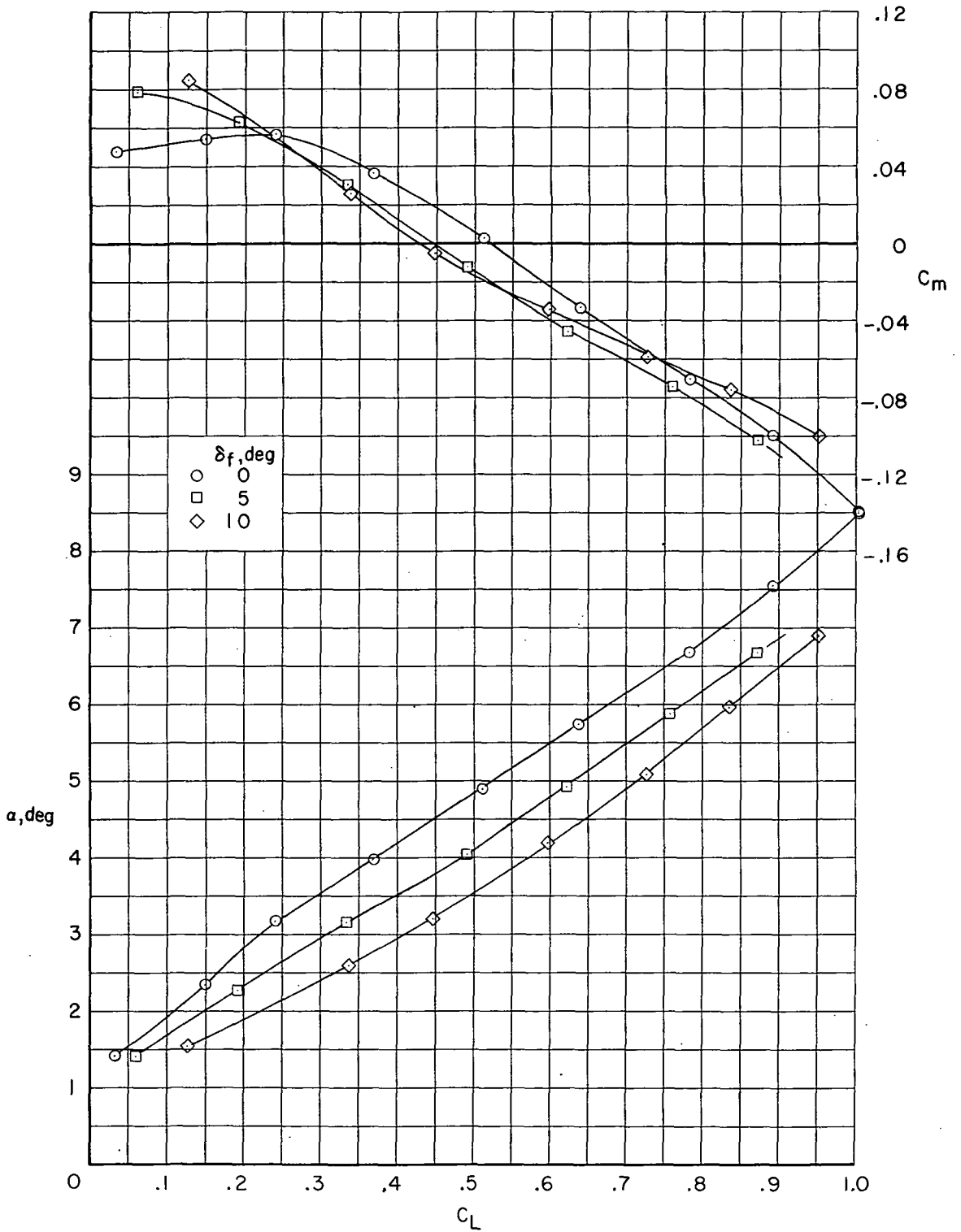
(f) $M = 0.88$. Transition rearward.

Figure 10. - Continued.



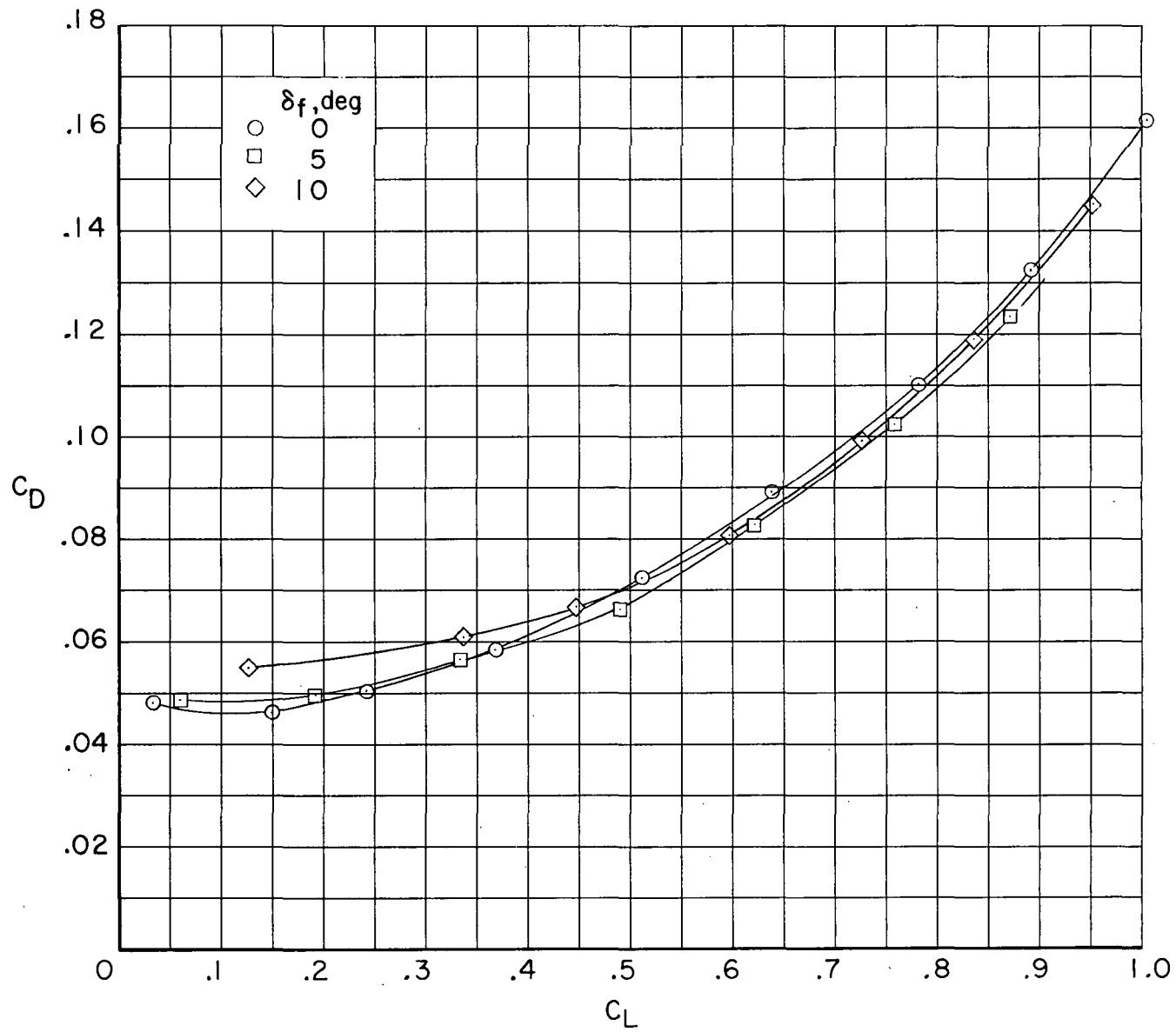
(f) $M = 0.88$. Transition rearward. Concluded.

Figure 10.- Continued.



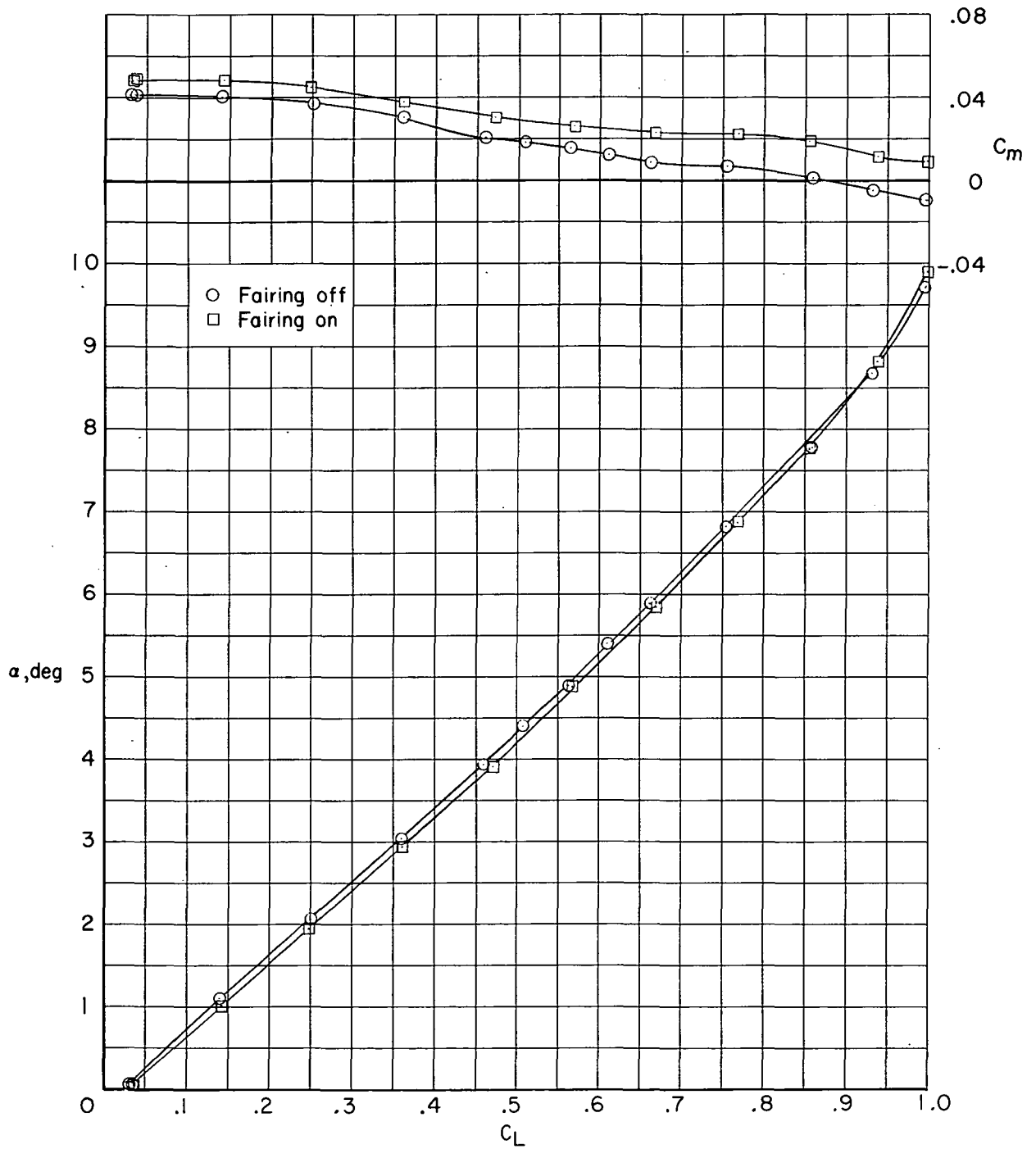
(g) $M = 0.91$. Transition rearward.

Figure 10.- Continued.



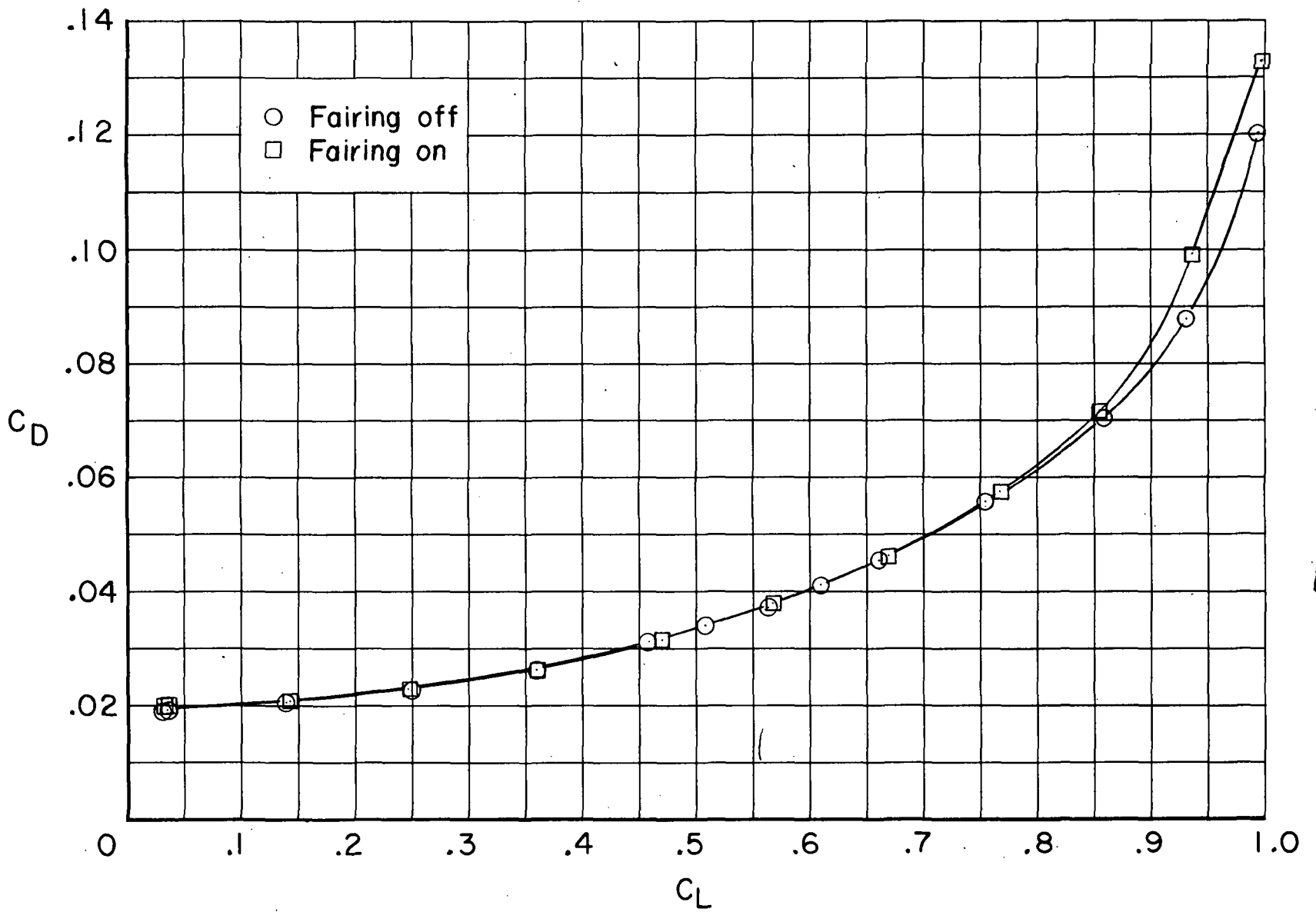
(g) $M = 0.91$. Transition rearward. Concluded.

Figure 10.- Concluded.



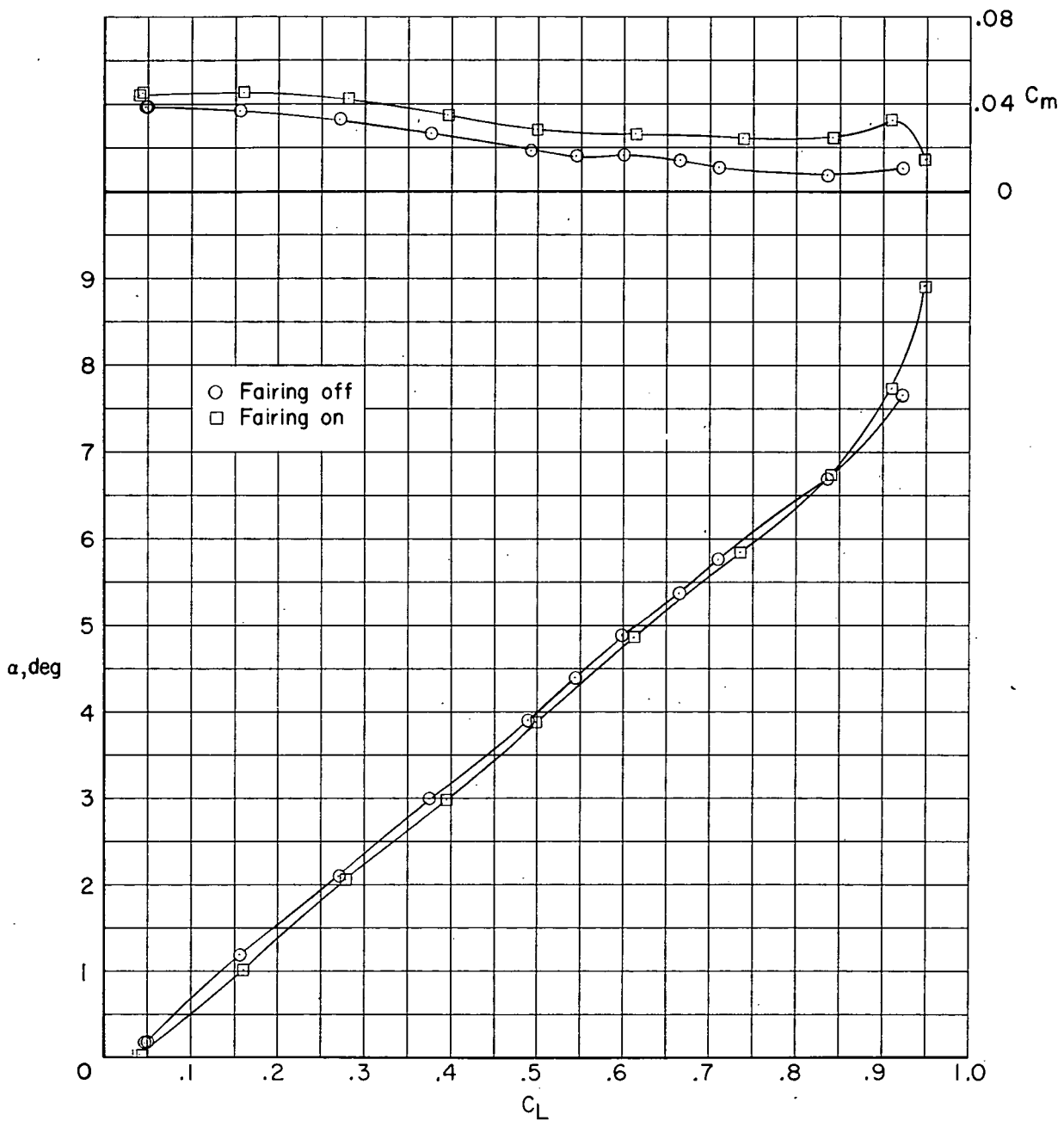
(a) $M = 0.60$.

Figure 11.- Effect of fuselage fairing on longitudinal aerodynamic characteristics of configuration with NACA 64A2XX airfoils and transition rearward. $\Lambda = 26^\circ$; $\delta_h = 0^\circ$; $i_w = 1^\circ$.



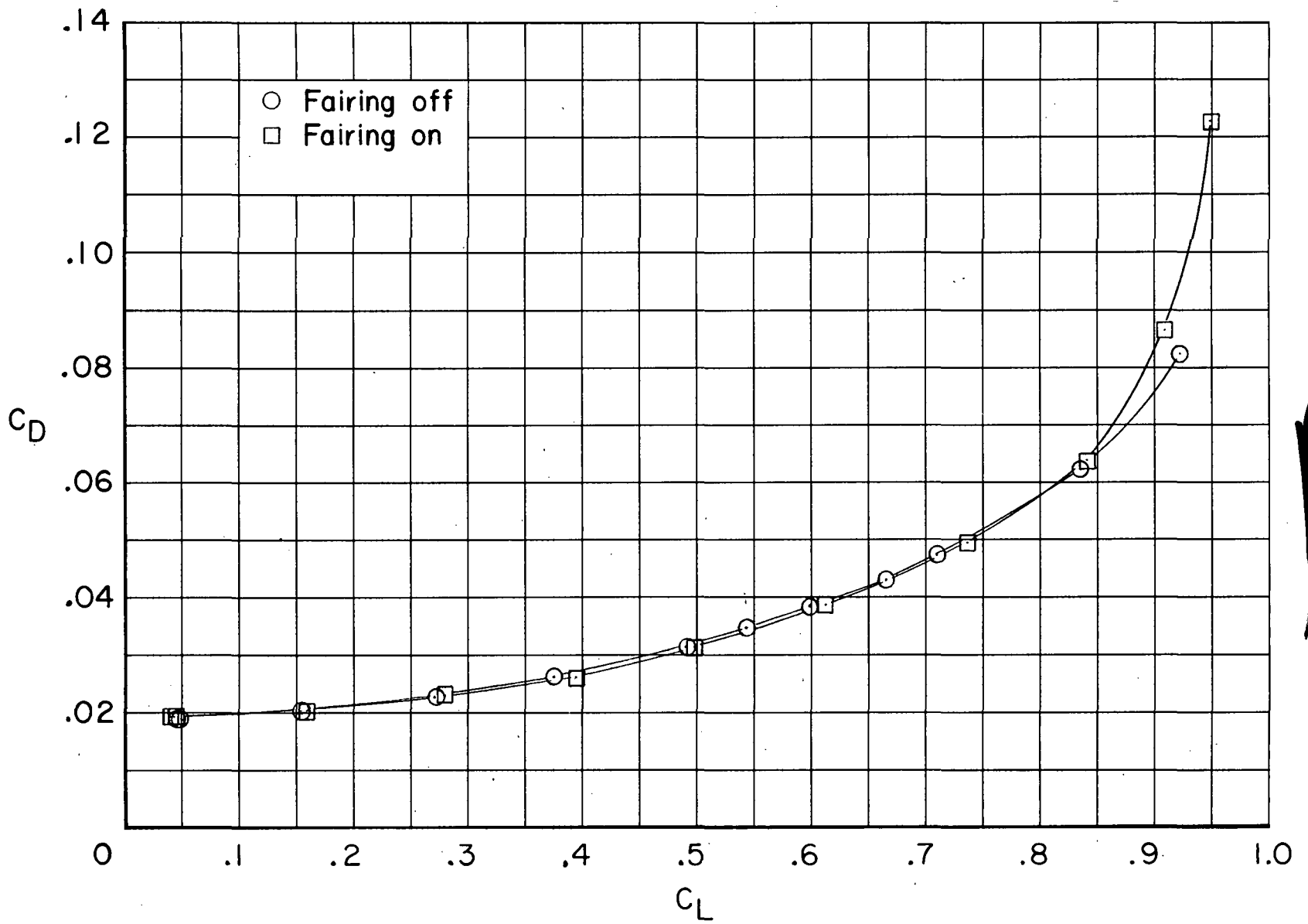
(a) $M = 0.60$. Concluded.

Figure 11. - Continued.



(b) $M = 0.70$.

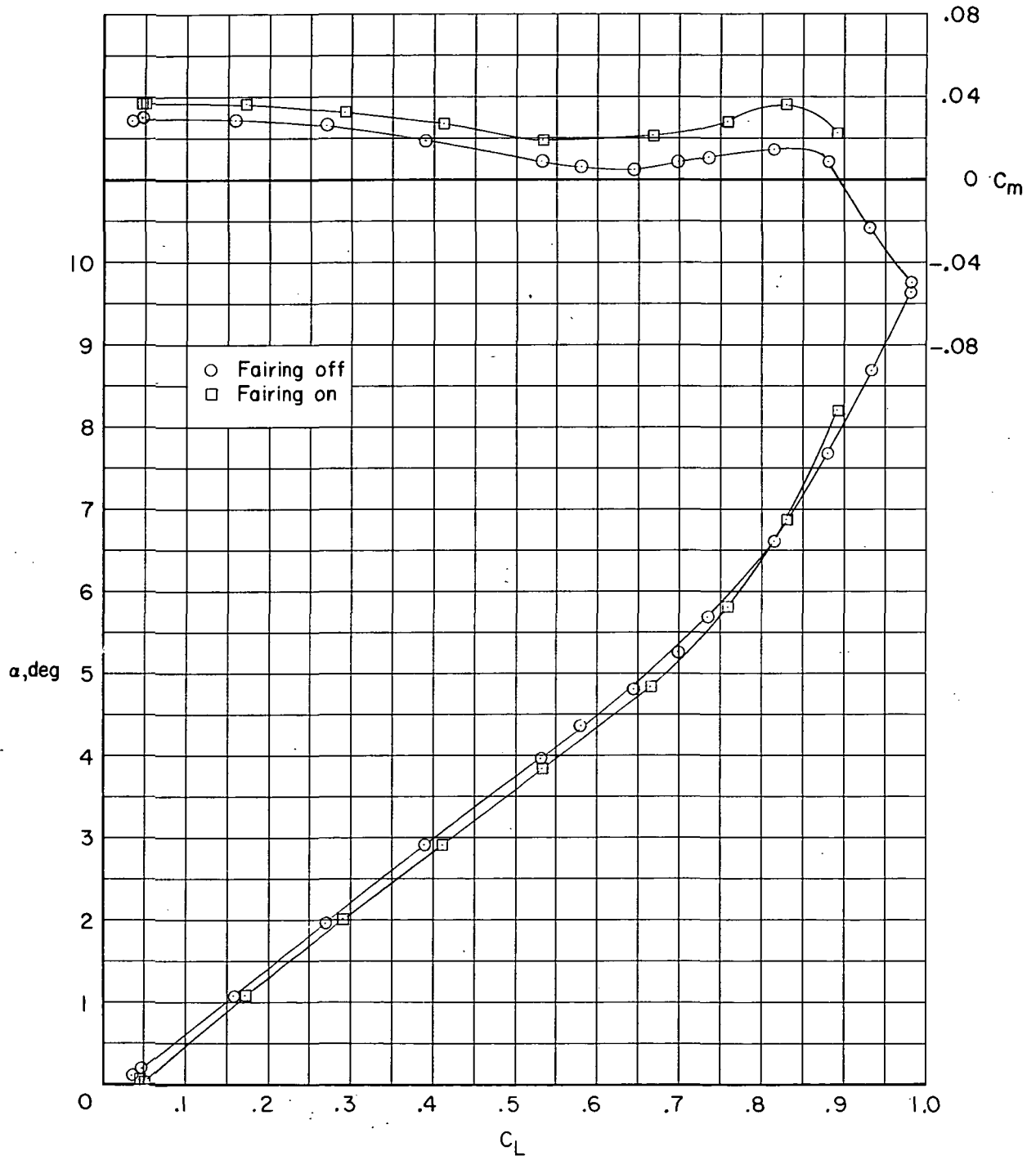
Figure 11.- Continued.



(b) $M = 0.70$. Concluded.

Figure 11.- Continued.

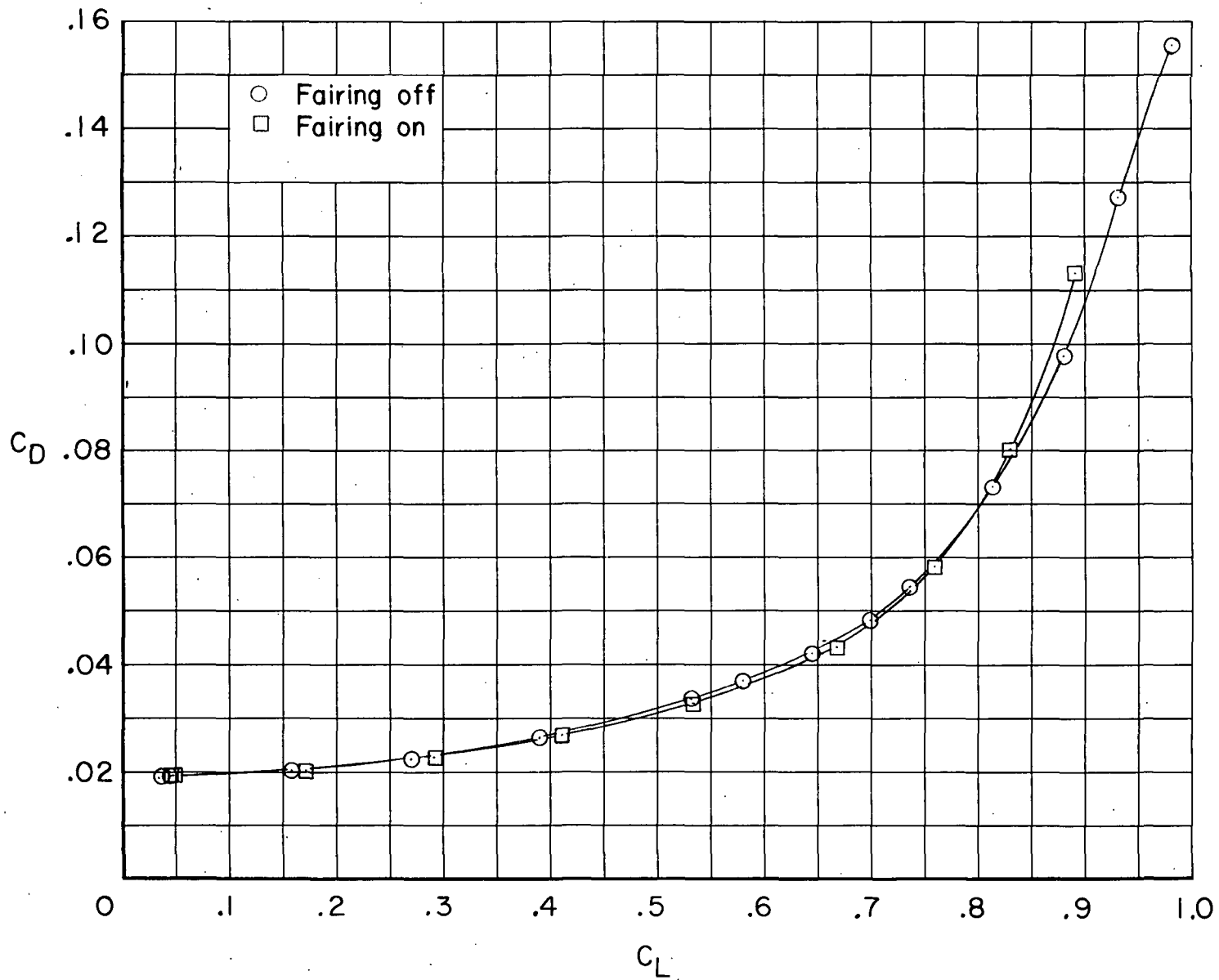
~~CONFIDENTIAL~~



(c) $M = 0.75$.

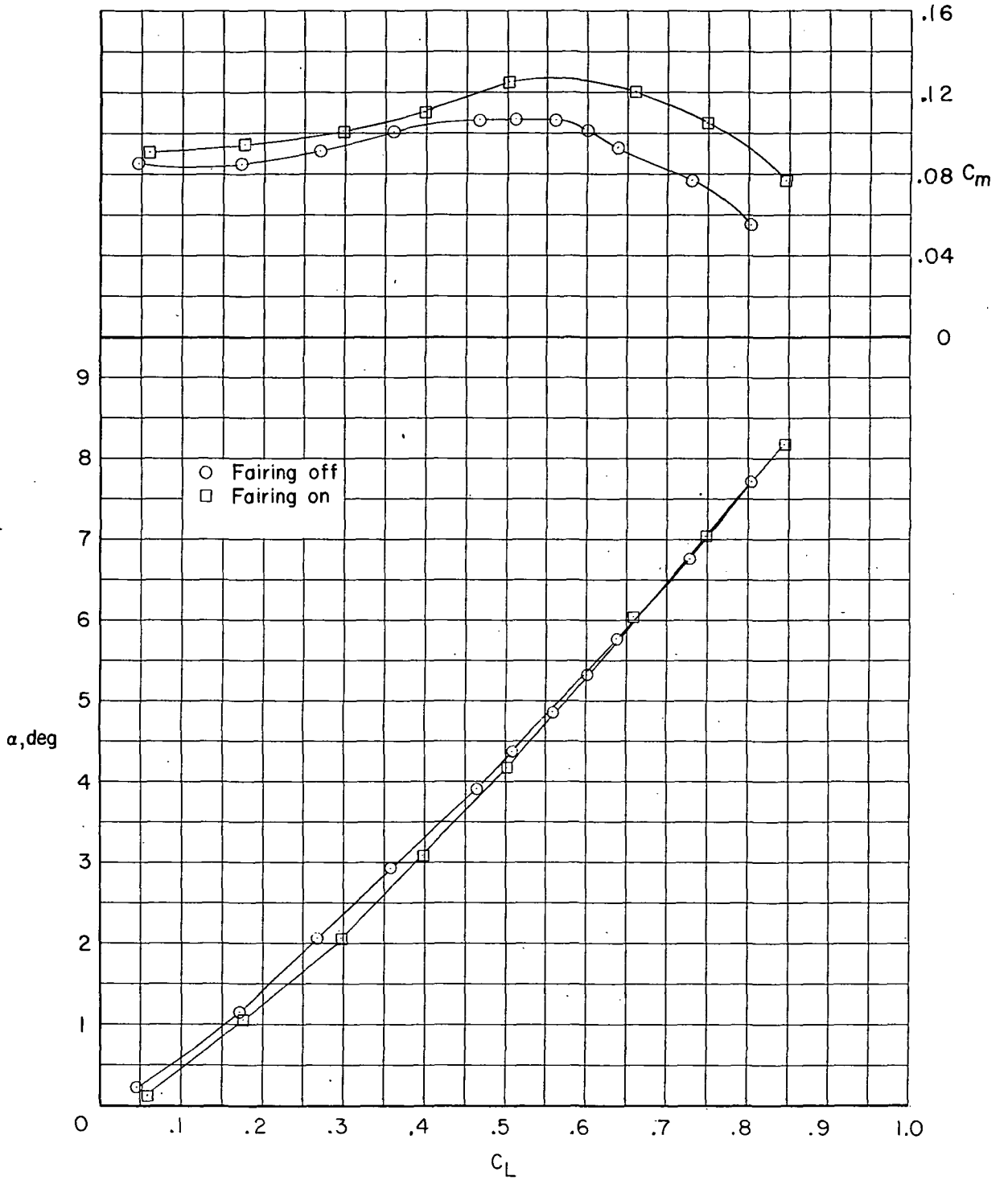
Figure 11.- Continued.

~~CONFIDENTIAL~~



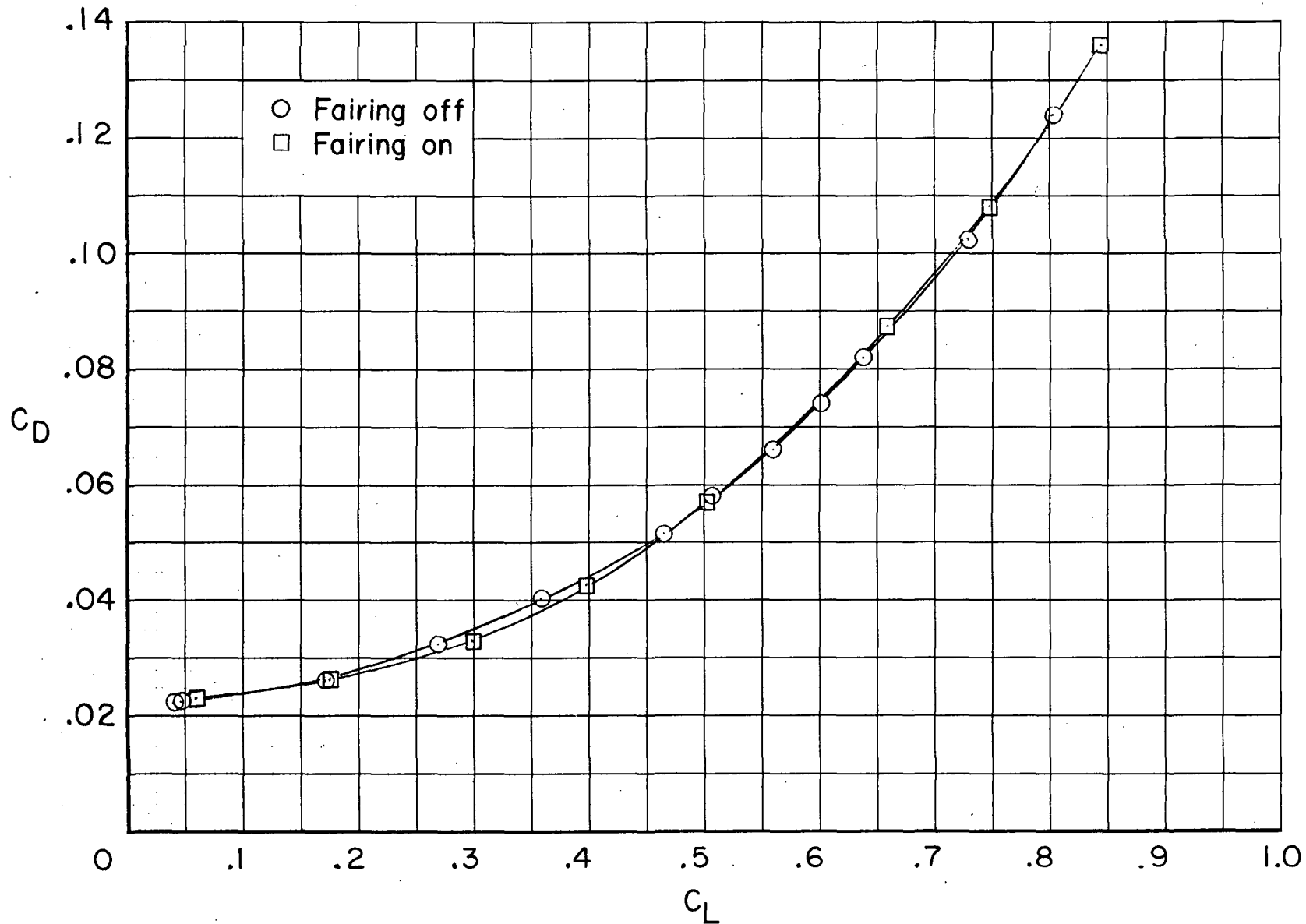
(c) $M = 0.75$. Concluded.

Figure 11.- Continued.



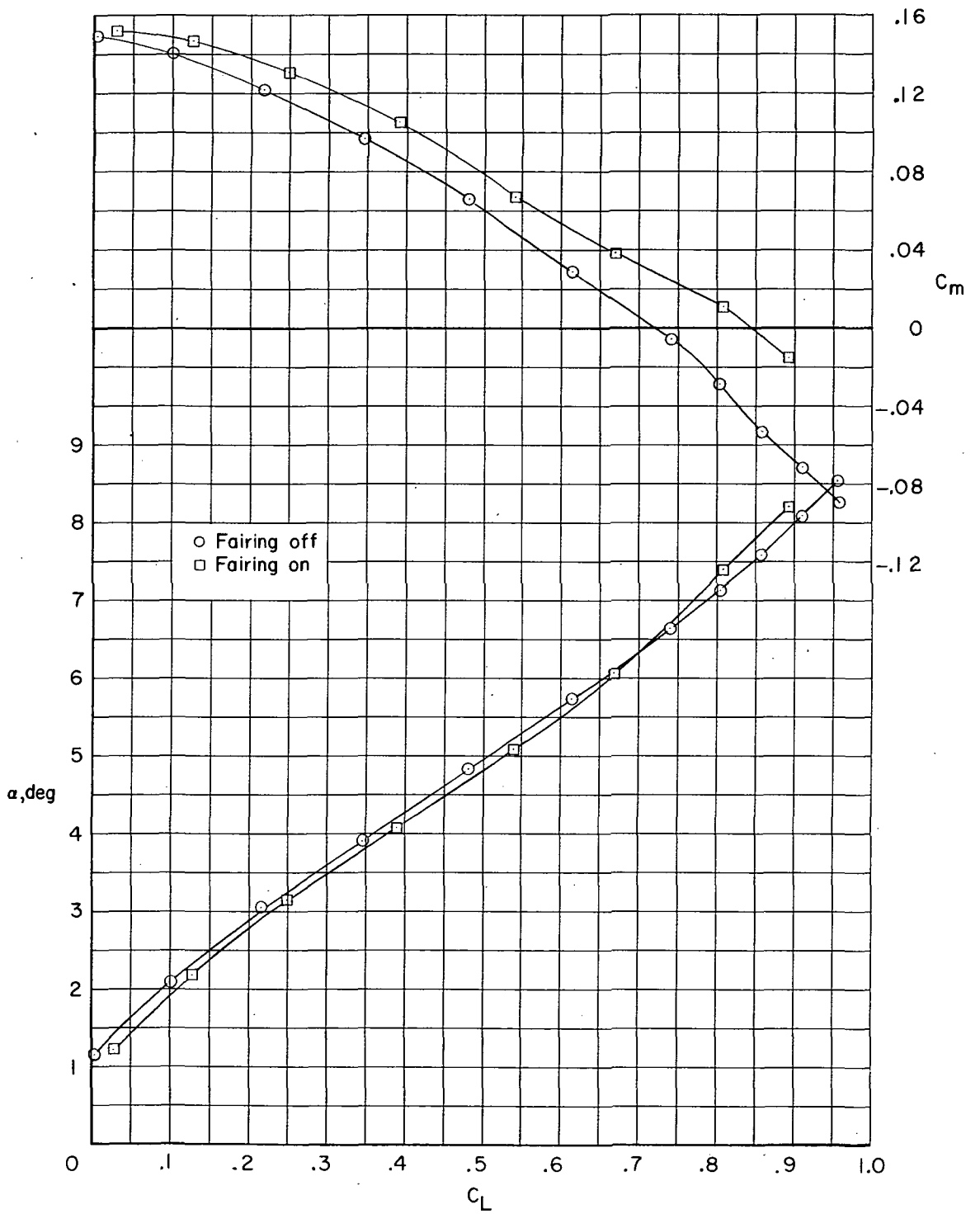
(d) $M = 0.85$.

Figure 11. - Continued.



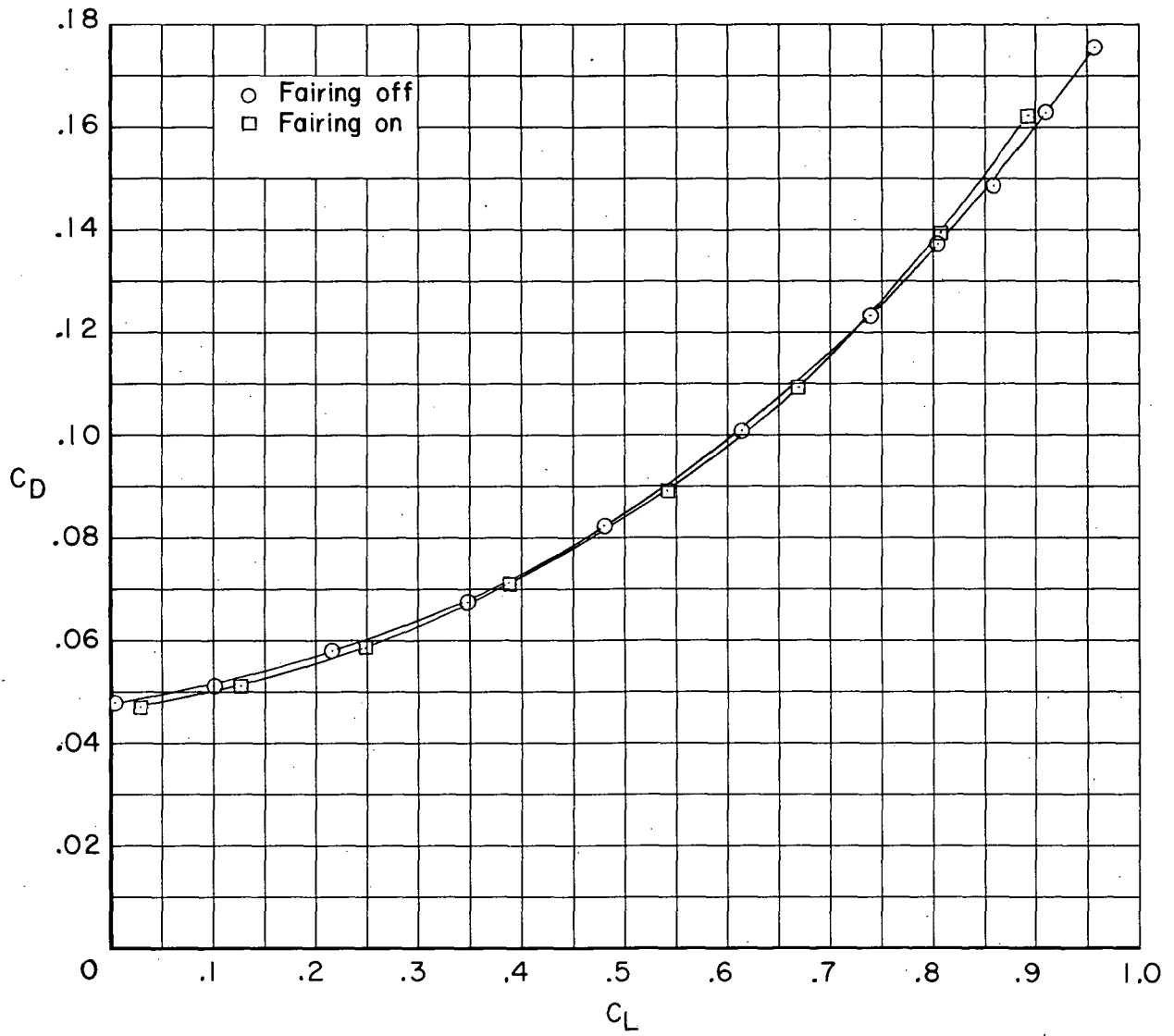
(d) $M = 0.85$. Concluded.

Figure 11.- Continued.



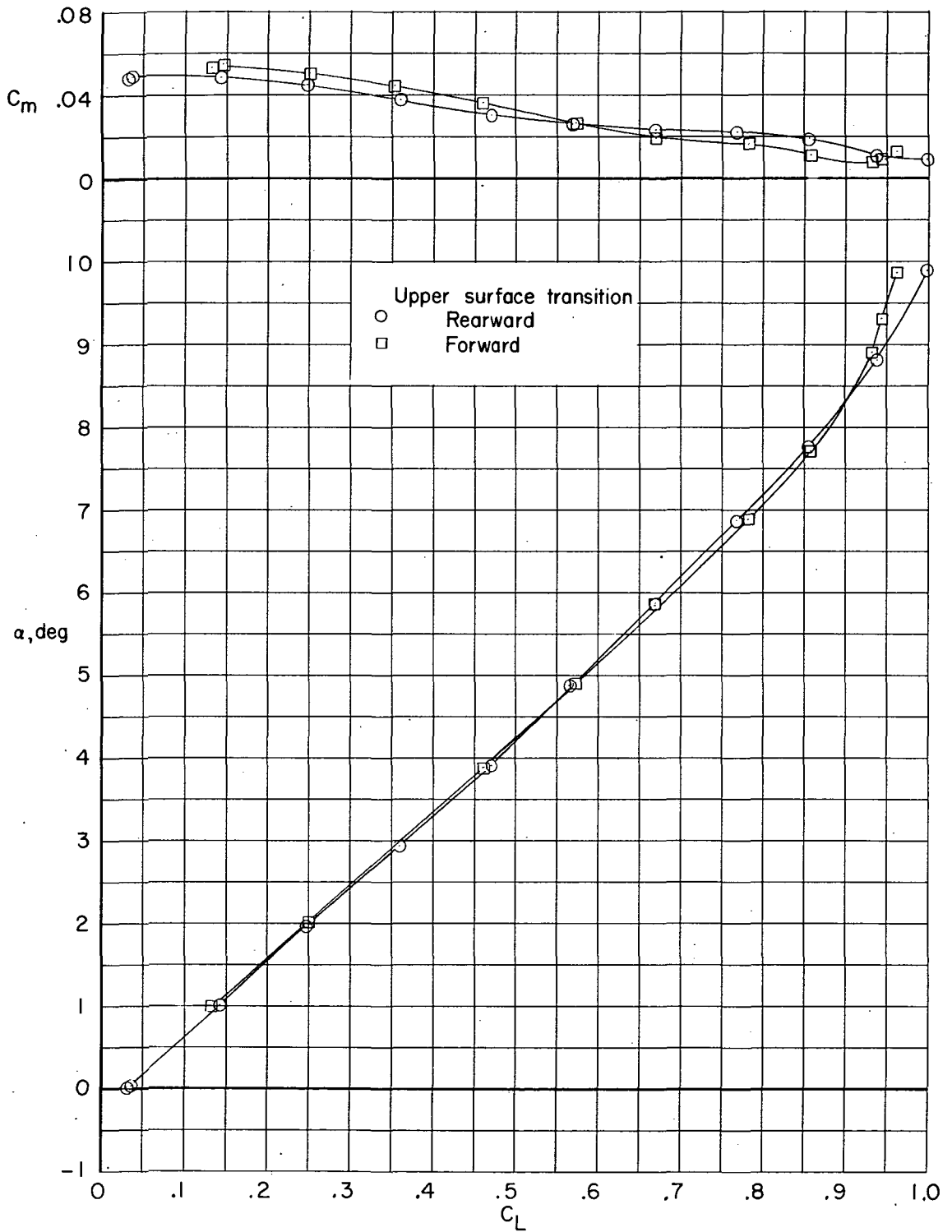
(e) $M = 0.91$.

Figure 11.- Continued.



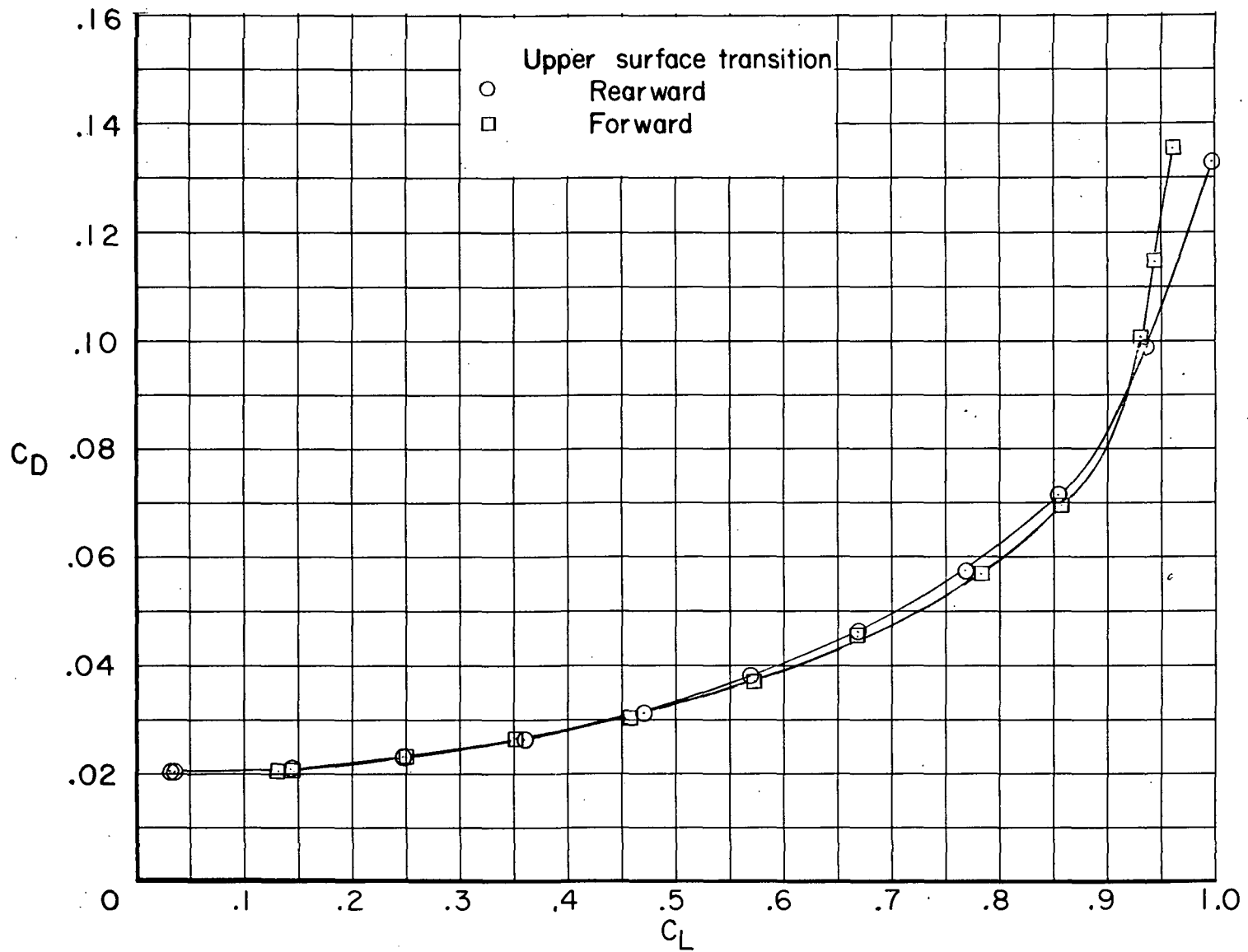
(e) $M = 0.91$. Concluded.

Figure 11.- Concluded.



(a) $M = 0.60$.

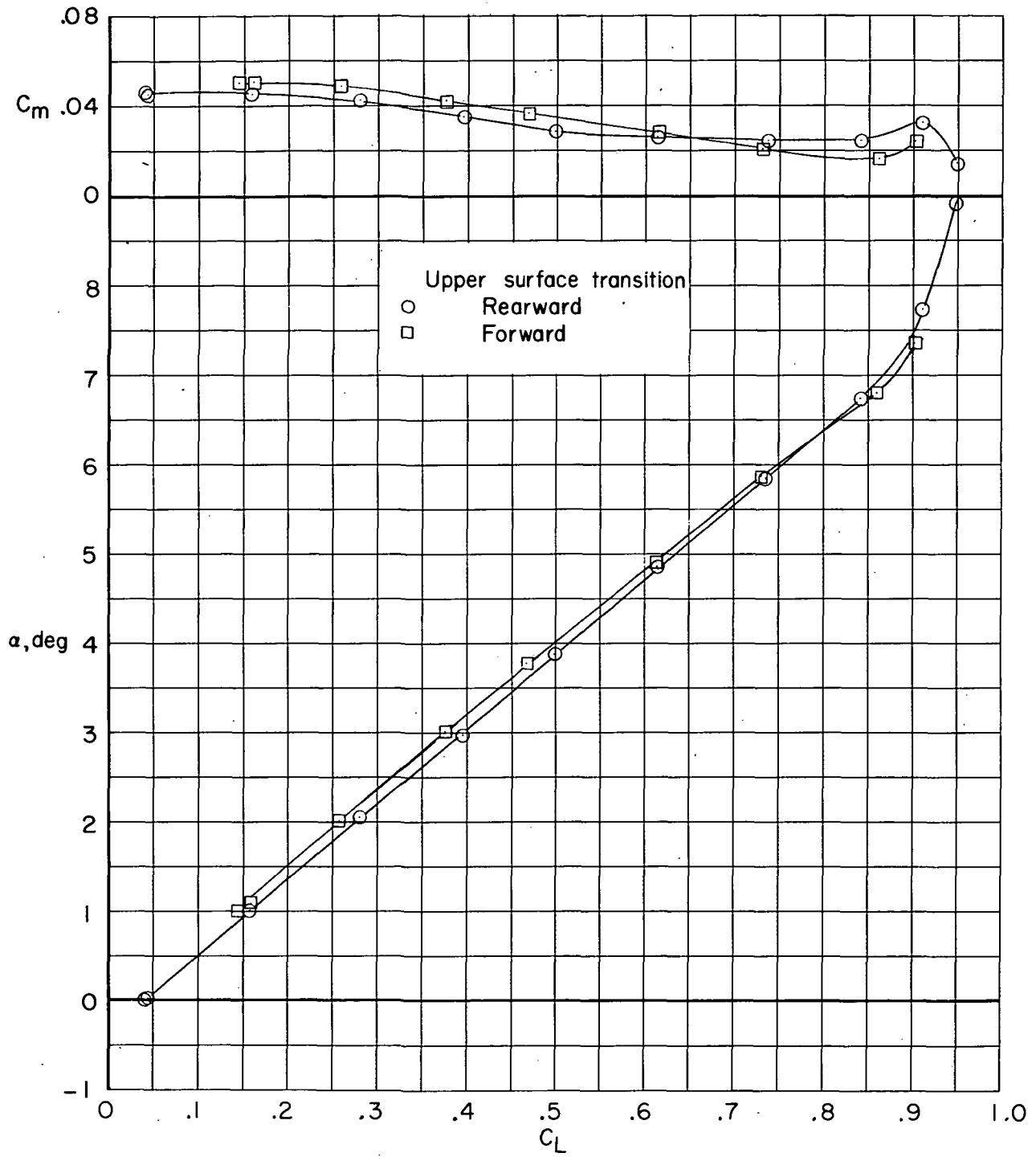
Figure 12.- Effect of upper surface transition location on longitudinal aerodynamic characteristics of configuration with NACA 64A2XX airfoils and fuselage fairing. $\Lambda = 26^\circ$; $\delta_h = 0^\circ$.



(a) $M = 0.60$. Concluded.

Figure 12. - Continued.

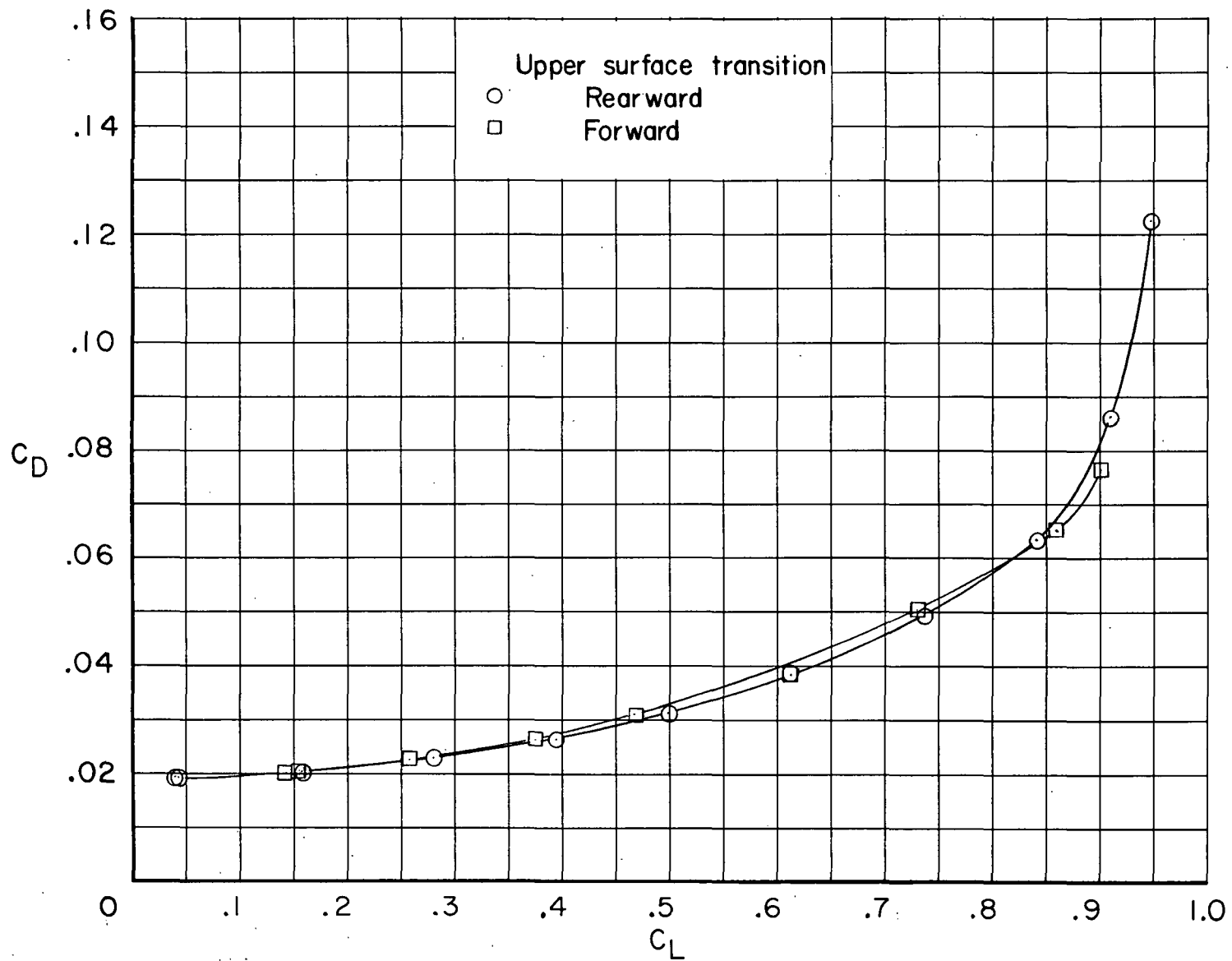
~~CONFIDENTIAL~~



(b) $M = 0.70$.

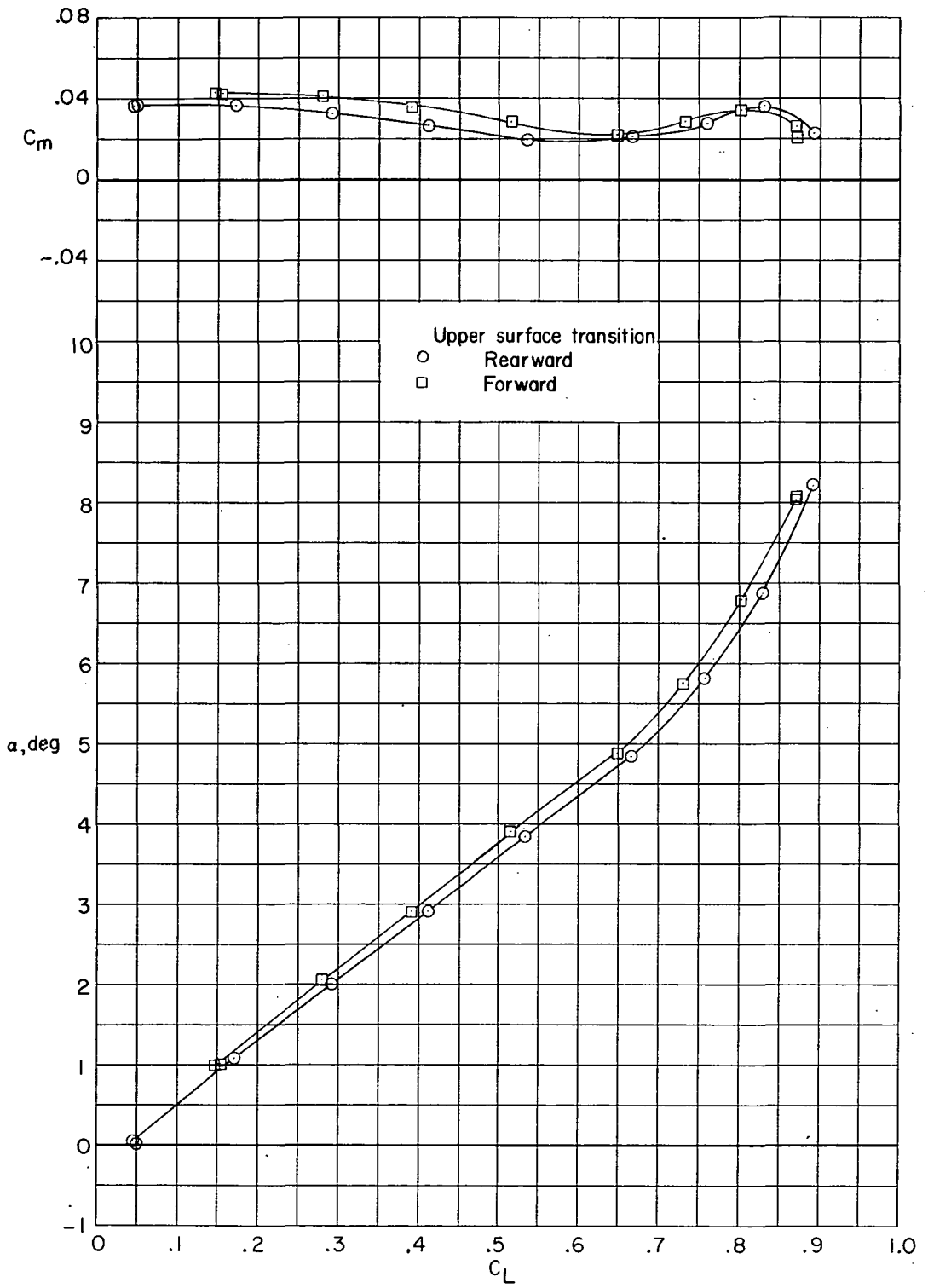
Figure 12.- Continued.

~~CONFIDENTIAL~~



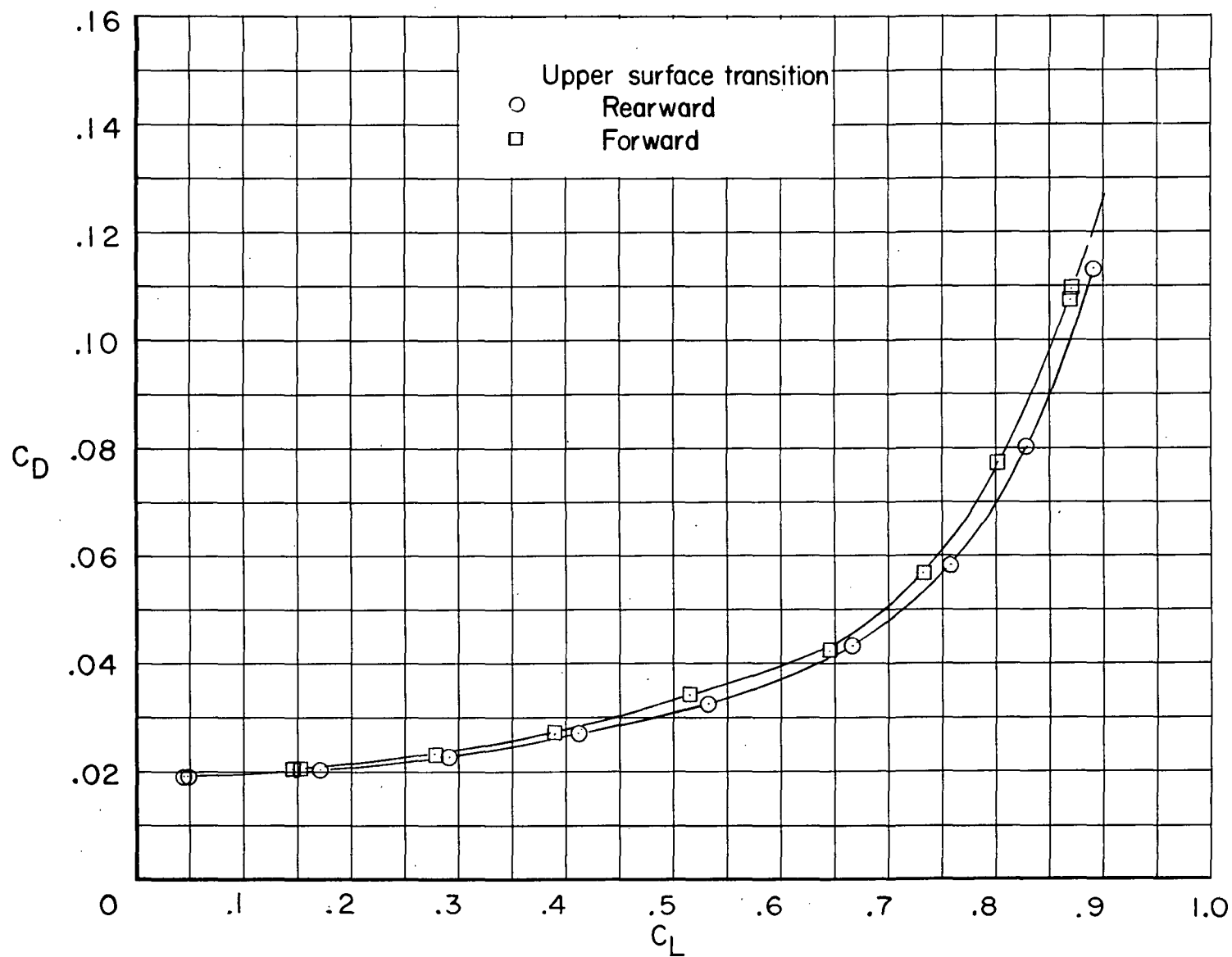
(b) $M = 0.70$. Concluded.

Figure 12.- Continued.



(c) $M = 0.75$.

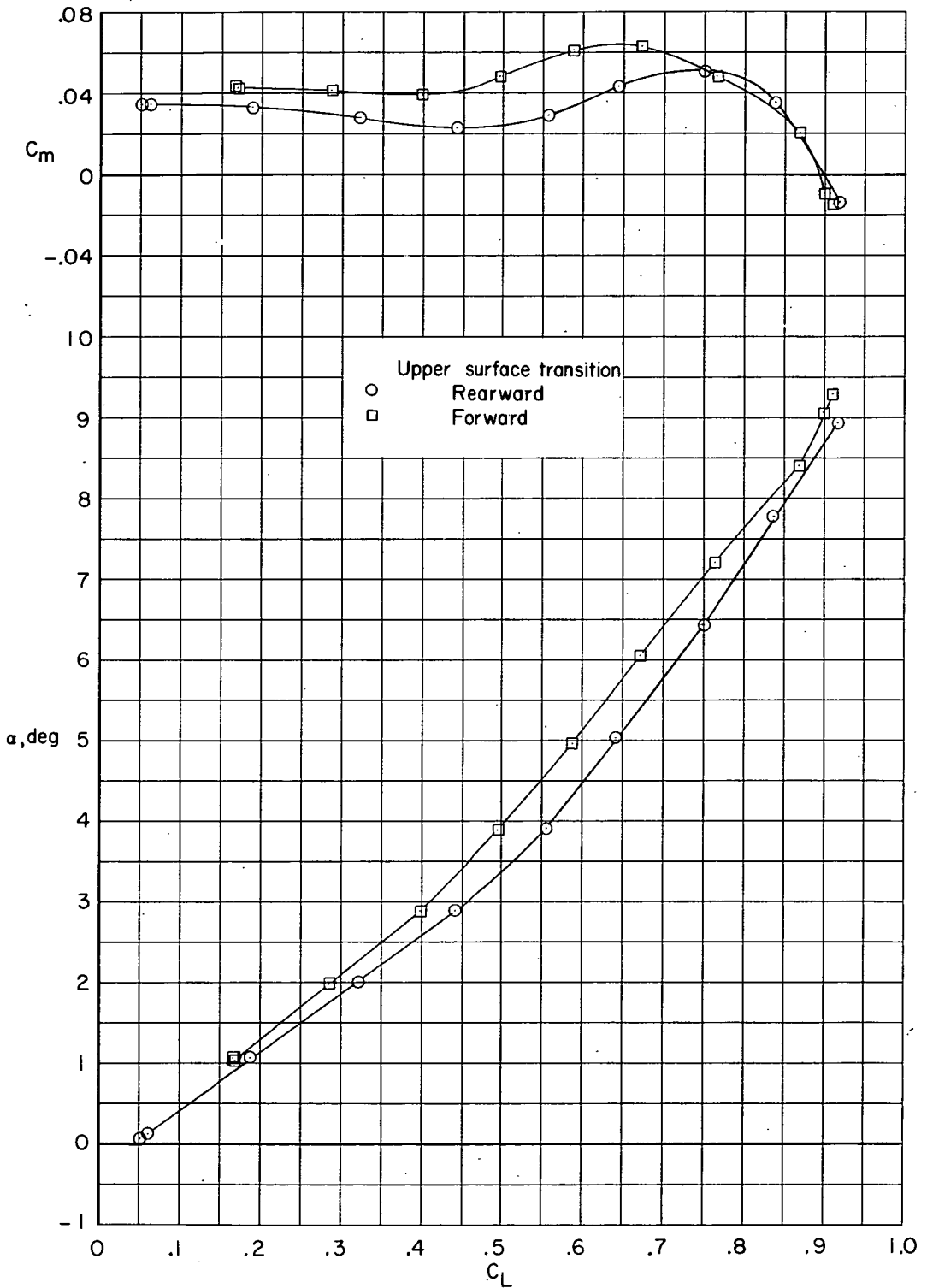
Figure 12. - Continued.



(c) $M = 0.75$. Concluded.

Figure 12. - Continued.

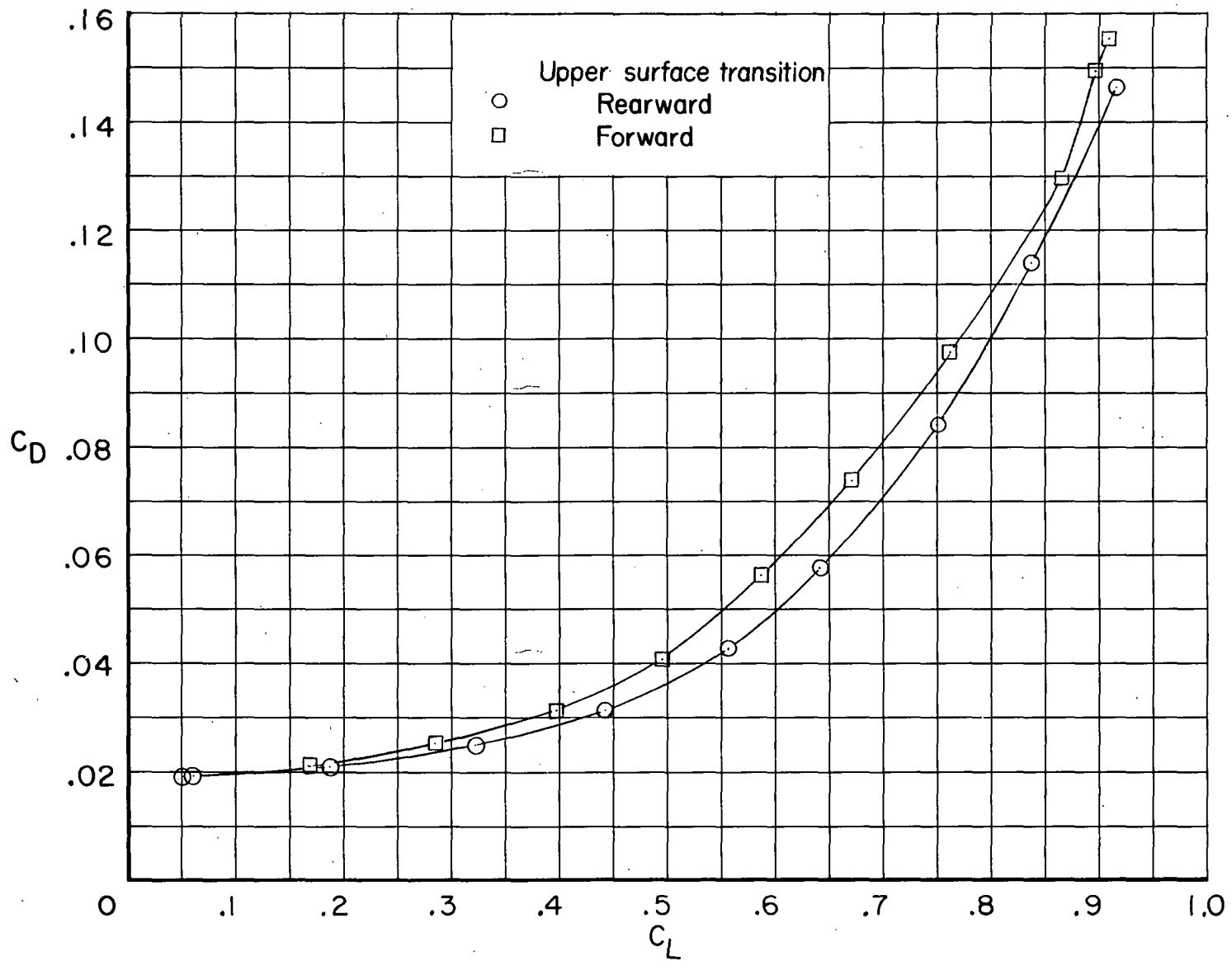
~~CONFIDENTIAL~~



(d) $M = 0.80$.

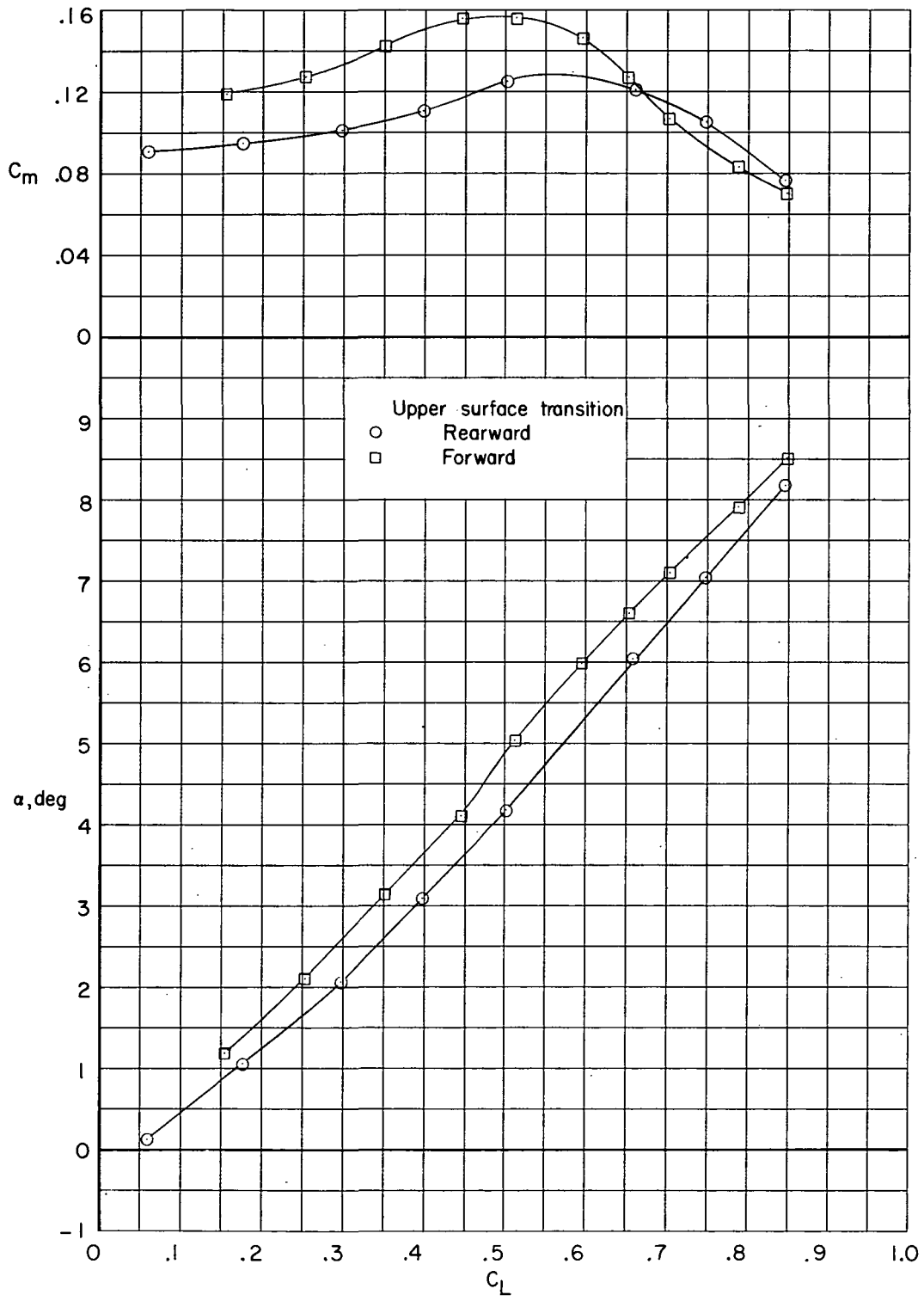
Figure 12. - Continued.

~~CONFIDENTIAL~~



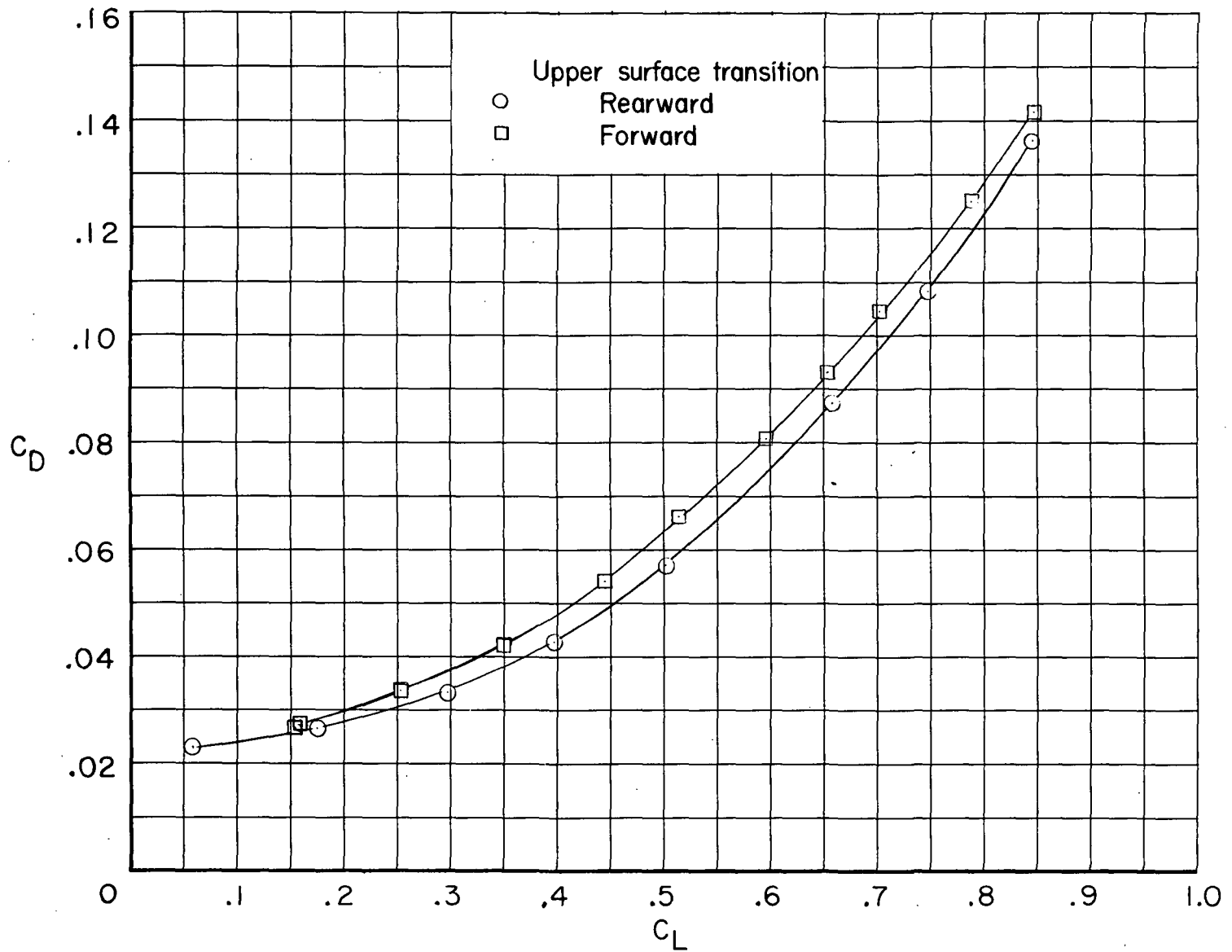
(d) $M = 0.80$. Concluded.

Figure 12. - Continued.



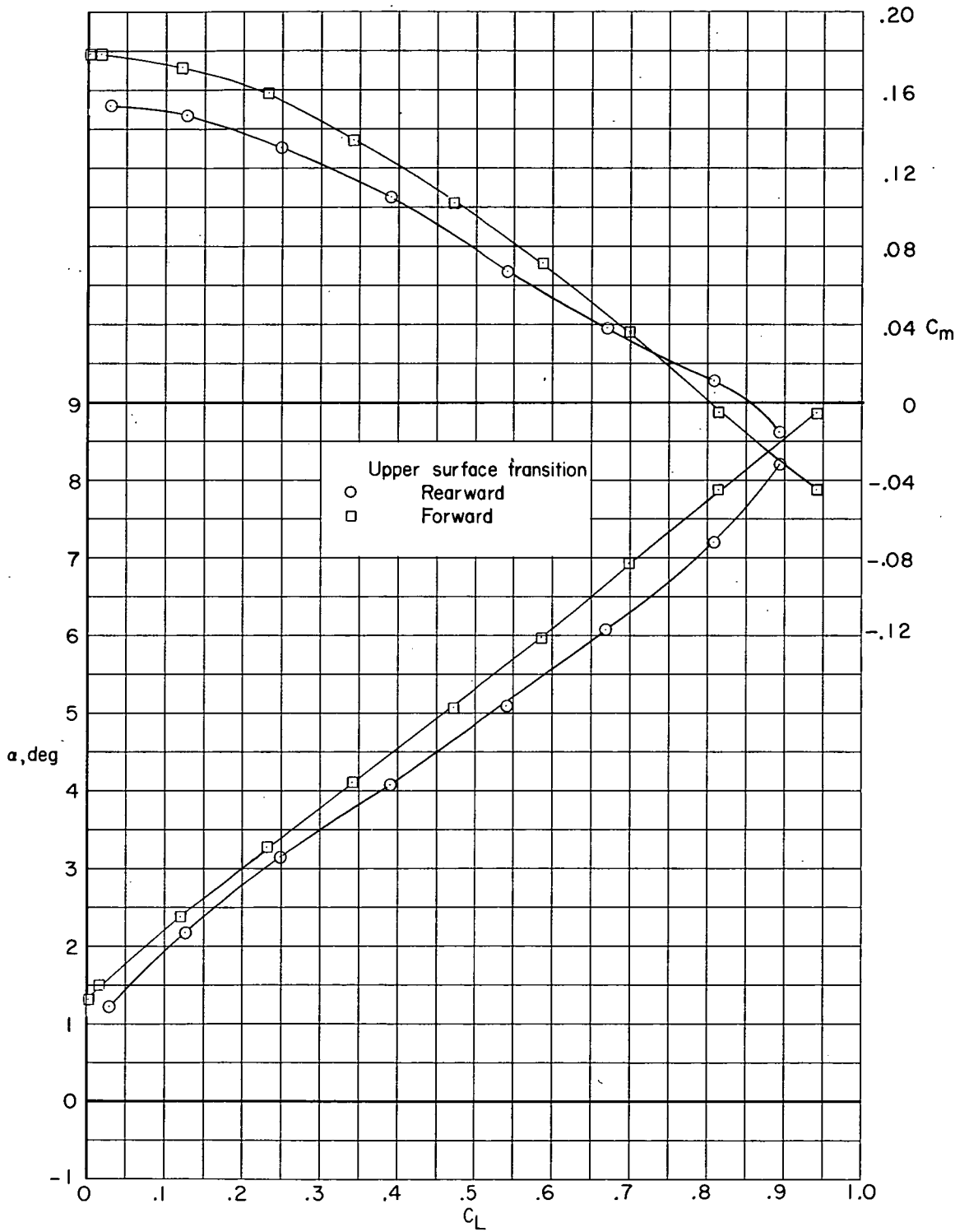
(e) $M = 0.85$.

Figure 12. - Continued.



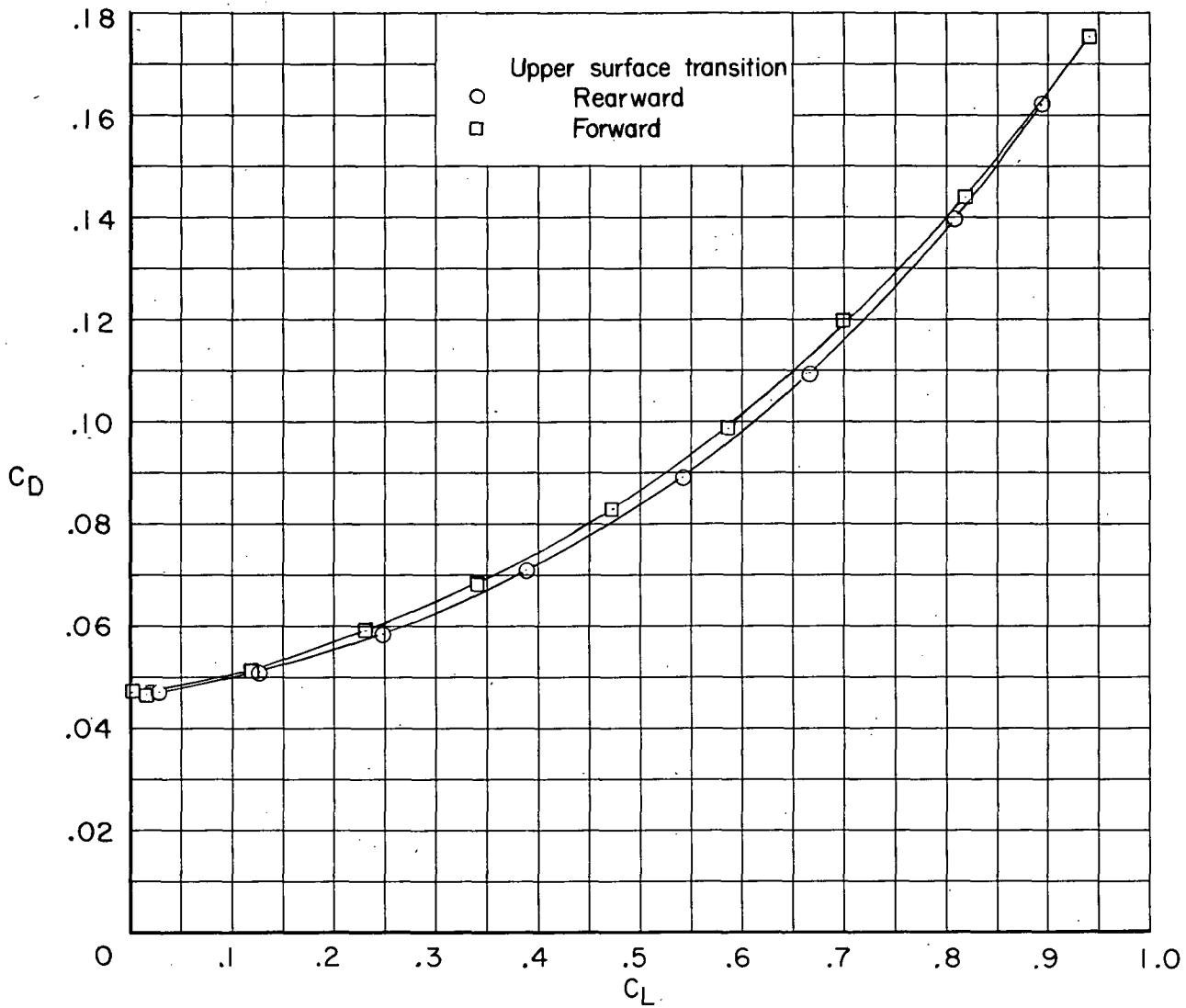
(e) $M = 0.85$. Concluded.

Figure 12. - Continued.



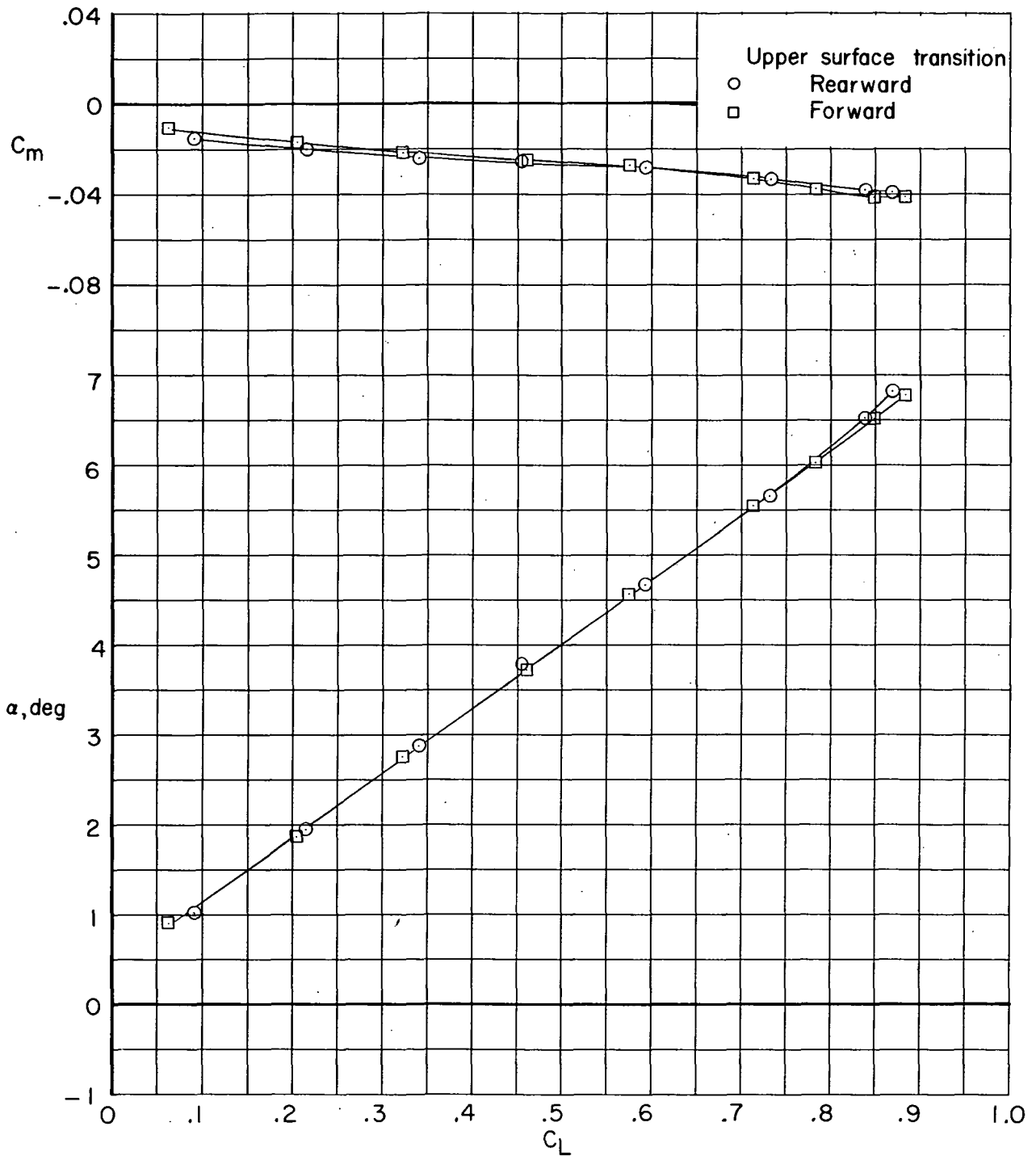
(f) $M = 0.91$.

Figure 12. - Continued.



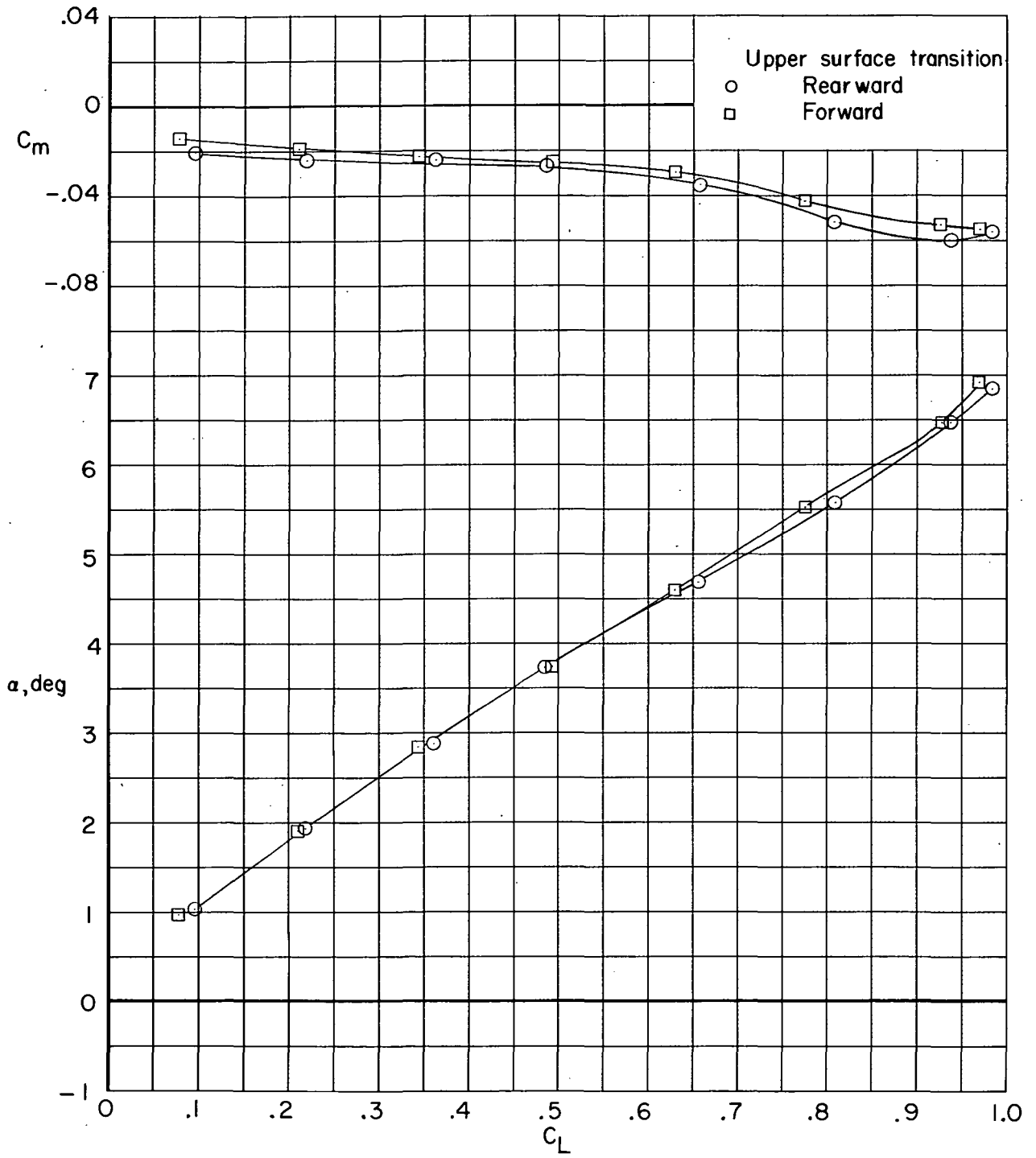
(f) $M = 0.91$. Concluded.

Figure 12. - Concluded.



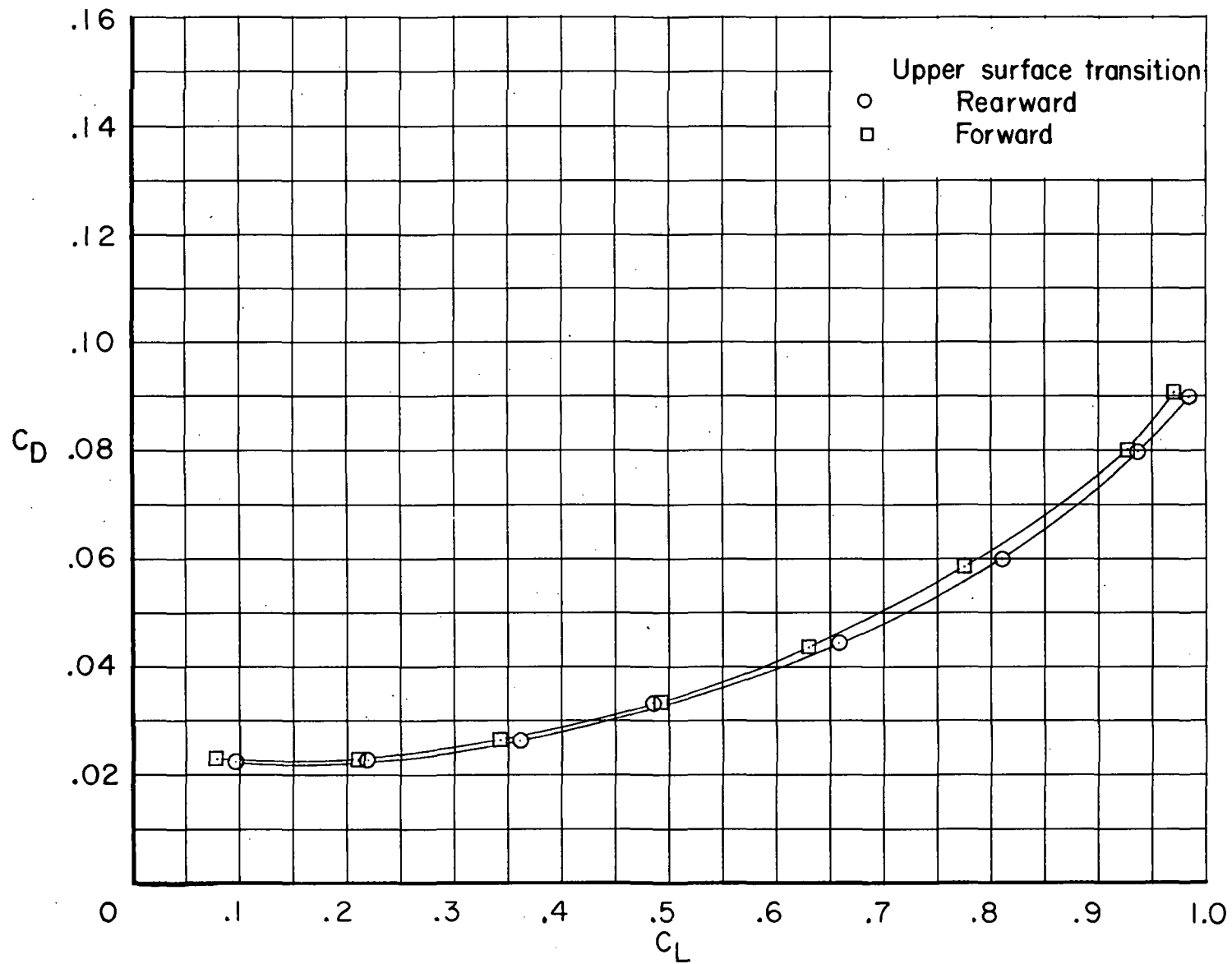
(a) $M = 0.75$.

Figure 13.- Effect of upper surface transition location on longitudinal aerodynamic characteristics of configuration with supercritical airfoil B and fuselage fairing. $\Lambda = 26^\circ$; $\delta_h = 0^\circ$; $i_w = -1^\circ$.



(b) $M = 0.80$.

Figure 13. - Continued.



(b) $M = 0.80$. Concluded.

Figure 13.- Concluded.

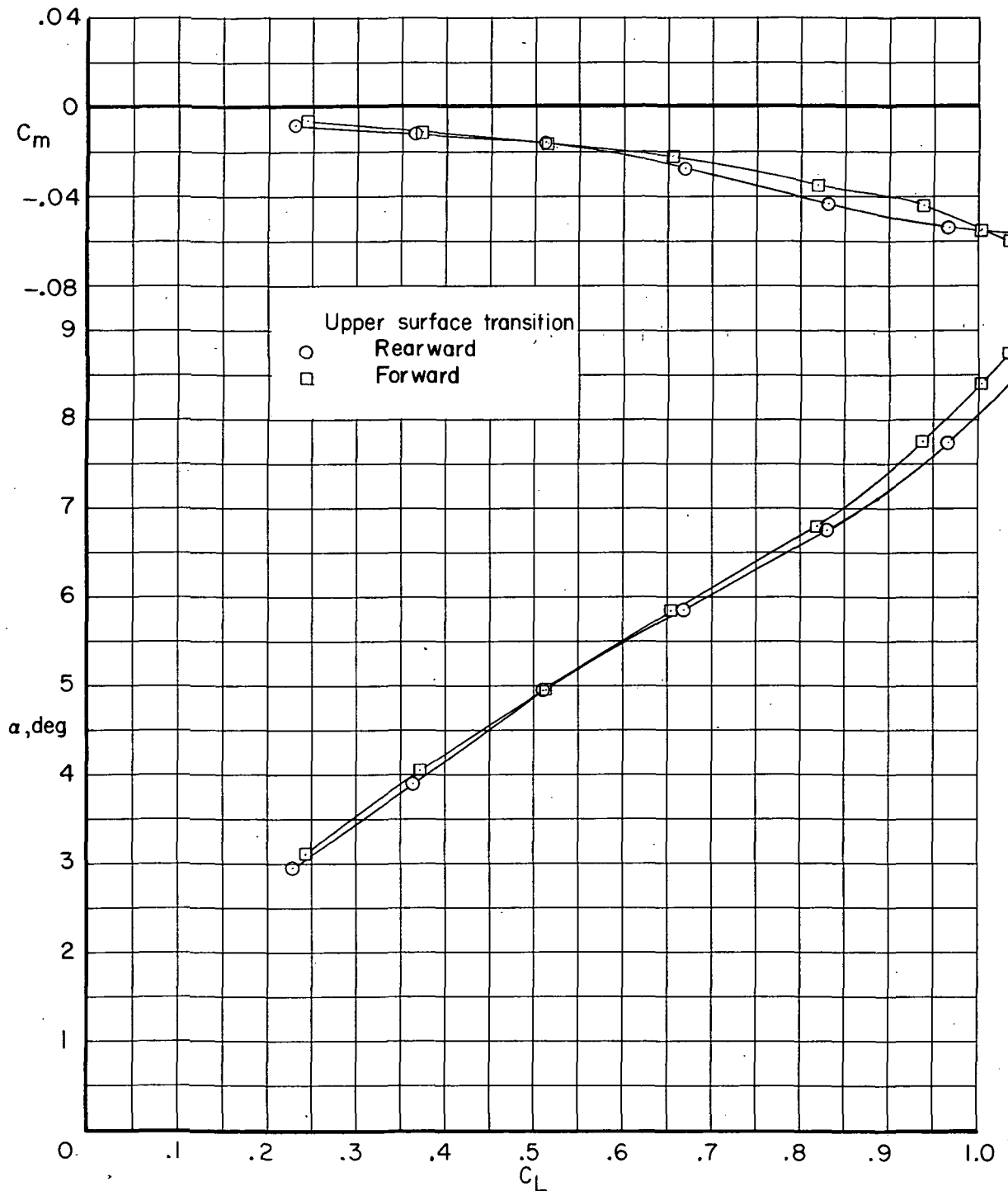


Figure 14.- Effect of upper surface transition location on longitudinal aerodynamic characteristics of configuration with supercritical airfoil C and fuselage fairing. $\Lambda = 26^\circ$; $\delta_h = 2^\circ$; $i_w = -3^\circ$; $M = 0.80$.

Upper surface transition

○ Rearward

□ Forward

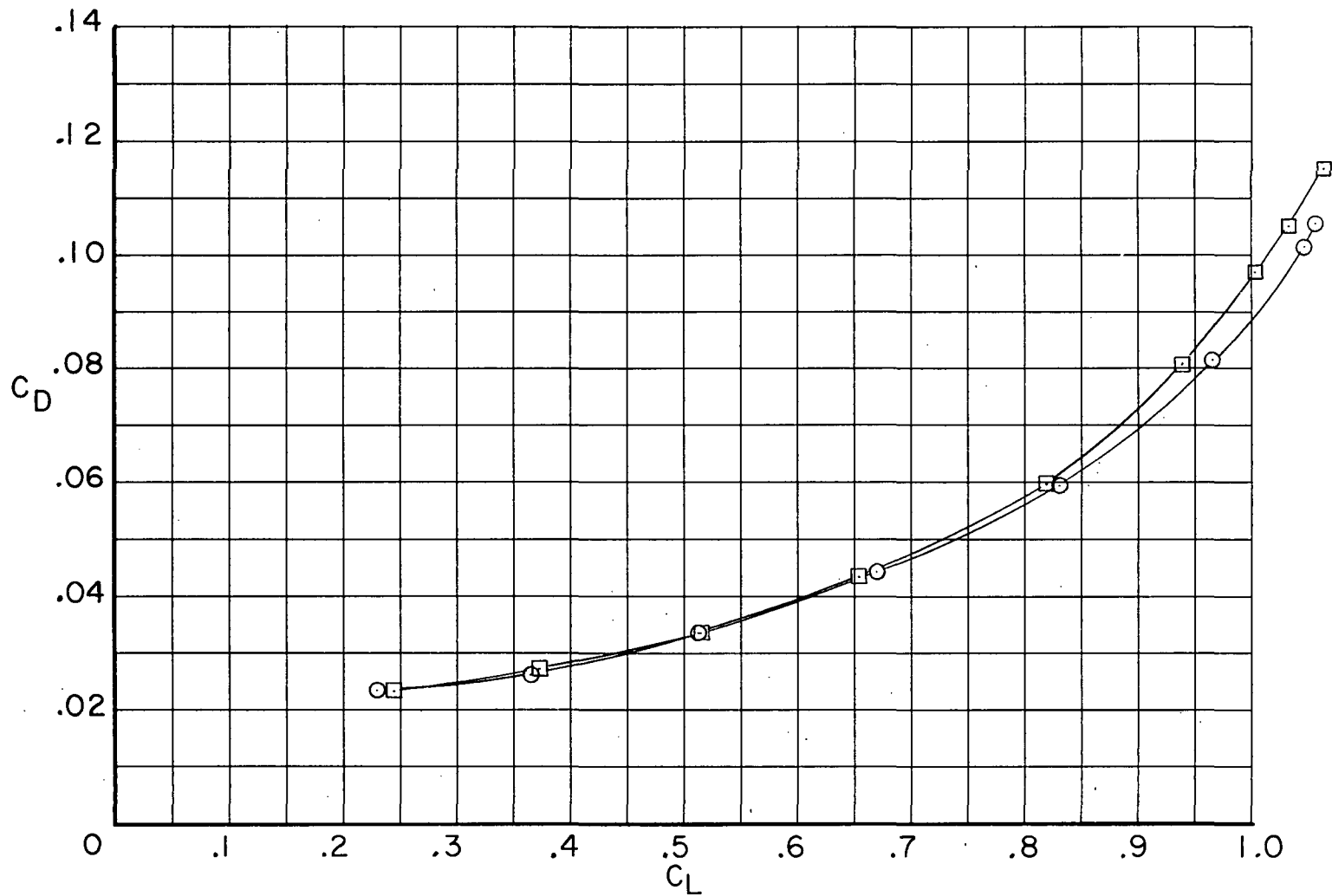
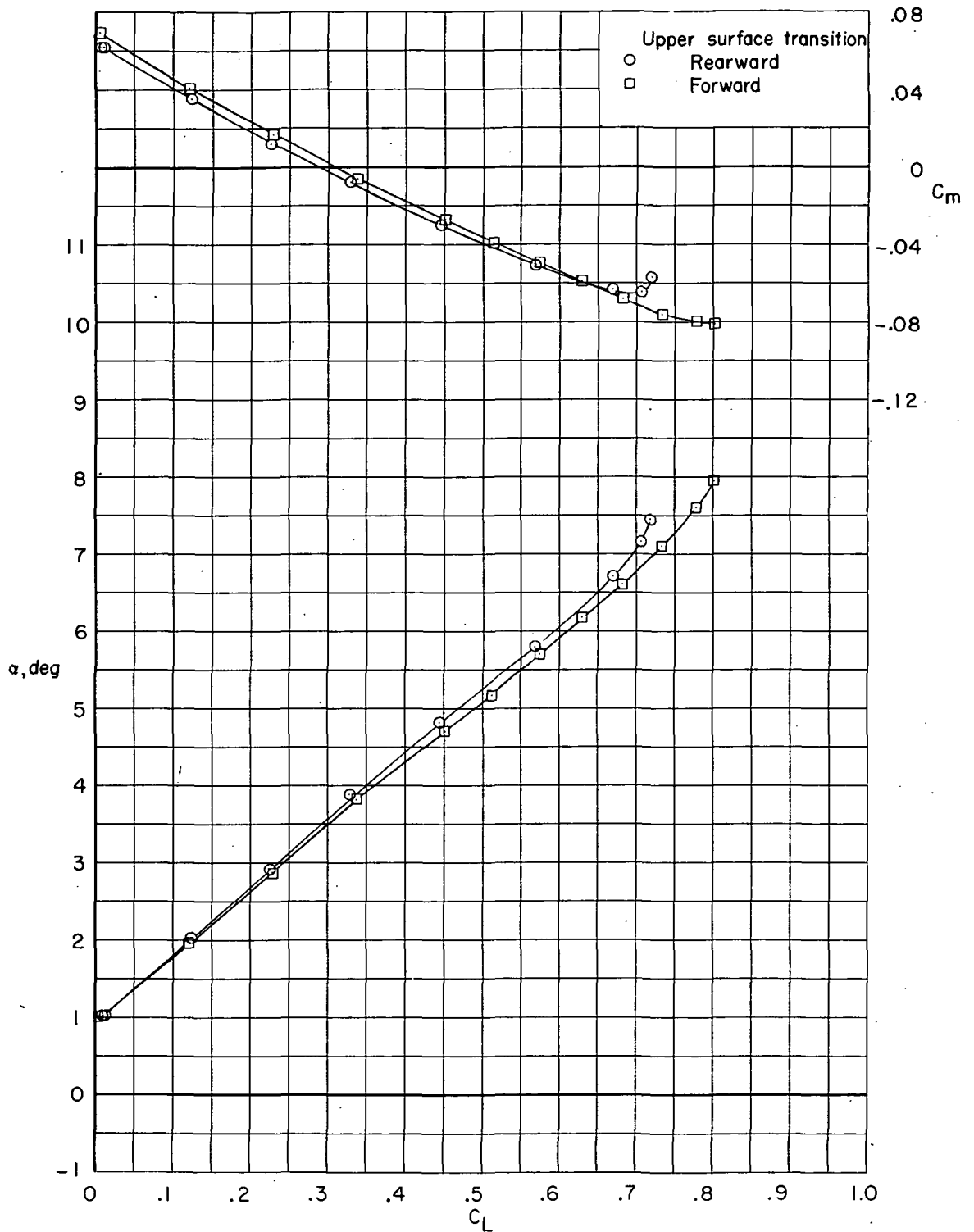
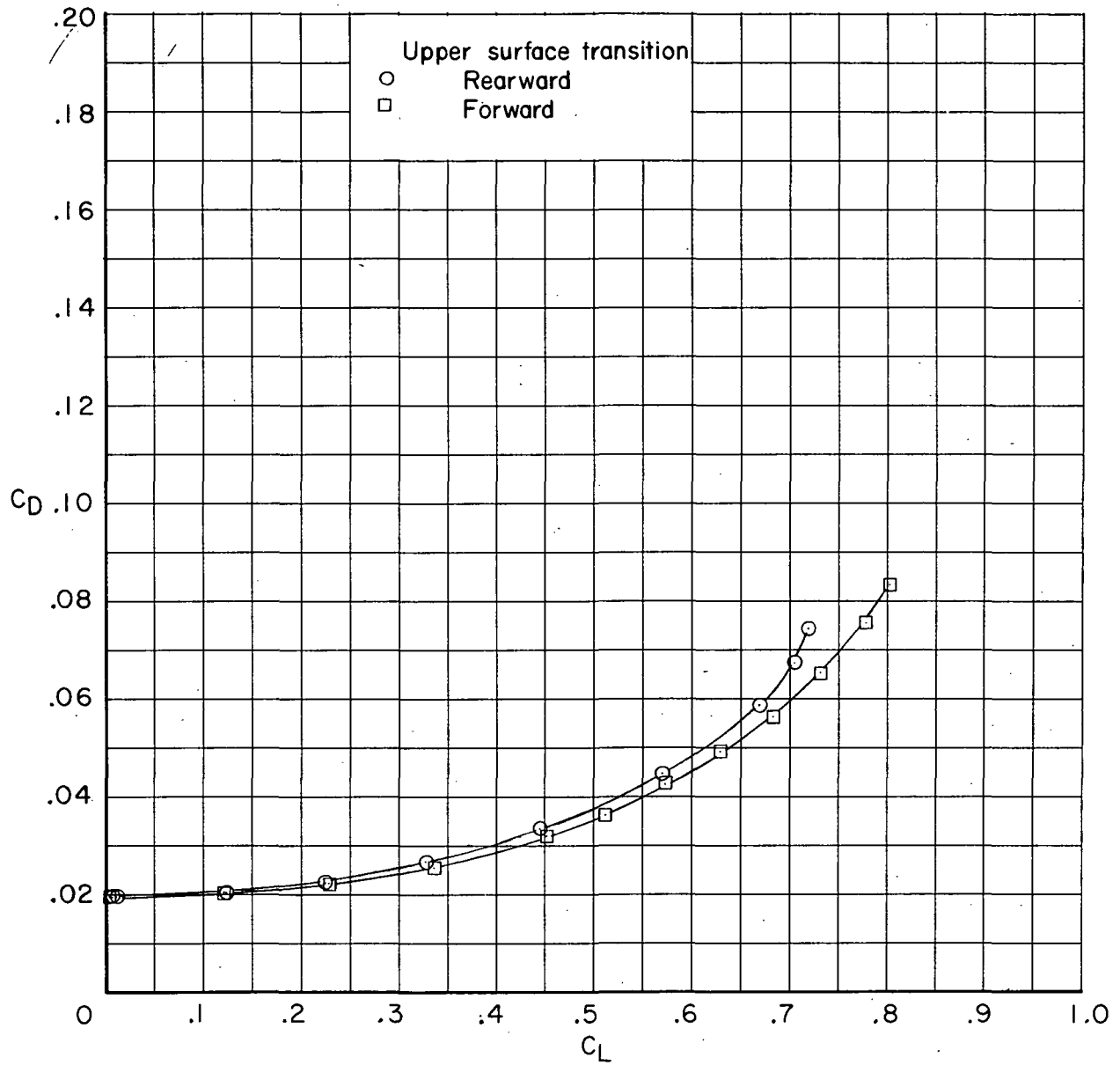


Figure 14.- Concluded.



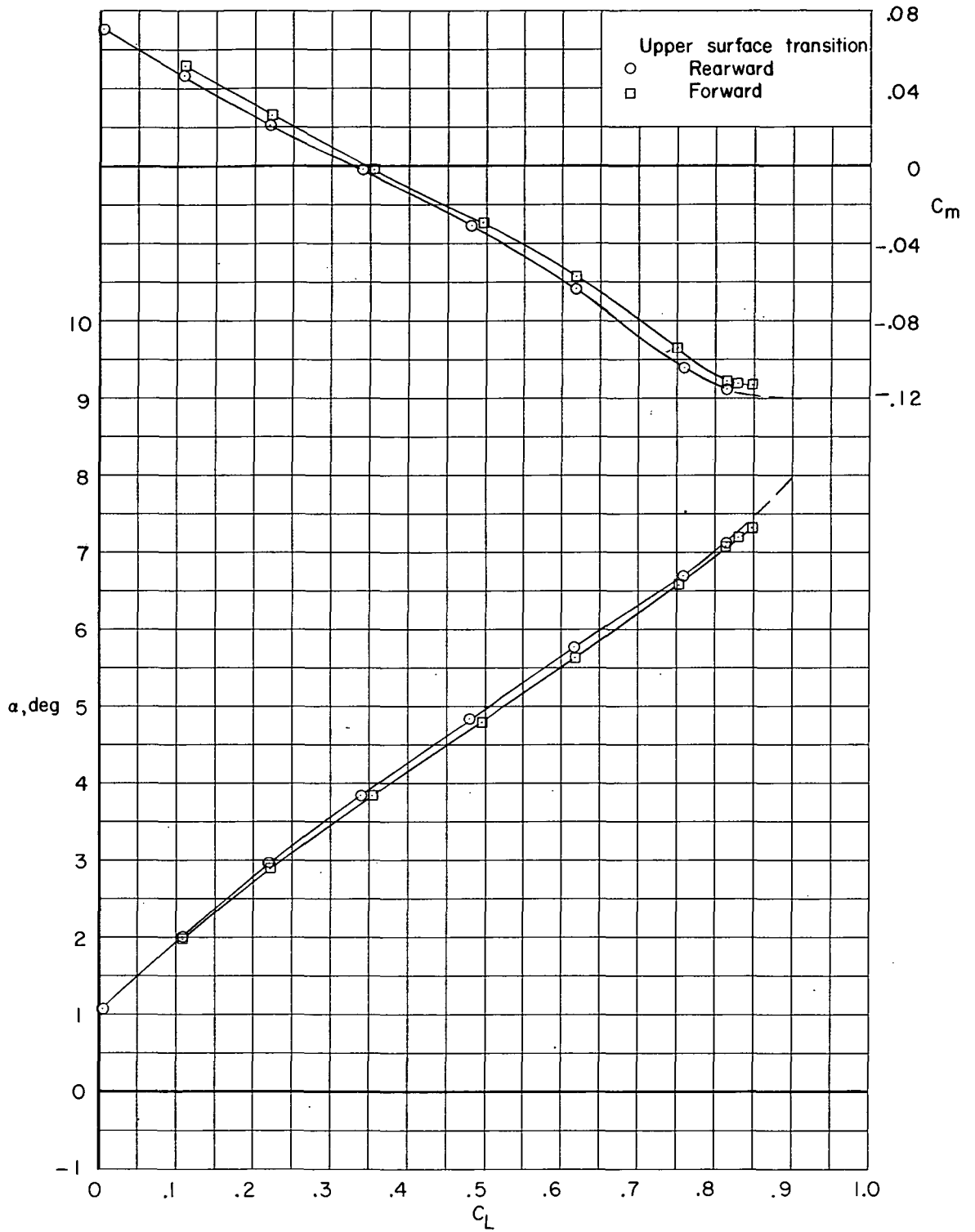
(a) $M = 0.80$.

Figure 15.- Effect of upper surface transition location on longitudinal aerodynamic characteristics of configuration with supercritical airfoil B and fuselage fairing. $\Lambda = 39^\circ$; $\delta_h = 0^\circ$; $i_w = -1^\circ$.



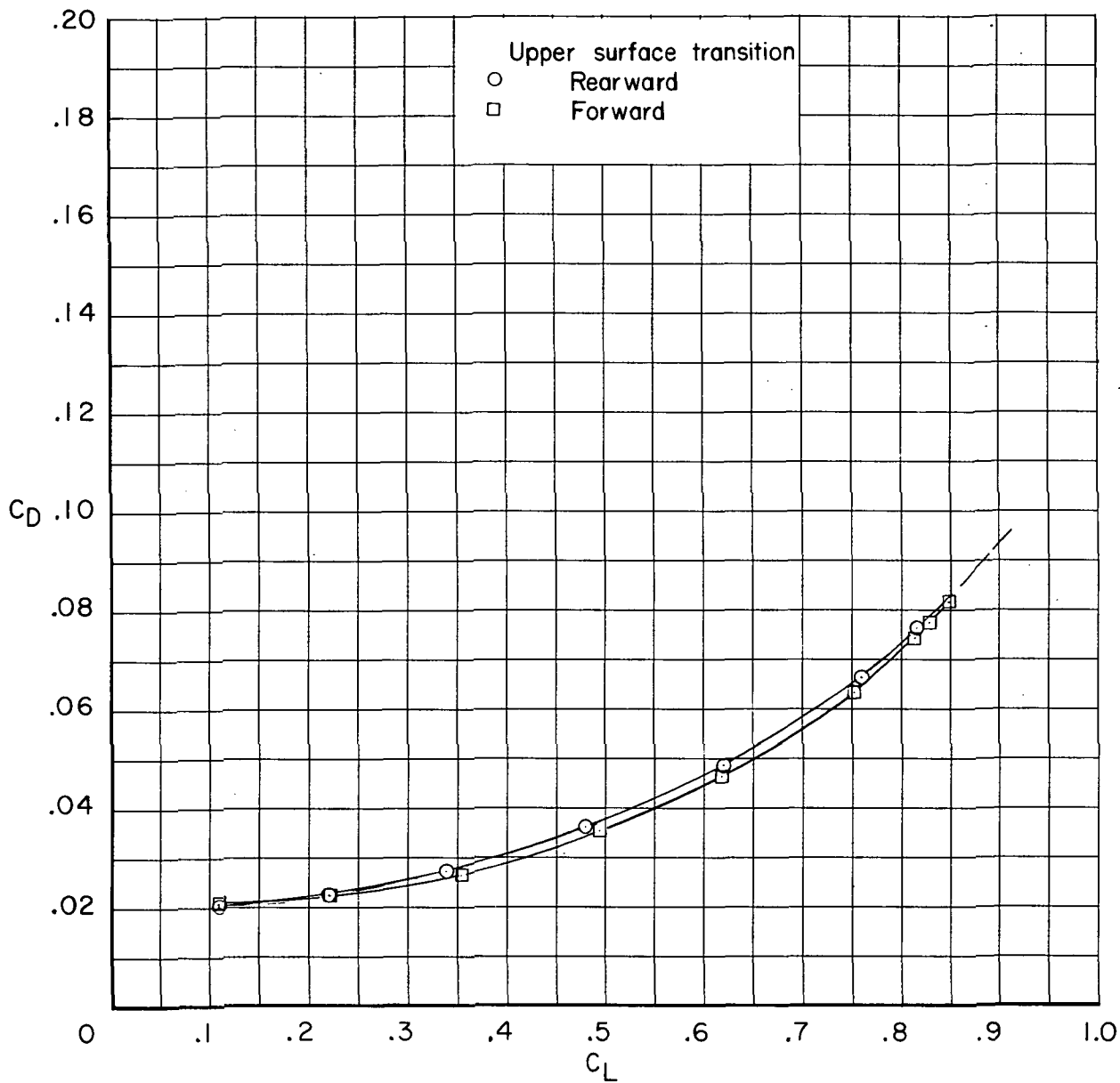
(a) $M = 0.80$. Concluded.

Figure 15.- Continued.



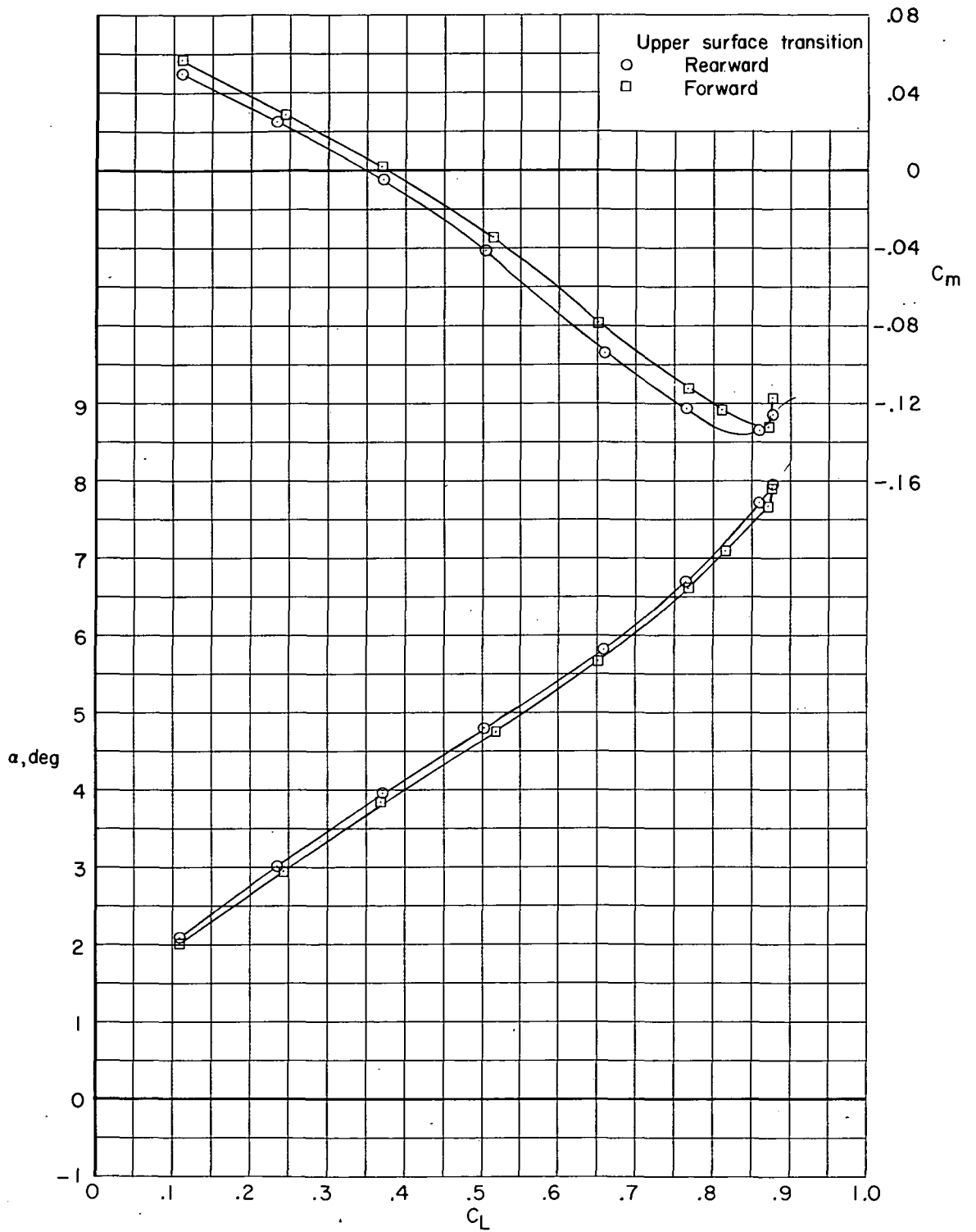
(b) $M = 0.85$.

Figure 15.- Continued.



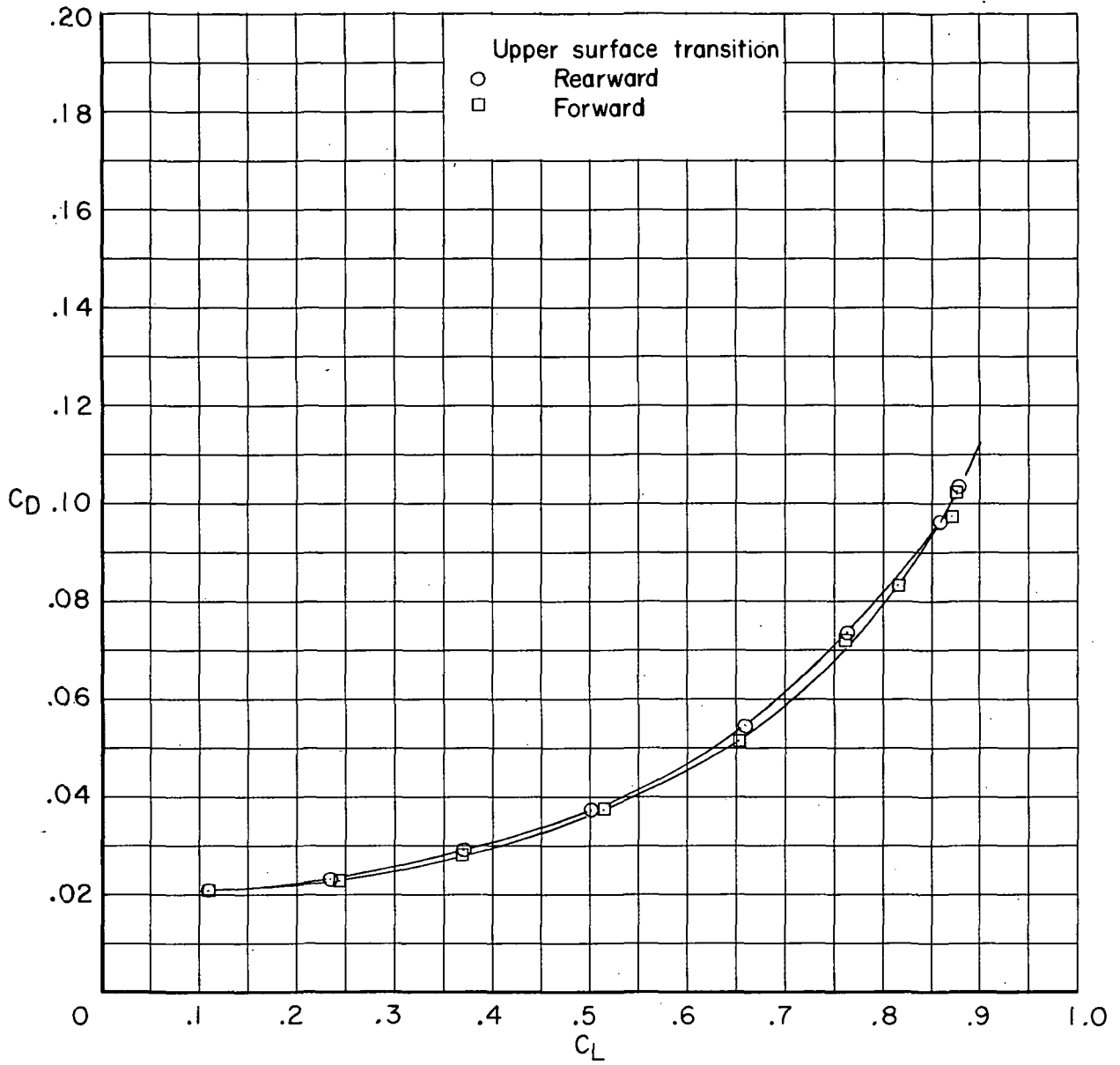
(b) $M = 0.85$. Concluded.

Figure 15. - Continued.



(c) $M = 0.88$.

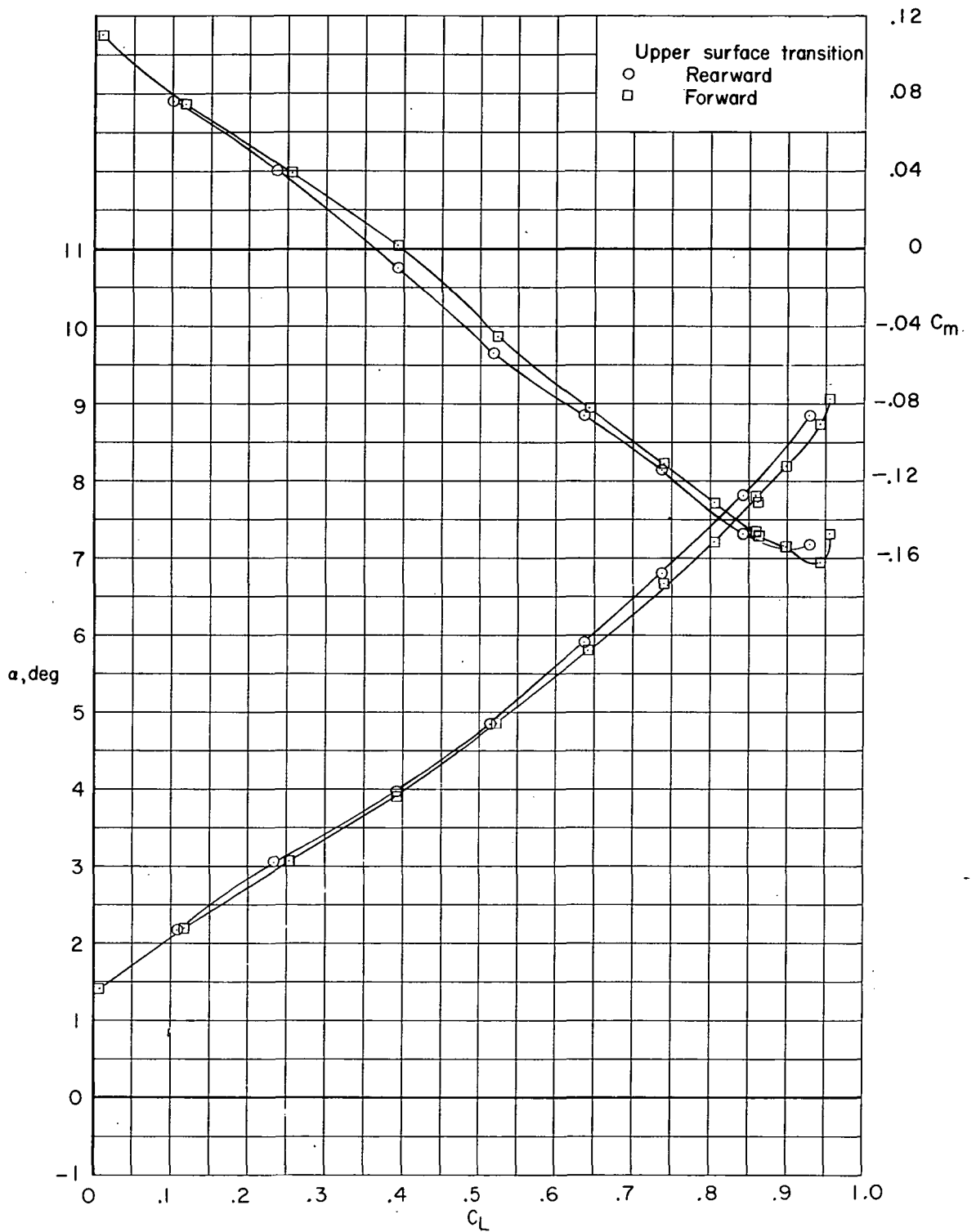
Figure 15.- Continued.



(c) $M = 0.88$. Concluded.

Figure 15.- Continued.

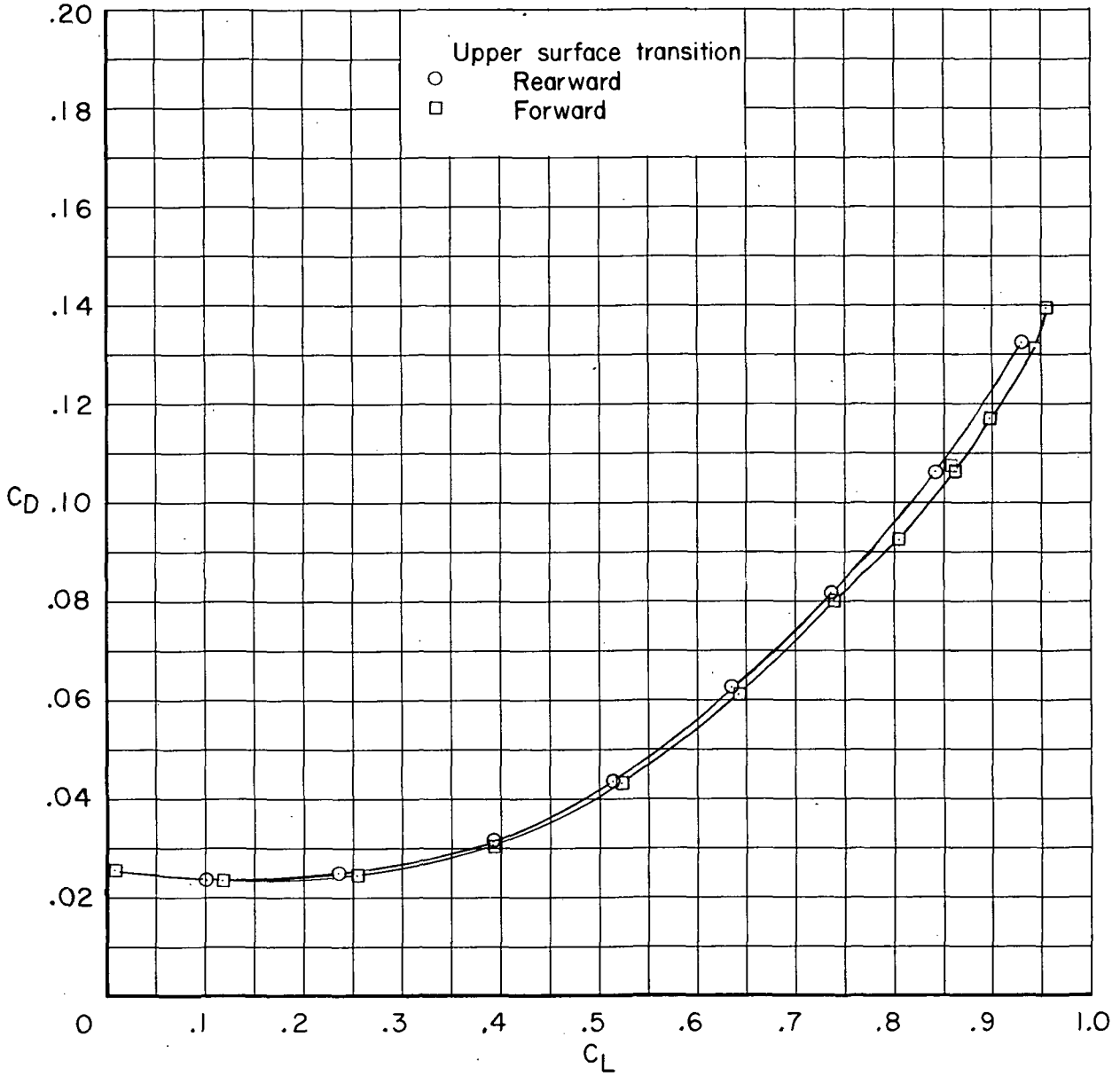
~~CONFIDENTIAL~~



(d) $M = 0.91$.

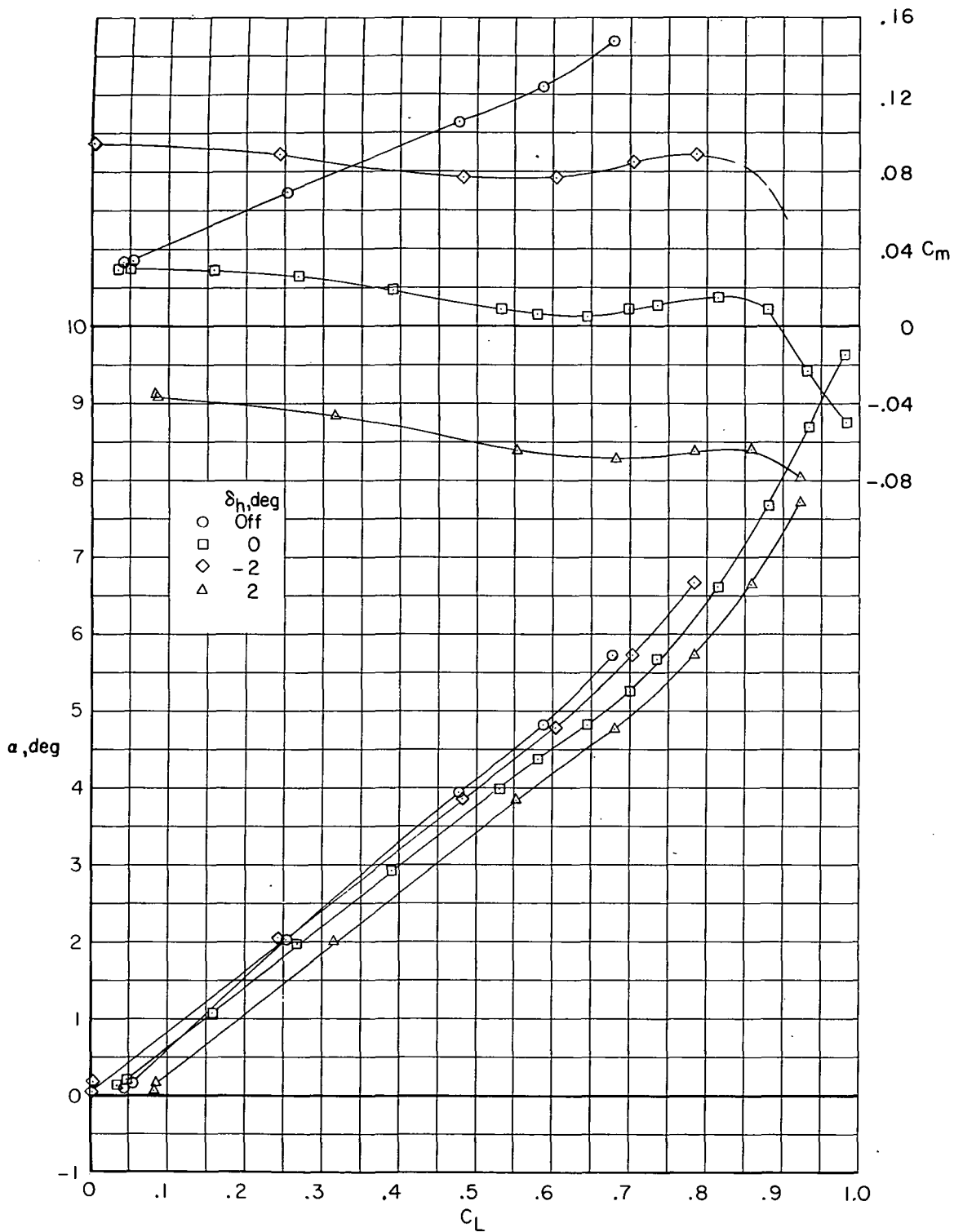
Figure 15.- Continued.

~~CONFIDENTIAL~~



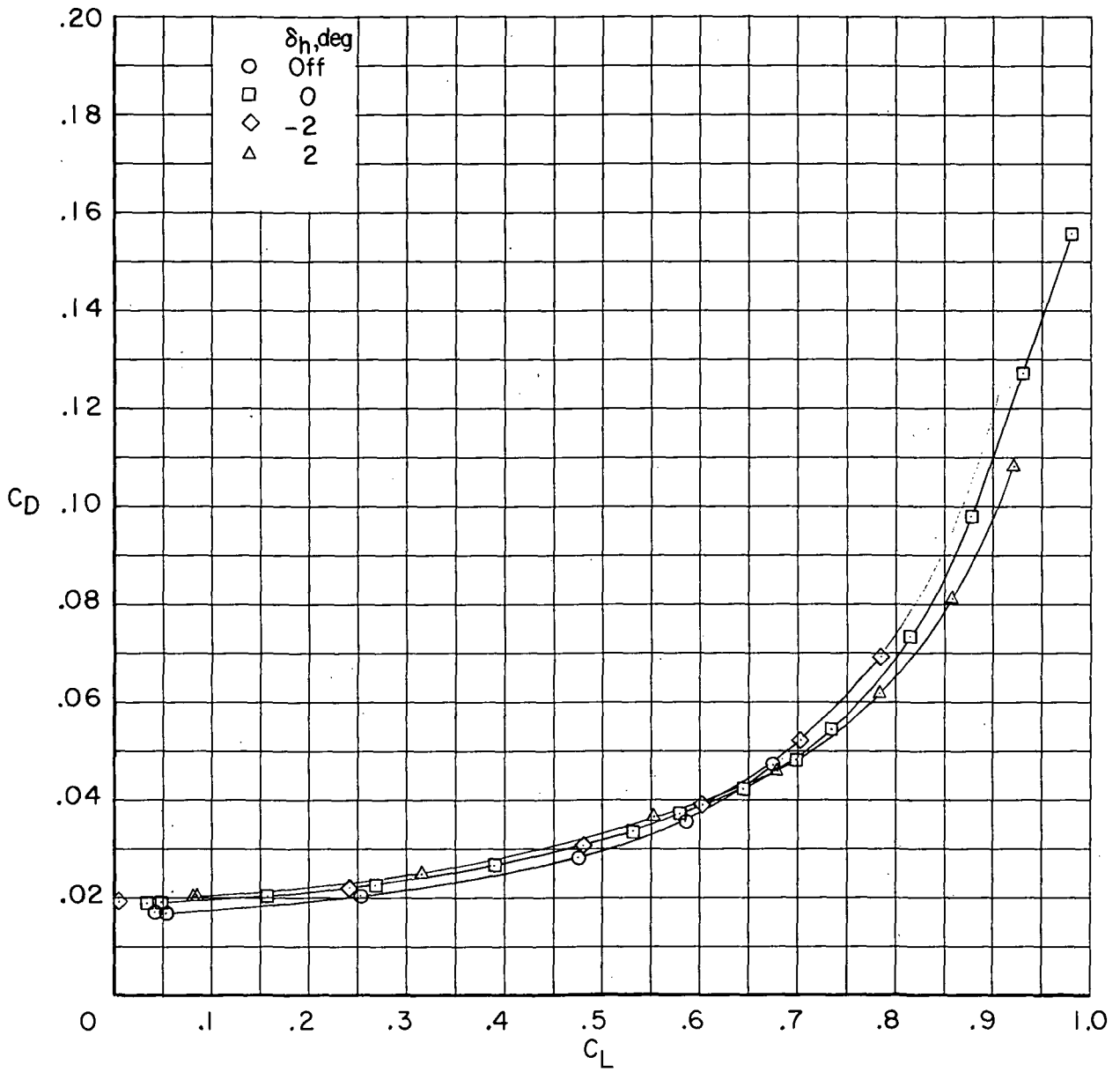
(d) $M = 0.91$. Concluded.

Figure 15.- Concluded.



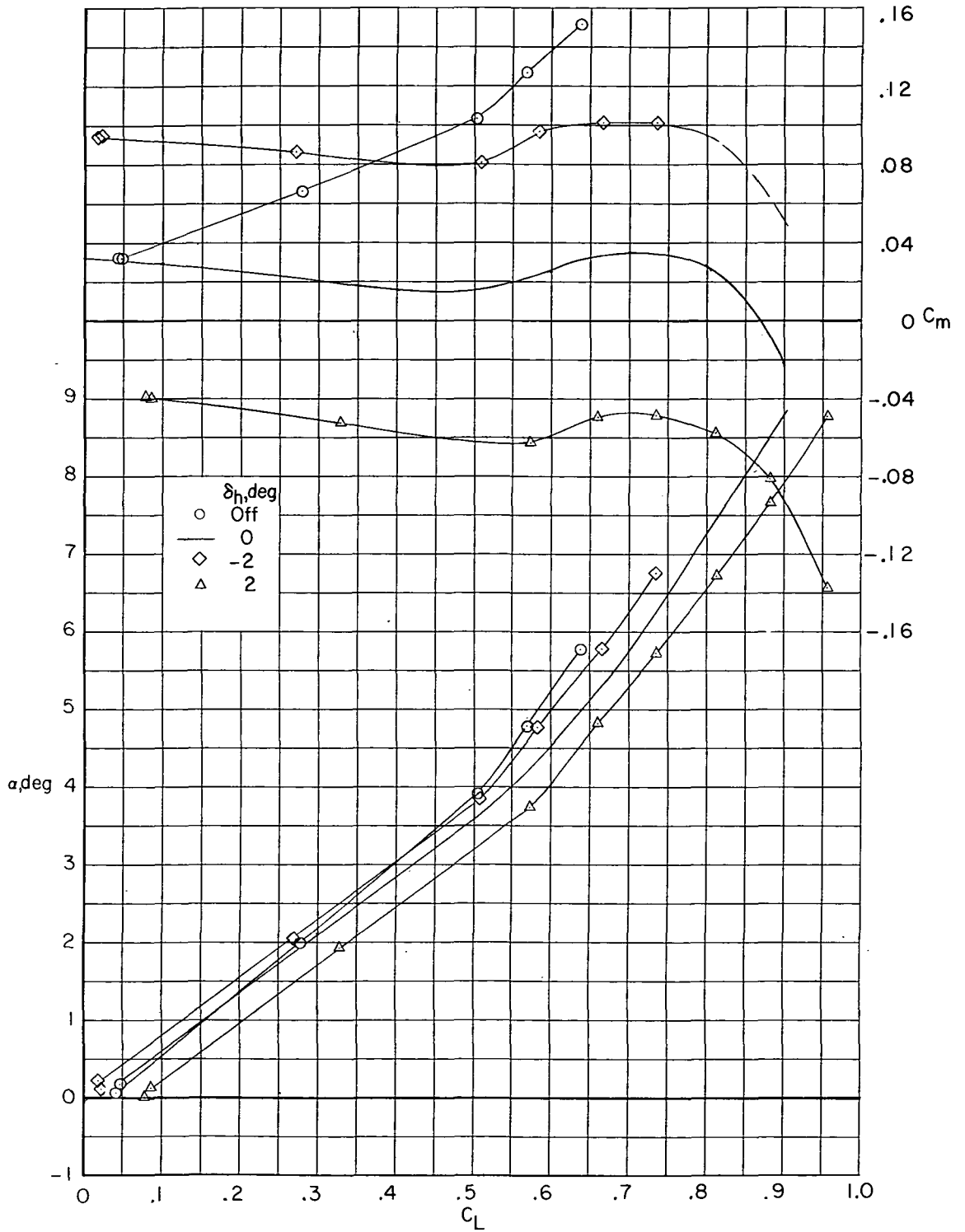
(a) $M = 0.75$.

Figure 16.- Effect of horizontal-tail deflection on longitudinal aerodynamic characteristics of configuration with NACA 64A2XX airfoil, fuselage fairing, and transition rearward. $\Lambda = 26^\circ$; $i_w = 1^\circ$.



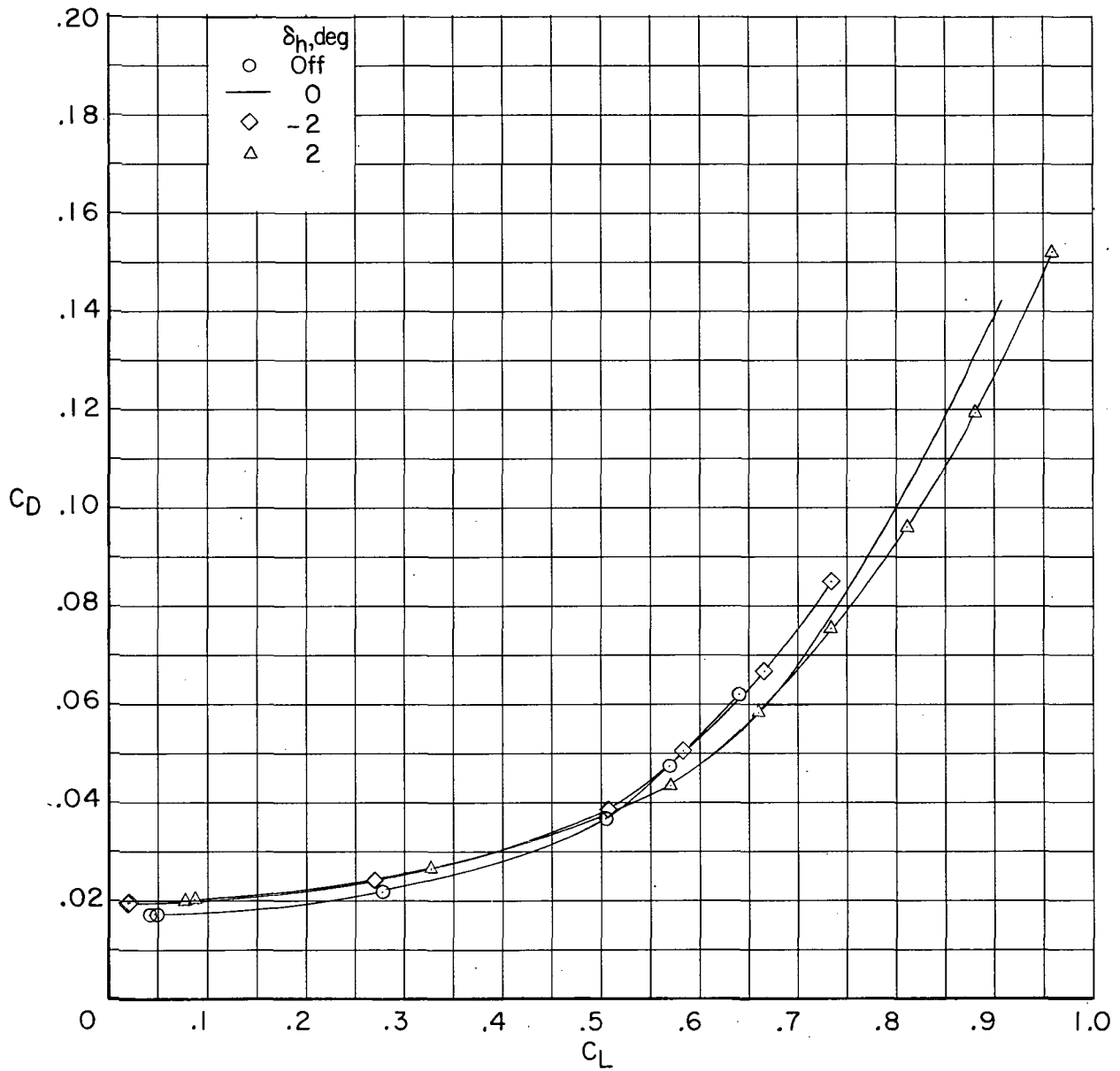
(a) $M = 0.75$. Concluded.

Figure 16.- Continued.



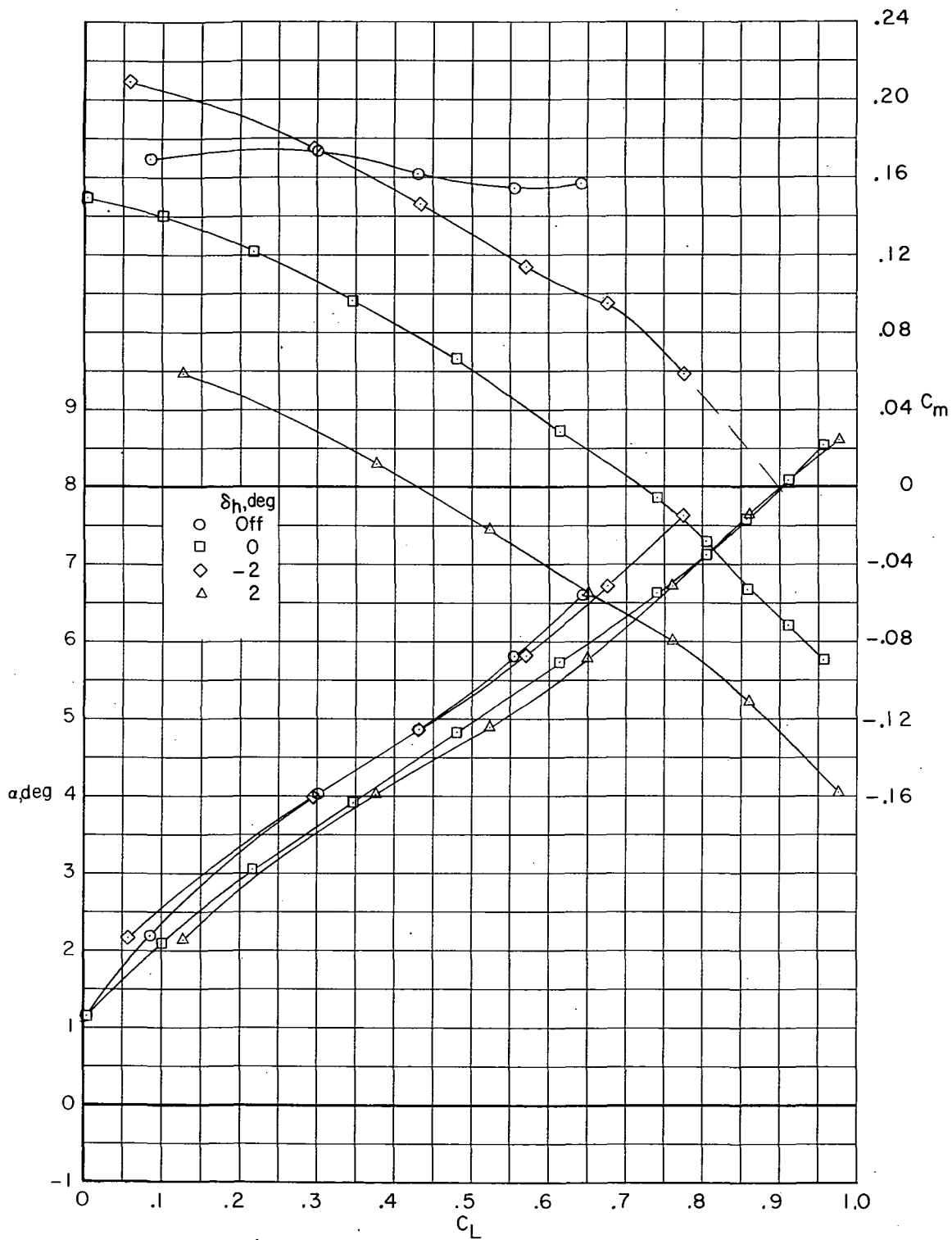
(b) $M = 0.80$.

Figure 16.- Continued.



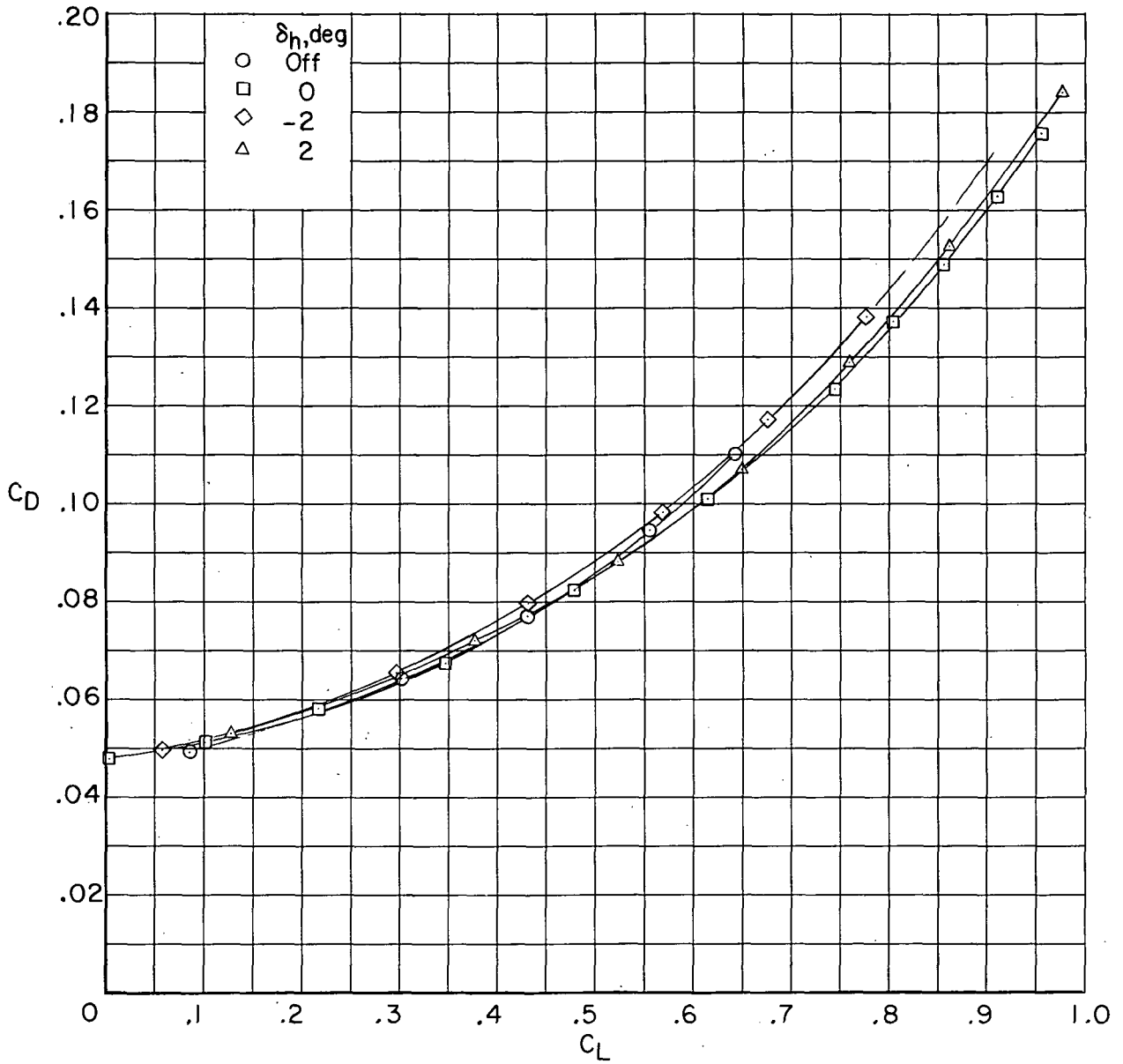
(b) $M = 0.80$. Concluded.

Figure 16.- Continued.



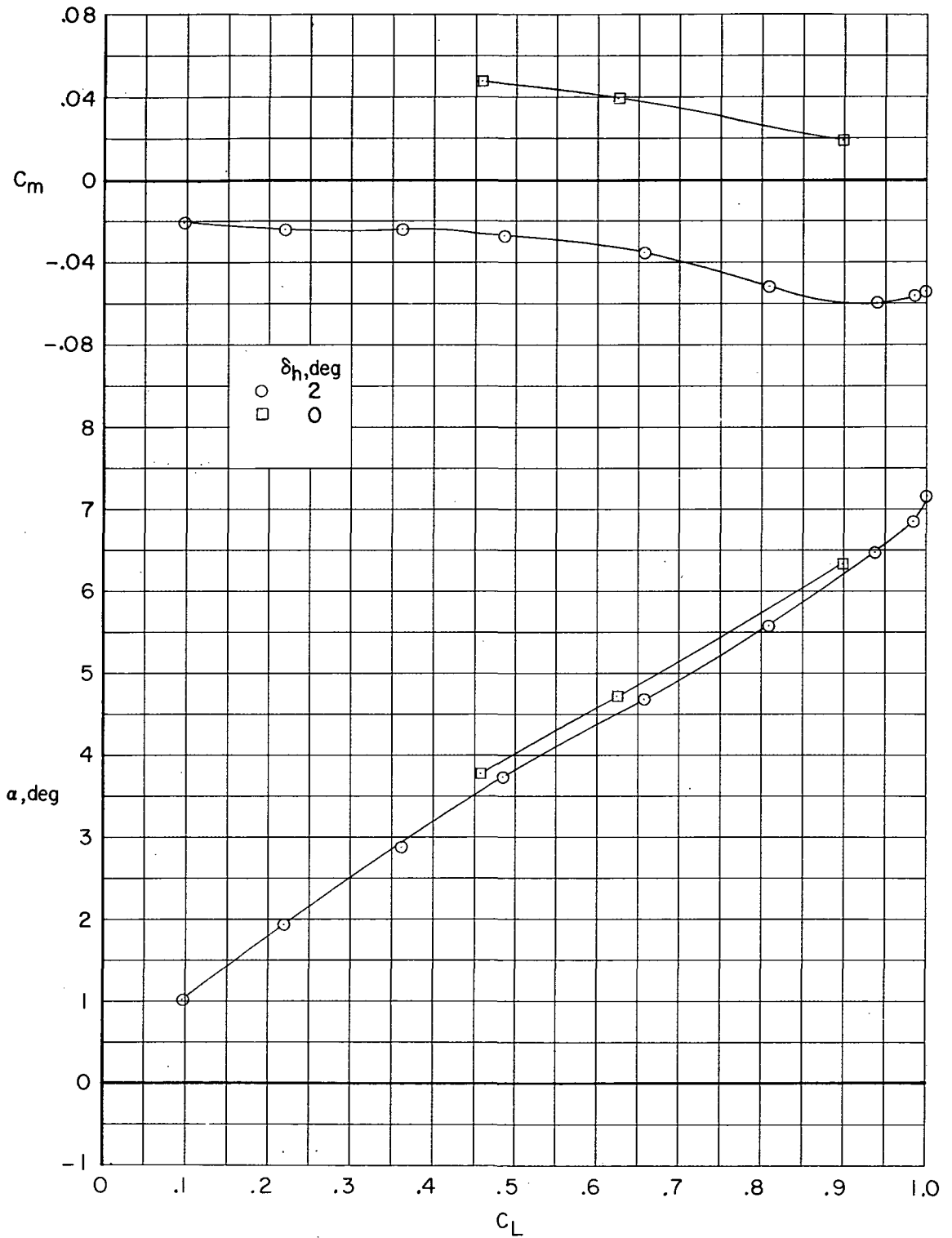
(c) $M = 0.91$.

Figure 16. - Continued.



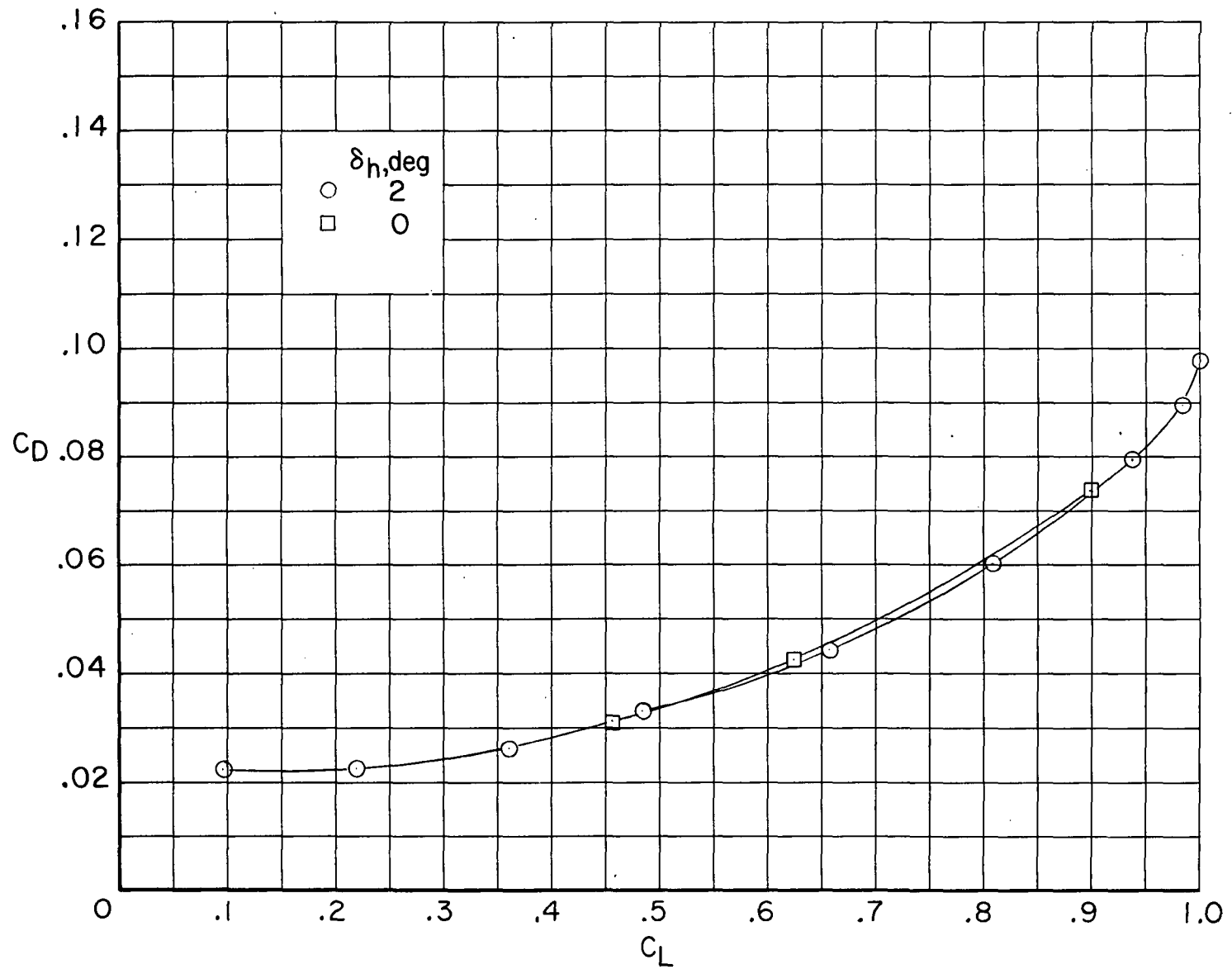
(c) $M = 0.91$. Concluded.

Figure 16.- Concluded.



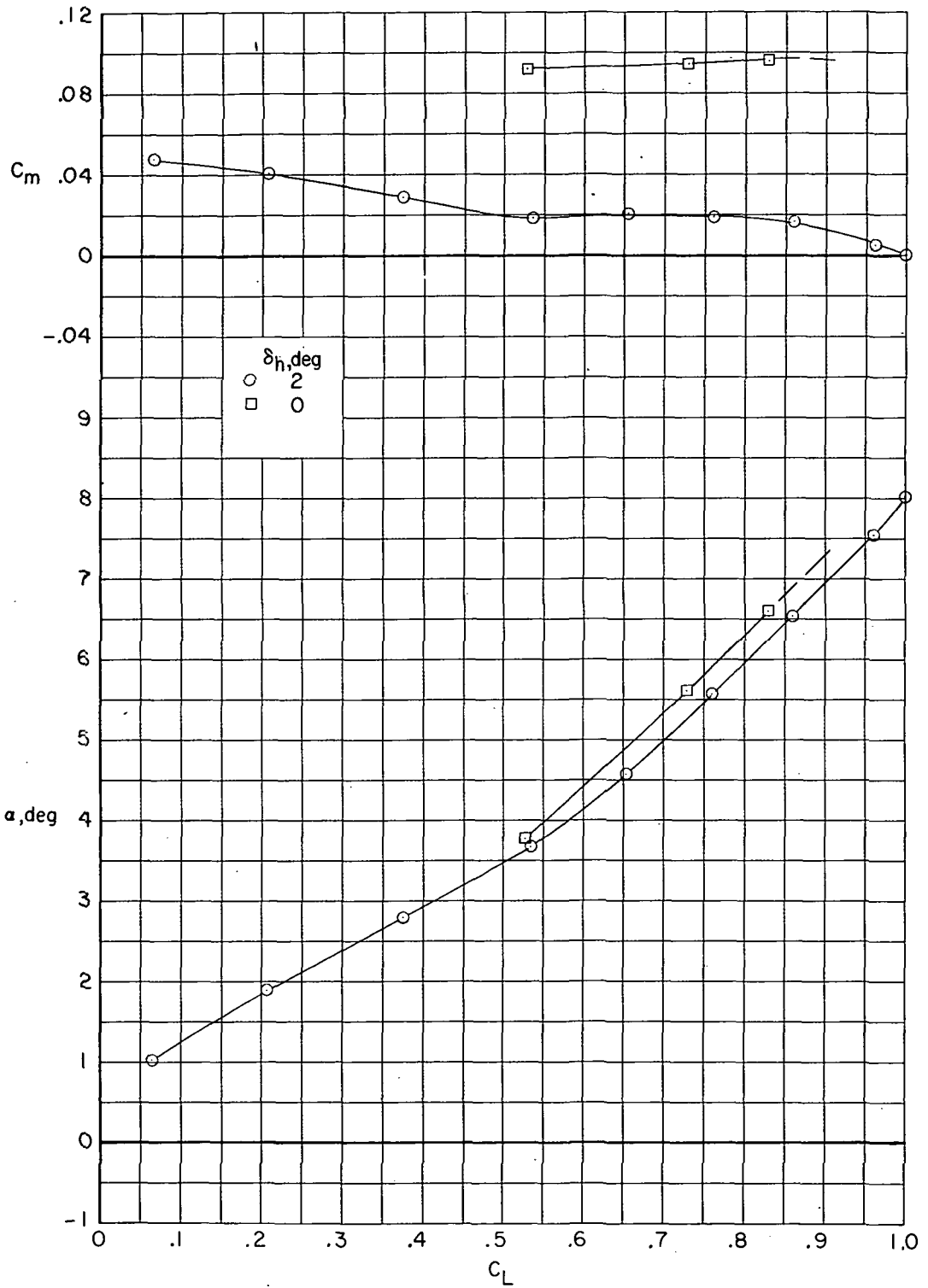
(a) $M = 0.80$.

Figure 17.- Effect of horizontal-tail deflection on longitudinal aerodynamic characteristics of configuration with supercritical airfoil B, fuselage fairing, and transition rearward. $\Lambda = 26^\circ$; $i_w = -1^\circ$.



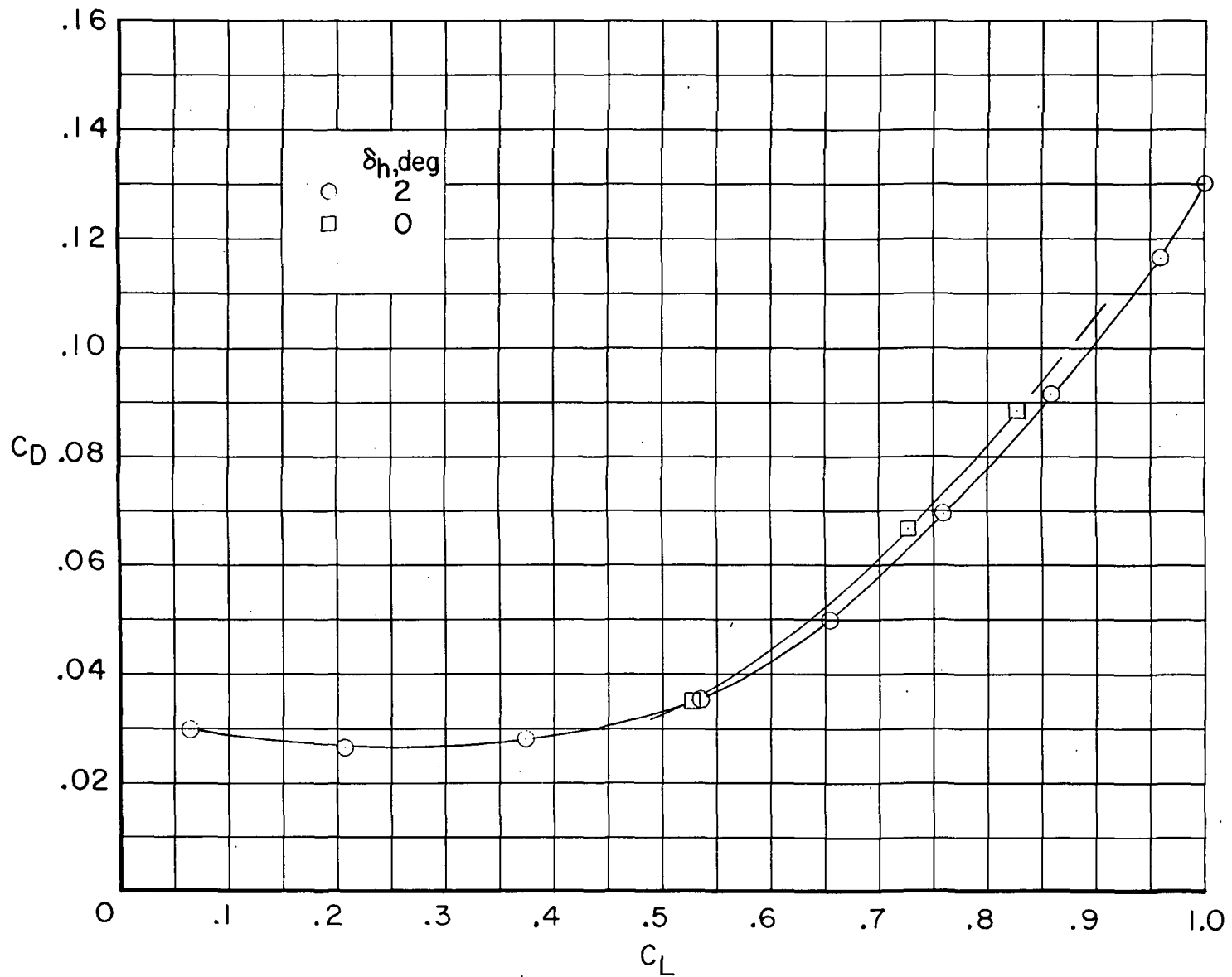
(a) $M = 0.80$. Concluded.

Figure 17.- Continued.



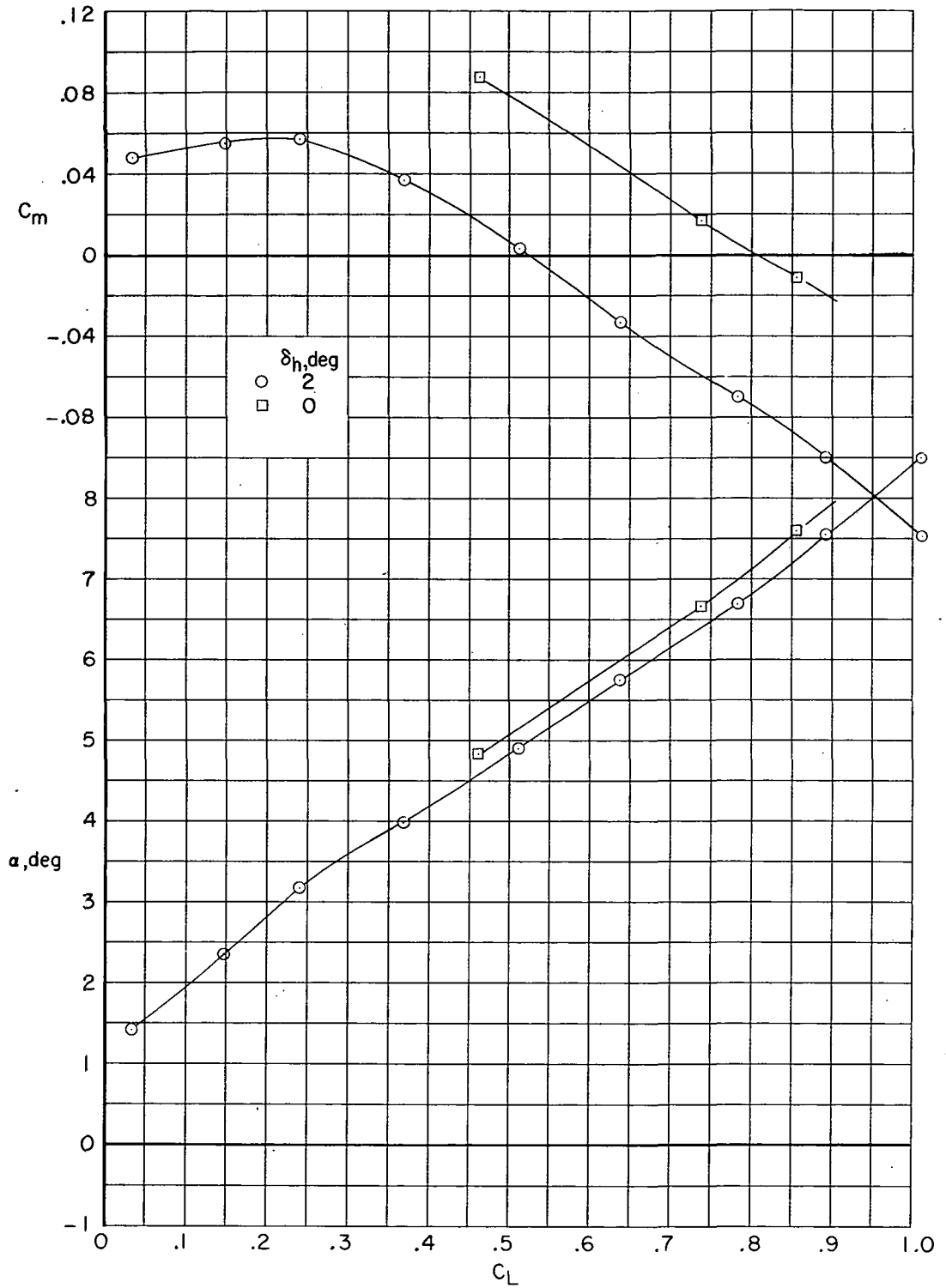
(b) $M = 0.85$.

Figure 17. - Continued.



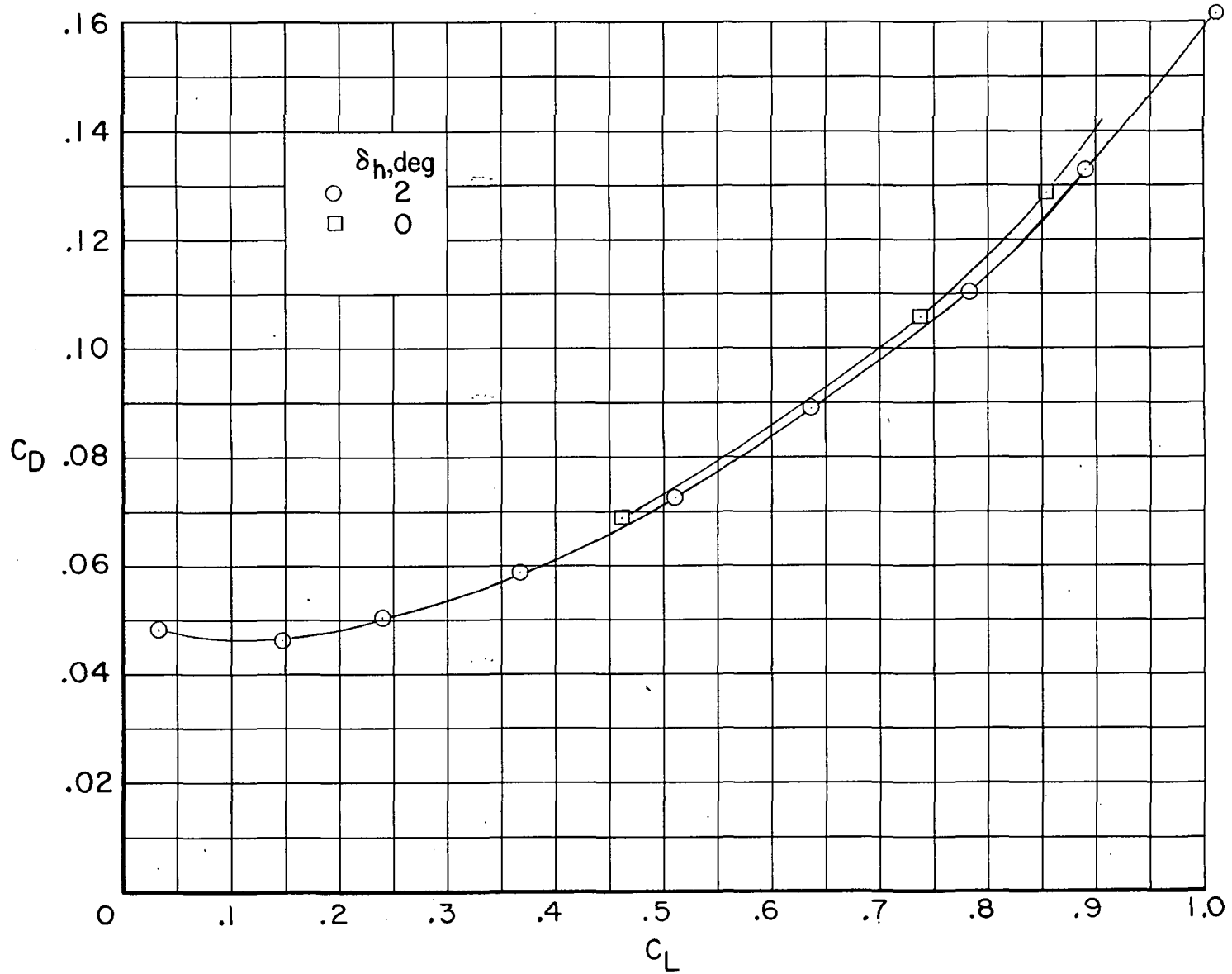
(b) $M = 0.85$. Concluded.

Figure 17.- Continued.



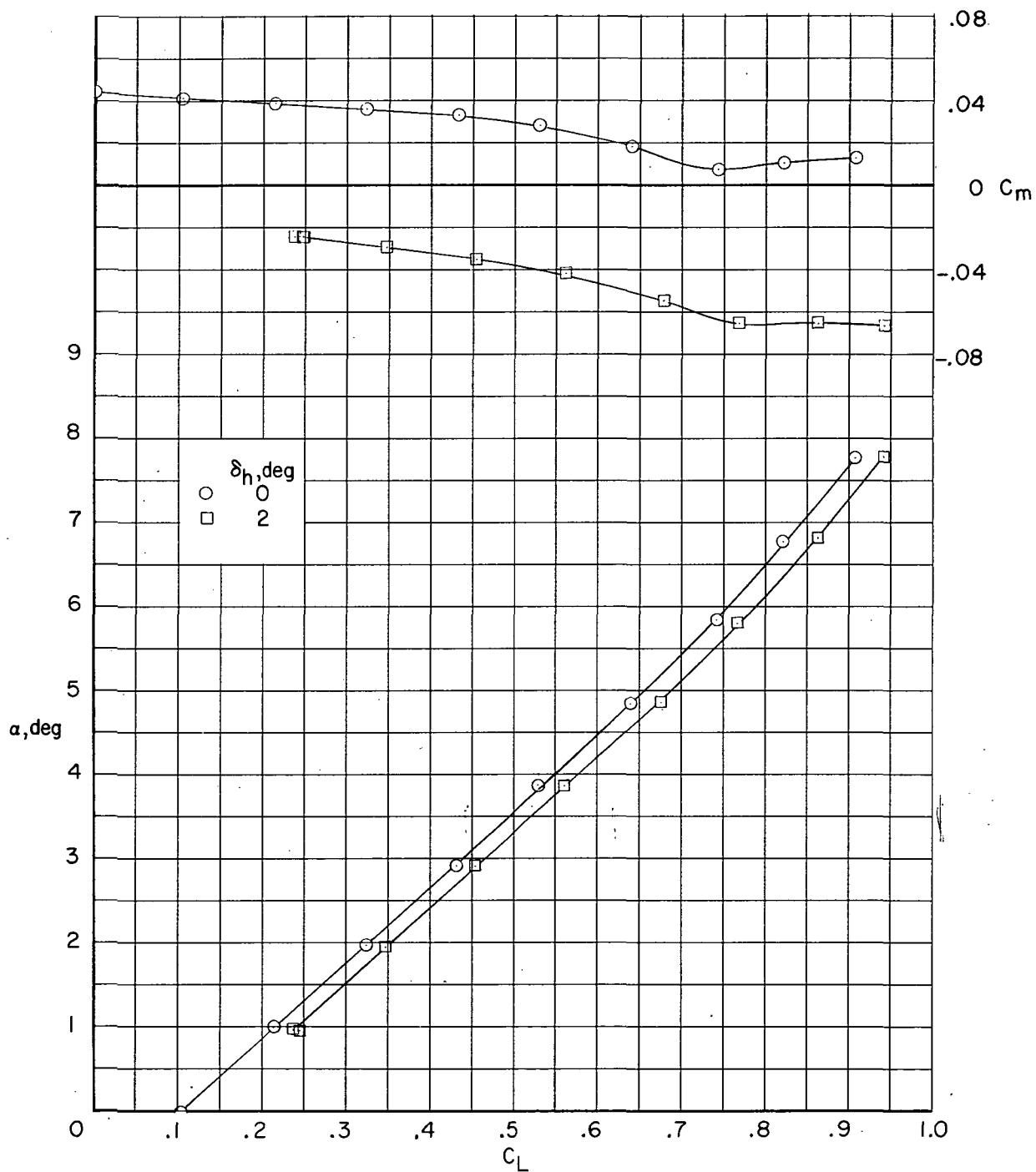
(c) $M = 0.91$.

Figure 17.- Continued.



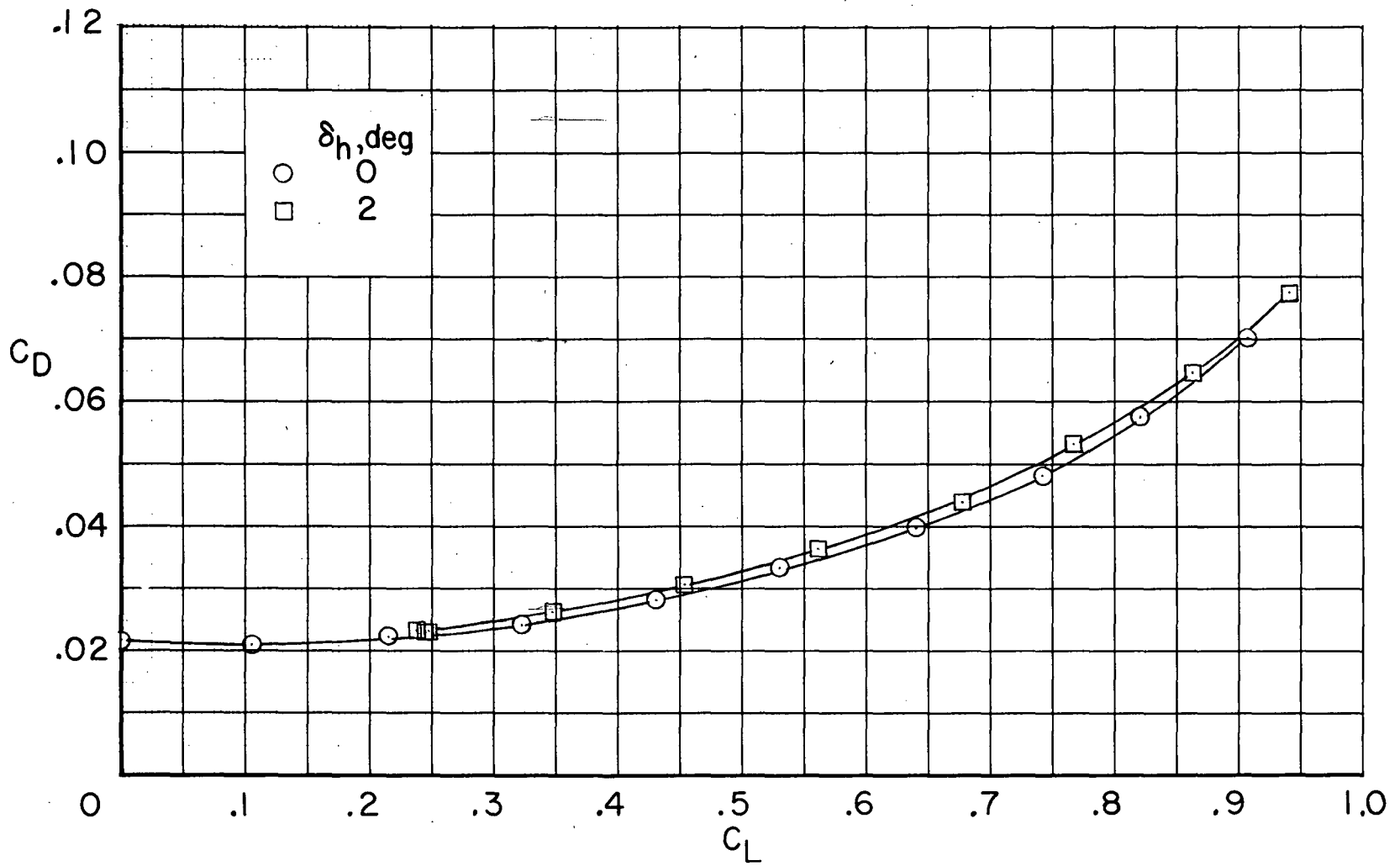
(c) $M = 0.91$. Concluded.

Figure 17.- Concluded.



(a) $M = 0.60$.

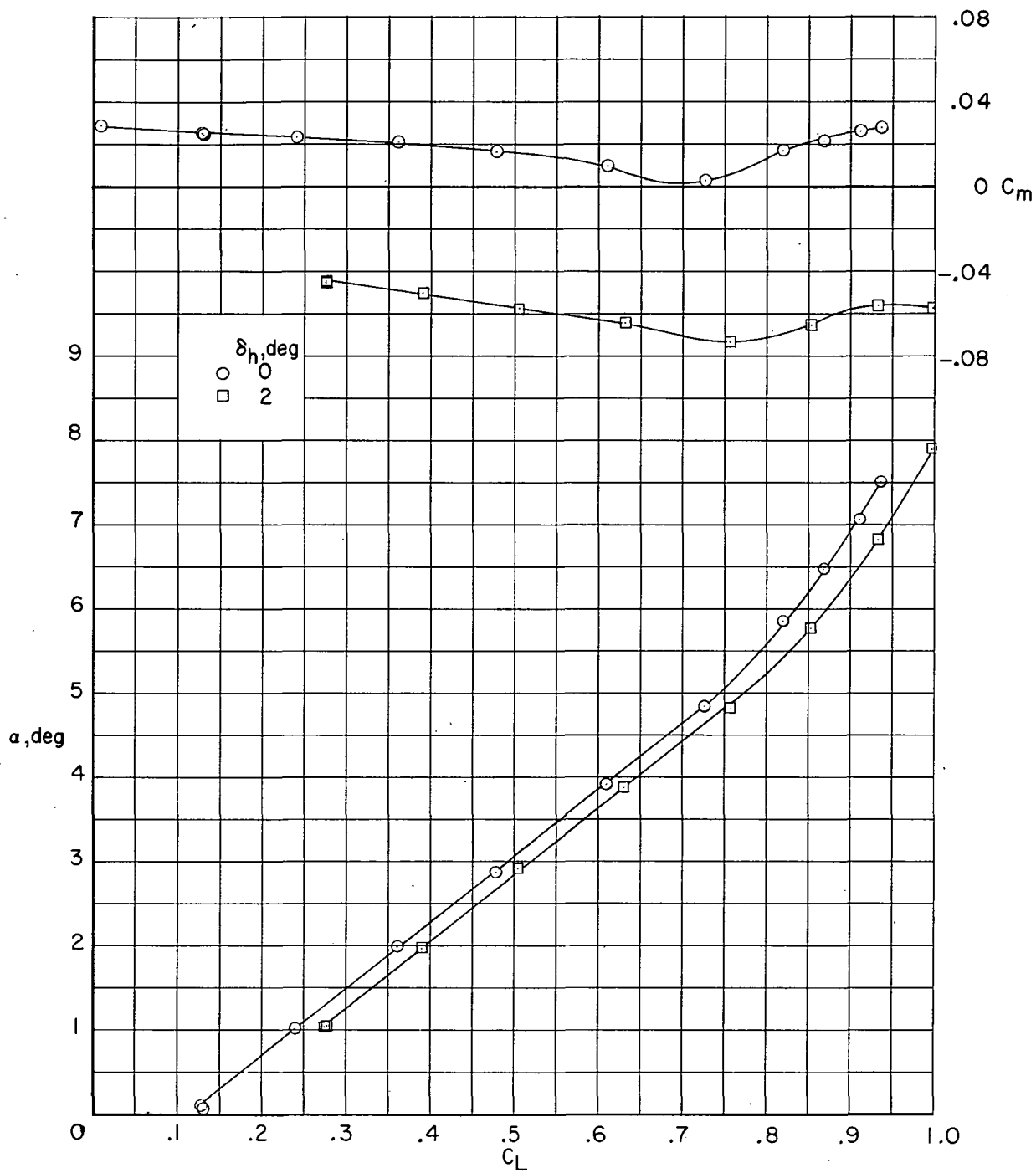
Figure 18.- Effect of horizontal-tail deflection on longitudinal aerodynamic characteristics in pitch of configuration with NACA 64A4XX airfoil, fuselage fairing, and transition rearward. $\Lambda = 26^\circ$; $i_w = 1^\circ$.



(a) $M = 0.60$. Concluded.

Figure 18.- Continued.

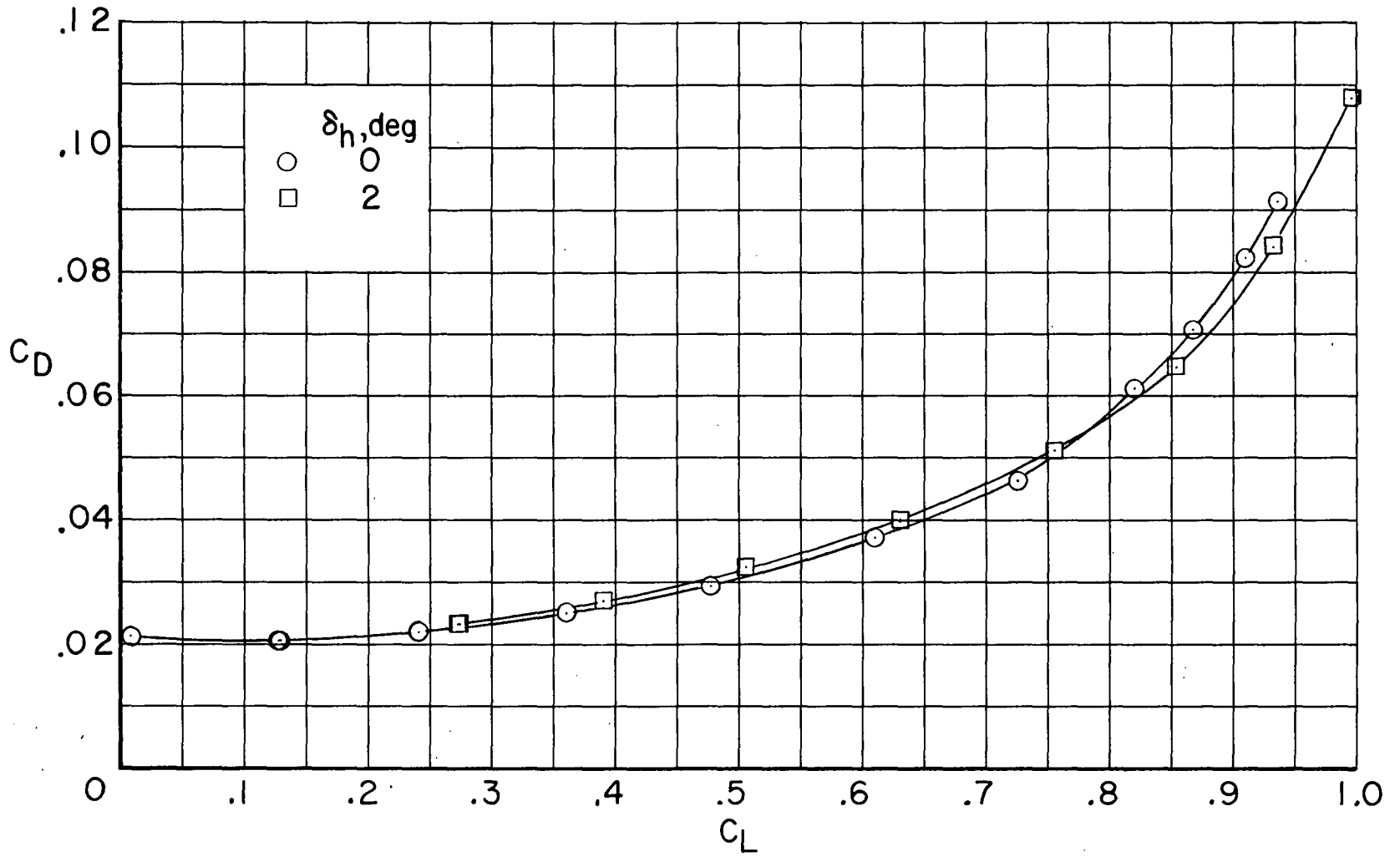
~~CONFIDENTIAL~~



(b) $M = 0.75$.

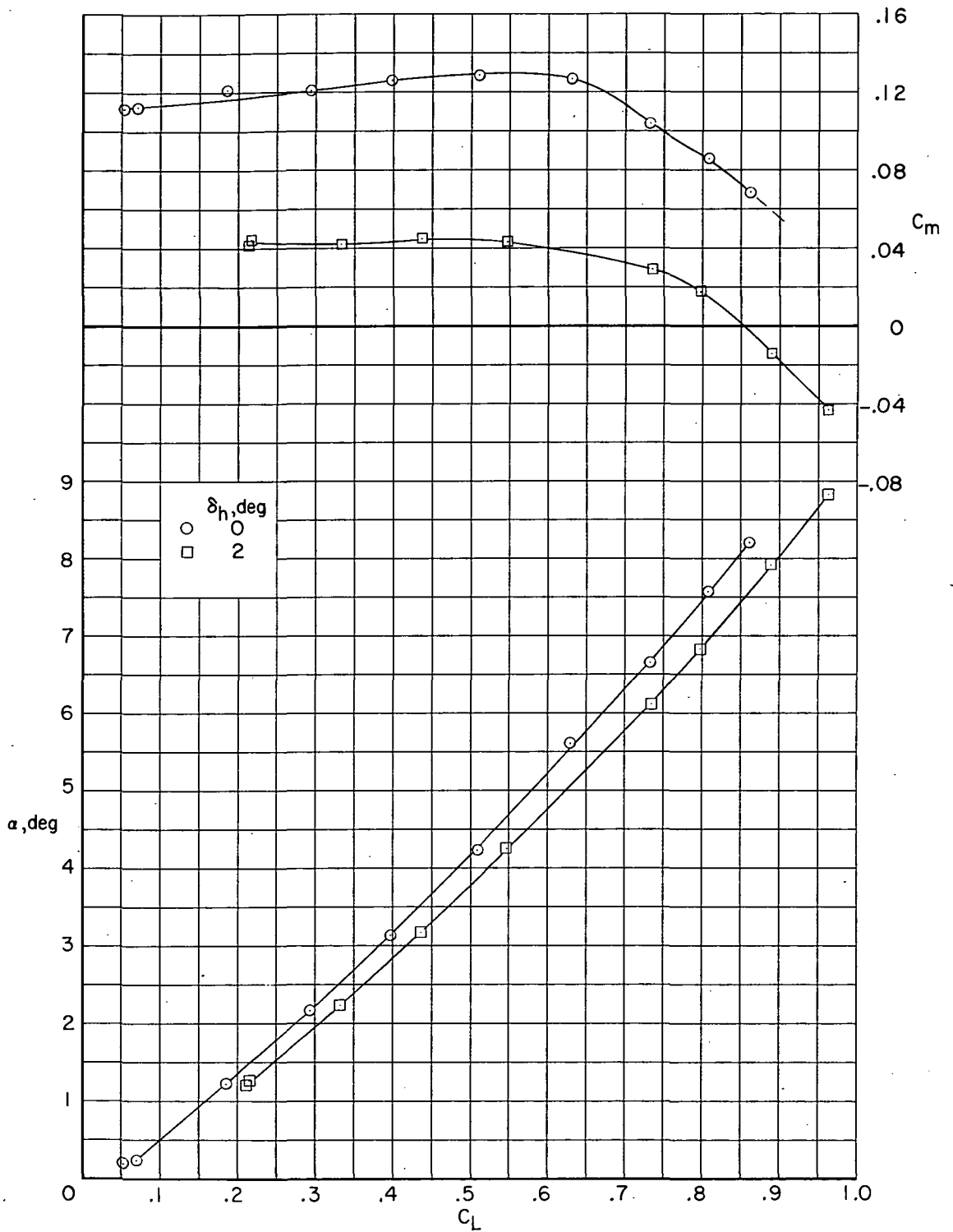
Figure 18.- Continued.

~~CONFIDENTIAL~~



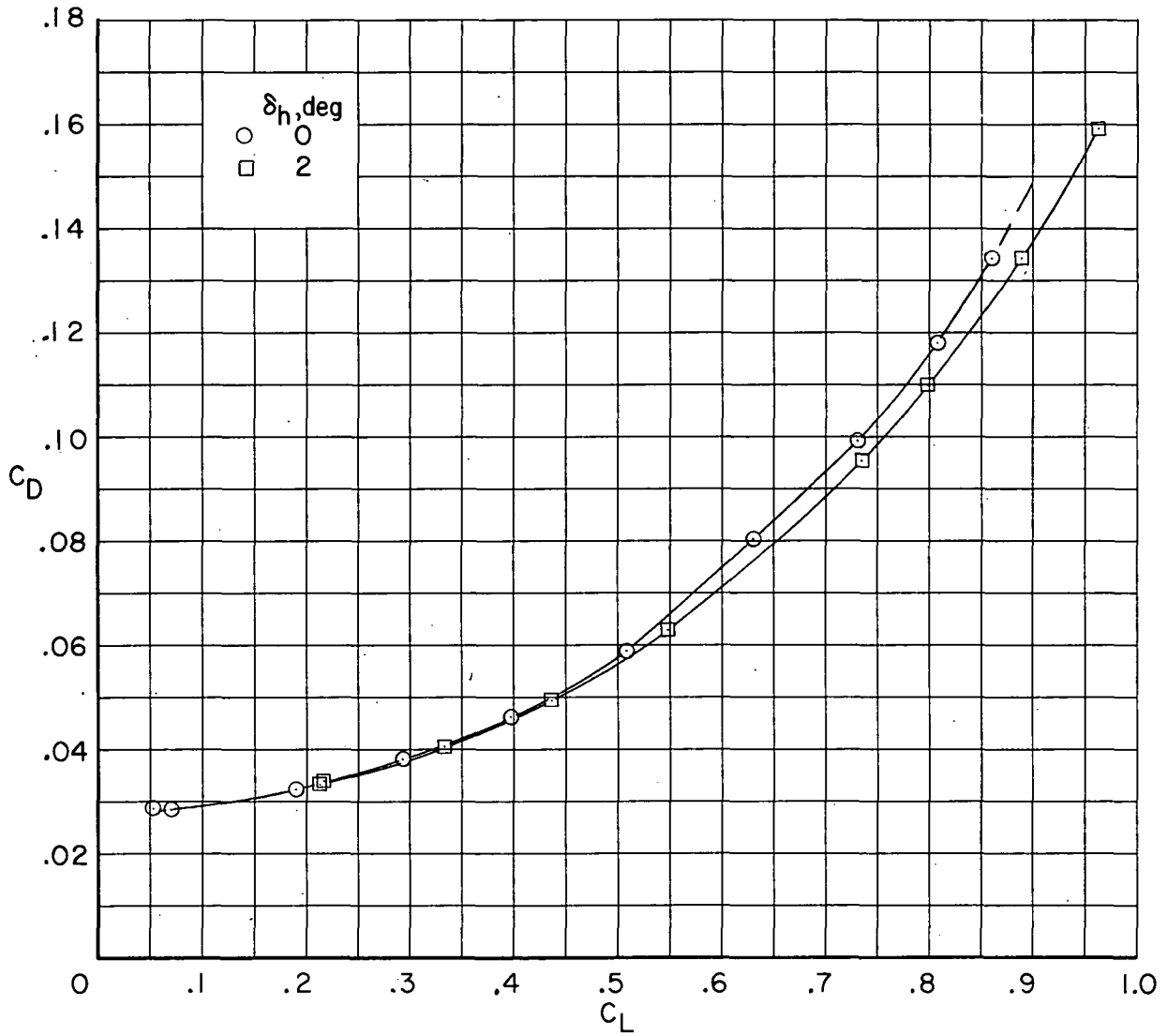
(b) $M = 0.75$. Concluded.

Figure 18.- Continued.



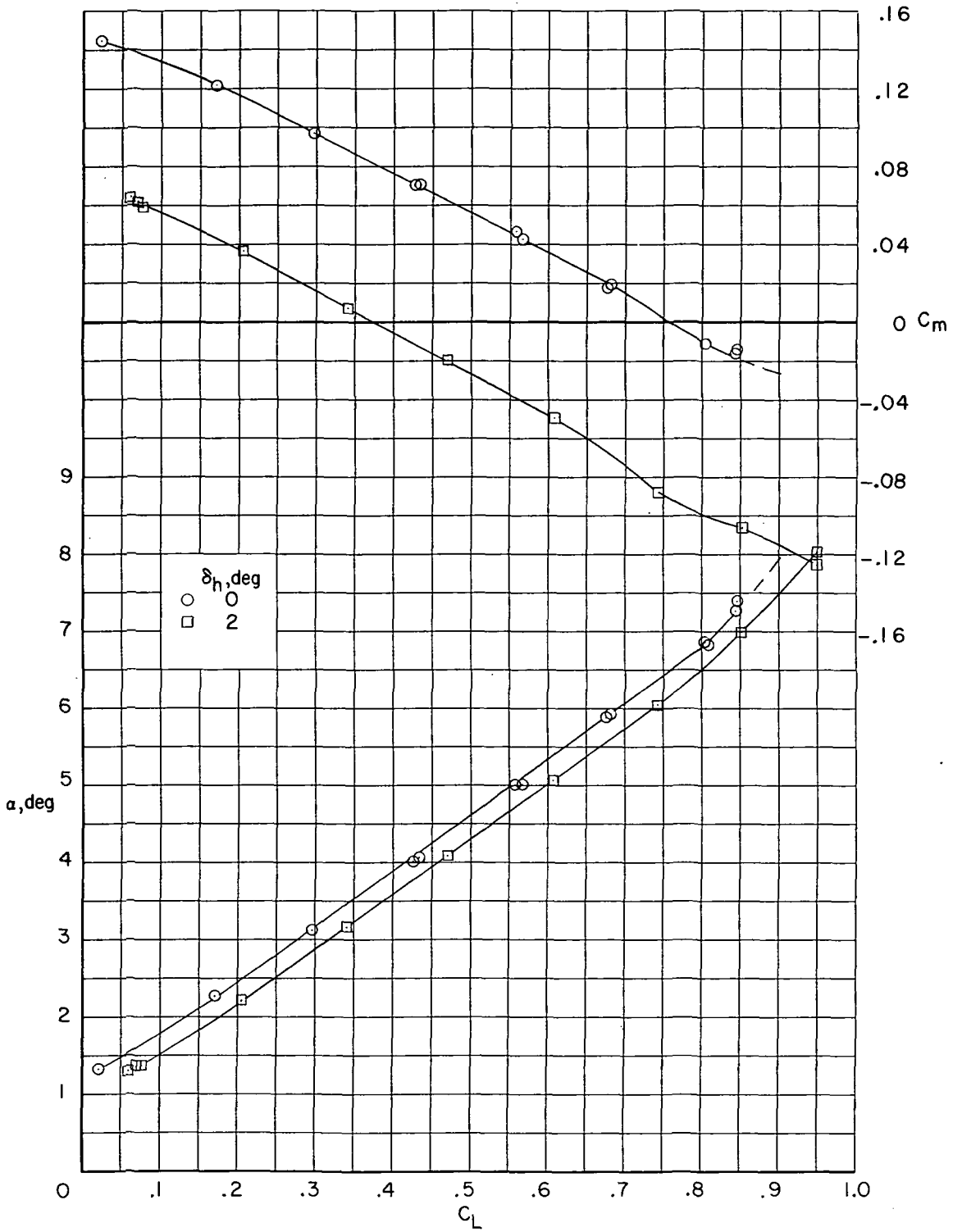
(c) $M = 0.85$.

Figure 18.- Continued.



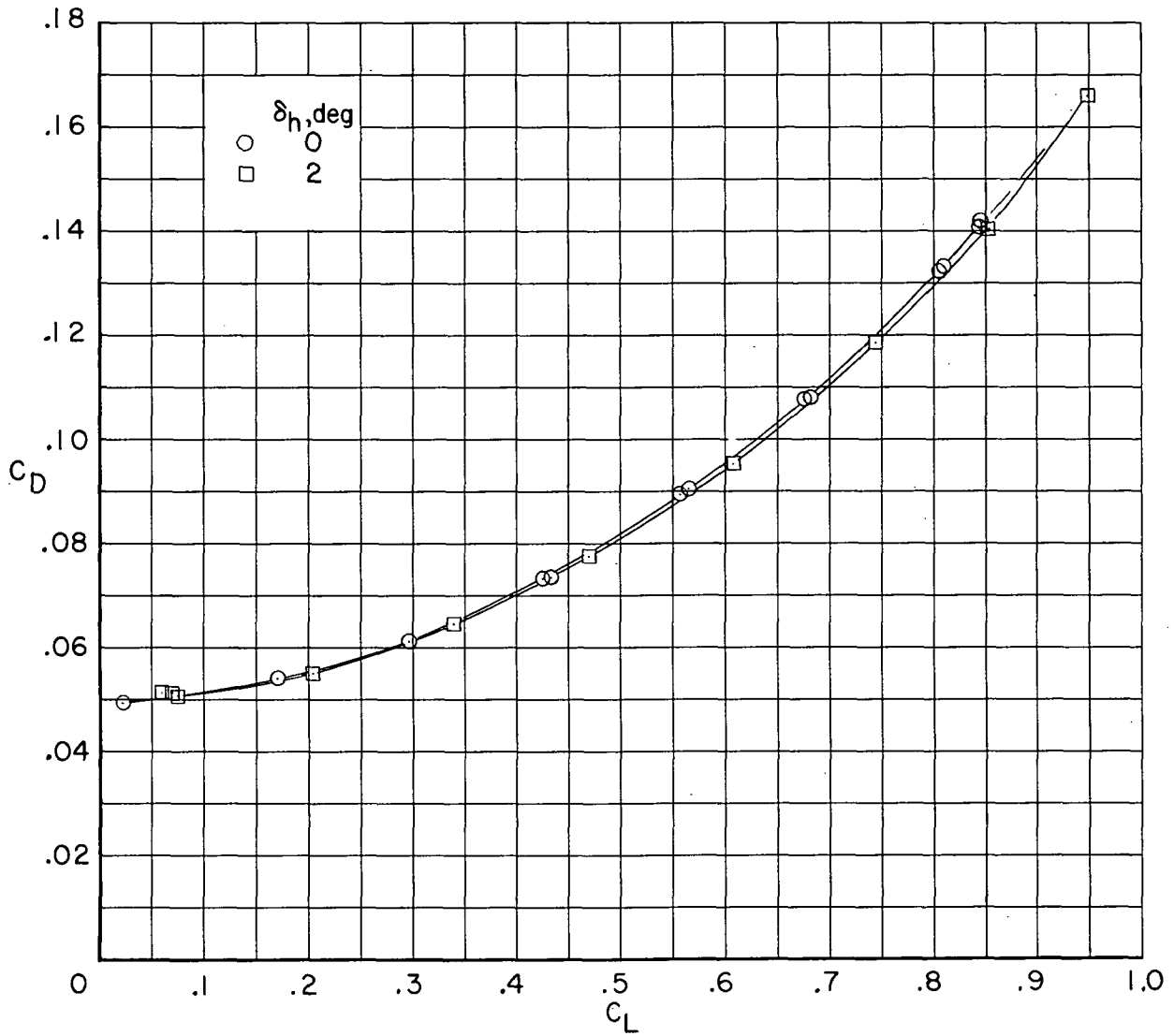
(c) $M = 0.85$. Concluded.

Figure 18. - Continued.



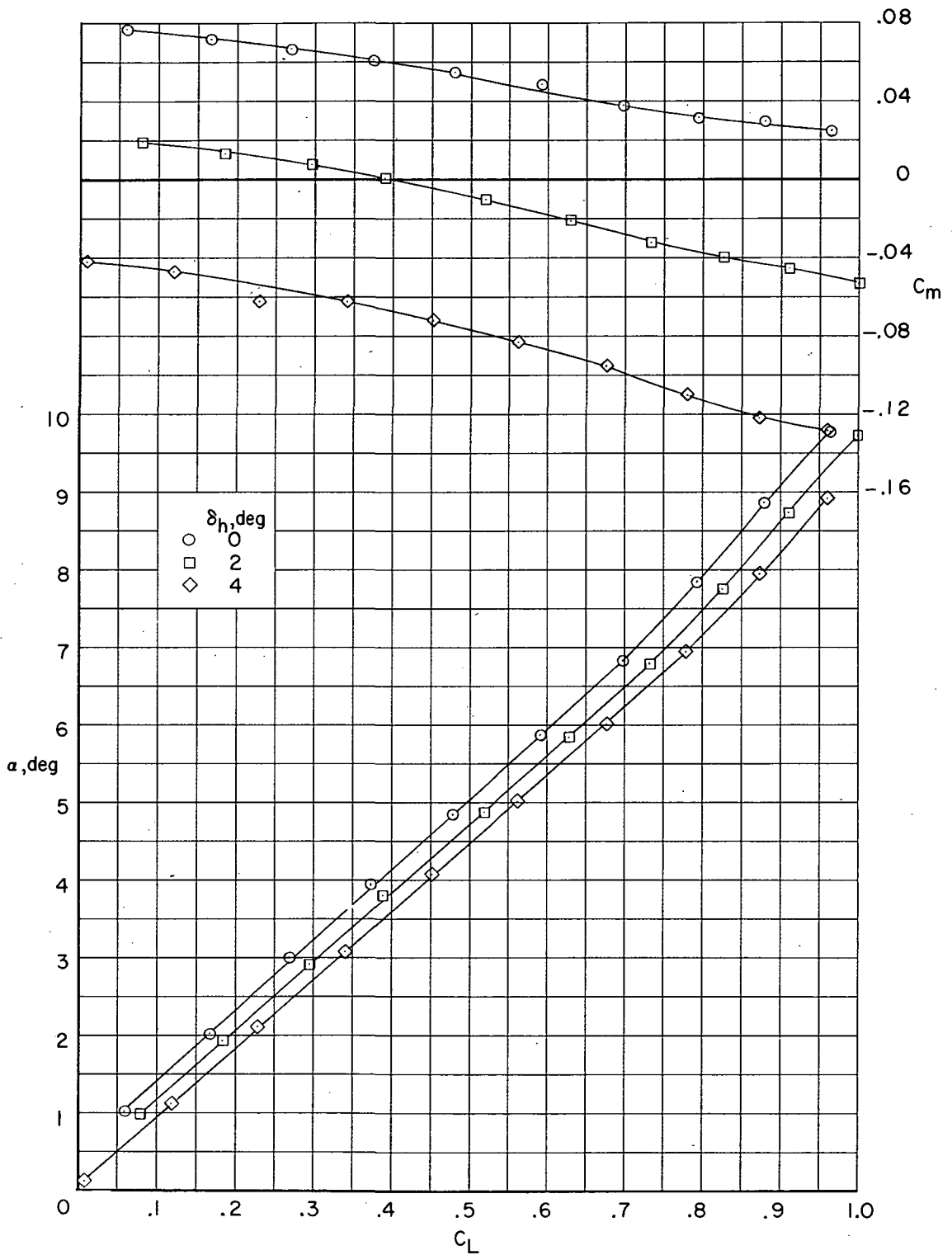
(d) $M = 0.91$.

Figure 18.- Continued.



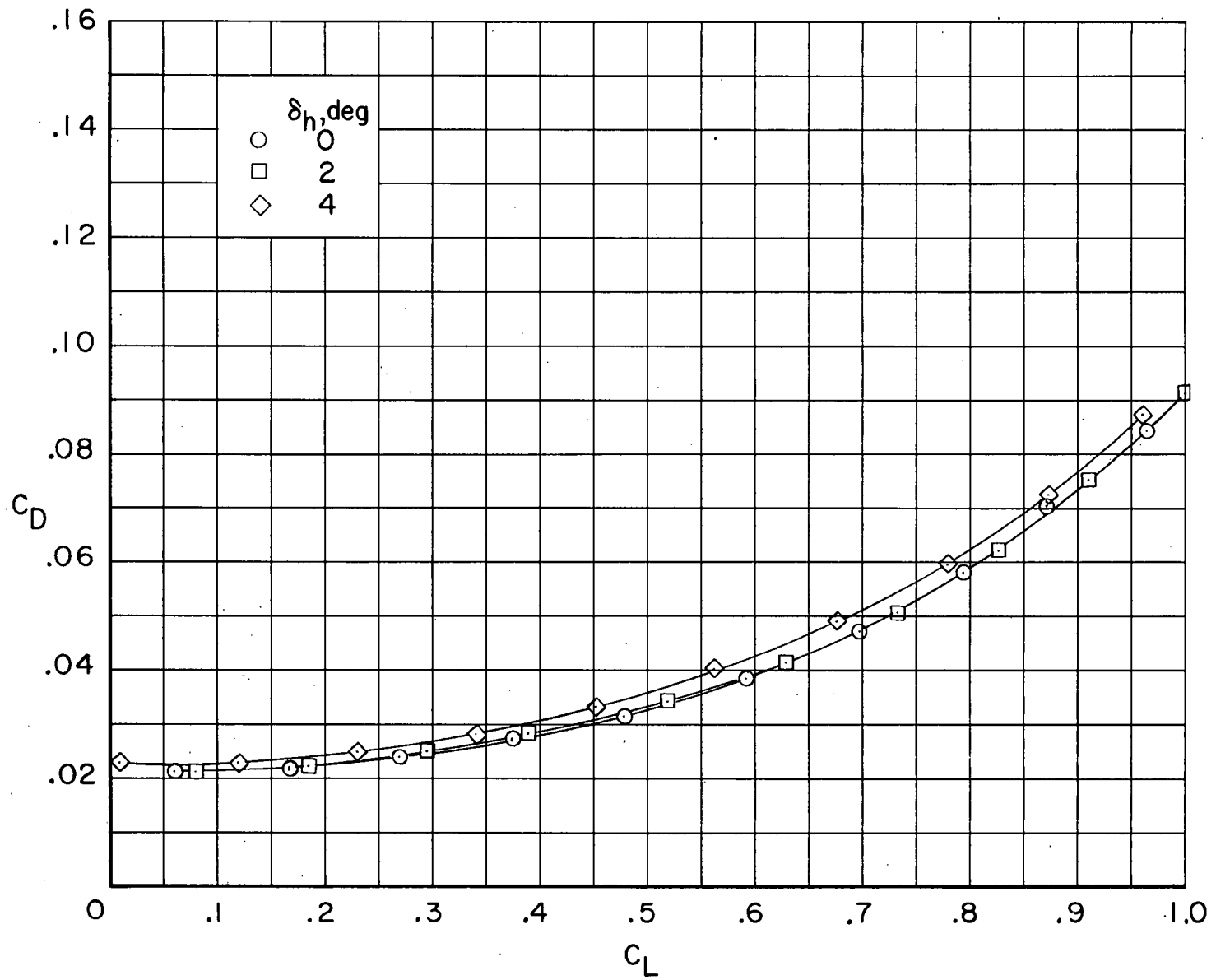
(d) $M = 0.91$. Concluded.

Figure 18.- Concluded.



(a) $M = 0.60$.

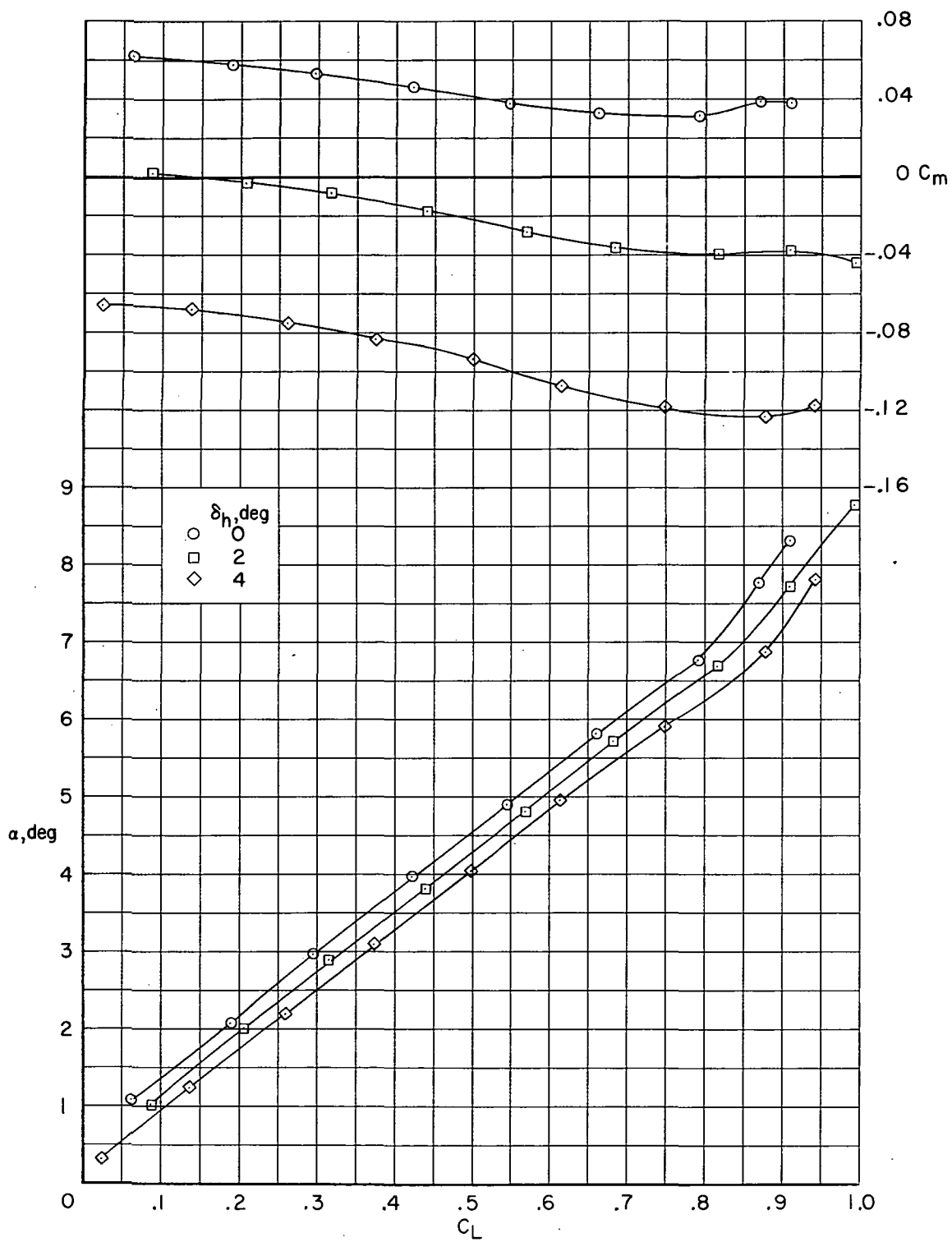
Figure 19.- Effect of horizontal-tail deflection on longitudinal aerodynamic characteristics of configuration with NACA 64A4XX airfoil, fuselage fairing, and transition rearward. $\Lambda = 26^\circ$; $i_w = -1^\circ$.



(a) $M = 0.60$. Concluded.

Figure 19.- Continued.

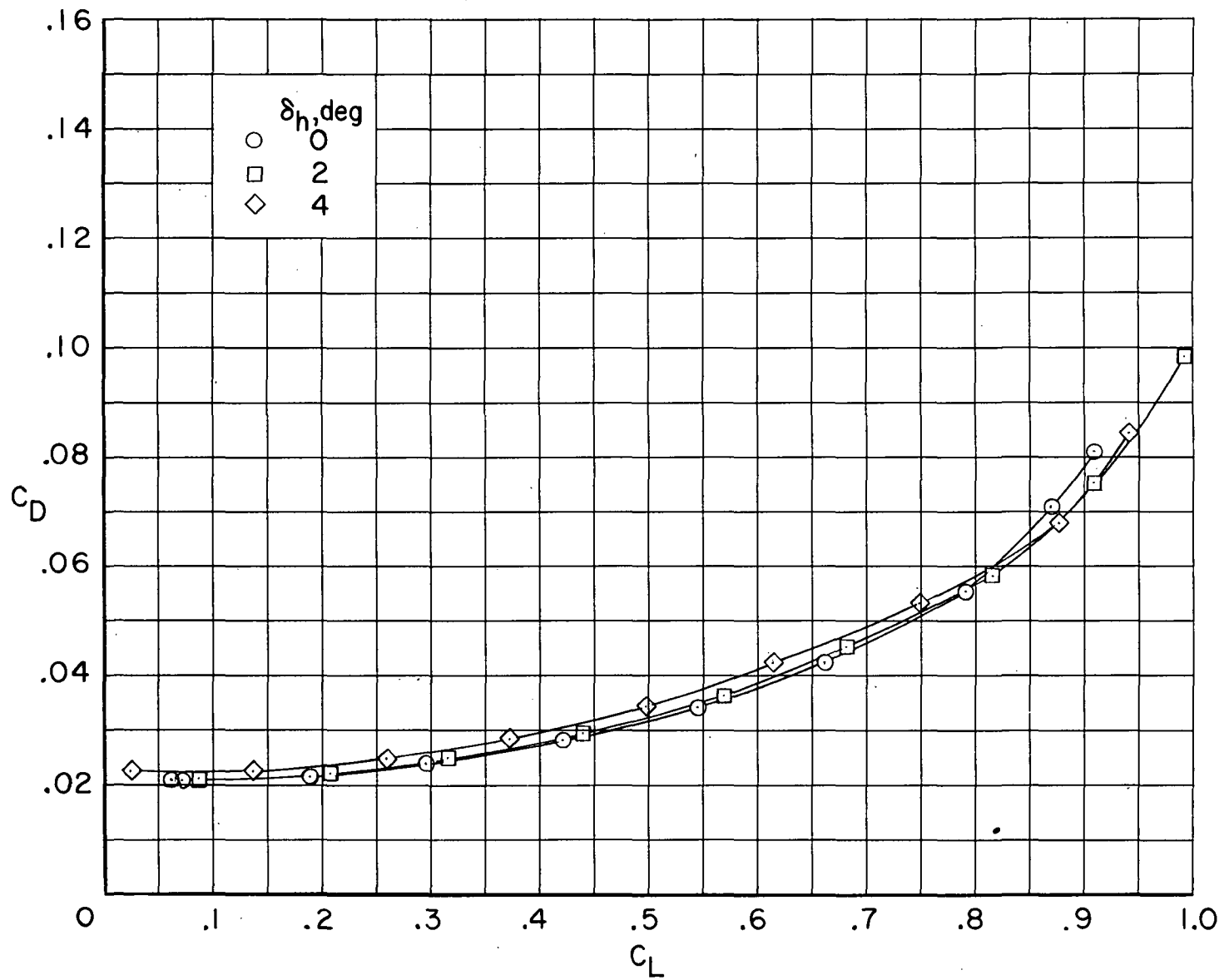
~~CONFIDENTIAL~~



(b) $M = 0.75$.

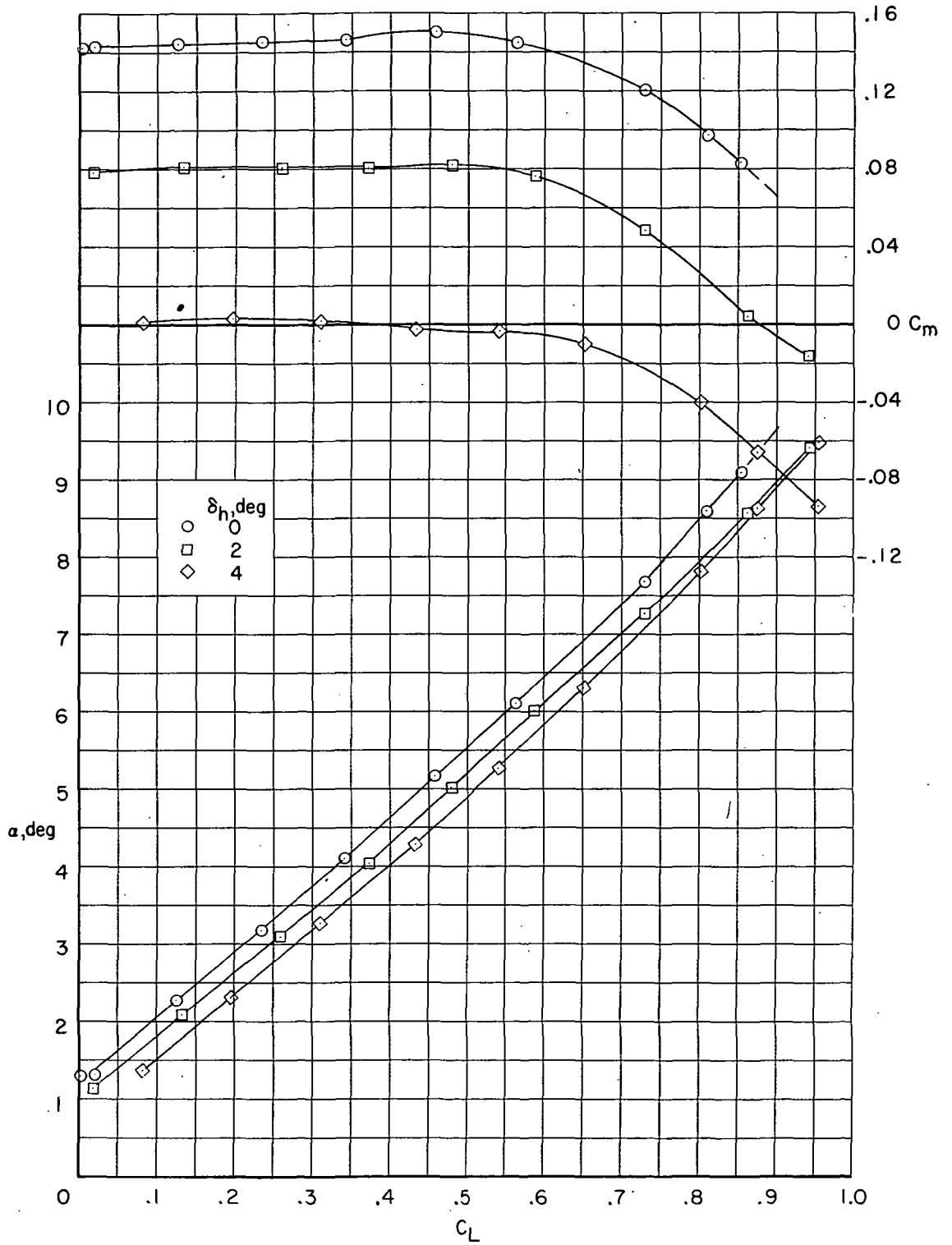
Figure 19. - Continued.

~~CONFIDENTIAL~~



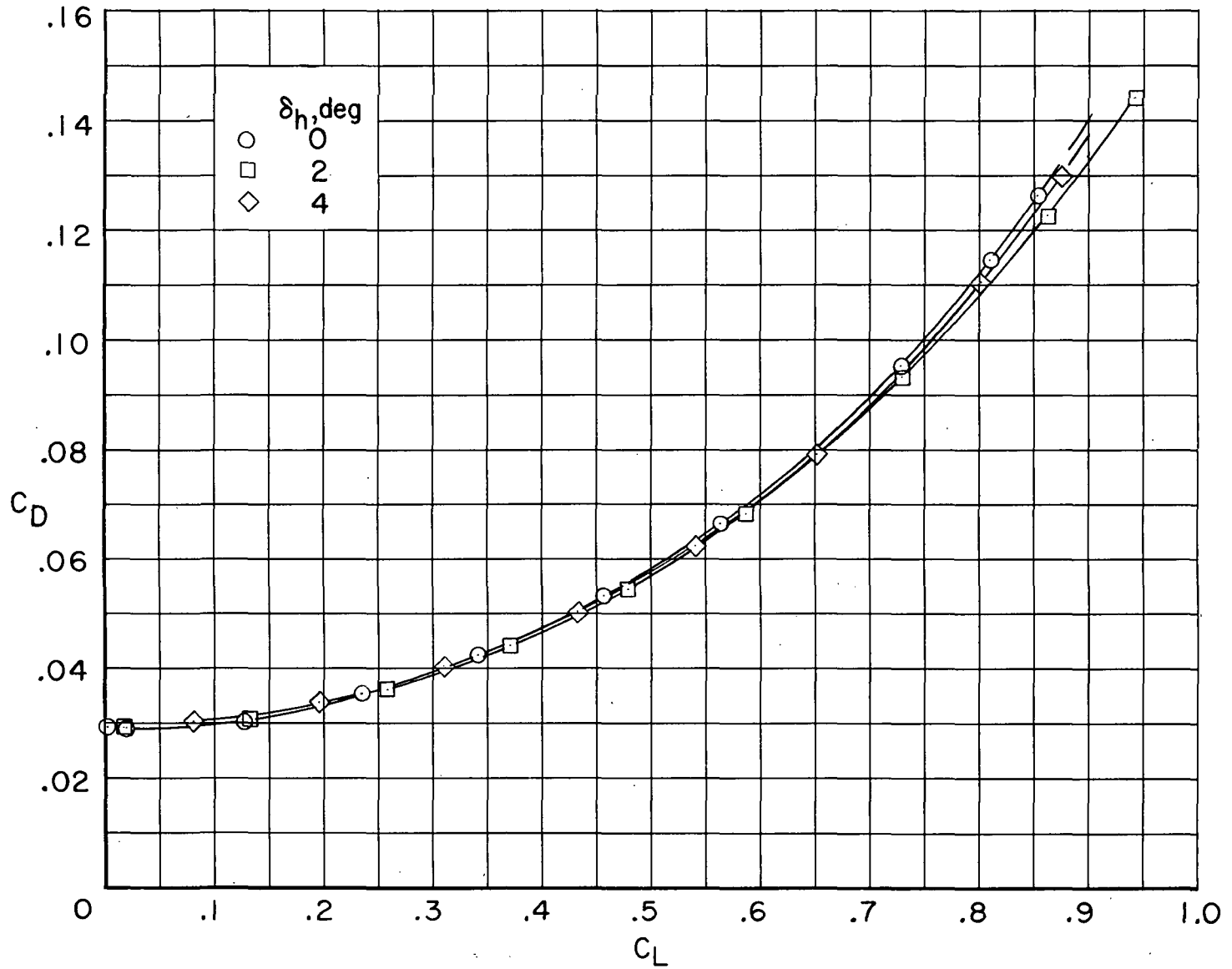
(b) $M = 0.75$. Concluded.

Figure 19. - Continued.



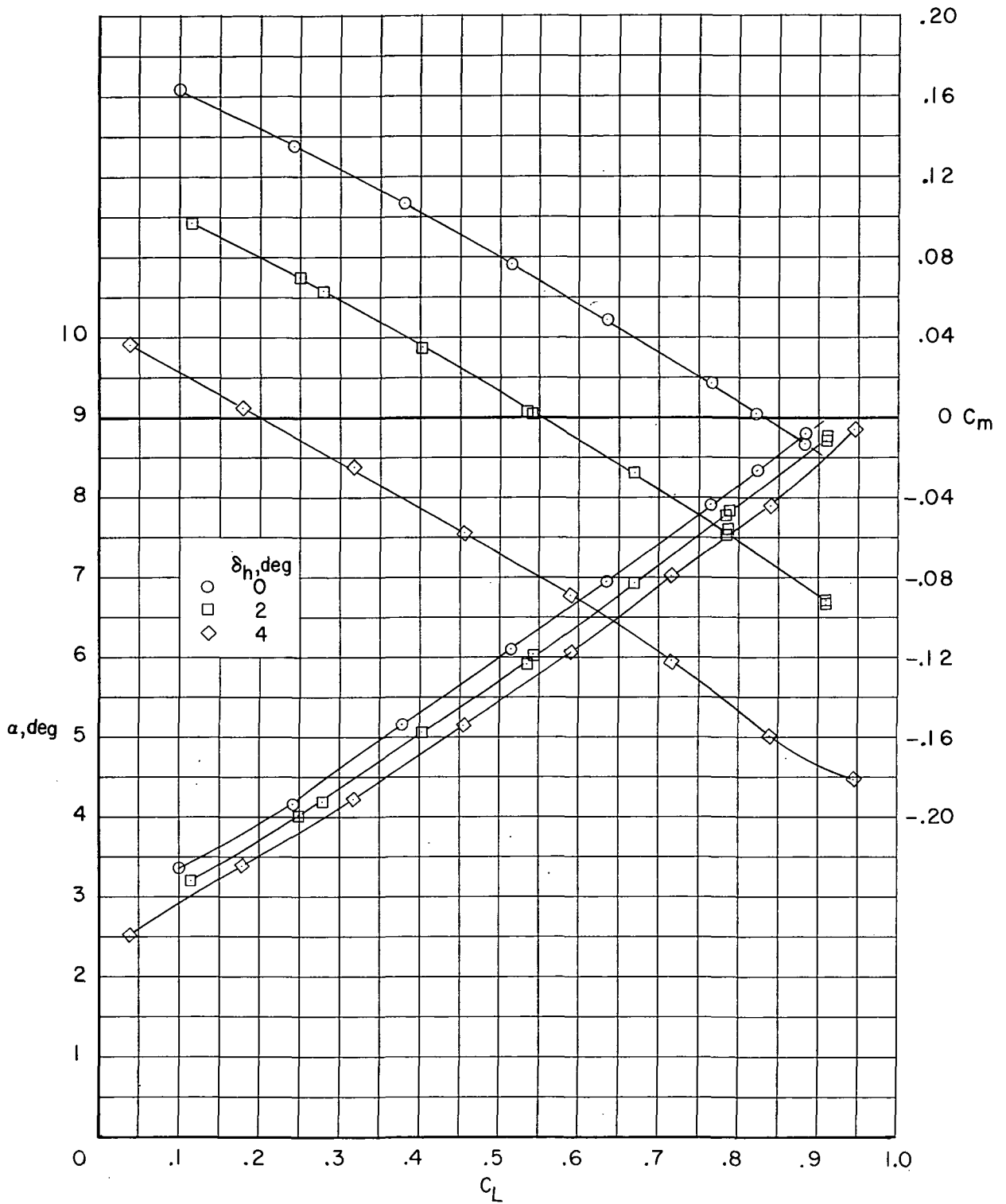
(c) $M = 0.85$.

Figure 19.- Continued.



(c) $M = 0.85$. Concluded.

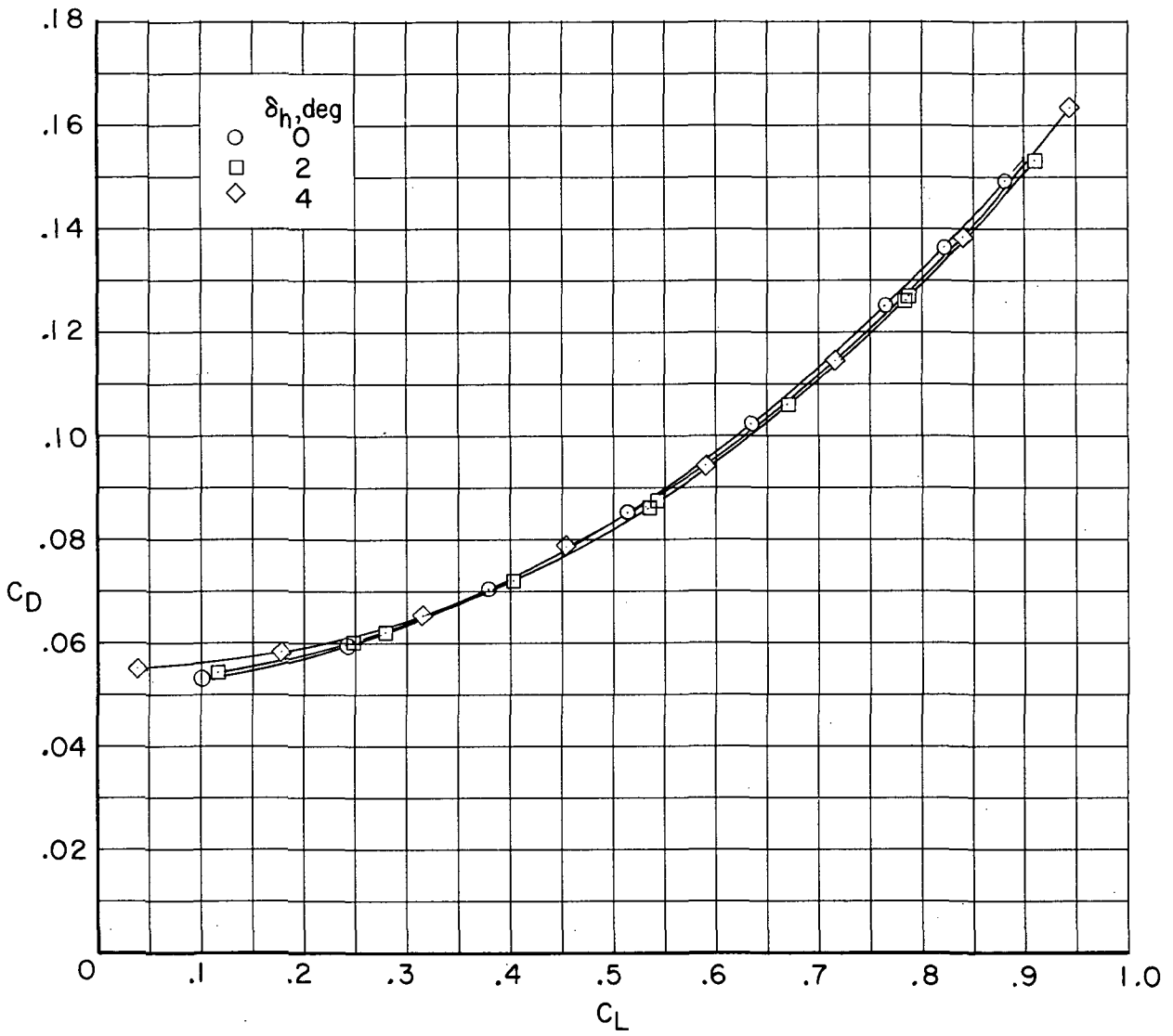
Figure 19.- Continued.



(d) $M = 0.91$.

Figure 19.- Continued.

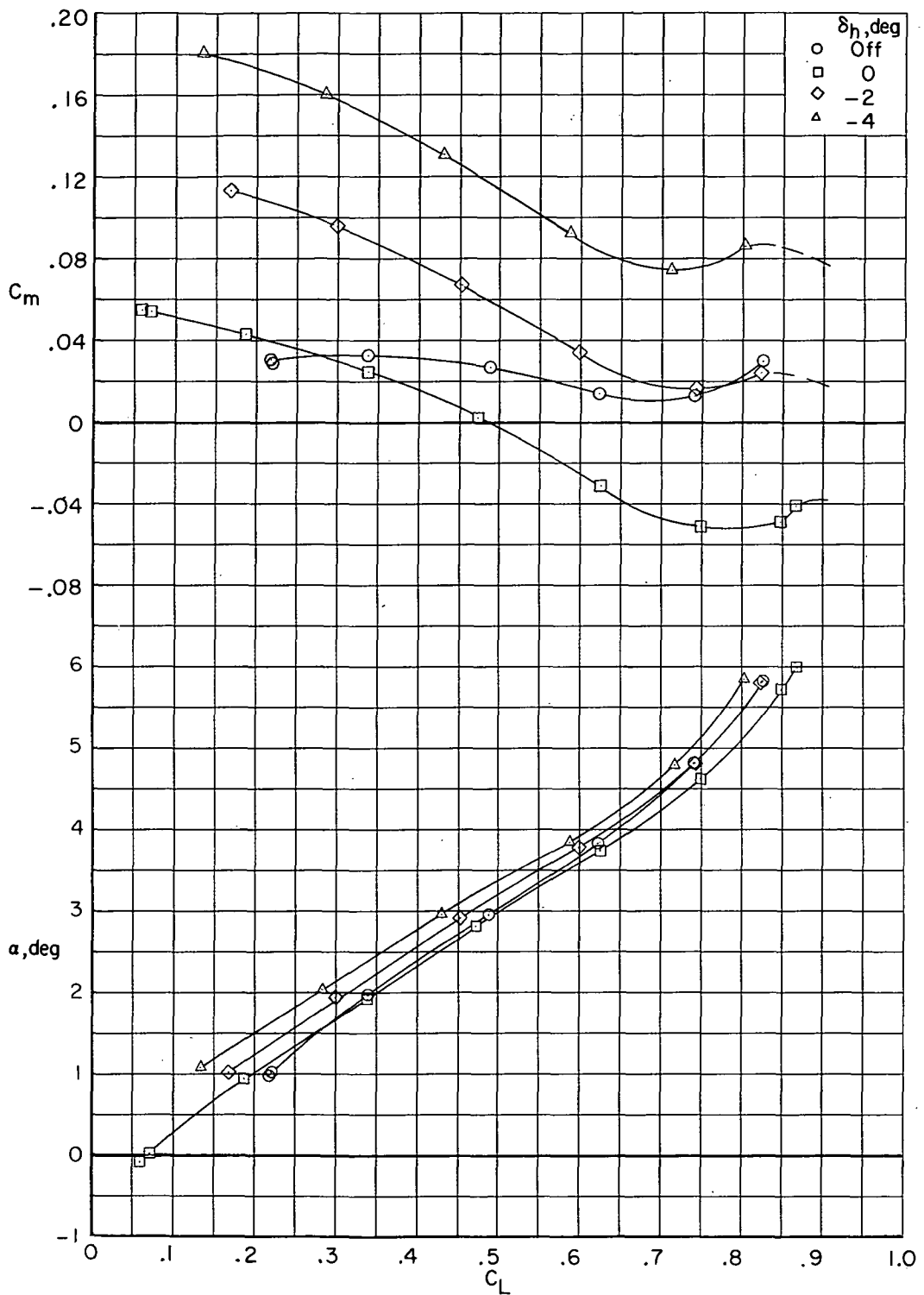
~~SECRET~~



(d) $M = 0.91$. Concluded.

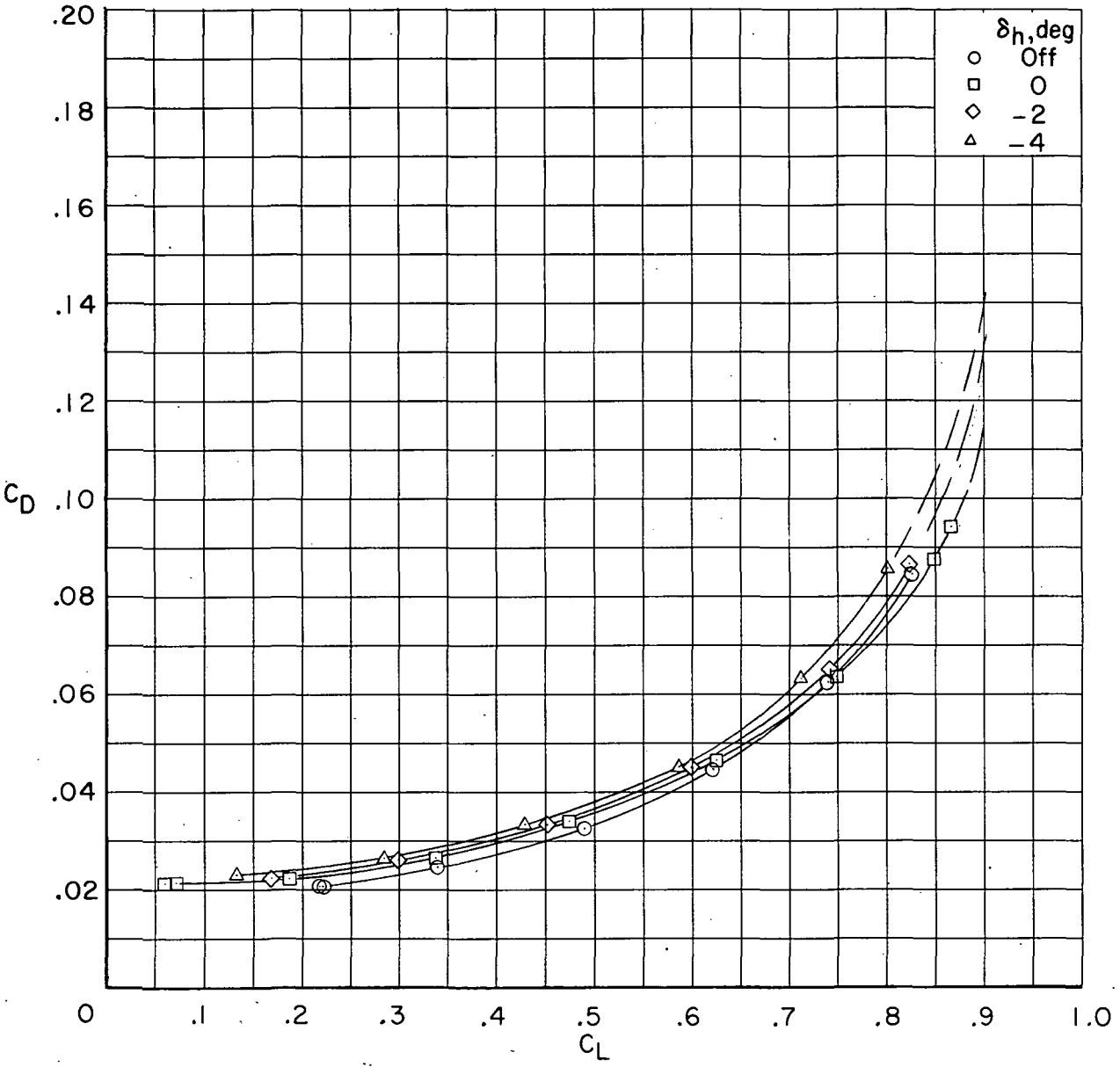
Figure 19.- Concluded.

~~SECRET~~



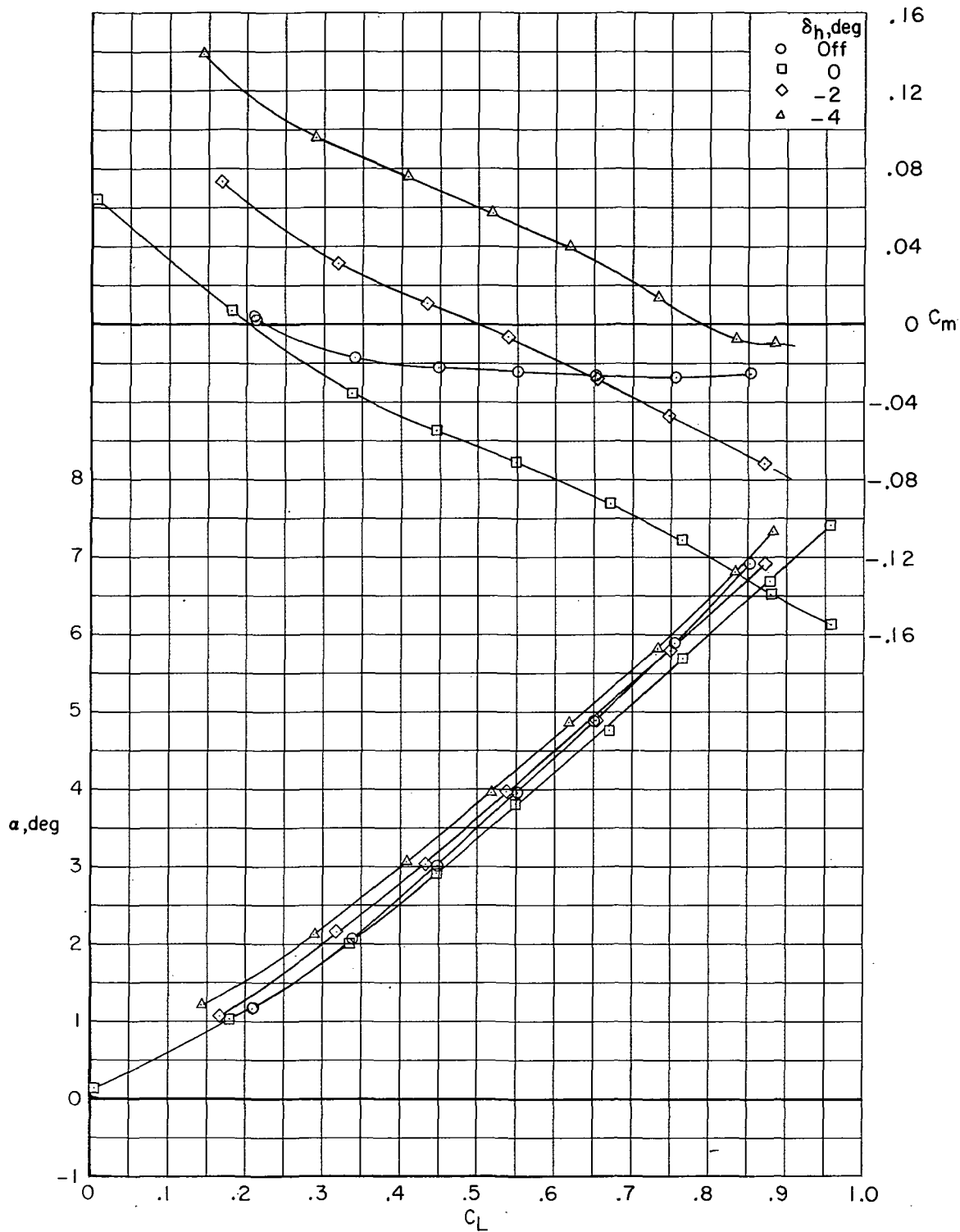
(a) $M = 0.85$.

Figure 20. - Effect of horizontal-tail deflection on longitudinal aerodynamic characteristics of configuration with supercritical airfoil B, fuselage fairing, and transition rearward. $\Lambda = 33^\circ$; $i_w = 1^\circ$.



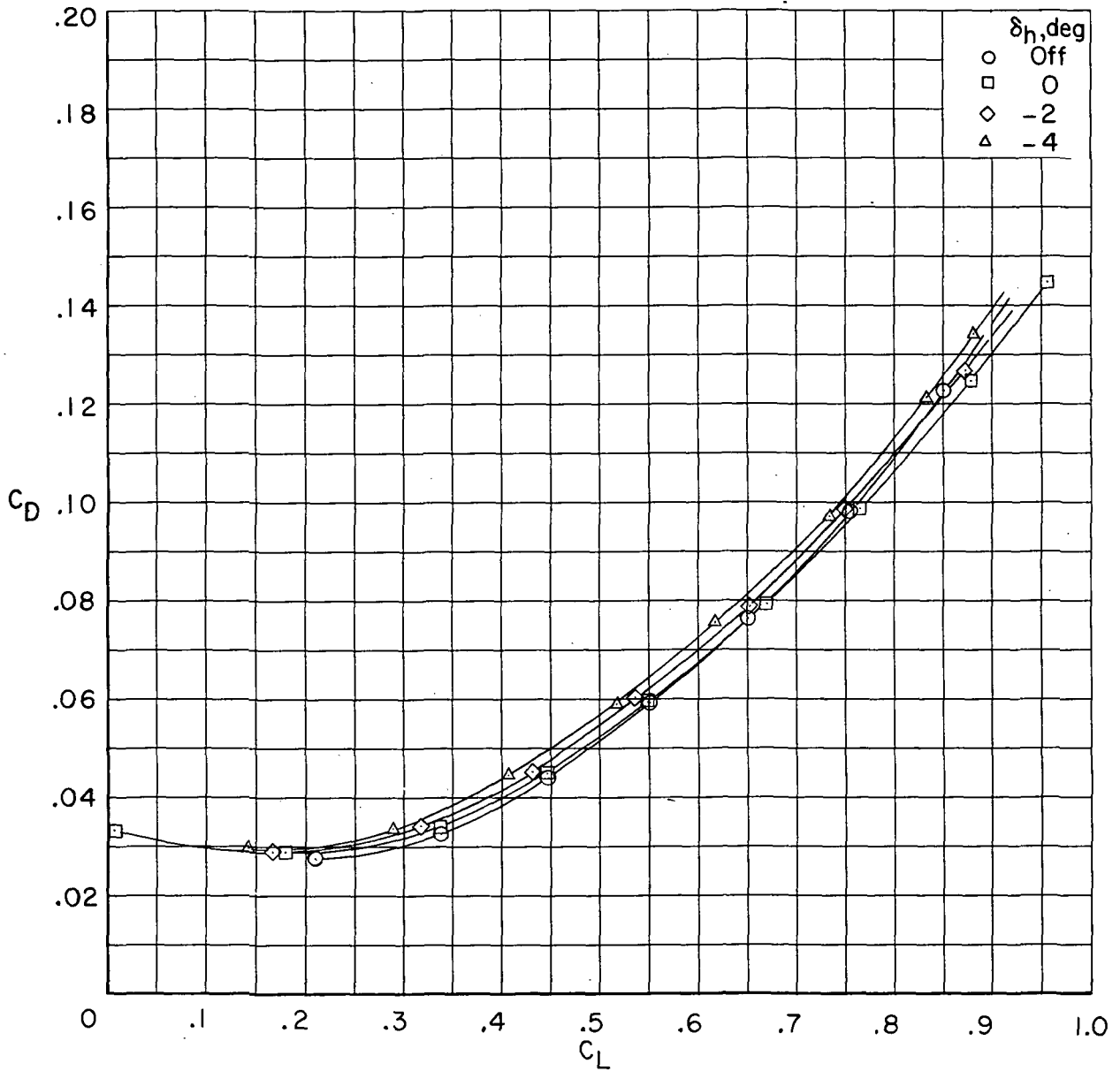
(a) $M = 0.85$. Concluded.

Figure 20. - Continued.



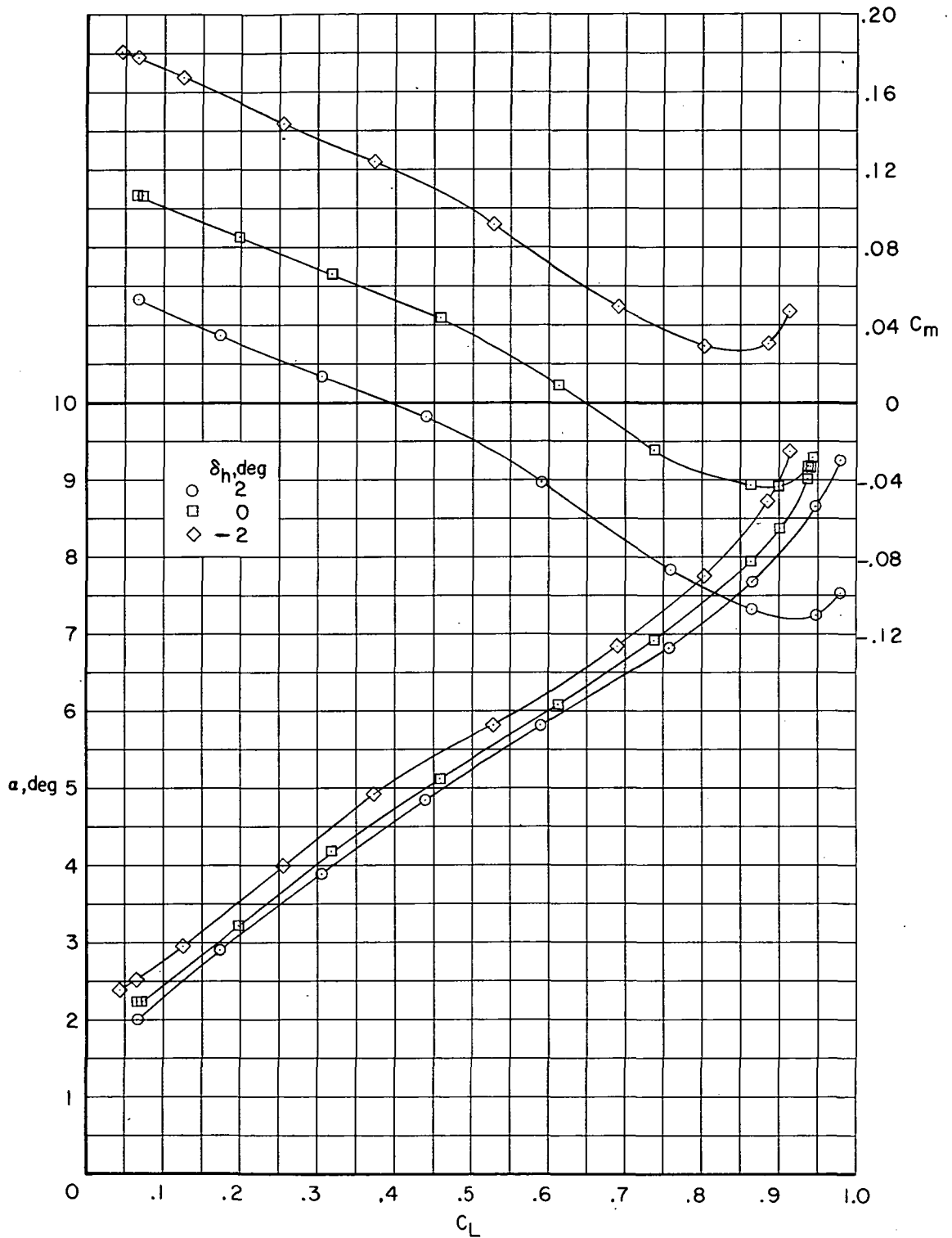
(b) $M = 0.91$.

Figure 20. - Continued.



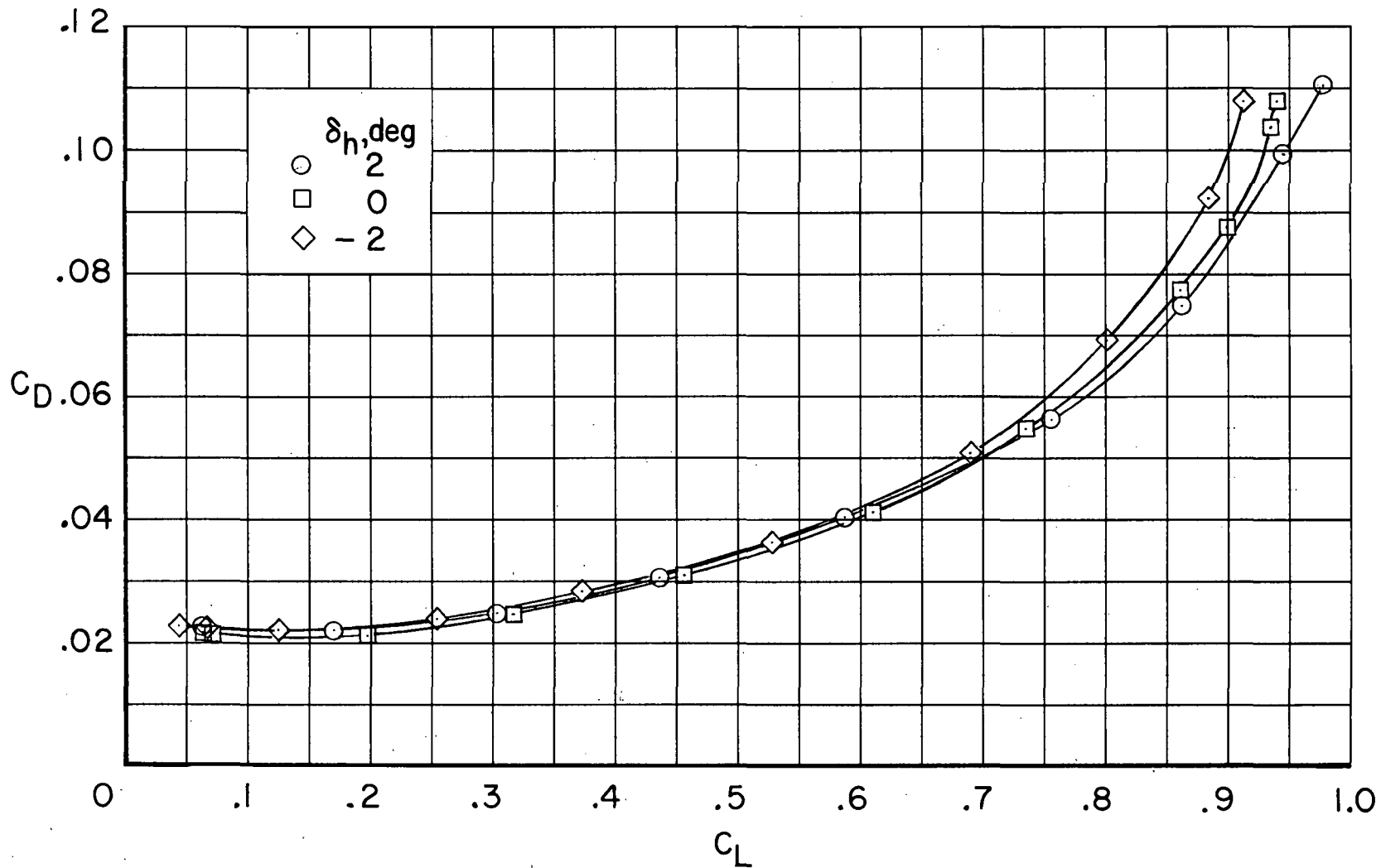
(b) $M = 0.91$. Concluded.

Figure 20.- Concluded.



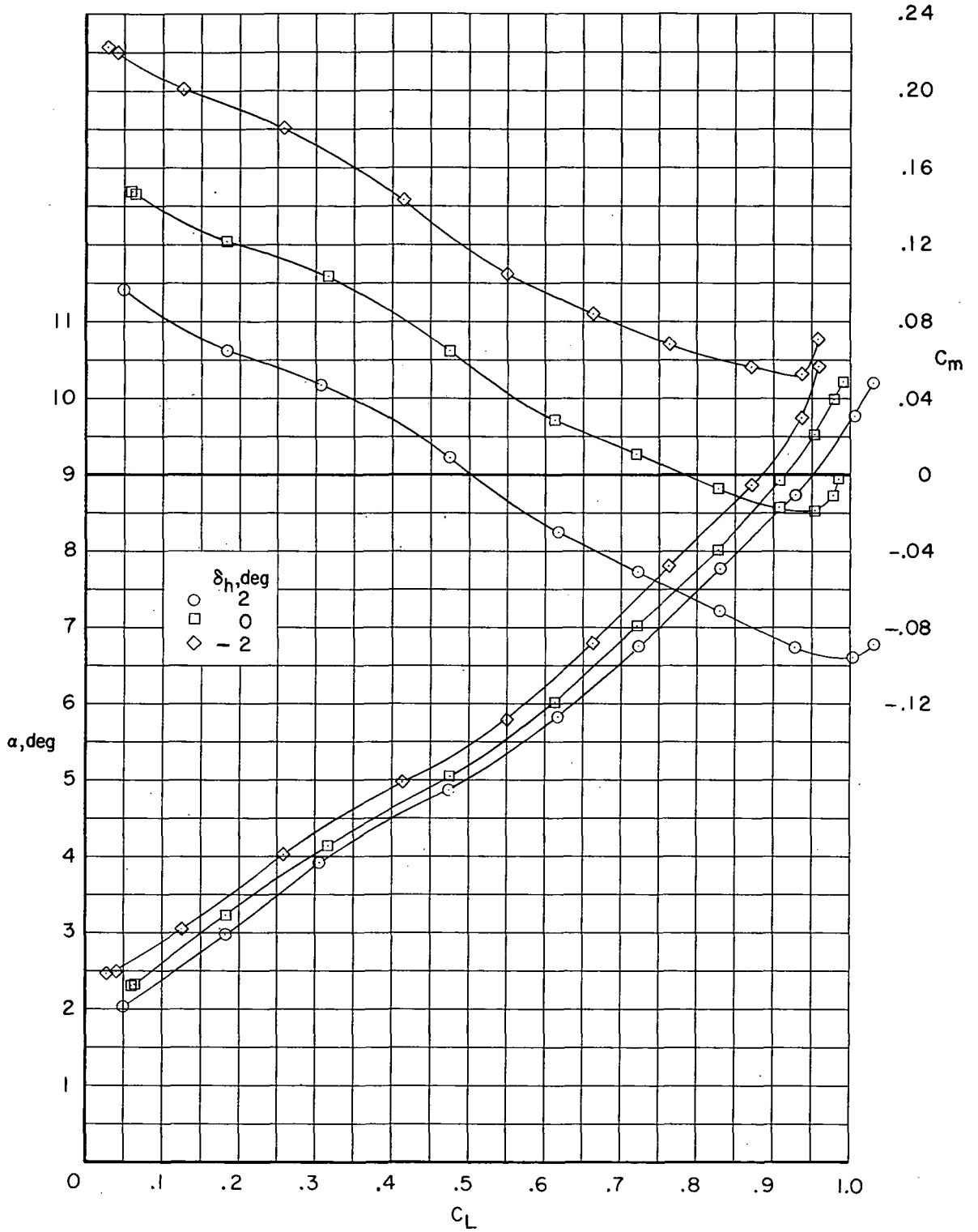
(a) $M = 0.85$.

Figure 21. - Effect of horizontal-tail deflection on longitudinal aerodynamic characteristics of configuration with supercritical airfoil C, fuselage fairing, and transition rearward. $\Lambda = 33^\circ$; $i_w = -3^\circ$.



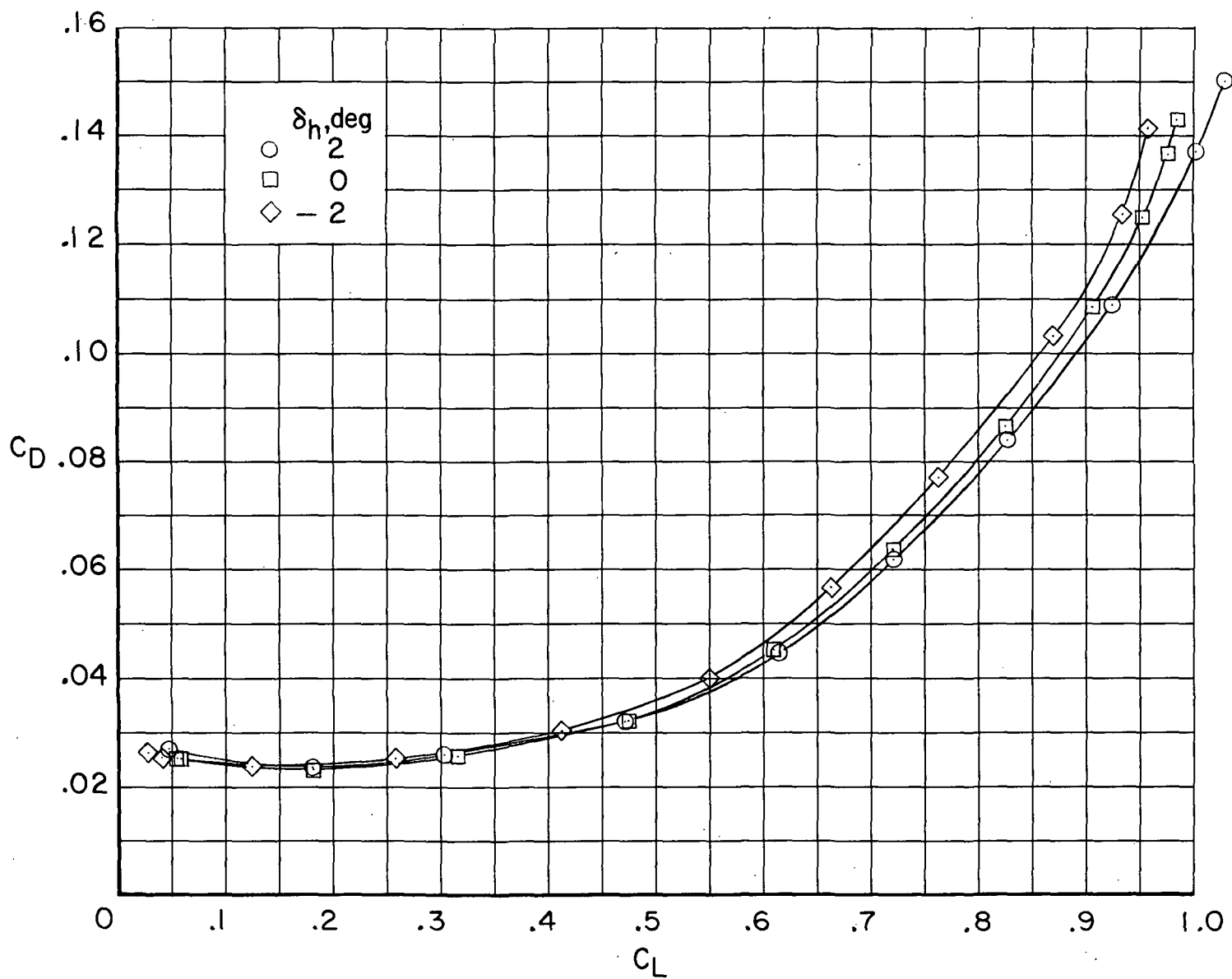
(a) $M = 0.85$. Concluded.

Figure 21.- Continued.



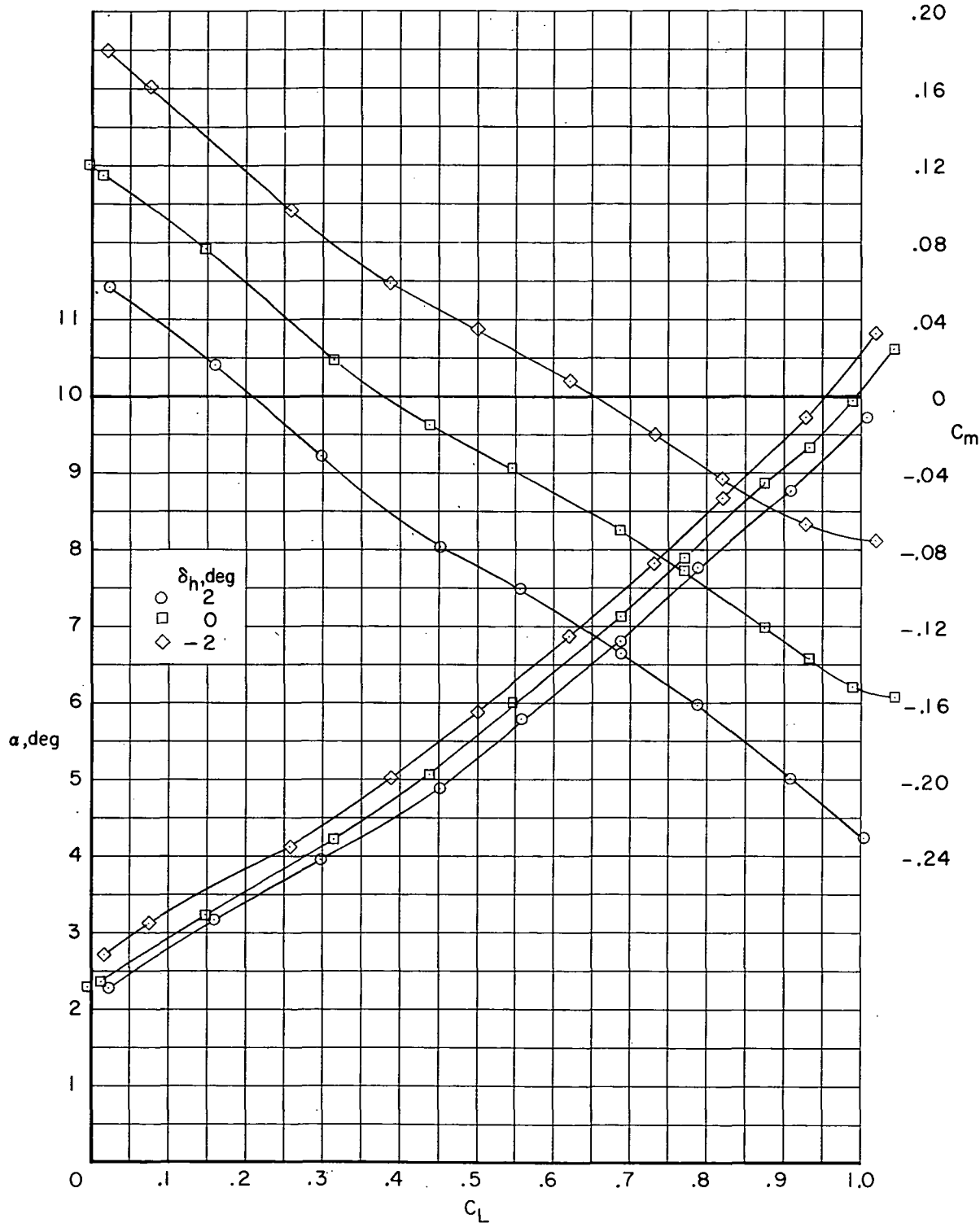
(b) $M = 0.88$.

Figure 21. - Continued.



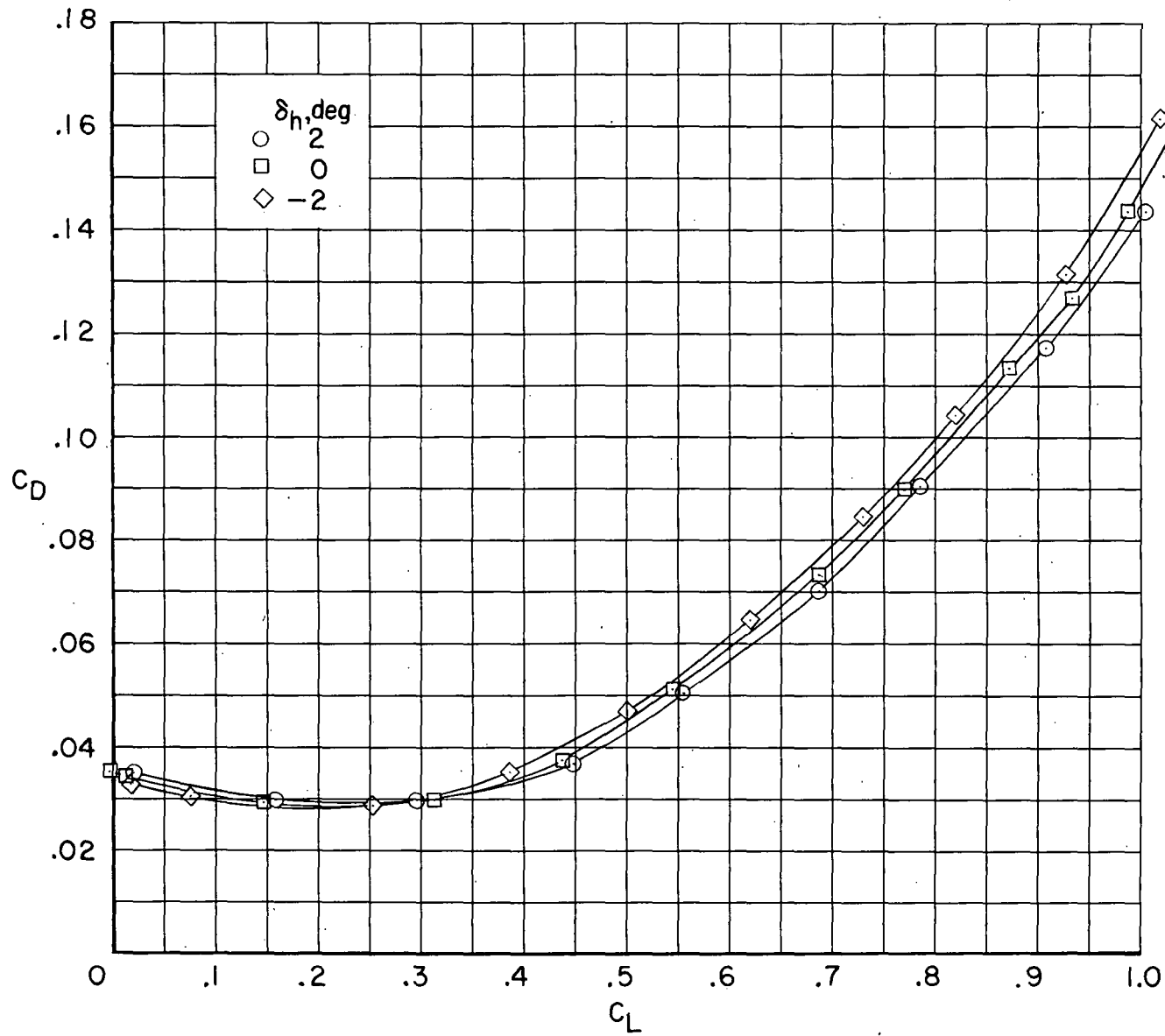
(b) $M = 0.88$. Concluded.

Figure 21.- Continued.



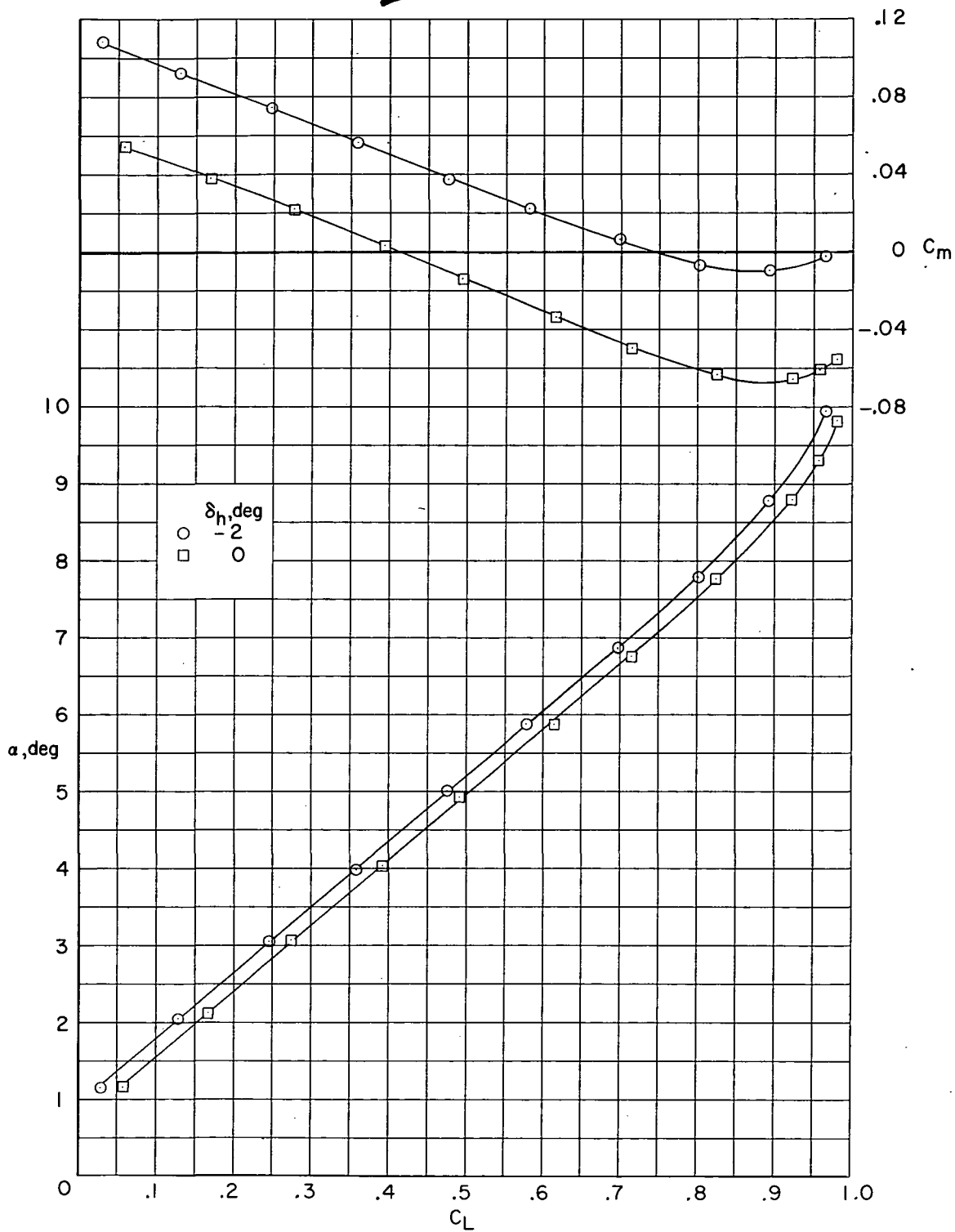
(c) $M = 0.91$.

Figure 21. - Continued.



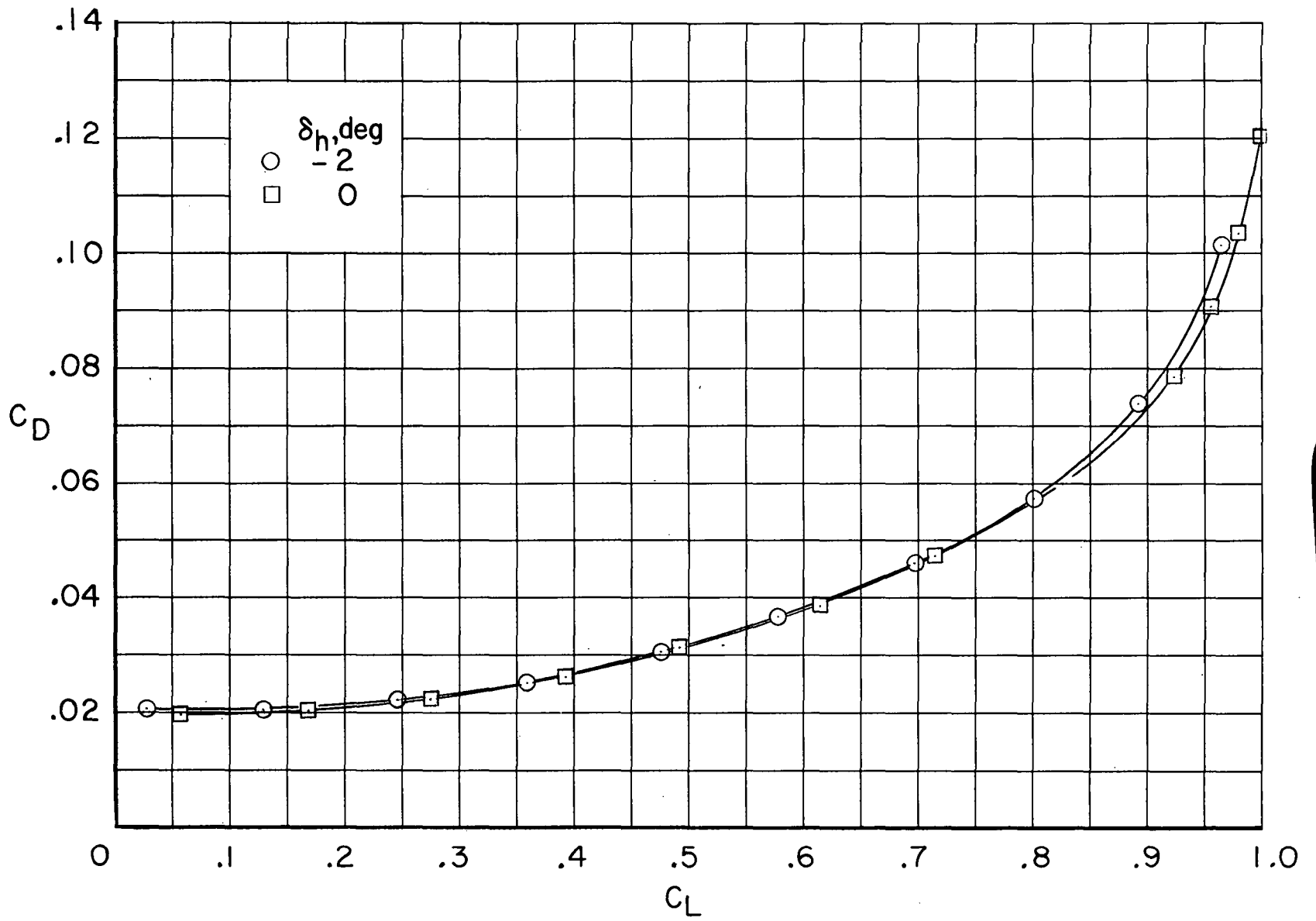
(c) $M = 0.91$. Concluded.

Figure 21.- Concluded.



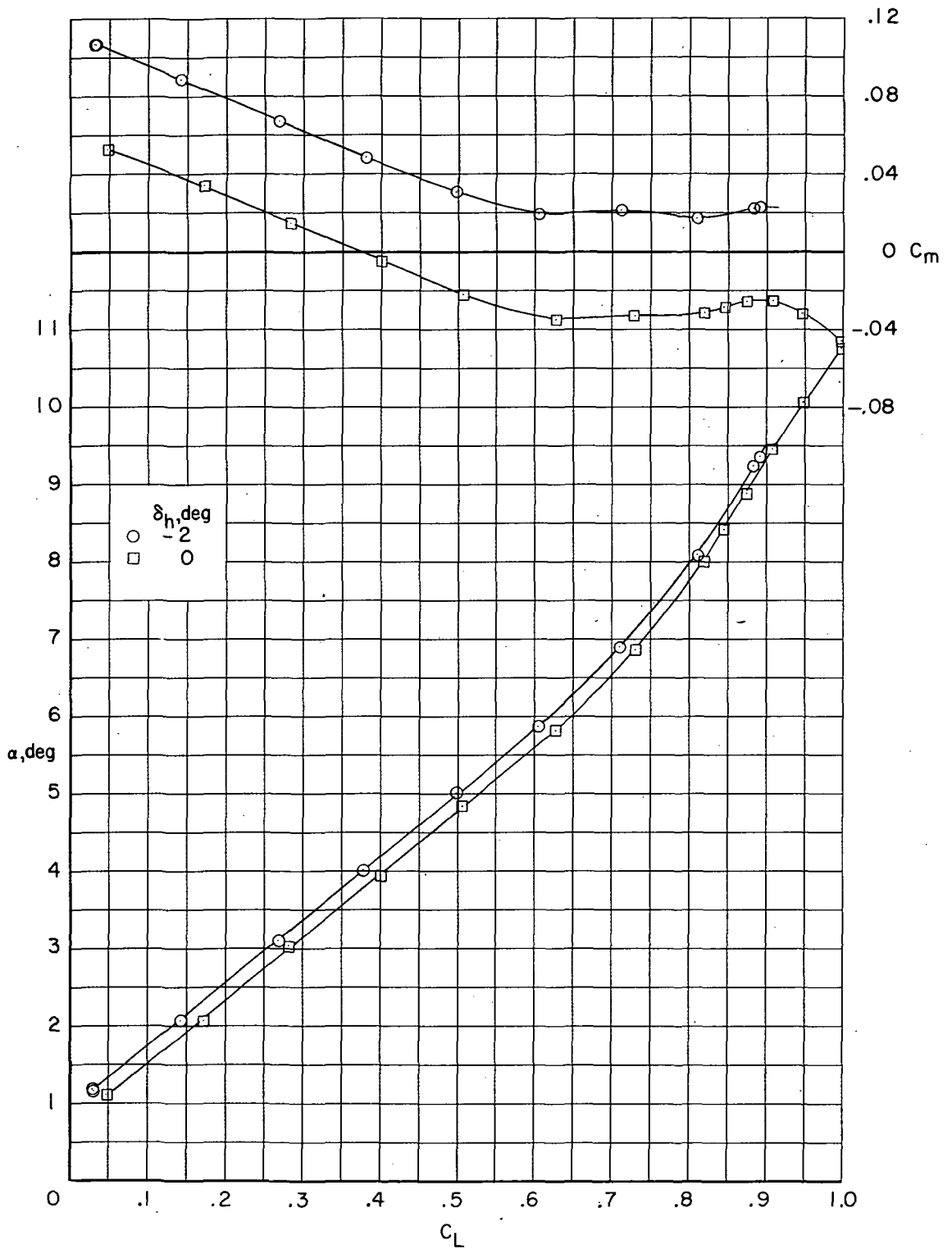
(a) $M = 0.75$.

Figure 22.- Effect of horizontal-tail deflection on longitudinal aerodynamic characteristics of configuration with NACA 64A4XX airfoil, fuselage fairing, and transition rearward. $\Lambda = 33^\circ$; $i_w = -1^\circ$.



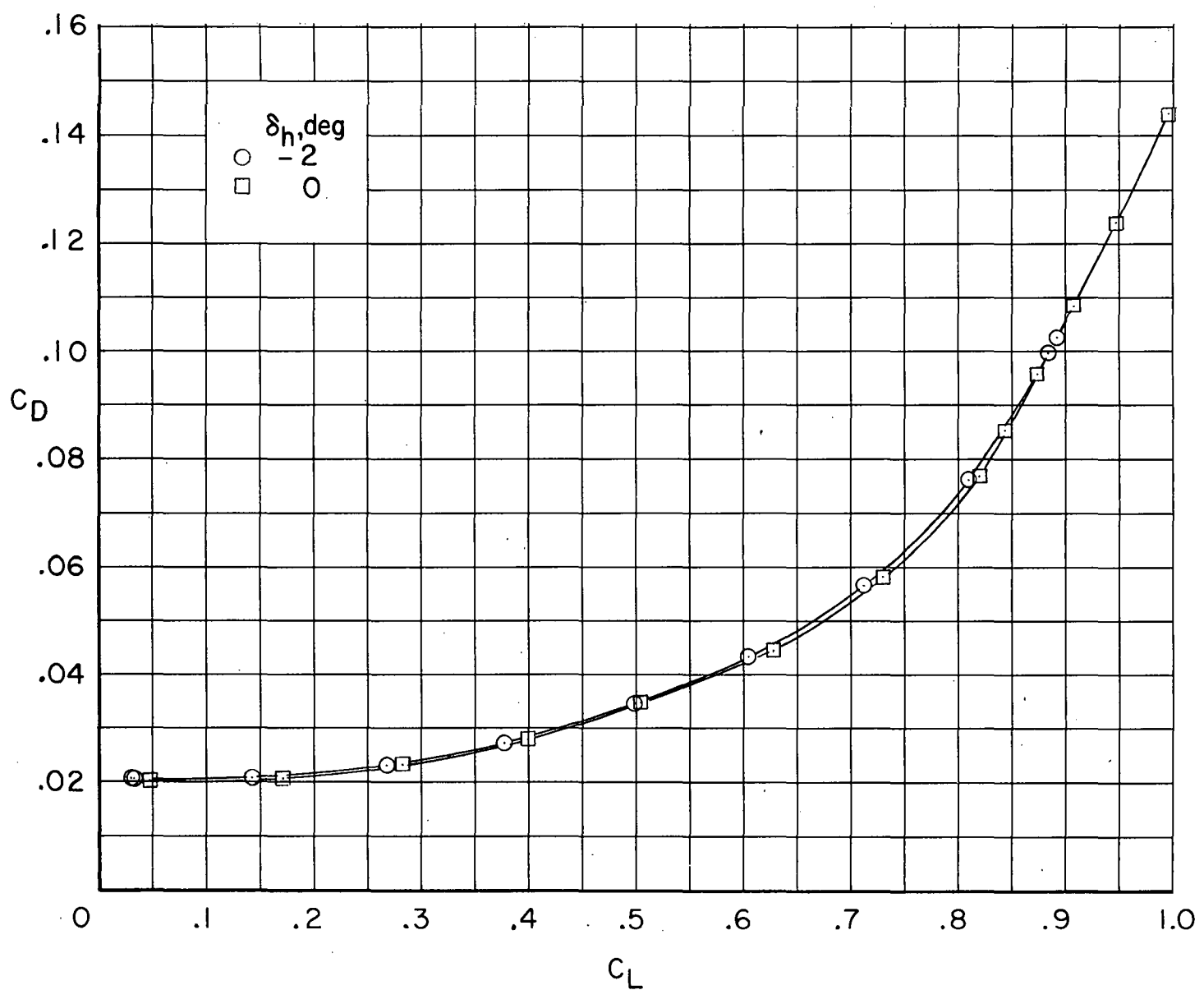
(a) $M = 0.75$. Concluded.

Figure 22. - Continued.



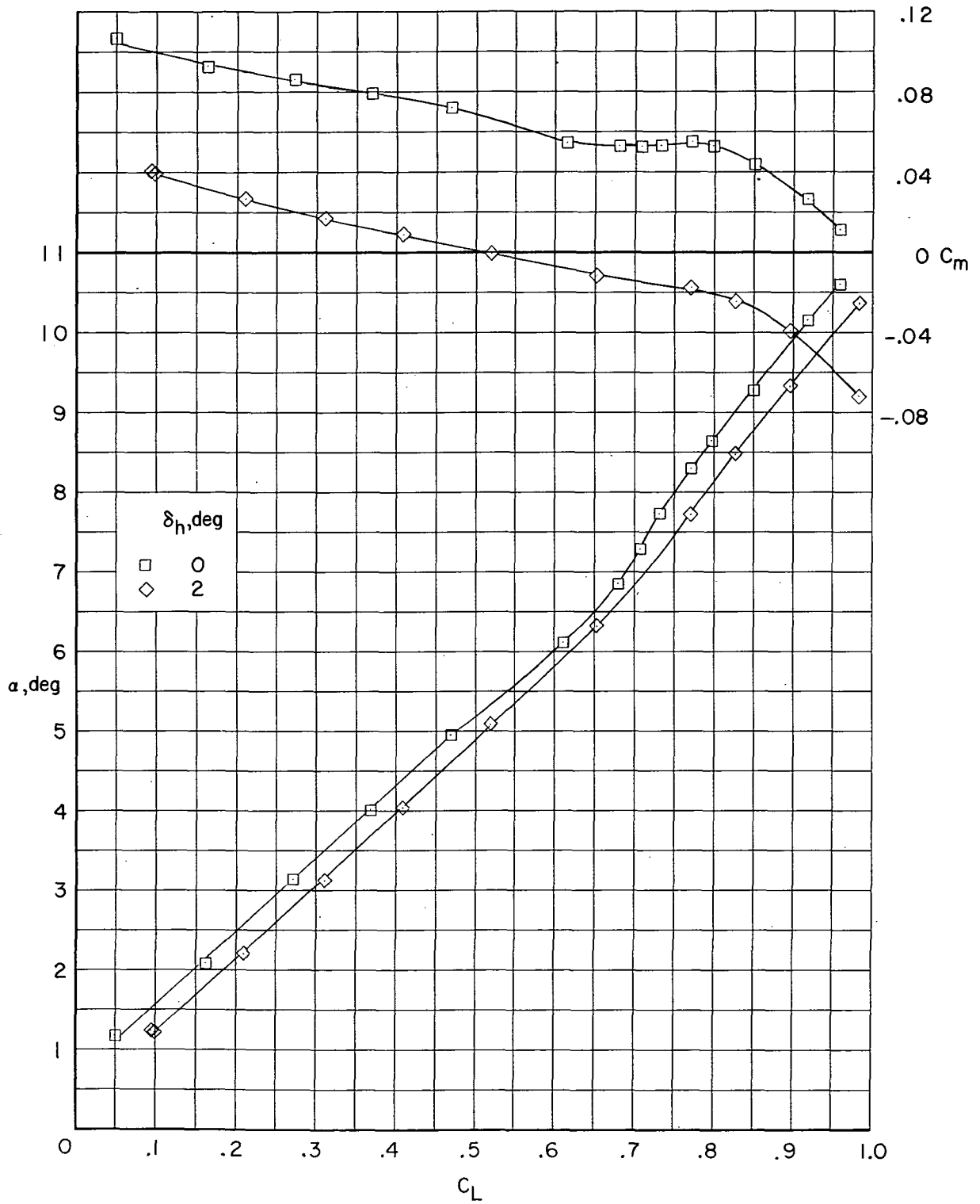
(b) $M = 0.80$.

Figure 22. - Continued.



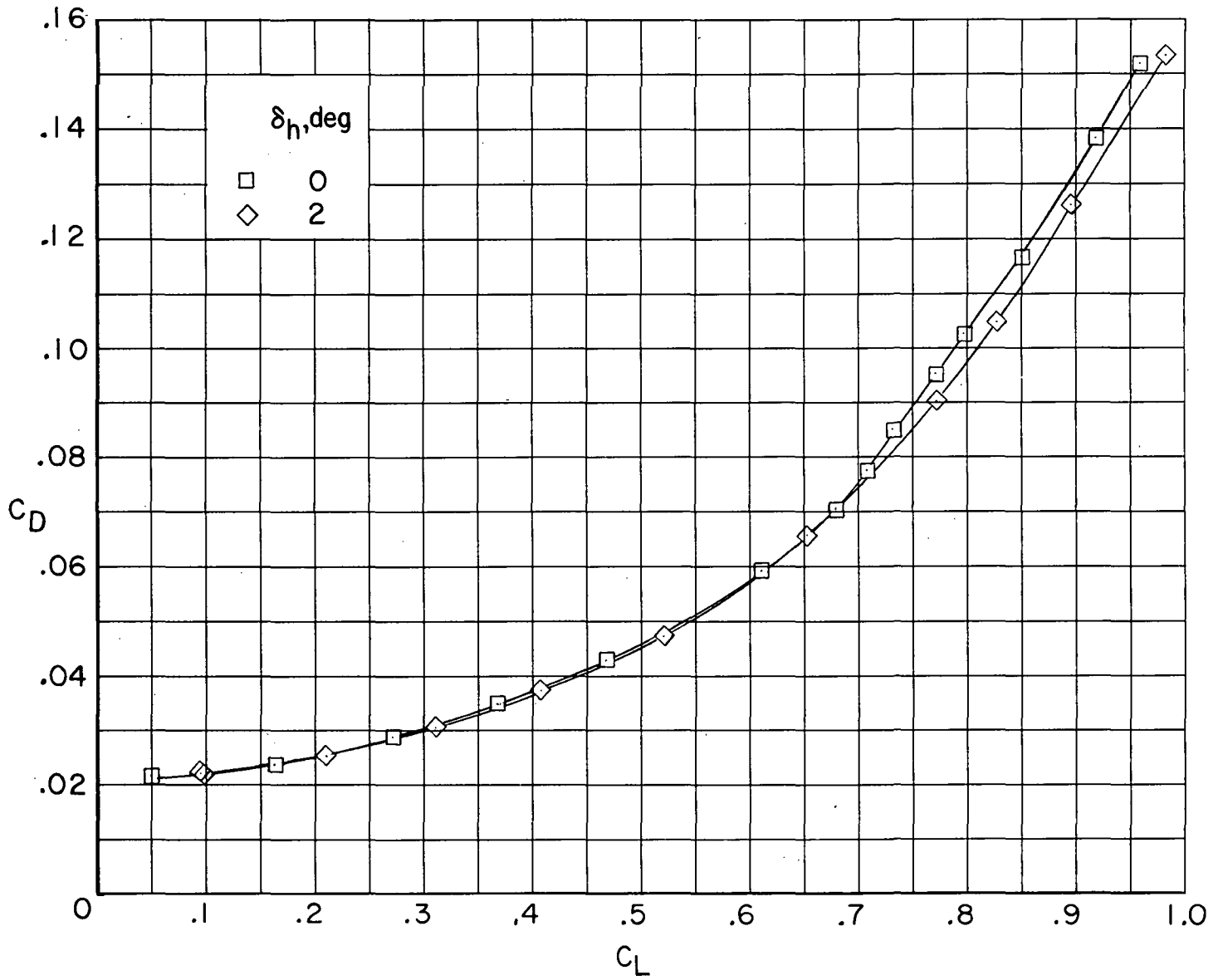
(b) $M = 0.80$. Concluded.

Figure 22.- Continued.



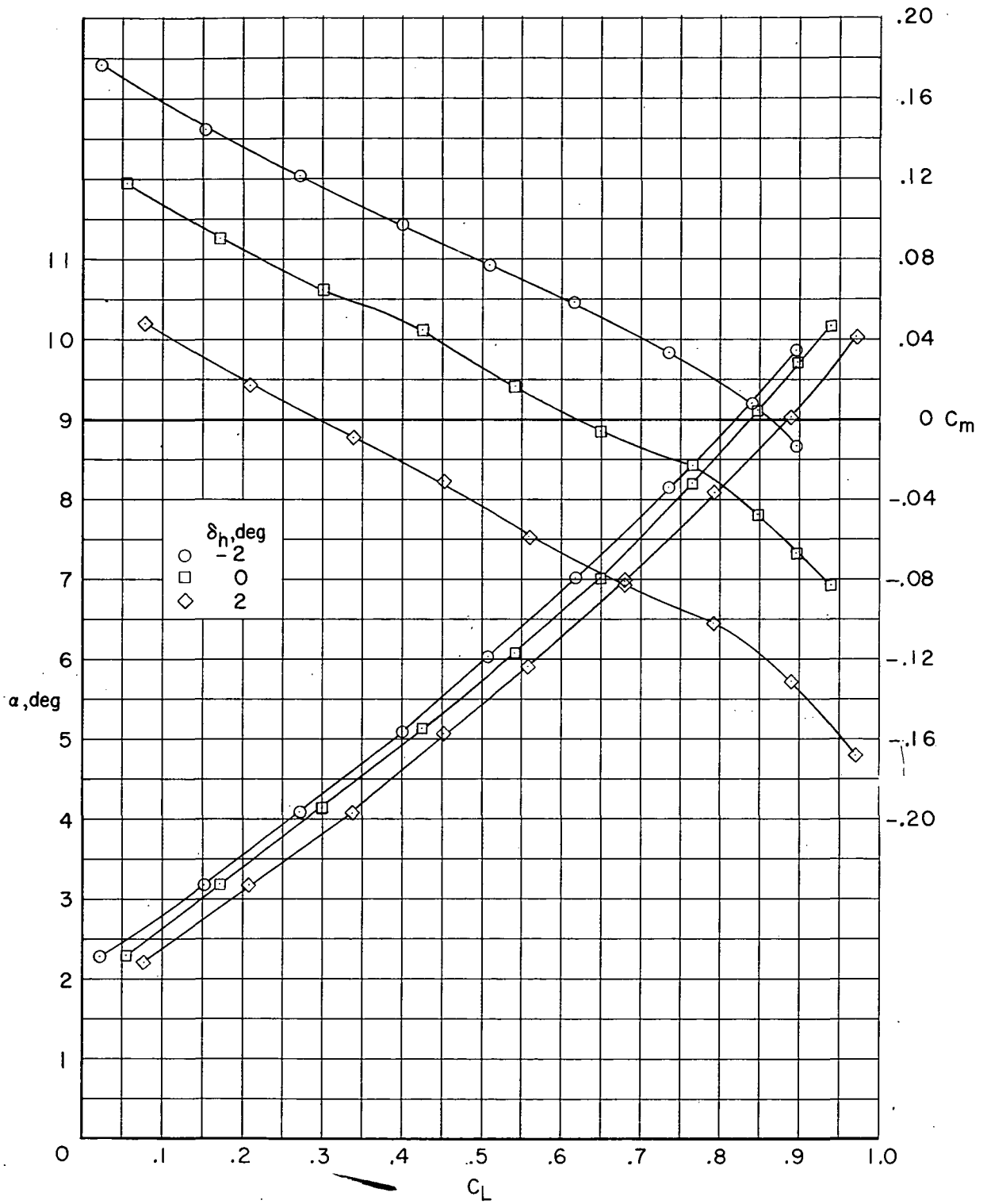
(c) $M = 0.85$.

Figure 22.- Continued.



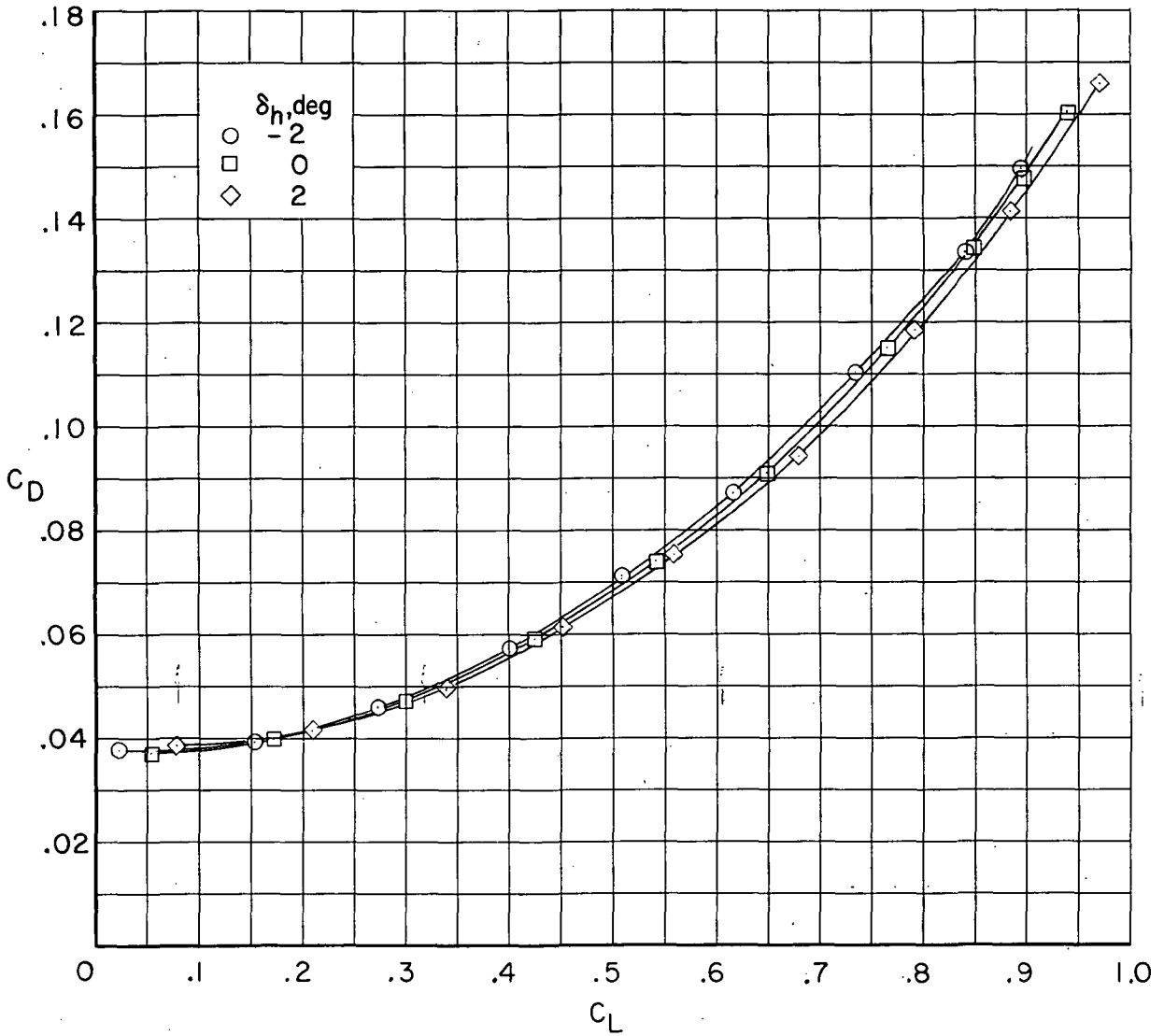
(c) $M = 0.85$. Concluded.

Figure 22. - Continued.



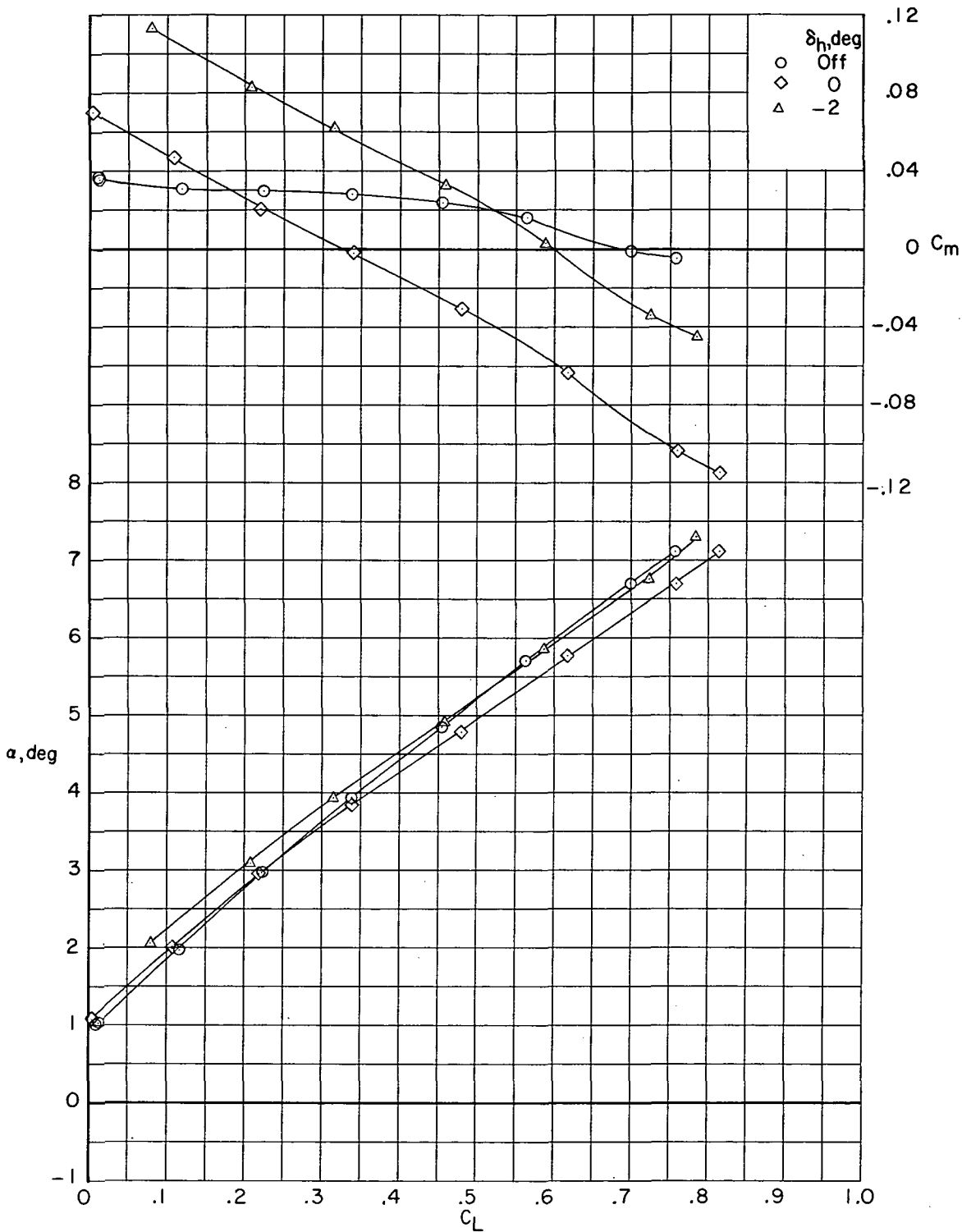
(d) $M = 0.91$.

Figure 22.- Continued.



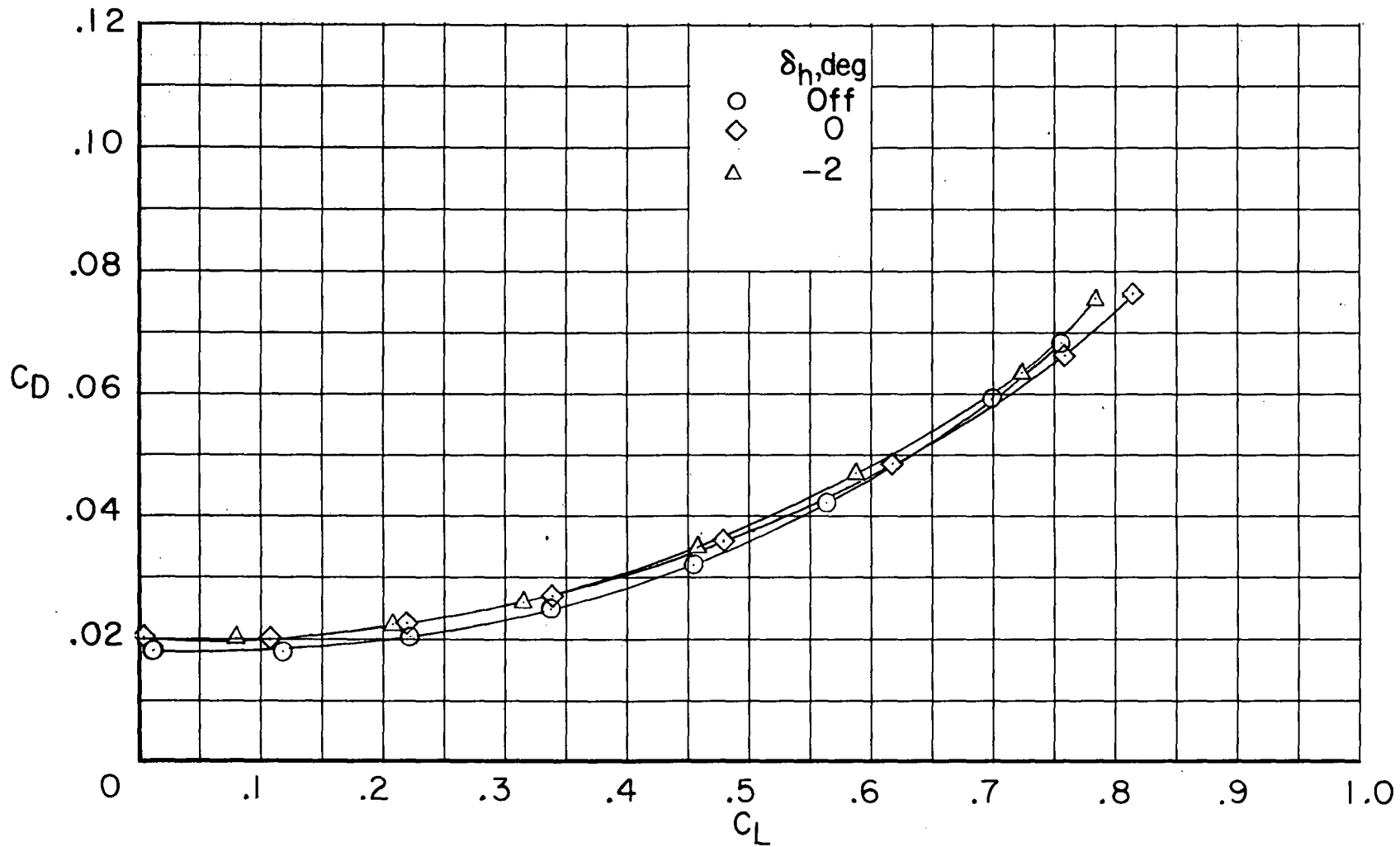
(d) $M = 0.91$. Concluded.

Figure 22.- Concluded.



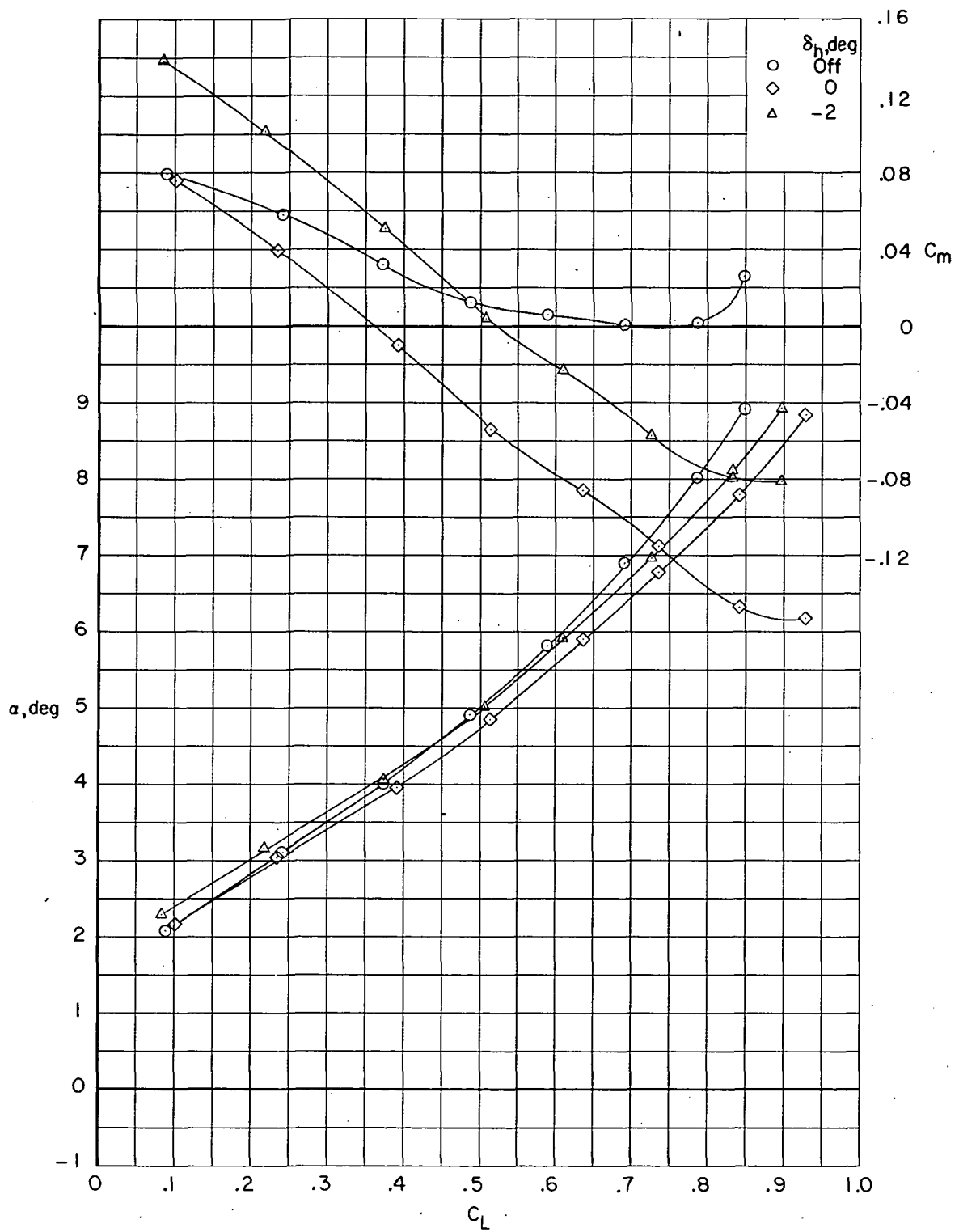
(a) $M = 0.85$.

Figure 23.- Effect of horizontal-tail deflection on longitudinal aerodynamic characteristics of configuration with supercritical airfoil B, fuselage fairing, and transition rearward. $\Lambda = 39^\circ$; $i_w = -1^\circ$.



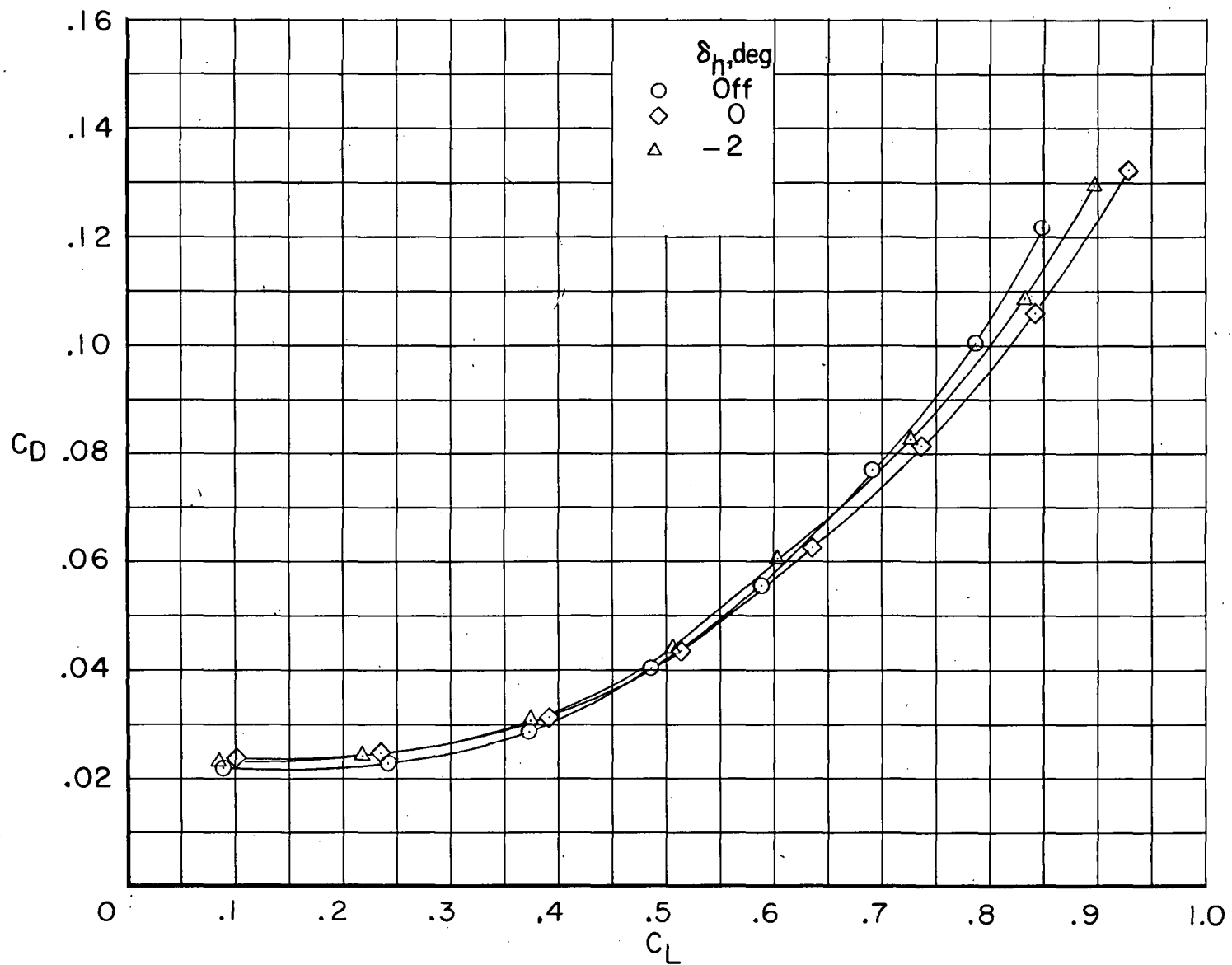
(a) $M = 0.85$. Concluded.

Figure 23. - Continued.



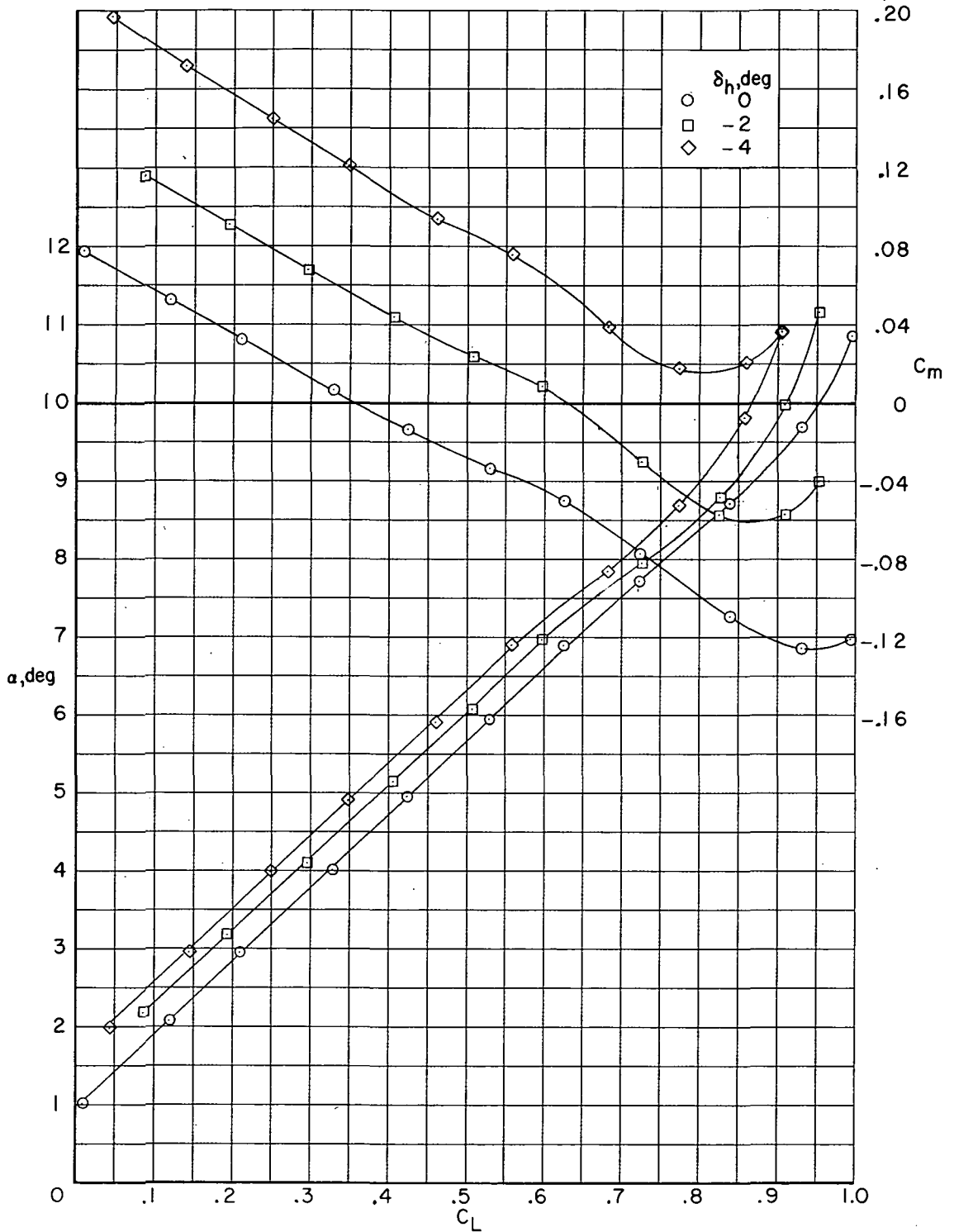
(b) $M = 0.91$.

Figure 23. - Continued.



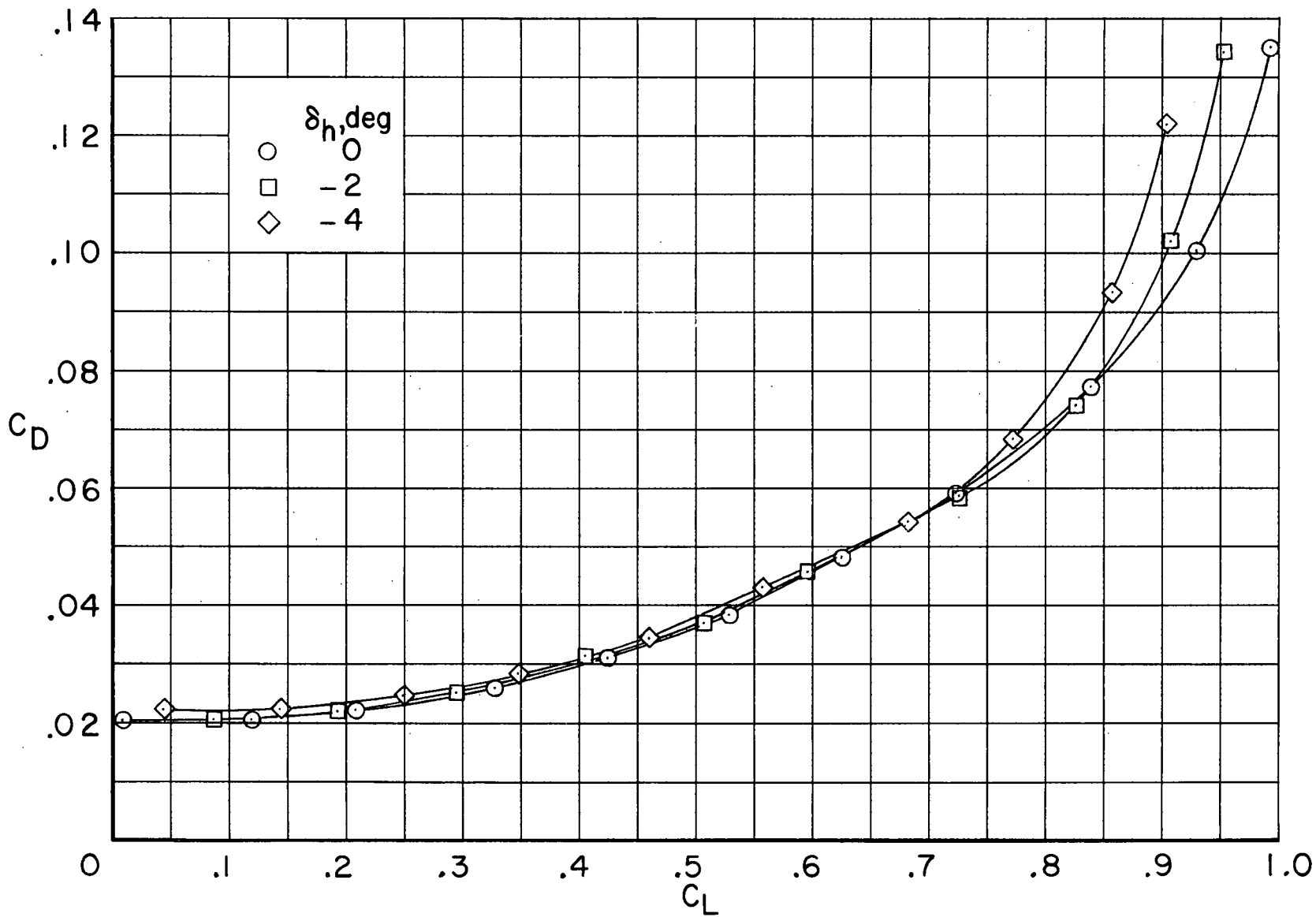
(b) $M = 0.91$. Concluded.

Figure 23.- Concluded.



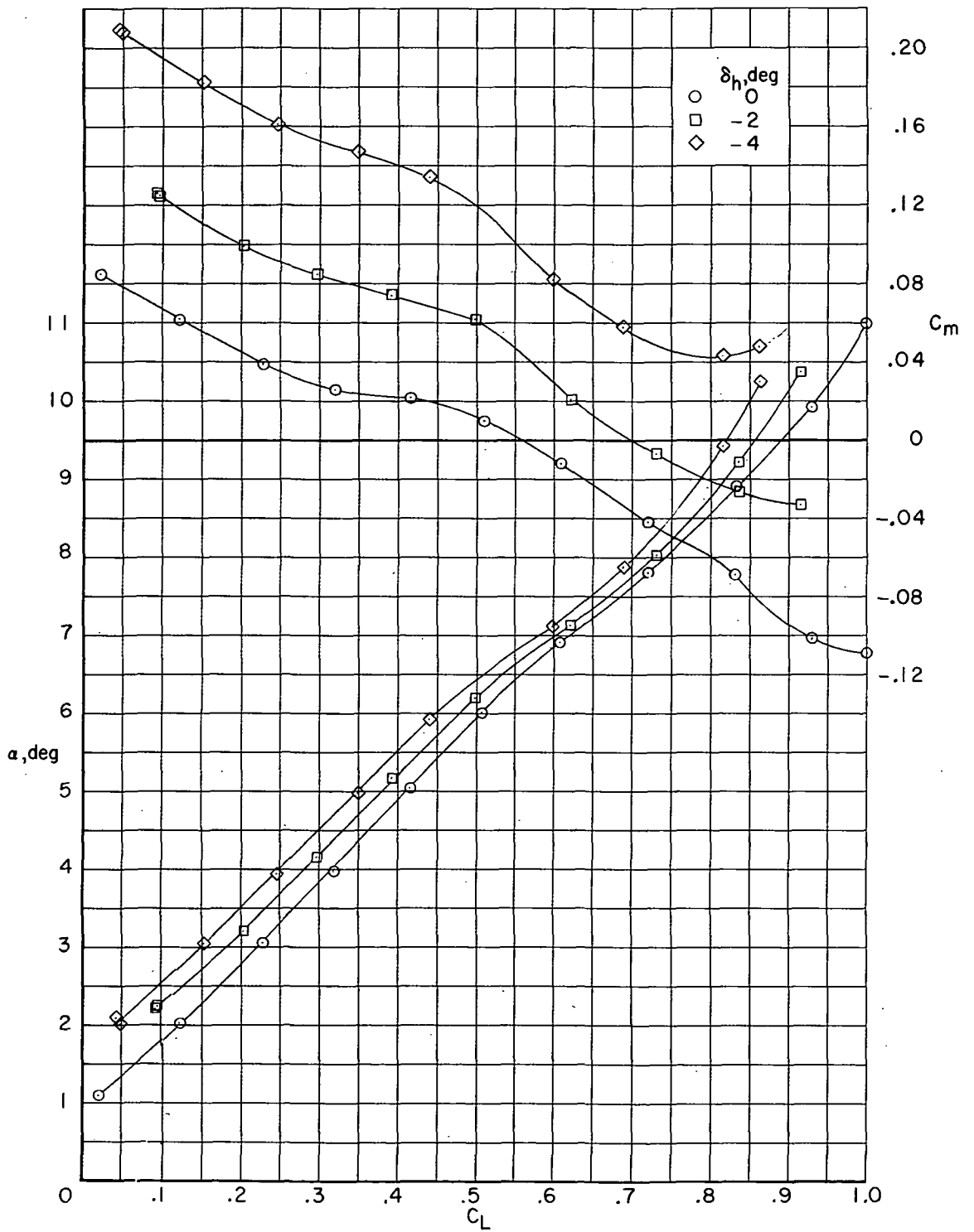
(a) $M = 0.80$.

Figure 24.- Effect of horizontal-tail deflection on longitudinal aerodynamic characteristics of configuration with NACA 64A4XX airfoil, fuselage fairing, and transition forward. $\Lambda = 39^\circ$; $i_w = -1^\circ$.



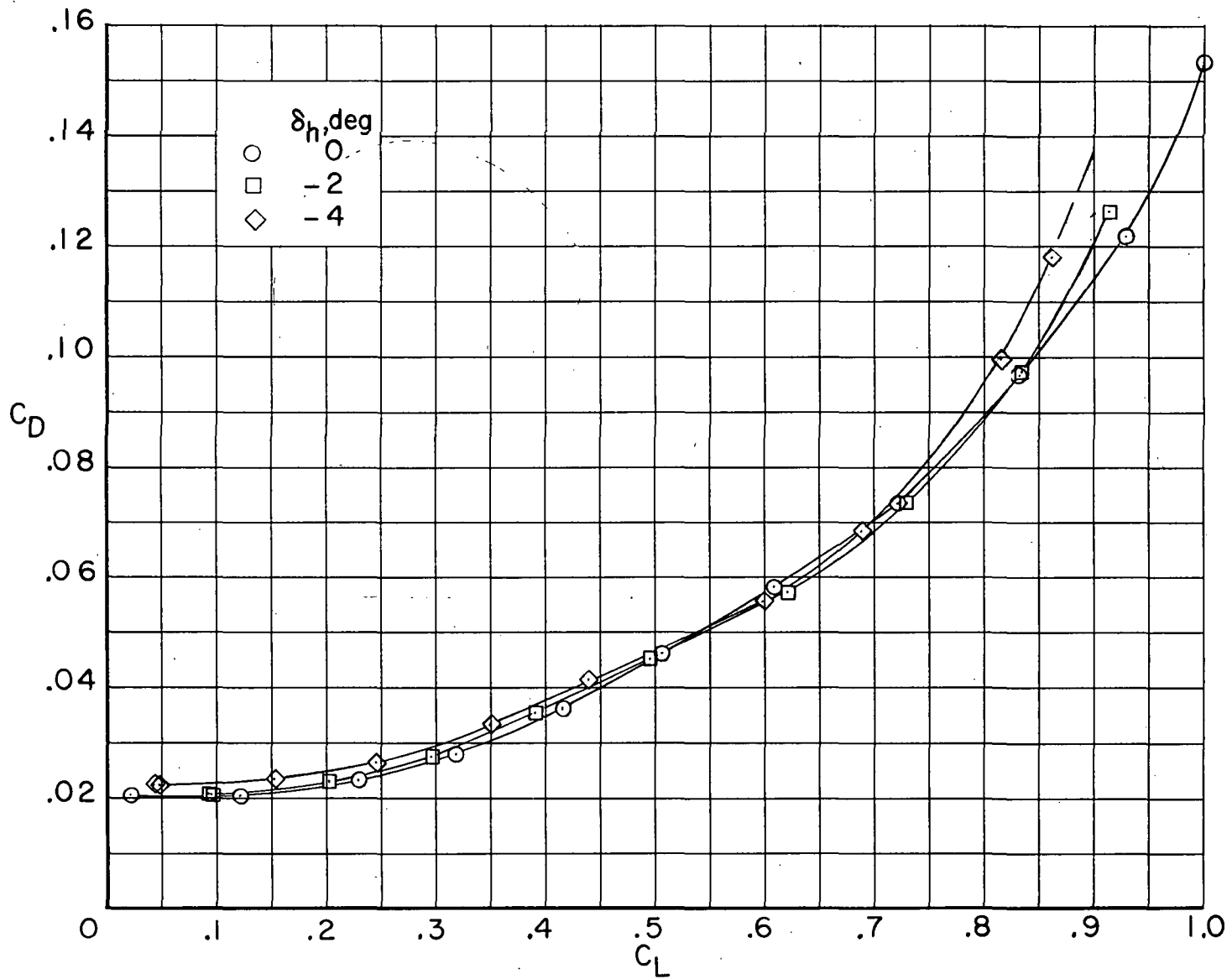
(a) $M = 0.80$. Concluded.

Figure 24.- Continued.



(b) $M = 0.85$.

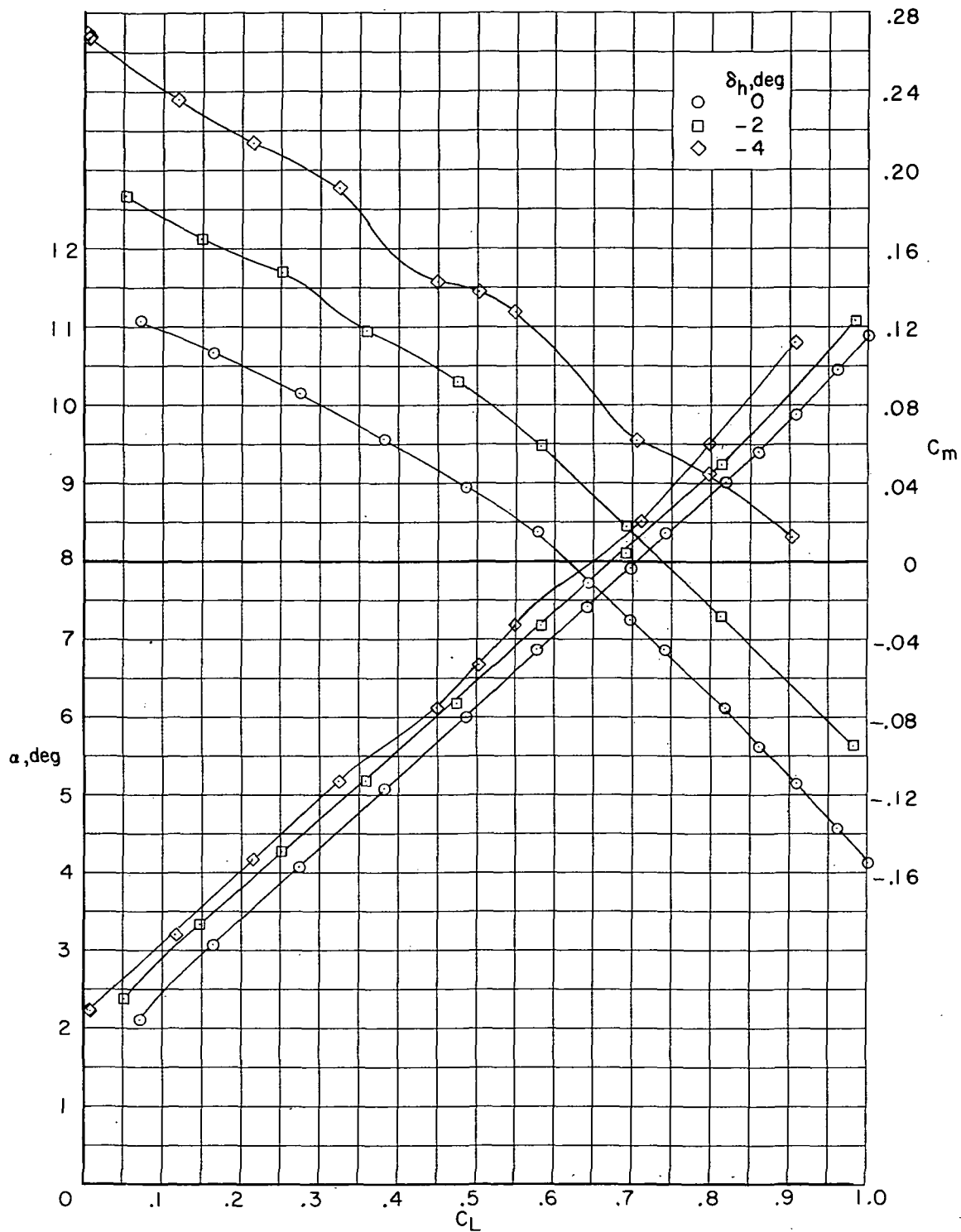
Figure 24. - Continued.



(b) $M = 0.85$. Concluded.

Figure 24.- Continued.

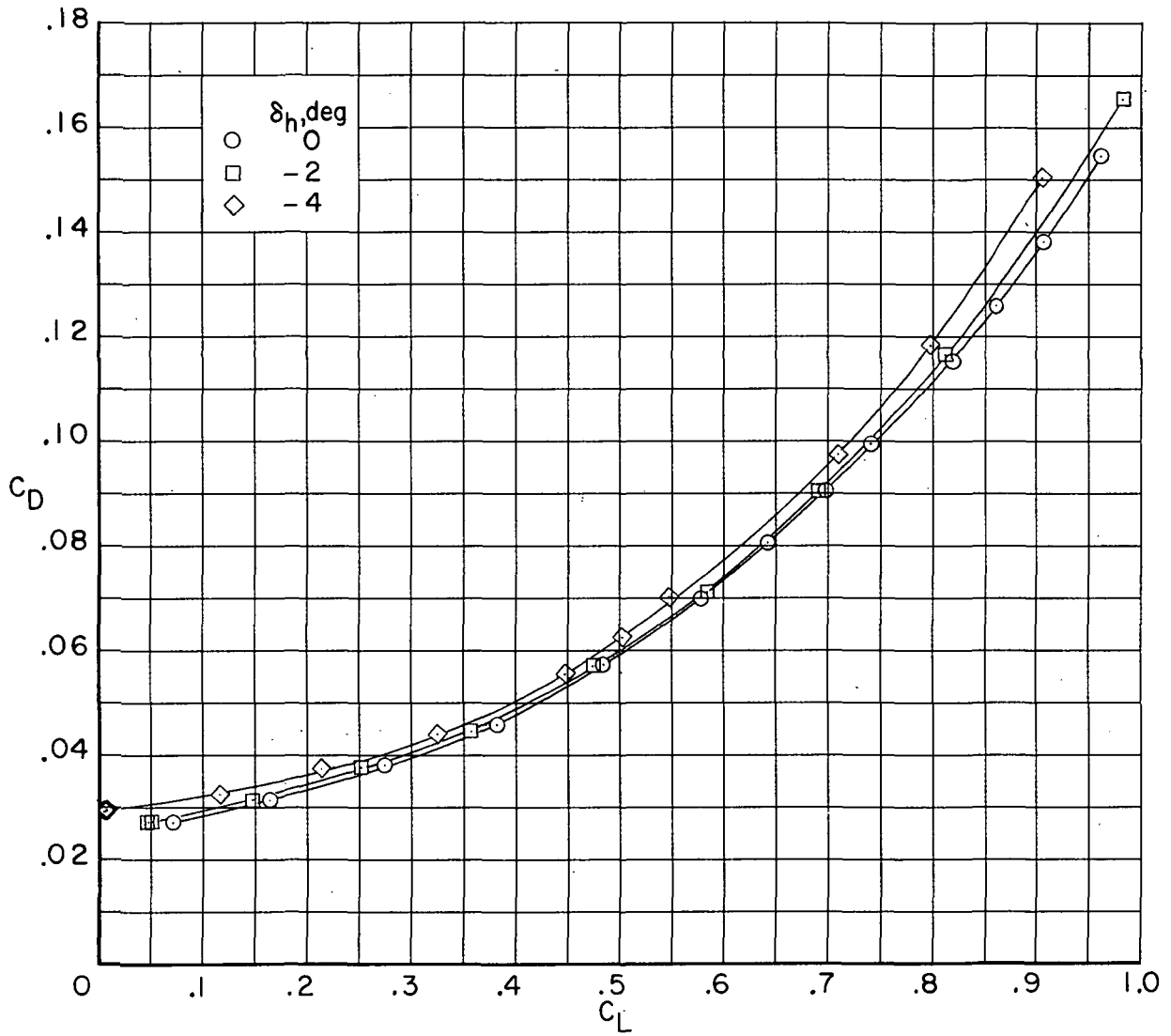
~~CONFIDENTIAL~~



(c) $M = 0.91$.

Figure 24.- Continued.

~~CONFIDENTIAL~~



(c) $M = 0.91$. Concluded.

Figure 24.- Concluded.

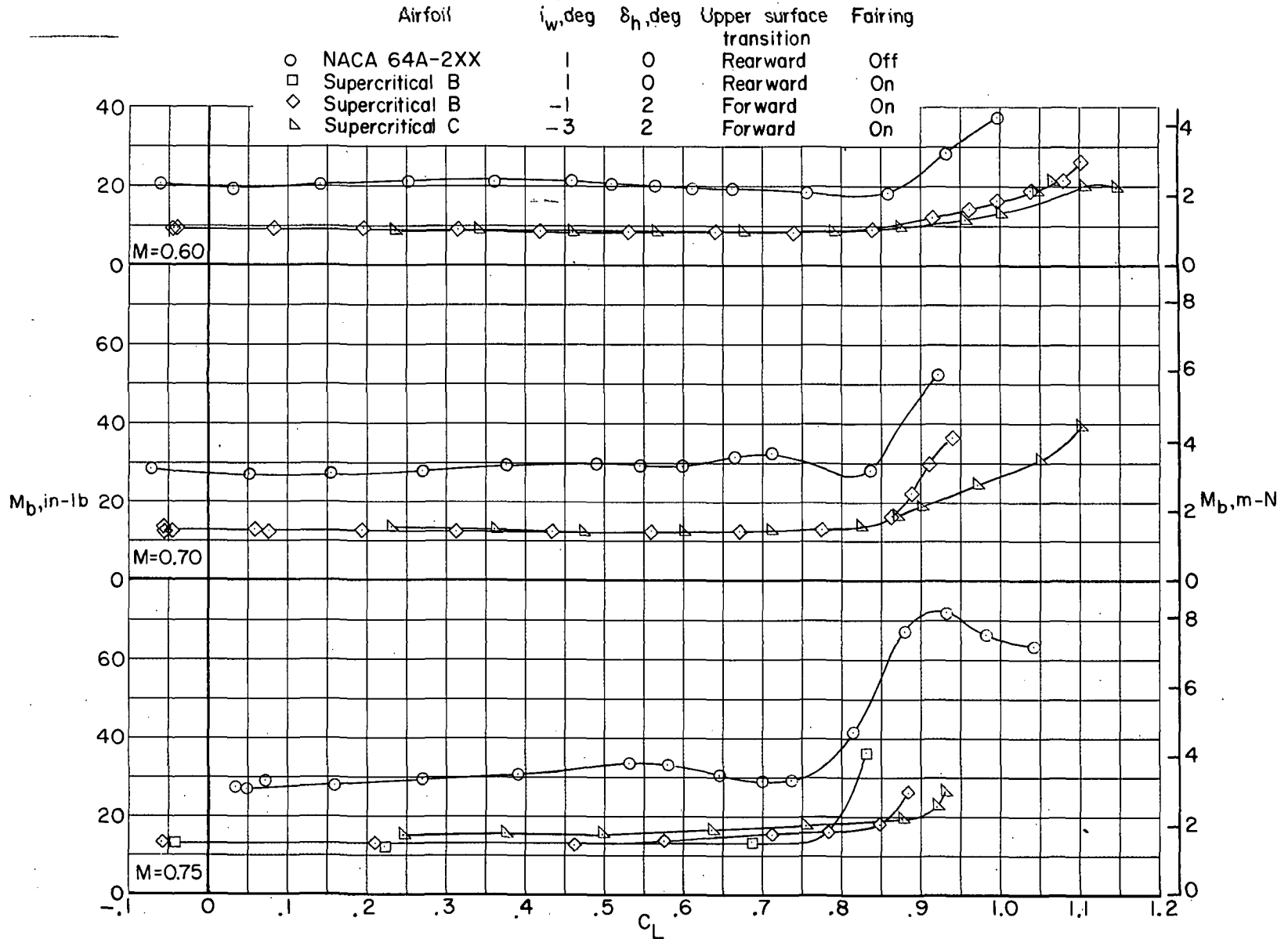


Figure 25.- Comparison of buffet characteristics of basic configuration with NACA 64A2XX and supercritical airfoils. $\Lambda = 26^\circ$.

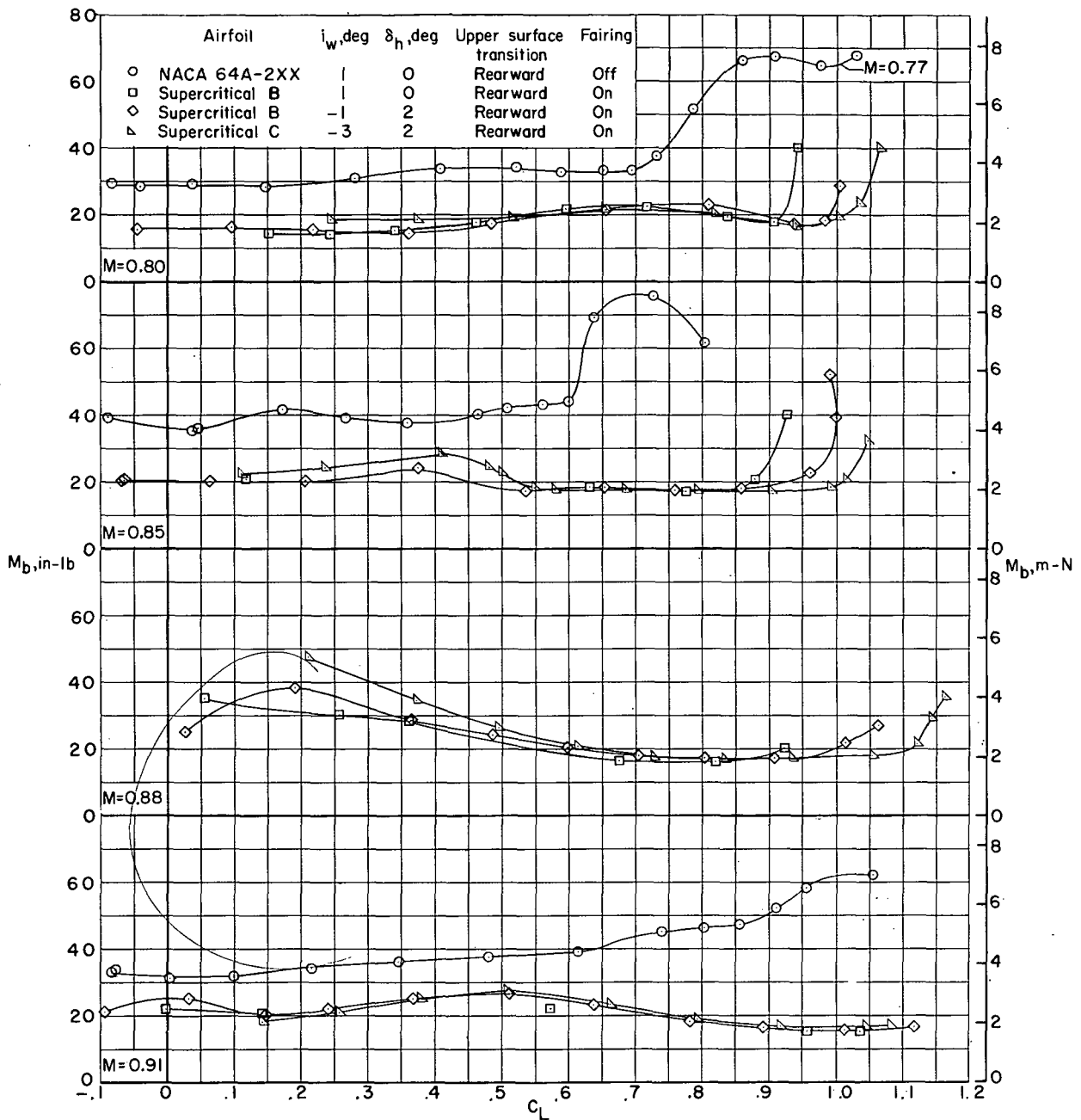


Figure 25. - Concluded.

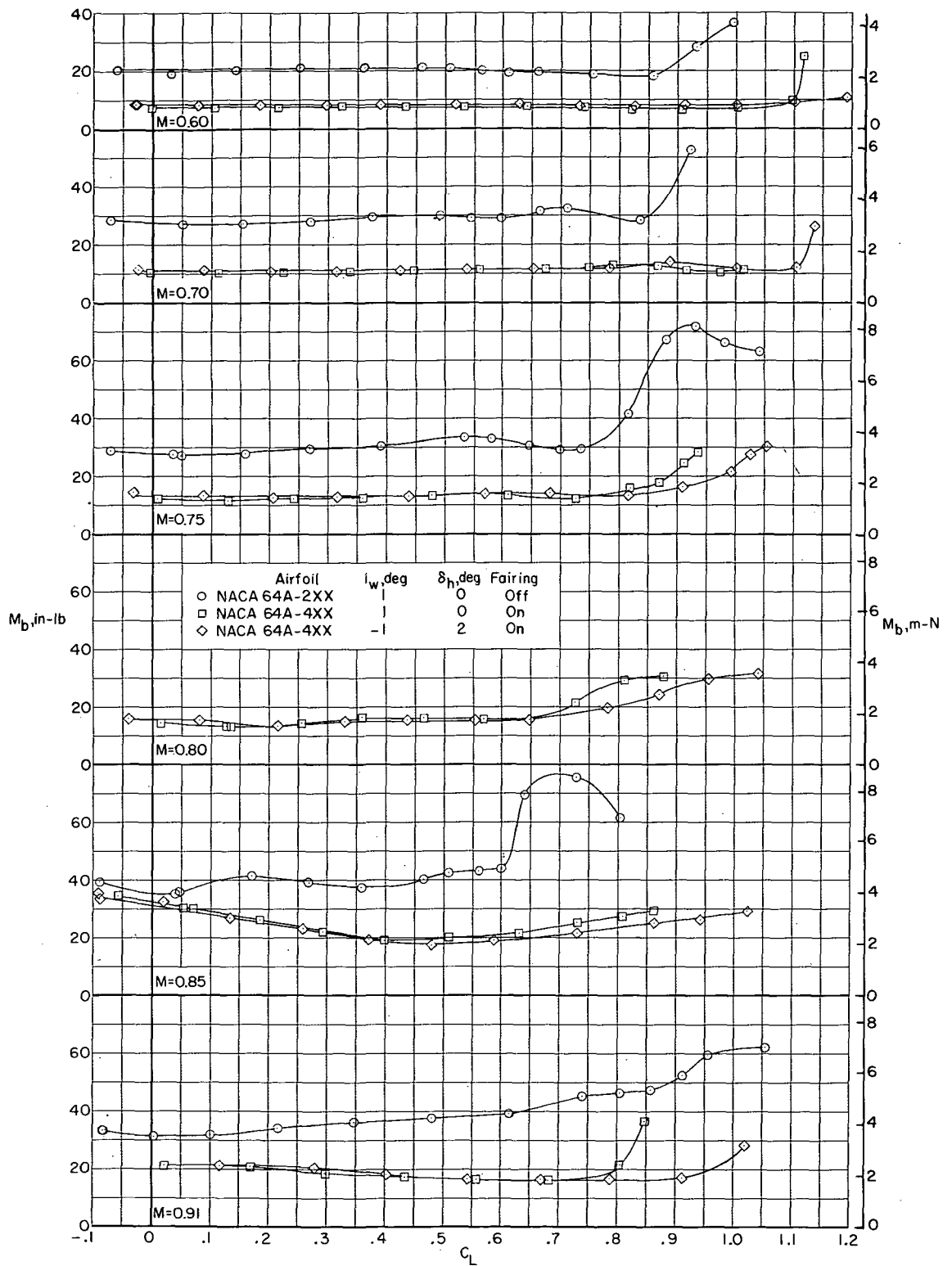


Figure 26.- Comparison of buffet characteristics for configurations with NACA 64A2XX and NACA 64A4XX airfoils and transition rearward. $\Lambda = 26^\circ$.

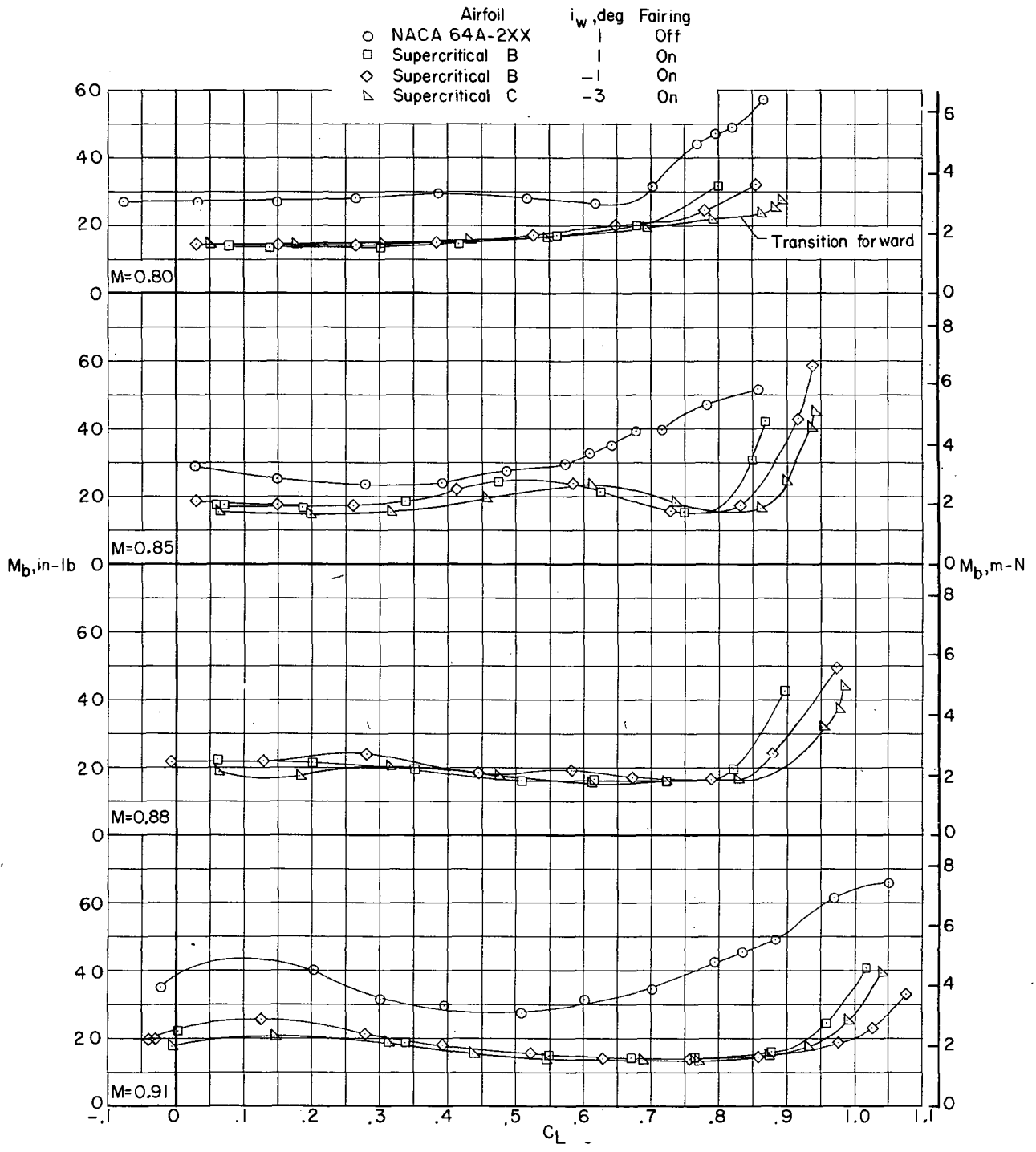


Figure 27. - Comparison of buffet characteristics of basic configuration with NACA 64A2XX and supercritical airfoils and upper surface transition rearward except as noted. $\Lambda = 33^\circ$; $\delta_h = 0^\circ$.

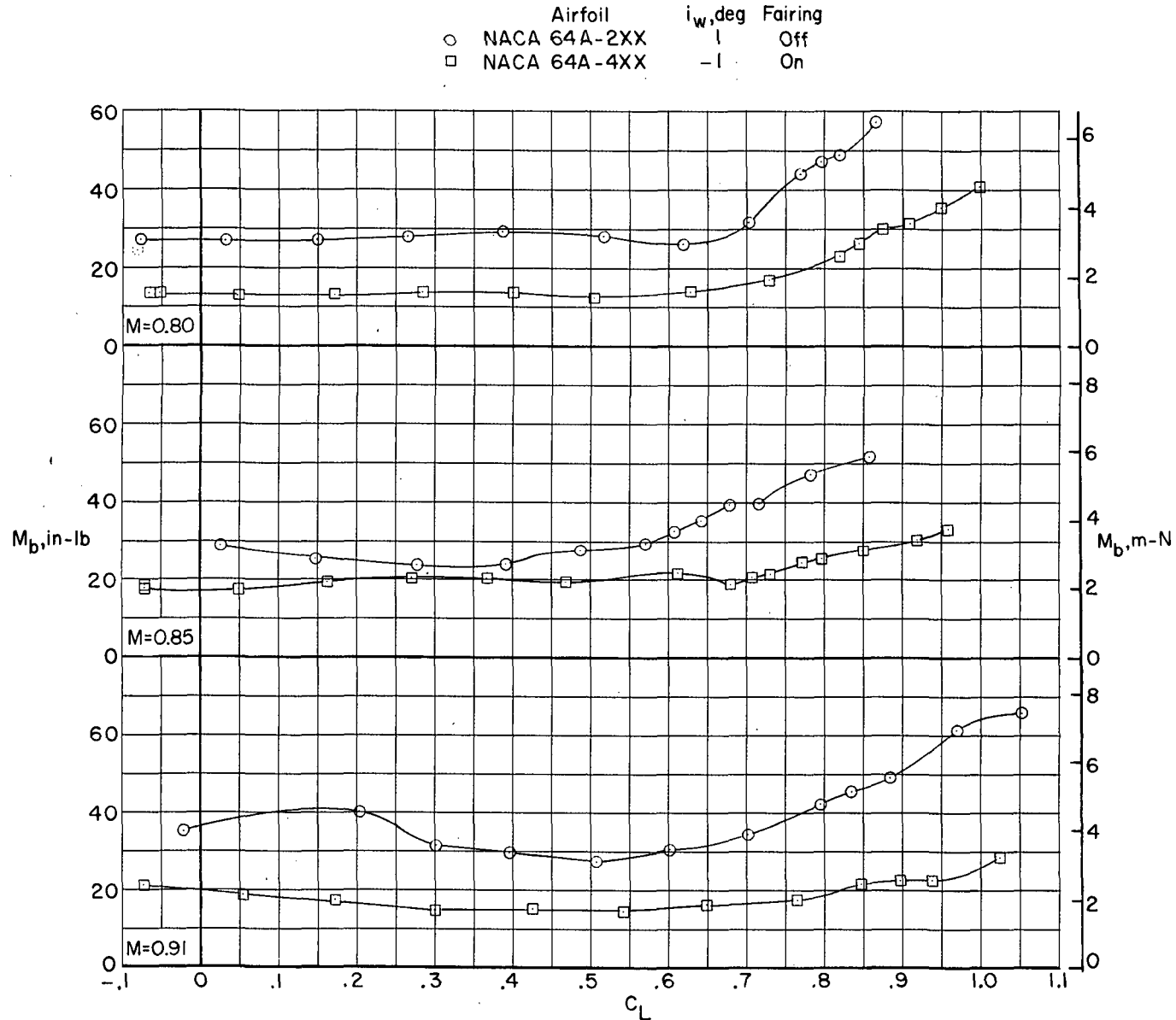


Figure 28.- Comparison of buffet characteristics of basic configuration with NACA 64A2XX and NACA 64A4XX airfoils and transition rearward. $\Lambda = 33^\circ$; $\delta_h = 0^\circ$.

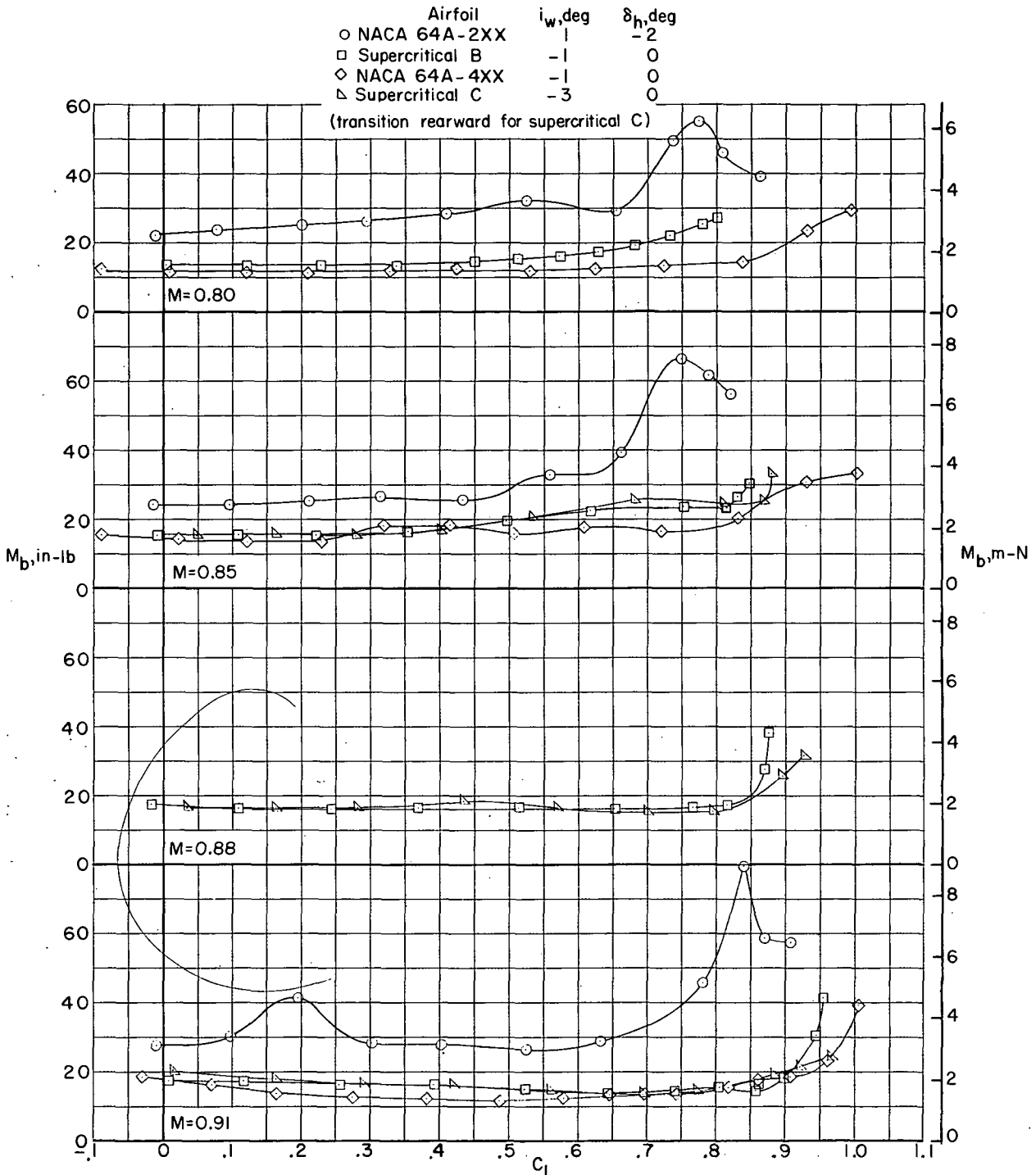
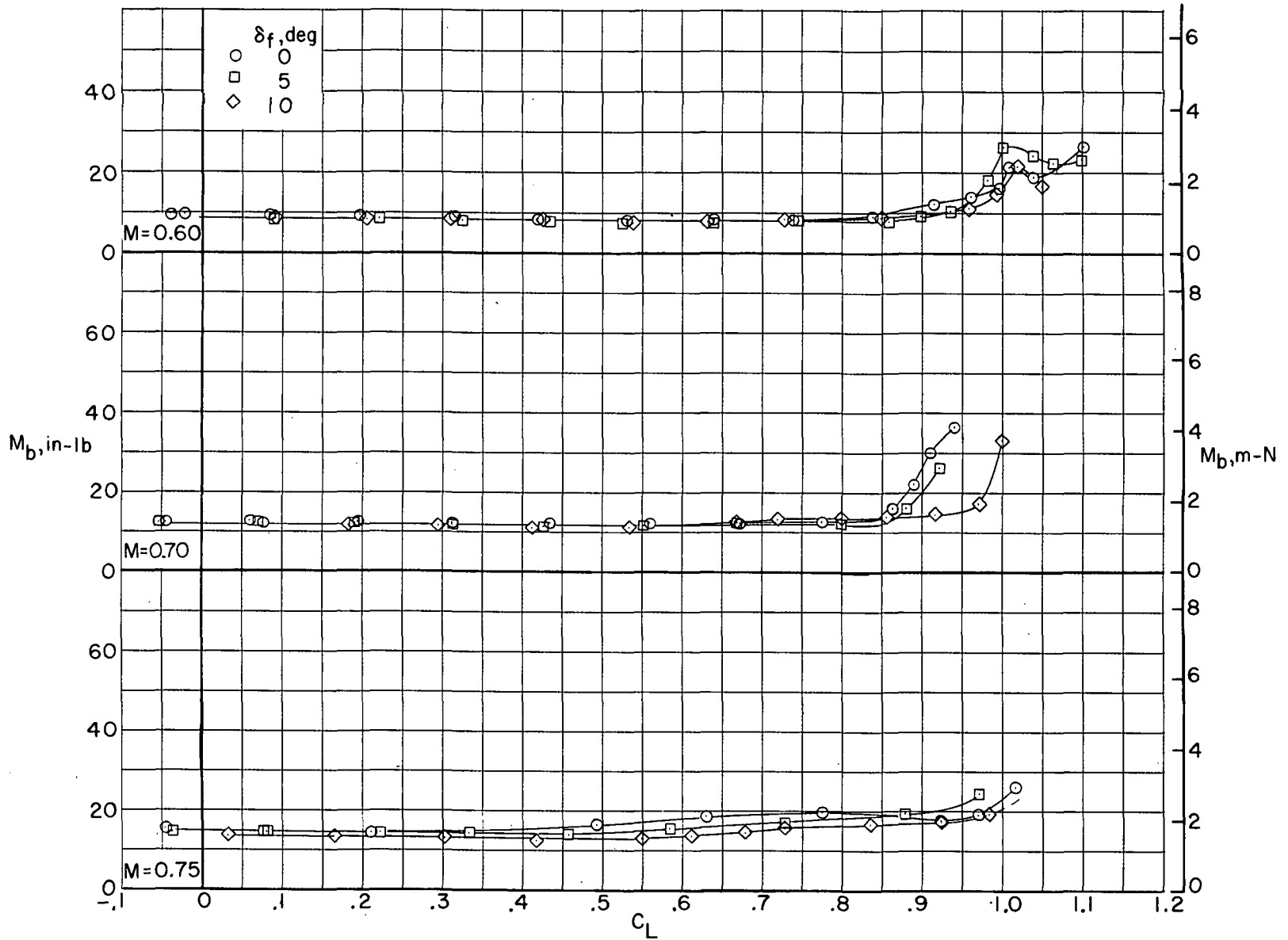
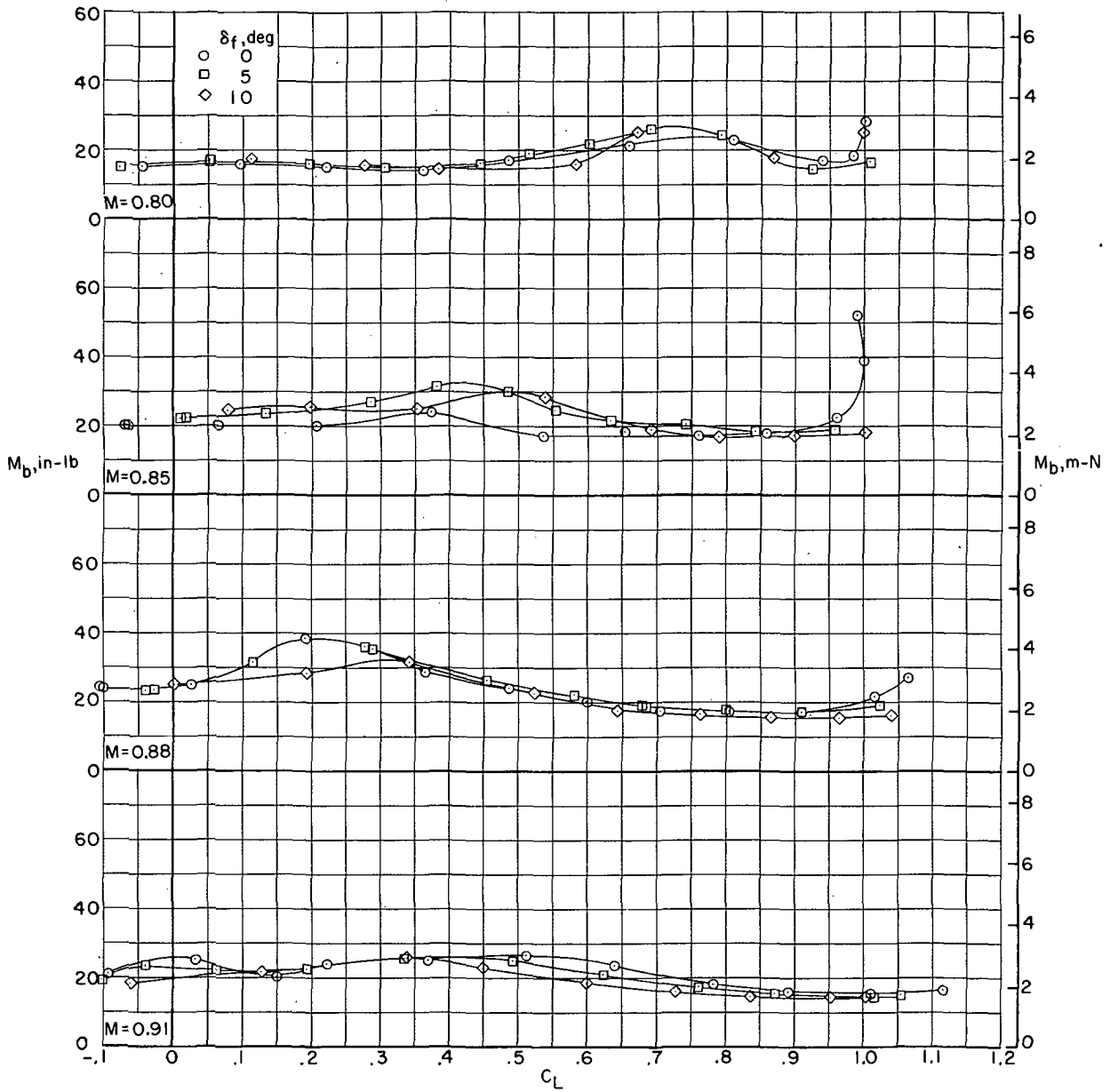


Figure 29.- Comparison of buffet characteristics for configurations with supercritical, NACA 64A2XX, and NACA 64A4XX airfoils, fuselage fairing, and upper surface transition forward except as noted. $\Lambda = 39^\circ$.



(a) Upper surface transition forward.

Figure 30.- Effect of trailing-edge flaps on buffet characteristics for configuration with supercritical airfoil B and fuselage fairing. $\Lambda = 26^\circ$; $\delta_h = 2^\circ$.



(b) Upper surface transition rearward.

Figure 30.- Concluded.



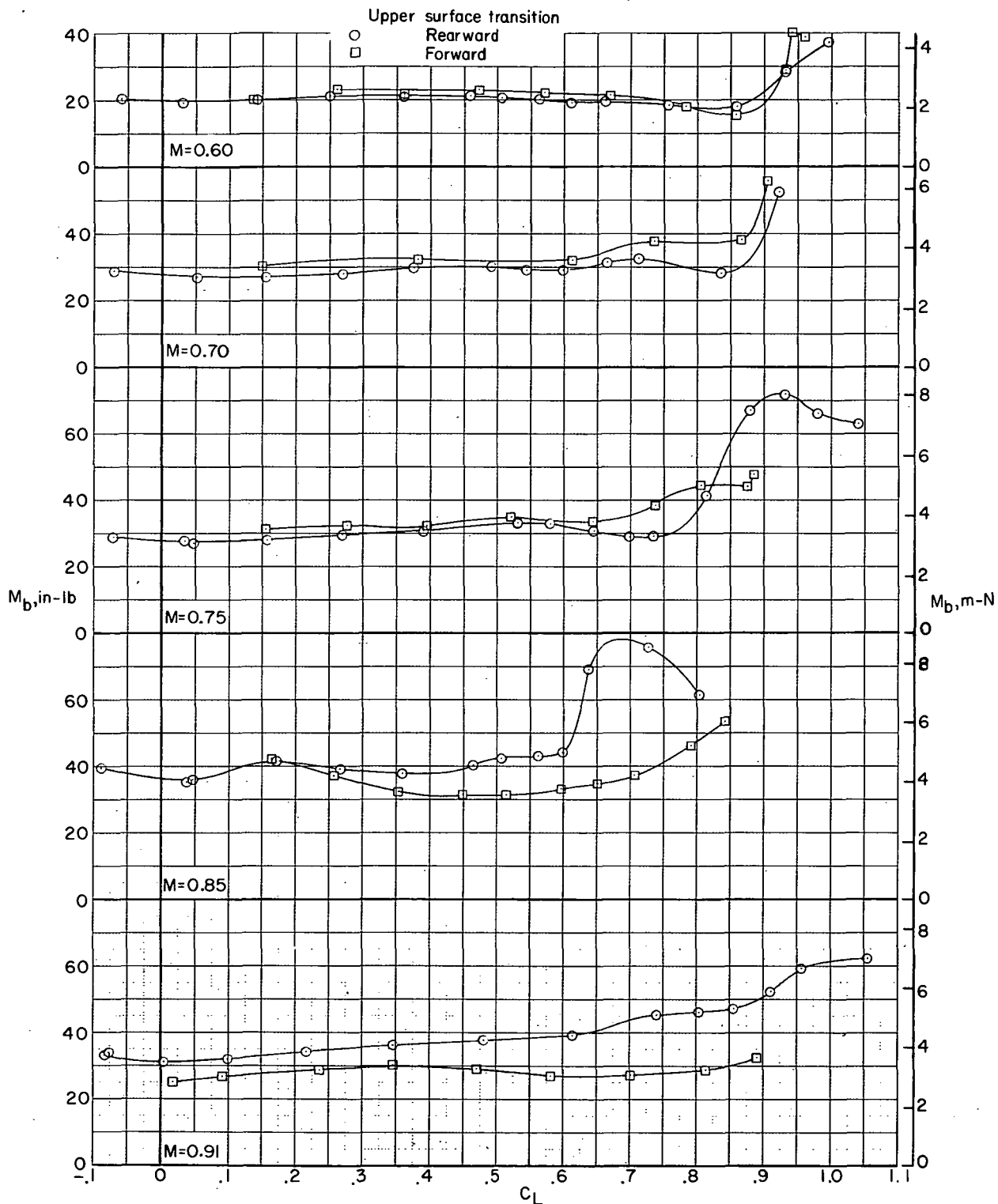


Figure 31. - Effect of upper surface transition location on buffet characteristics for configuration with NACA 64A2XX airfoils and fuselage fairing. $\Lambda = 26^\circ$; $\delta_h = 0^\circ$; $i_w = 1^\circ$.

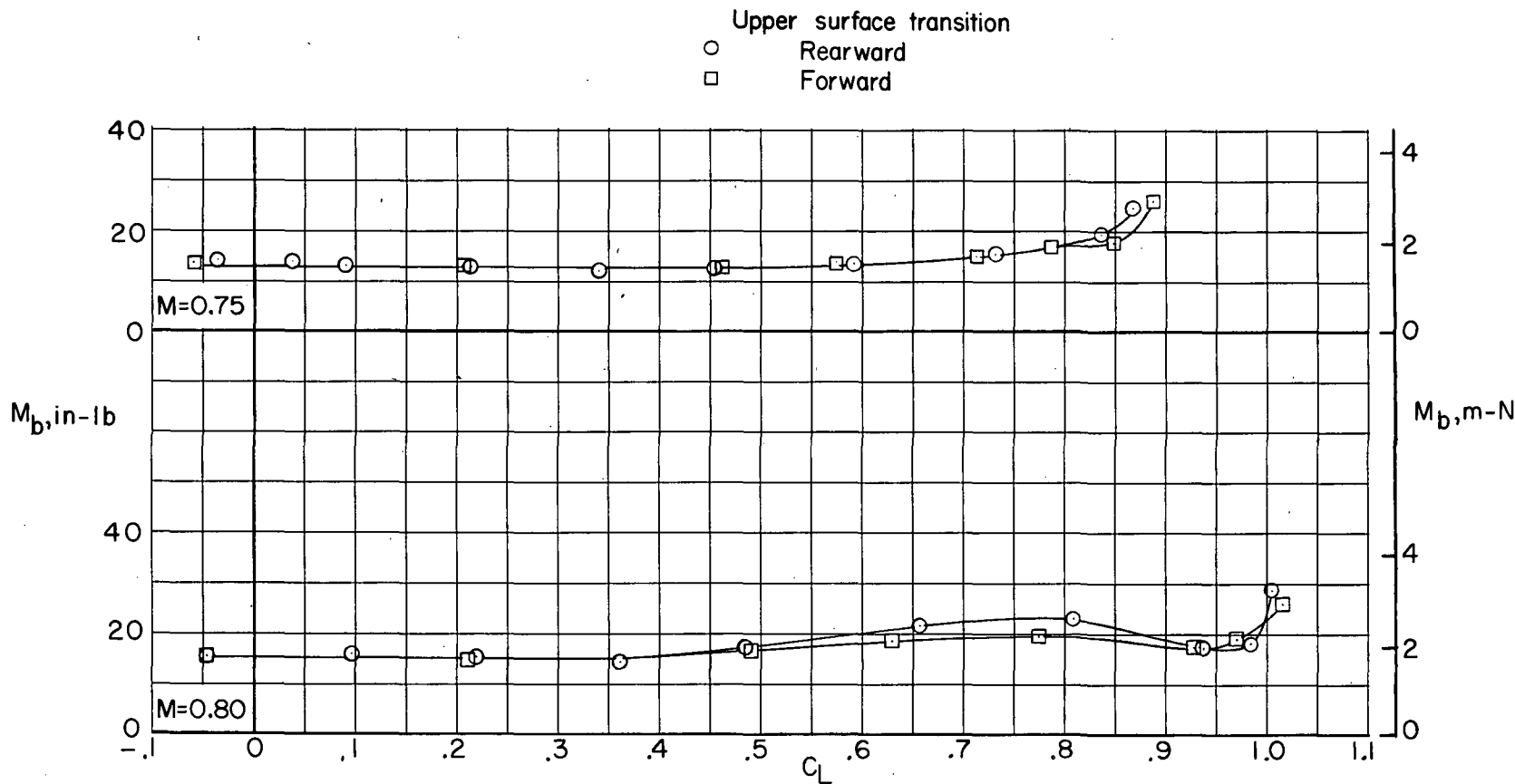


Figure 32. - Effect of upper surface transition location on buffet characteristics for configuration with supercritical airfoil B and fuselage fairing. $\Lambda = 26^\circ$; $\delta_h = 2^\circ$.

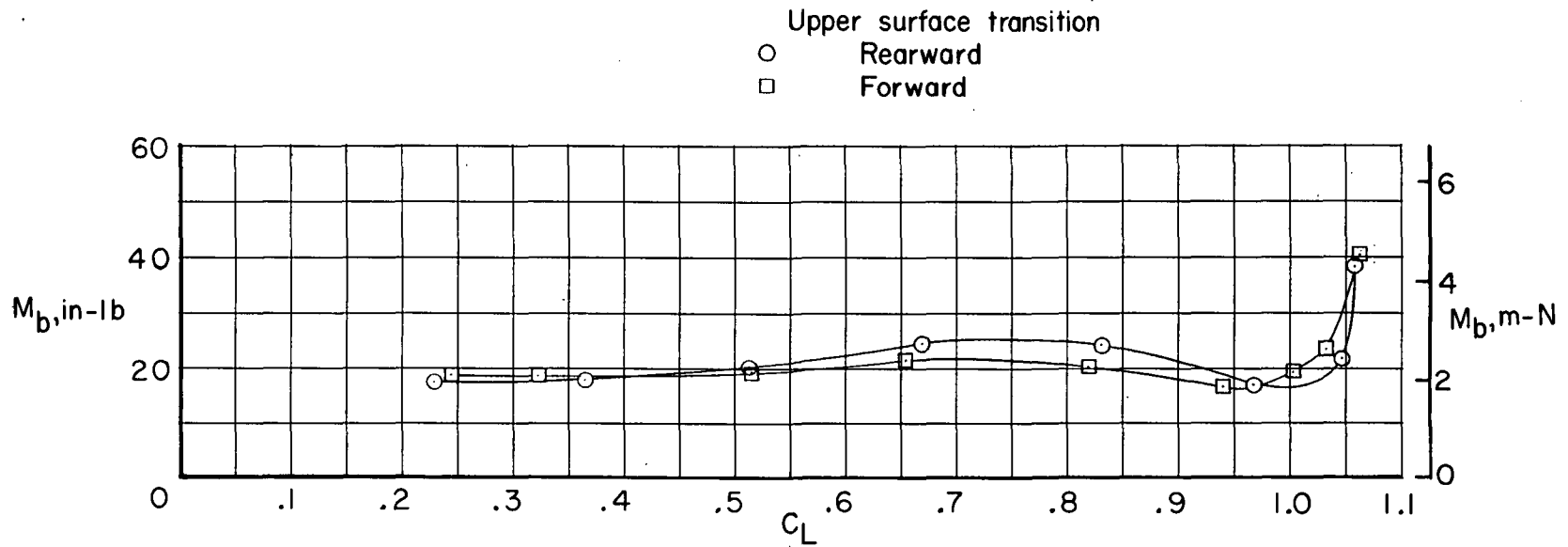


Figure 33.- Effect of upper surface transition location on buffet characteristics for configuration with supercritical airfoil C and fuselage fairing. $\Lambda = 26^\circ$; $i_w = -3^\circ$; $\delta_h = 2^\circ$; $M = 0.80$.

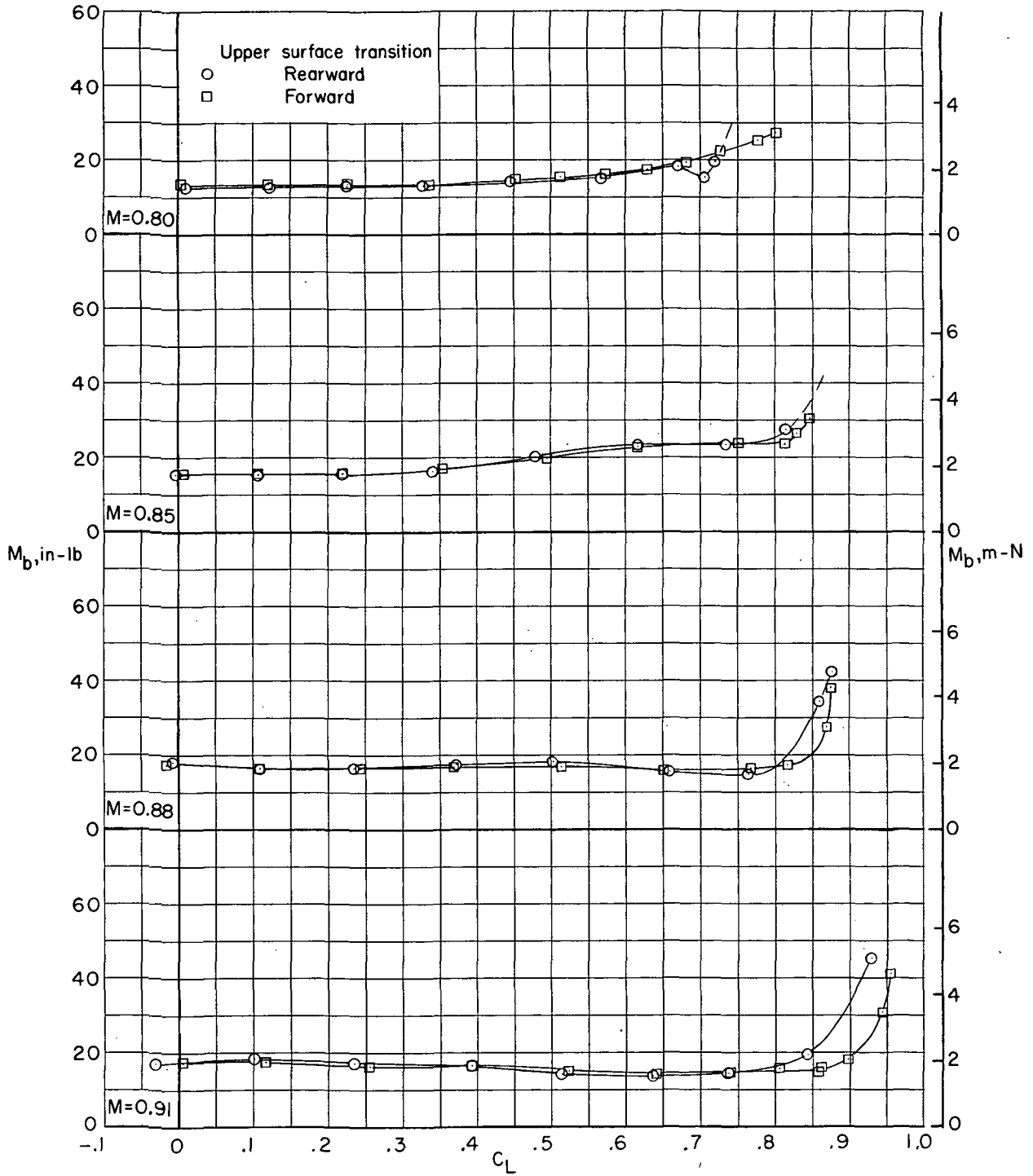
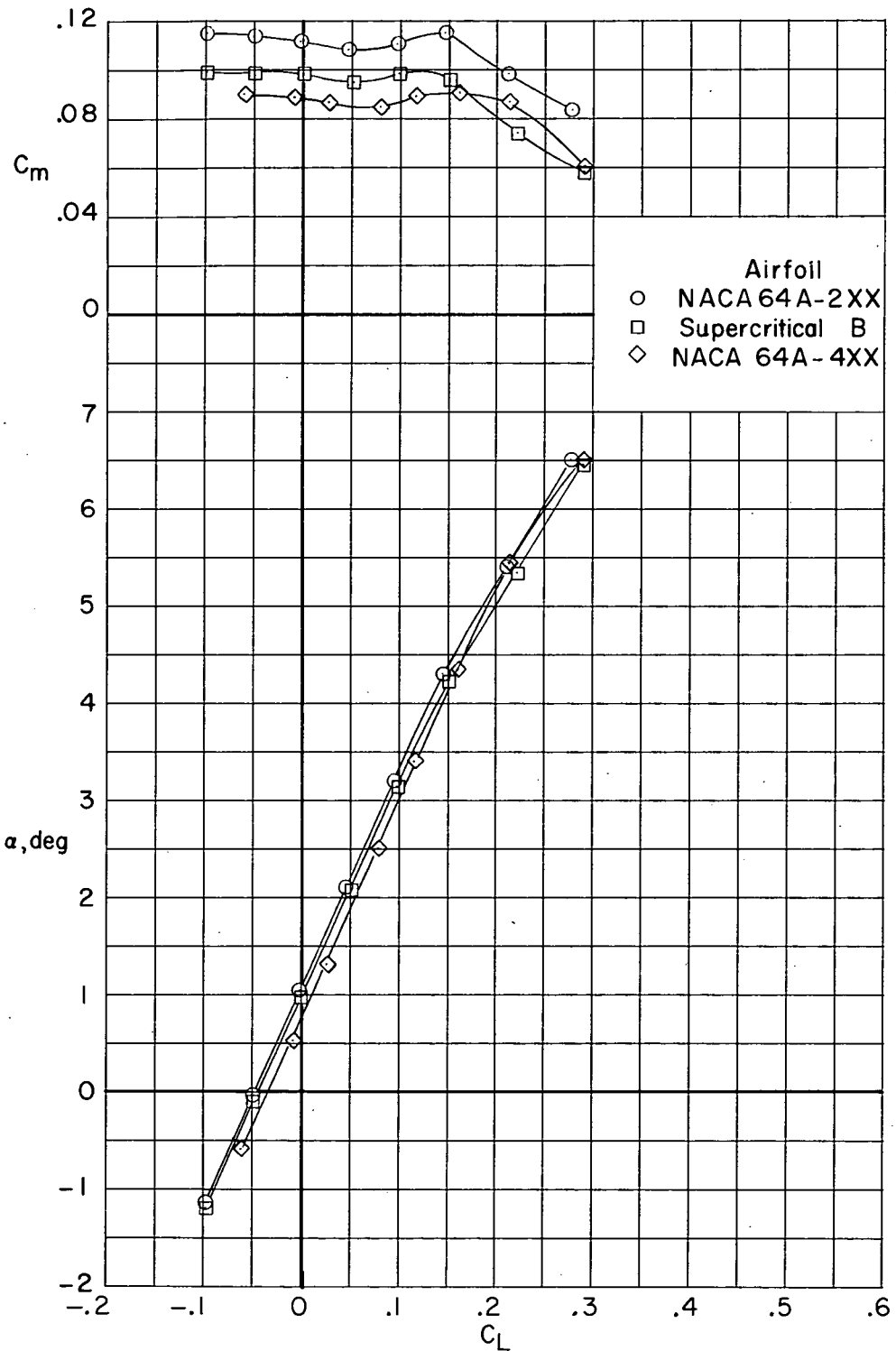
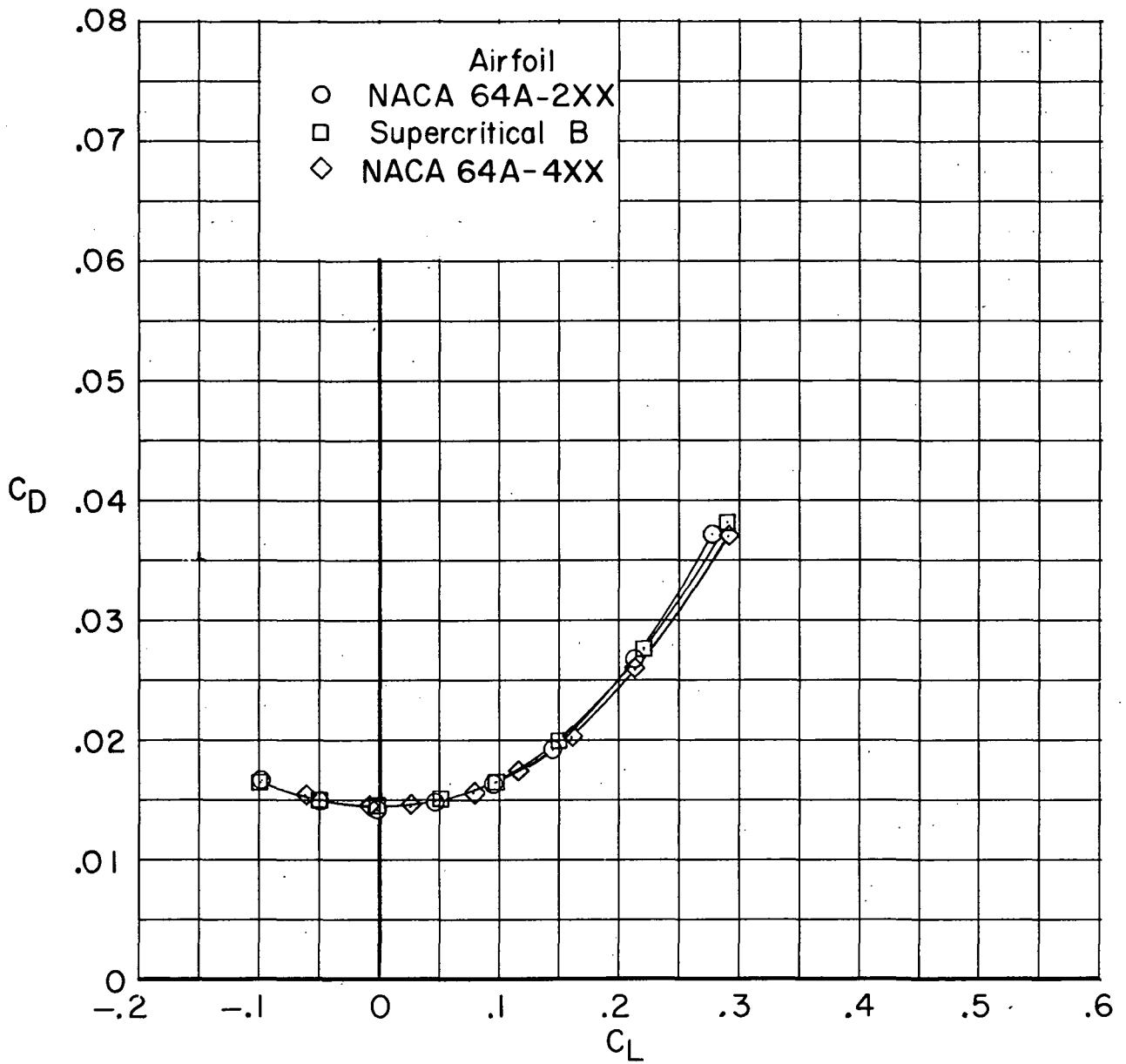
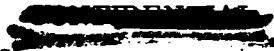


Figure 34.- Effect of upper surface transition location on buffet characteristics for configuration with supercritical airfoil B and fuselage fairing. $\Lambda = 39^\circ$; $\delta_h = 0^\circ$.



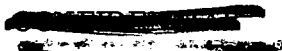
(a) $M = 0.95$.

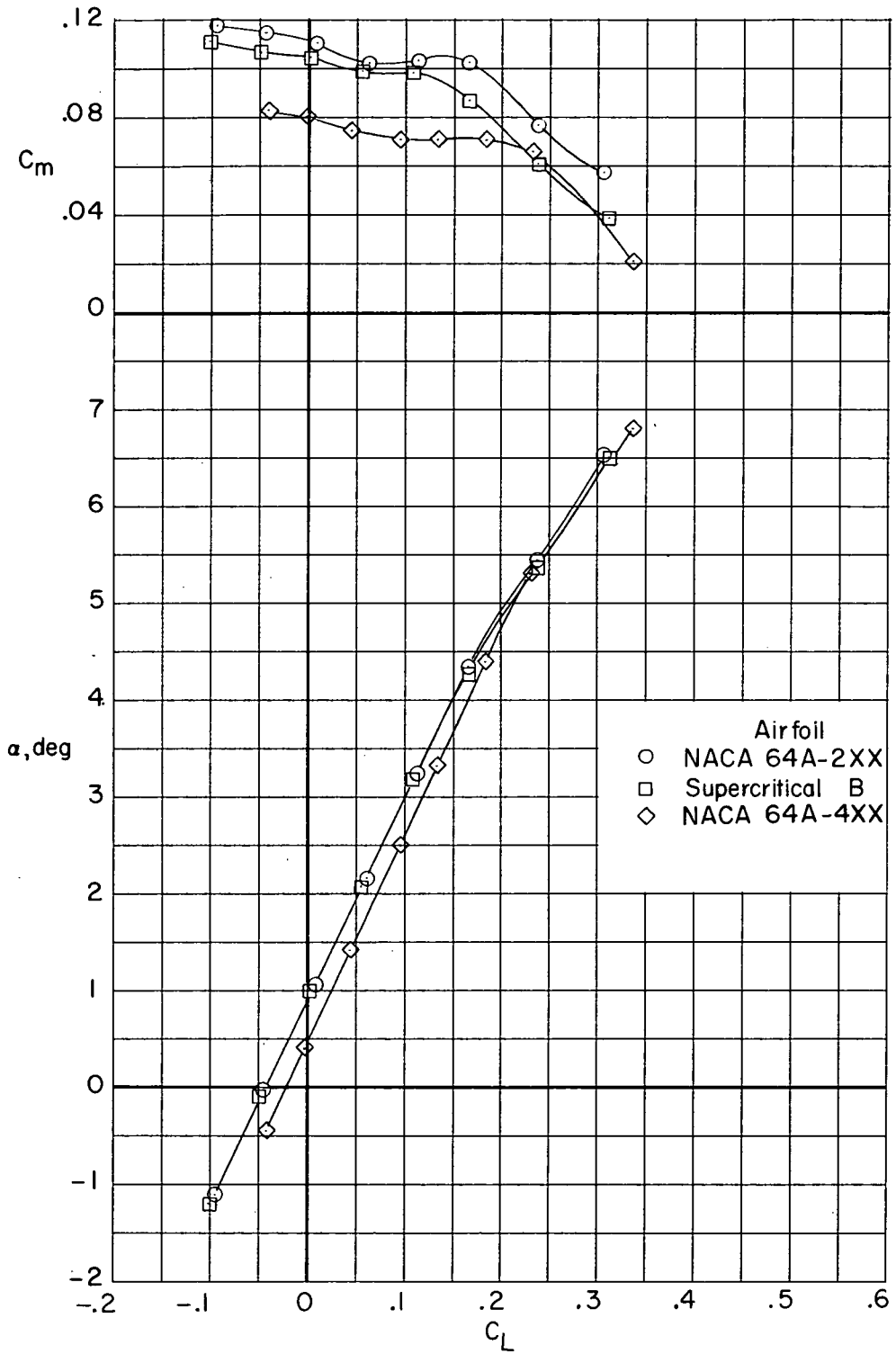
Figure 35.- Comparison of longitudinal aerodynamic characteristics for configuration with NACA 64A2XX, supercritical, and NACA 64A4XX airfoils, fuselage fairing, and transition rearward. $\Lambda = 72.5^\circ$; $i_w = 1^\circ$; $\delta_h = \text{Off}$.



(a) $M = 0.95$. Concluded.

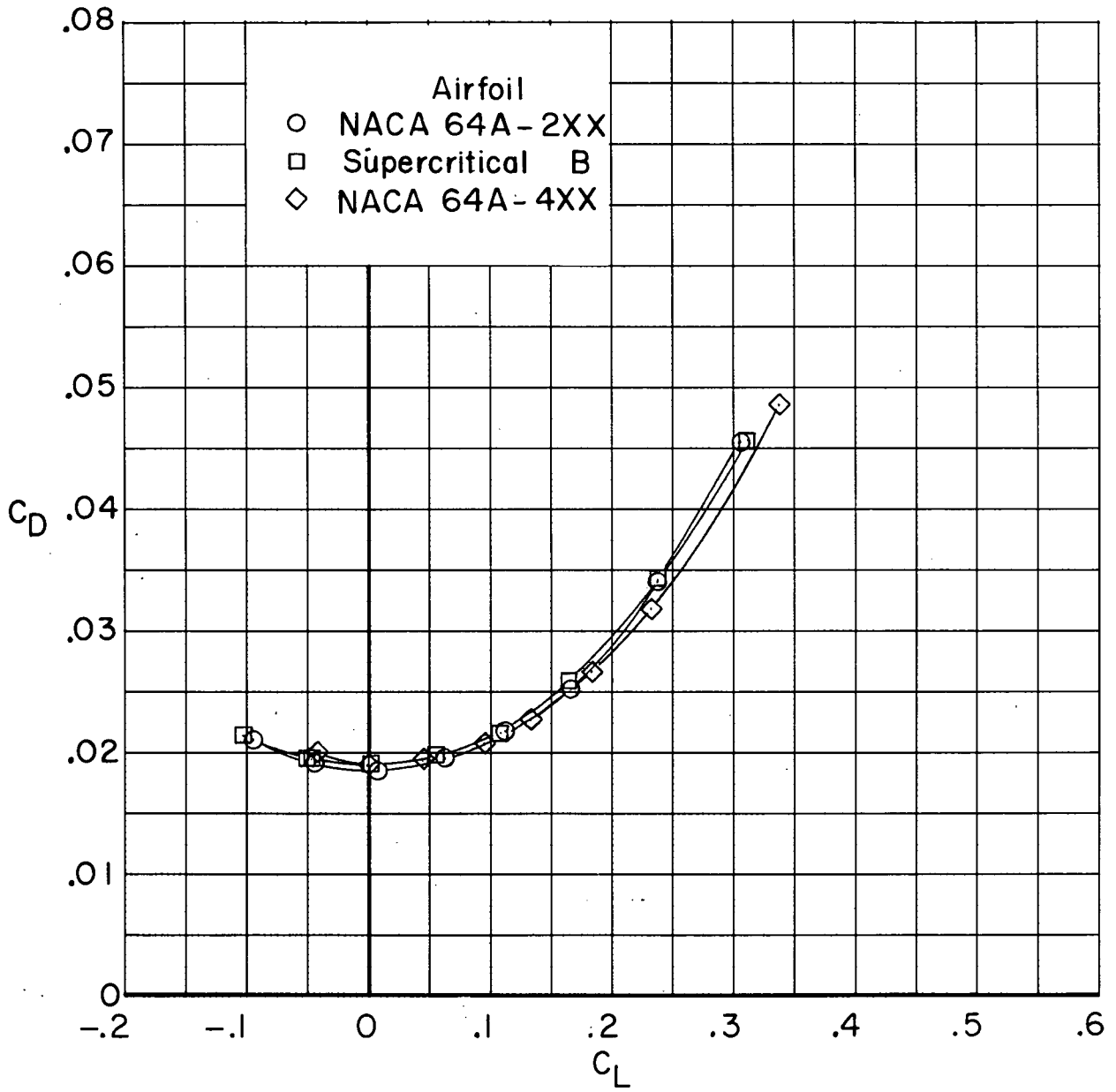
Figure 35.- Continued.





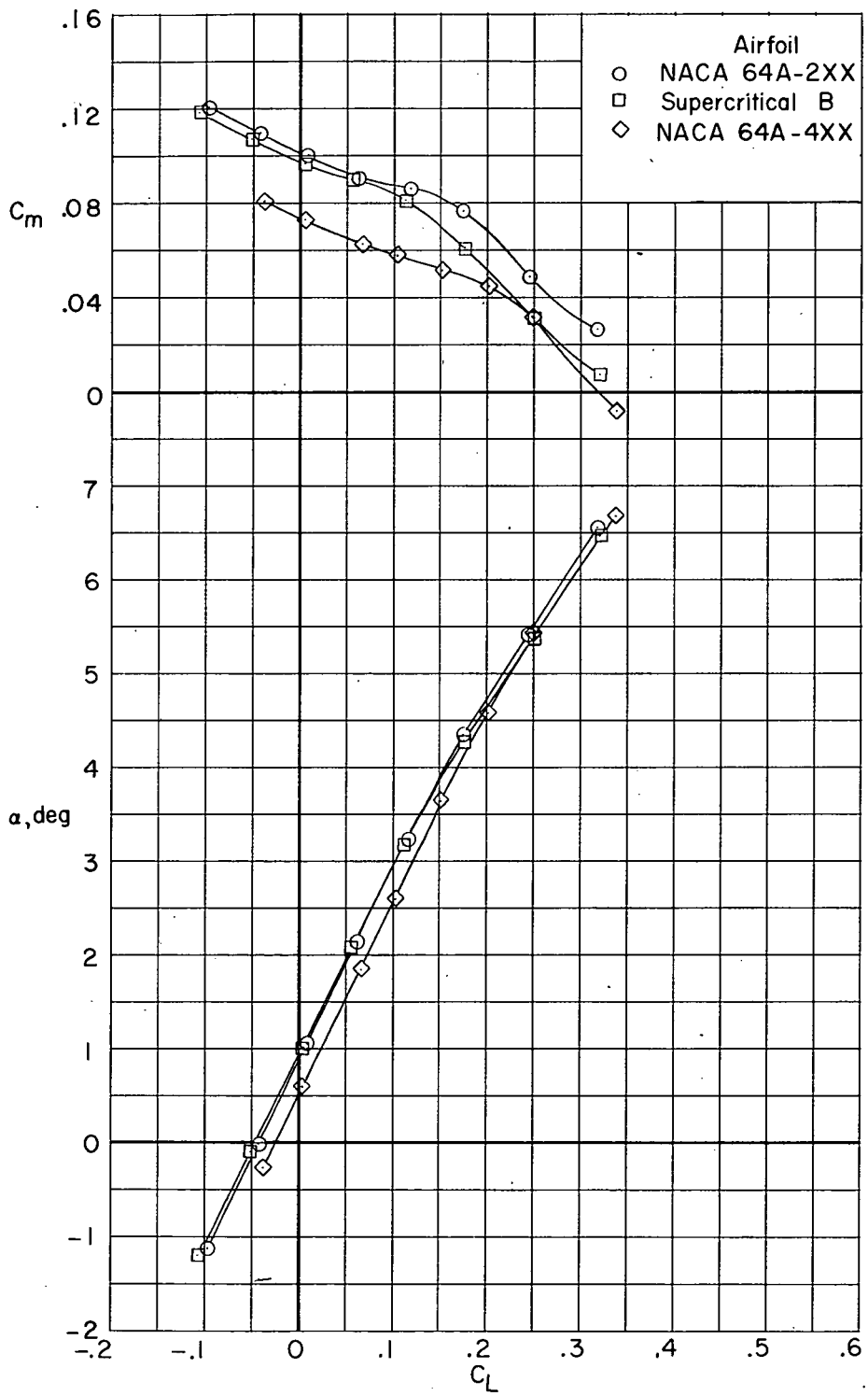
(b) $M = 1.00$.

Figure 35. - Continued.



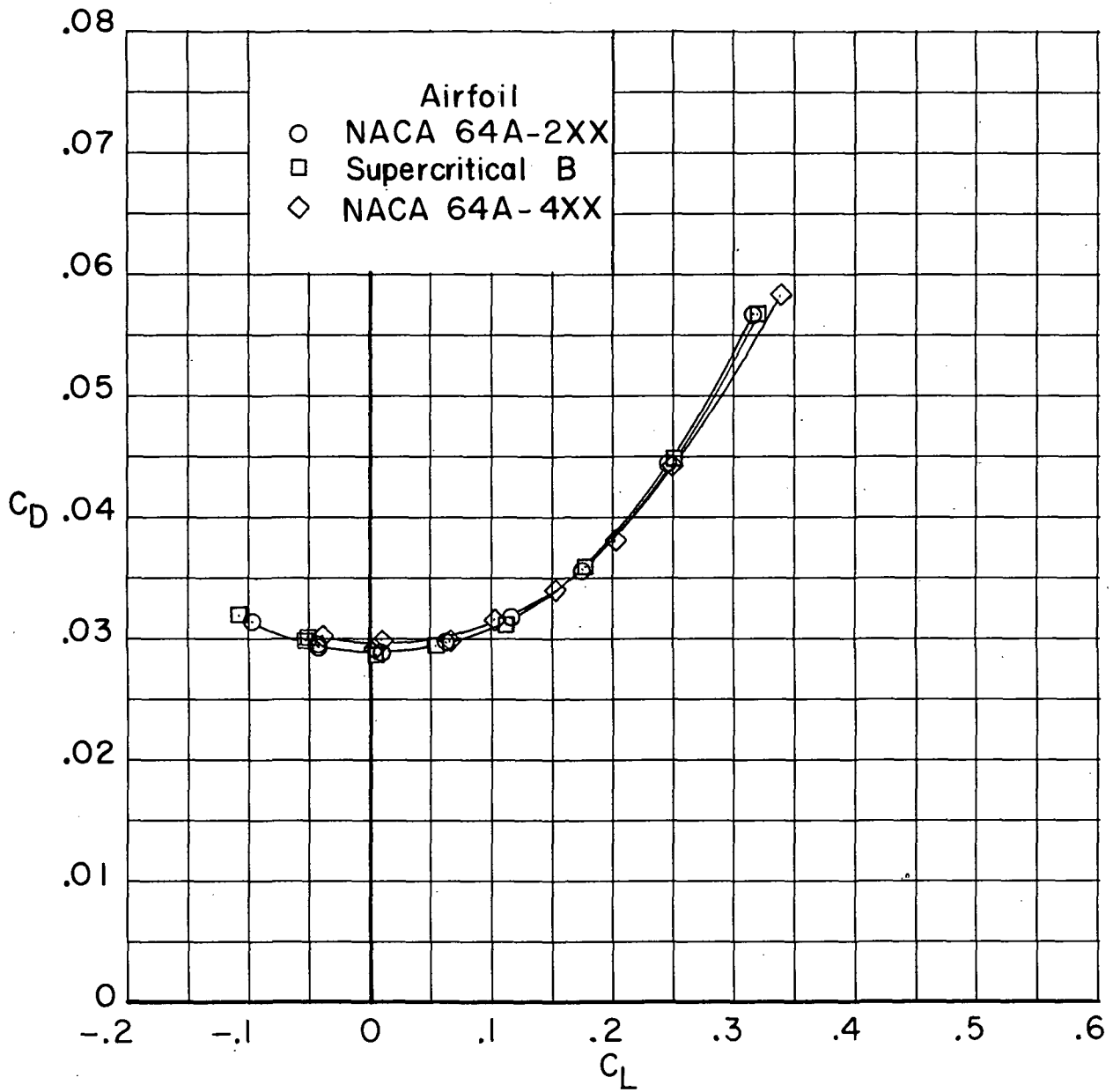
(b) $M = 1.00$. Concluded.

Figure 35.- Continued.



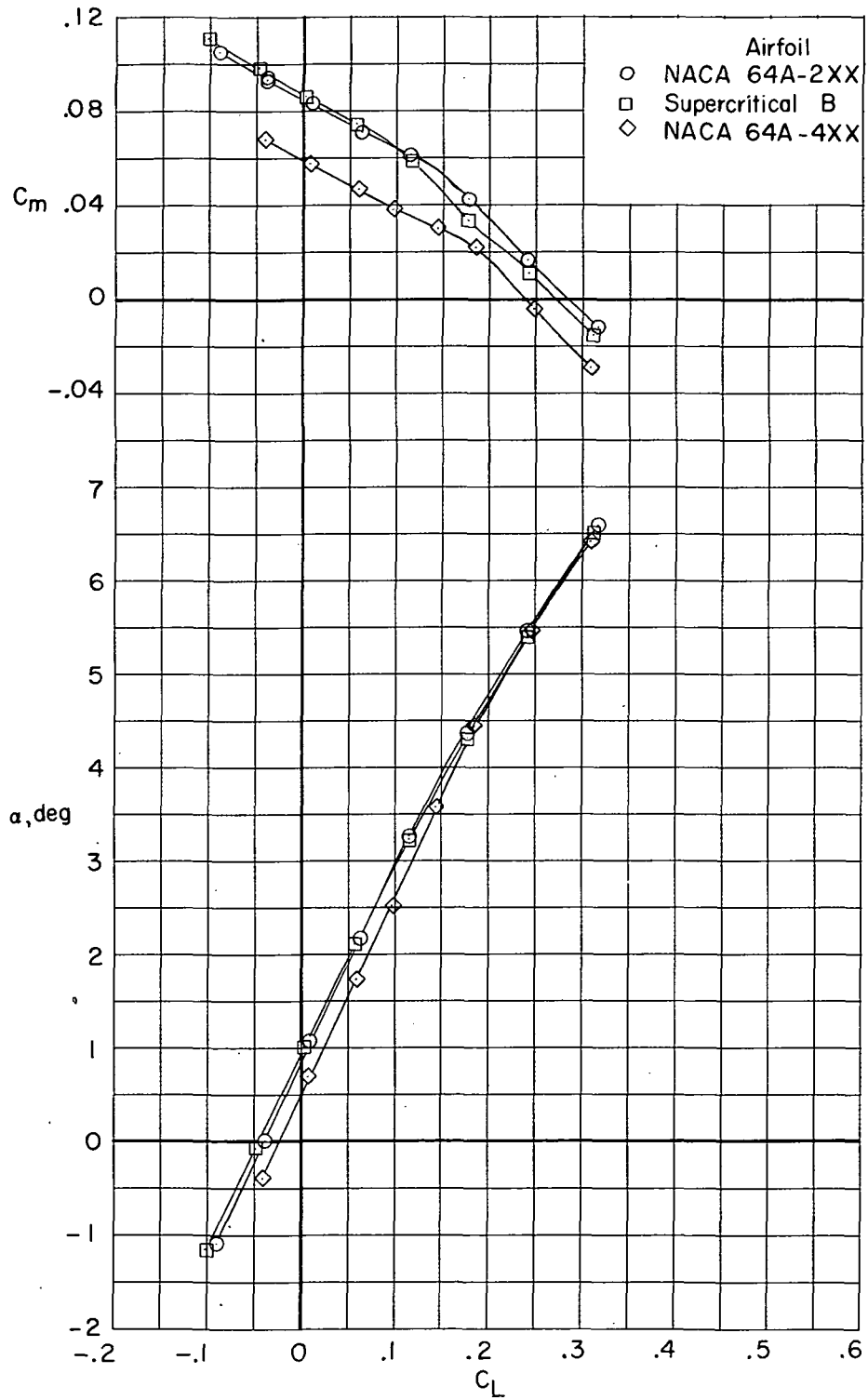
(c) $M = 1.03$.

Figure 35.- Continued.



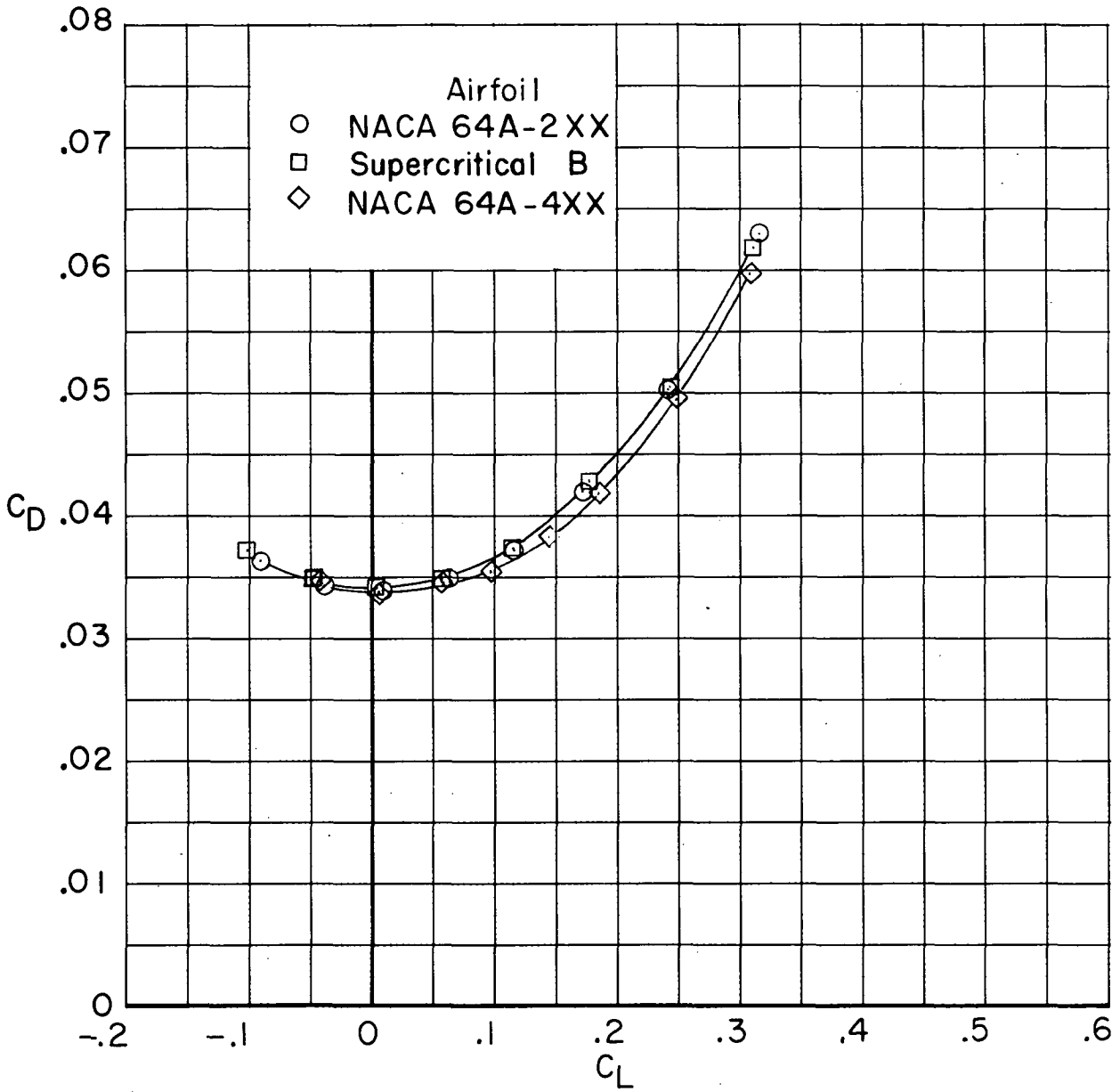
(c) $M = 1.03$. Concluded.

Figure 35. - Continued.



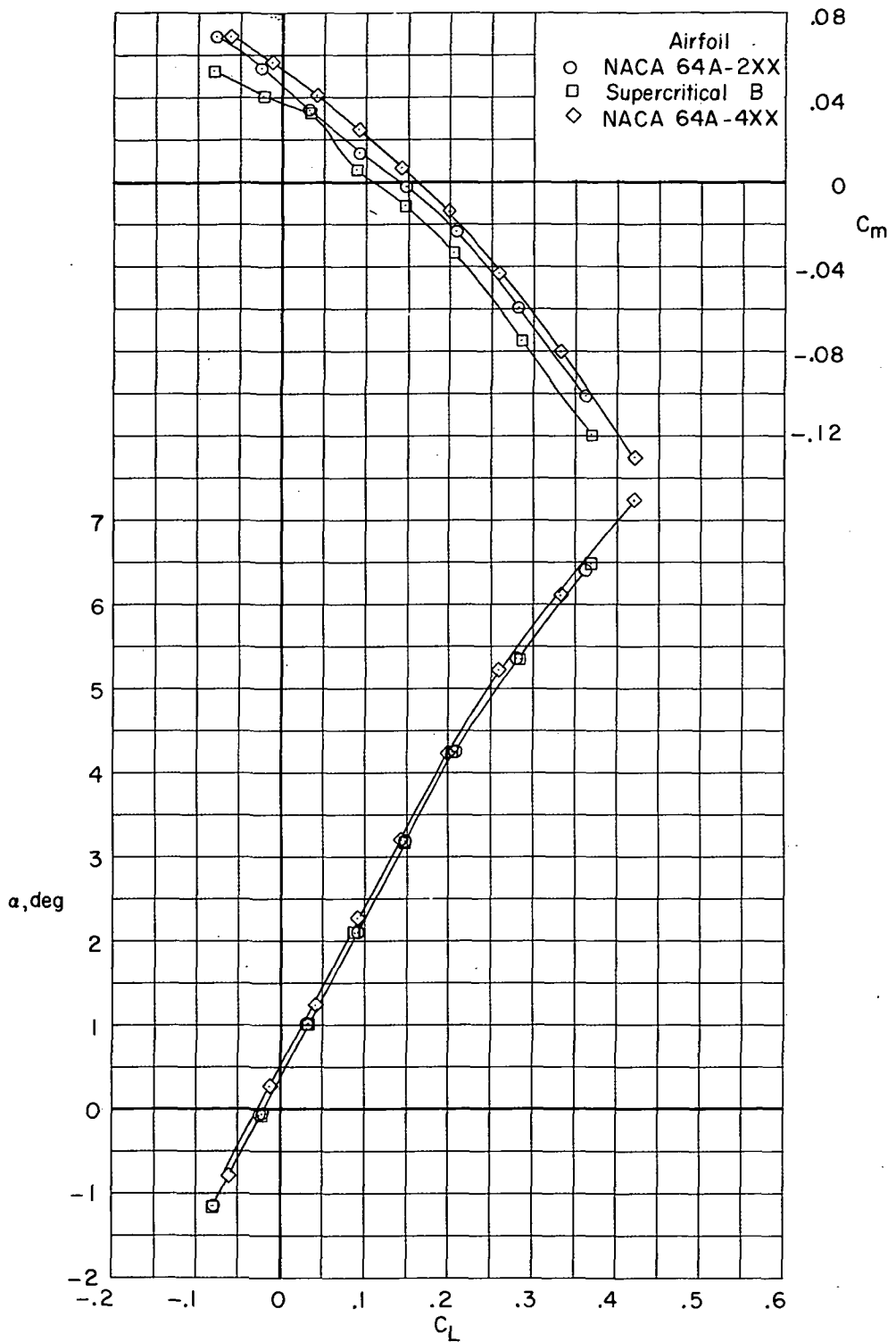
(d) $M = 1.20$.

Figure 35.- Continued.



(d) $M = 1.20$. Concluded.

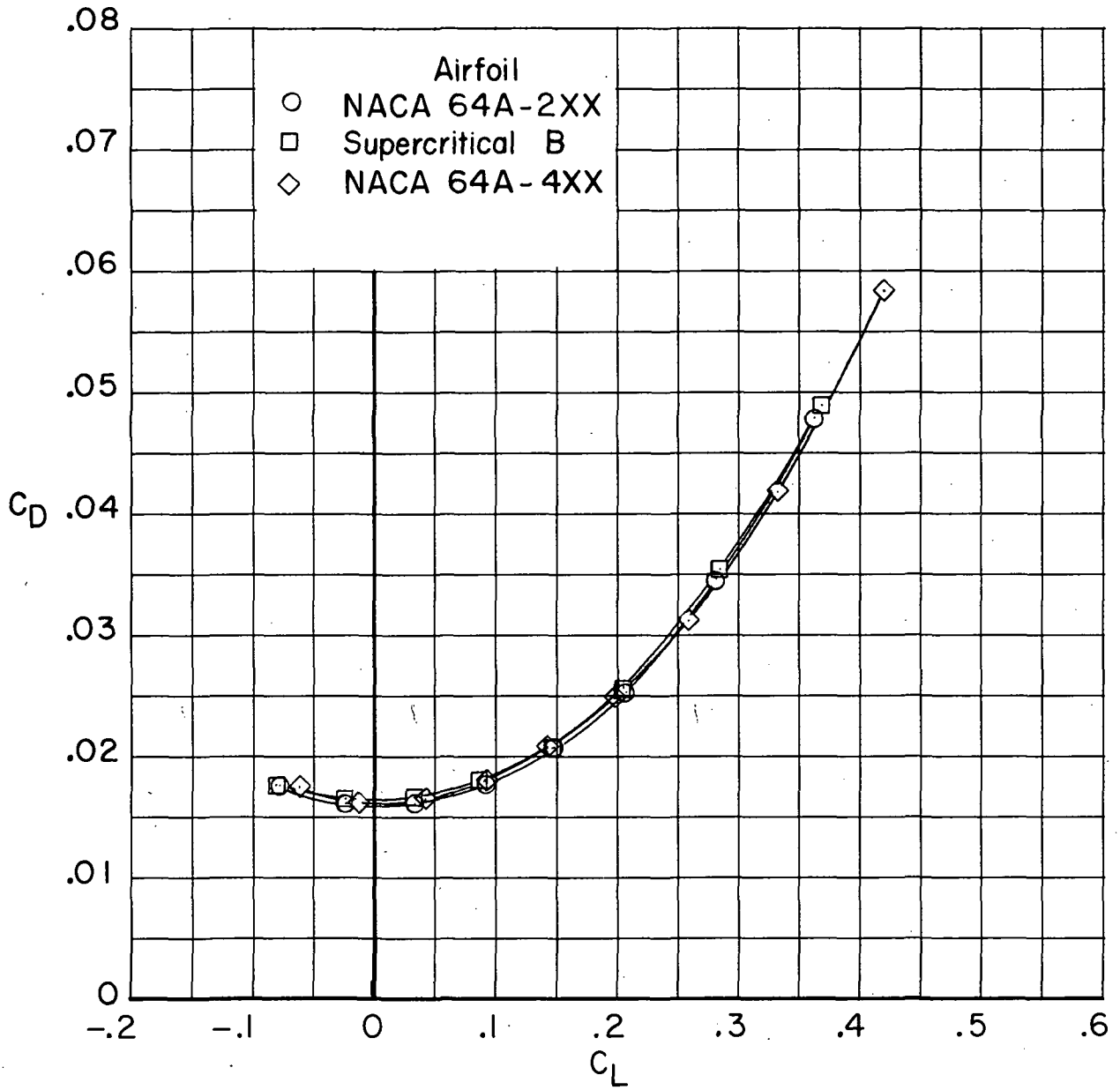
Figure 35. - Concluded.



(a) $M = 0.95$.

Figure 36.- Comparison of longitudinal aerodynamic characteristics for configuration with NACA 64A2XX, supercritical, and NACA 64A4XX airfoils, fuselage fairing, and transition rearward. $\Lambda = 72.5^\circ$; $i_w = 1^\circ$; $\delta_h = 0^\circ$.

~~CONFIDENTIAL~~

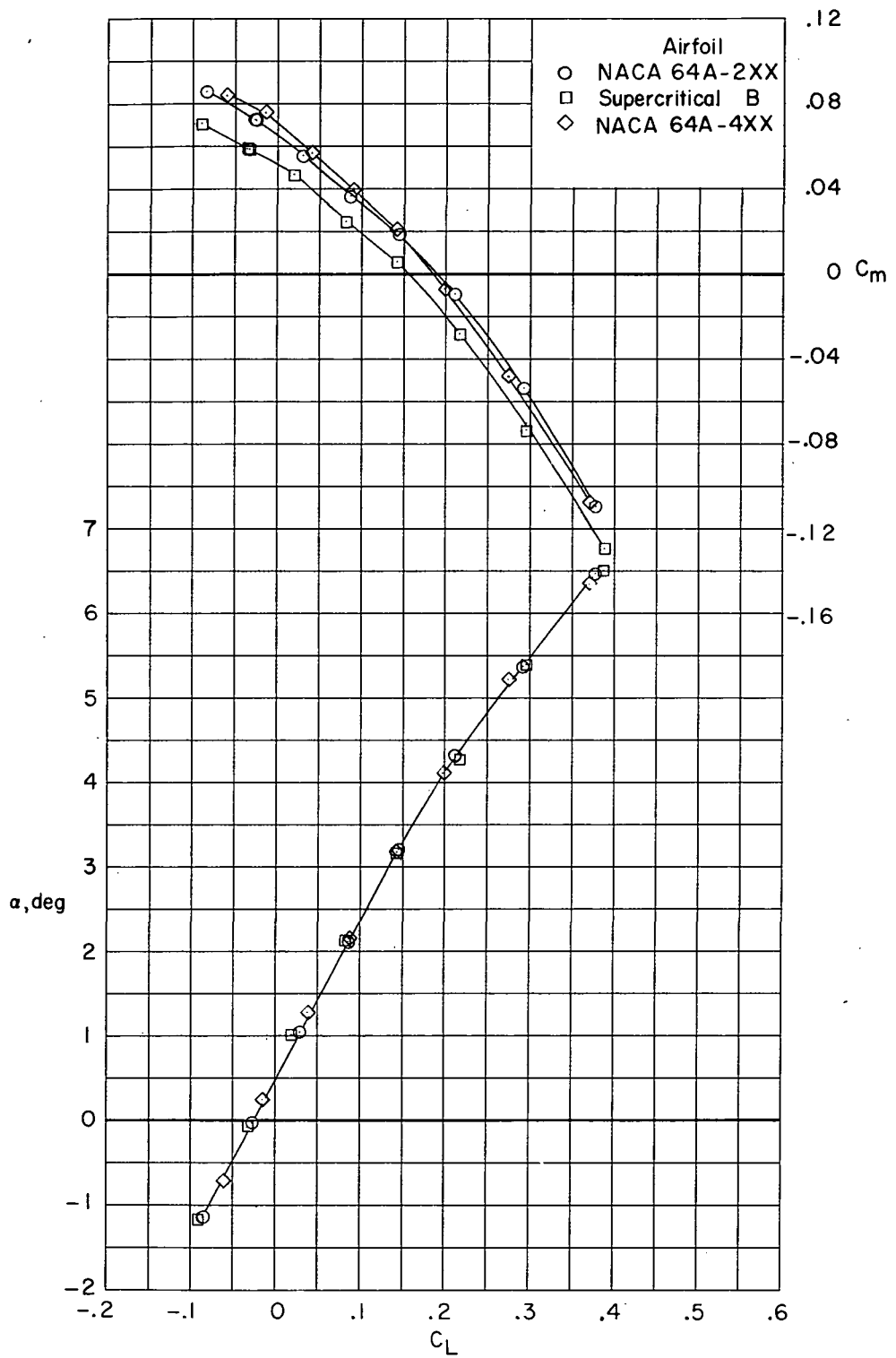


(a) $M = 0.95$. Concluded.

Figure 36.- Continued.

~~CONFIDENTIAL~~

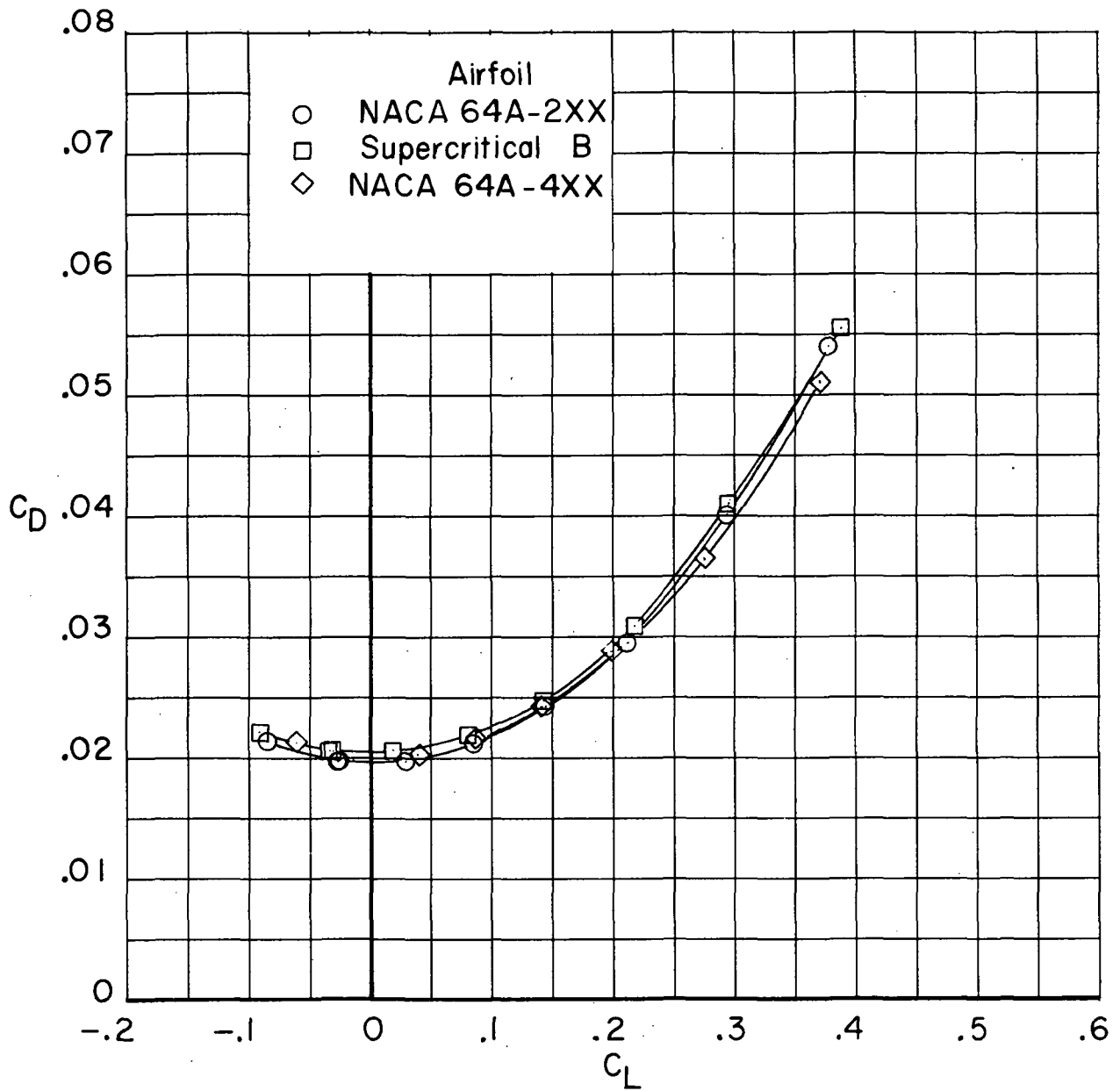
~~CONFIDENTIAL~~



(b) $M = 1.00$.

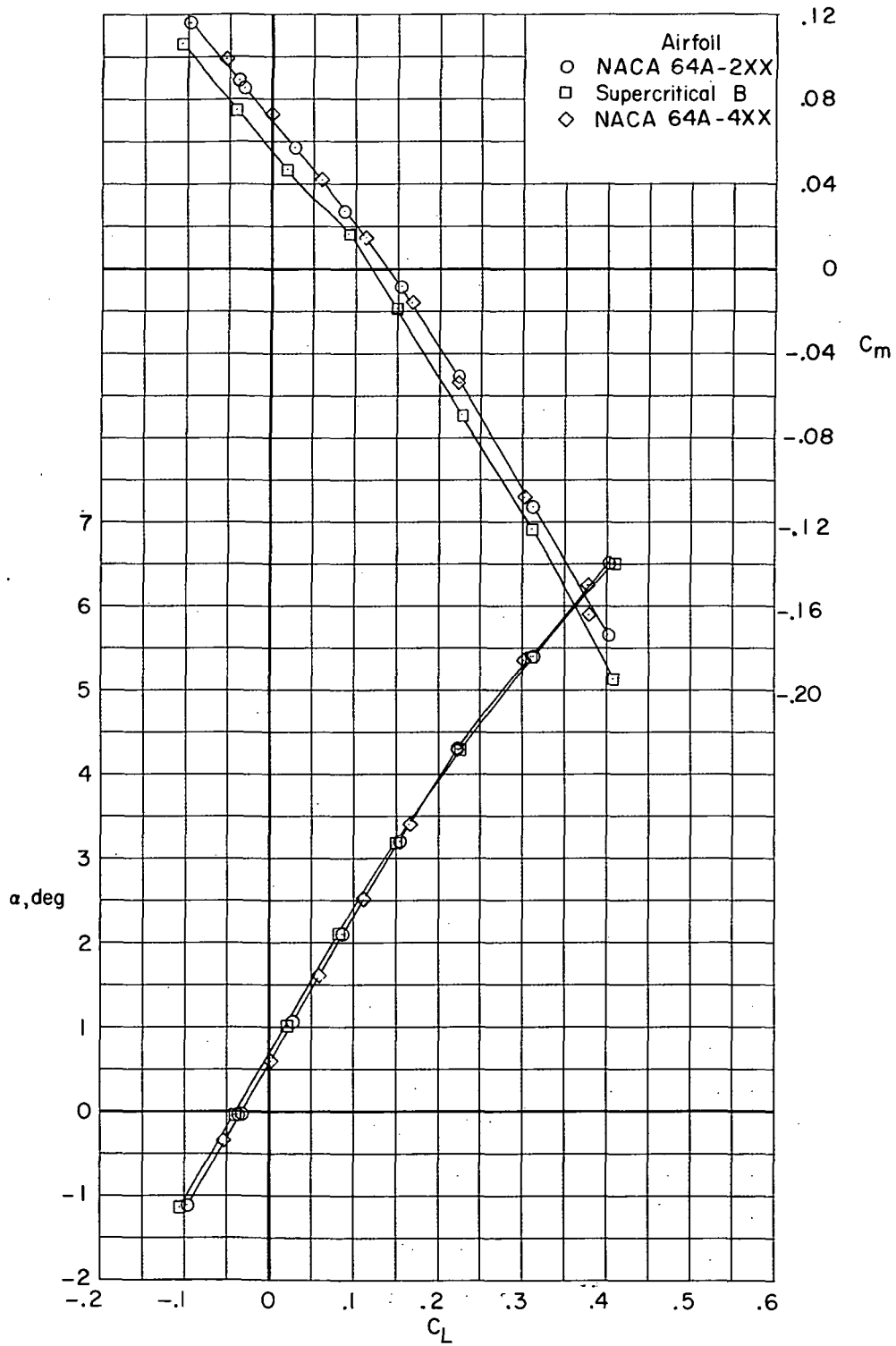
Figure 36.- Continued.

~~CONFIDENTIAL~~



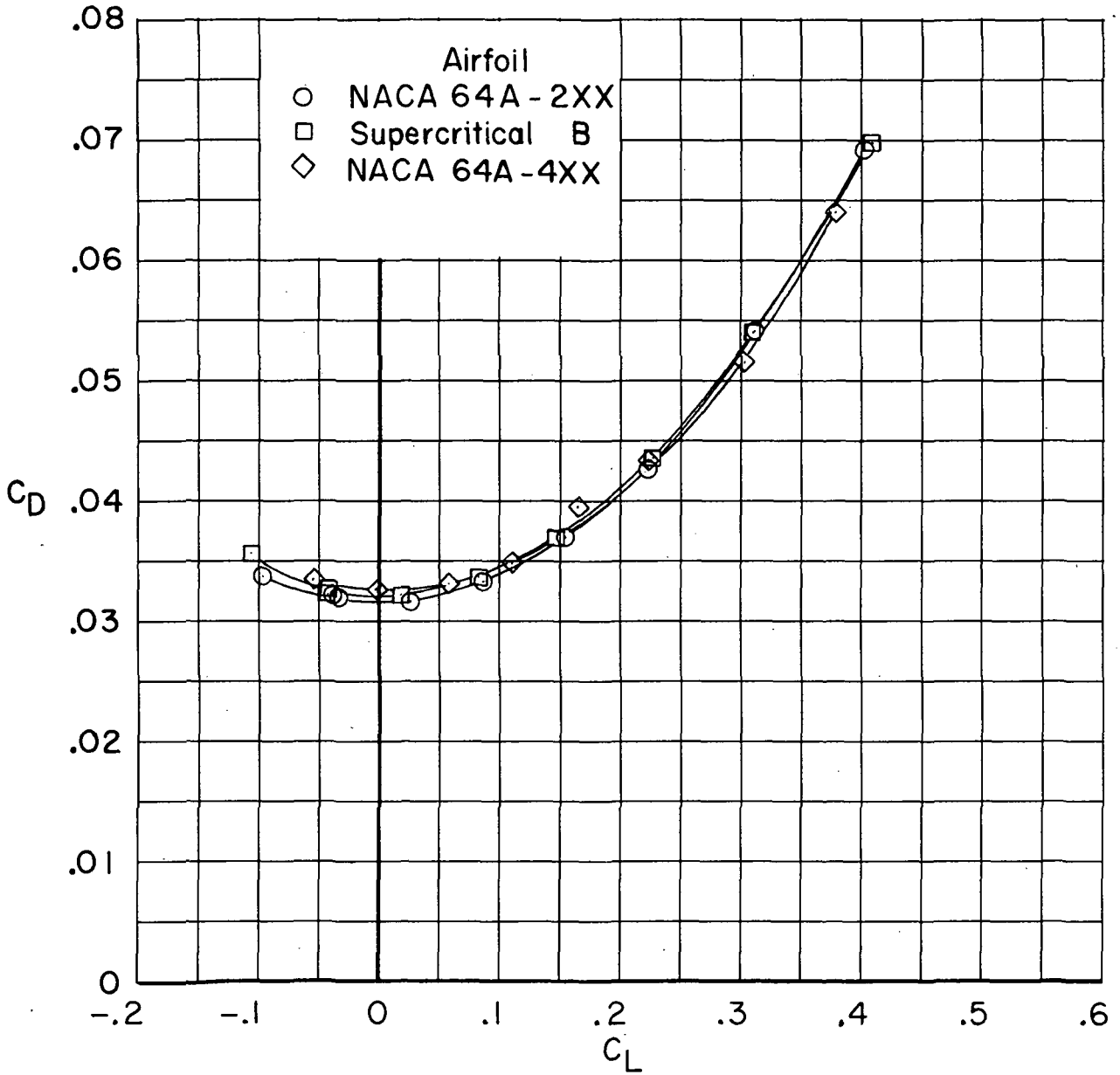
(b) $M = 1.00$. Concluded.

Figure 36. - Continued.



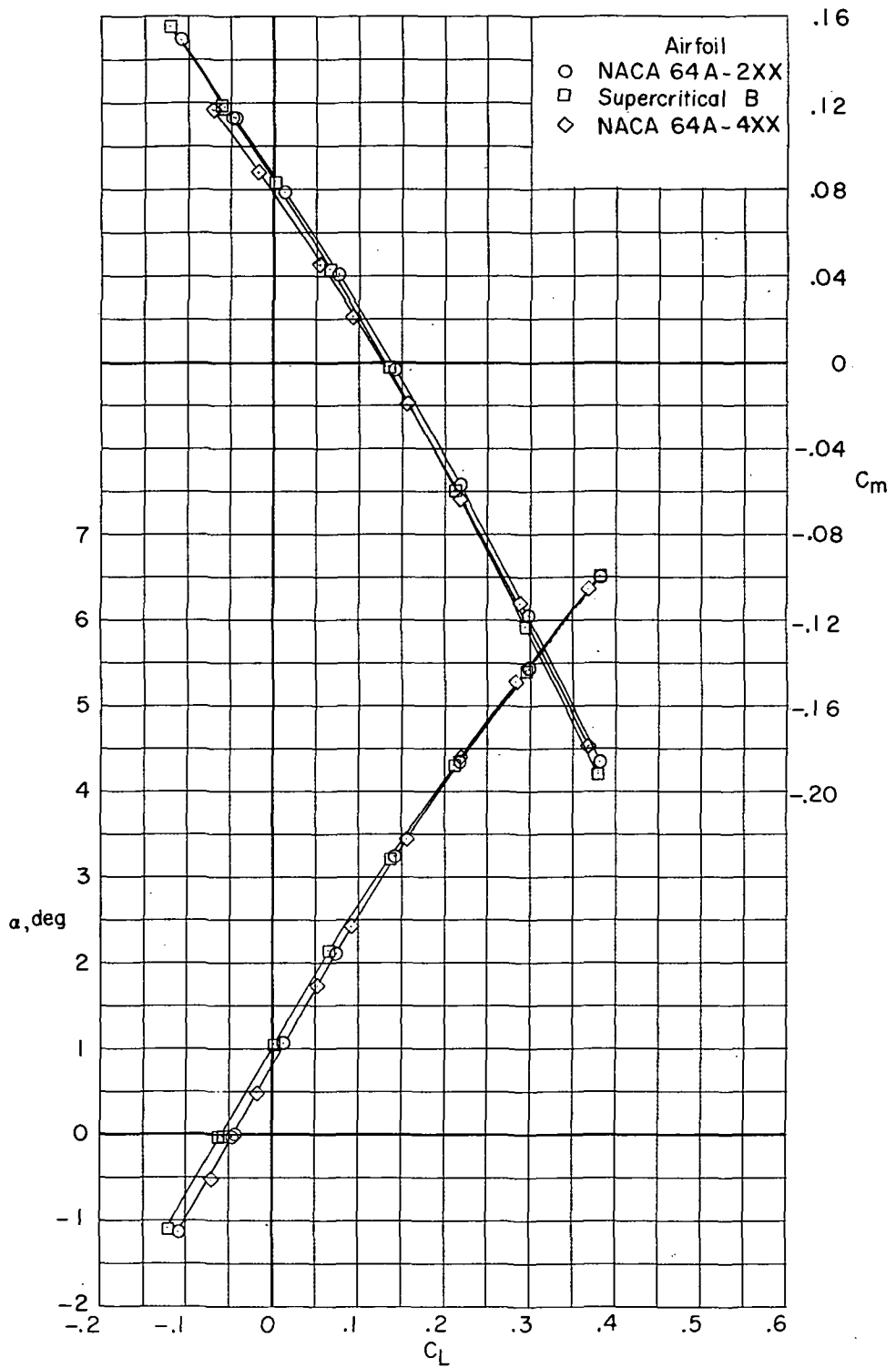
(c) M = 1.03.

Figure 36.- Continued.



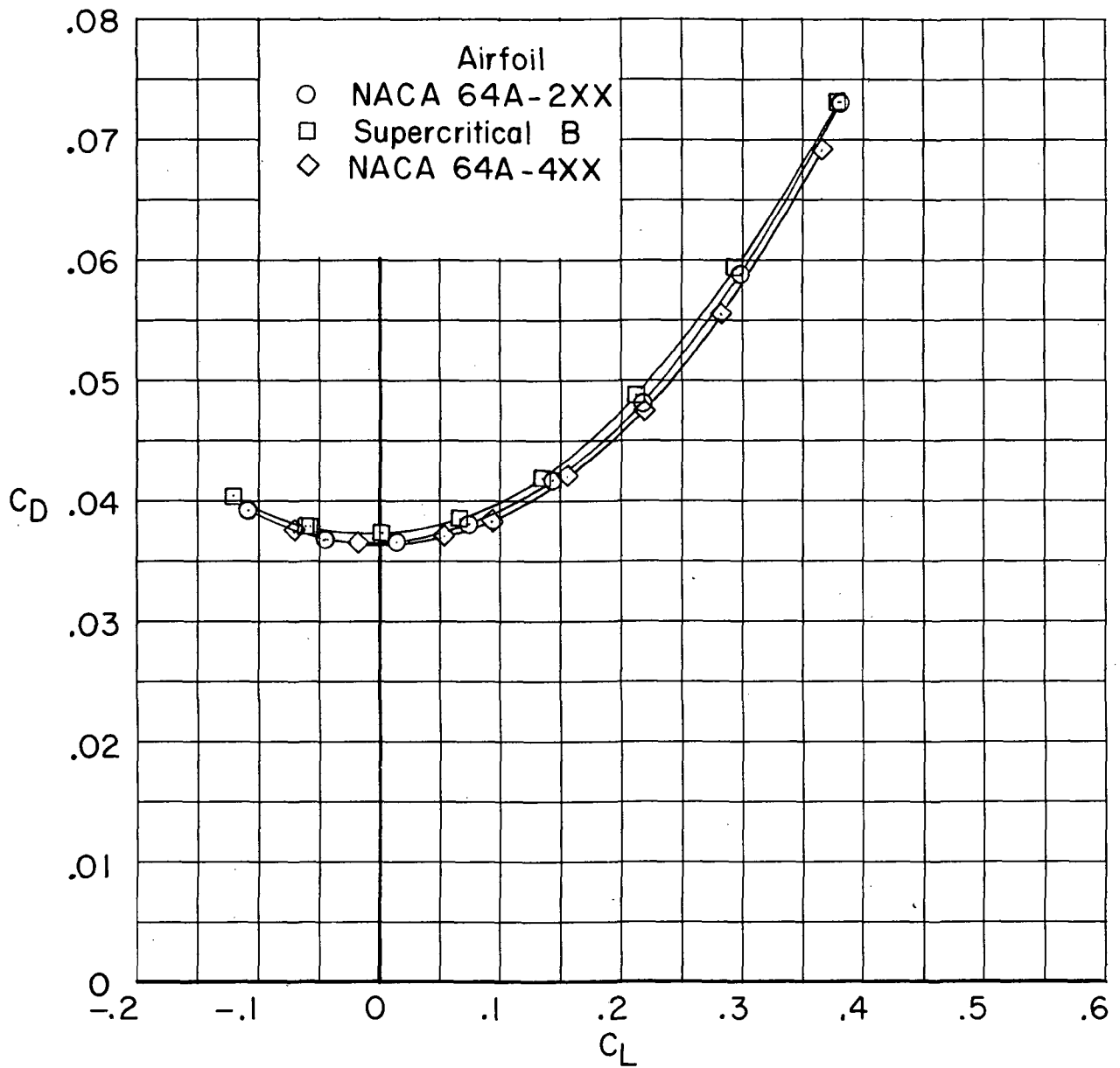
(c) $M = 1.03$. Concluded.

Figure 36.- Continued.



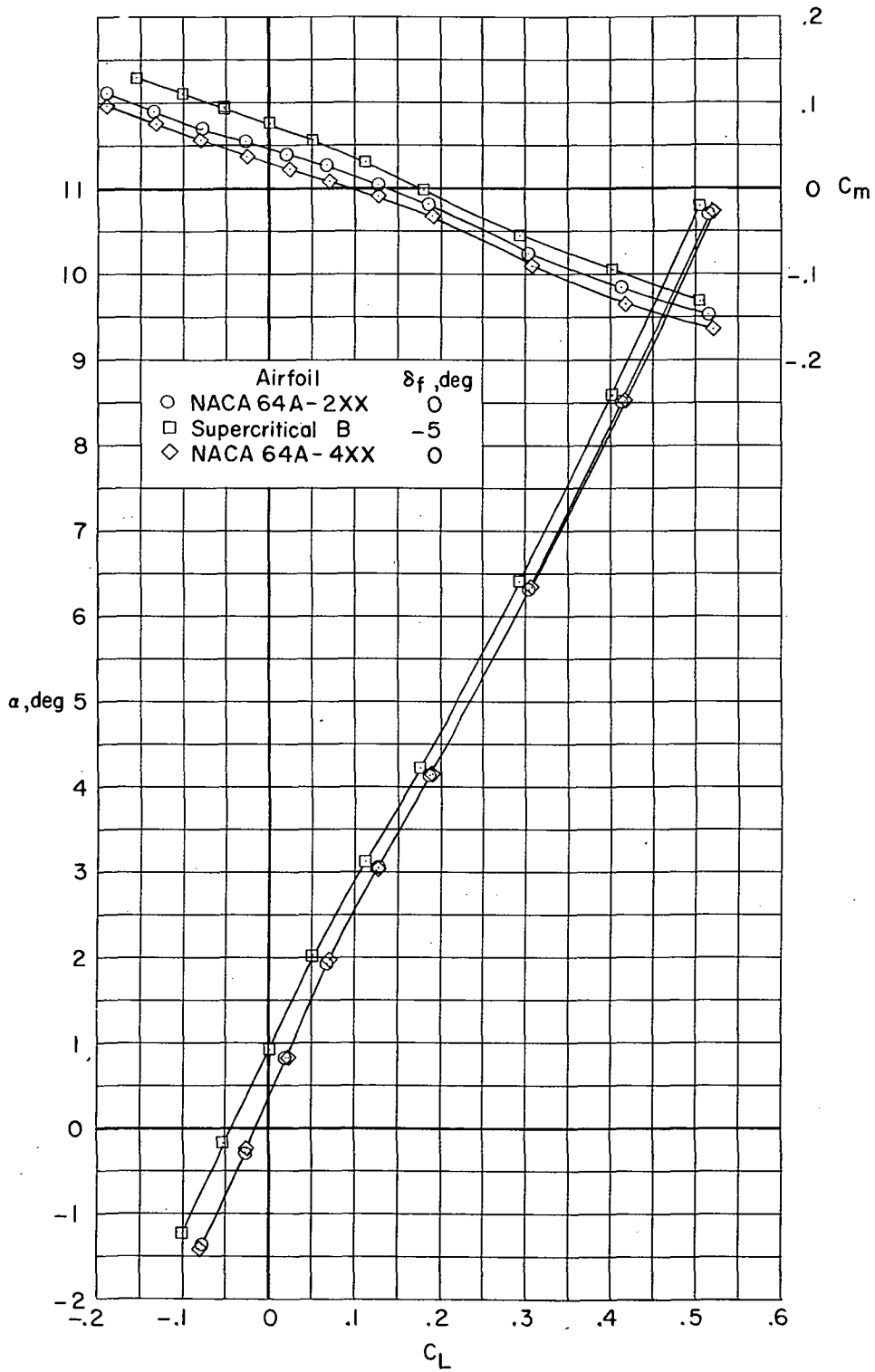
(d) $M = 1.20$.

Figure 36.- Continued.



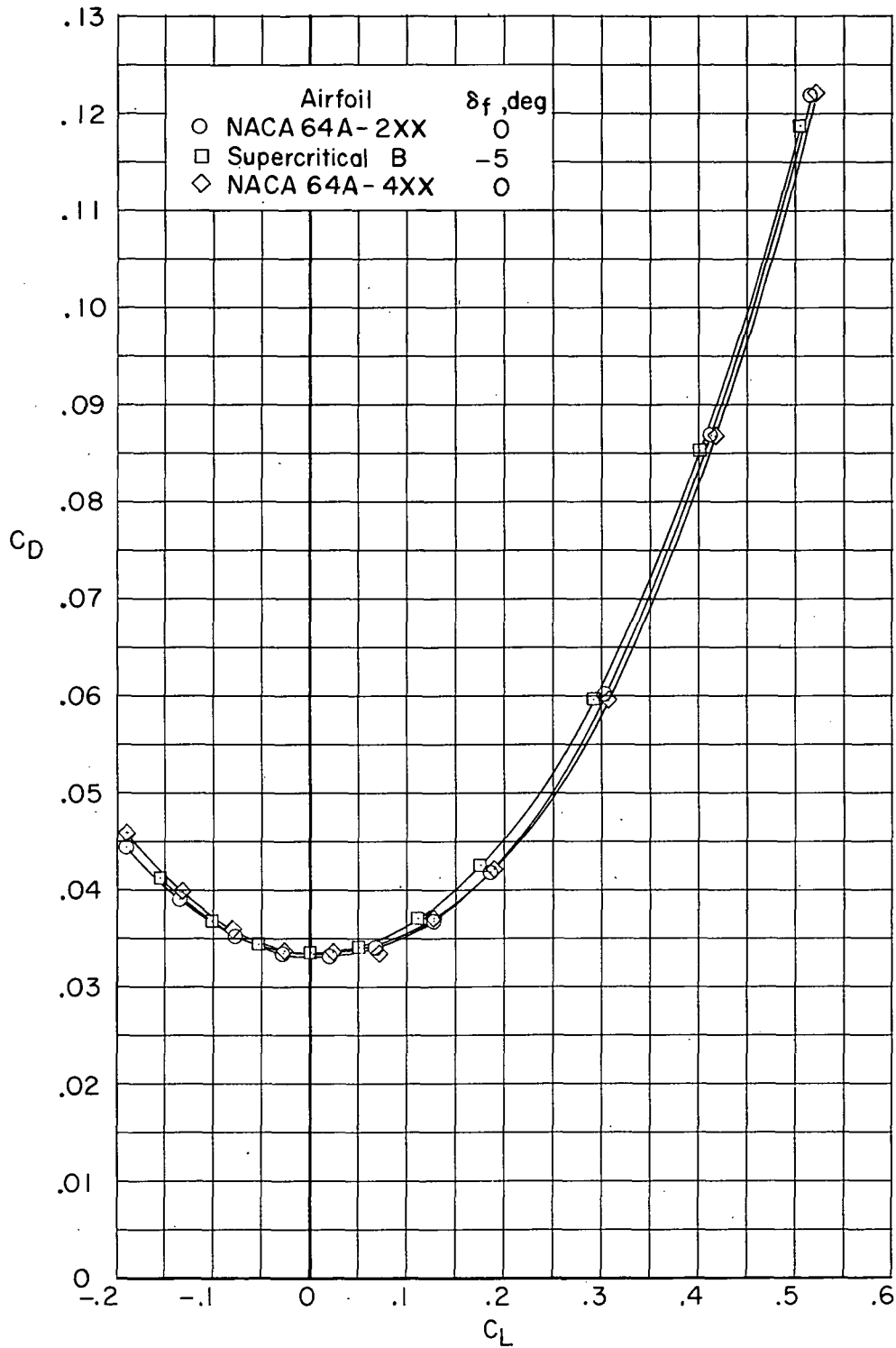
(d) $M = 1.20$. Concluded.

Figure 36.- Concluded.



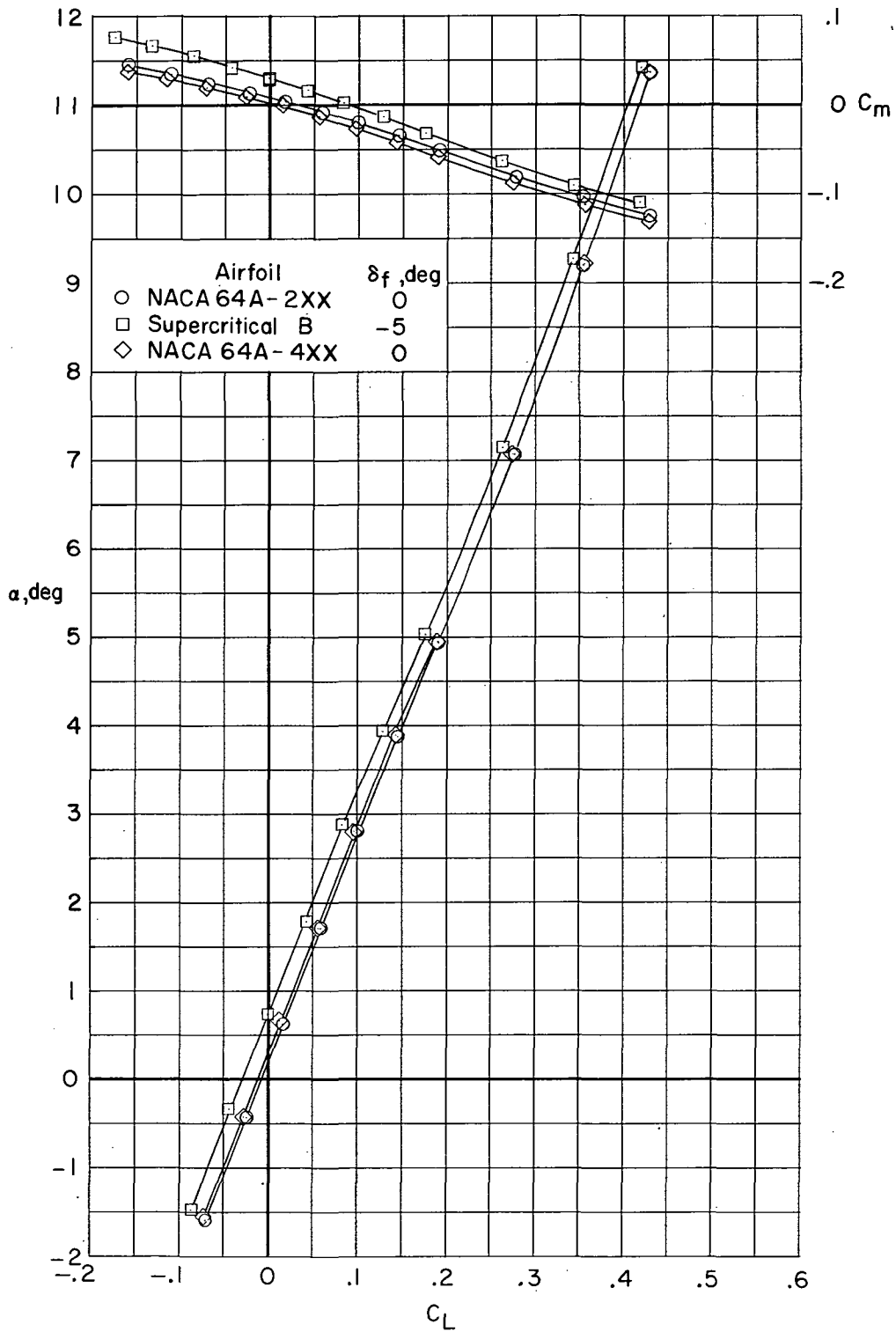
(a) $M = 1.60$.

Figure 37.- Comparison of longitudinal aerodynamic characteristics for configuration with NACA 64A2XX, supercritical, and NACA 64A4XX airfoils and transition forward. $\Lambda = 72.5^\circ$; $i_w = 1^\circ$; $\delta_h = \text{Off}$.



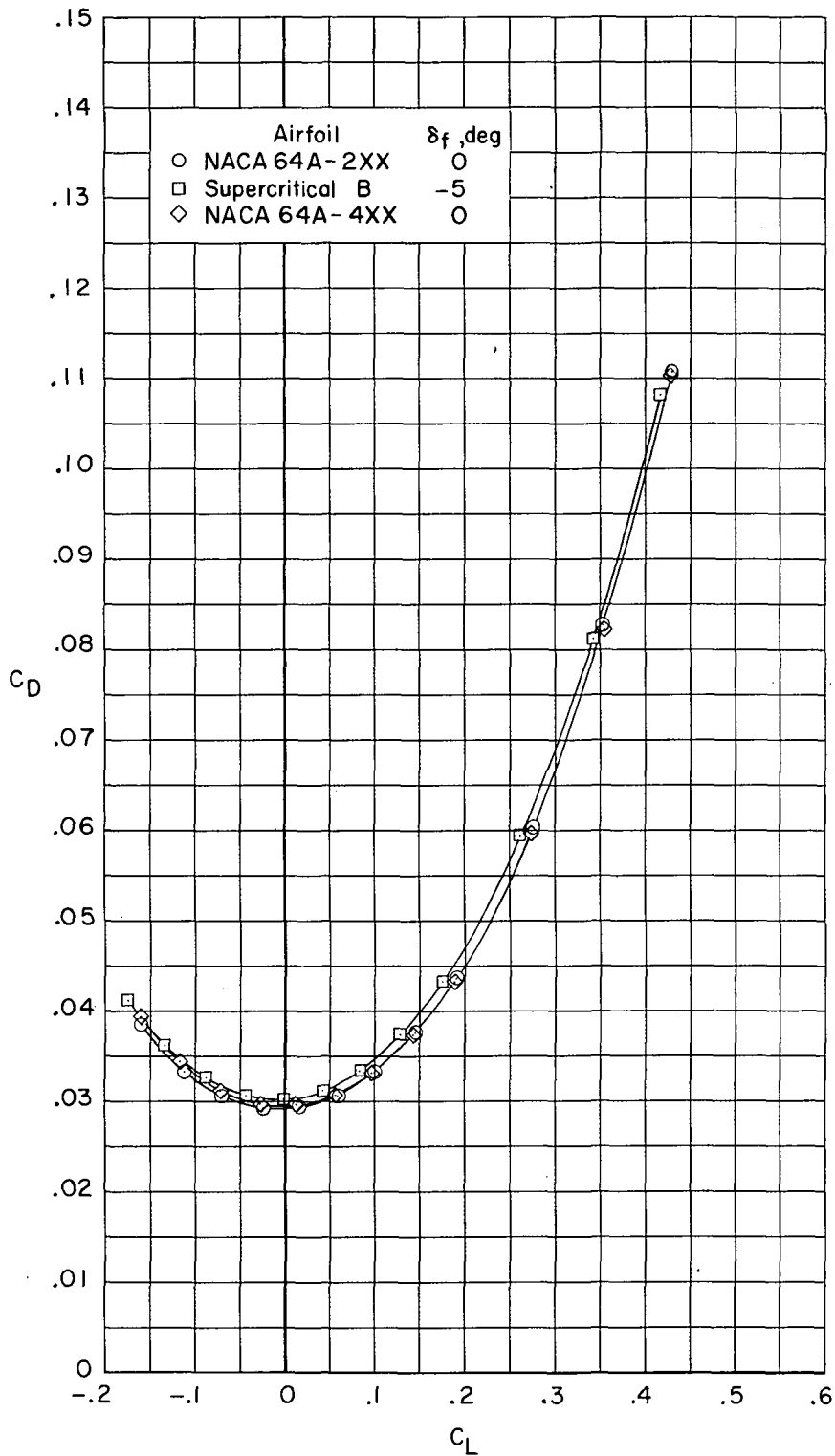
(a) $M = 1.60$. Concluded.

Figure 37.- Continued.



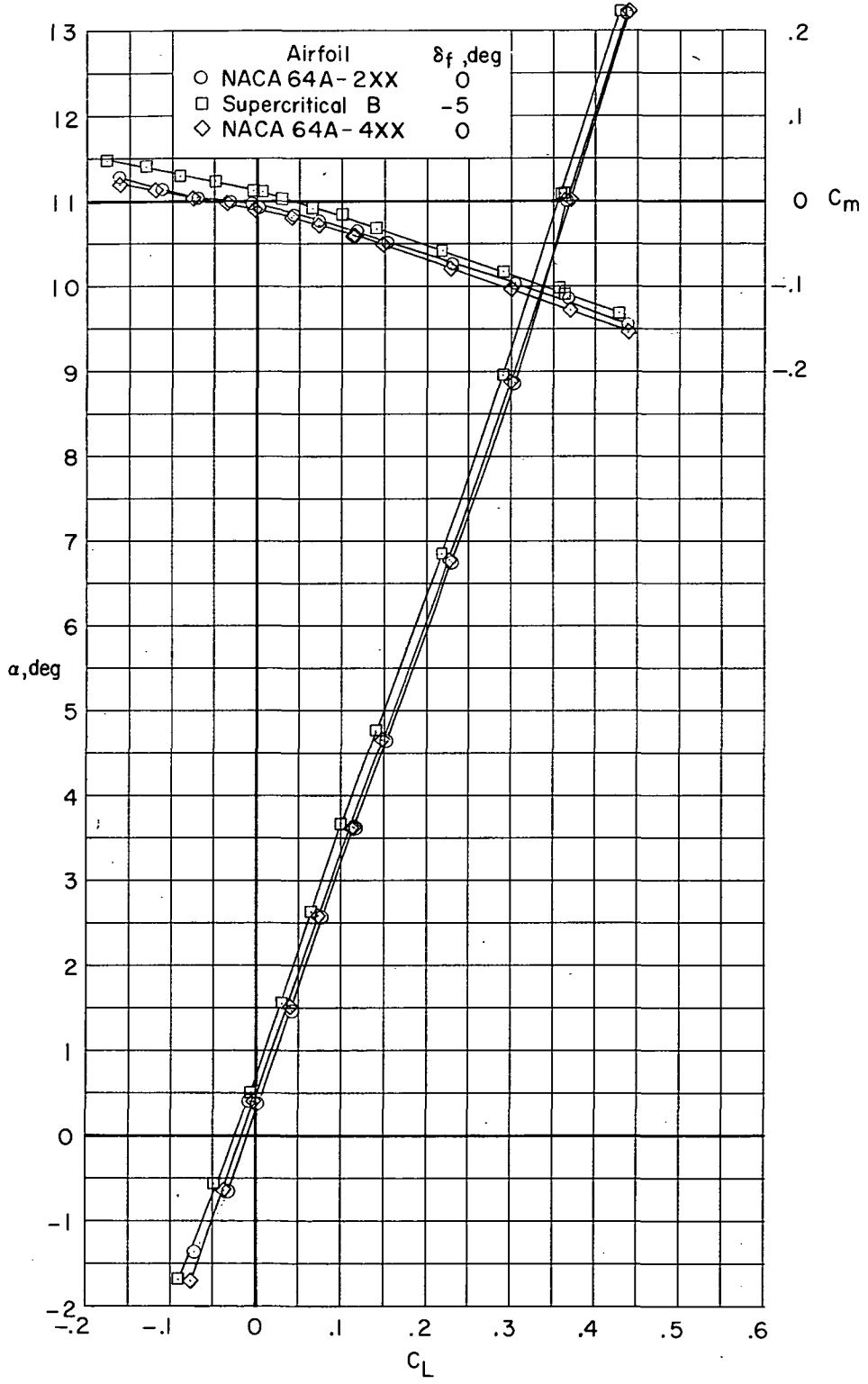
(b) $M = 2.16$.

Figure 37.- Continued.



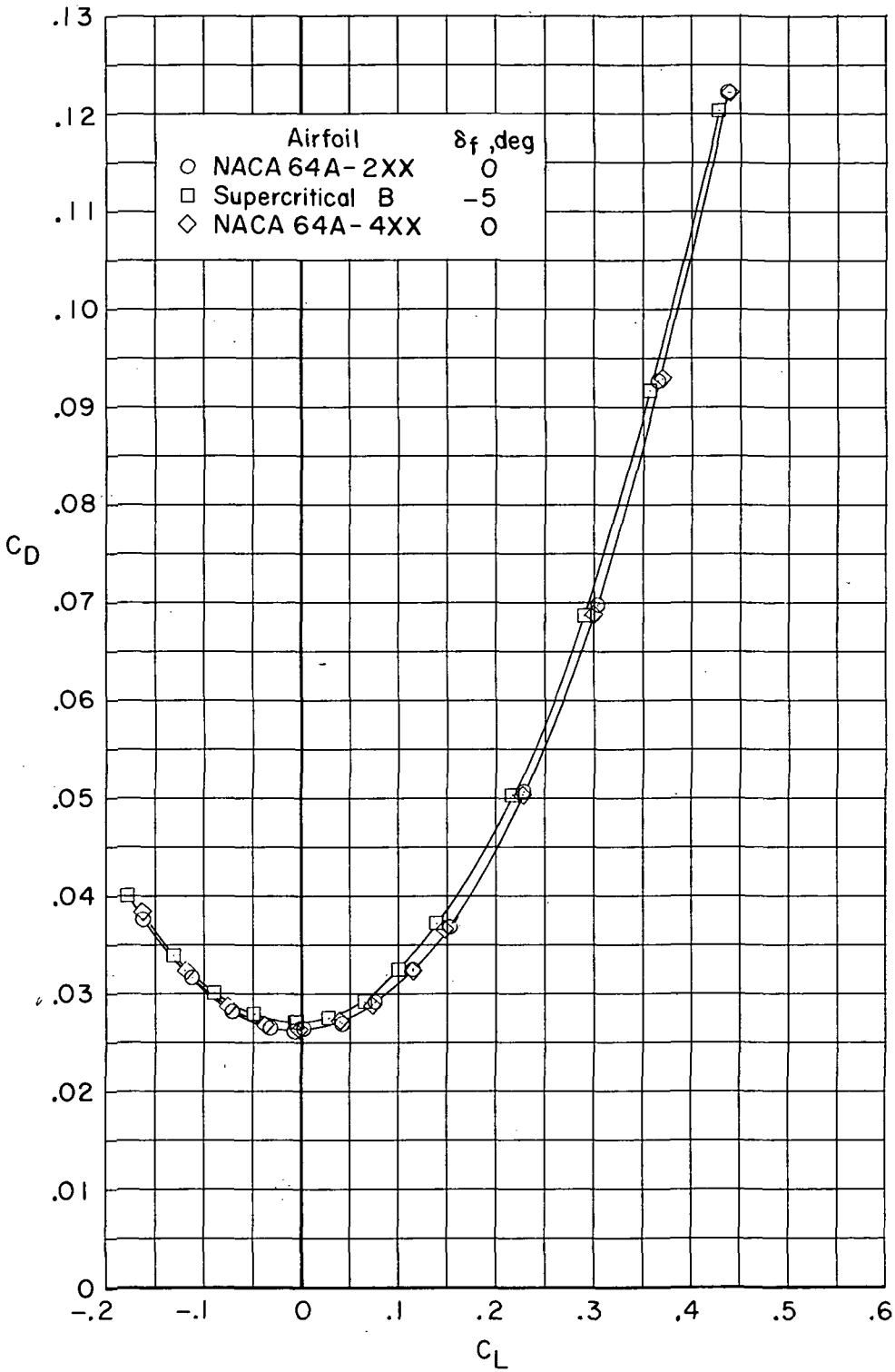
(b) $M = 2.16$. Concluded.

Figure 37.- Continued.



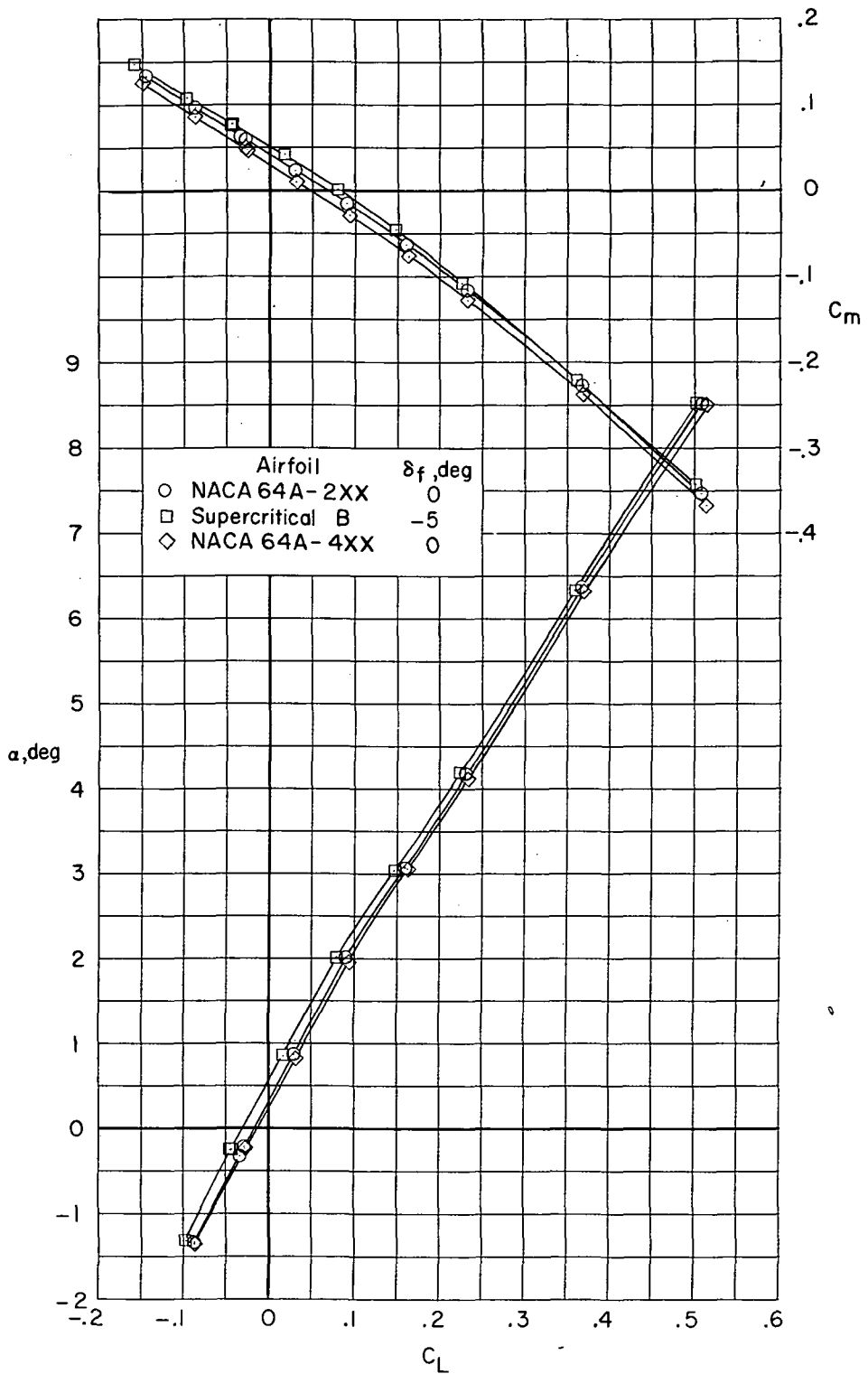
(c) $M = 2.50$.

Figure 37. - Continued.



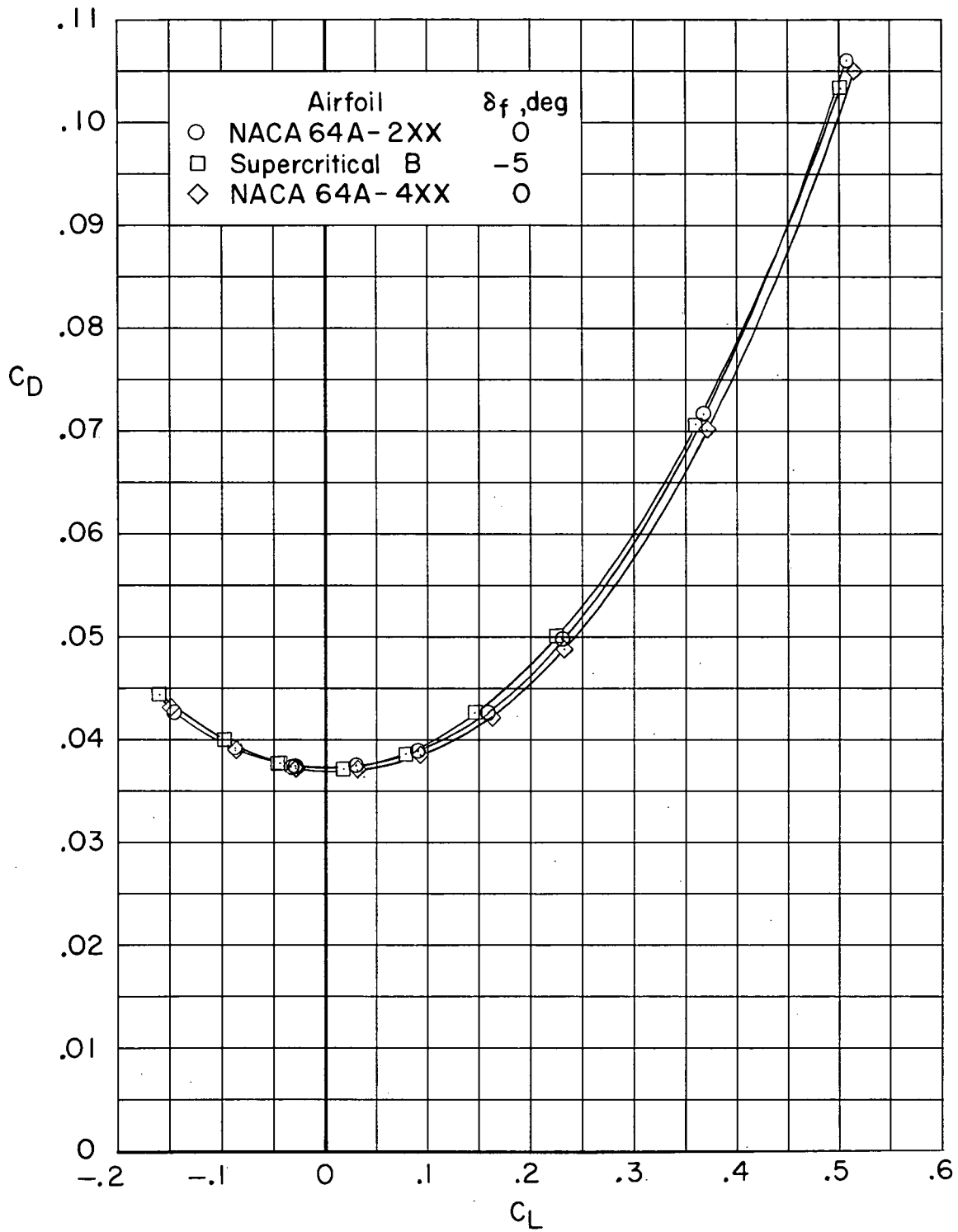
(c) $M = 2.50$. Concluded.

Figure 37.- Concluded.



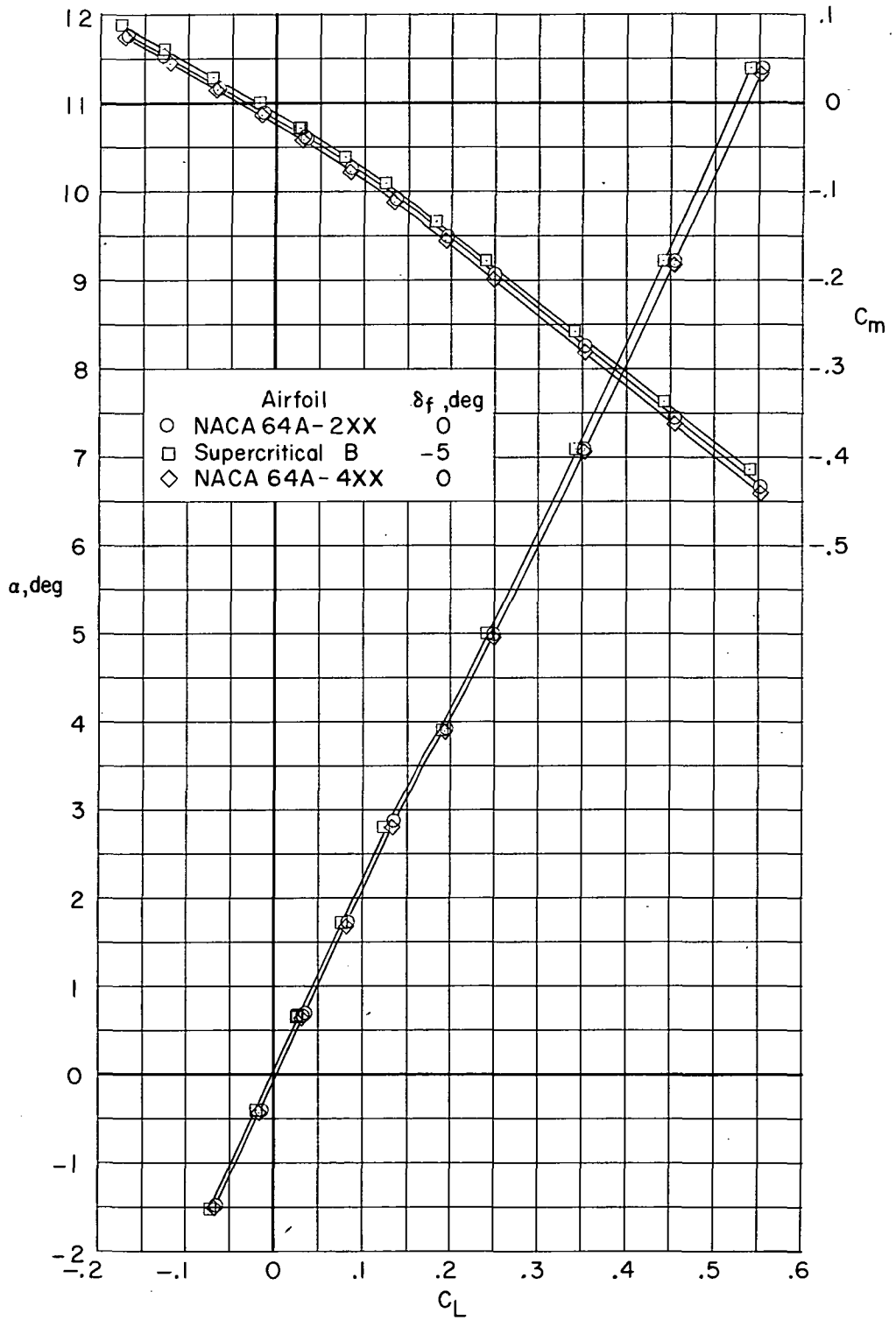
(a) $M = 1.60$.

Figure 38.- Comparison of longitudinal aerodynamic characteristics for configuration with NACA 64A2XX, supercritical, and NACA 64A4XX airfoils and transition forward. $\Lambda = 72.5^\circ$; $i_w = 1^\circ$; $\delta_h = 0^\circ$.



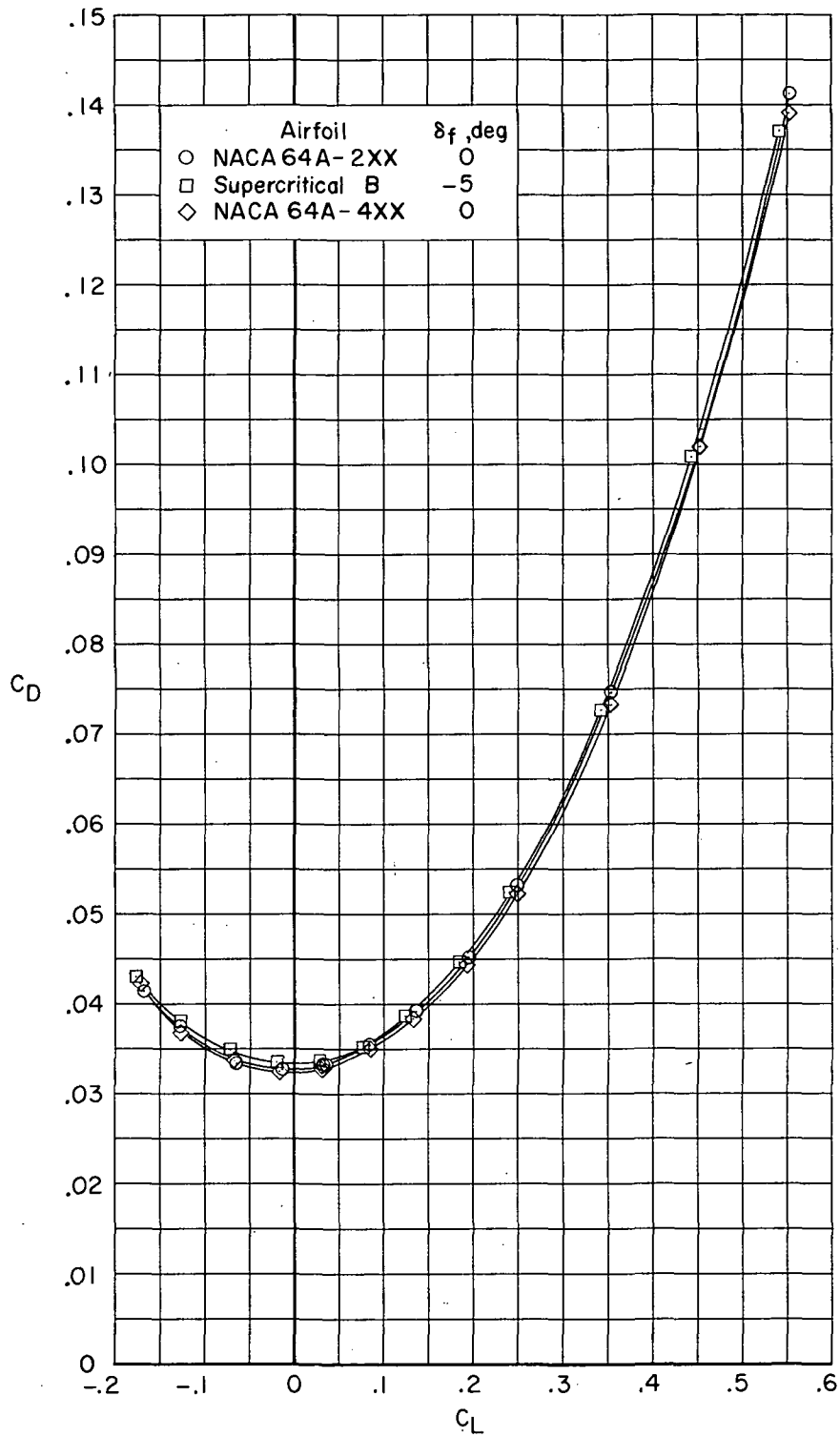
(a) $M = 1.60$. Concluded.

Figure 38.- Continued.



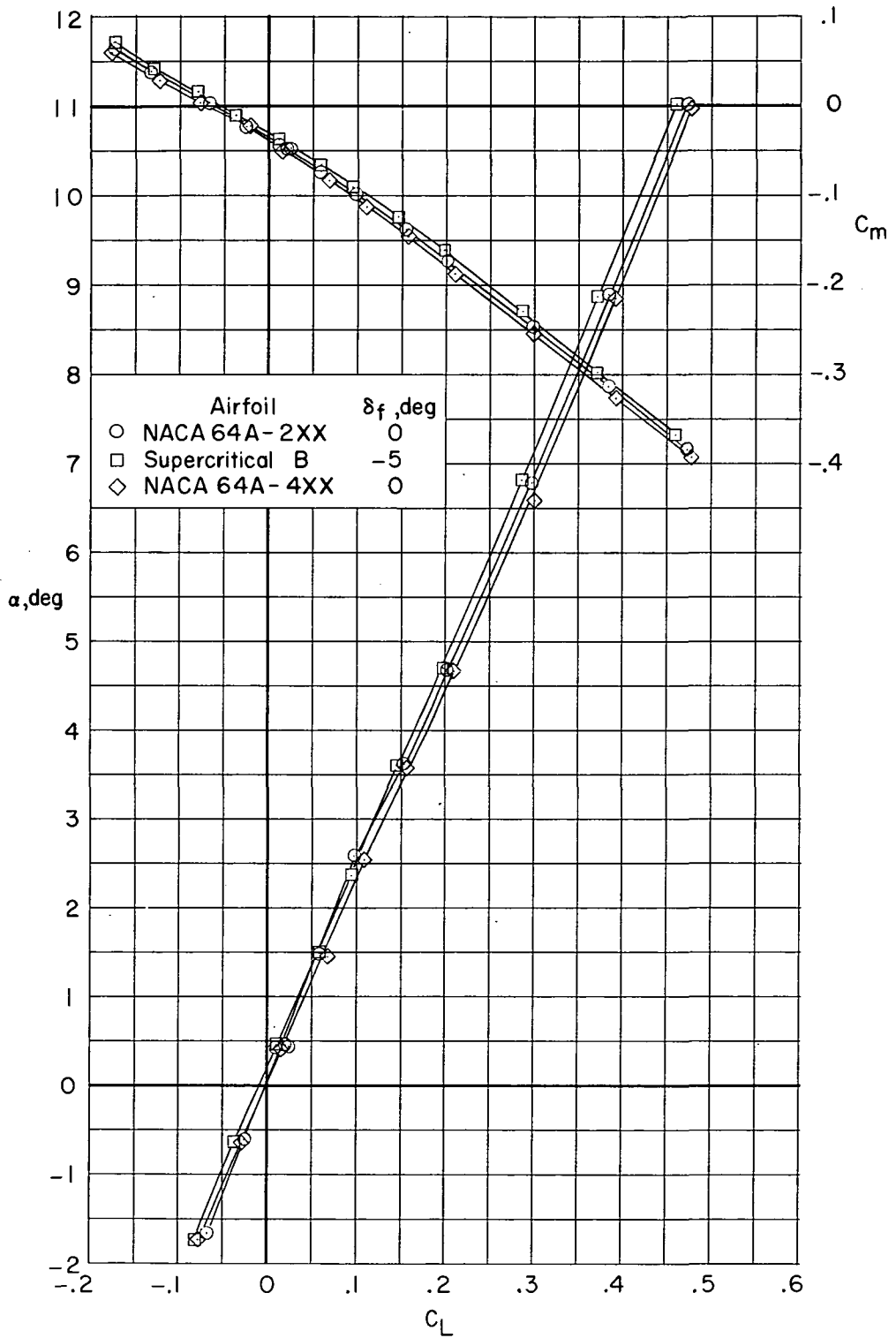
(b) $M = 2.16$.

Figure 38.- Continued.



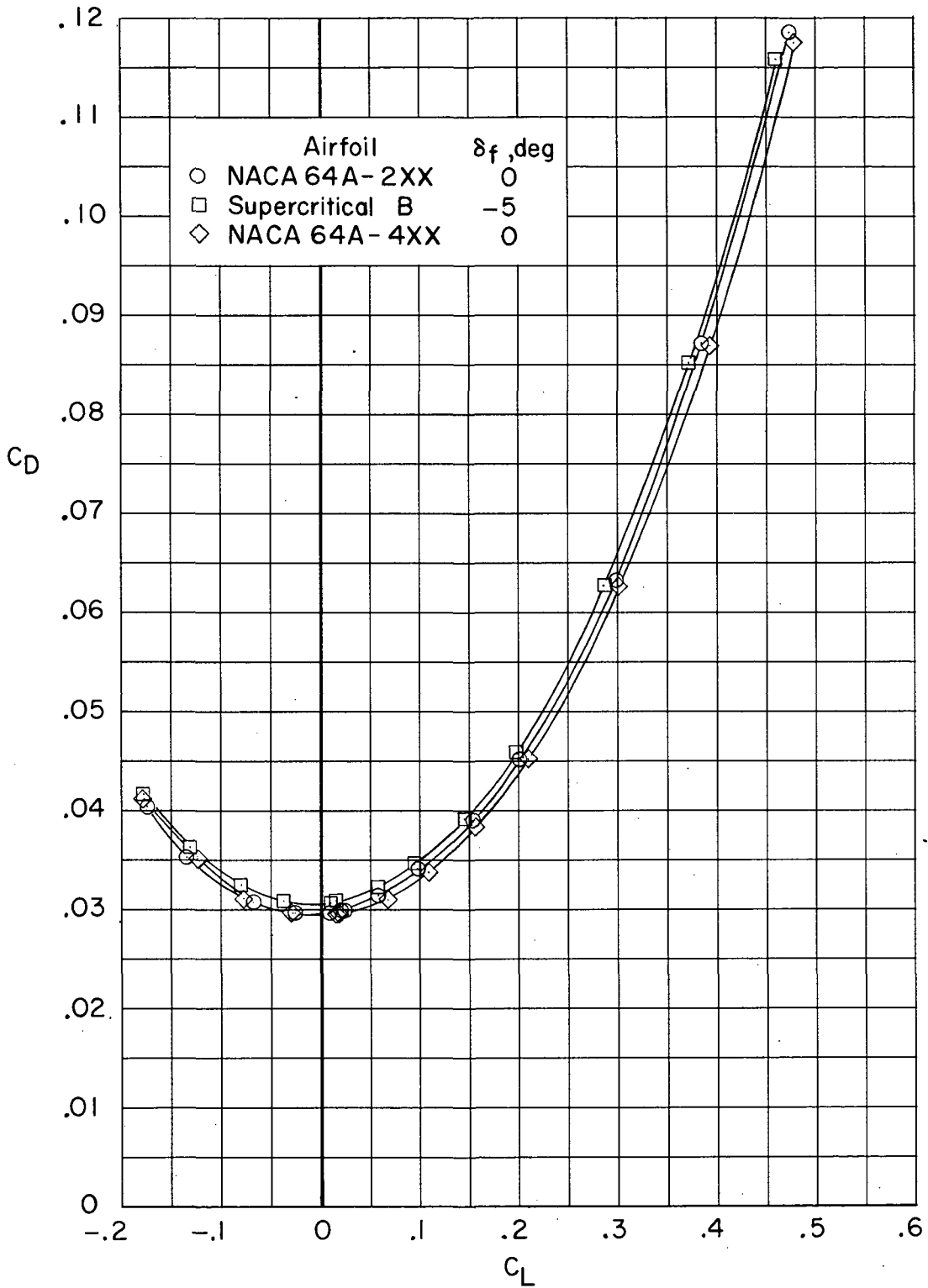
(b) $M = 2.16$. Concluded.

Figure 38. - Continued.



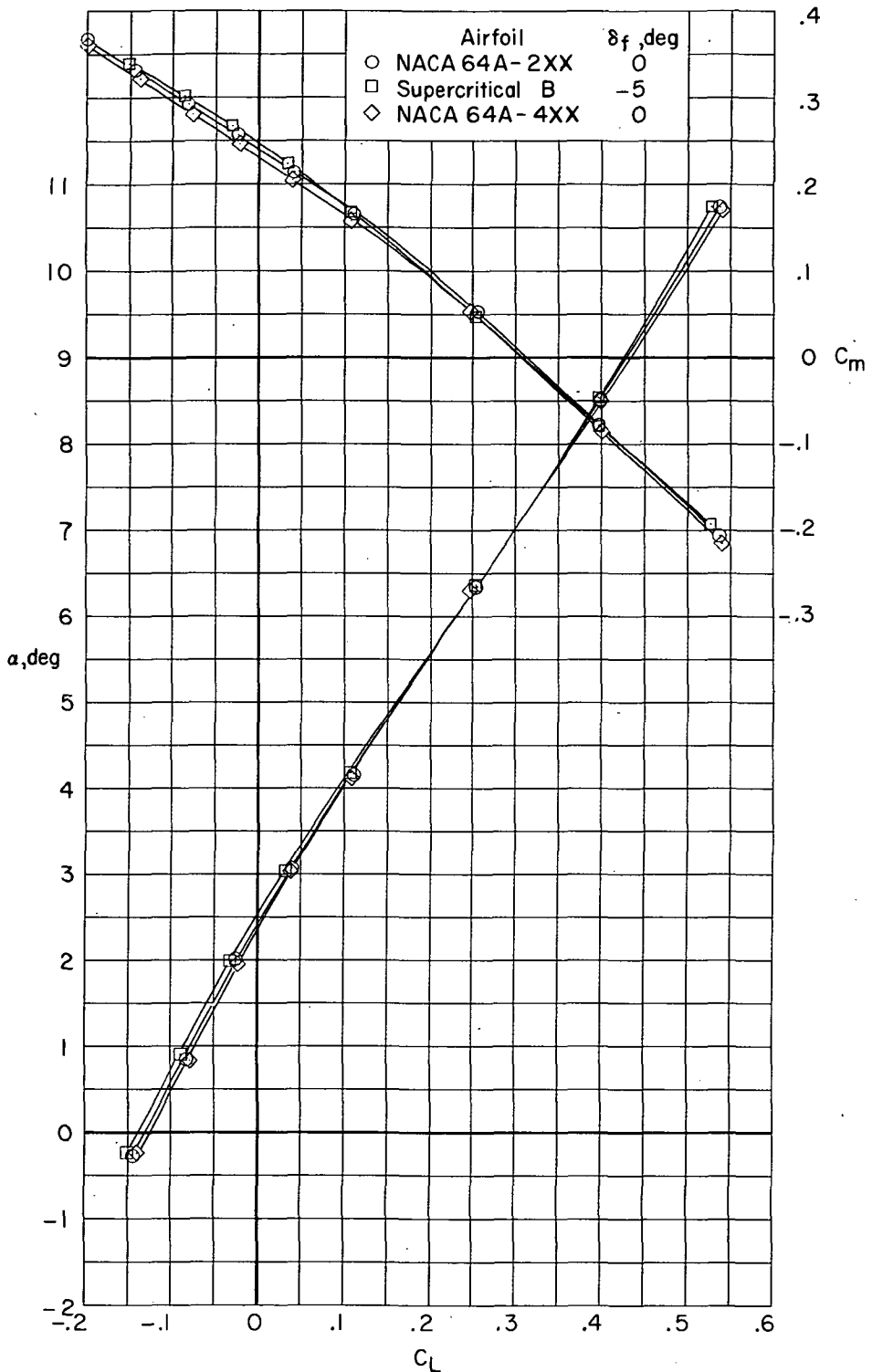
(c) $M = 2.50$.

Figure 38.- Continued.



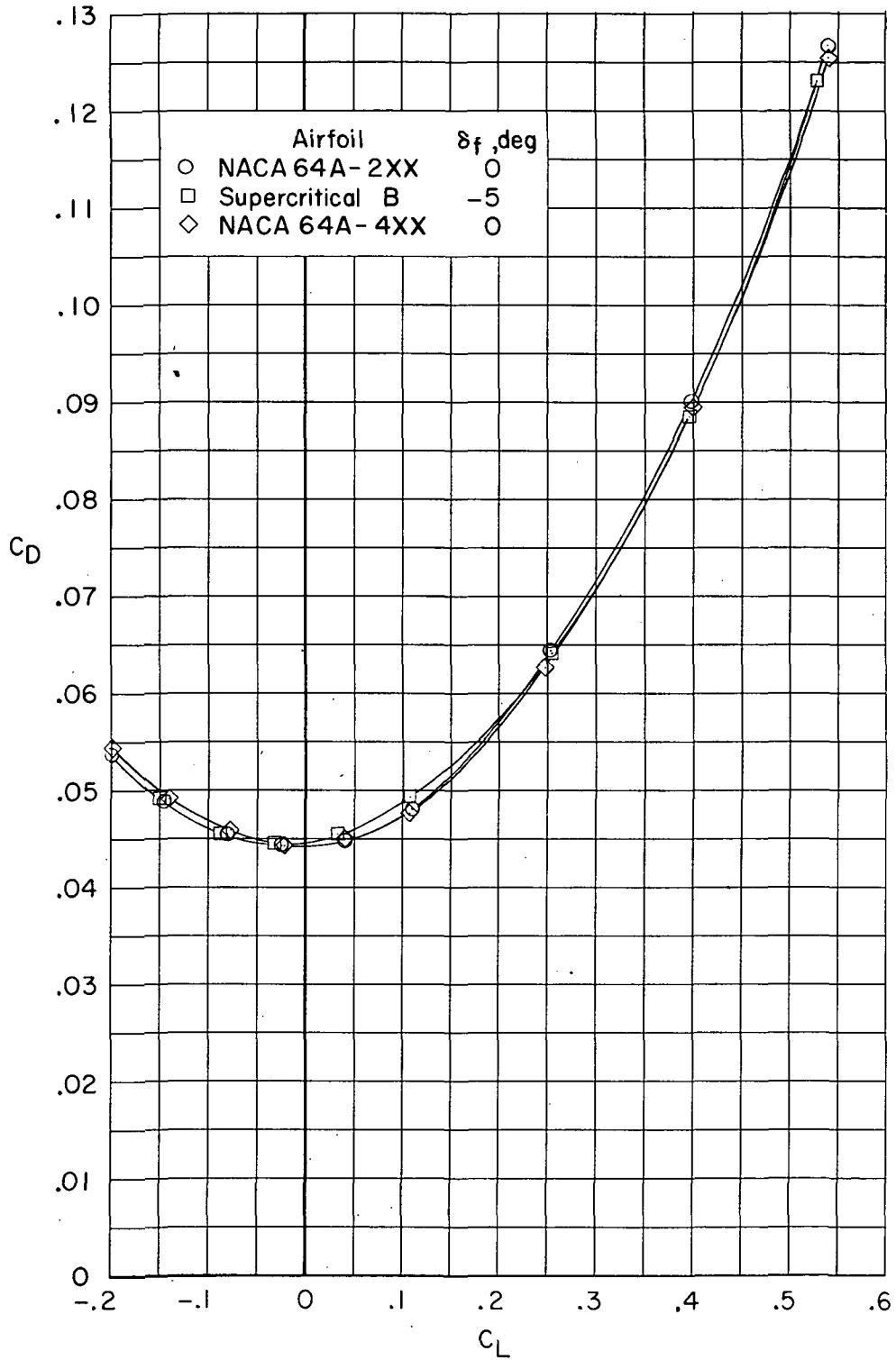
(c) $M = 2.50$. Concluded.

Figure 38.- Concluded.



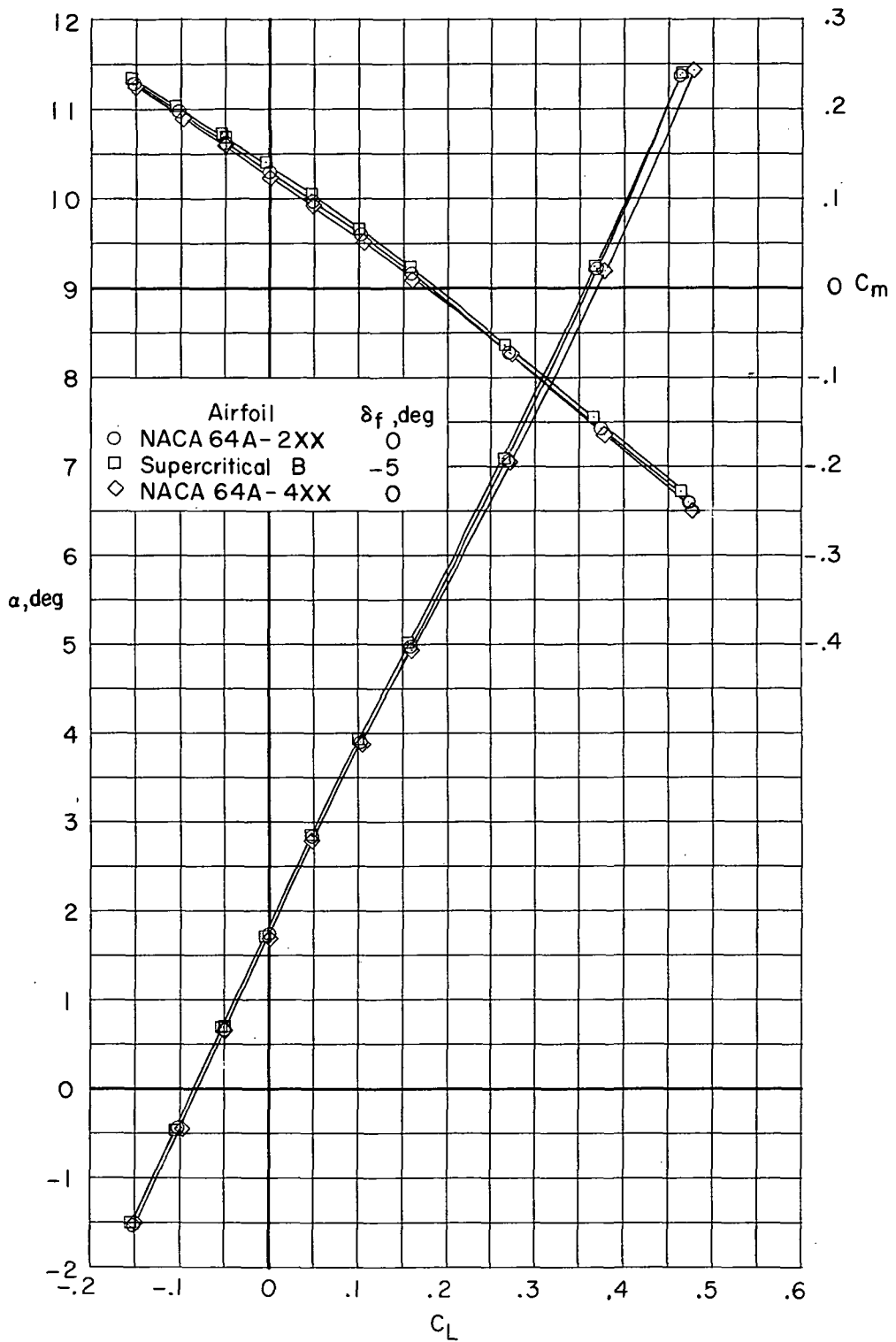
(a) $M = 1.60$.

Figure 39.- Comparison of longitudinal aerodynamic characteristics for configuration with NACA 64A2XX, supercritical, and NACA 64A4XX airfoils and transition forward. $\Lambda = 72.5^\circ$; $i_w = 1^\circ$; $\delta_h = -10^\circ$.



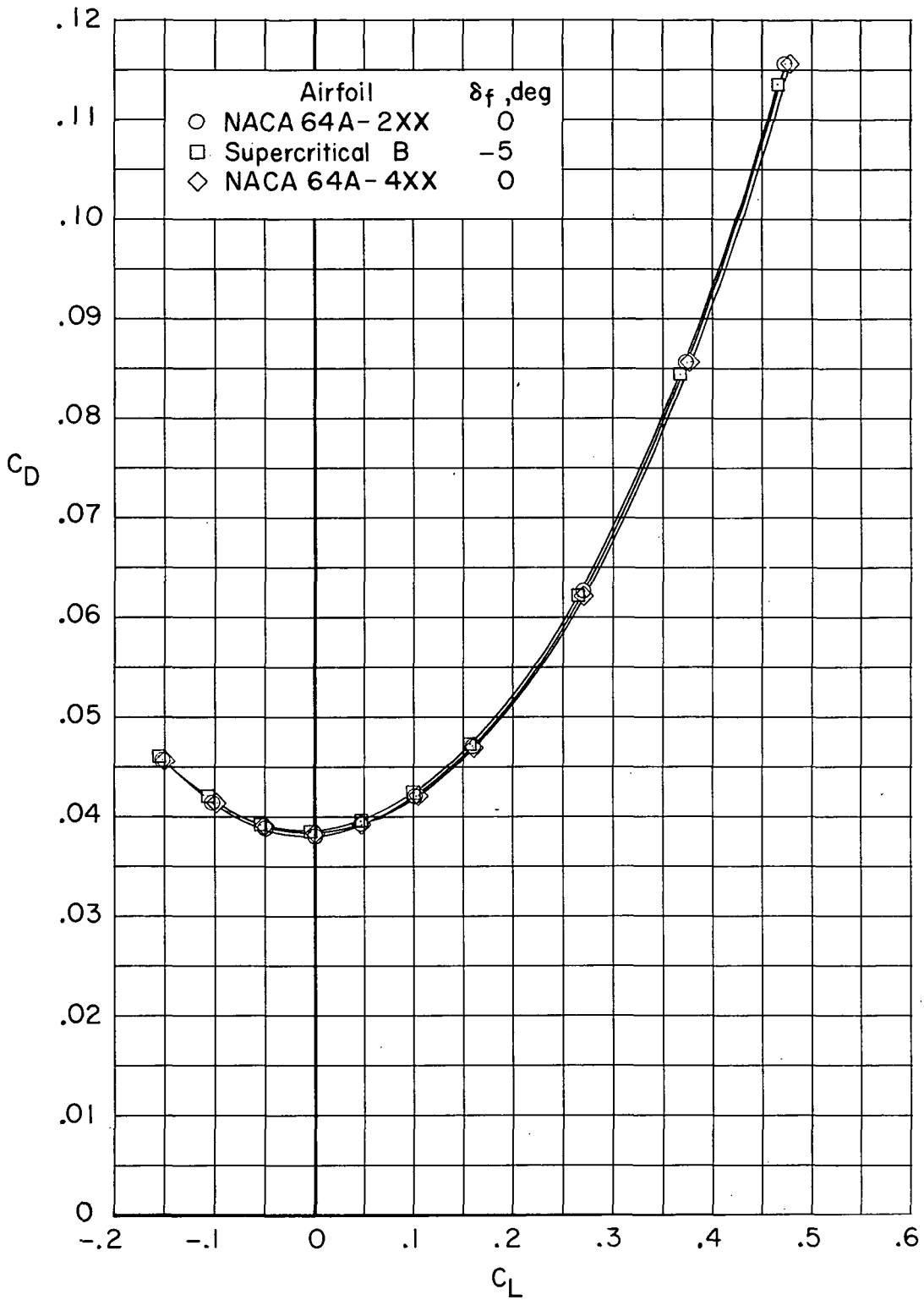
(a) $M = 1.60$. Concluded.

Figure 39.- Continued.



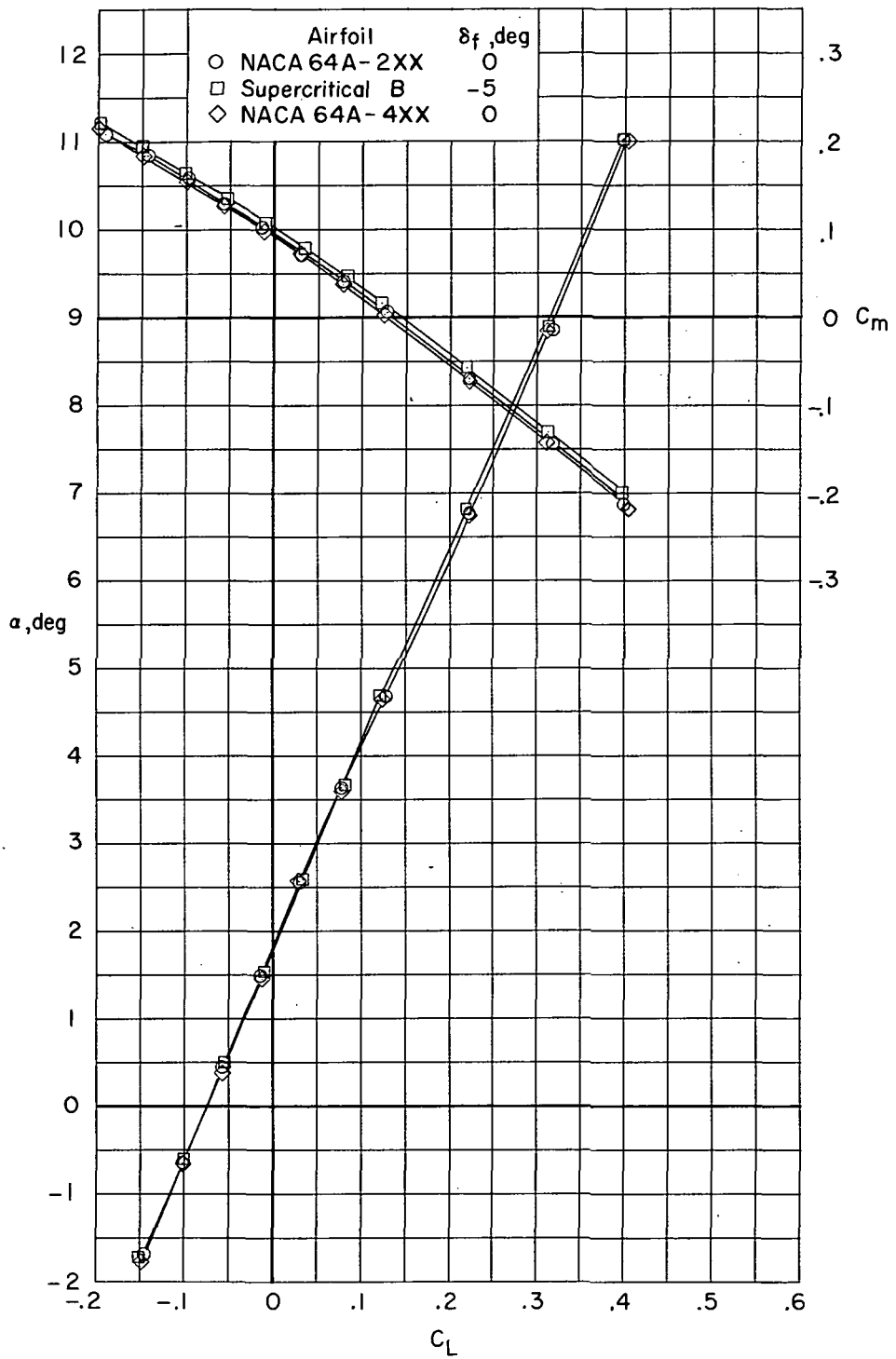
(b) $M = 2.16$.

Figure 39.- Continued.



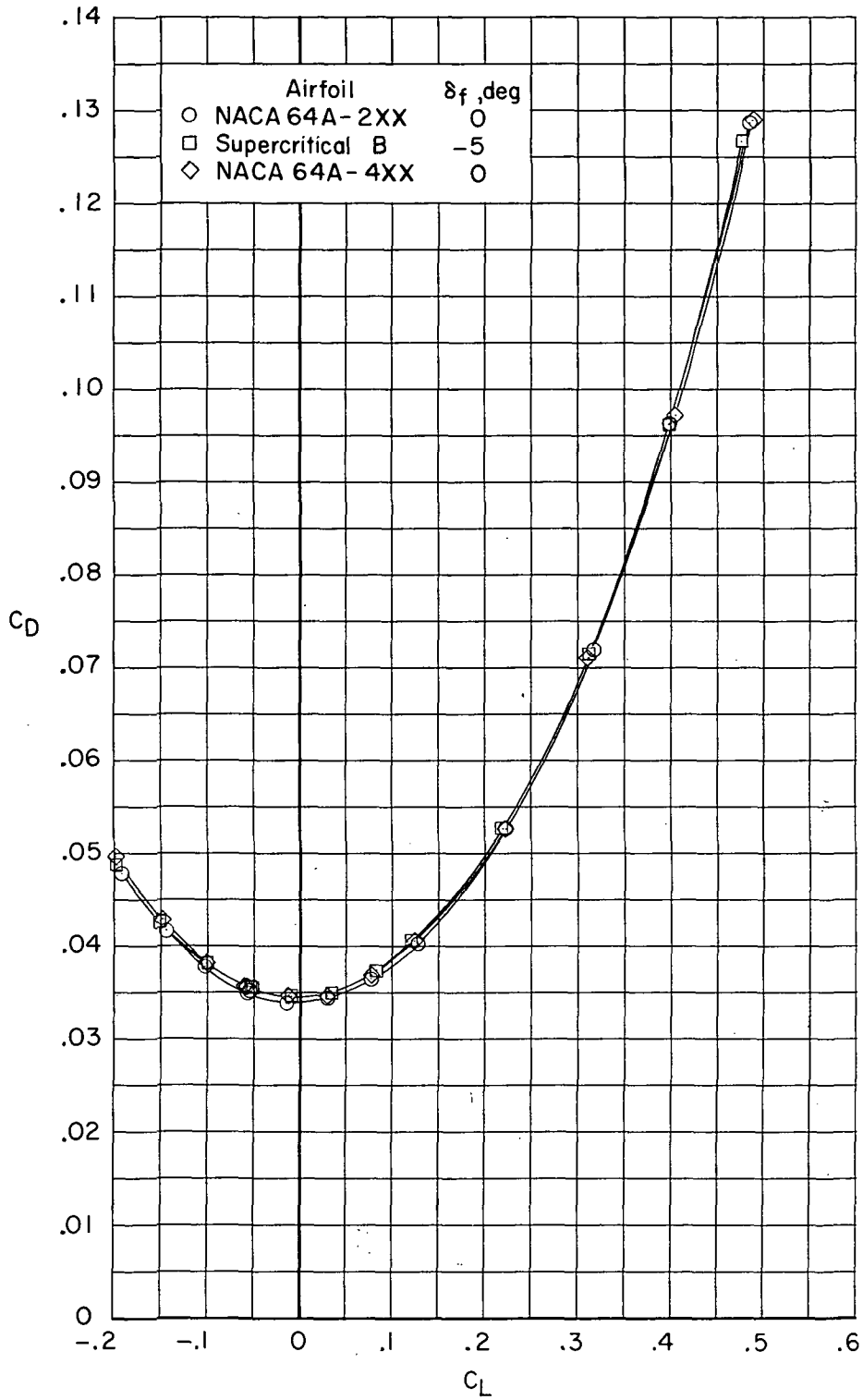
(b) $M = 2.16$. Concluded.

Figure 39. - Continued.



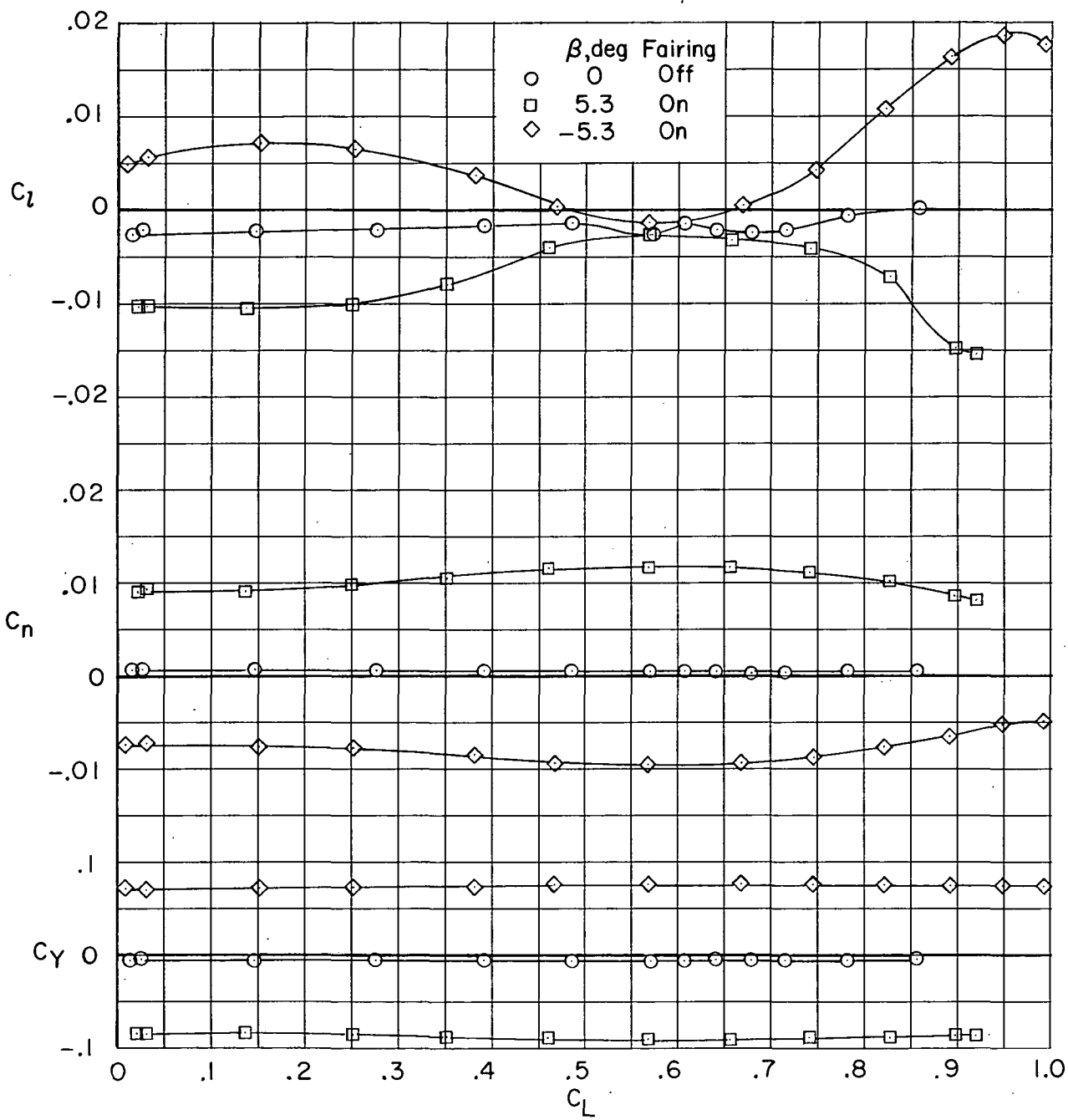
(c) $M = 2.50$.

Figure 39.- Continued.



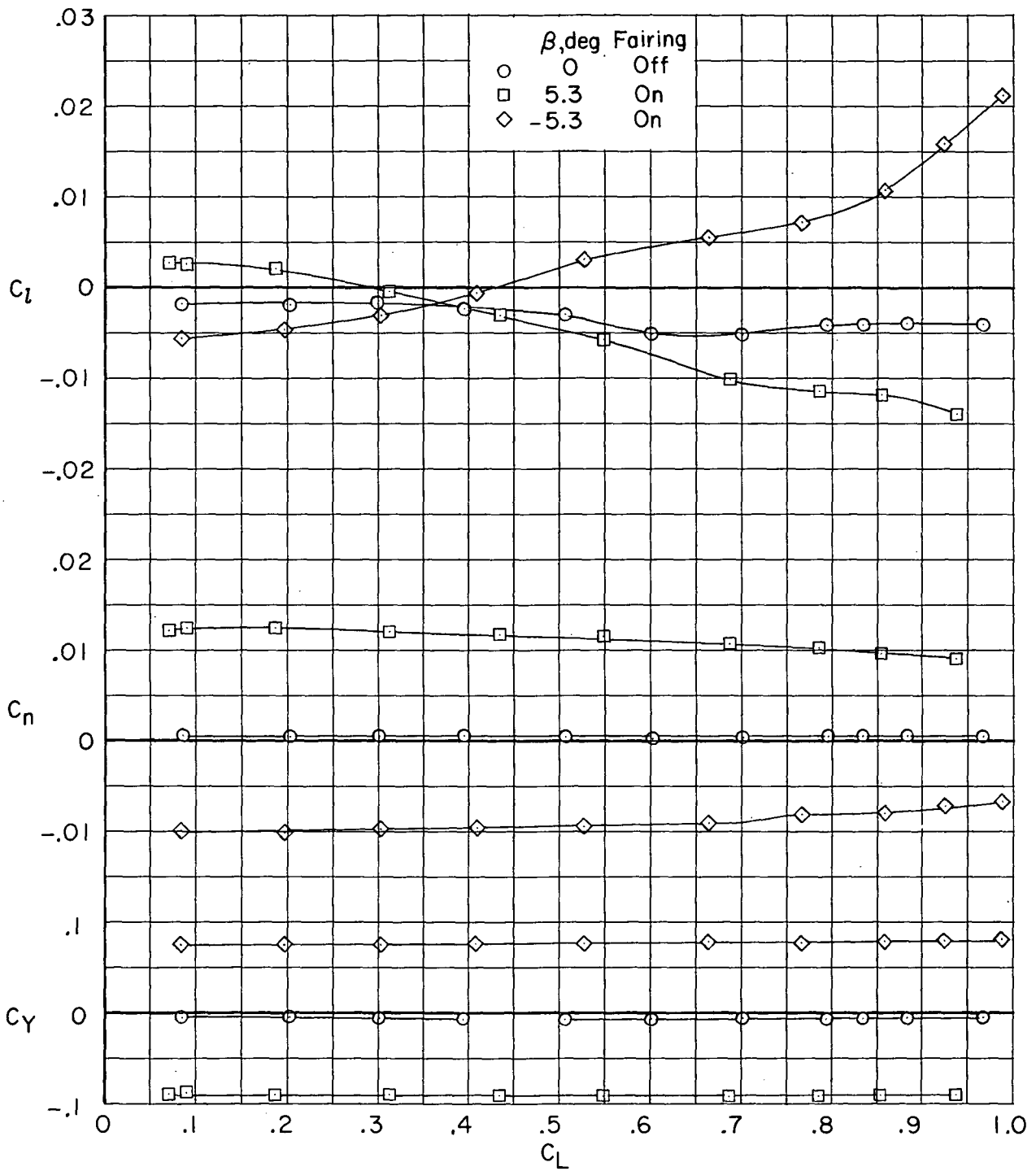
(c) $M = 2.50$. Concluded.

Figure 39. - Concluded.



(a) $M = 0.85$.

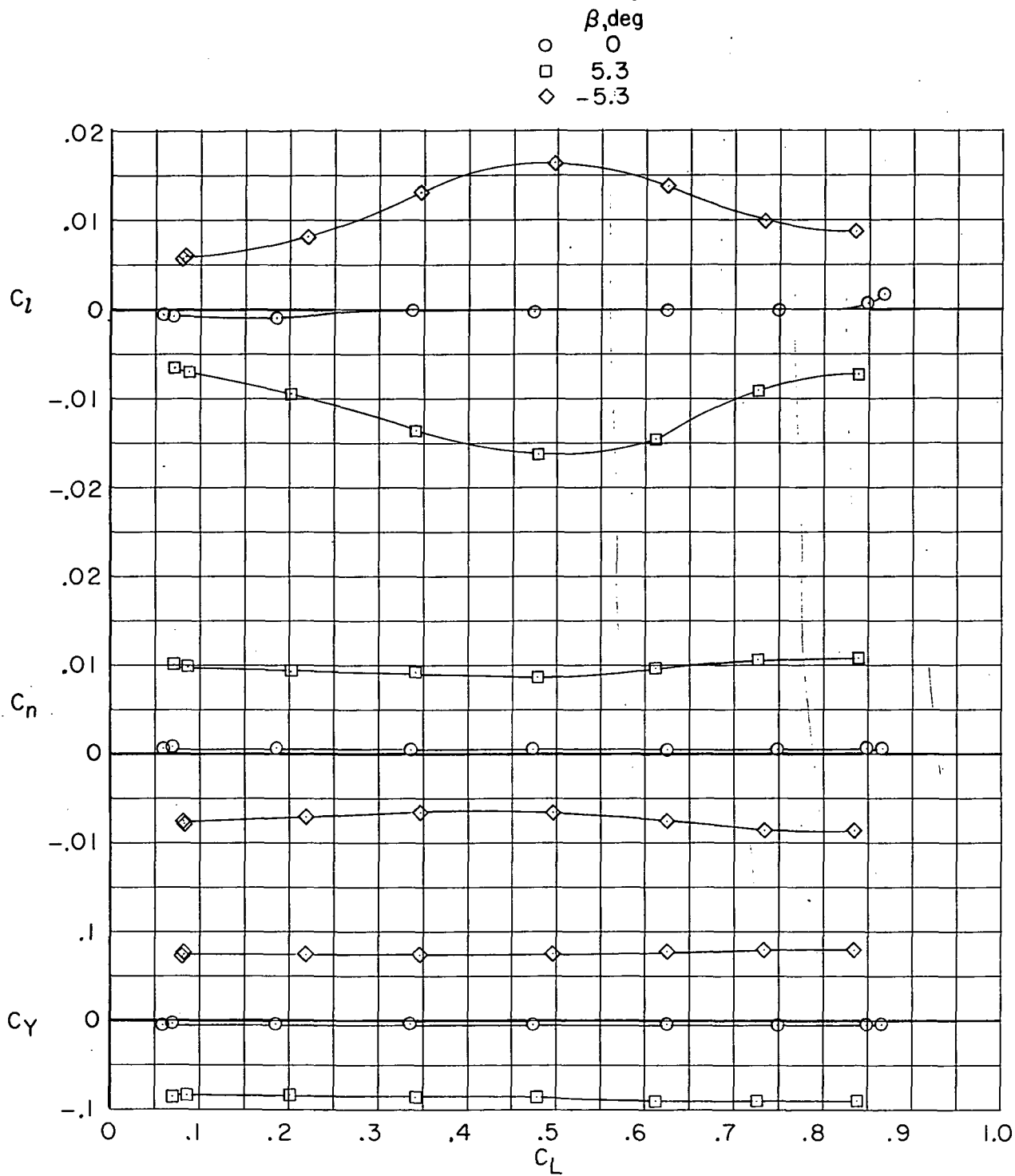
Figure 40.- Lateral-directional aerodynamic characteristics for configuration with NACA 64A2XX airfoils and transition rearward. $\Lambda = 33^\circ$; $i_w = 1^\circ$; $\delta_h = 0^\circ$.



(b) $M = 0.91$.

Figure 40. - Concluded.

~~CONFIDENTIAL~~

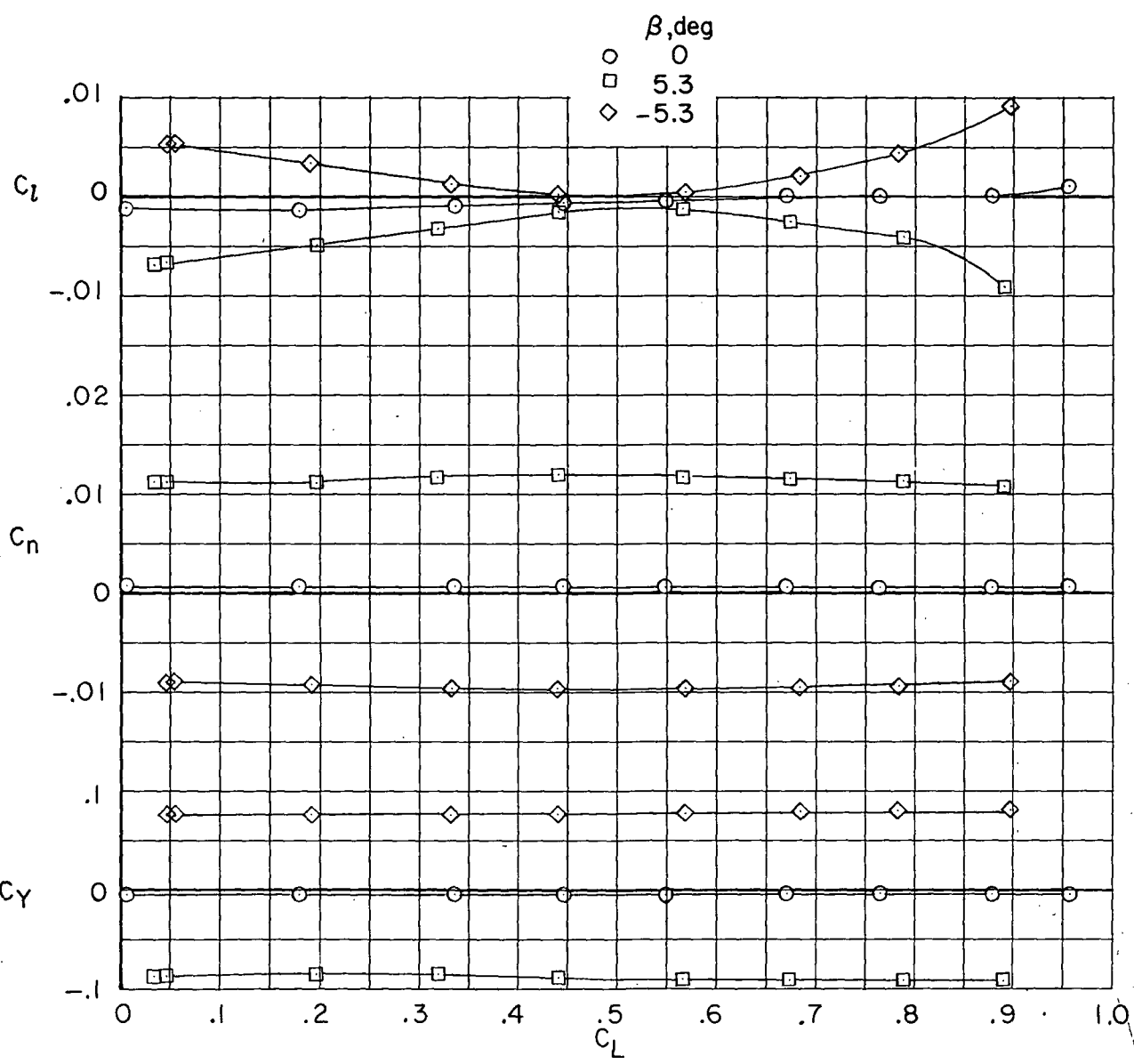


(a) $M = 0.85$.

Figure 41. - Lateral-directional aerodynamic characteristics for configuration with supercritical airfoil B, fuselage fairing, and transition rearward.

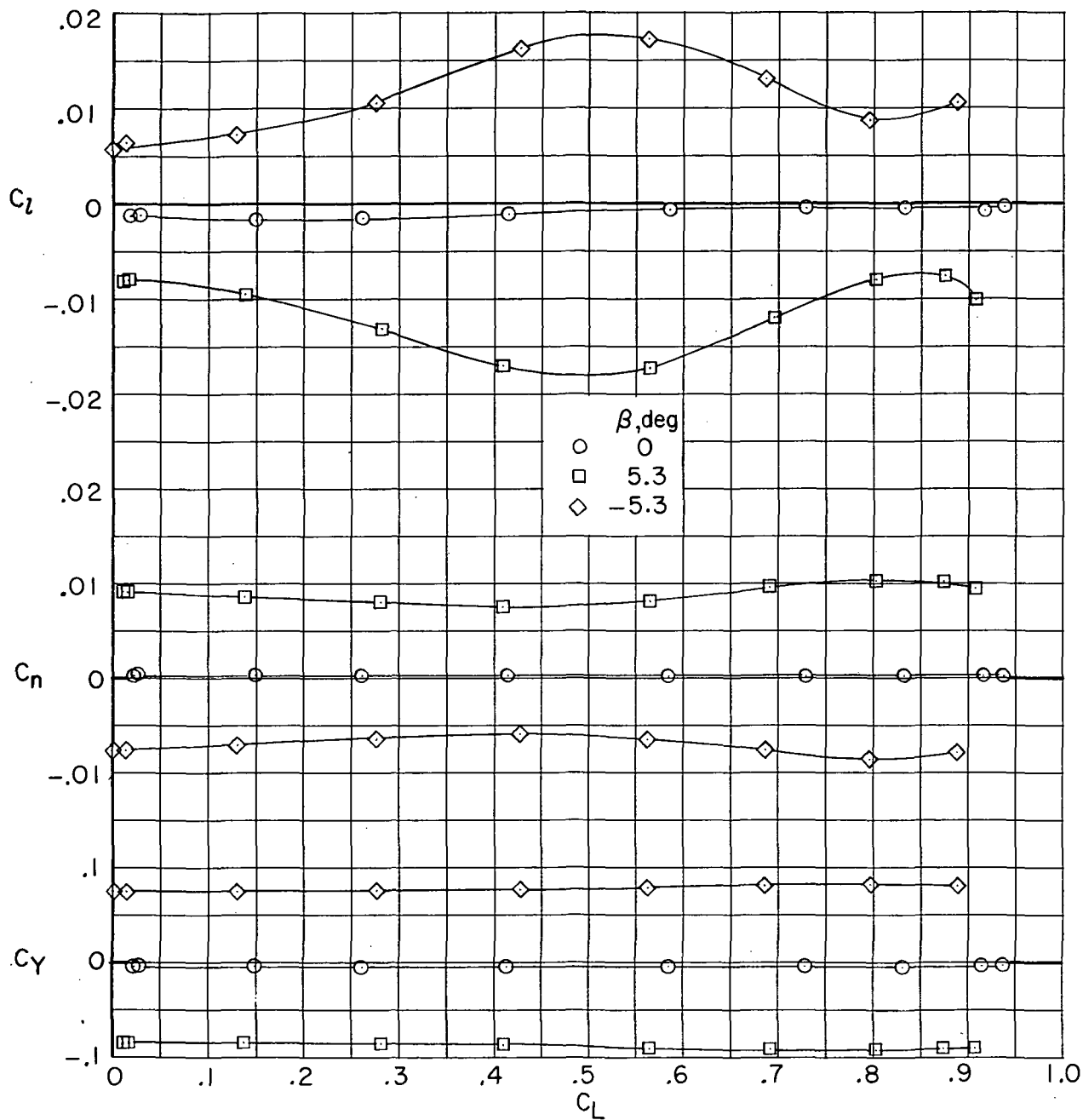
$\Lambda = 33^\circ$; $i_w = 1^\circ$; $\delta_h = 0^\circ$.

~~CONFIDENTIAL~~



(b) $M = 0.91$.

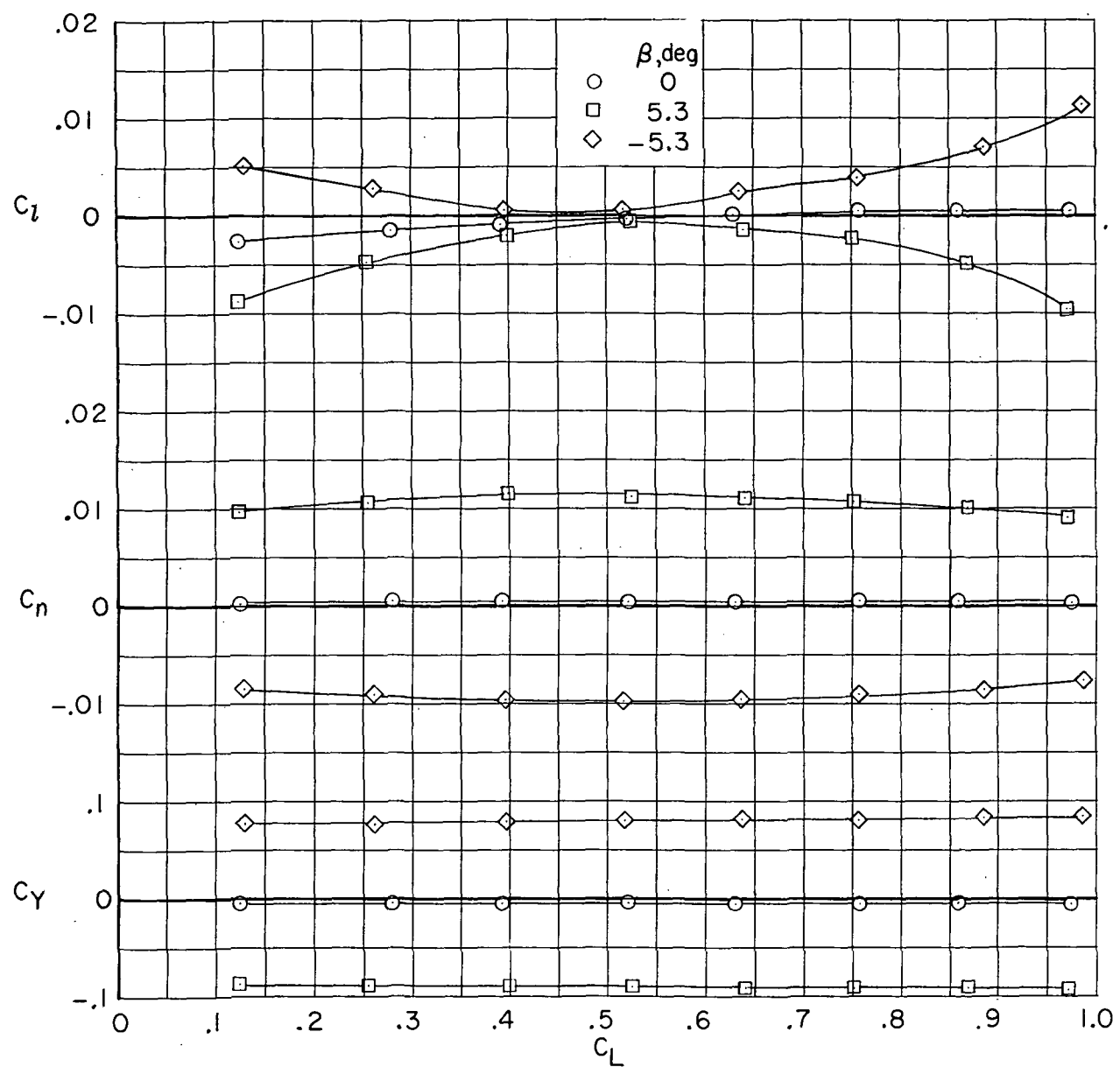
Figure 41. - Concluded.



(a) $M = 0.85$.

Figure 42.- Lateral-directional aerodynamic characteristics of configuration with supercritical airfoil B, fuselage fairing, and transition rearward. $\Lambda = 33^\circ$; $i_w = -1^\circ$; $\delta_h = 0^\circ$.

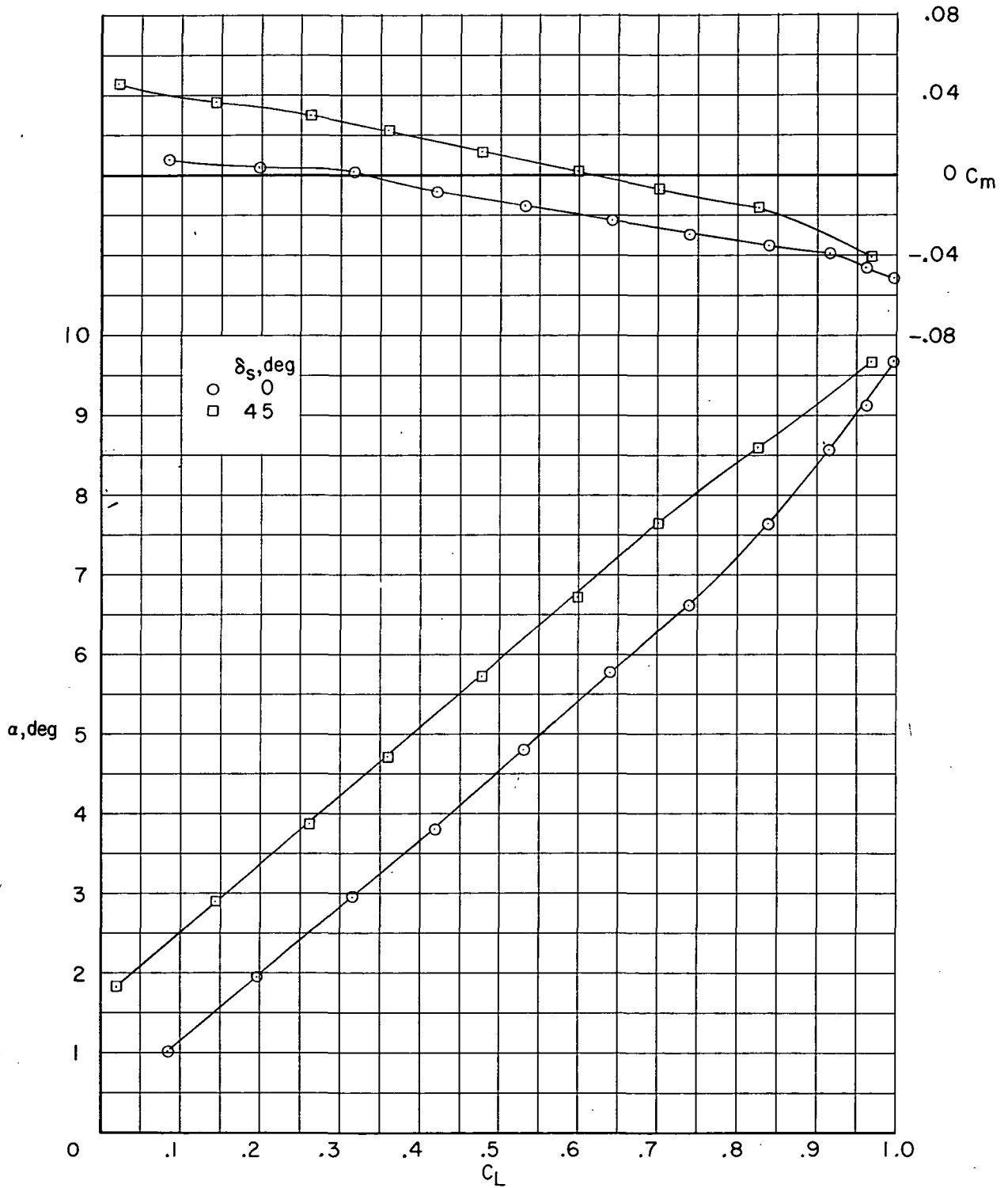
~~CONFIDENTIAL~~



(b) $M = 0.91$.

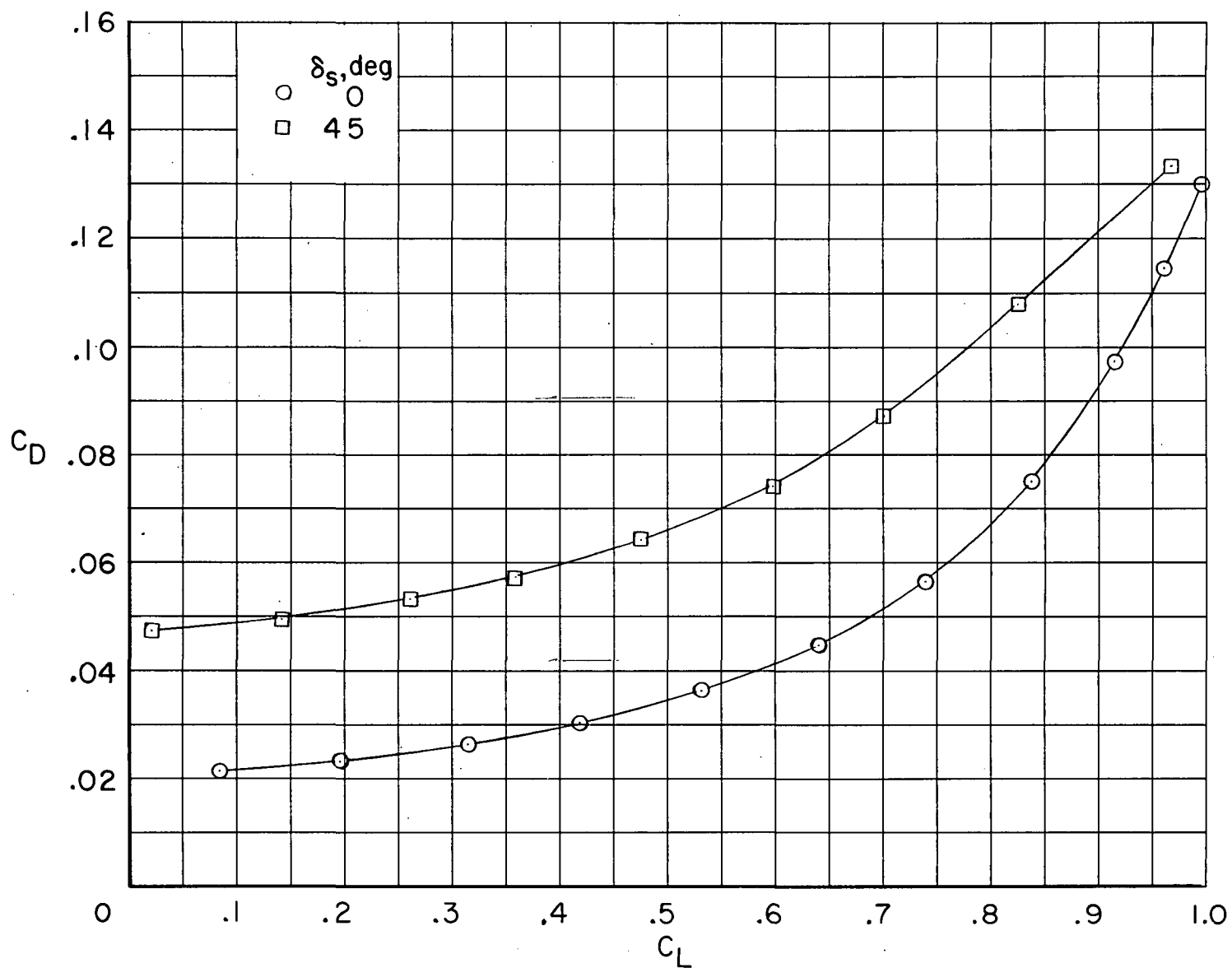
Figure 42.- Concluded.

~~CONFIDENTIAL~~



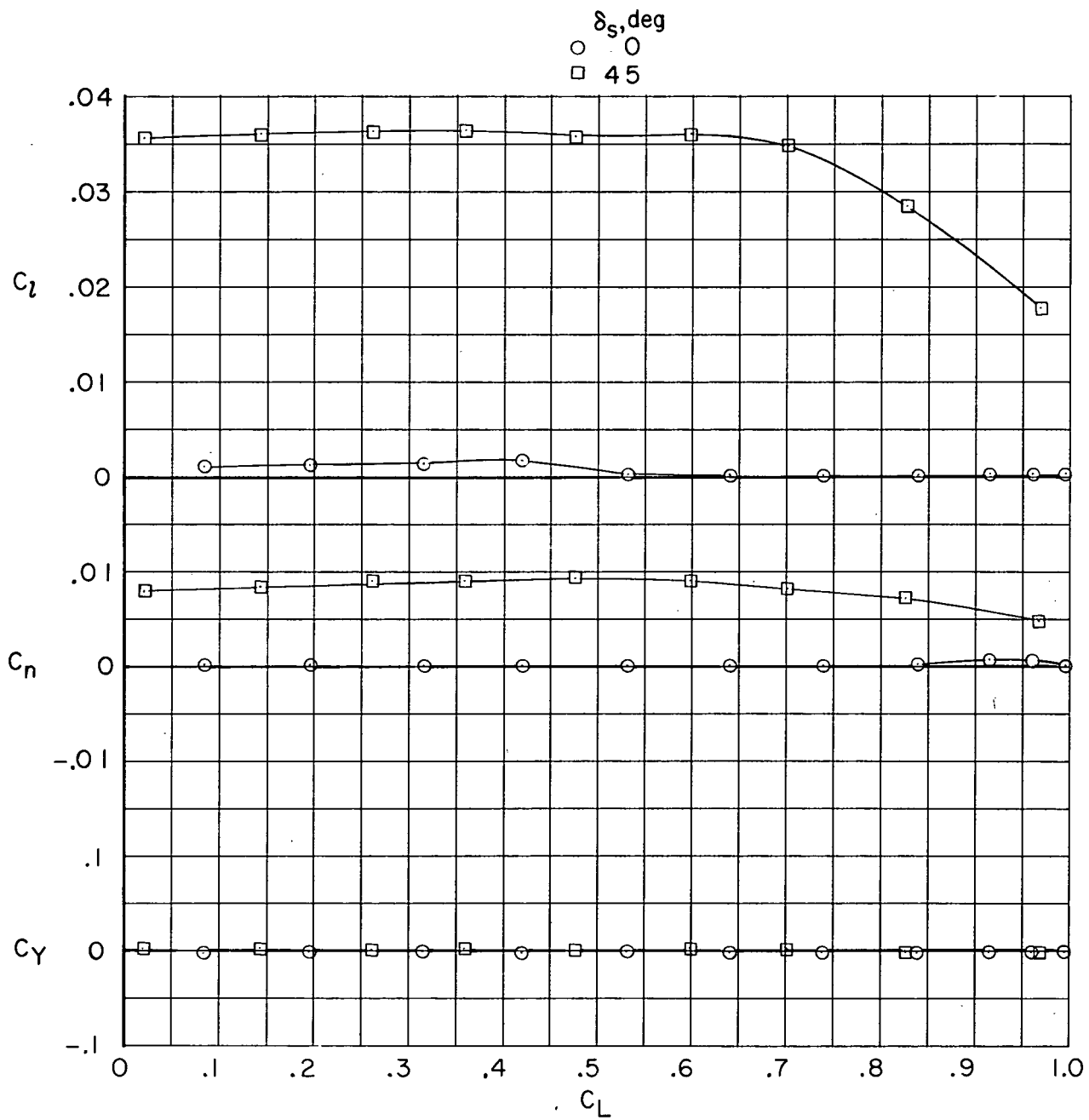
(a) $M = 0.60$.

Figure 43.- Effect of spoiler deflection on longitudinal and lateral-directional aerodynamic characteristics of configuration with supercritical airfoil B, fuselage fairing, and upper surface transition forward. $\Lambda = 26^\circ$; $i_w = -1^\circ$; $\delta_h = 0^\circ$.



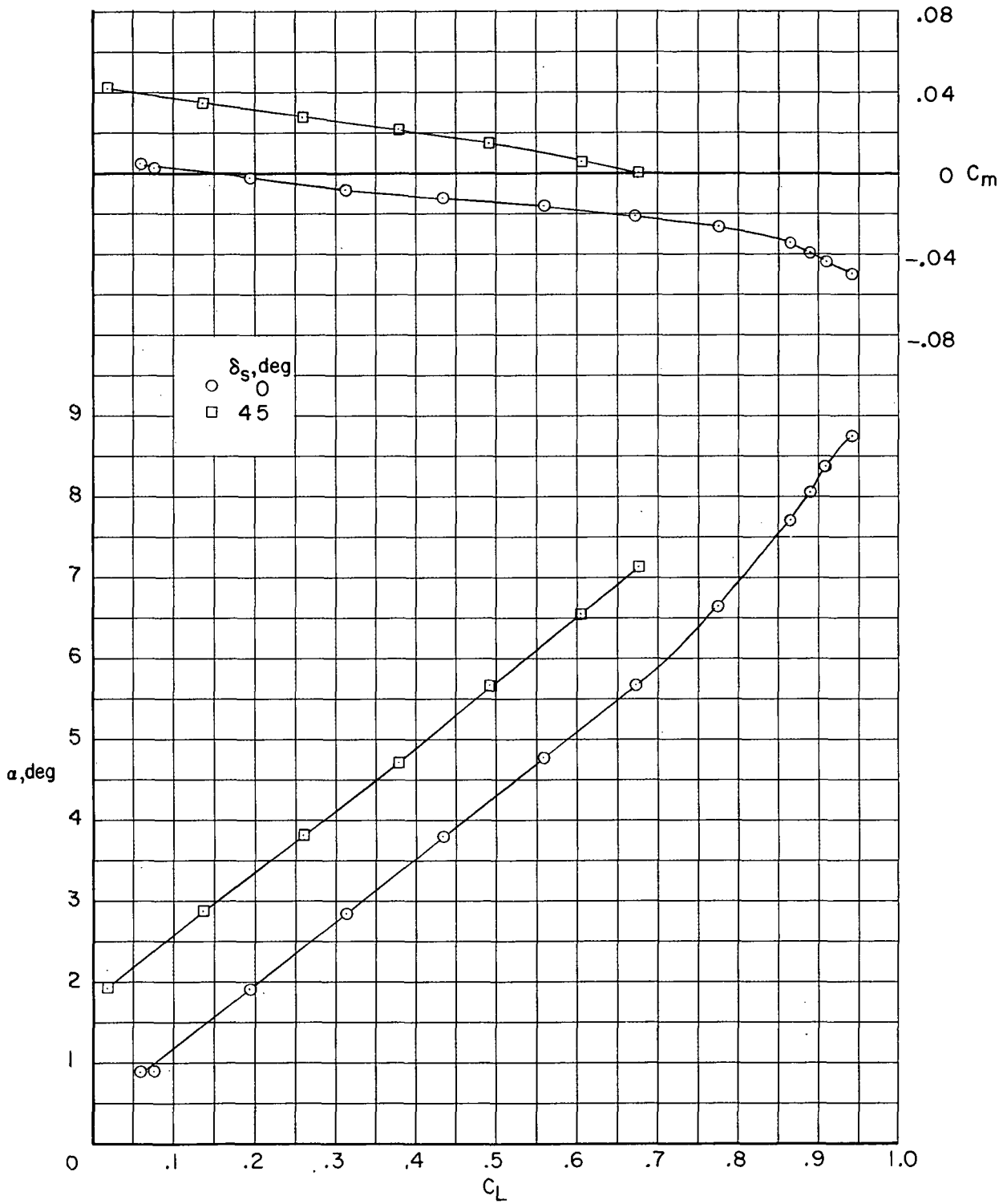
(a) $M = 0.60$. Continued.

Figure 43. - Continued.



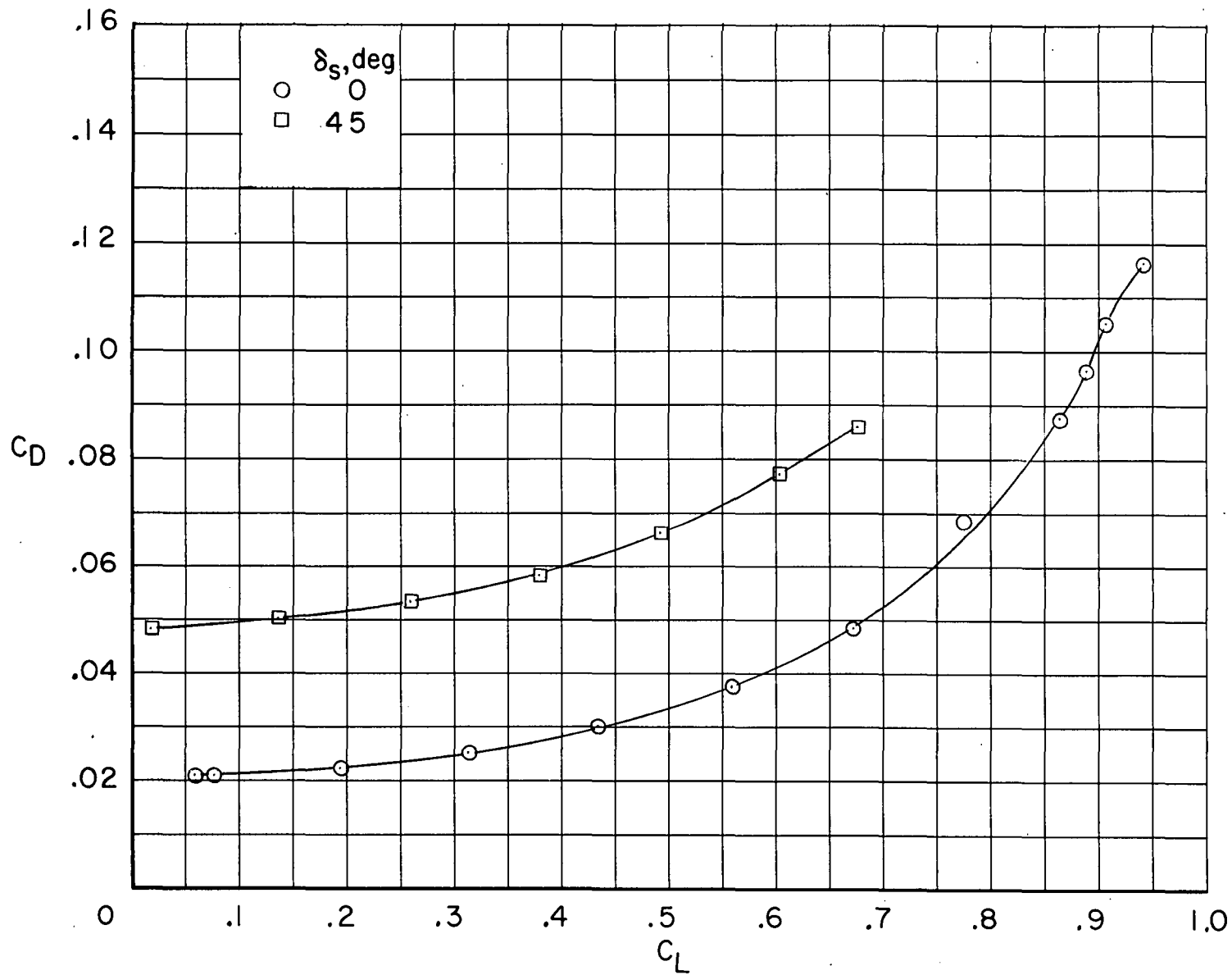
(a) $M = 0.60$. Concluded.

Figure 43.- Continued.



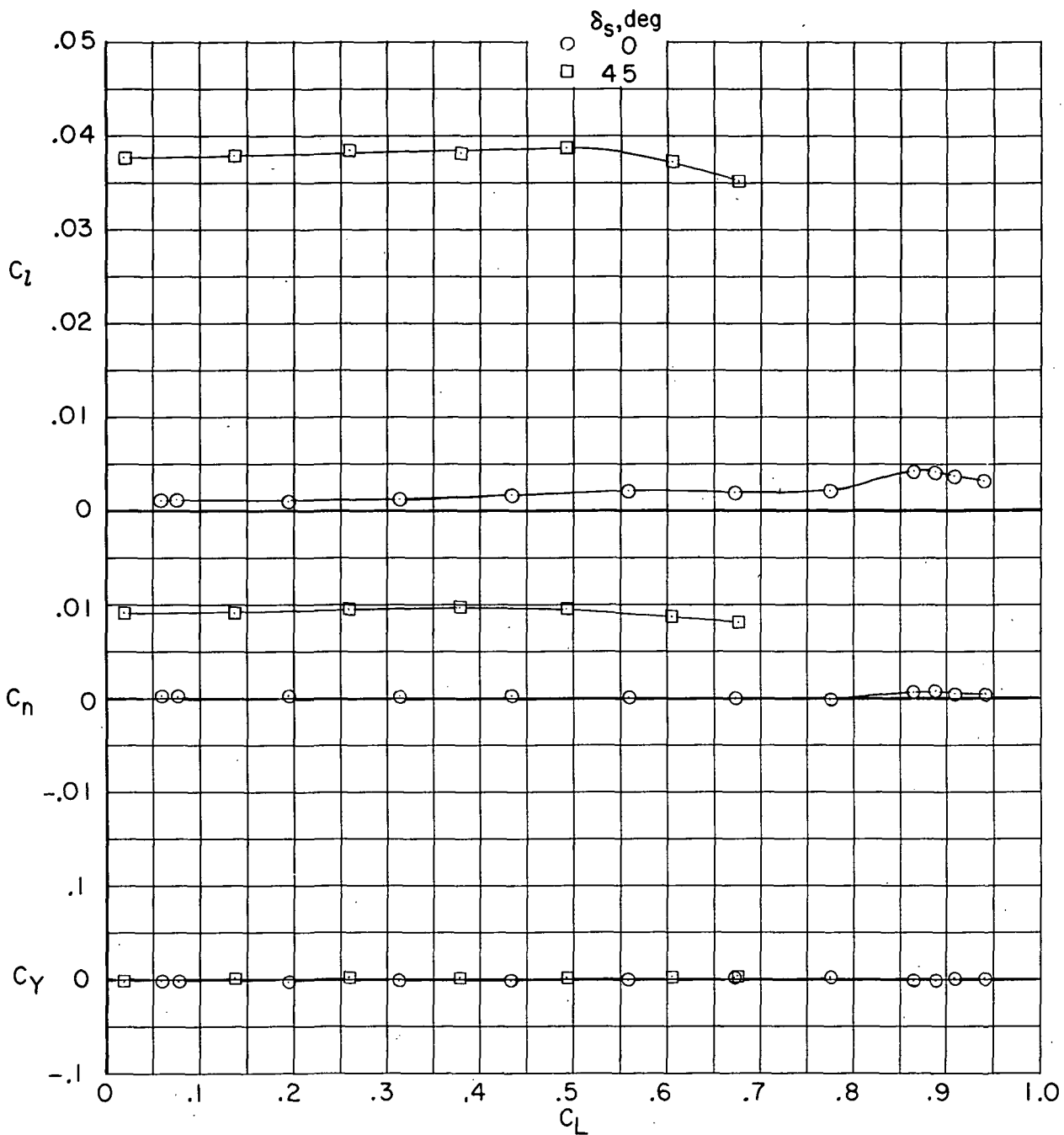
(b) $M = 0.70$.

Figure 43.- Continued.



(b) $M = 0.70$. Continued.

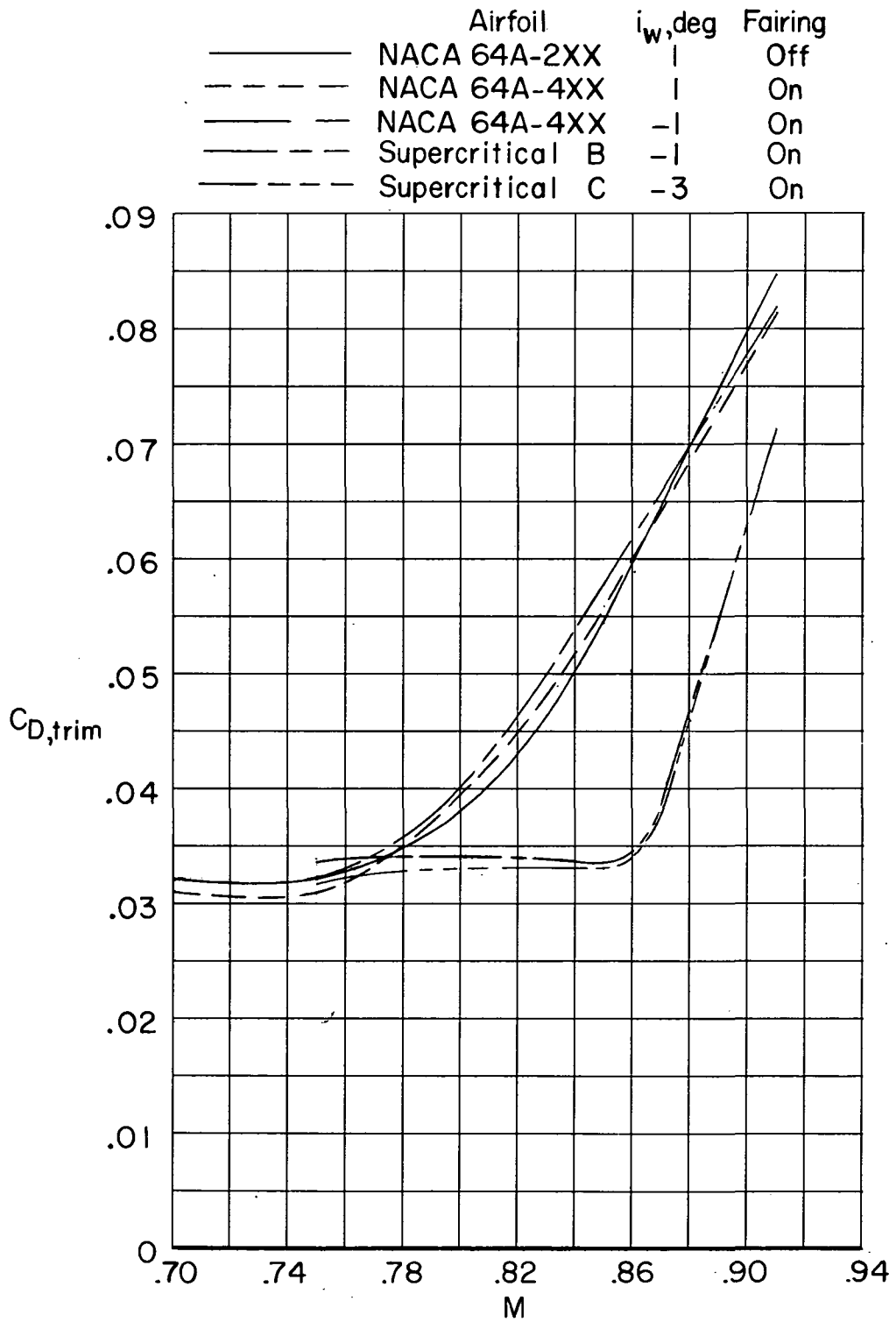
Figure 43.- Continued.



(b) $M = 0.70$. Concluded.

Figure 43.- Concluded.

~~CONFIDENTIAL~~

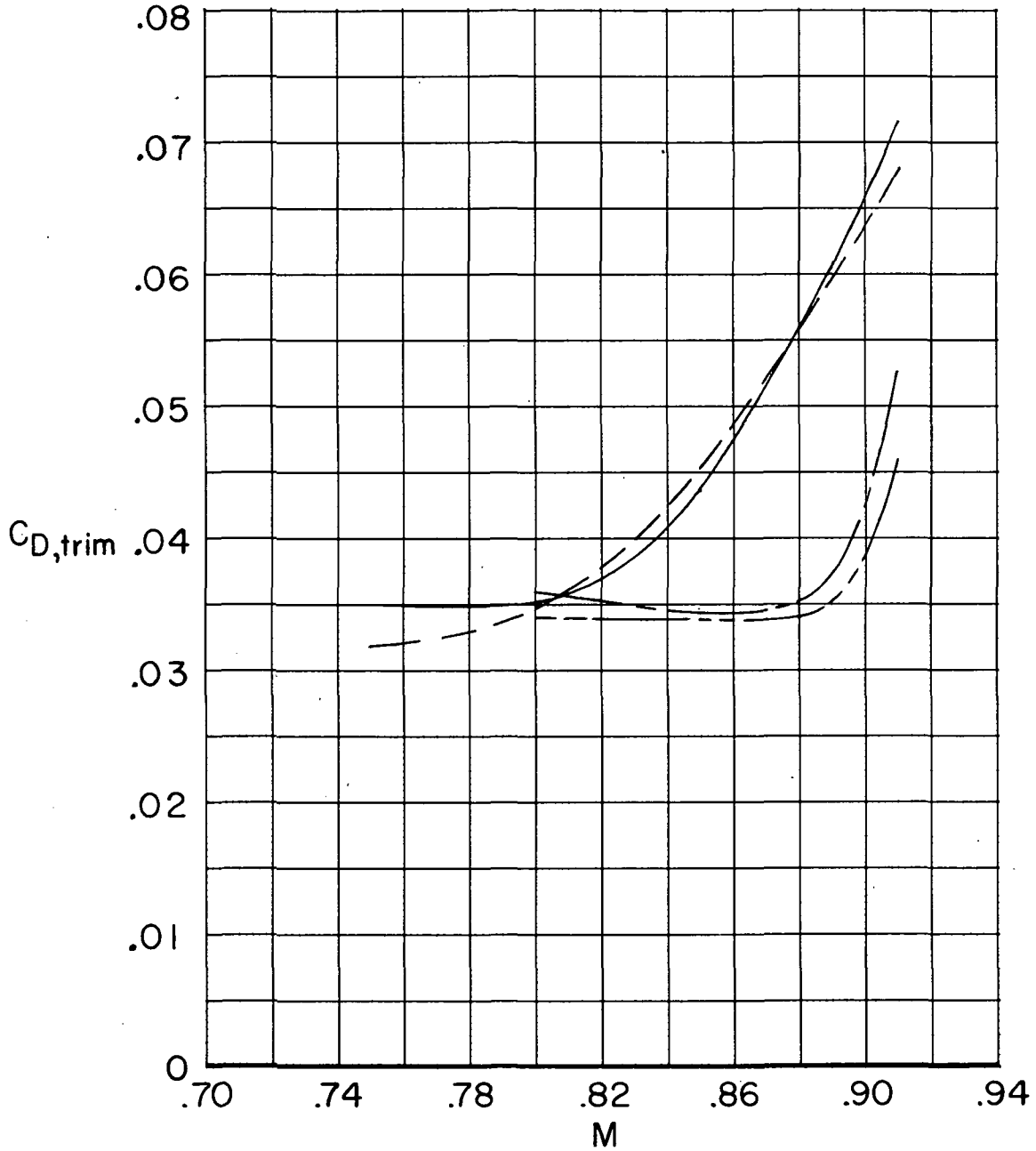


(a) $\Lambda = 26^\circ$.

Figure 44.- Variation with Mach number of trimmed drag characteristics. $C_L = 0.50$.

~~CONFIDENTIAL~~

	Airfoil	i_w, deg	Fairing
—————	NACA 64A-2XX	1	Off
- - - - -	NACA 64A-4XX	-1	On
—————	Supercritical B	-1	On
- - - - -	Supercritical C	-3	On

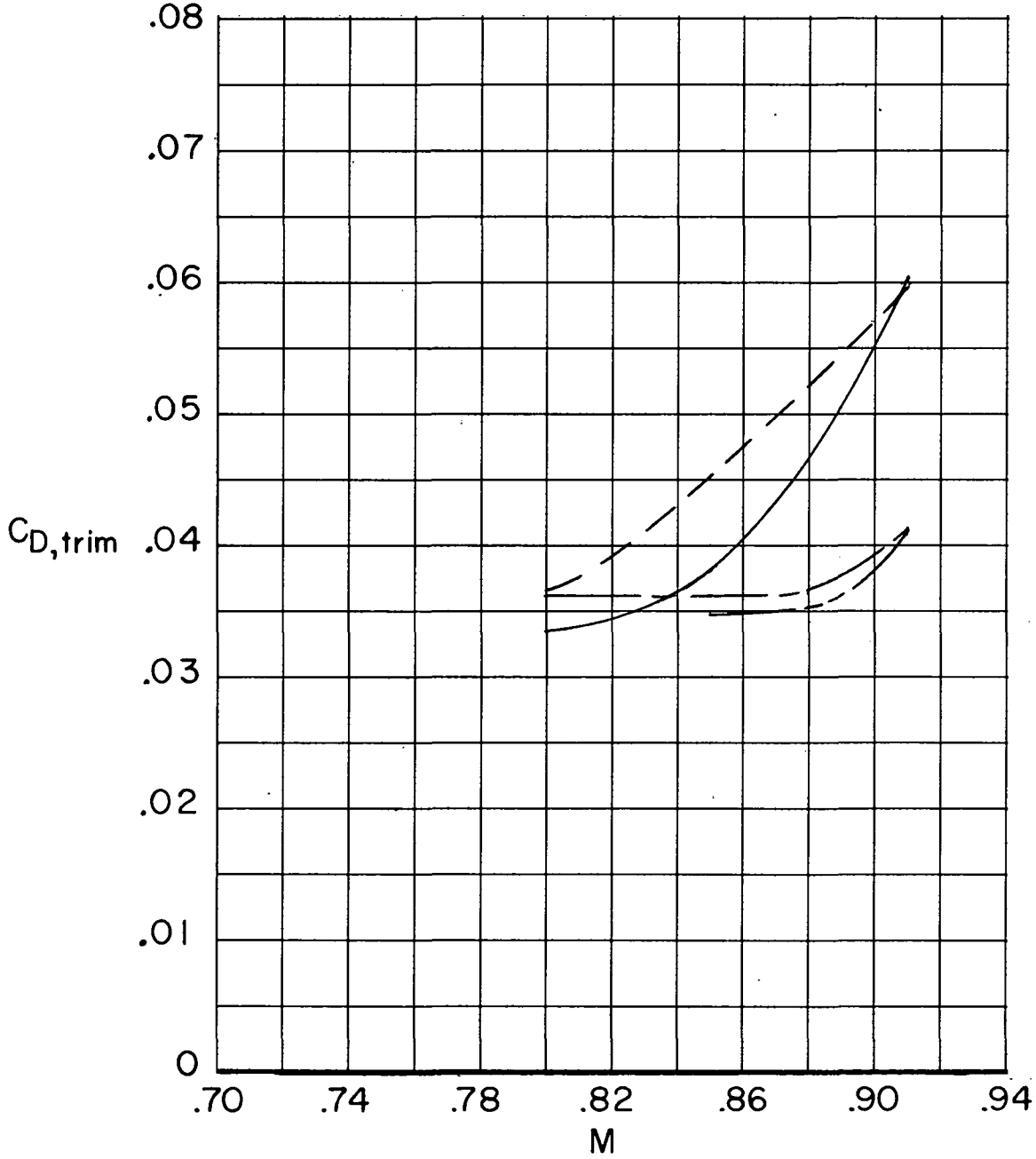


(b) $\Lambda = 33^\circ$.

Figure 44. - Continued.

~~CONFIDENTIAL~~

	Airfoil	i_w , deg	Fairing
—————	NACA 64A-2XX	1	Off
-----	NACA 64A-4XX	-1	On
——— —	Supercritical B	-1	On
——— - -	Supercritical C	-3	On

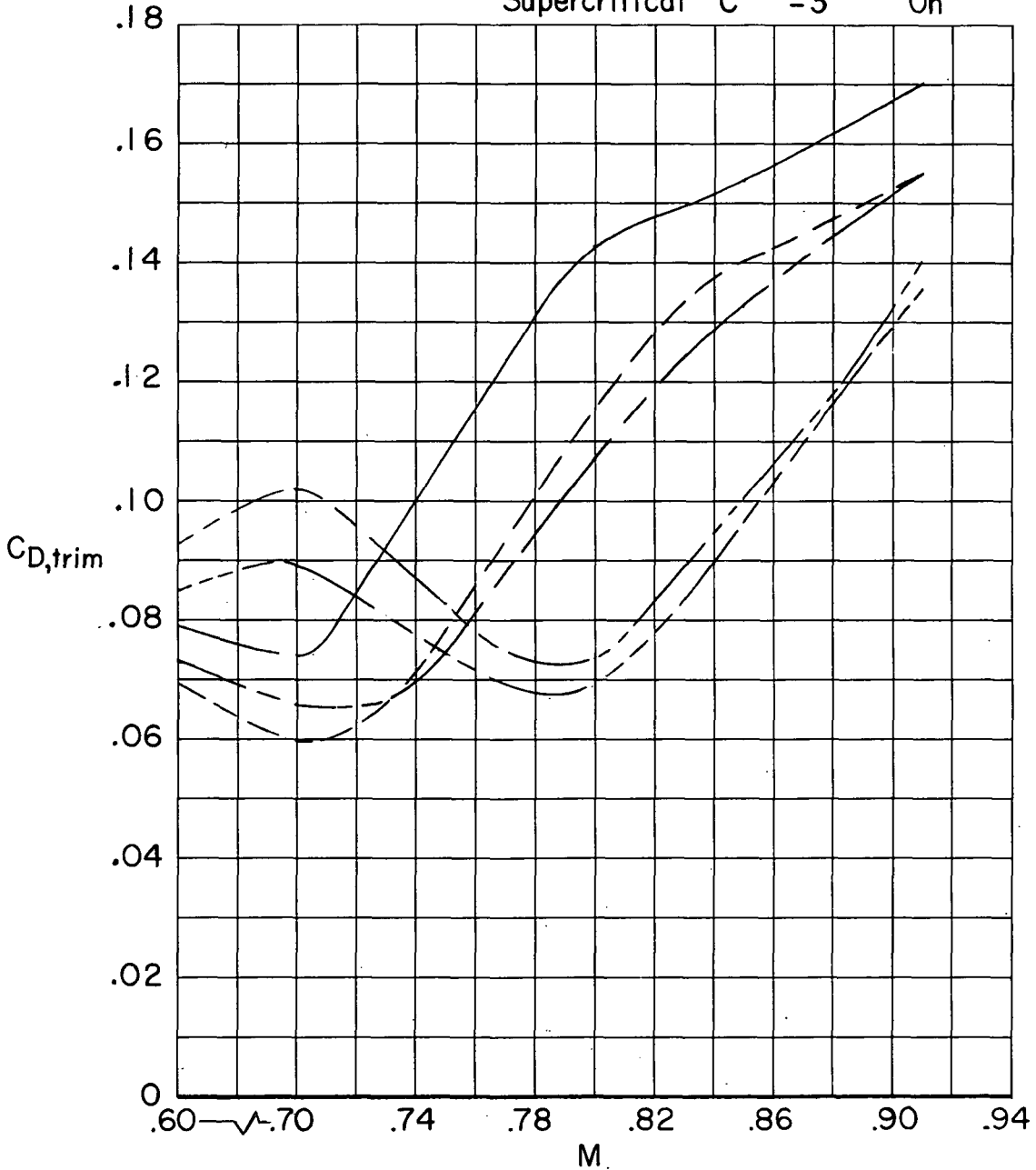


(c) $\Lambda = 39^\circ$.

Figure 44.- Concluded.

~~CONFIDENTIAL~~

	Airfoil	i_w, deg	Fairing
—————	NACA 64A-2XX	1	Off
-----	NACA 64A-4XX	1	On
—————	NACA 64A-4XX	-1	On
-----	Supercritical B	-1	On
-----	Supercritical C	-3	On

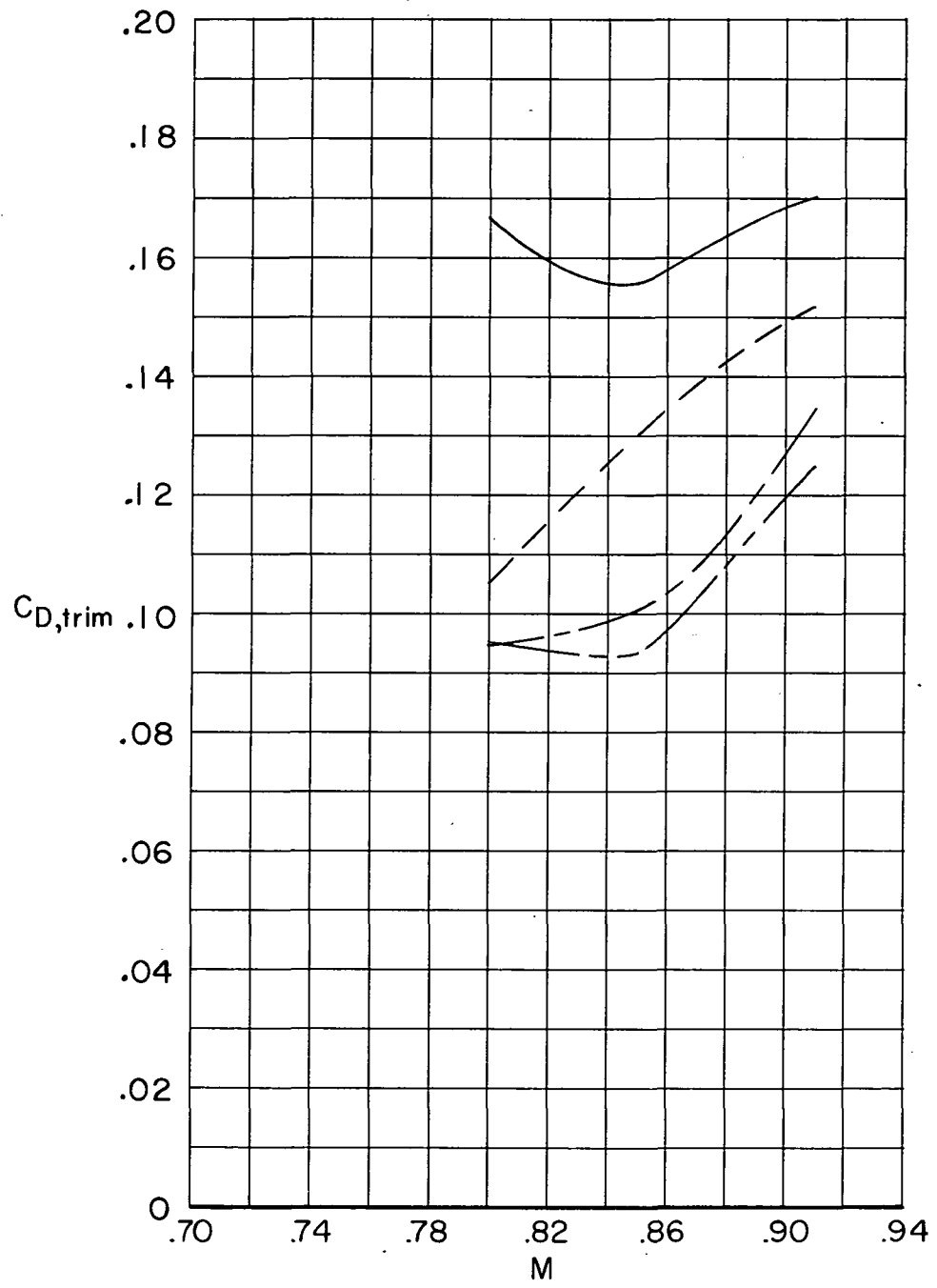


(a) $\Lambda = 26^\circ$.

Figure 45.- Variation with Mach number of trimmed drag characteristics. $C_L = 0.90$.



	Airfoil	i_w, deg	Fairing
————	NACA 64A-2XX	1	Off
-----	NACA 64A-4XX	-1	On
———	Supercritical B	-1	On
———	Supercritical C	-3	On



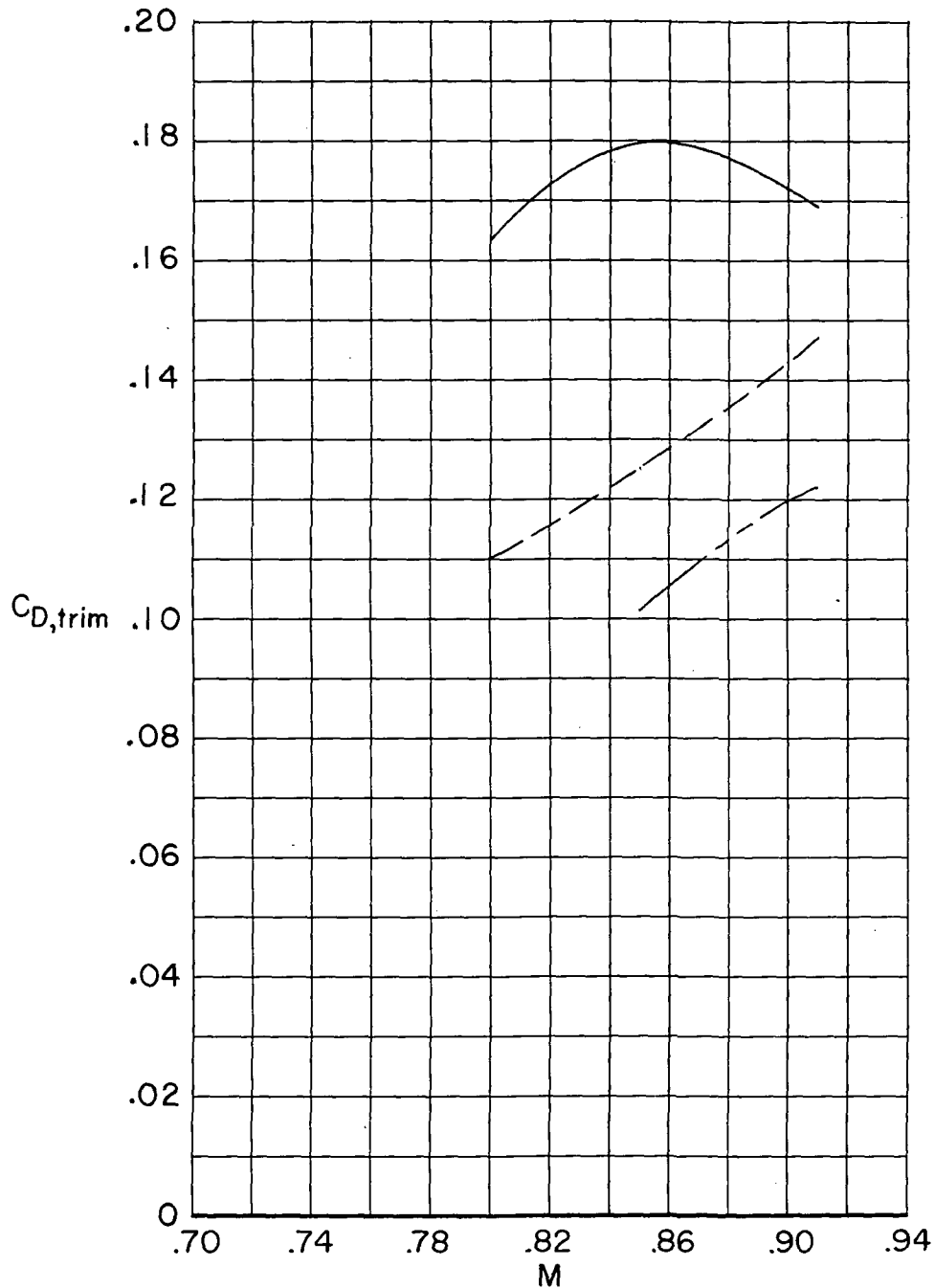
(b) $\Lambda = 33^\circ$.

Figure 45. - Continued.



~~CONFIDENTIAL~~

	Airfoil	i_w, deg	Fairing
—————	NACA 64A-2XX	1	Off
-----	NACA 64A-4XX	-1	On
-----	Supercritical C	-3	On



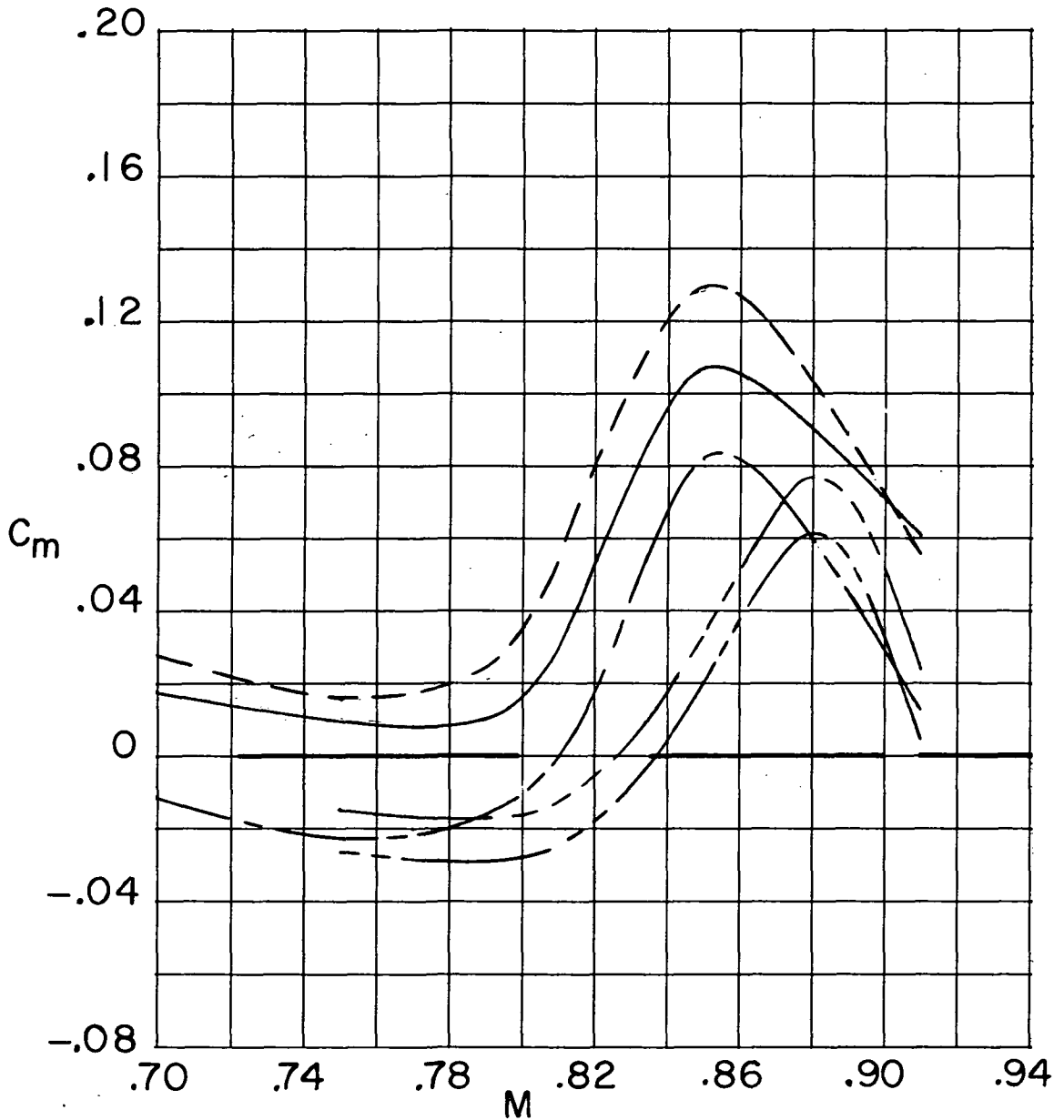
(c) $\Lambda = 39^\circ$.

Figure 45.- Concluded.

~~CONFIDENTIAL~~

~~CONFIDENTIAL~~

	Airfoil	i_w, deg	δ_h, deg	Fairing
—————	NACA 64A-2XX	1	0	Off
- - - - -	NACA 64A-4XX	1	0	On
—————	NACA 64A-4XX	-1	2	On
—————	Supercritical B	-1	2	On
- - - - -	Supercritical C	-3	2	On

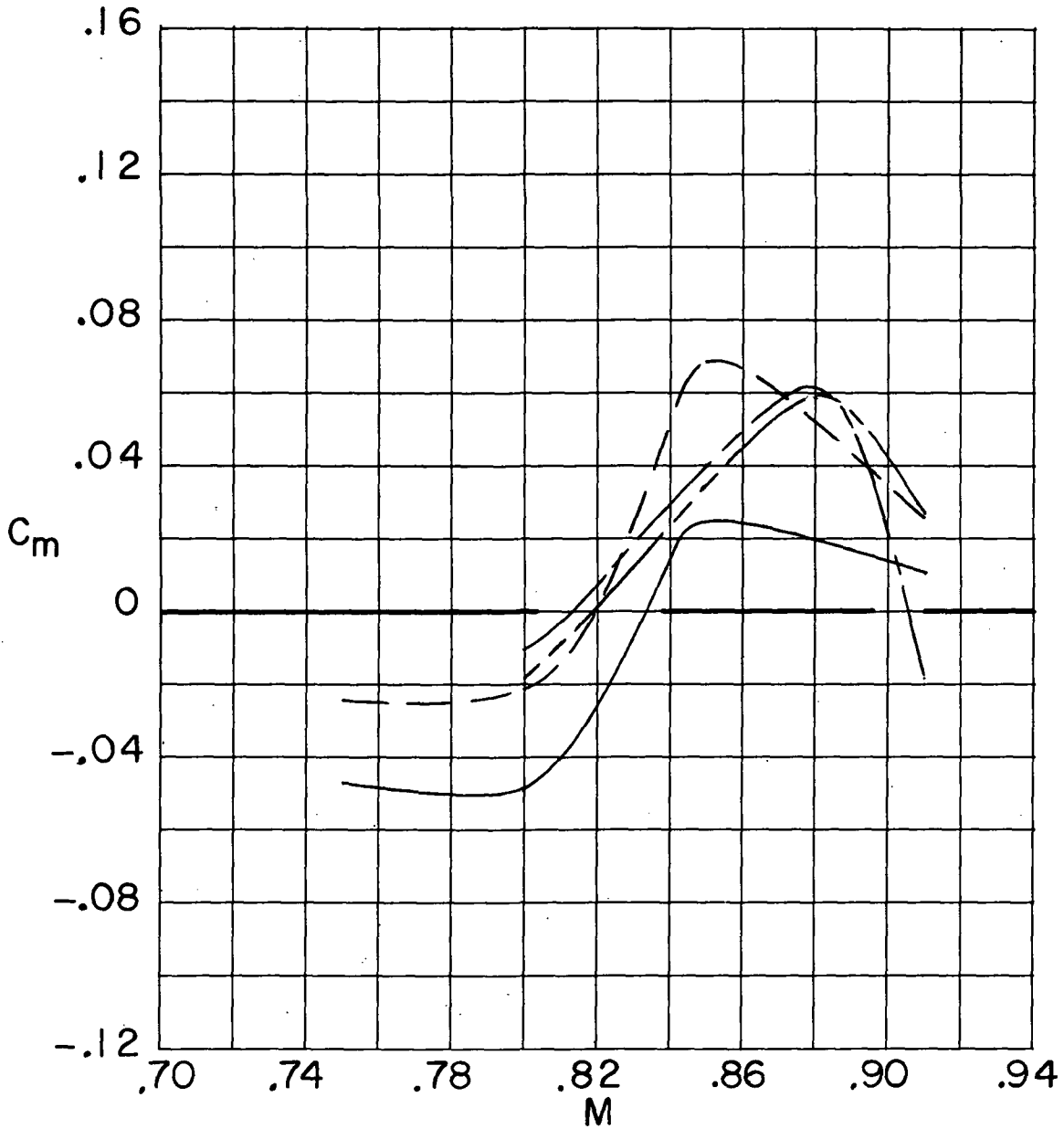


(a) $\Lambda = 26^\circ$.

Figure 46.- Variation with Mach number of pitching-moment characteristics. $C_L = 0.50$.

~~CONFIDENTIAL~~

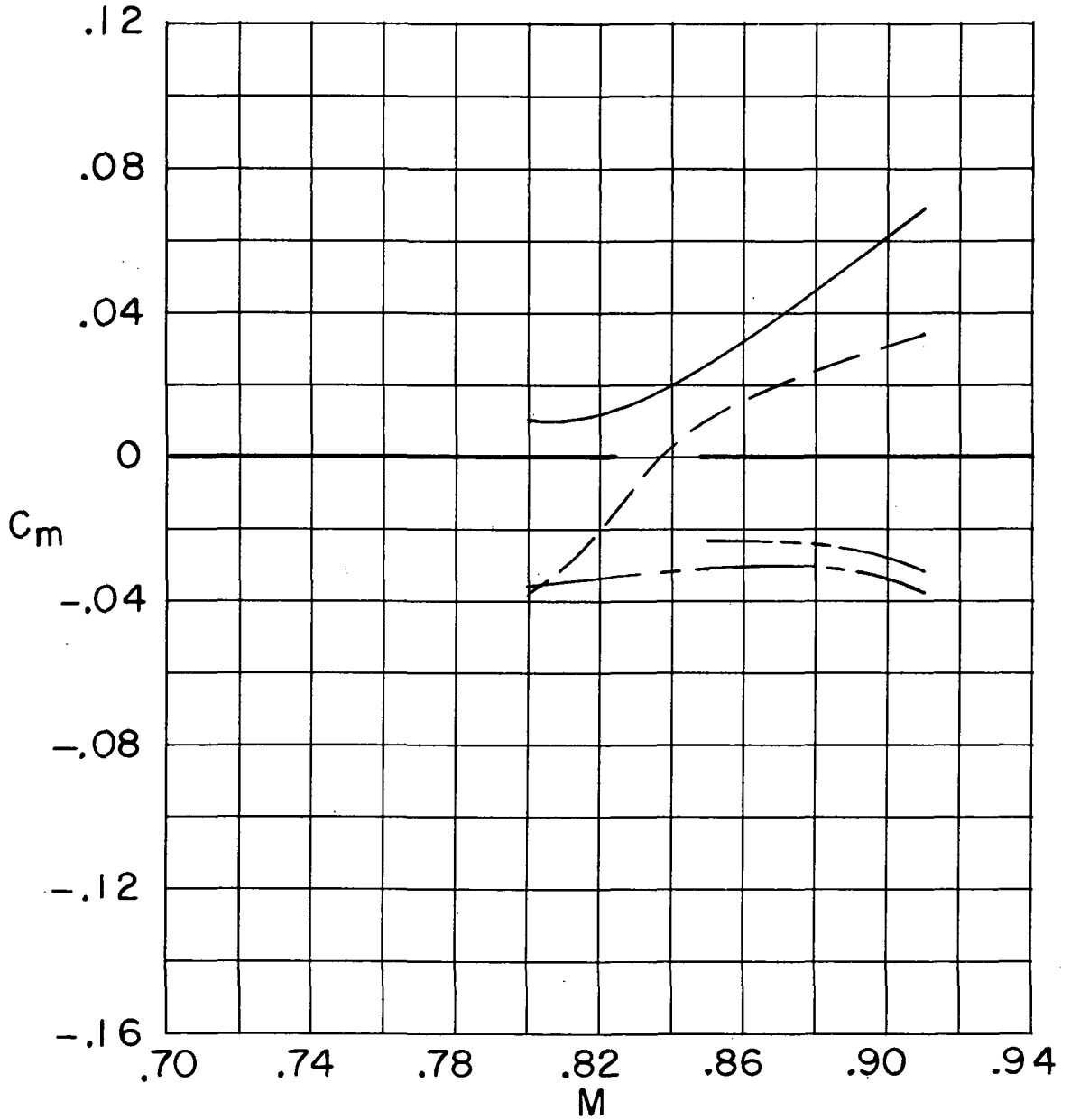
	Airfoil	i_w, deg	δ_h, deg	Fairing
————	NACA 64A-2XX	1	0	Off
— — —	NACA 64A-4XX	-1	0	On
—— —	Supercritical B	-1	0	On
— — —	Supercritical C	-3	0	On



(b) $\Lambda = 33^\circ$.

Figure 46. - Continued.

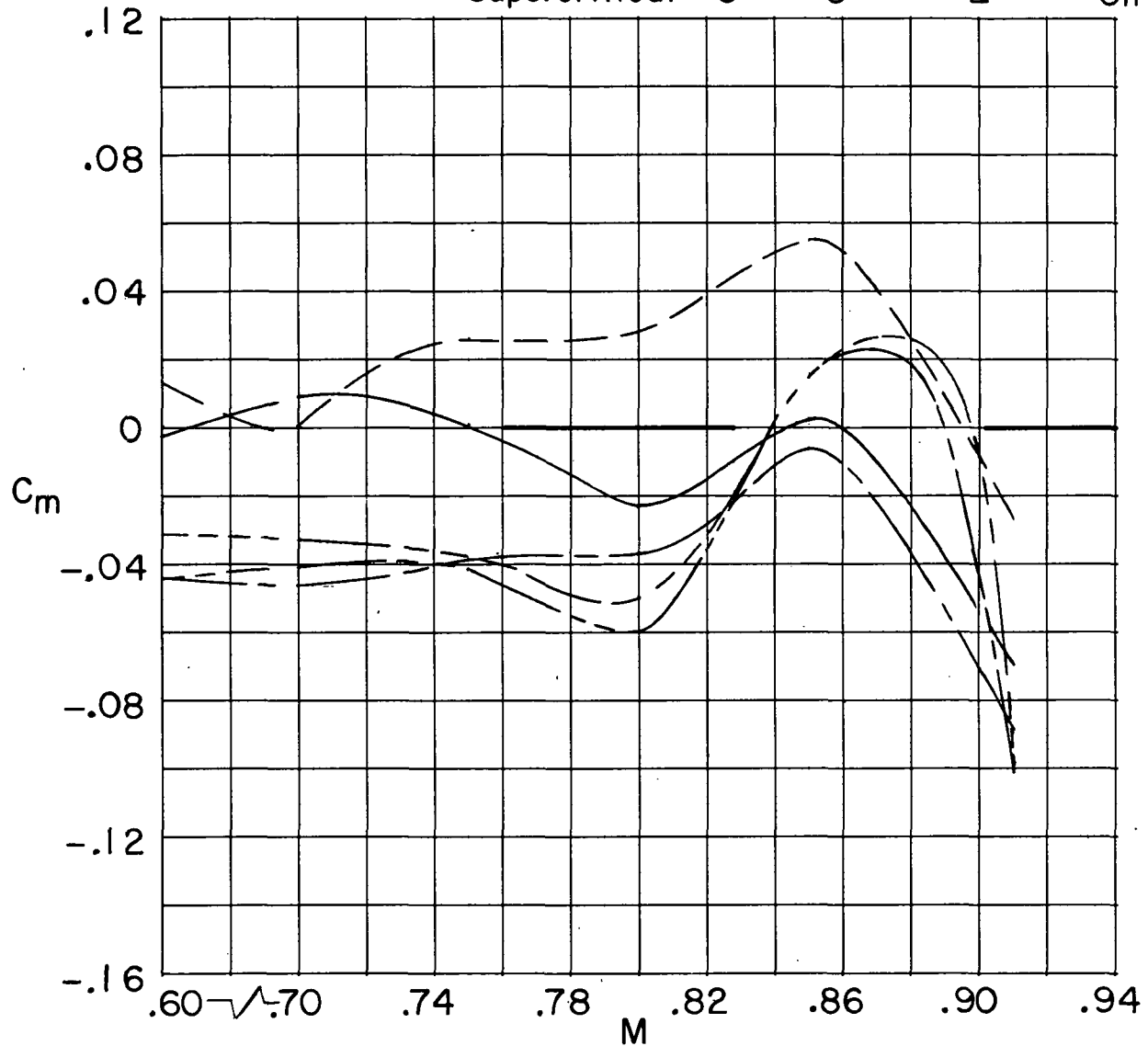
	Airfoil	i_w, deg	δ_h, deg	Fairing
————	NACA 64A-2XX	1	-2	Off
- - - -	NACA 64A-4XX	-1	0	On
————	Supercritical B	-1	0	On
- - - -	Supercritical C	-3	0	On



(c) $\Lambda = 39^\circ$.

Figure 46.- Concluded.

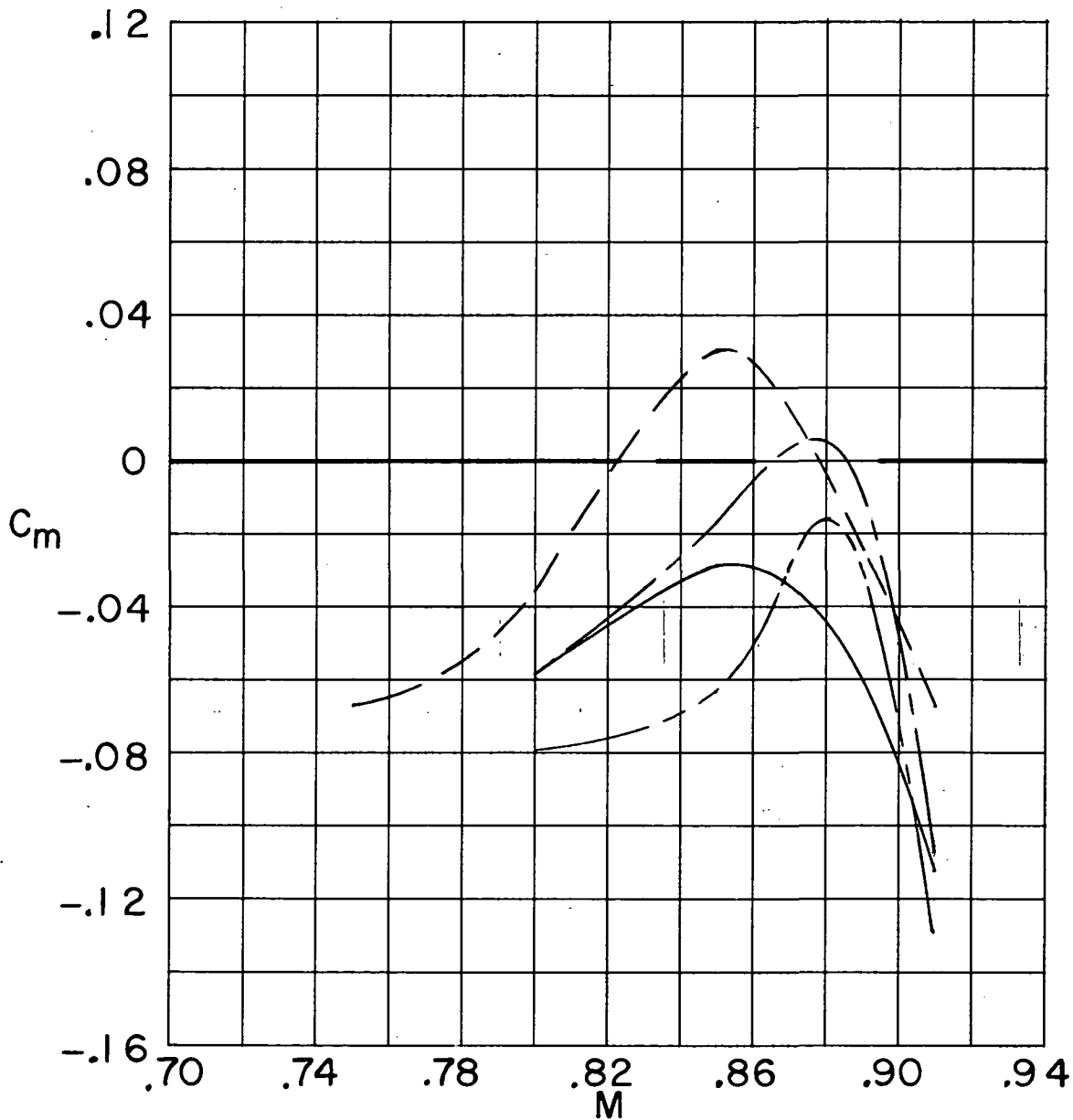
	Airfoil	i_w, deg	δ_h, deg	Fairing
—————	NACA 64A-2XX	1	0	Off
-----	NACA 64A-4XX	1	0	On
—————	NACA 64A-4XX	-1	2	On
-----	Supercritical B	-1	2	On
-----	Supercritical C	-3	2	On



(a) $\Lambda = 26^\circ$.

Figure 47.- Variation with Mach number of pitching-moment characteristics. $C_L = 0.90$.

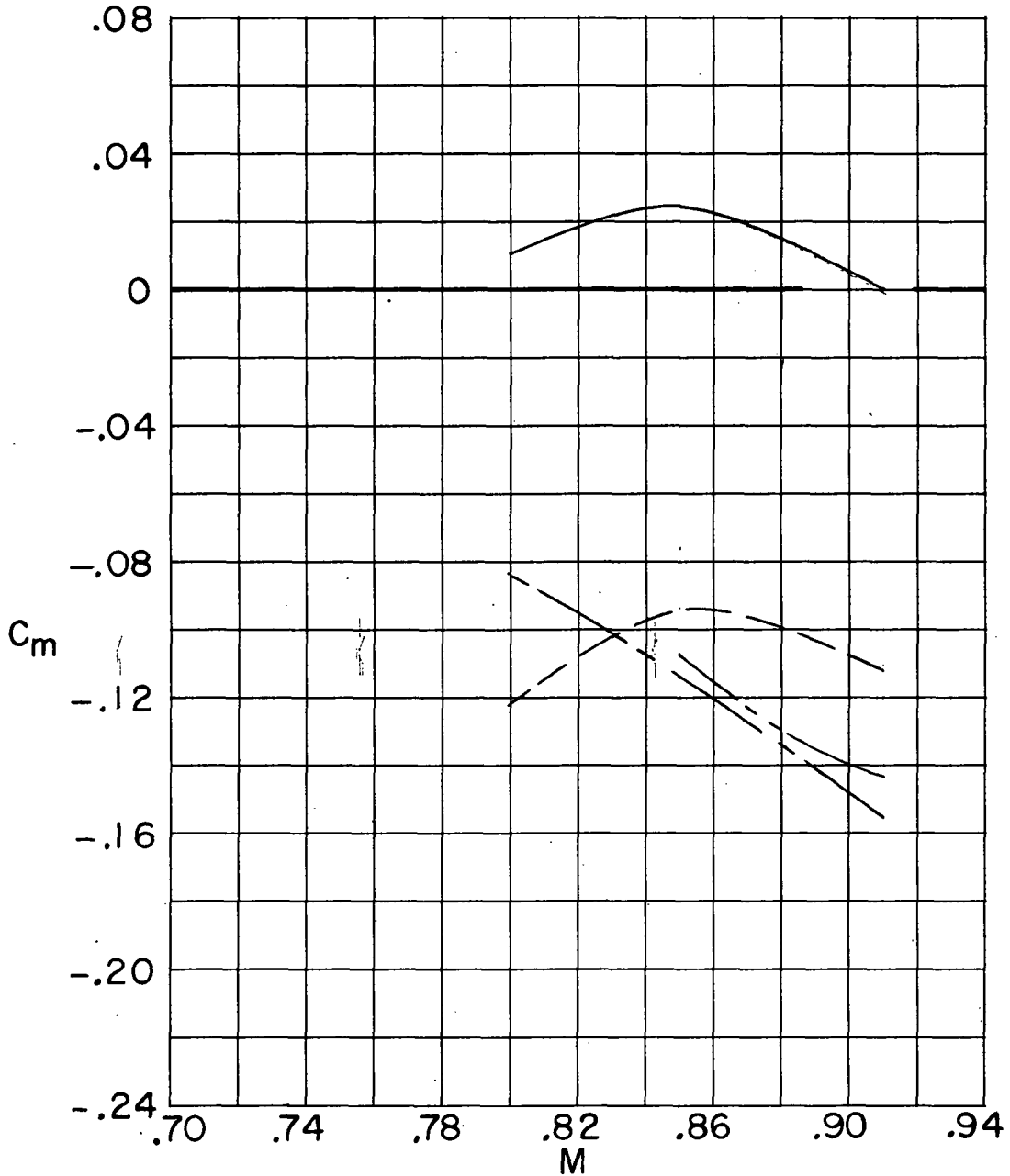
	Airfoil	i_w, deg	δ_h, deg	Fairing
—————	NACA 64A-2XX	1	0	Off
-----	NACA 64A-4XX	-1	0	On
—————	Supercritical B	-1	0	On
-----	Supercritical C	-3	0	On



(b) $\Lambda = 33^\circ$.

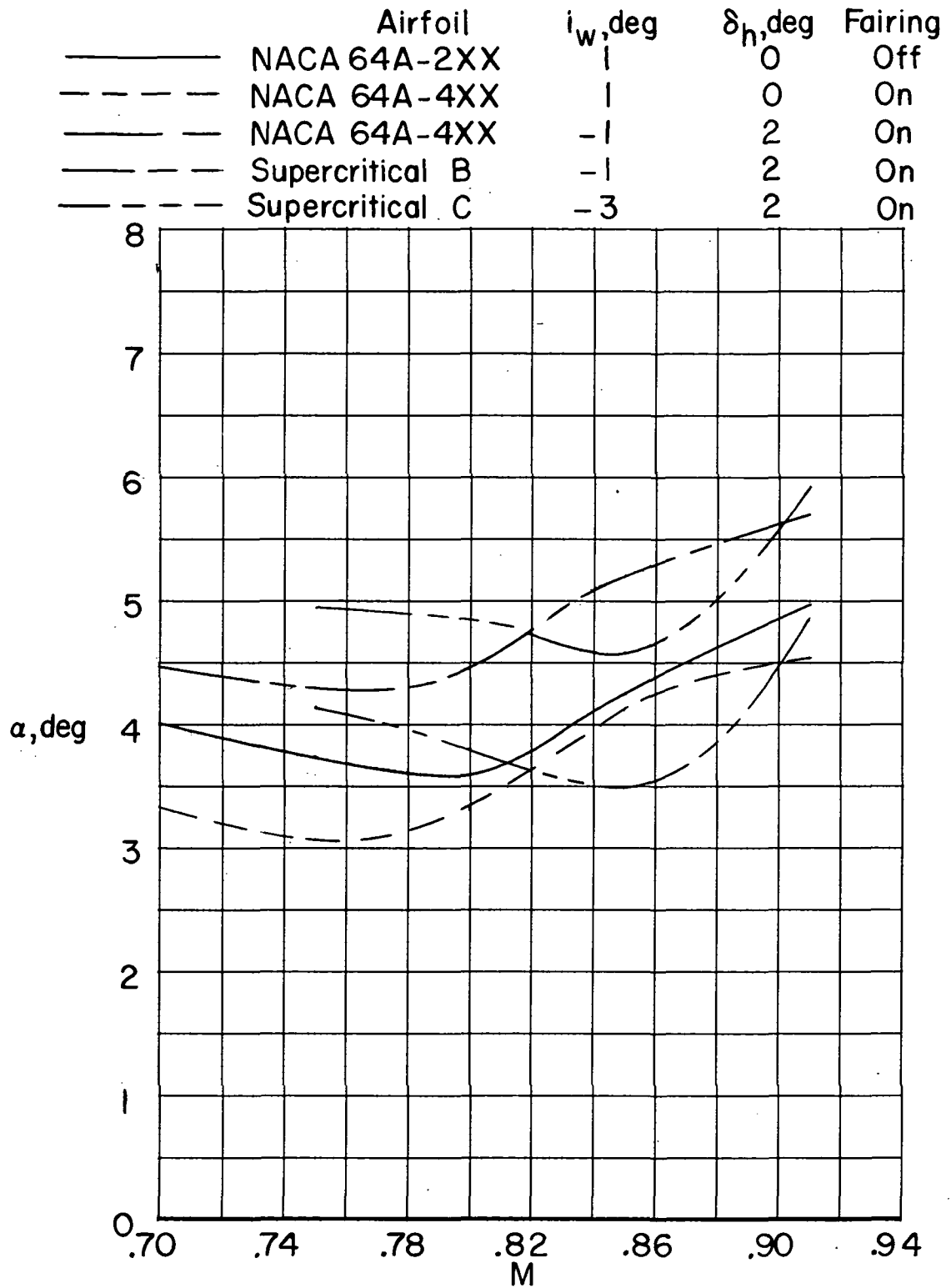
Figure 47.- Continued.

	Airfoil	i_w, deg	δ_h, deg	Fairing
—————	NACA 64A-2XX	1	-2	Off
- - - - -	NACA 64A-4XX	-1	0	On
—————	Supercritical B	-1	0	On
- - - - -	Supercritical C	-3	0	On



(c) $\Lambda = 39^\circ$.

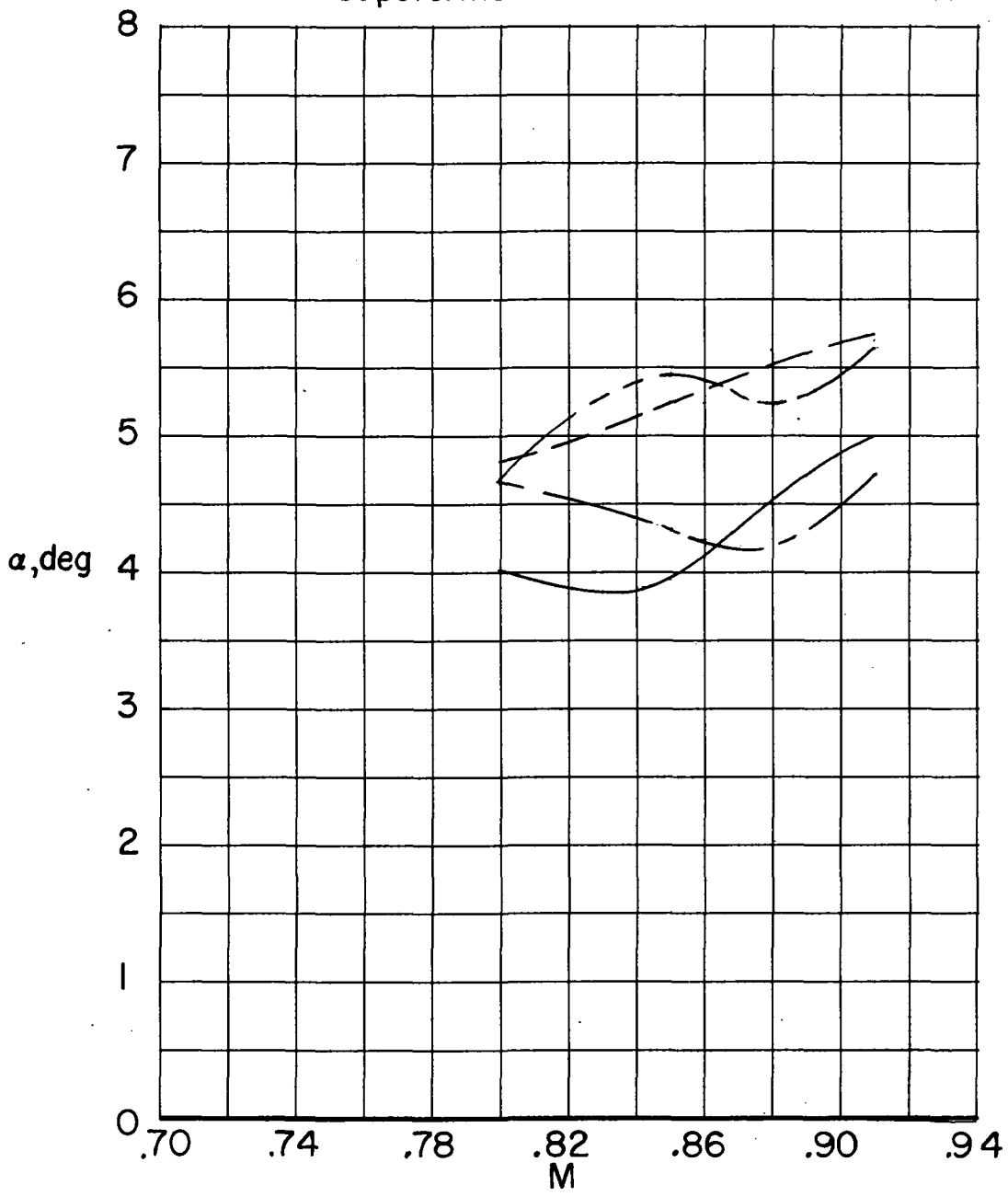
Figure 47.- Concluded.



(a) $\Lambda = 26^\circ$.

Figure 48.- Variation with Mach number of angle-of-attack characteristics. $C_L = 0.50$.

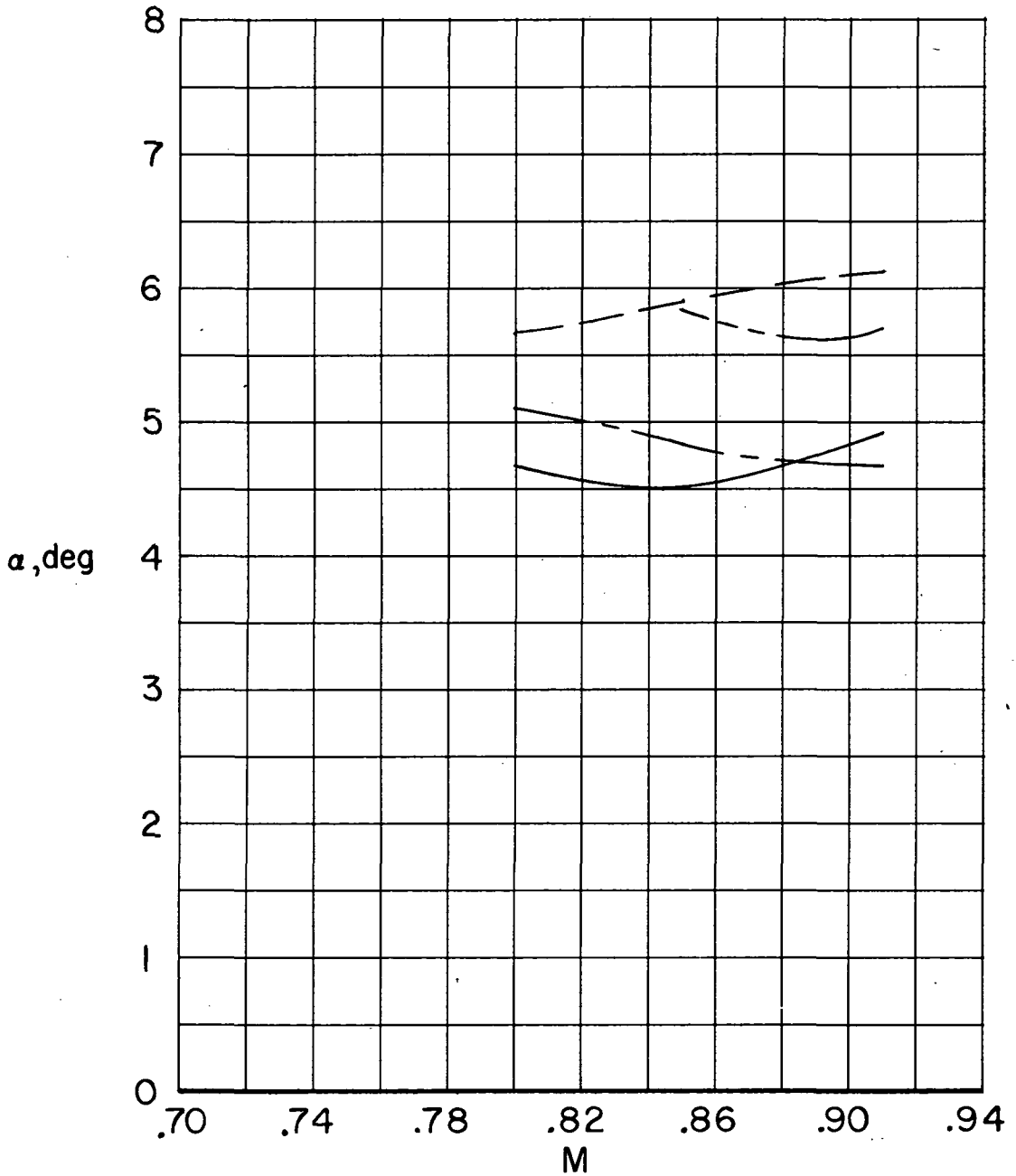
	Airfoil	i_w, deg	δ_h, deg	Fairing
—————	NACA 64A-2XX	1	0	Off
-----	NACA 64A-4XX	-1	0	On
—————	Supercritical B	-1	0	On
-----	Supercritical C	-3	0	On



(b) $\Lambda = 33^\circ$.

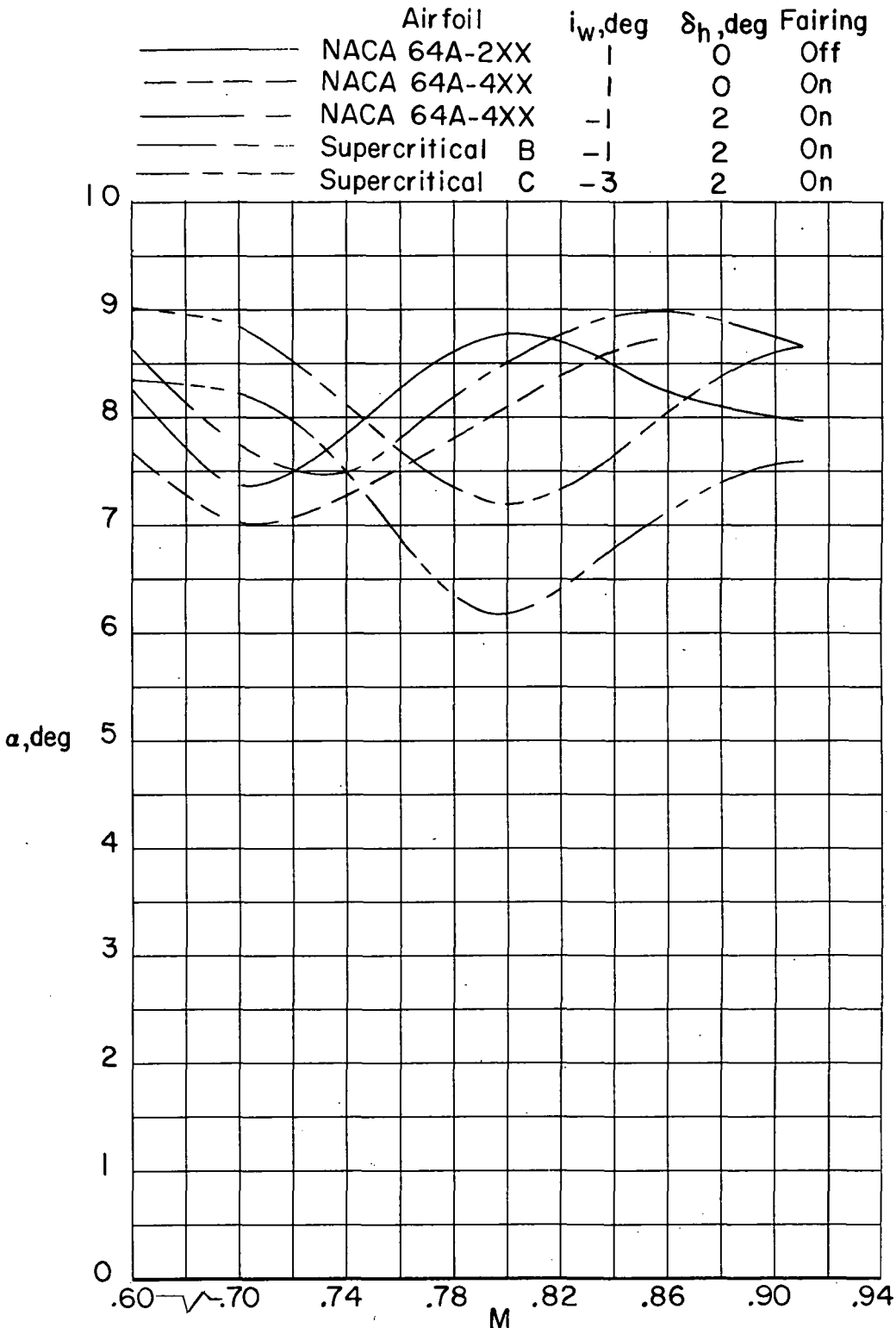
Figure 48. - Continued.

	Airfoil	i_w , deg	δ_h , deg	Fairing
————	NACA 64A-2XX	1	-2	Off
- - - -	NACA 64A-4XX	-1	0	On
————	Supercritical B	-1	0	On
- - - -	Supercritical C	-3	0	On



(c) $\Lambda = 39^\circ$.

Figure 48. - Concluded.

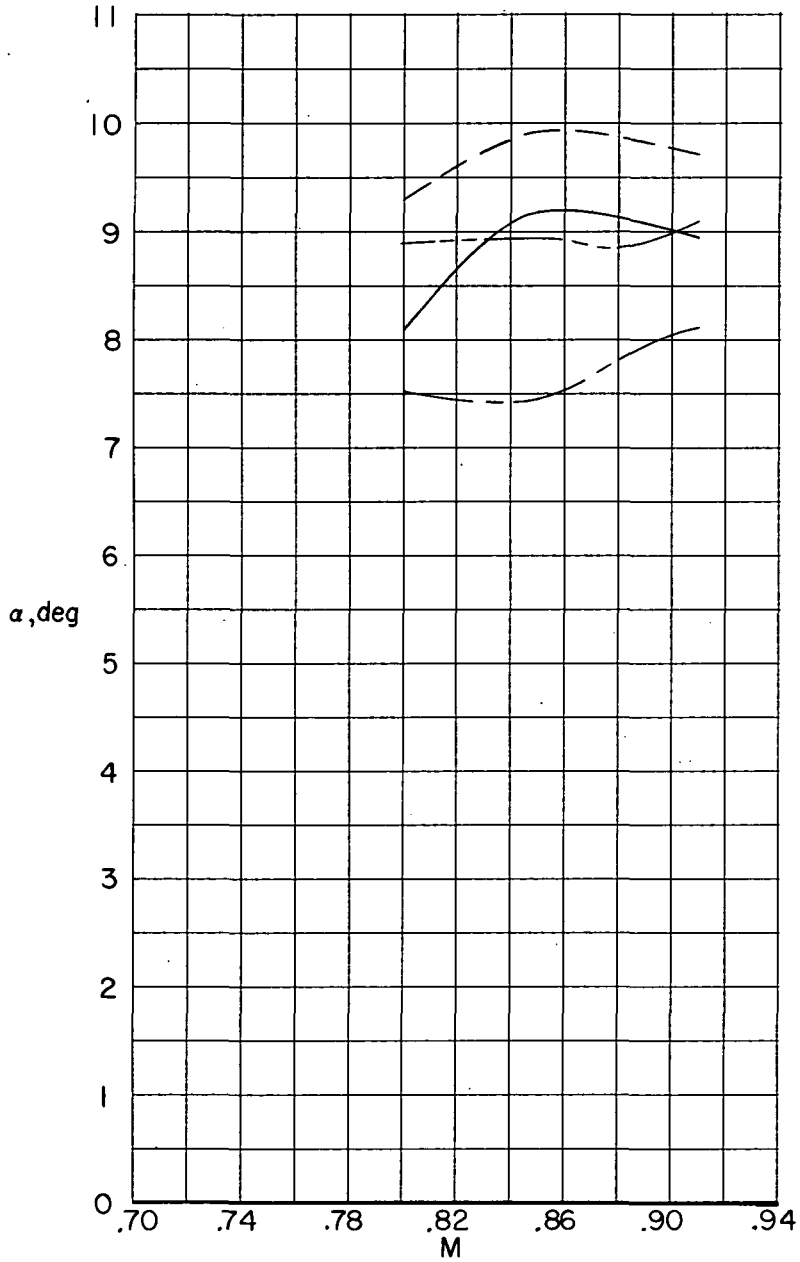


(a) $\Lambda = 26^\circ$.

Figure 49.- Variation with Mach number of angle-of-attack characteristics. $C_L = 0.90$.

~~CONFIDENTIAL~~

	Airfoil	i_w, deg	δ_h, deg	Fairing
—————	NACA 64A-2XX	1	0	Off
-----	NACA 64A-4XX	-1	0	On
-----	Supercritical B	-1	0	On
-----	Supercritical C	-3	0	On

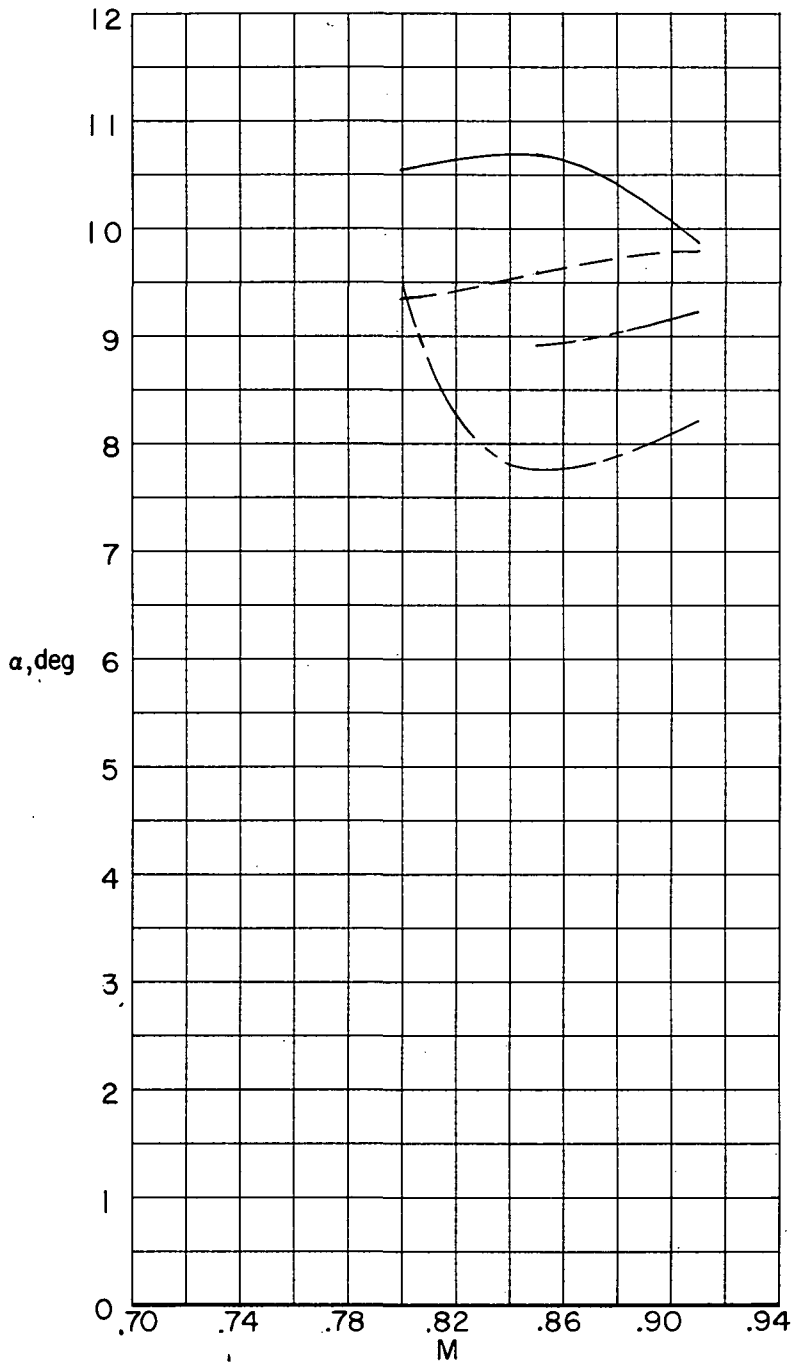


(b) $\Lambda = 33^\circ$.

Figure 49.- Continued.

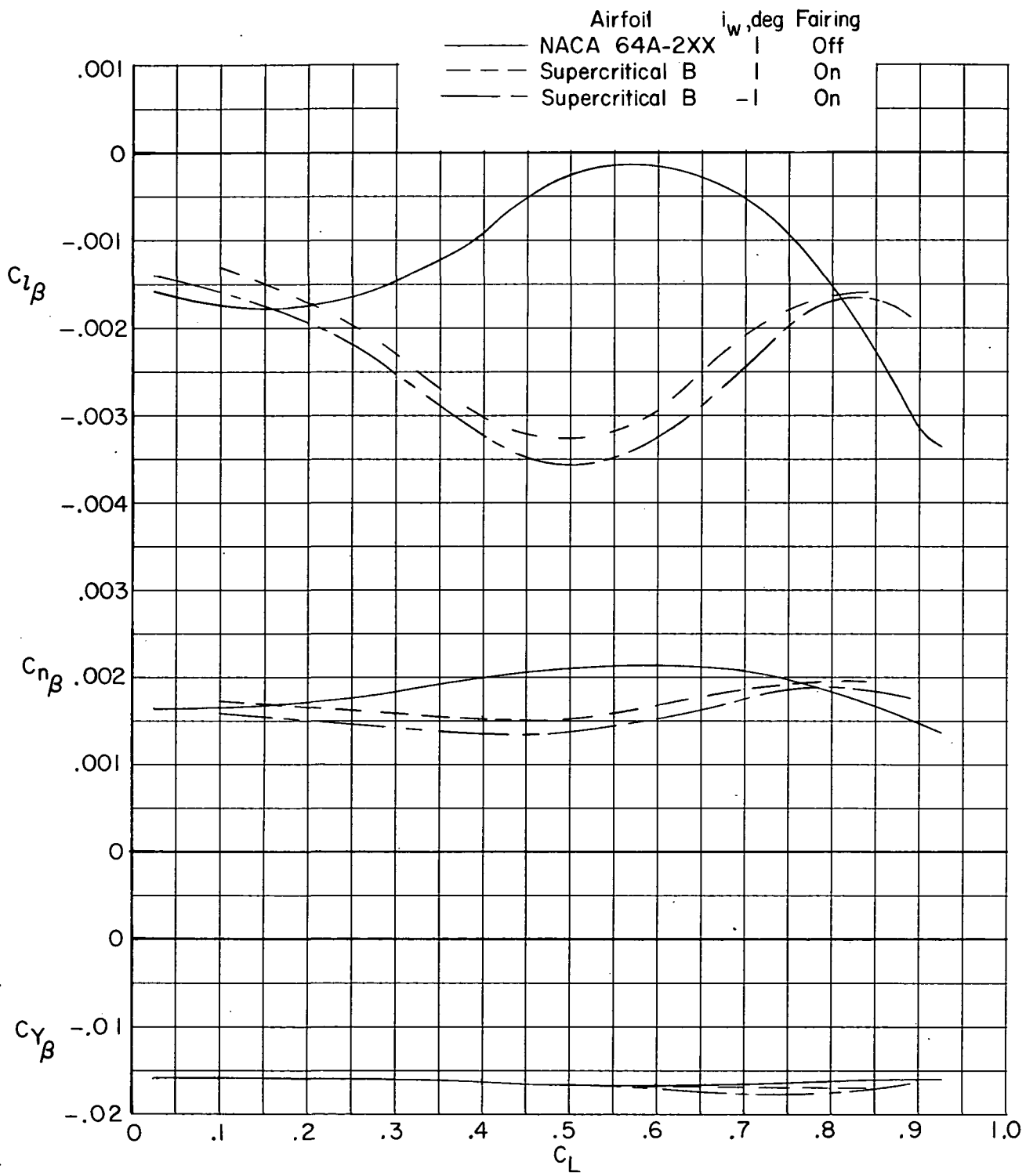
~~CONFIDENTIAL~~

	Airfoil	i_w, deg	δ_h, deg	Fairing
—————	NACA 64A-2XX	1	-2	Off
-----	NACA 64A-4XX	-1	0	On
—————	Supercritical B	-1	0	On
-----	Supercritical C	-3	0	On



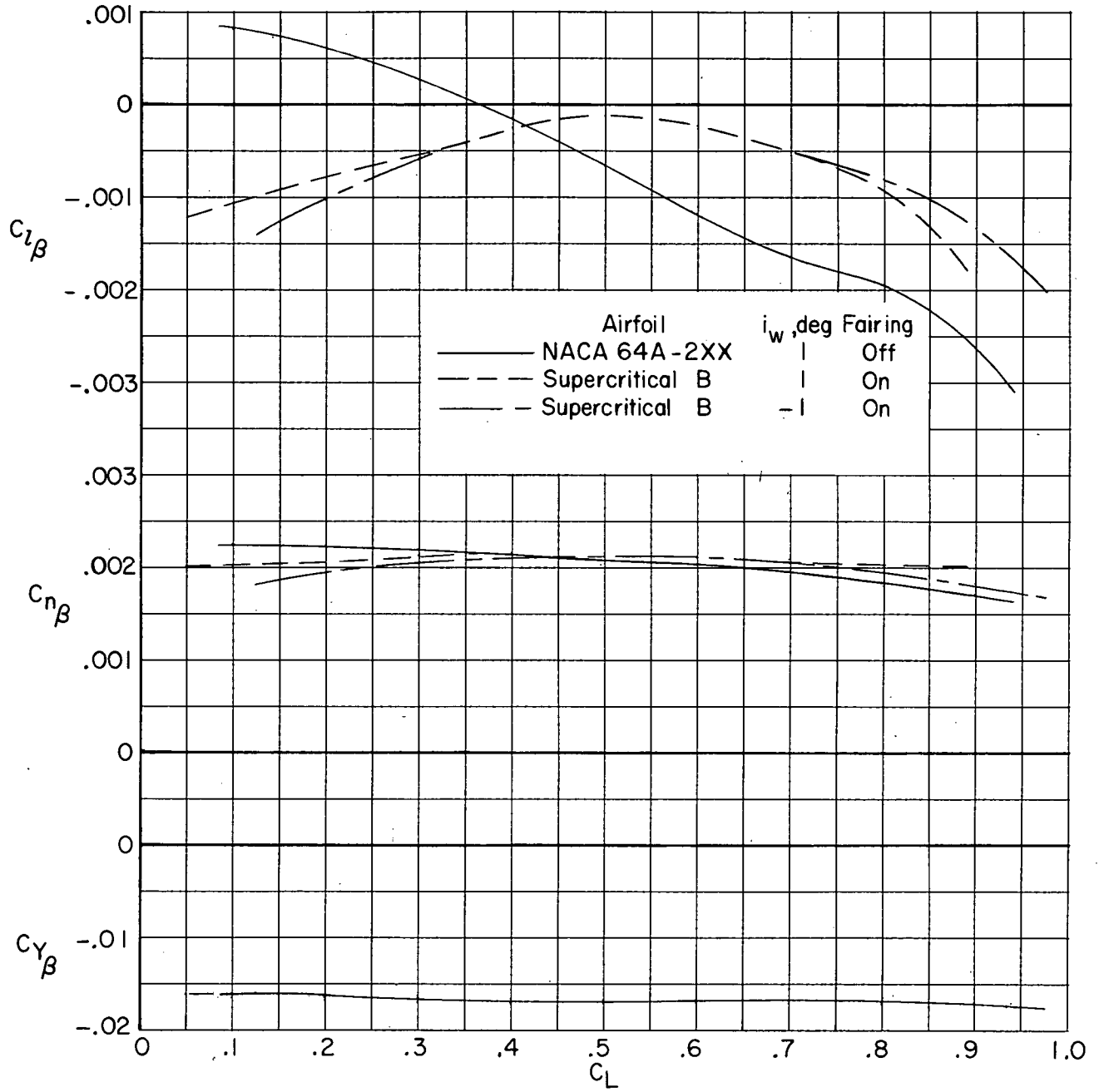
(c) $\Lambda = 39^\circ$.

Figure 49.- Concluded.



(a) $M = 0.85$.

Figure 50.- Variation with lift coefficient of sideslip derivatives. $\Lambda = 33^\circ$; $\delta_h = 0^\circ$.



(b) $M = 0.91$.

Figure 50. - Concluded.

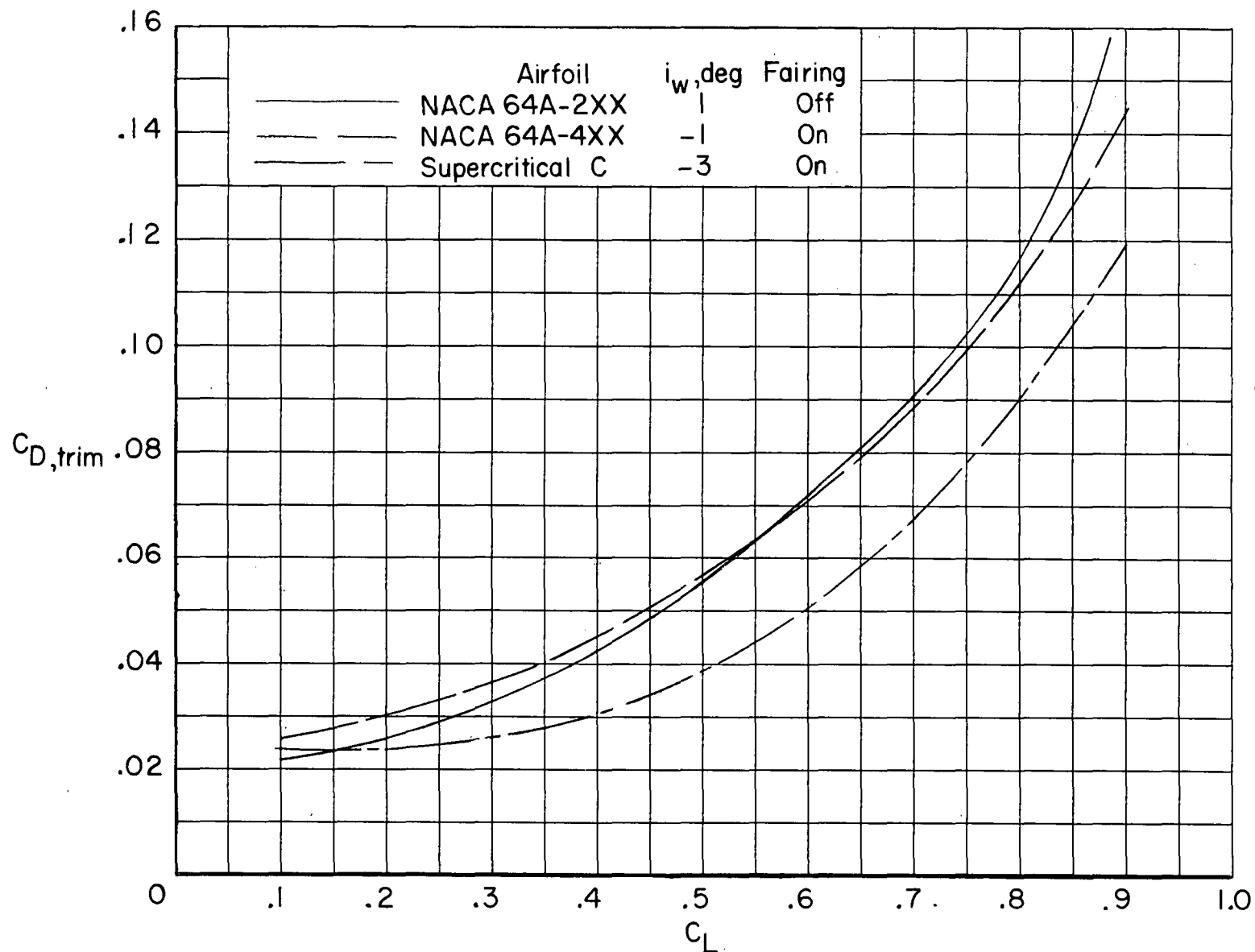


Figure 51.- Comparison of trimmed lift-drag polars for leading-edge sweep of 39° at Mach number of 0.90. Transition rearward.

~~CONFIDENTIAL~~

"The aeronautical and space activities of the United States shall be conducted so as to contribute . . . to the expansion of human knowledge of phenomena in the atmosphere and space. The Administration shall provide for the widest practicable and appropriate dissemination of information concerning its activities and the results thereof."

—NATIONAL AERONAUTICS AND SPACE ACT OF 1958

NASA SCIENTIFIC AND TECHNICAL PUBLICATIONS

TECHNICAL REPORTS: Scientific and technical information considered important, complete, and a lasting contribution to existing knowledge.

TECHNICAL NOTES: Information less broad in scope but nevertheless of importance as a contribution to existing knowledge.

TECHNICAL MEMORANDUMS: Information receiving limited distribution because of preliminary data, security classification, or other reasons.

CONTRACTOR REPORTS: Scientific and technical information generated under a NASA contract or grant and considered an important contribution to existing knowledge.

TECHNICAL TRANSLATIONS: Information published in a foreign language considered to merit NASA distribution in English.

SPECIAL PUBLICATIONS: Information derived from or of value to NASA activities. Publications include conference proceedings, monographs, data compilations, handbooks, sourcebooks, and special bibliographies.

TECHNOLOGY UTILIZATION PUBLICATIONS: Information on technology used by NASA that may be of particular interest in commercial and other non-aerospace applications. Publications include Tech Briefs, Technology Utilization Reports, and Technology Surveys.

Details on the availability of these publications may be obtained from:

SCIENTIFIC AND TECHNICAL INFORMATION OFFICE
NATIONAL AERONAUTICS AND SPACE ADMINISTRATION

Washington, D.C. 20546

~~CONFIDENTIAL~~